NASA/TM—2002-211700

Experimental Investigation of Water Droplet Impingement on Airfoils, Finite Wings, and an S-Duct Engine Inlet

Michael Papadakis and Kuohsing E. Hung
Wichita State University, Wichita, Kansas

Giao T. Vu
Boeing Airplane Company, Wichita, Kansas

Hsiung Wei Yeong
Wichita State University, Wichita, Kansas

Colin S. Bidwell
Glenn Research Center, Cleveland, Ohio

Marlin D. Breer
Boeing Airplane Company, Wichita, Kansas

Timothy J. Bencic
Glenn Research Center, Cleveland, Ohio

October 2002

The NASA STI Program Office . . . in Profile

Since its founding, NASA has been dedicated to the advancement of aeronautics and space science. The NASA Scientific and Technical Information (STI) Program Office plays a key part in helping NASA maintain this important role.

The NASA STI Program Office is operated by Langley Research Center, the Lead Center for NASA's scientific and technical information. The NASA STI Program Office provides access to the NASA STI Database, the largest collection of aeronautical and space science STI in the world. The Program Office is also NASA's institutional mechanism for disseminating the results of its research and development activities. These results are published by NASA in the NASA STI Report Series, which includes the following report types:

- TECHNICAL PUBLICATION. Reports of completed research or a major significant phase of research that present the results of NASA programs and include extensive data or theoretical analysis. Includes compilations of significant scientific and technical data and information deemed to be of continuing reference value. NASA's counterpart of peer-reviewed formal professional papers but has less stringent limitations on manuscript length and extent of graphic presentations.

- TECHNICAL MEMORANDUM. Scientific and technical findings that are preliminary or of specialized interest, e.g., quick release reports, working papers, and bibliographies that contain minimal annotation. Does not contain extensive analysis.

- CONTRACTOR REPORT. Scientific and technical findings by NASA-sponsored contractors and grantees.

- CONFERENCE PUBLICATION. Collected papers from scientific and technical conferences, symposia, seminars, or other meetings sponsored or cosponsored by NASA.

- SPECIAL PUBLICATION. Scientific, technical, or historical information from NASA programs, projects, and missions, often concerned with subjects having substantial public interest.

- TECHNICAL TRANSLATION. English-language translations of foreign scientific and technical material pertinent to NASA's mission.

Specialized services that complement the STI Program Office's diverse offerings include creating custom thesauri, building customized databases, organizing and publishing research results . . . even providing videos.

For more information about the NASA STI Program Office, see the following:

- Access the NASA STI Program Home Page at ***http://www.sti.nasa.gov***

- E-mail your question via the Internet to help@sti.nasa.gov

- Fax your question to the NASA Access Help Desk at 301–621–0134

- Telephone the NASA Access Help Desk at 301–621–0390

- Write to:
  NASA Access Help Desk
  NASA Center for AeroSpace Information
  7121 Standard Drive
  Hanover, MD 21076

NASA/TM—2002-211700

Experimental Investigation of Water Droplet Impingement on Airfoils, Finite Wings, and an S-Duct Engine Inlet

Michael Papadakis and Kuohsing E. Hung
Wichita State University, Wichita, Kansas

Giao T. Vu
Boeing Airplane Company, Wichita, Kansas

Hsiung Wei Yeong
Wichita State University, Wichita, Kansas

Colin S. Bidwell
Glenn Research Center, Cleveland, Ohio

Marlin D. Breer
Boeing Airplane Company, Wichita, Kansas

Timothy J. Bencic
Glenn Research Center, Cleveland, Ohio

National Aeronautics and
Space Administration

Glenn Research Center

October 2002

Acknowledgments

Funding for this work was provided by NASA through NASA Glenn Research Grants NAG3–1775 and NAG3–1985. The authors would like to thank the following NASA Glenn personnel: Tom Bond, Chief, Icing Branch, for his support, John R. Oldenburg and Robert F. Ide for performing droplet size and distribution as well as LWC measurements during the impingement tests and for their useful comments and suggestions, the IRT personnel for their extensive support with the impingement tests, Dave Sheldon for his engineering support with the wind tunnel models, Harold E. Addy and Charlie Andracchio for their assistance with the surface pressure measurements, Howard Broughton and co-op student Joel Feldman for their contributions to the development of the CCD data reduction system. The support received from Victor Canacci, NYMA, during the uniformity tests is also acknowledged. The authors would like to thank Frank Lynch, Abdi Khodadoust, Kichio Ishimitsu, and Anil Shah of the Boeing Company for making the three-element high lift wing model available for testing. Thanks are also due to: Baily Vittal, Katharine Treml, and Brian Treml of the Allison Advanced Development Company for providing the S-duct and for their support during the impingement tests; Mike Hinson and Reuben Chandrasecharan of the Bombardier/Learjet Company for providing the 25 percent and full-scale business jet tail models. Finally, the extensive contributions of Art Porter, Arief Rachman, Wadii Benjilany, and Michael Davis, Wichita State University, to this project are acknowledged

The Aerospace Propulsion and Power Program at
NASA Glenn Research Center sponsored this work.

Available from

NASA Center for Aerospace Information
7121 Standard Drive
Hanover, MD 21076

National Technical Information Service
5285 Port Royal Road
Springfield, VA 22100

Available electronically at http://gltrs.grc.nasa.gov

Experimental Investigation of Water Droplet Impingement on Airfoils, Finite Wings, and an S-Duct Engine Inlet

Michael Papadakis and Kuohsing E. Hung
Wichita State University
Wichita, Kansas

Giao T. Vu
Boeing Airplane Company
Wichita, Kansas

Hsiung Wei Yeong
Wichita State University
Wichita, Kansas

Colin S. Bidwell
National Aeronautics and Space Administration
Glenn Research Center
Cleveland, Ohio

Marlin D. Breer
Boeing Airplane Company
Wichita, Kansas

Timothy J. Bencic
National Aeronautics and Space Administration
Glenn Research Center
Cleveland, Ohio

Abstract

Validation of trajectory computer codes, for icing analysis, requires experimental water droplet impingement data for a wide range of aircraft geometries as well as flow and icing conditions. This report presents improved experimental and data reduction methods for obtaining water droplet impingement data and provides a comprehensive water droplet impingement database for a range of test geometries including an MS(1)-0317 airfoil, a GLC-305 airfoil, an NACA 65_2-415 airfoil, a commercial transport tail section, a 36-inch chord natural laminar flow NLF(1)-0414 airfoil, a 48-inch NLF(1)-0414 section with a 25% chord simple flap, a state-of-the-art three-element high lift system, a NACA 64A008 finite span swept business jet tail, a full-scale business jet horizontal tail section, a 25%-scale business jet empennage, and an S-duct turboprop engine inlet. The experimental results were obtained at the NASA Glenn Icing Research Tunnel (IRT) for spray clouds with median volumetric diameter (*MVD*) of 11, 11.5, 21, 92 and 94 microns and for a range of angles of attack. The majority of the impingement experiments were conducted at an air speed of 175 mph corresponding to a Reynolds

number of approximately 1.6 million per foot. The maximum difference of repeated tests from the average ranged from 0.24% to 12% for most of the experimental results presented. This represents a significant improvement in test repeatability compared to previous experimental studies. The increase in test repeatability was attributed to improvements made to the experimental and data reduction methods. Computations performed with the LEWICE-2D, and LEWICE-3D computer codes for all test configurations are presented in this report. For the test cases involving median volumetric diameters of 11 and 21 microns, the correlation between the analytical and experimental impingement efficiency distributions was good. For the median volumetric diameters of 92 and 94-micron cases, however, the analysis produced higher impingement efficiencies and larger impingement limits than the experiment. It is speculated that this discrepancy is due to droplet splashing and breakup experienced by large droplets during impingement.

Executive Summary

Ice accretion on critical aerodynamic surfaces can significantly degrade aircraft performance and safety. Ice protection systems are employed on most commercial aircraft to reduce or eliminate the adverse effects of ice accretion. The design of ice protection systems requires knowledge of local and total droplet impingement intensities in order to determine energy levels per unit area for ice protection. In addition, the water impingement limits are needed for determining the extent of the surface area to be protected. A number of trajectory computer codes have been developed over the years for predicting water impingement characteristics of internal and external aerodynamic surfaces. The application of these codes to icing analysis for ice protection system design and certification requires validation against experimental data.

The first experimental water impingement database was developed by the National Advisory Committee for Aeronautics (NACA) in the 1950's using a dye tracer technique. In 1984, a research program was initiated to develop improved experimental and data reduction methods for measuring water impingement and to obtain experimental impingement data for a range of modern wings and engine inlets. This research program was sponsored by the National Aeronautics and Space Administration (NASA) and by the Federal Aviation Administration (FAA) and was conducted by personnel from the Wichita State University (WSU) and the Boeing Company. The program included two major tunnel entries and analysis of the extensive data was completed in 1993.

A peer review of NASA icing research activities conducted in 1994 and results from an industry survey conducted in 1995 indicated that additional experimental water droplet impingement data were needed, including data for supercooled large droplet (SLD) conditions which were not available. To address the concerns of its industrial partners, the Icing Technology Branch at NASA Glenn Research Center awarded a research grant to Wichita State University (WSU) in 1996 to begin work on modernizing and expanding the water droplet impingement database. The accomplishments of this new research program, which was completed in 2000, are summarized below:

1. Significant improvements were made to the experimental method including automation of the WSU 12-nozzle spray system and development of a new laser sheet method for setting cloud uniformity.
2. Extensive experiments were conducted to identify the effect of key experimental parameters on the repeatability of the impingement results.
3. A new, very efficient data reduction method based on a CCD array camera was developed for extracting the raw experimental impingement data from the dye-laden blotter strips.
4. Experiments were performed to assess the accuracy of the new data reduction method and extensive comparisons were made with results obtained using the laser reflectometer developed in the 1980's.
5. Experimental impingement data were obtained for six two-dimensional airfoils, a modern high lift system, three finite swept tails and an S-duct engine inlet. Data were obtained for median volumetric diameters of 11, 11.5, 21, 92 and 94 microns.
6. Correlation of the experimental impingement data with analysis data obtained with the LEWICE-2D and LEWICE-3D computer codes was performed.

Nomenclature

AOA	Angle of Attack
BJ	Business Jet
BJE	Business Jet Empennage
CCD	Charge-Coupled Device
DAQ	Data Acquisition
DIO	Digital Input Output
FAA	Federal Aviation Administration
FS	Full-Scale
FSSP	Forward Scattering Spectrometer Probe
IRT	Icing Research Tunnel
LE	Leading Edge
LWC	Liquid Water Content
MAC	Mean Aerodynamic Chord
MVD	Median Volumetric Diameter
OAP	Optical Array Probe
PDPA	Phase Doppler Particle Analyzer
RCM	Reference Collector Mechanism
PC	Personal Computer
SLD	Supercooled Large Droplets
SSR	Solid State Relay
TE	Trailing Edge
WRP	Wing Reference Plane
WSU	Wichita State University
A_f	Frontal area of a body projected parallel to freestream velocity direction
A_∞	Area perpendicular to freestream direction, defined by the tangent trajectories

c	Model chord length
C_D	Droplet drag coefficient
C_f	Nozzle flow coefficient
d	Droplet diameter
D	Droplet diameter
D_{max}	Maximum droplet diameter in clouds of non-uniform droplet size
D_{min}	Minimum droplet diameter in clouds of non-uniform droplet size
D_{MVD}	Droplet diameter based on MVD
E	Total impingement efficiency in clouds of non-uniform droplet size
g	Acceleration due to gravity
Highlight	Reference point on test geometry for measuring impingement efficiency. For the single element airfoils and three finite swept tails tested the highlight was located at the leading edge (x/c=0). For the three-element configuration, the highlight was located at the leading edge of each element. For the S-duct inlet, the highlight locations are defined in Fig. 22h. A summary of highlight locations for the models tested is provided in Appendix A.
K	$\rho_{droplet} \cdot V_\infty \cdot MVD^2 / (18 \cdot \mu \cdot c)$, droplet inertia parameter
K_0	$K \cdot \lambda / \lambda_s$, Modified droplet inertia parameter
L	Characteristic dimension of a body
M	Mach number of airflow relative to droplet
M_∞	Freestream Mach number of airflow
Re_c	Reynolds number based on chord length
Re_V	Reynolds number of airflow relative to droplet
Re_{MVD}	Reynolds number based on MVD and free stream speed
R_n	Normalized reflectance
S	Surface distance from highlight
$S_{\beta max}$	Surface distance from highlight to location of maximum impingement efficiency
S_u	Surface distance from highlight to impingement limit on upper surface
S_l	Surface distance from highlight to impingement limit on lower surface
t	Time; Airfoil thickness
U_i	Initial droplet velocity
V	Potential flow velocity dimensionless with V_∞
V_i	Initial potential flow velocity
V_∞	Freestream airspeed
$\dot{W}$	Water flow rate from WSU spray nozzles
W	Engine inlet mass flow
x,y	Cartesian coordinates
x_l	Chordwise distance corresponding to the impingement limit on the lower surface
x_u	Chordwise distance corresponding to the impingement limit on the upper surface
α	Angle of attack
β	Local impingement efficiency

ΔP	P_{water}-P_{air}
δ_{ij}	Kronecker delta
ϕ	Impingement parameter $(\mathrm{Re}_{MVD})^2/K$
λ	True range of droplet as projectile injected into still air
λ_s	Range of droplet as projectile following Stokes' law
μ	Absolute air viscosity
ρ	Air density
ρ_ω	Density of water

1.0 Introduction

Aircraft flying at subsonic speeds through clouds below 8000 meters (approximately 26,000 ft) can be subject to ice formation on critical aerodynamic surfaces which can lead to deterioration of aircraft aerodynamic performance and handling qualities. Ice accretion results from small, supercooled droplets (droplets cooled below freezing), usually 5 to 50 microns in diameter, which can freeze upon impact with the aircraft surface. Ice protection systems are employed on most commercial aircraft to reduce or eliminate the adverse effects of ice accretion. The design of ice protection systems requires knowledge of local and total droplet impingement intensities in order to determine energy levels per unit area for ice protection. In addition, the water impingement limits are needed for determining the extent of the surface area to be protected. Thus, experimental water droplet impingement data are important to the development and certification of ice protection systems.

Experimental impingement data are also needed for the validation of trajectory computer codes, which play a significant role in aircraft icing analyses. A number of trajectory computer codes have been developed over the years for predicting the water impingement characteristics of internal and external aerodynamic surfaces. These codes are commonly used by industry as a cost-effective tool for evaluating icing protection requirements for aircraft components and to assist in the testing and certification of ice protection systems.

Several efforts in water droplet impingement research, including the work by the NACA in the 1950's and the research in the 1980's and 1990's, can be found in Refs. 1-7. These efforts have generated experimental impingement data for a range of conditions within the current icing certification requirements.

Recently, ice accretions resulting from supercooled large droplets (SLD) have become a safety concern in the aviation community. These icing conditions are outside the icing certification envelope as defined in Appendix C of FAR Part 25. As a result, regulatory authorities are currently evaluating large droplet icing effects and safety issues. To expand the range of application of current icing analysis codes beyond the

current icing certification envelope would require experimental impingement data for large droplets.

This report includes small and large droplet impingement data for a range of aerodynamic surfaces. The experimental data were obtained in 1997 and in 1999 at the NASA Glenn Icing Research Tunnel (IRT) facility. The selection of test models and conditions for the impingement tests was based on an industry survey conducted in 1995.

2.0 Background

The first extensive water droplet impingement database was developed by NACA in the 1950's. A dye-tracer technique was developed for measuring local impingement efficiency on aircraft aerodynamic surfaces (Ref. 1). In this technique, water containing a small amount of water-soluble dye was injected in the form of droplets into the air stream ahead of the body by means of spray nozzles. The surface of the body was covered with blotter material upon which the dyed water impinged and was absorbed. At the point of impact and droplet absorption, a permanent dye deposit (dye trace) was obtained. The impingement limits were obtained directly from the rearmost dye trace on the absorbent material.

Data analysis consisted of removing the dyed blotter strips from the body and punching out small segments of the blotter material for the determination of local impingement characteristics. The dye was dissolved out of each segment in a known quantity of water. The weight of dye in this solution was determined by the amount of light of a suitable wavelength transmitted through the solution by use of a calibrated colorimeter (colorimetric analysis). The weight of water that impinged at any surface location per unit time was determined from the weight of dye collected per unit area, and from knowledge of the original concentration of the dye in the water droplets.

The liquid water content in the cloud was determined using an aspirating device (Refs. 1, 2). This device consisted essentially of a tube, which sucked in the approaching air and cloud droplets at the freestream velocity (inlet velocity ratio 1) so that both the air streamlines and droplets entered the tube along straight-line paths. The dyed droplets were deposited on a filter mounted within the tube, leaving a dye trace that could be analyzed using colorimetric analysis. The droplet size distribution was determined by comparing experimental local impingement rates on cylinders of different sizes with theoretical predictions of droplet trajectories and impingement points using a differential analyzer.

Between 1955 and 1958 NACA personnel developed a water droplet impingement database for a wide range of cylinders, airfoils sections, bodies of revolution and a supersonic inlet (Refs. 1–5). Table 1 provides a selected list of test geometries and conditions used by NACA personnel for water droplet impingement testing. For most test configurations, the NACA method was sufficiently accurate. The

error in evaluating maximum local impingement efficiency varied from 10 to 25 percent (Refs. 1, 2). The major limitations of the NACA method included reduced spatial resolution and a laborious and time-consuming process for reducing the experimental data. In addition, the uncertainty in measuring the LWC and MVD values of the spray clouds used in the impingement tests was considerable.

In 1984, a research program was initiated to further expand and update the experimental water droplet impingement database and to provide much needed impingement data for aircraft inlets and modern wing sections. This program was sponsored by the NASA Glenn Research Center in Cleveland, Ohio and the FAA Technical Center in Atlantic City, New Jersey. The work was performed by researchers at Wichita State University and Boeing. During this research program, an experimental method similar to the one used in the early 1950's by NACA researchers was developed for measuring local impingement efficiency (Ref. 6). A new method for extracting the impingement data from the blotter strips was also developed. In this method, the amount of dye trace on a blotter strip obtained in a given time interval was converted into local impingement efficiency distribution using a laser reflectance spectroscopy method. Tests showed that the new data reduction method was significantly more efficient than the method of colorimetric analysis used in the 1950's by NACA personnel.

To generate the required spray clouds for the impingement tests a twelve-nozzle spray system was fabricated. This system was designed to have a very fast on/off response because the spray duration had to be very short (approximately 2–4 sec) to avoid saturation of the blotter paper. For the reflectance method to be accurate, dye penetration into the blotter paper had to be kept to a minimum.

The first series of impingement tests were conducted in September of 1985 in the NASA IRT for a period of four weeks. The geometries tested included a four-inch cylinder, a NACA 65_2-015, an MS(1)-0317 supercritical airfoil, three simulated ice shapes, an axisymmetric engine inlet model and a Boeing 737-300 engine inlet model. The configurations tested are given in Table 2. The second and final series of impingement tests were performed in the IRT facility during April of 1989 and lasted for approximately four weeks. Models tested during this phase of the research program included two simulated ice shapes, a Natural Laminar Flow airfoil section NLF(1)-0414F, an infinite span 30 degree swept MS(1)-0317 wing, a finite span 30 degree swept NACA 0012 wing, and a Boeing 737-300 engine inlet model. Details of the test geometries and conditions are given in Table 3. The experimental impingement data obtained during the 1985 and 1989 impingement tests can be found in Refs. 6 and 7. In summary, the water droplet impingement research program conducted between 1984 and 1993 was successful and considerably expanded the impingement database.

A peer review of NASA Glenn icing research activities conducted in 1994 indicated that additional water droplet impingement data were needed. Large droplet impingement data were also requested in response to a recent commuter aircraft icing related accident which has raised the question of the effect of ice accretion due to Supercooled Large Droplets (SLD) on aircraft performance and handling characteristics

(Refs. 8, 9). Preliminary studies of the effect of SLD on the ice accretion characteristics of a full-scale Twin-Otter wing section were reported in Ref. 10. Icing tests conducted with large droplets of 99 and 160 microns MVD demonstrated that an ice ridge formed aft of the active portion of the deicer boot. Potential adverse effects due to this ice ridge formation on the aerodynamic characteristics of aircraft include large loss in lift, increase in drag and pitching moment, and in severe cases aileron hinge moment reversal and aileron snatch as discussed in Ref. 11.

Currently, the Aviation Rulemaking Advisory Committee (ARAC)—Ice Protection Harmonization Working Group (IPHWG) is considering rulemaking addressing aircraft operations in SLD icing conditions. These conditions are outside the current icing certification envelopes. Current droplet trajectory and ice accretion computer codes are not validated for SLD conditions and they will need to be validated so that they can be used as a means of compliance (Ref. 12). Experimental data is needed to assess the validity and acceptability of droplet trajectory codes for SLD conditions.

To address the concerns of the icing community, the Icing Technology Branch at NASA Glenn Research Center awarded a research grant to Wichita State University (WSU) in 1995 to begin work on modernizing and expanding the water droplet impingement database. WSU and NASA conducted an industry survey in November of 1995 to identify geometries and conditions to be considered for the next series of water droplet impingement tests.

Survey participants were chosen from a database of scientists and engineers kept by the NASA Glenn Icing Branch. Surveys were sent to anyone who was believed to be interested in the goals of this program. A total of 54 surveys were sent out. About 50% of the surveys were received back. Table 4 shows a summary of the survey participants by company. Table 5 provides geometries requested by industry group. Geometries ranged from wings, inlets, S-ducts to radomes. Conditions specified included drop sizes from 15 to 4,000 microns, airspeeds from 0–500 mph, a wide range of angles of attack and inlet mass flows.

Survey participants were invited to attend a workshop at NASA Glenn on December 8, 1995, to discuss concerns, experimental tasks and priorities, test models and test conditions. The workshop results were compiled and were distributed to all survey participants in the form of a second questionnaire for further comments and inputs. Responses from the second questionnaire were used to define a test matrix for future impingement tests in the NASA Glenn IRT facility.

In December of 1996, NASA awarded a second grant to WSU to improve the experimental method developed during the 1984 to 1993 research program and to develop of a more efficient reflectance method based on a CCD camera for extracting the impingement data from the blotter strips. In addition, extensive impingement tests were planned in the NASA Glenn Icing Research Tunnel with a range of two-dimensional airfoils, and finite wings and a turboprop S-duct engine inlet.

The first series of the IRT impingement tests was conducted during the period of July 25 to September 7, 1997. The second series of impingement tests was conducted from January 31 to March 1, 1999. A total of 11 wind tunnel models were tested during these two IRT entries. Test models included six two-dimensional airfoils, a two-dimensional high-lift system, three swept horizontal tails and an engine inlet S-duct. Tests were performed for a range of angles of attack and for median volumetric diameters of 11, 11.5, 21, 92 and 94 microns. The 92-94 MVD case was selected to provide SLD impingement data.

Detailed descriptions of the experimental and data reduction methods used to generate the impingement data and all the experimental impingement data obtained during the 1997 and 1999 IRT entries are presented in the following sections of this report.

3.0 Droplet Trajectory Equation and Impingement Parameters

The non-dimensional form of the droplet trajectory equations and non-dimensional impingement parameters that are commonly used in the presentation of theoretical and experimental impingement data are presented in this section. The dependent impingement parameters are defined for clouds with uniform and non-uniform droplet size distributions.

3.1 Differential Equation of Particle Trajectory

The forces acting on a small spherical droplet moving in the steady flow of air involve droplet drag, weight, and buoyancy (Ref. 13). The fluid dynamic drag arising from the relative (slip) velocity of air with respect to the droplet acts as the predominant force on a droplet. The development of the droplet trajectory equations is based on a simplified approach, taken by researchers as early as the 1940's. In this approach, the quasi-steady motion of small spherical droplets moving in the steady flow of air is considered and it is assumed that the motion of droplets does not disturb the airflow. The main assumptions used in the derivation of the particle trajectory equations are summarized below (see Ref. 13):

1. Single phase (air) flow about the body; flow field is not disturbed by the presence of droplets
2. Quasi-steady-state approximation: at each instant and position, the steady state drag and other forces act on the particle
3. The drag coefficient for stationary sphere applies
4. Particles are assumed to be solid and spherical in shape
5. Particles do not rotate and have no lift and no moment
6. All drops which strike the airfoil deposit on the surface. Droplets do not splash/breakup during the impingement process
7. Droplets do not interact with other droplets

8. Compressible or incompressible potential flow field of the gas phase about the body
9. Viscous flow effects such as thick boundary layer formation and flow separation are not considered.

Using the above assumptions and applying Newton's second law, the non-dimensional form for the particle trajectory equation is obtained:

$$\frac{dU_i}{dt} = \frac{C_D(Re_v)\cdot Re_v\cdot(V_i - U_i)}{24K} - \frac{(1-\sigma)\cdot g\cdot L\cdot \delta_{i2}}{V_\infty^2} \qquad (3\text{-}1)$$

where $K = \rho_p V_\infty d^2 / 18\mu\ L$, inertia parameter of droplet

d = Droplet diameter
μ = Absolute air viscosity
V_∞ = Freestream speed
t = Time, dimensionless with L/V_∞

σ = ρ/ρ_p, density ratio of air to particle
L = Characteristic dimension of body
Re_V = Reynolds number of airflow relative to droplet
U_i = i^{th} directional component of particle velocity, dimensionless with V_∞
V_i = i^{th} directional component of air velocity, dimensionless with V_∞

The above mathematical model is valid for icing conditions within the intermittent and continuous maximum icing envelopes defined in the Federal Aviation Regulation, Part 25, Appendix C. The maximum concentration and mean volumetric diameter (*MVD*) of droplets for these icing conditions are as follows:

	Intermittent Maximum	Continuous Maximum
LWC	3.0 g/m^3	0.8 g/m^3
MVD	50 μm	40 μm

For the concentrations and sizes of droplets expected to occur within icing clouds, the assumptions of undisturbed airflow and spherical shape (due to surface tension) of droplets are valid.

The droplet drag coefficient, C_D in Eq. 3.1 is a function of the relative Reynolds number. It is an analytical form of the standard drag curve and the Cunningham drag correction factor for molecular slip and compressibility effect. The C_D is given in the following form:

$$C_D(M, Re_v) = \frac{C_{D_{inc}}(Re_v)}{G(M/Re_v)} \qquad (3.2)$$

where

$C_{D_{inc}}$ = Incompressible sphere drag coefficient

$G(M/Re_v)$ = Cunningham drag correction factor

M = Mach number of airflow relative to droplet

From Stokes' law of drag, the incompressible sphere drag coefficient can be expressed as:

$$C_{D_{inc}}(Re_v) = C_{D_{Stokes}}(Re_v)\left(1 + \frac{Re_v^{2/3}}{6}\right) \tag{3.3}$$

where

$$C_{D_{Stokes}}(Re_v) = \frac{24}{Re_v}$$

This equation agrees to within about 5% of the standard drag curve in the range of $0 \le Re_v \le 1000$ and for particles of diameter less than or equal 1 mm.

The Cunningham drag correction factor was proposed by Carlson and Hoglund (Ref. 14) with following empirical fit to available experimental data for the ranges of $M \le 0.2$ and $Re_v \le 1000$:

$$G\left(\frac{M}{Re_v}\right) = \frac{A}{B} \tag{3.4}$$

where

$$A = 1 + (M/Re_v)\left[3.82 + 1.28e^{(-1.25\,Re_v/M)}\right]$$

$$B = 1 + e^{\left(-0.427M^{-4.63} - 3\,Re_v^{-0.88}\right)}$$

The numerator, *A* in Eq. 3.4 represents the drag reduction factor to account for the incompressible drag due to the molecular slip or rarefaction effects. The denominator, *B* in Eq. 3.4 is the additional correction to account for the Mach number dependence of the particle drag (compressibility) in continuum flow.

3.1.1 Large Droplet Effects

A number of droplet trajectory codes have been developed over the years which use the trajectory equation discussed in this section. These codes have been extensively tested for icing conditions within the FAA, Part 25, Appendix C envelope and in general, have demonstrated good agreement with experimental impingement data.

Currently, there is need to extend the application of these trajectory codes to icing clouds with median volumetric diameters greater than 40 μm which fall outside the Appendix C envelop. For large droplet clouds, some of the assumptions made in deriving the trajectory equation may not be valid. In addition, computation of large droplet impingement may require improvements to the existing numerical models to account for physical phenomena such as droplet splashing and breakup that have been observed in recent experimental impingement studies with large droplets. The impact of these phenomena on the simulation of the impingement characteristics of aerodynamic surfaces can be considerable as demonstrated in section 7 of this report where large

droplet experimental and computational impingement data are compared for a range of aerodynamic surfaces.

3.2 Impingement Parameters

Spray cloud characteristics and droplet impingement parameters for clouds with a range of drop sizes are discussed below.

3.2.1 Liquid Water Content (*LWC*)

The liquid water content (*LWC*) of a cloud is the amount of water contained in a given volume of cloud. *LWC* is usually expressed in grams of water per cubic meter of cloud. LWC_{max} values for icing clouds according to the Appendix C icing envelopes are presented in section 3.1. For simulated icing clouds inside the icing tunnels, the *LWC* is controlled by the water and /or air pressures of the spray system used to create the spray clouds.

3.2.2 Cloud Droplet Distribution

The distribution of droplets in a cloud can be expressed in various forms (Ref. 6). Briefly, the following four types of distributions are most commonly used:

1. Number density of droplets versus droplet diameter
2. Percent of liquid water content versus droplet diameter
3. Percent of liquid water content versus droplet diameter normalized to median volumetric diameter.
4. Percent cumulative liquid water content versus droplet diameter normalized to median volumetric diameter.

A distribution which has been employed in various analytical studies is the Langmuir "D". This distribution and other similar ones were established by Langmuir (Ref. 15) from natural-icing cloud measurements made on Mt. Washington. The rate of deposition of ice on slowly rotating cylinders exposed to supercooled clouds blowing over the summit was correlated with that of theoretical calculations. Reference 6 provides comparisons of Langmuir "D" distribution and the droplet distributions produced by the WSU spray system used in the 1985 impingement tests. A dimensionless Langmuir "D" distribution is shown in Fig. 1a.

3.2.3 Median Volumetric Diameter (*MVD*)

The Median Volumetric Diameter (*MVD*) of a droplet distribution is defined as the droplet diameter for which half the total liquid water content is contained in droplets larger than the median and half in droplets smaller than the median. Given a droplet distribution, the *MVD* can be calculated as follows:

1. For a continuous distribution, if $n(D)$ is the number of particles per unit sampling volume having diameters between D and $D+dD$ (volumes between V and $V+dV$) then D_{MVD} can be calculated from

$$\frac{\frac{\pi}{2}\rho_\omega \int_{D_{min}}^{D_{MVD}} n(x)\, x^2 dx}{\frac{\pi}{2}\rho_\omega \int_{D_{min}}^{D_{max}} n(x)\, x^2\, dx} = 0.5 \tag{3.5}$$

2. For a discrete distribution, if the particle number density is given in N discrete groups such that $n_i(D_i)$ is the number of the particles in group i having diameters between D and $D+dD$ then, Eq. 3.5 can be written as

$$\frac{\frac{\pi}{6}\rho_\omega \sum_{i=1}^{K} n_i(D_i) D_i^3}{\frac{\pi}{6}\rho_\omega \sum_{i=1}^{N} n_i(D_i) D_i^3} = 0.5 \tag{3.6}$$

where

D_K = the diameter of group K, is equal to the MVD (D_{MVD})

ρ_ω = density of water, Kg/m^3

3.2.4 Local Impingement Efficiency ($\bar{\beta}$)

Considering a body in a cloud with uniform droplet size distribution, the local impingement efficiency β for any point on the body surface is defined as the local droplet flux rate at the body surface normalized to the freestream flux rate. Referring to Fig. 1b, β is defined as the ratio of that infinitesimal area dA_∞ to the corresponding impingement area on the body surface dA_S. This definition follows from the continuity of droplet mass flow.

For a continuous non-uniform cloud distribution, the impingement efficiency is given by the following expression

$$\bar{\beta} = \frac{1}{\omega_t} \int_0^{\omega_t} \beta \, d\omega \tag{3.7}$$

where β is a function of drop size and therefore can be expressed as a function of ω, the liquid content for a given drop size.

For a discrete cloud distribution, β is defined as the weighted average of the local impingement efficiency values due to each droplet group in the cloud. Let ω_t be the liquid water content of the cloud, $\Delta\omega_i$ be the partial liquid water content contained in the droplets of size (d_i), in the group (i) of the distribution, and N be the total number of discrete size droplet groups available. For a body exposed to a cloud with such a droplet distribution, the local impingement efficiency due to a single droplet group of size d_i is β_i, where β is defined in figure 1b. The local impingement efficiency due to all N groups in the distribution over an infinitesimal area of the body is given by the following expression

$$\bar{\beta} = \frac{1}{\omega_t} \sum_{i=1}^{N} \beta_i \Delta\omega_i \tag{3.8}$$

3.2.5 Total Impingement Efficiency ($\bar{E}$)

The total impingement efficiency of a three dimensional body exposed to a cloud of droplet distribution is defined as

$$\bar{E} = \frac{1}{A_f} \int_{s_l}^{s_u} \bar{\beta}\, dA_s \tag{3.9}$$

where

A_f is the projected frontal area of the body

dA_s is an infinitesimal impingement area on the surface of the body

S_u and S_l represent the upper and lower impingement limits on the body

3.2.6 Impingement Limits

Droplets which start out at freestream position y_∞ (Fig. 1c) with respect to a reference line that pass through the highlight (most forward point at α=0°) of a body downstream will impinge at some location on that body. As these initial freestream droplet positions increase in distance from the reference line they will impinge farther back along the surface of the body until a maximum distance $y_{\infty,max}$ is obtained. This limiting trajectory is defined as the tangent trajectory to the body at point P (Fig. 1c). Any droplets starting at a freestream location farther from the reference line than $y_{\infty,max}$ will miss the body entirely. The distance S_m measured along the body surface from the highlight of the body to point P is called the limit of impingement. This distance is usually expressed in dimensionless form by dividing S_m by the characteristic length (L) of the body.

For two-dimensional flow, there are two impingement limits, an upper and lower (for external flow, e.g., airfoil section) or an outer and inner (for partly internal flow, e.g., engine inlet). For three-dimensional flow, the limits of impingement may vary spanwise along the surface of a finite wing or circumferentially along the surface of an engine inlet. For a droplet distribution that varies from D_{min} to D_{max}, the impingement limits can be established for each droplet size. The maximum impingement limits are defined by the impingement limits of the largest droplet diameter of the distribution.

3.2.7 Summary of Droplet Impingement Parameters

Table 6 provides a list of definitions and expressions for key non-dimensional parameters that affect the droplet trajectory such as droplet inertia parameter K, droplet modified inertia parameter K_0, Reynolds number based on MVD, Re_{MVD}, true droplet range λ, and independent impingement parameter ϕ, which represents the deviation of the droplet drag force from Stoke's law and is defined is such a way that the droplet diameter, d, has been eliminated. These non-dimensional impingement parameters are also useful in linking the impingement data presented in this report with early

experimental and numerical studies of airfoil water impingement characteristics (Refs. 1 and 2). In some of these early studies, the impingement characteristics of bodies were in some cases presented in terms of non-dimensional impingement parameters such as K and ϕ. Note that the definitions in Table 6 are based on the reference length, typically the airfoil chord for two-dimensional sections or the mean aerodynamic chord (MAC) for finite span wings.

4.0 Experimental Method

4.1 Wind Tunnel Facility

The impingement tests were conducted in the NASA Glenn Icing Research Tunnel (IRT). The IRT is a closed-loop refrigerated wind tunnel with a 6-ft high by 9-ft wide by 20-ft long test section and a maximum speed of 430-mph (empty test section). A plan view of the IRT circuit is shown in Fig. 2. The tunnel circuit operates at or below atmospheric pressure, and the test section static temperature can be controlled between –40 °F to +40 °F. All test models were installed on the tunnel turntable using the floor mounting plate (See Fig. 3). A view of the IRT test section is given in Fig. 4. Two sets of nozzles are available in the IRT facility for generating spray clouds and include the standard and MOD-1 type nozzles. The basic IRT nozzle design is shown in Fig. 5. The IRT spray system consists of 10 spray bars with 54 nozzle locations per spray bar. Only 129 nozzles are currently being used to generate the required icing clouds. The IRT spray system is capable of simulating icing clouds with MVDs in the range of 14 to 40μm, and Liquid Water Content (LWC) of 0.3 to 3 g/m^3 as shown in Figs. 6 and 7. Recently, a small number of large droplet calibrations have been performed permitting the generation of icing clouds with MVDs in the range 70 to 270 microns. Further details regarding the IRT facility are provided in Ref. 16.

4.2 Test Models and Instrumentation

Details of the eleven test models used in the experimental investigation and related instrumentation are given below.

4.2.1 MS(1)-0317 Airfoil

The MS(1)-0317 airfoil is representative of modern medium speed airfoils. It was designed in the mid 1970's for general aviation aircraft (Ref. 17). This two-dimensional airfoil was constructed out of Fiberglass skin, which was epoxied to an aluminum spar and aluminum ribs. The interior of the airfoil model was filled with foam. An aluminum plate was installed at each end of the model for mounting in the IRT test section. The model had a nominal span of 72 inches and a chord of 36 inches and it was mounted vertically in the test section. A total of 49 static pressure taps were available for this airfoil. These taps were located in the chordwise direction 35.5 inches above the tunnel floor. The MS(1)-0317 airfoil section and model installation details are given in Figs. 8a-8c. Impingement data for this airfoil were obtained during the 1985 IRT impingement tests performed by WSU and Boeing. These data were used to verify the experimental set up for the 1997 and 1999 water droplet impingement tests.

4.2.2 GLC-305 Airfoil

This airfoil is representative of general aviation business jet wing sections. It was constructed at the NASA Glenn Research Center out of Fiberglass with two 2-inch thick wooden spars and seven 1-inch thick ribs as described in Ref. 18. It had 36-inch chord, 72-inch span and 3.123-inch maximum thickness (t_{max} = 8.7% chord) at x/c = 0.4. The airfoil was instrumented with 44 static pressure taps distributed in the chordwise direction at a span location 33 inches above the tunnel floor. The airfoil section geometry and installation in the IRT test section are shown in Figs. 9a–9c.

4.2.3 NACA 65_2-415 Airfoil

This airfoil is representative of general aviation wing sections. Airfoils suitable for low speed general aviation aircraft should have low drag and gentle stall characteristics with relatively high thickness ratio to keep structural weight low and to provide sufficient space for fuel (Ref. 19). The NACA 6-series airfoils were designed to have low profile drag in a limited range of lift coefficient (drag bucket). Aerodynamic performance characteristics for the NACA 65_2-415 airfoil are provided in Ref. 20.

The single element NACA 65_2-415 wind tunnel model was designed and fabricated at Wichita State University. It was made out of aluminum, and had 72-inch span and 36.53-inch chord which was truncated to 36 inches during manufacturing to allow for sufficient trailing edge thickness for installation of a pressure port at the trailing edge. The maximum thickness for this airfoil was 5.486 inches (t/c = 0.15) and was located at approximately 40% chord. The center of rotation of the airfoil was at 50% chord. The airfoil was instrumented with 79 pressure taps at the mid span location which corresponded to the IRT centerline. Twelve additional pressure taps were placed in the chordwise direction one foot above and below the centerline taps (6 taps on each side) and nine more taps were distributed spanwise at the 70% chord station on the upper surface of the airfoil. The 21 additional pressure taps were used to verify that two-dimensional flow was maintained for the angles of attack used in the impingement tests. The airfoil section geometry and installation in the IRT test section are shown in Figs. 10a–10c.

4.2.4 Commercial Transport Tail Section

This airfoil was provided by NASA Glenn Research Center and was representative of horizontal tail sections used in large commercial transport aircraft. The model was constructed out of Fiberglass skin 3/8-inch thick with two 2-inch thick wooden spars and seven 1-inch thick ribs (Ref. 18). The airfoil had 36-inch chord, 72-inch span and a maximum thickness of approximately 9% chord (3.23 inches) at x/c = 0.34. It was instrumented with 44 static pressure taps distributed in the chordwise direction at a span location 33 inches above the tunnel floor. Two thirds of the static ports were located in the forward 50% portion of the chord length. Figures 11a–11c show the airfoil geometry and model installation in the IRT test section.

4.2.5 36-in and 48-in NLF(1)-0414 Airfoils

The Natural Laminar Flow NLF(1)-0414 airfoil was designed in the early 1980's for general aviation applications. Airfoil design performance features at a Reynolds number of 10 million and Mach number of 0.4 included lift coefficient of 0.4, drag coefficient of 0.0027 at an angle of attack of approximately –1°, 70% chord laminar flow on both surfaces, and maximum lift coefficient of 1.83 at a stall angle of attack of 17.8° (Ref. 21). The NLF(1)-0414 airfoil had a maximum thickness to chord ratio of 0.143. The maximum thickness on the upper surface was 8.3% chord at x/c = 0.418 while that on the lower surface was 6% chord at x/c = 0.515.

Two NLF(1)-0414 airfoils were tested, a 36-inch single element airfoil and a 48-inch two-element section. Both models spanned the height of the IRT test section (72 inches).

The 36-inch airfoil was provided by NASA Glenn and was constructed out of Fiberglass. The airfoil had a trailing edge thickness of 0.055 inches and it was instrumented with five pressure taps. The airfoil section and model installation details are depicted in Figs. 12a–12c.

The 48-inch two-element airfoil shown was fabricated at WSU out of aluminum and had a simple 25% chord full span flap as shown in Fig. 13a. The deflection of the control surface was adjustable in 5-degree increments from –35° to +35°. The pivot location of the control surface was at x = 37.584 in, y = –0.116 in. The leading edge radius of the control surface was 1.584 inches and the trailing edge thickness was 0.057 inches. The gap between the control and the main element was 0.2 inches. The 48-in model was instrumented with 124 pressure taps, which were distributed as shown in Table 7. Figures 13b–13c show the model installation in the IRT test section.

4.2.6 NACA 64A008 Swept Tail

This was a full-scale reflection plane tail model consisting of the outboard portion (44% to 100% semi-span) of a general aviation business jet tail. The tail tip consisted of a semi-cylindrical cap. Geometry and model installation details are provided in Figs. 14a–14d. The model was fabricated at NASA Glenn Research Center out of aluminum and it was instrumented with 60 pressure taps which were equally divided between two spanwise stations 24 and 43 inches above the tunnel floor as shown in Fig. 14c. The tail airfoil was a symmetric 8% thick NACA 64A008 section and it was constant from root to tip. The location of maximum thickness for this airfoil section was at x/c = 0.39. The Mean Aerodynamic Chord (MAC) of the finite swept tail model was 37.65 inches and was located approximately 22 inches above the tunnel floor.

4.2.7 25%-Scale Business Jet Empennage (BJE)

The horizontal tail of the BJE consisted of a tapered swept planar planform (i.e., no twist and no dihedral) with an 8% chord thick airfoil section from root to tip. The location of the maximum thickness was at approximately 38% local chord. The airfoil section was in the streamwise direction and its chord length was 16.35 inches at the root and 7.04 inches at the tip. The tail sweep was 29.098 degrees at leading edge and

11.066 degrees at the trailing edge. The tail mean aerodynamic chord (MAC) was 12.31 inches, the tail span was 51.575 inches and the tail area was 603.135 in^2. The aspect ratio of the horizontal tailplane was 4.4. The incidence of the horizontal tail was –8 degrees with respect to the body axis. Thus, a body angle of attack (AOA) of $+8^\circ$ corresponded to a geometric angle of attack of 0° at the tail.

The elevator had a leading edge sweep of 17.28 degrees with its leading edge at 68% of local chord. The elevator hinge line was at 73.32% chord location. The elevator surface behind the hinge line had a geometric mean chord of 3.072-inch and a planform area (left + right elevators) of 152.784 in^2.

The right side of the tail surface was instrumented with 126 pressure taps distributed at three spanwise locations corresponding to 25%, 55% and 85% semi-span. Each spanwise location had 42 static pressure ports. Fig. 15a shows the geometry of the airfoil section. The installation of this model in the IRT test section is shown in Figs. 15b–15e.

4.2.8 Full-Scale Business Jet Horizontal Tail

This model was a half-span full-scale version of the 25%-scale BJE horizontal tail described above. The full-scale tail was truncated at approximately 44.5% semi-span so that it could be installed in the IRT test section as a reflection plane model. The non-truncated half span full-scale horizontal tail consisted of a tapered swept planar planform (i.e., no twist and no dihedral) with an 8% chord thick airfoil section that remained the same from root to tip. The airfoil section is shown in Fig. 16a. The chord length was 65.4 inches at the root and 28.16 inches at the tip. The maximum airfoil thickness was at approximately 38% local chord. The tail mean aerodynamic chord (MAC) was 49.249 inches. The tail sweep was 29.098 degrees at the leading edge and 11.066 degrees at the trailing edge. The half tail span was 103.15 inches and the half tail planform area was 33.509 ft^2 (4825.30 in^2). The aspect ratio of the non-truncated horizontal tail was 4.4. The elevator had a leading edge sweep of 17.28 degrees and its leading edge was at 68% of the airfoil chord. Note that the airfoil chord varied linearly in the spanwise direction. The elevator hinge line was at 73% chord location and the elevator surface behind the hinge line had a geometric mean chord of 12.288 inch and a planform area of 8.49 ft^2 (left elevator). For the truncated model tested, the root chord was 48.82 inch and the tip chord was 28.16 inch as shown in Fig. 16b. The truncated tail model had a 57-inch span starting at 44.5% semi-span of the non-truncated model and extending to the tail tip (100% semi-span). Model installation details are presented in Figs. 16b and 16c.

4.2.9 Three-Element High Lift System

This high lift airfoil section was selected to address the needs of large transport airframers. The three-element section was designed in the early 1990s (Refs. 22 and 23). It is an advanced high lift system, which is representative of modern transport wing designs.

The three-element airfoil was an all aluminum model with 72 inches span and 36 inches nested chord. The configuration consisted of a slat, a main element and a flap.

The flap and slat elements were rigged to the main element with four one-piece steel brackets. Only the landing configuration was considered in this investigation. For this case, the slat deflection was 30° leading edge down and the flap deflection was 30° trailing edge down. Deflection of the high-lift components was set with respect to the main element wing reference plane (WRP) as shown in Fig. 17a. The slot size between the main element and the high lift components was defined in terms of the overhang (OH) and the gap. Overhang is the horizontal distance from the trailing edge of the upstream element and the leading edge of the downstream element. The overhangs for the slat and flap were –0.9 and +0.09 inches respectively. Gap is the minimum distance between the trailing edge of the upstream element and the leading edge of the downstream element. For the slat, the gap was 1.062 inches and for the flap it was 0.457 inches. The installation of the three-element airfoil in the IRT test section is shown in Figs. 17b–17c.

A total of 128 static pressure taps were available on this model. These taps were distributed along a single chordwise row at mid-span (36 inches above the tunnel floor) and along three spanwise rows, two on the upper surface of the flap and one on the upper surface of the slat. The distribution of the pressure ports is given in Table 8.

4.2.10 Comparison of Airfoil Sections Tested

Figures 18–21 compare the airfoil sections for the 2D and 3D wing models tested during the 1997 and 1999 impingement tests. Coordinates for the airfoil sections of the models tested can be found in Appendix B.

4.2.11 S-duct Engine Inlet

This model consisted of a full-scale bifurcated inlet S-duct representative of modern turboprop aircraft. The S-duct inlet configuration is depicted in Fig. 22a. The test article was actual flight hardware and was provided by the Allison Advanced Development Company. A bifurcated inlet of the type tested protects the engine from ingesting foreign objects primarily in the form of runway debris, ice, birds, etc. The bifurcated inlet requires scavenge air in addition to the scheduled engine airflow, thus causing greater mass flow rate at the highlight plane. The sizing criterion of the scavenge duct is based on the minimum required air flow to preclude any objects from entering the engine flow path at a critical operating point such as normal takeoff (Ref. 24). The main features of the S-duct inlet are depicted in Figs. 22b and 22c. Details of the inlet cross-section are provided in Figs. 22d, 22e and 22f. As shown in Figs. 22d–22e the inlet three-dimensional shape is a combination of two-dimensional elliptical cross-sections that are stacked on a three-dimensional spine line. The complete geometry definition for this model is available in electronic format from NASA Glenn Research Center. The installation of the inlet in the IRT test section is shown in Fig. 22g. Blotter strip locations for this model are provided in Fig. 22h.

The inlet was instrumented with an array of 30 static pressure taps. Four static pressure taps were installed circumferentially at four axial locations in the duct upstream of the splitter nose. An additional four static taps were placed circumferentially near the

engine inlet plane. The remaining 10 taps were located on the splitter nose and along the lower wall of the scavenge duct.

The main inlet mass flow was simulated and recorded using the IRT mass flow system. To determine the scavenge duct flow a calibrated Dantec Flow Master Probe type 54N60 was provided by the Allison Company. The Dantec probe used was a temperature compensated thermal anemometer probe with an accuracy of ±2.5%.

Tunnel airspeeds and inlet mass flow conditions used during the impingement tests of the S-duct engine inlet are summarized below:

Tunnel Air Speed mph	Main Inlet Flow (Core Flow) lbm/s	Scavenge Duct Flow lbm/s	Capture Area Ratio (Includes scavenge flow)
130	23	1.57 ± 0.04	0.84
170	23	2.08 ± 0.05	0.65

4.3 Dye Tracer Method

The dye-tracer technique was initially developed by NACA (Ref. 1) and was modified by Papadakis et al. (Ref. 6). The modified dye-tracer method was used in the 1997 and 1999 IRT impingement tests. In this method, distilled water containing a known concentration of blue dye (0.3g of FD&C Blue No. 1 dye per 1 liter of water) was injected into the air stream of the IRT in the form of a droplet spray cloud using a specially designed 12-nozzle spray system. The test model was covered with thin strips of blotter paper (James River Paper Company Verigood 100# Blotting Paper) in areas of interest and was exposed to the spray cloud. The amount of dye-mass per unit area of blotter strip obtained in a given time interval was measured using reflectance spectroscopy. The water impingement characteristics of a test model were obtained from the concentration and location of the dye distribution on the blotter paper.

4.4 Spray System

All 1997 and 1999 impingement tests were conducted using a twelve-nozzle spray system developed by personnel at Wichita State University. The IRT spray system was not used in this study because it was not designed for the short duration sprays (typically 2–18 seconds) required to prevent saturation of the blotter paper used in the dye tracer method.

The WSU spray system was originally developed in 1985 but it was significantly modified for the 1997 and 1999 impingement tests. The system was designed to use the standard or MOD-1 IRT spray nozzles shown in Fig. 5. Details of the original WSU spray system can be found in Ref. 6. Briefly, the original system developed in 1985 provided blue dye solution under pressure from a high pressure supply tank to each of the 12 nozzles via high-pressure rubber hoses as shown in Fig. 23. Pressure for the supply tank was obtained from a 125-psig airline, and was set to the required level using a mechanical pressure regulator. A separate 100-psig high mass flow air source (atomizing air manifold) provided air to the nozzle assemblies for atomizing the water.

The atomizing air pressure was set by a mechanical pressure regulator. Fast acting solenoid valves were used to turn the spray on and off. During testing, the main air supply solenoid was turned on several seconds before the spray was initiated to allow the air pressure to stabilize. Next, the 12 water solenoid valves were turned on and a spray cloud was produced. The median volumetric diameter (MVD) of the spray cloud was set by varying the air-to-water pressure ratio. The duration of the spray was controlled by a timer developed to turn on and off the air and water solenoid valves. System pressure adjustments and monitoring were done manually and as a result, during the 1985 and 1989 tests it was difficult to maintain consistent performance between sprays.

One of the main goals of the research effort described in this report was to improve the repeatability of the experimental impingement data which in previous experimental studies was found to exhibit considerable variation. Studies conducted by the WSU/Boeing research group showed that spray system consistency had a large effect on the repeatability and quality of the experimental impingement data. Thus, a significant effort was directed during this new research program in improving and monitoring spray system performance.

A number of electronic pressure transducers were added to the spray system at strategic locations to monitor the air and water pressures during each test. The pressure transducer selected for monitoring water pressure was the SETRA 206. A pressure transducer was installed in each water line just upstream of the nozzle and also at the water tank. The pressure of the atomizing air was measured at the regulator with a SETRA 204 transducer. In addition, three SETRA 206 transducers were used to monitor atomizing air pressures at selected nozzles. These transducers were added to the longest airline corresponding to each group of four nozzles. Pressure transducer information is provided in Table 9. Prior to each IRT test entry, the NASA Glenn flow calibration lab tested and calibrated all the pressure transducers used in the WSU spray system.

A sensitive flow meter was added to the spray system to monitor water volume flow rate. This instrument measured the water volume flow rates in the range 0.02 to 1 gallon per minute with an accuracy of 0.2% full scale (FS). This flow meter was also calibrated by the NASA Glenn flow calibration lab.

The pressure regulators for setting the tank water pressure and the nozzle air pressure were modified so that the pressures could be set remotely from the tunnel control room. A miniature Electro-pneumatic transducer was added to each pressure regulator and was used to adjust and maintain the required air and water pressure levels in the spray system. During the 1999 IRT test, an automatic feedback control was incorporated in both the water and air pressure regulating units. The desired pressure levels for both air and water could be pre-set into the spray system control program to enhance the accuracy and repeatability of the spray system performance.

The NASA Glenn Standard nozzles used in the 1985 and 1989 impingement tests were replaced with the NASA Glenn MOD-1 nozzles. This was done for two reasons. First, the MOD-1 nozzles have a lower flow rate (approximately 1/3) for a given air pressure and delta pressure (P_{water}–P_{air}) than the standard nozzles so that longer spray times could be achieved without saturating the blotter strips. Longer spray times are desirable because they result in more stable sprays. Second, large MVD calibration data were available for these nozzles. One of the objectives of the 1997 and 1999 impingement tests was to produce data for MVD sizes of the order of 100 μm.

A new stainless steel pressure tank with 30-gallon capacity was installed. The new larger capacity tank replaced the 9-gallon aluminum tank used previously. A set of 12 brackets were designed and built for mounting the twelve-nozzle spray system to the new IRT spray bars. The new brackets allowed for a more precise installation of the 12 nozzle assemblies. The installation of the WSU spray system in the IRT facility for 1997 impingement tests, and the location of the twelve-nozzle spray system on the IRT spray bars as well as the tabulated coordinates of each spray nozzle with respect to the IRT spray bars are shown in Figs. 24–25. The locations of the WSU spray nozzles for the 1999 impingement tests are given in Figs. 26–27. A close up of one of the WSU nozzle assemblies is provided in Fig. 28. The stainless steel pressure tank for storing the dyed solution and the main air and water pressure lines and the air and water pressure regulators are shown in Figs. 29–31a.

The improved twelve-nozzle spray system is shown in Fig. 31b. This system was assembled and tested extensively at WSU before it was shipped to NASA Glenn for the water droplet impingement tests. During the impingement tests at the NASA Glenn IRT facility, several detailed analyses of recorded spray system parameters were performed. The results showed that the system was capable of maintaining air and water pressures to within ±1 psi from the required settings as demonstrated in Tables 10a and 10b.

Note that the IRT water spray system was not used for the impingement tests. However, during the 1997 impingement tests, IRT spray bar air was used to enhance cloud uniformity. In addition, during the 1997 and 1999 impingement tests, the IRT spray bars were activated periodically between impingement tests to maintain the required relative humidity level in the tunnel air stream.

4.5 Spray System Data Acquisition and Control

A personal computer system with related hardware and software was developed to control and monitor the performance of the spray system and to store and analyze spray system performance parameters. This system consisted of a Pentium 100Mhz PC system with a data acquisition (DAQ) board, and a digital I/O (DIO) board, thirteen (13) solid-state relay (SSR) digital signal conditioning modules installed on two backplane boards, a transducer control panel, a shielded I/O connector block (SCB) and a cable adapter board. A schematic of the main hardware units is given in Fig. 32. The DAQ board was used to read and process the signals from all transducers. This board had 32 input differential channels and a sampling rate capability of up to 500,000 samples per second. The DIO board was a high-speed, 32 bit parallel digital I/O ISA interface. This

board was used to turn on selected SSR relay units, which in turn activated the associated solenoid valves of the spray system. Each of the twelve nozzle assemblies had one solenoid valve. In addition, a solenoid valve was installed on the main air supply, which provided high-pressure air for atomizing the water sprays from the twelve nozzles.

The control software was developed using LabVIEW, a graphical programming language for data acquisition and control, data analysis and data presentation. The LabVIEW software provided a Windows driven menu system for controlling and monitoring the performance of the spray system. The user could select any combination of nozzles and transducers from the windows menu, specify spray time duration, plot the transducer signals in real time, and store a range of impingement test parameters as well as other information related to each test. All test parameters and transducer voltages were written out to a Microsoft Excel file at the end of each test.

During an impingement test the system software activated the solenoid valves by sending a command to the DIO board. Data from the DAQ board were recorded at regular time intervals for the complete duration of the spray. The sampling rate varied from approximately 9 to 18 points per second depending on spray duration. For long sprays, the lower sampling rate was used. This was done to keep the size of the output files to a manageable level.

4.6 Cloud Uniformity

Cloud uniformity is critical to obtaining repeatable and accurate impingement data. The three main parameters involved in the description of a spray cloud are droplet size, droplet distribution and LWC. Of these three parameters, LWC distribution is the most difficult to control. Extensive tests were conducted to set the location of the twelve spray nozzles so as to obtain a 2-ft high by 3-ft wide uniform cloud region centered in the IRT test section. Since perfect uniformity is practically not obtainable, for the purpose of the impingement tests, uniformity was accomplished when LWC variation within the region of interest was within ±15% of the average.

Cloud uniformity was measured using two methods. In one method, a 6-ft by 6-ft stainless steel grid with horizontal and vertical increments 6 inches apart was used to determine cloud uniformity. The plane of the grid was normal to the flow and passed through the center of the turntable. Blotter squares, approximately 1.25 inches in size, were attached to this grid at 6 inch horizontal and vertical increments to cover the required 2-ft by 3-ft area (35 blotter strips were used during each cloud uniformity test). The tunnel was brought up to test speed and the blotters were sprayed. The dye distribution on each blotter was determined using the CCD reflectometer described in section 5 of this report. Next, the nozzles were adjusted to make the dye distribution and therefore the LWC more uniform. This grid/blotter method, which was laborious and time consuming, was similar to the one presented in Refs. 6 and 7. Figure 33 shows the uniformity grid (with/without blotter squares) installed in the IRT test section.

The second method for determining cloud uniformity was recently developed at NASA Glenn (Ref. 25). In this method, a 15-watt Argon-Ion laser beam was split into two beams, which were directed to sheet projectors or to a galvanometer using optic fibers. The light from the sheet projectors or the galvanometers was passed through large (64cm long) cylindrical lenses, which produced a laser sheet that spanned the tunnel width. By using only one or both of the cylindrical lenses, the height of the laser sheet could be adjusted to 2-ft or 4-ft respectively. The laser sheet was set approximately normal to the flow and was located a small distance upstream of the uniformity grid. The uniformity grid was left in the test section and was used for reference. The installation of the Argon-Ion laser beam system and its key components are shown in Figs. 34–36. The location of the 2-ft and 4-ft high laser sheet planes with respect to the IRT test section is shown in Fig. 37.

A 14 bit CCD array camera was installed on the IRT spray bars between bars four and five and 21 inches to the left (looking upstream) of the vertical support beam as shown in Figs. 24 and 26. The camera was placed inside an airfoil fairing to minimize disturbance to the flow. Uniformity tests were conducted with all lights off in the test section and with the lights in the control room dimmed. With the tunnel set to the required airspeed (175 mph), the spray system was activated for approximately 30 to 50 seconds. The intensity of the scattered laser light from the droplets crossing the laser sheet was recorded using the CCD camera installed on the IRT spray bars. High intensity regions in the recorded image corresponded to high LWC and vice versa. Using camera software, the image could be analyzed to determine variations in LWC within the desired uniformity region. Figure 38 shows example images of clouds obtained with the CCD camera.

Extensive tests were conducted with the laser sheet method for all spray conditions selected for the impingement tests. The images obtained were used to adjust the locations of the nozzles until the desired LWC distribution was obtained. This method was found to be considerably more efficient than the grid/blotter method. In addition, the high resolution of the laser sheet technique proved valuable in understanding the effect of individual nozzles on the cloud LWC distribution. To verify the results obtained with the new uniformity method, a small number of tests were conducted with the grid and blotter strips. The results obtained showed good correlation with the laser sheet test results for all MVD conditions.

4.7 MVD and LWC Measurements

Droplet size and distribution measurements for all spray conditions were determined using the NASA Glenn Forward Scattering Spectrometer Probe (FSSP) and the Optical Array Probe (OAP) shown in Figs. 39 and 40 respectively. Details regarding these probes can be found in Ref. 26. The LWC measurements were performed with the NASA Glenn hot wire King Probe Model KLWC-5 described in Ref. 27. Briefly, the King Probe operates on the theory that when a heated wire is maintained at a constant temperature, any excess power consumed by the wire is in proportion to the mass of water impacting on it. The installation of the King Probe in the IRT test section is shown in Fig. 41.

Two series of droplet and LWC measurements were conducted during each of the six-week IRT test entries in 1997 and 1999. One was conducted near the start of testing after the uniformity tests were completed and a second near the end of the impingement tests. Each series of droplet size, droplet distribution, and LWC tests consisted of several repeated measurements of the desired spray cloud conditions. MVD and LWC measurements were performed for all spray conditions used in the experiments. Short and long duration sprays were used in the LWC measurements to determine the effect of cloud unsteadiness on LWC. Traces of LWC as a function of time showed no significant impact of spray duration on the average LWC. Measured MVD and LWC distributions during the 1997 and 1999 IRT tests are summarized in Fig. 42a–42c. MVD sizes and corresponding spray system air and water pressure settings are given in Tables 10a and 10b. Note that all data presented in Fig. 42 were obtained at the center of the IRT test section.

Extensive tests were also conducted with the FSSP and King probes in 1997 and in 1999 to identify the impact of relative humidity on the cloud characteristics. These tests showed that the effect of relative humidity on LWC was considerable particularly for the 11-micron MVD case. Based on the relative humidity studies, it was decided to conduct all impingement tests at a relative humidity of 75% ± 5%.

4.8 Reference Collector Mechanism

Local LWC measurements were obtained with a device called the Reference Collector Mechanism (RCM) at all locations in the IRT test section corresponding to test model blotter strip locations. The purpose of these measurements was to correct the impingement data for local variations in LWC. The LWC measurements were performed with the reference collector mechanism described in Ref. 6. Due to test model installation, size, and angle of attack, blotter strips on each model tested resulted at different locations within the 2-ft high by 3-ft wide uniformity region established from the uniformity tests. By measuring the local LWC within the 2-ft by 3-ft test area, the effect of variation in cloud uniformity could be corrected, thus improving the accuracy and repeatability of the experimental impingement data. The RCM had six short blades and one long blade as shown in Fig. 43. Each blade was 0.2 inches wide and 1 inch in chord as shown in Fig. 44. The length (span) of the blades was 2 inches for the short blades and 9 inches for the long blade.

The collector mechanism was placed in the empty IRT test section with its collector blades positioned as close as possible to the blotter strip locations on the test models. Since test model location varied depending on model installation and angle of attack, the collector mechanism had to be tested at several positions. For the collector tests, blotter strips 0.2 inches wide were placed on the collector blades so that the plane of each blotter strip was normal to the flow. The collector mechanism was tested at the same airspeed and cloud conditions as the test models. In addition, the spray duration for the collector tests was identical to that used for the airfoil tests Figure 45 shows the location of the collector blades with respect to the uniformity grid with the reference collector mechanism placed on the IRT turntable center. The locations of the reference

collector blades with respect to the blotter strip locations on the MS(1)-0317 airfoil at an angle of attack of zero degrees are shown in Fig. 46.

The impingement data from the collector blotter strips were analyzed using the data reduction methods described in section 5 and the amount of dye in the freestream was determined at all locations of interest. The collector dye mass per unit area and its impingement efficiency were used to obtain the LWC in the freestream which was then used to convert the raw impingement data for each test model into impingement efficiency distributions. Table 11 provides computed impingement efficiency values for the collector blades for all test MVDs as well as the LWC measurements obtained with the King Probe during the 1997 and 1999 tests. Table 11 shows that the collector blades had high impingement collection efficiency. This is attributed to the small chord and thickness of the collector blades.

4.9 Test Matrix

Models and conditions for the 1997 (7/25/97 to 9/7/97) and 1999 (1/31/99 to 3/1/99) IRT tests are provided in Table 12a and 12b respectively. All tests were conducted at a total air temperature of 48°F ± 8°F and a relative humidity of 75% ±5%.

4.10 Surface Pressure Measurements

Most of the models tested were equipped with surface pressure taps as discussed in section 4.2. Surface pressures for each model were obtained prior to the impingement tests. Pressure measurements were performed with the IRT electronically scanned pressure (ESP) system. Six 32-port (±5 psid) ESP modules were available in the IRT, providing a total of 192 pressure channels. One port in each module was used for a check pressure; thus 31 channels per module were available for test data, or a total of 186 ports. The ESP system applied a three-point pressure calibration to all port transducers. The calibration pressures were measured with precision digital quartz transducers. This on-line three-point calibration ensured that measurement errors were not greater than ±0.1% of full-scale. The standard calibration interval was every 400 cycles (approximately 15 minutes). The experimental pressure data were used to validate the computed pressure distributions prior to performing the impingement analyses.

4.11 Impingement Test Procedure

To obtain water droplet impingement data for a test model the following steps were performed.

1. The spray system air and dyed water pressures were set to produce the required MVD. Pressure settings for all MVD sizes used in the impingement tests are given in Tables 10a and 10b for the 1997 and 1999 tests respectively.
2. Blotter strips were attached at the required locations on the forward part of the test model with aluminum tape. The blotter strips were approximately 1.5 inches wide and had various lengths, depending on model geometry, angle of attack and MVD size. For the majority of the models the blotter strips were rectangular in shape. For the swept NACA 64A008, 25%-scale BJE, and full-scale business

jet tail section, however, V-shape blotter strips were used so that the blotter strip was in the streamwise direction. Each blotter strip was marked on its backside with the run number, test model and location on the model.

3. The tunnel airspeed and in the case of the S-duct the inlet mass flow was set to the required value, the spray system was activated for a short period of time and a dye deposit was obtained on the blotter strips. The spray time duration varied from approximately 2 to 18 seconds depending on MVD size as shown in Table 10.
4. The tunnel airspeed was reduced to idle, the blotter strips were carefully removed from the model and were placed in the control room to dry prior to being stored. The model was wiped clean and new blotter strips were placed on the model for the next test.

Each test condition was repeated three to four times (i.e., 3 to 4 tests per condition) to establish a measure of test repeatability. In some cases as many as 10 repeats were performed over a period of two days to better determine the repeatability of the experimental technique.

Periodically, the collector mechanism was tested between model tests to provide the required local LWC measurements for reducing the model impingement results.

5.0 Data Reduction Method

Two methods have been developed over the years for reducing impingement data. The first method was developed by NACA in the 1950's and was based on colorimetric analysis (Ref. 1). The second method was developed by WSU/Boeing in the 1980's and was based on diffuse reflectance spectroscopy (Refs. 6, 28 and 29). This method was significantly more efficient than colorimetric analysis and provided higher resolution impingement data. In an effort to further increase the efficiency of the data reduction process to the point where the data could be reduced on-line, a new implementation of the diffuse reflectance spectroscopy method was developed during the course of this research program. Details of the data reduction methods and the semi-automated systems developed for extracting and analyzing the data from the blotter strips are presented below.

5.1 Reflectance Spectroscopy

The data reduction methods used in this work rely on the assumption that when a dye-laden blotter strip is illuminated by a light source the intensity of light scattered by the dyed paper is a measure of the dye mass per unit area of the paper. Regions on the blotter strip corresponding to high impingement rates are darker in color and reflect less light than those corresponding to low impingement rates. Regions with no dye accumulation are white and scatter the maximum amount of light. The relation between dye concentration and reflectance is not linear and is defined from calibration tests. To enhance the sensitivity of the reflectance method, the dye must have a strong absorption at the wavelength of the light source used for illuminating the blotter strips.

For improved accuracy, dye penetration normal to the blotter surface should be kept to a minimum since the data reduction method relies on surface reflectance measurements. The acceptable level of dye penetration depends on the data reduction system and is determined from experiments.

5.2 Reflectance Calibration Curves

The reflectance calibration curve relates normalized reflectance from the dye-laden blotter strip to dye mass and therefore water impingement on the blotter strip. The curve is a standard against which the reflectance of each blotter strip is compared during the data reduction process.

To produce the reflectance calibration curve, approximately 30 rectangular blotter samples each 1.5-inch wide by 15-inch long were prepared over the course of this research program. Each blotter sample was sprayed with blue dye solution until a uniform blue color density was obtained over the whole rectangular blotter sample. By varying the spraying time and the concentration of the dye solution, blotters with a wide range of uniform color densities were obtained covering the spectrum from very light blue to dark blue color. Next, three circular disks each 1.13-inch in diameter were punched out from each of the rectangular blotter samples. The average reflectance of each of the discs was measured using both the laser and CCD reflectometers described below. The dye mass from each disc was extracted by the WSU chemistry lab using the method of colorimetric analysis described in Ref. 6. Next, the dye mass from each blotter disc was divided by the disc area to provide the dye mass per unit area. The normalized reflectance calibration curves shown in Figs. 47-50 were produced by plotting the normalized reflectance from each disc sample against the corresponding dye mass per unit area. In these curves, a normalized reflectance value of 1 corresponds to the white blotter paper and indicates zero dye mass. More than 70 dye-laden blotter discs were used to define the laser and CCD calibration curves shown in figures 47–50.

5.3 Data Reduction Systems

Two systems were used to reduce the raw impingement data obtained during the 1997 and 1999 impingement tests. The first system was a laser reflectometer, which was developed and tested extensively during the 1985 and 1993 research programs conducted by WSU and Boeing Company. The second system made use of a CCD array camera for digitizing the images of the dyed blotter strips, which were then stored for later analysis.

A prototype CCD data reduction system was developed in 1992 at Wichita State University. This system consisted of an 8-bit Cohu 4080 CCD camera with a Dipex frame grabber connected to a personal computer. Tests showed that this system was capable of extracting impingement data from dyed blotter strips. However, it was determined that a system with a resolution higher than 8-bits was required to accurately resolve the variation in blue color density, particularly near the region of maximum impingement. Further development of the method was hindered by the cost of high-resolution cameras at that time.

In 1995, Bragg et al. (Ref. 30) developed a method based on a 14-bit CCD camera array which was used to analyze impingement data from tests conducted with a NACA 65_2-015 airfoil. Good correlation with other published experimental data for this airfoil was demonstrated.

The main advantages of a CCD data reduction system are speed and spatial resolution. Such a system has the capability of providing on-line data reduction during impingement testing.

The Laser and CCD data reduction systems used in this work are described below.

5.3.1 Laser Reflectometer

The main components of the laser reflectometer are depicted in Fig. 51a and include: (a) a red He-Ne laser with a wavelength of 632.8 nm, (b) a rotating drum for mounting the blotter strips, (c) a convergent lens for focusing the reflected light from the blotter strip onto a silicon photodetector and (d) a EG&G silicon photodetector for converting the reflected light collected by the lens into a voltage (V_1) which is stored for further analysis, and (e) a splitter glass plate and another silicon photodetector for monitoring fluctuations in laser light intensity. The voltage (V_2) from the second photodetector is also stored and is used in the data analysis. Details of the laser reflectometer can be found in Ref. 6.

A PC based digital data acquisition system was developed to control the operation of the reflectometer and to analyze and plot the impingement data. Note that the maximum absorption of the blue dye selected for the impingement tests occurred at 629.5 nm, which is very close to the wavelength of the laser, thus, ensuring that small changes in dye color density could be resolved by the system.

The process of converting the raw color density distribution from a dye-laden blotter strip into impingement efficiency distribution involved a number of steps. First, the raw reflectance versus surface distance data (see Fig. 51b) were extracted by mounting each blotter strip on the drum of the laser reflectometer and scanning the strip along its length as shown in Fig. 52a and 52c. The voltages V_1 and V_2 from the two photodetectors obtained during a scan were stored on disk and were used to generate the raw reflectance values shown in Fig. 51b. Note that V-shape strips and long rectangular blotter strips had to be scanned in segments because the reflectometer could only accommodate rectangular strips with a maximum length of 16.5 inches. The raw reflectance data from each segment of the blotter were then combined using a computer program and were stored for further analysis. The spatial resolution of the reflectometer was 47 data points per inch. To convert the raw reflectance values into impingement distributions a FORTRAN program developed during the course of this research was used. The steps involved in generating the final impingement distribution curves are outlined below:

1. The raw reflectance values stored in electronic format during the data extraction process were divided by the reflectivity of the bare (white) blotter paper to obtain normalized reflectance data using the equation below.

$$R_n = \frac{\text{Raw reflectance of dyed blotter paper}}{\text{Raw reflectance of white blotter paper}} = \frac{(V_1/V_2)_{\text{Dyed blotter paper}}}{(V_1/V_2)_{\text{White blotter paper}}} \quad (5.1)$$

   The raw reflectance of the white blotter paper was determined by scanning several sample white strips to obtain an average value. This value was verified at the beginning and end of each data reduction session.
2. The normalized reflectance data were converted into dye mass per unit area using the laser calibration curves in Figs. 47 and 48.
3. The impingement efficiency for each data point recorded was obtained from the following equation.

$$\beta = \frac{\text{Local Dye Mass per Unit Area}}{\text{Average Collector Dye Mass per Unit Area}} \times \beta_{Collector} \quad (5.2)$$

   Collector strips were reduced prior to the model strips since the collector dye mass was required to define the impingement efficiency of each test model. The value of $\beta_{Collector}$ is a function of MVD and is given in Table 11.

5.3.2 Charge-Coupled Device (CCD) Reflectometer

A schematic diagram of the CCD system developed by WSU is given in Fig. 53a. The system consisted of a Pentium 200 MHz PC, a CCD array camera with 14-bit resolution, a camera electronics unit, a camera PC controller, a 24 mm Nikkor lens, four (4) Quartz halogen lamps with precision beam control, four 629nm band pass filters one for each lamp, two power supplies for the lamps, a camera stand, a 1.5-ft wide by 2.5-ft long non-reflecting glass sheet, and a portable dark room for reducing the data.

The data from each dye-laden blotter strip were extracted as follows. Each strip was placed on the table inside the dark room next to a reference scale. The highlight mark on the blotter strip was aligned with a fixed mark on the reference scale. The non-reflecting glass was placed on top of the blotter to keep the blotter flat on the table. The halogen lights were set to the required intensity level by adjusting the voltage and amperage of the two power supplies. Light from each lamp was passed through a 600 nm ±40 nm filter to enhance light absorption by the blue dye on the strip. The camera shutter was activated through the PMIS software and it was kept open for a specified time period, which was determined during the system calibration. A 512 by 512 pixel array image of the blotter strip was obtained and it was stored on disk for later analysis. The camera was capable of resolving nearly 14 bits (or approximately 16000) of intensity values of scattered light from the blotter strip. The blue strip was removed and a white reference strip was placed on the table in exactly the same location. The

process was repeated and a 512 by 512 image of the white strip was obtained and stored. The raw reflectance from the white strip was used to normalize the raw reflectance from the dyed strip. Figure 53b shows a typical raw intensity plot obtained from PMIS software for a tested blotter strip. Note that, the lower intensity values on the plot correspond to the darker (dyed) region on the blotter strip.

Windows driven software, written in PV-WAVE command language and in Microsoft FORTRAN, were developed for the CCD data reduction system to process the images from the dyed strips into impingement distributions. The process for generating the impingement efficiency distributions involved the following steps:

1. Each dyed strip image and the corresponding white strip image were read using the PV-WAVE software developed. Both images were corrected using the bias, dark, flatfield and reference images, which were obtained and stored during the calibration of the CCD array camera.
2. Using the computer mouse, a rectangular region was selected on the white strip image. This region was processed by the software to provide an average intensity value for the white paper.
3. For a rectangular dye-laden blotter strip, a region that was large enough to cover the complete extent of dye impingement was selected using the computer mouse as shown in Fig. 52b. The location of the highlight point on the strip (typically the point on the leading edge of the test geometry corresponding to x/c=0) and a length scale were defined for determining surface distance along the strip. For a V-shape strip, four points were selected by the user as shown in Fig. 52d to define the extent of impingement.
4. The software produced an array of dye intensity versus surface distance for the dyed strip. These values were normalized by the average white blotter paper intensity value to produce an array of normalized intensity (i.e., 0 to 1) distribution versus surface distance, which was stored for further analysis.

Because impingement tests were repeated a number of times for each test condition, several blotter strips were produced for each condition tested. A FORTRAN program was developed to process the normalized intensity values from several blotter strips into a single array of averaged normalized intensity versus surface distance. This array was converted into dye mass ($\mu g/cm^2$) versus surface distance using the calibration curve shown in Fig. 49 and 50. Next the local impingement efficiency values were obtained from Eq. 5.2, which is identical to the one used for processing the data from the laser reflectometer.

6.0 Analysis Methods

Analytical results for the two-dimensional test cases involving the MS(1)-0317, NACA 65_2-415, commerical transport tail section, GLC 305 and NLF(1)-0414 airfoils were obtained with the LEWICE-2D code version 1.6. This code is a panel-based ice accretion prediction code that applies a time-stepping procedure to calculate the shape of an ice accretion. The potential flow field is calculated in LEWICE 1.6 (Ref. 31) using the Douglas Hess-Smith 2-D panel code. This potential flow field is then used to calculated the trajectories of particles and the impingement points on the body. Note that the impingement analysis for the three-element high lift system was obtained with theLEWICE3D code and a 2-D incompressible Navier-Stoke based flow solver (INS2D).

Three-dimensional analysis for NACA 64A008 finite swept wing, 25%-scale business jet empennage, full-scale business jet horizontal tail, and s-duct engine was performed on a single processor (R12000) of an SGI Octane computer. The following steps were required to complete the impingement analysis for the three-dimensional configurations.

1. The grid for the trajectory calculations was constructed using the ICEGRID code
2. The PMARC code was used to generate the velocities on this grid and to generate the surface velocities needed in the LEWICE-3D code.
3. The impingement analysis was performed with the LEWICE-3D code using the panel model and the surface velocity information obtained in step 2 above.

6.1 Grid Generation - ICEGRID

TheICEGRID program was developed at Glenn Research Center by Bidwell and Coirier specifically for the task of optimizing trajectory calculations in the LEWICE-3D code for the panel code interface. ICEGRID automatically produces grids which are optimal for trajectory calculations. An optimal grid for trajectory calculation should have a minimum number of cells, allow for quick traversal (for velocity interpolation), and have clustering of cells near regions of impingement. The tri-binary, multi-block grid structure coupled with a feature that generates refinement only external to the surface of the geometry results in a program that generates grids with a minimum number of cells and which are quickly traversed. The use of refinement regions and functions within the program allows the user to easily control cell size and density in any region of the grid. The ICEGRID program also produces a minimum of grid points which reduces the panel code calculation times. The program requires the surface geometry and an input file describing the grid volume and refinement parameters. The code refines the grid near regions of interest which can include the geometry, parts of the geometry, and lines or points input by the user. The code is similar to an oct-tree method (Ref. 32) in that it recursively divides the original grid volume until the refinement criteria for each cell have been met. The code will not refine cells internal to the geometry. ICEGRID is different from most oct-tree methods in that the grid volume is allowed to be multiply skewed, multiblock and different refinement functions can be used in any direction. This last feature is where the code really differs from the oct-tree methods in that it allows a given cell to be divided into 8, 4 or 2 cells depending on the refinement function instead of the

oct-tree method which divides a cell into 8 cells if the refinement is required. This results in grids with much fewer cells for cases where gridding requirements are disparate in the different directions (e.g. swept wings which have a much smaller cell size requirement in the chordwise direction than in the spanwise direction). The grids used in the impingement analysis of the swept tail models are shown in Figs. 54–56. The grids were all swept to align with the leading edge of each model and were only generated for one side of the symmetry plane.

Cell size is critical in producing accurate droplet trajectories. The panel and grid cell size must be similar and small enough to resolve the velocity gradients in the vicinity of the wing. Specific grid properties for each swept tail model are summarized below:

Geometry	No of Grid Points	Min Chordwise/surface normal grid spacing	Min Grid Cell Size - Spanwise	Max Cell Size for grid
NACA 64A008	216,708	0.159 cm	5.08 cm	40.64 cm
Full-Scale BJ Tail	259,066	0.159 cm	5.08 cm	40.64 cm
25%-scale BJ Tail	224,582	0.04 cm	1.27 cm	10.16 cm

The grid plane at y = 0 shows the major features of the grid. It took approximately one hour of CPU time to generate each of the grids.

6.2 Flow Solver - PMARC

PMARC is a first order 3D potential flow panel code (Ref. 33). Geometries are represented with quadrilateral surface panels which have constant doublet and source distribution. The formulation used in PMARC results in a solution that is second order accurate allowing for accurate flow solutions with fewer panels and less CPU time than other first order methods. The disadvantage of this method is that because a numerical differentiation is used to generate the velocity distribution careful panelling is required to prevent numerical errors. The code can generate solutions for internal and external compressible flows and can handle a large number of panels (approximately 10,000).

For the current study, PMARC computations were performed using a steady, isolated flow with a y = 0 plane of symmetry as shown in Figs. 54c, 55c and 56c. The swept 64A008 panel model contained 2303 panels, the full-scale business jet tail section panel model contained 2162 panels and the 25%-scale business jet empennage panel model contained 2162 panels. Flow solutions were calculated for two angles-of-attack (0°, 6.25° for the NACA 64A008 model; 1°, 6° for the full-scale business jet tail section and 2°, 7° for the 25%-scale business jet empennage model. In cases where surface pressure information was available (i.e. the swept NACA 64A008 model and the 25%-scale business jet empennage model) an attempt to match the analytical and experimental pressure distributions was made by varying the analytical angle-of-attack. In these cases, the analytical and experimental angles-of-attack were different. Matching the pressure distributions ensured that the experimental and analytical flow models had

similar flow fields which is the key in the consistency of the collection efficiency comparisons (Ref. 34). The flow solutions and velocity calculations took approximately 150 minutes for each of the cases.

6.3 Impingement Analysis - LEWICE-3D

The LEWICE-3D grid based code incorporates trajectory, heat transfer and ice shape calculation into a single computer program. This code can handle generic multiblock structured grid based flow solutions, unstructured grid based flow solutions, simple cartesian grids with surface patches, and adaptive grids with surface patches. The latter two methods allow the use of generic panel code input which is a computationally efficient method for generating ice shapes. The code can handle overlapping and internal grids and can handle multiple planes of symmetry. Calculations of arbitrary streamlines and trajectories are possible. The code has the capability to calculate tangent trajectories and impingement efficiencies for single droplets or droplet distributions. Ice accretions can be calculated at arbitrary regions of interest in either a surface normal or tangent trajectory direction. The LEWICE-3D code has been used in previous calculations for isolated wings, inlets, ducts, and full aircraft configurations (Refs. 35–41).

The methodology used in the LEWICE-3D analysis is desribed in Ref. 42. In general, the trajectory analysis requires six basic steps for each section of interest at each time step as follows:

1. In the first step the flow field is generated by the user.
2. Surface streamlines are calculated during the second step. The surface streamline analysis uses a variable step size fourth-order Runge-Kutta integration scheme developed by Bidwell (Ref. 40).
3. In the third step, tangent trajectories are calculated at the region of interest.
4. In step 4, an array of particles is released between the tangent trajectories. These impacting particles are used to calculate collection efficiency as a function of surface position. The trajectory analysis is basically that of Hillyer Norment (Ref. 43) with modifications by Bidwell. At the heart of the trajectory analysis is the variable step predictor-corrector integration scheme developed by Krogh (Ref. 44).
5. Step 5 involves interpolating or extrapolating the collection efficiencies onto the streamlines.

LEWICE-3D calculation times varied for the different cases depending upon the drop size and the number of trajectories. The LEWICE-3D calculation times are heavily dependent upon grid size and structure because the largest portion of the LEWICE-3D calculation time (greater than 99%) is spent calculating velocities at specified points, which involves searching through the grid tree structure for the cell in which the point is located. The trajectory integration time for the cases varied from 0.02–0.05 seconds. Approximately 100 trajectories were required for each drop size at each section of interest for the droplet impingement calculations. This resulted in calculation times of approximately 250–500 seconds for each of the tail cases (2 sections-of-interest, 27 bin distribution).

The S-duct engine inlet analysis was comprised of two tasks. The grids and flow solutions using the NPARC flow solver were provided by the engine manufacturer. NASA Glenn generated the trajectory analysis using the LEWICE-3D program.

There were six blocks of grid systems with a total of 997,450 grid points as shown in Fig. 57. A multi-block Navier-Stokes flow solver (NPARC) was used to obtain the internal flow solution for a Reynolds number of 591,290 based on a reference length of approximately 16 inches (see Fig. 22f) and a Mach nubmer of 0.22.

The trajectory analysis was conducted with the LEWICE-3D program with an eight-bin distribution representing the IRT cloud for each of the three droplet sizes used in the experimental investigation. The Monte-Carlo collection efficiency method was used to generate the collection efficiencies on the inlet outer and inner surfaces. Each bin of the distribution required about 1,000,000 droplet trajectory calculations and took about 240 hours on a single 300 MHz SGI Octane processor to complete.

7.0 Results and Discussion

In this section, the accuracy of the experimental and data reduction methods is discussed and sources of error are identified. Results from studies performed during the experimental investigation are used to quantify the effect of test variables on test repeatability. Experimental impingement data for all models tested are presented and are compared with analysis data obtained with the LEWICE-2D and LEWICE-3D computer codes discussed in section 6. All the experimental data are averaged data from repeated tests. Geometric, flow and droplet parameters for the airfoil and finite wing models used during the impingement tests are summarized in Table 13.

7.1 Repeatability of Experimental Method

Test repeatability is an important indicator of the quality of the experimental method. Repeatability is defined as the maximum percent difference of repeated test runs from the average. Typically, the maximum difference is observed at the point of maximum impingement efficiency. Previous experimental investigations (Refs. 1–7 and 30) have demonstrated test repeatability in the range of 10%–30%. The main contributor to this uncertainty has been the experimental method and in particular, the repeatability of the spray clouds.

An uncertainty analysis presented in Ref. 30 showed that errors in spray time, dye concentration, spray system pressures, tunnel velocity and cloud unsteadiness due to spray bar-induced turbulence alone were responsible for 14% variation in β_{max}. Tests performed during the present investigation have identified and quantified the uncertainty of important experimental variables and their effect on test repeatability. In general, the results obtained support the findings in Ref. 30 with one significant exception: relative humidity was found to be critical to test repeatability.

7.1.1 Spray System Performance and Repeatability

The spray system is an important component of the experimental method and is directly responsible for the repeatability of the spray cloud. Important spray system variables include air and water pressures, spray duration, and nozzle performance. In addition, since spray system pressures are set based on information gathered from pressure transducers distributed throughout the system, the accuracy of these devices is critical to spray system performance. The accuracy of the pressure transducers used in this work is presented in Table 9.

Experimental results presented in Table 10 and Figs. 58 and 59 indicate that the twelve-nozzle spray system was capable of maintaining water and air pressures to within ± 1 psi. A detailed error analysis was performed using the calibration equations for the MOD-1 nozzles provided by NASA (Refs. 45 and 46). This analysis showed that variations of ±1 psi in spray system pressures would result in ±0.5 microns error for the 11.5-micron MVD and ± 1 micron error for the 21-micron MVD. These results are supported by repeated FSSP and OAP measurements presented in Fig. 42. Computations performed with LEWICE-2D (Ref. 31) showed that the errors in β_{max} due to ±0.5 microns, and ±1 micron error in MVD were of the order of ±1% (i.e., $\Delta\beta = .01$) for the 11.5-micron and 21-micron cases as demonstrated in Fig. 60a. The effect of the MVD uncertainty on the impingement limits can be estimated from Fig. 60b. All computations were performed with monodispersed (i.e., single drop size) droplet distributions.

The NASA Glenn MOD-1 nozzles used in this investigation have a very thin water tube with a diameter of 0.0155 inches (0.4 mm). A bent or clogged water tube can cause significant changes in cloud uniformity. It is very difficult to estimate the error due to nozzle characteristics. The approach taken in this work was to carefully select and check all nozzles used in the 12-nozzle spray system. The first step was to select nozzles with very similar flow coefficients (C_f). The flow coefficient of a nozzle is defined as

$$C_f = \frac{\dot{W}}{\sqrt{\Delta P}}$$

Where, $\dot{W}$ is the water flow rate in gallons per minute and ΔP is the differential pressure between the water and air supplied to the nozzle in psi. The flow coefficients of the 12 nozzles selected varied from 0.00398 to 0.00406 as shown in Figs. 25 and 27. Next, each MOD-1 nozzle was visually inspected to verify that its water tube was aligned with the nozzle axis. To help prevent nozzle clogging, the water solution from the tank was filtered prior to entering the MOD-1 nozzle assemblies. Since filtering does not eliminate the problem of nozzle clogging, a very sensitive flow meter was installed in the spray system. During each test, the flow rate from all 12 nozzles was monitored. Tests performed with partially clogged nozzles showed that the flow meter could easily detect changes in the total flow rate even with a single nozzle partially clogged. Flow rates corresponding to each test MVD case are presented in Table 10. Figure 61 shows the

variation in the 12-nozzle water flow rate for selected tests conducted during the 1999 IRT entry. As an added precaution, a video camera was installed near the entrance of the test section to monitor the nozzles during each test. Finally, each time the spray system pressures were adjusted to change the MVD size, two to three spray tests were performed to verify that all nozzles were spraying consistently.

Repeatability of spray duration is important to the accuracy of the experimental results. Spray duration was controlled by the PC timer unit, which was accurate and repeatable. However, another factor, which affects spray duration and cannot be controlled easily, is nozzle on/off performance. This is related to the MOD-1 nozzle design and solenoid on/off response. During the evaluation of the spray system, each nozzle was videotaped from the start to the end of a spray test. By counting video frames (30 frames per second), it was determined that the spray required approximately 0.06 seconds to reach full strength after activation of the solenoid valves. Upon de-activation of the solenoid valves, however, the spray "shut off" time varied from 0.2 to 0.4 seconds depending on nozzle. In summary, the variation in spray duration was approximately 0.2 seconds between tests. Since spray duration was set according to MVD size, the variation in spray duration for the 1997 impingement tests was 1% for the 18 seconds spray (MVD = 11.5μm), 3% for the 6 seconds spray (MVD = 21μm), and 7% for the 3 seconds spray (MVD = 92μm). Shorter sprays were selected for the larger MVDs to avoid blotter paper penetration by the dye solution. Note that during the 1999 IRT tests, spray times were reduced as shown in Table 10b. This was done to enhance the sensitivity of the data reduction method by further limiting dye penetration into the blotter paper. For the new spray times selected the variation in spray duration was 2% for the 9 seconds spray (MVD = 11 μm), 4.7% for the 3.8 seconds spray (MVD = 21μm), 9.5% for the 2.2 seconds spray (MVD = 94μm).

Figures 62 and 63 show typical spray system air and water pressure histories for each of the three MVD cases used in the 1997 and 1999 impingement tests respectively. A small transient period, approximately 0.5 to 1 seconds in duration is observed in the pressure traces for some of the test cases. This transient behavior was also observed during the MVD and LWC measurements with the FSSP, OAP and KING probes. Basically, the cloud MVD and LWC stabilized to their final values within 0.5 to 1 seconds.

7.1.2 Cloud Uniformity

Cloud uniformity and in particular LWC uniformity, is the most challenging aspect of the experimental method and contributes significantly to the experimental uncertainty. During the course of the 1997 and 1999 impingement tests, extensive cloud uniformity tests were performed using the laser sheet as well as the grid and blotter method. The objective of the uniformity tests was to adjust the WSU spray nozzle locations in order to produce spray clouds with uniform LWC over a 2-ft high by 3-ft wide area at the center of the IRT test section. This area was determined to be sufficient for testing the wind tunnel models selected for the impingement tests. Figures 64–66 show typical cloud uniformity results in terms of normalized reflectance for the 11, 21, and 94-micron MVD cases obtained with the grid and blotter method during the 1999 IRT entry. Note that

the sharp reflectance spikes in these figures (normalized reflectance values close to 1.0) correspond to the grid bars which were spaced 6 inches apart in both the horizontal and vertical directions. The results presented show that in most cases the cloud uniformity was in the range of ±10% to ±15% from the average within the area of interest.

However, in spite of the extensive efforts made to obtain a spray cloud with uniform LWC, local variations within the test area are usually present and these variations could significantly affect the quality of the experimental data. These local variations are the result of the large number of variables that influence the spray cloud characteristics. Parameters such as nozzle performance, spray system settings, model geometry, angle of attack, relative humidity, tunnel turbulence level, etc. could affect the LWC distribution in the wind tunnel test section. Furthermore, the interaction between these variables was not easy to assess. For example, high spray system air pressures required for certain cloud conditions could increase the level of turbulence in the tunnel and the level of cloud unsteadiness. This is why it is so important that local LWC measurements are made at exactly the same locations as the model strips. Typical local LWC measurements performed with the collector mechanism are presented in Figs. 67a and 67b in terms of normalized reflectance. Variation in normalized reflectance was between –2.8% and +1.4% from the average and corresponded to a dye mass density (i.e., LWC) variation from +9% to –4% respectively. Thus, although the variation in LWC within the 2-ft by 3-ft area of interest was ±10% to ±15%, local LWC measurements exhibited less variation.

However, measurement of local LWC does not eliminate the effect of cloud non-uniformity. This is because the collector mechanism and the model are not subjected to exactly the same flow field. The presence of a lifting wing modifies the flow field, particularly in high lift situations. Thus, although blotter strips on the wing and collector could be placed so that they corresponded to the same physical location in the test section, the dye impinging on model and collector strips could originate from spatial locations in the cloud with different values of LWC.

7.1.3 Relative Humidity

The effect of relative humidity on the experimental impingement data was partially investigated by the WSU/Boeing team during the 1985 and 1989 impingement tests at NASA Glenn. However, attempts to quantify the effect of relative humidity were not successful. Recently, experiments conducted by Bragg et al. (Ref. 30) showed that relative humidity did not have a significant effect on spray clouds produced with three NASA Glenn STANDARD nozzles. This conclusion was drawn from cloud droplet distribution measurements for five humidity levels varying from 10% to 63%.

During the present investigation, extensive tests were performed to quantify the effect of relative humidity on cloud droplet distribution and LWC, since these parameters are directly related to the repeatability of the experimental impingement data. Droplet distributions and LWC measurements were conducted for relative humidity levels ranging from 55% to 95%. Droplet measurements were obtained with the NASA Glenn

FSSP probe while LWC measurements were performed with the NASA Glenn KING probe. Results from this study are presented in Table 14, and in Figs. 68a and 68b.

Table 14 shows that relative humidity had a significant effect on droplet count and LWC but not on cloud MVD. The effect of relative humidity on cloud LWC for MVDs of 11, 11.5, 21, 92 and 94 microns is demonstrated Figs. 68a and 68b. For the 1997 IRT tests and for the 11.5μm MVD, increasing the relative humidity from 60% to 90% increased LWC from 0.01 to 0.12 g/m^3. Thus, a 30% increase in relative humidity increased the local LWC by a factor of 12. Similar tests conducted during the 1999 IRT tests showed that a 30% increase in relative humidity resulted in a threefold increase in cloud LWC. Relative humidity had a smaller but still significant effect on the LWC for clouds with larger MVDs. For instance, tests conducted during the 1997 IRT entry showed that for the 21μm cloud, a 30% increase in relative humidity increased LWC from 0.12 to 0.21 g/m^3 while for the 92μm case, the same increase in humidity increased LWC from 0.18 to 0.28 g/m^3.

The results of the relative humidity study demonstrate that changes in relative humidity of the order of ±10% could result in large variations in the impingement results and that the repeatability of the data can be adversely affected by changes in relative humidity. In particular, if the collector and the models are tested at different relative humidity levels, the experimental error can be considerable. It should be noted that the NASA Glenn MOD-1 nozzles used in the 1997 and 1999 impingement tests have lower flow rates (approximately 1/3 lower) than the STANDARD nozzles. Therefore, spray clouds produced with the MOD-1 nozzles could be more sensitive to changes in relative humidity.

7.1.4 Dye Recirculation

Dye recirculation could adversely affect the experimental impingement results. Several tests were conducted to investigate the possibility of dye recirculation in the tunnel. Initially, blotter strips were attached on the IRT spray bars near the tunnel centerline so that the blotters were facing upstream. After two days of testing, the blotter strips were scanned with the CCD reflectometer. No dye trace was found. Five weeks after the start of the impingement tests, the tunnel turning vanes upstream and downstream of the refrigeration section, which was located just upstream of the IRT spray bars, were examined for dye deposits. Several turning vanes were wiped with a clean wet cloth to determine if dye deposits were present. Small traces of dye were found in the vanes upstream of the refrigeration section. However, no dye trace was found downstream of the refrigeration section. To investigate the possibility of dry dye powder recirculation in the tunnel, several wet blotter strips and a wet cloth were attached to the IRT spray bars facing upstream. The blotters and cloth were moistened periodically to make sure that they remained wet between impingement tests. After two days of testing, the blotters and cloth were examined for dye deposits. No visible dye traces were observed. Thus, it is concluded that dye recirculation was not a problem in the present investigation.

7.2 Repeatability of Data Reduction Methods

A discussion on accuracy and repeatability of the data reduction methods is presented in this section. Key factors affecting the data reduction method include: blotter paper consistency, calibration curve relating normalized reflectance to dye mass, depth of dye penetration into the blotter, uniformity of blotter strip illumination and performance of hardware components.

7.2.1 Blotter Paper Characteristics

It is advisable to select a thin blotter paper for the impingement tests since a thin paper conforms better to the surface of the test model and minimizes aerodynamic interference. The paper should also retain its texture throughout the testing and it should be chemically inert to the dye and water. Its composition should minimize dye diffusion in the lateral direction. Furthermore, the paper should be mechanically strong to withstand the aerodynamic forces experienced during testing.

Three types of white blotter paper were evaluated for the impingement tests: a James River Paper Company 100# Verigood blotting paper (VG100#) with a thickness of 0.53 mm, a James River 80# Verigood blotting paper (VG80#) with a thickness of 0.45 mm, and a Whatman WH3MM Chromatography paper (W3MM) with a thickness of 0.35 mm. To determine the consistency in the reflectance properties of these papers, a large sample of blotter strips were scanned with both data reduction systems. The results obtained showed that the VG100# and W3MM papers exhibited ±2% variation in raw reflectance from the average. Reflectance variation for the VG80# was in the range of ±3% to ±4%. It should be noted that some of the variation observed was due to the data reduction systems.

Several dye-laden blotter paper samples were produced with all three types of blotter paper to define the normalized reflectance versus dye mass calibration relation for each paper. The data for the laser reflectometer are presented in Fig. 69. Corresponding data for the CCD data reduction system are depicted in Fig. 70. Note that these are not the final calibration data for the data reduction systems. They are presented here to demonstrate the effect of paper characteristics on the calibration curve and on the data reduction process.

The reflectance versus dye mass relation exhibited a steep decline in normalized reflectance for low dye mass densities followed by a more gradual decline. As the dye mass density increased beyond a certain value, the slope decreased significantly and in some cases it was close to zero. In the region of the calibration curve where the slope is nearly zero (saturation region), the accuracy of the data reduction method is considerably reduced. That is, a small error in normalized reflectance can produce a large error in dye mass. Thus, the saturation region limits the usable range of the calibration curve. The usable range of the calibration curve corresponds to the region of the curve where small errors in reflectance measurements do no result in large errors in dye mass per unit area. It is desirable to have a reflectance calibration curve with a wide usable range because during testing, a range of dye densities is usually obtained on the blotter strips due to the variation in test conditions and impingement intensity.

Figures 69 and 70 show that the start of the saturation region for the VG80# occurred at a dye mass density near 1.5 g/cm^2. For the VG100# and W3MM papers the saturation range occurred at dye mass densities greater than 2.5 g/cm^2. Thus, the VG100# and W3MM papers were selected for further evaluation during for the 1997 IRT impingement tests. Tests with a number of airfoil models showed that the W3MM was easier to apply to the model surface. Its resistance to dye penetration, however, was low and in many cases the level of dye penetration was high even for short spray times. The VG100# paper was prone to creasing in regions of high surface curvature such as the sharp leading edge of a thin airfoil. However, this paper was considerably more resistant to dye penetration and it provided the best overall performance during the impingement tests. The VG100# paper was used exclusively for all impingement tests conducted in 1999. Note that the spray duration and the concentration of the blue dye solution were determined from the reflectance and penetration characteristics of the VG100# blotter paper used in the impingement tests.

7.2.2 Blotter Paper Illumination

To eliminate the influence of external light sources on reflectance measurements, the data reduction was performed in a dark room. Thus, the only light source was that used in the illumination of the blotter strips.

The laser reflectometer relies on a point measurement technique and the illumination of the blotter paper is accomplished using a He-Ne laser beam 1mm in diameter. For practical purposes, the intensity of the incident light over the 1mm diameter area of the blotter paper can be assumed uniform. Laser light intensity could be affected by variations in laser power output. However, this problem was eliminated with the use of the glass splitter plate shown in Fig. 51a. Details on the use of the splitter plate to account for laser power fluctuations during the data reduction process can be found in Ref. 6. Another advantage of the laser reflectometer is that the intensity of the laser beam is powerful enough to penetrate below the surface of the blotter paper. Thus, reflectance measurements are less sensitive to dye penetration as long as dye penetration into the blotter is limited to less than 20% of the blotter thickness.

The CCD data reduction method measures reflectance over a large area of the blotter strip simultaneously. For this system, uniform illumination of the blotter strip is very important in obtaining accurate results. In addition, dye penetration into the paper can affect the accuracy of the reflectance measurements because the illumination intensity from the four halogen lamps used to in the CCD system was not high enough to penetrate below the surface of the blotter paper. Thus, dye penetration into the blotter must be maintained to very low levels when the CCD data reduction system is used to extract the impingement data.

7.2.3 Repeatability of Data Reduction Systems

To establish the repeatability of the data reduction systems, a white VG100# blotter strip was scanned with the laser and the CCD reflectometers several times over a period of two months. Four randomly selected scans obtained with each data reduction

system are presented in Figs. 71 and 72 for 1997 and 1999 tests respectively. The results indicate that the variation in the four reflectance measurements obtained with the laser reflectometer and the CCD system was approximately ±1% from the average.

7.3 Pressure Distributions

Experimental pressure distributions for the all models tested are compared with analysis results from LEWICE-2D, LEWICE-3D, INS2D and NPARC in Figs. 73–82. Note that the first two computer codes use potential flow methods for the computation of the flow field. INS2D is an incompressible Navier-Stokes code while NPARC uses the full Navier-Stokes equations to simulate internal or external flows. In order to match the experimental pressure, the angles of attack in the computations were slightly adjusted by approximately –2.0 to 2.5 degrees depending on the model tested. The adjustments made in the angles of attack used in the computations of the airfoil/wing flow fields were mainly due to airfoil trailing edge thickness, viscous effects and tunnel wall effects. For example, the trailing edge of the MS(1)-0317 was blunt with a thickness of approximately 1% chord, however, for the computations, a sharp trailing edge was generated by extending the airfoil chord. This extension resulted in higher circulation for a given angle of attack. Another reason for the reduction in angle of attack used in the computations is tunnel flow angularity, which was found to be approximately –0.5°. Good correlations can be found for all cases between experimental and computational data after modifying the computational angles of attack.

Experimental and computational pressure distributions for the multi-element airfoil are depicted in Fig. 81. The flow computations were performed with the INS2D computer code (Refs. 47, 48) using a Chimera grid. For this case, acceptable correlation between the experimental and computational results was obtained without having to modify the experimental angle of attack. The discrepancies observed over the slat surface could be due to the small tunnel angularity and tunnel wall effects.

Experimental and computed pressure distributions for the S-Duct engine inlet are presented in Figs. 82a–82c for a freestream velocity of 170 mph and an inlet mass flow of 23 lbm/sec. The computed pressure distributions were obtained with the NPARC Navier-Stokes code (Ref. 49). Good agreement between experiment and analysis is demonstrated at most inlet locations. However, for the axial location X=37.24 in Fig. 82c considerable differences between the computed and experimental pressure distributions were observed.

7.4 Impingement Results

7.4.1 Test Repeatability

Test repeatability is an important indicator of the quality of the experimental results. For the purpose of this discussion, repeatability is defined as the maximum percent difference of repeated tests from the average. Typical test repeatability in previous experimental investigations (Refs. 1–6) was in the range 10% to 30%. The large variation in the test data was attributed to a number of factors that influence the experimental results as discussed in Refs. 1, 2, 6, 30 and 50. A discussion of potential sources of errors affecting the impingement data was presented in sections 7.1 and 7.2.

During the 1997 and 1999 impingement tests, 3 to 4 tests were performed for each test condition and in a limited number of cases as many as 11 tests were conducted to assess the repeatability of the experimental data. Selected test repeatability data are presented in Figs. 83–94 and in Table 15 for all eleven models tested during the 1997 and 1999 IRT entries and for most of the test conditions. The results presented in these figures indicate that the maximum difference of repeated tests from the average was as follows:

- MS(1)-0317 airfoil (1997 IRT tests) 3.0% to 12.0%
- MS(1)-0317 airfoil (1999 IRT tests) 3.0% to 11.0%
- GLC 305 airfoil 4.9% to 16.0%
- NACA 65_2-415 airfoil 7.0% to 17.0%
- Commercial Transport Tail Section 1.7% to 9.8%
- NLF-0414 (36-inch chord) 0.2% to 14.0%
- NLF-0414 (48-inch chord) 0.8% to 11.0%
- NACA 64A008 Swept Tail 3.2% to 12.0%
- 25%-Scale Business Jet Horizontal Tail 3.2% to 14.0%
- Full-Scale Business Jet Horizontal Tail 1.6% to 8.7%
- Three-element High Lift System 5.6% to 17.0%
- S-Duct Engine Inlet 4.6% to 13.0%

In summary, the data presented indicate that the maximum difference of repeated tests from the average was

- 0.24% to 12% for 82 out of the 93 cases presented
- 13.00% to 17% for 11 out of the 93 cases presented

For the test conditions where 11 tests were performed to assess test repeatability, the maximum difference from the average was similar to that obtained using only 3 to 4 test runs.

This is a significant improvement in test repeatability compared to previous experimental efforts. The effort to improve the repeatability of the experimental impingement data continues. Currently, work is being done to further enhance the accuracy of the data reduction methods and to develop new methods for measuring local LWC in the vicinity of the test model using a laser sheet method.

All experimental data presented in Figs. 83-94 were reduced with the laser reflectometer. Note that the laser reflectometer uses point reflectance measurements at two to three locations along the width of a blotter strip (see Fig. 52a) to generate the value of the local impingement efficiency. Thus, impingement results obtained with the laser reflectometer tend to exhibit larger variation from the average. Corresponding repeatability data (not shown) obtained with the CCD data reduction system exhibited less variation from the average by approximately 1 to 2 percentage points compared to the laser reflectometer. This is because at any model surface location the CCD system

averages data from a large portion of the width of the blotter strip which reduces the effect of local variations in impingement characteristics between test runs. The laser illumination method used in the laser reflectometer, however, can penetrate below the surface of the blotter paper and as a result, dye penetration errors are minimized as explained in section 5 of this report.

7.4.2 Experimental and LEWICE Impingement Data

All the experimental impingement curves presented in this section are the average of the three to four tests conducted for each impingement condition. Prior to averaging the experimental data, the individual experimental impingement curves were smoothed using a three point moving average technique. Unless stated otherwise, the experimental impingement data presented were reduced using the laser reflectometer.

A summary of key geometric as well as aerodynamic and impingement parameters for the two-dimensional airfoils and the three finite wing model tested are provided in Table 16. The symbol $S_{\beta max}$ in Table 16 denotes the surface location corresponding to the maximum impingement efficiency. The symbols S_u and S_l are the upper and lower impingement limits defined as the locations on the model surface where the local impingement efficiency was 0.01% (i.e., $\beta = 0.0001$). The non-dimensional chordwise locations for S_u and S_l are denoted by x_u/c and x_l/c.

Experimental impingement data for the eleven models tested and for all test conditions are compared with LEWICE-2D and LEWICE-3D predictions in Figs. 95–107. For ease of reference, a summary of all impingement data obtained during the 1997 and 1999 IRT tests is provided in Appendix A. The impingement data are presented in the form of local impingement efficiency versus surface distance in mm. Surface distance was measured with respect to a reference point on each test model termed the highlight. Surface distance was negative along the suction side (typically the airfoil upper surface) and positive along the pressure side of an airfoil or finite span tail model. For all models tested, the highlight was located at the leading edge corresponding to a surface distance of 0 mm. The surface distance resolution for the experimental data was 0.50 mm (0.02 inch). For clarity of presentation, symbols were placed at every 5th point in the experimental curves. Caution was exercised in the placement of these symbols so as not to miss the location of the peak efficiency.

With the exception of the S-duct case, the LEWICE impingement results presented in the figures were obtained with the measured FSSP+OAP droplet distributions shown in Fig. 42 which were divided into 27 bins to simplify the computations. Note that the version of LEWICE distributed to the public is limited to a maximum of 10 bins for approximating droplet distributions. For the S-duct inlet an 8-bin approximation of the experimental droplet distributions was used. For the LEWICE computations the experimental angles of attack were adjusted as discussed in section 7.3 to match the experimental pressure distributions.

Figures 108–116 show experimental impingement limits plotted on the airfoil surface for the six two dimensional test models and the three finite tail models tested.

Figures 117–125 show the experimental impingement distributions plotted on the airfoil surface. These plots are for illustration purposes only and they are not to scale. The plots were constructed by plotting the local impingement efficiency value at a given surface location normal to the surface of the airfoil. All β values were scaled by c/20 where c is the chord length of the airfoil in mm. The resulting plots resemble ice accretions and are useful in demonstrating the magnitude and extent of impingement as a function of angle of attack and MVD size.

A. MS(1)-0317 Airfoil

This airfoil was tested by the WSU/Boeing research group in 1985 and it was used as a calibration model for the IRT impingement tests conducted in 1997 and 1999. Comparisons between test data obtained in 1985 and in 1997 were presented in Ref. 50 and showed good overall agreement.

Experimental impingement data at the mid-span location (36 inches above the tunnel floor) of the MS(1)-0317 airfoil are presented in Figs. 95a–95f for angles of attack of 0° and 8° and MVDs of 11.5, 21 and 92μm. The data presented in Fig. 95 were obtained during the 1997 IRT entry. For all cases, three impingement curves are presented for each angle of attack. Two of the curves are the experimental data reduced with the CCD data reduction system and the laser reflectometer while the third curve is analysis data obtained with the LEWICE-2D code. The computations were performed for an angle of attack of -1.85° (instead of 0°) and for 6.15° (instead of 8°) to match the experimental pressure distributions as shown in Fig. 73. The experimental data obtained in 1999 for an angle of attack of 0° and MVDs of 11, 21 and 94 micron are presented in Fig. 96. The experimental and analytical impingement efficiency distributions presented in Figs. 95 and 96 indicate the following general trends:

1. Experimental data reduced with the laser reflectometer and the CCD data reduction systems were in very good overall agreement. In some cases, however, the laser reflectometer produced higher impingement efficiency values near the region of maximum impingement efficiency. This is evident in the 1997 data presented in Fig. 95. The reason for the observed discrepancy was attributed to a small level of dye penetration into the blotter, which could not be detected by the current set up of the CCD data reduction system. In 1999, the spray times were reduced to minimize dye penetration into the blotter. Note that the 1999 experimental impingement data obtained with the laser and CCD reflectometers are in better overall agreement compared to the 1997 data.
2. For the $\alpha = 0^\circ$ case, the maximum impingement efficiency occurred along the upper surface (s = –1 to –6 mm) near the leading edge for all MVDs. Maximum values of β were 0.32–0.33 (laser), 0.26 (CCD) for MVD = 11.5 and 11μm; 0.50 (laser), 0.41 (CCD) for MVD = 21μm; 0.68 (laser), 0.59 (CCD) for MVD = 92 and 94 μm. The extent of the impingement limits increased with MVD size as expected.

3. At the higher angle of attack, α = 8°, the location of maximum impingement efficiency was shifted to the lower surface of the airfoil. For this case, the values of maximum β were 0.25 for MVD = 11.5 μm, 0.51 for MVD = 21 μm, and 0.76 for MVD = 92 μm. Once again, the extent of the impingement limits increased with MVD size.
4. Analysis results obtained with the corrected angles of attack and with the measured droplet distributions (solid line) were in good correlation with the experimental results for the 11-μm, 11.5-μm and 21-μm MVD cases. However, for the 92-μm and 94-μm MVDs, the computed impingement efficiencies were considerably higher and the impingement limits were greater than the experiment.
5. Analysis impingement data obtained with uncorrected angles of attack (not shown) were shifted to the right with respect to the experimental data.
6. Experimental data obtained in 1997 and in 1999 for α = 0° and MVDs of 11, 11.5, 21, 92 and 94 microns were in very good agreement in all cases as shown in Fig. 97 indicating that the experimental methodology was consistent and repeatable.

B. GLC 305 Airfoil Section

Experimental and LEWICE impingement data for angles of attack of 1.5° and 6° and MVDs of 11.5, 21 and 92 micron are compared in Figs. 98a–98f. All data are for the mid-span station (36 inches above the tunnel floor) and were obtained during the 1997 IRT entry. The LEWICE computations presented were obtained for angles of attack 1.6° and 5.25° to match the experimental pressure distributions as shown in Fig. 74. The measured FSSP+OAP droplet distributions were used to compute the impingement characteristics. For both angles of attack tested, good agreement between LEWICE and experiment is demonstrated for the 11.5 and 21-micron MVD cases but once again, large differences are observed for the 92-micron case. The maximum impingement efficiency for the α = 1.5° was on the lower surface of the airfoil in the proximity of the leading edge. Maximum experimental impingement efficiencies for this angle of attack were 0.47, 0.66 and 0.76 for the 11.5, 21 and 92-micron MVDs respectively. For all MVD cases the extent of impingement was greater on the lower surface than on the upper surface as shown in Figs. 98a–98c. For the case of α = 6°, the location of the maximum impingement efficiency was further aft on the lower surface as expected and the maximum experimental impingement efficiencies were 0.43, 0.60 and 0.72 for the 11.5, 21 and 92-micron MVDs respectively.

C. NACA 652-415 Airfoil

Experimental and LEWICE impingement data for this airfoil obtained at the mid-span location (36 inches above the tunnel floor) during the 1997 IRT entry are presented in Figs. 99a–99c for α = 0° and in Figs. 99d–99f for α = 8°. The LEWICE computations presented in Figs. 99a–99f were obtained for angles of attack –0.55° and 6.55° to match the experimental pressure distributions as shown in Fig. 75.

For the $\alpha = 0^\circ$ case, the point of maximum impingement for this airfoil was at the leading edge and the maximum impingement efficiency was 0.45, 0.62 and 0.73 for the 11.5, 21 and 92-micron cases respectively. As expected, the impingement limits increased with MVD size. Overall, agreement with the LEWICE was very good for the 11.5-μm case. For the 21-μm MVD, the LEWICE impingement tails were higher in magnitude and extent than the experimental data. Notable differences were observed between LEWICE and experiment for the 92-μm MVD case. The magnitude and extent of impingement computed by LEWICE were considerably greater than the experiment for this MVD.

As angle of attack was increased to 8°, the following trends were observed in the experimental data. The point of maximum impingement moved toward the lower surface, maximum impingement efficiency decreased with respect to the $\alpha = 0^\circ$ case for all MVDs and the limit of impingement moved toward the leading edge on the upper surface and toward the trailing edge on the lower surface. Agreement with the LEWICE data was good for the 11.5 and 21-micron cases. For the 92-μm case, large discrepancies between the LEWICE and the experimental data were observed. Once again, the analysis produced more water impingement than the experiment.

D. Commercial Transport Tail Section

Experimental results from the 1997 IRT entry and LEWICE data for this model are compared in Figs. 100a-100f for an angle of attack of 0° and 4°. The experimental results correspond to the mid-span station (36 inches above the tunnel floor). The LEWICE computations presented in Figs. 100a-100f were obtained for angles of attack 0° and 4°. Note that for this airfoil the experimental and computational angles of attack were the same as shown in Fig. 76. Correlation between experimental and analysis was good for MVDs of 11.5 and 21 microns for both angles of attack. The 92-micron data show the same discrepancy between analysis and experiment that was observed with the other test models. The maximum experimental impingement occurred at the leading edge for $\alpha = 0^\circ$ for all MVDs with maximum impingement efficiency of 0.47, 0.60 and 0.76 for the 11.5, 21 and 92-micron cases respectively. At $\alpha = 4^\circ$ the impingement curves shifted toward the lower surface and the maximum impingement efficiency values were 0.41, 0.54 and 0.74 for 11.5, 21 and 92-micron spray clouds respectively.

E. 36-in and 48-in NLF(1)-0414 Airfoils

Two airfoils with chordlengths of 36 and 48 inches were tested in 1999 to provide impingement data for two different scales. In addition, the 48-in airfoil had a 25% chord control surface to measure the effect of simple flap or aileron deflection on impingement characteristics. The experimental and LEWICE data presented in Figs. 101a–101f are for the 36-inch airfoil and include angles of attack of 0° and 8° and all MVD cases tested. For the 48-inch airfoil, the experimental and LEWICE data are presented in Figs. 102a-102o and include $\alpha = 0^\circ$, 4°, and 8° with a flap deflection of $\delta = 0^\circ$ and $\alpha = 0^\circ$ with a flap deflection of $\delta = 15^\circ$. Note that the experimental data shown in the figures correspond to the mid-span location. The angles of attack used in the LEWICE

computations to match the experimental pressure distributions for $\alpha = 0^\circ$, and 8° with a flap deflection of $\delta = 0^\circ$ were as follows: -1° and 5.5° for the 36 inch chord model and -0.75° and 6° for the 48-inch model as shown in Figs. 77 and 78 respectively.

Experimental and LEWICE impingement data for an angle of attack of 0 degrees and for MVDs of 11, 21 and 94 micron are compared in Figs. 101a–101c and 102a–102c for the 36-in and 48-in airfoils respectively. Maximum impingement efficiency for the 36-in airfoil was 0.45, 0.60, and 0.77 for the 11, 21 and 94-micron cases respectively. Corresponding maximum impingement efficiencies for the 48-in airfoil were 0.40, 0.55 and 0.75. Thus, for each MVD case the 36-inch airfoil had higher maximum impingement efficiency and the impingement limits were further aft (in percent chord) than the 48-inch section as expected. For both airfoils and for all MVDs the maximum impingement efficiency occurred at the upper surface close to the leading edge. Good agreement between the experimental and LEWICE data was demonstrated for the 21-micron case. For the 11-micron case, however, the maximum experimental impingement efficiency was approximately 6% higher for the 36-inch airfoil and 12% higher for the 48-in airfoil than corresponding LEWICE values. The experimental data for the 94-micron MVD had considerably smaller impingement limits and maximum impingement efficiency than the LEWICE results.

Experimental and LEWICE impingement data for an angle of attack of 4 degrees and for MVDs of 11, 21 and 94 micron are compared in Figs. 102d–102f for the 48-in airfoil. Maximum impingement efficiency for this case was 0.38, 0.52, and 0.72 for the 11, 21 and 94-micron cases respectively. Good agreement between the experimental and LEWICE data was demonstrated for all but the 94-micron case.

Experimental and LEWICE impingement data for an angle of attack of 8° and for MVDs of 11, 21 and 94 micron are compared in Figs. 101d–101f and 102g–102i for the 36-inch and 48-inch airfoils respectively. Maximum impingement efficiency for the 36-in airfoil was 0.37, 0.57, and 0.75 for the 11, 21 and 94-micron cases respectively. Corresponding maximum impingement efficiencies for the 48-inch airfoil were 0.36, 0.51 and 0.70. As observed with the $\alpha = 0^\circ$ case, for fixed MVD the 36-inch airfoil had higher maximum impingement efficiency and larger impingement limits (in percent chord) than the 48-inch section as expected. For both airfoils and for all MVDs the maximum impingement efficiency moved further aft along the lower surface as the angle of attack was increased from 0 to 8 degrees. For the 36-inch airfoil, good correlation between the LEWICE and the experimental data was demonstrated for the 11 and 21-micron cases but not for the 94-micron case. In the case of the 48-inch section, LEWICE produced lower impingement efficiencies than the experiment for the 11-micron case. In general, good agreement between the experiment and analysis was observed for the 21-micron case. For the 94-micron case, the impingement efficiency obtained with LEWICE was considerably higher than the experiment.

Referring to Figs. 101e, 102e and 102h corresponding to test cases $\alpha = 8^\circ$, MVD=21 μm, 36-inch section, $\alpha = 4^\circ$, MVD=21 μm, 48-inch section, and $\alpha = 8^\circ$,

MVD=21 μm, 48-inch section a small "hump" was observed in the experimental impingement data between S=30mm and S=90 mm. The LEWICE data did not exhibit this feature. The reason for this difference between the analysis and the experiment is not known.

The effect of the 25% chord flap deflection on the impingement characteristics of the 48-inch NLF(f)-0414 airfoil is shown in Figs. 102j–102o. The data presented in these figures are for an angle of attack of 0 degrees and a flap deflection of 15 degrees trailing edge down. The peak impingement efficiencies for this case were 0.41, 0.55 and 0.75 for the 11, 21 and 94-micron cases respectively. Note that these values are nearly the same as the ones obtained with the flap at 0 degrees. However, the flap deflection caused the location of the maximum impingement efficiency to move from 2 mm along the upper surface to 6 to 7 mm along the lower surface. In addition, the impingement curve was shifted to the right as a result of deflecting the flap. Good agreement between the experimental and LEWICE data was demonstrated for all but the 94-micron case. Figures 102k, 102m and 102o show the impingement distribution on the lower surface of the flap element for the 11, 21 and 94-micron cases respectively. In all cases, droplet impingement extended to the trailing edge of the flap and the impingement intensity increased as the cloud MVD was increased.

F. NACA 64A008 Finite Swept Tail

This model was tested during the 1997 IRT entry. Impingement data for this reflection plane model were obtained at two stations A (inboard) and B (outboard) corresponding to 36 and 44 inches above the tunnel floor respectively. The chord lengths at stations A and B were 32.76 inch and 29.52 inch respectively. Station B was approximately 5 inches from the tail tip. All blotter strips were V shaped to permit alignment of the blotters with the streamwise direction.

Analysis data for this geometry were obtained with the LEWICE-3D code. Experimental data reduced with the laser reflectometer are provided for station A only. Data for station B were practically the same as that for station A and have not been plotted. Analysis data are provided for both the A and B locations. The experimental data are for angles of attack of 0 and 6 degrees and for all three cloud MVDs.

In Figs. 103a–103c, the experimental results are compared with computational data for an α of 0°. The correlation is good for the 11.5 and 21-micron cases but not for the 92-micron MVD. The maximum impingement efficiencies for all MVDs occurred at the leading edge as expected for a symmetric airfoil. The magnitudes of the peak efficiencies in the experimental data were 0.45, 0.61 and 0.71 for the 11.5, 21 and 92-micron cases respectively. LEWICE-3D computations showed very small differences between the impingement efficiency distributions obtained at stations A and B.

Impingement results for α = 6° are presented in Figs. 103d–103f. The experimental results show a shift in the impingement curves toward the lower surface of the tail. The maximum impingement efficiencies occurred on the lower surface near the leading edge and had magnitudes of 0.45, 0.61 and 0.70 for the 11.5, 21, and 92-micron

cases respectively. Agreement between analysis and experiment was good for the 11.5 and 21-micron MVDs but not for the 92-micron case where the analysis predicted substantially higher impingement values and larger impingement limits. Once again no notable differences between the station A and B results were observed in the LEWICE-3D data presented.

G. 25%-Scale Business Jet Empennage (BJE)

This model was tested in 1999 to obtain impingement data for the horizontal tail of a modern business jet. In general, tailplanes are inverted wings so that the suction side of the airfoil corresponds to the lower surface of the tail while the pressure side of the airfoil is the upper surface of the tail. Typically, tailplanes operate at negative angles of attack for downward (i.e., negative) lift so as to balance the aircraft in pitch. The horizontal tail was set at –8 degrees with respect to the body axis. Thus, a body angle of attack, α_b, of +8° corresponded to a geometric tail angle of attack, α_t, of 0°. The horizontal tail was tested at two tail angles of attack, α_t = –1 and –6 degrees.

Impingement data were obtained using V-shape blotter strips at two spanwise locations A and B corresponding to the 25.5% and 55.4% tail semi-span locations as shown below:

- A (Inboard) : 19.2-in from the tail tip, (25.78–19.2)/25.78=0.255 semi-span
- B (Outboard) : 11.5-in from the tail tip, (25.78–11.5)/25.78=0.554 semi-span

These spanwise locations were selected because the tail was instrumented with pressure taps at these locations to provide pressure information for the validation of the computed flow field used in the impingement analysis. Another constraint in the selection of these spanwise locations was that they had to be within the region of cloud uniformity.

Experimental and LEWICE-3D impingement data for this model are compared in Figs. 104a–104c (inboard location) and in 104g-104i (outboard location) for a tail angle of attack of –1° and in Figs. 104d–104f (inboard location) and in 104j–104l (outboard location) for a tail angle of attack of –6°. Note that in these figures, the surface distance from the highlight is divided into "Suction Side" and "Pressure Side" instead of "Upper Surface" and "Lower Surface". For all other airfoil and finite span tail geometries tested, the lower surface of the airfoil or tail was the pressure side. However, since the 25%-scale horizontal tailplane was tested as an inverted wing the pressure side was the upper surface.

LEWICE-3D computations were performed for tail angles of attack of –2 and –7 degrees instead of the experimental values of –1 and –6 degrees to match the experimental pressure distributions as shown in Fig. 80.

The maximum collection efficiency and the extent of impingement increased with increasing drop size and the impingement region was shifted towards the pressure side

of the tail as the tail angle of attack was increased (more negative). Good overall agreement between the LEWICE-3D and the experiment impingement data was observed in all cases tested except for the 94-micron MVD cases. The experimental and computational impingement results for the two spanwise stations were nearly the same for all MVDs and angles of attack tested. The maximum experimental collection efficiencies for the 25%-scale model ranged from 0.6 to 0.81 as the cloud MVD was increased from 11 to 94 microns. Peak efficiencies were 1% to 4% higher for the –1 degree tail angle of attack case than for the –6 degree case. The high impingement peak efficiencies obtained with this model were attributed to its small chord length and to its thin profile which had a maximum thickness to chord ratio of 0.08.

H. Full-Scale Business Jet Tail Section

The left side (with respect to the pilot) of a full-scale business jet horizontal tail was tested in 1999 to provide full-scale data for the 25%-scale horizontal tail model discussed above. The geometric characteristics of the 25%-scale and the full-scale tails were identical. The semi-span of the full-scale horizontal tail was 103.16 inches and was considerably larger than the height of the tunnel, thus the tail was truncated at approximately 44.5% semi-span so that it could be installed in the IRT test section as a reflection plane model. The truncated half tail model was the outboard 57-inch portion (44.5% to 100% semi-span) of the non-truncated full-scale half tail.

Impingement data were obtained using V-shape blotter strips at two tail spanwise locations A and B corresponding to the 72.4% and 79.6% tail semi-span locations of the non-truncated model as shown below:

- A (Inboard) : 28.5-in from the tail tip, (103.16–28.5)/103.16=0.724 semi-span
- B (Outboard) : 21.0-in from the tail tip, (103.16–21.0)/103.16=0.796 semi-span

These spanwise locations were selected to be within the uniform cloud region. In addition, the inboard loaction was selected to match as close as possible the outboard location tested with the 25%-scale model which was at 55.5% semi-span. The difference between the inboard location on the full-scale and the outboard location tested with the 25%-scale model was approximately 17% semi-span which was considerable. However, experimental impingement data obtained with the NACA 64A008 and the 25%-scale swept tail models showed little variation in the impingement distributions with spanwise location over a considerable spanwise distance. Thus, considering the test constraints associated with full and sub-scale model testing in the same wind tunnel facility, it was felt that the comparison of the the full-scale tail data obtained at the 72.4% semi-span station with the 25%-scale data obtained at the 55.5% semi-span could provide useful information regarding scaling effects.

Another significant difference between the full-scale and sub-scale models was the chord Reynolds number because both models were tested at the same air speed. The Reynolds number of the truncated full-scale model was 4.3 million while that of the 25%-scale model was 1.49 million. However, because the tests were conducted at low tail angles of attack, and the Reynolds numbers were in the turbulent range for both

models the difference between the two test model flow fields were not significant, even though the difference in Reynolds number for the two models was considerable. Finally, it should be noted that the truncated full-scale tail had a lower aspect ratio than the full span 25%-scale model. However, studies performed with computational flow dynamics showed that the effect of lowering the model aspect ratio on the pressure distribution at the impingement locations tested was small for the low angles of attack used in this study.

Experimental and LEWICE-3D impingement data for the truncated full-scale horizontal tail are presented in Figs. 105a–105h for all test configurations and tail spanwise locations. The results presented indicate the following:

1. Spanwise location had a small effect on the impingement distributions. In general the peak impingement efficiencies were in the range 0.44 to 0.75.
2. LEWICE and experimental data were in good agreement for the 11 and 21-micron MVD cases but not for the 94-micron MVD case.
3. Only the 21-micron MVD was tested for the 6 degree tail angle of attack case. For this case, the impingement curves were shifted to the right as the angle of attack was increased from 1 to 6 degrees indicating more impingement on the lower surface (pressure side) of the tail as expected. The peak impingement efficiencies, however, did not change with angle of attack as shown in Table 16.

Comparison of full-scale impingement data obtained at the 72.4% (inboard) semi-span location (Figs. 105a–105c and 105d) with corresponding 25%-scale data obtained at the 55.5% (outboard) semi-span station (Figs. 104g–104i and 104k) showed that the peak efficiencies where higher for the sub-scale model by 18% for the 11-micron MVD case, 15% for the 21-micron MVD case and 10% for the 94-micron MVD case. In addition, the chordwise extent of impingement for the sub-scale model was greater in all cases as demonstrated in Table 16.

I. Three-element High Lift System

This model was tested during the 1997 IRT entry. Experimental impingement data for this model are presented in Figs. 106a–106v. The experimental data presented are for $\alpha = 0^\circ$ and 4° with slat deflection of 30° and flap deflection of 30° (i.e., landing configuration, see Fig. 17a). The highlight location corresponding to a surface distance, S, of 0 mm, was at the leading edge of each element.

LEWICE-3D impingement data were obtained for $\alpha = 0^\circ$ only since analysis flow field data were not available for the 4 degree angle of attack case. The flow field about this model was computed using the INS2D incompressible Navier-Stokes code (Refs. 47 and 48). The LEWICE-3D computations were performed with the measured (FSSP+OAP) droplet distributions which were divided into 27-bins for the impingement computations. Impingement analysis data are presented for all three elements.

Experimental and analysis data for $\alpha=0^\circ$ and MVDs of 11.5, 21 and 92 microns are compared in Figs. 106a through 106k. In most cases, the computed and

experimental impingement efficiency distributions for the slat and flap elements were in good agreement. For the main element, however, the LEWICE results were considerably higher than the experimental data. The reason for this discrepancy is not clear.

The experimental data show that β_{max} for all MVD cases occurred near the leading edge of the slat. The impingement intensity on the main element was very low and in general the impingement efficiency was less than 10%. The impingement limits for the main element varied from the upper surface to the start of the cove region (step) on the lower surface. In general, droplet impingement in the cove region of the main element occurred near the trailing edge for the 11.5 and 21-micron cases only. The extent of impingement in the cove region was approximately 30 to 50 mm long and the magnitude ranged from nearly zero to approximately 0.15 for the 11.5-micron case and to 0.05 for the 21-micron case as shown in Figs. 106j and 106k respectively. In both cases, the maximum impingement occurred at the trailing edge of the main element. The impingement limit for the lower surface of the flap extended to the flap trailing edge. In general, the LEWICE results for the slat and flap elements exhibited the same trends as those observed in the experimental data. Discrepancies between the experimental and the computed impingement data for the slat and flap elements were mainly due to differences in the experimental and computational flow fields. Multi-element flow fields pose significant challenges for flow analysis tools due to the complex viscous flow regions that develop in the gaps between adjacent elements. It is interesting to point out that the LEWICE impingement data for the 92-micron case exhibited better agreement with the experimental data for this model compared to the other models tested. Furthermore, for the 92-micron case the magnitude of the impingement efficiencies predicted by LEWICE for the flap element were less than the experimental values.

Experimental impingement data for $\alpha = 4^\circ$ and MVDs of 11.5 and 21 and 92 micron are presented for the slat, main and flap elements in Figs. 106l–106v. The maximum impingement on the slat and flap did not vary significantly from the $\alpha = 0^\circ$ case while the maximum impingement on the main element increased significantly as demonstrated in Figs. 106o–106q and in Table 17. The impingement limit on the lower surface of the flap extended to the trailing edge of this element for all MVD cases tested. In general, for the 4 degrees angle of attack case, droplet impingement in the cove region of the main element was similar to that observed for the $\alpha = 0^\circ$ case as shown in Figs. 106u and 106v for the 11.5 and 21-micron cases respectively.

J. S-Duct Engine Inlet

Experimental impingement data for this inlet were obtained during the 1999 IRT entry for the following test cases:

1. $\alpha = 0^\circ$, V = 170 mph, MVD = 11, 21, 94 micron
   Main inlet Flow = 23 lb/s, Scavenge Flow =2.08 lb/s
   Capture Area Ratio (CAR) = 0.60 (does not include scavenge flow)
   Capture Area Ratio (CAR) = 0.65 (includes scavenge flow)
   Blotter Strip Locations: A, B, C, D

2. $\alpha = 0^\circ$, V = 130 mph, MVD= 21, 94 micron
   Main inlet Flow = 23 lb/s, Scavenge Flow =1.57 lb/s
   Capture Area Ratio (CAR) = 0.80 (does not include scavenge flow)
   Capture Area Ratio (CAR) = 0.84 (includes scavenge flow)
   Blotter Strip Locations: A, B, C, D

The locations of the four blotter strips A, B, C and D are shown in Fig. 22h and where as follows:

Strip A: Inlet outer lip at circumferential location $\theta = 180^\circ$. For this strip S=0 mm (highlight) in the impingement plots corresponds to the highlight of the engine outer lip.

Strip B: Inlet interior sidewall at circumferential location $\theta = 90^\circ$ extending from 10.7 to 27.6 inches in the axial direction with respect to the inlet outer lip highlight.

Strip C: Apex corner (also referred to as splitter nose) at axial location x = 27.5 inches with respect to the inlet outer lip highlight. For this strip, S=0 mm in the impingement plots corresponds to the most forward (upstream) point on the apex corner. The strip was used to obtain impingement data along a section on the inlet vertical plane of symmetry on the splitter surface dividing the main flow from the scavenge flow.

Strip D: Lower surface of torque tube in engine duct at circumferential location $\theta = 180^\circ$ extending from 27.5 inches to 37.5 inches with respect to the inlet outer lip highlight. For this strip, S=0 mm in the impingement plots corresponds to the downstream end of the blotter strip which was located behind the small ramp on the torque tube at an axial location 28 inches form the inlet outer lip highlight as shown in Fig. 22h.

The experimental impingement data presented in Figs. 107a–107o indicate the following:

- Test Case 1 (CAR=0.65): The experimental data presented in Figs. 107a–107c indicate that water impingement at locations A and B increased progressively as the droplet size was increased from 11 to 94 microns. Note that for the 11-micron case practically no impingement was observed along the inlet side wall (Strip B). The maximum and total impingement at location C (splitter nose) increased dramatically as the cloud MVD was increased from 11 to 94 microns as demonstrated in Figs. 107d–107f. Note that most of the impingement occurred on the scavenge duct side indicating that the inlet performed as designed; that is the water droplets were directed away from the engine by the scavenge flow. Only for the 94-micron case was there substantial impingement on the inlet side of the splitter nose surface. The experimental data for strip D shown in Figs. 107g–107i indicate considerable total impingement on the lower side of the inlet torque tube particularly for the 21 and 94-micron MVD cases. The maximum impingement intensity occurred near the small ramp on the torque tube surface and it did not vary significantly with drop size.

- Test Case 2 (CAR=0.84): the total and maximum experimental water impingement intensity at location A increased progressively as the droplet size was increased from 21 to 94 microns (Figs. 107j–107k). For these two drop sizes, the maximum impingement efficiency was 0.45 and 0.58 respectively. Water impingement along the interior sidewall of the inlet at location B was nearly zero for the 21-micron MVD case and increased to about 10% for the 94-micron case. In general, the total impingement at station B was less than for Test Case 1. Water impingement for station C (Figs. 107l–107m) exhibited the same trends with MVD size as for the 0.65 capture area ratio case (Test Case 1). However, both the total and maximum levels of impingement efficiency were a little higher for Test Case 2. The impingement trends for station D (Figs. 107n–107o) were similar to those obtained with Test Case 1 but the total and maximum impingement were higher for Test Case 2.

LEWICE-3D computations were performed for Test Case 1 only since analysis flow data were not available for Test Case 2. The engine flow field was computed with the NPARC Navier-Stokes computer code and was provided by the inlet manufacturer. In general, the agreement between LEWICE-3D and experiment was good in terms of impingement trends. However, in some cases considerable differences were observed between the LEWICE-3D and the experimental impingement intensities and impingement limits. These differences are to some extent attributed to differences between the computed and the experimental flow fields as demonstrated in Fig. 82.

7.5 Large Droplet Impingement Issues

The comparisons of LEWICE results with the experimental data presented in section 7.4 demonstrated good overall agreement for the 11 and 21-micron MVD cases. In most cases, however, for the 92 and 94-micron spray clouds LEWICE predicted much higher local impingement efficiencies and impingement limits than observed in the experiment. Possible reasons for the large differences between analysis and experiment are explored in this section. Analysis data and exploratory tests conducted at the Goodrich icing tunnel in December of 1998 as well as tests performed during the 1999 IRT entry are used to support the discussion below.

7.5.1 Errors in Measuring MVD (92–94 μm cloud)

A number of computations were conducted to establish the required change in cloud MVD in order to match analysis data with the experiment. The assumption was that measurement errors with the FSSP and OAP probes may have been the main reason for the large differences observed between the analysis and experimental data. These studies showed that a reduction of 30–35 microns in the 94-micron MVD size would have been necessary in order to bring the analysis data close to the experiment.

Even with an MVD of 60 microns, the overall behavior of the analytical impingement distribution did not match that of the experiment as shown in Figs. 126–129. Further reductions in MVD size were investigated but did not improve the correlation. For example a 35 micron size MVD would have been necessary to match the experimental peak efficiency of the MS-317 airfoil for $\alpha = 0^{\circ}$ and MVD = 94 μm.

However, in this case the impingement limits would have been considerably smaller than the experiment. In any case, it is very unlikely that the NASA FSSP+OAP measurements were off by 30 to 60 microns consistently over repeated runs during two IRT entries.

7.5.2 Droplet Splashing and Breakup

Another hypothesis for the lower impingement efficiencies observed in the experimental investigation is droplet splashing and breakup which is discussed in some detail in Refs. 51–54. The basic assumption is that large droplets in the cloud, some considerably larger in diameter than the cloud MVD, deform upon impact and breakup into smaller droplets. The smaller droplets "bounce" forward (upstream) with some velocity and are carried downstream by the airflow. Thus, the amount of water that remains on the surface is considerably reduced. This hypothesis is also supported by experimental data obtained by other investigators during low speed large droplet impingement tests performed for engineering applications not related to aircraft icing as discussed in Refs. 52–54. The significance of this hypothesis, if proven true, is that trajectory and icing codes will have to be calibrated for large droplet impingement and ice accretion analyses.

A. Studies at the Goodrich Icing Tunnel

Exploratory tests to investigate large droplet splashing and breakup were performed at the Goodrich Icing Tunnel in Uniontown, Ohio. Tests were conducted for warm (no ice) conditions and for various icing conditions. A Droplet Size and Velocity measuring device (Phase Doppler Particle Analyzer—PDPA) was used to measure droplet size and axial velocities near the leading edge of an airfoil for cases tested. The hypothesis was that if droplet breakup and splashing occurred, small droplets with negative axial velocities would have been present near the leading edge of the airfoil.

Figures 130–132 show the droplet and velocity distributions as well as the velocity versus droplet size at the leading edge of a 21-inch two-dimensional NACA-0012 model. The tunnel airspeed, temperature, and MVD for the data presented in these figures were 175 mph, 31 $^{\circ}$F and 104 μm respectively. In Fig. 131, a bimodal velocity distribution with a significant number of negative velocity counts is shown. In Fig. 132, small particles with negative velocities near the leading edge of the airfoil are evident. These observations, although not conclusive, support the hypothesis of large droplet splashing and breakup.

B. Studies at the NASA Icing Research Tunnel

During the 1999 IRT impingement tests, a number of studies were conducted with the MS-0317 airfoil to investigate droplet splashing. Tests were conducted at different air speeds with a large droplet (MVD = 94 micron) cloud. The droplet impingement near the leading edge was visualized with a laser sheet normal to the span of the airfoil. A video camera was installed on the tunnel ceiling window with its lens set at a small angle with respect to the airfoil span and looking at the airfoil leading edge region near the mid-span location. The speed of the tunnel was adjusted in increments of 25 mph from 50 to

200 mph and the region of impingement was videotaped. By increasing the speed of the airflow, the momentum of the particles was increased. When the air speed was increased beyond 100 mph, the region of impingement in the proximity of the leading edge exhibited significantly greater laser light scattering suggesting that the number of small particles was increased. The smaller particles present near the region of impingement were assumed to be the result of large droplet splashing.

7.5.3 Future Work

Tests are currently being planned to investigate large droplet splashing and breakup. These tests will include cloud and droplet impingement visualization methods to determine what happens to large droplets during impingement.

8.0 Summary and Conclusions

An overview of previous impingement work was presented along with results from a recent industry survey indicating that a considerable expansion of the available impingement database was needed. A new impingement research program for providing the data requested by industry was outlined. The objectives of this program were to improve the experimental and data reduction methods for obtaining and reducing water droplet impingement data, and to perform extensive wind tunnel tests to expand the available impingement database.

Significant improvements made to the experimental method developed by WSU and Boeing in the 1980's and a new data reduction method for extracting the water droplet impingement data from the blotter strips were presented. An extensive discussion, supported by measurements performed, on known sources of error in the experimental and data reduction methods was provided.

Extensive wind tunnel tests were conducted at the NASA Glenn Icing Research Tunnel to expand the water droplet impingement database and to provide large droplet impingement data. Tests were conducted with five single element airfoils; an airfoil with a simple flap, a high-lift system, three swept wings and an S-duct engine inlet. The single element airfoils had maximum thickness ratios in the range of 8% to 17% and were representative of sections used in general aviation and large commercial transport aircraft. Test conditions included freestream speeds in the range of 130 mph to 176 mph, a range of angles of attack and cloud median volumetric diameters of 11, 11.5, 21, 92 and 94 micron. Each experimental condition for each test model was repeated 2 to 3 times and in some cases as many as 10 times to establish a measure of test repeatability. Additional tests were also performed to investigate the repeatability of spray system performance and its effect on LWC and droplet distribution. Comparisons of experimental and analysis impingement data obtained with the NASA Glenn LEWICE-2D and LEWICE-3D codes were performed. Below is a summary of key findings based on the work performed.

1. Automation of the WSU twelve nozzle spray system resulted in improved spray system performance. The WSU spray system with automated pressure feedback control was able to maintain air and water pressures at the spray nozzles to within 1 psi from the required settings.
2. Repeated droplet distribution measurements showed that the variation in cloud MVD was ± 0.5 μm from the average for the 11.5 and 21-μm clouds and ± 2 μm from the average for the 92 and 94-μm clouds.
3. A new method involving an Argon laser sheet and a CCD camera for determining cloud LWC uniformity was evaluated during this experimental investigation. Results from this new method were found to be in good correlation with the grid/blotter method developed previously. The laser sheet uniformity technique was considerably faster, less laborious and increased the resolution of the uniformity data compared to the grid and blotter method.
4. A CCD reflectometer was developed for extracting the raw impingement data from the dye-laden blotter strips. The main advantage of the CCD system was its ability to reduce the experimental impingement data in a very short time allowing for on-line data reduction. This allowed for quick evaluation of the impingement data during the 1997 and 1999 impingement experiments. The main drawbacks of the current CCD reflectometer design included difficulty in obtaining uniform blotter strip illumination, particularly for long strips, and decreased accuracy in regions where dye penetration into the blotter had occurred.
5. The laser reflectometer was found to be more accurate than the CCD reflectometer in reducing the impingement data. This instrument allowed for a more uniform illumination of the blotter strip over the region of interest and was less sensitive to dye penetration into the blotter paper. The experimental impingement data presented in this report were reduced with the laser reflectometer.
6. Relative humidity studies performed during the 1997 and 1999 IRT tests showed that the impact of relative humidity on LWC was considerable particularly for the 11 and 11.5-μm spray clouds.
7. The maximum difference of repeated impingement tests (3 to 10 repeats) from the average was in the range of 0.24% to 12% for approximately 85% of the test cases and 13% to 17% for the remaining 15% of the test cases. This is a significant improvement in test repeatability compared to previous experimental investigations where variations in the range of 10% to 30% were observed in the experimental data. The number of repeats performed per test condition is not sufficient to establish a statistical average. However, the maximum differences recorded were consistent for the 500 impingement tests conducted to generate the experimental data presented in this paper. Thus, it would be reasonable to conclude that the experimental method used was repeatable.
8. General impingement trends for the single element airfoils tested were as follows:
   a. For a fixed angle of attack, the total and maximum impingement efficiencies and the impingement limits increased with MVD as expected.
   b. In general, for a fixed MVD, the maximum impingement efficiency decreased with angle of attack. The total impingement efficiency, did not exhibit clear trends with angle of attack. For some models the total impingement efficiency increased as the angle of attack was increased. In other cases, however, the total impingement efficiency decreased as the angle of attack was increased.

c. In most cases, for the same MVD and angle of attack the thin airfoils (t/c = 8% to 9%) resulted in higher maximum impingement efficiencies than the thicker airfoils (t/c = 14% to 17%).

9. Impingement results for a 48-inch chord NLF-0414 airfoil with a 25% simple flap showed that for an angle of attack of 0 degrees, a flap deflection of 15 degrees trailing edge down did not have a significant effect on the magnitude of maximum and total impingement efficiencies compared to the nested flap case. However, for the flap deflection case, the extent of impingement along the lower surface of the airfoil increased considerably compared to the nested flap case. Water impingement was observed on the lower surface of the flap element in all cases and was found to extend all the way to the trailing edge.
10. Experimental impingement data for the three-element high lift system tested, showed considerable impingement on the slat and flap elements. For α=0°, the impingement efficiency on the main element was less than 10% and extended all the way to the start of the cove. For α=4°, the impingement on the slat and flap was not significantly different than for the α=0°case. However, the magnitude of the maximum and total impingement on the main element was considerably increased at the higher angle of attack. For both angles of attack tested, impingement in the cove region of the main element was observed for the 11.5 and 21-micron cases only For both angles of attack, impingement along the flap lower surface extended to the trailing edge of the flap.
11. For the three swept tail configurations tested, the experimental and analysis impingement data presented showed little variation with spanwise location. Water impingement was increased as the MVD size of the cloud was increased. In addition, the impingement region was shifted towards the pressure side of the wing as the angle of attack was increased. The extent of water impingement was considerably greater at the higher angles of attack.
12. Impingement scaling experiments conducted with 36-inch and 48-inch chord NLF-0414 airfoils and with a full-scale and a 25%-scale business jet swept tails showed that for the same air speed, angle of attack and MVD size the smaller scale models resulted in higher impingement efficiencies. The chordwise extent of impingement was also greater for the smaller scale models.
13. Experimental impingement data for the S-Duct engine inlet showed considerable impingement along the engine outer lip, the splitter nose dividing the engine flow from the scavenge flow, and along the lower surface of the torque tube located in the engine flow duct. Some impingement was also observed along the interior sidewall of the main inlet duct for the 21 and 94-micron MVD cases. In general, the impingement intensity at all inlet locations tested increased as the droplet size was increased from 11 to 94 microns. For each MVD case, total and maximum impingement efficiencies at stations C and D corresponding to the apex corner and lower surface of the torque tube, increased as the inlet capture area ratio was increased.
14. In general, good agreement between the experimental results and analysis data obtained with the NASA Glenn LEWICE-2D and LEWICE-3D computer codes was demonstrated for the 11, 11.5 and 21-micron cases. However, for the 92 and 94-micron cases the analysis produced considerably higher overall impingement than the experiment for nine out of the eleven models tested and for all angles of attack.

15. Exploratory tests conducted with the 94-micron spray cloud and with various test models suggest that droplet splashing may be the main reason for the discrepancy observed between the experimental and the LEWICE data. These preliminary findings are supported by recent research efforts in large droplet impingement performed for engineering applications unrelated to aircraft icing. More research is needed to further explore phenomena associated with large droplet impingement for icing applications.

Table 1 Test geometries and conditions for NACA impingement tests (1955-1958).

NACA TN #	Geometry	MVD (μm)	α (deg.)	V_∞ (mph)
3338	Cylinders (Diam. = 2,4 and 6 inches, Span = 1 ft)	7.6, 12, 14.8	0	175
4092	Spheres (Diam. 5.92, 18 inch)	11.5, 12.7, 16.7-18.6	0	181
4092	Ellipsoids (minor axis 30 and 20 inch) with fineness ratios of 2.5 and 3.0	11.5, 12.7, 16.7-18.6	0, 3, 6	181
4092	Conical (30°) with 18.93 inch base radius- RPMs = 0, 600, 800, 1200	11.5, 12.7, 16.7-18.6	0, 3, 6	181
3564	NACA 0011, 87 inch chord, 6 foot span	22-59	0 to 9.3	175 - 275
3839	Joukowski 0015, NACA: 65_1-206, 65_2-206, 65_1-212, 65_2-212, 63_2-015, 65_2-216 chord lengths: 13-96 inches	11.5, 16.7, 18.6	0 to 12	175
4151	NACA 65A004 (unswept) 19 inch cord, 42 inch span		11	275
4155	NACA 65A004, 6 ft chord, 42 inch span removable L.E., flap angle: -15° to 15°	11-19	0 to 12	125 - 276
4268	Supersonic inlet with – conical center body	11.5, 16.7, 19.4	0 to 4.2	179

Table 2 Test matrix for 1985 impingement tests (all tests were conducted at a freestream speed of 165 mph, each test condition was repeated 2-3 times, Ref. 6).

Geometry	MVD (μm)	α (deg.)	Mass Flow (lbm/sec)
Cylinder (2, 4 inches in diameter)	16.5, 20.4	0	NA
NACA 65_2-015 airfoil (13 inch chord)	16.5, 20.4	0, 8	NA
MS(1)-0317 airfoil (36 inch chord)	16.5, 20.4	0, 8	NA
Rime Ice Shape	20.4	0	NA
Small Glaze Ice Shape on 2-in diameter cylinder	20.4	0	NA
Large Glaze Ice Shape on 2-in diameter cylinder	20.4	0	NA
Axisymmetric Engine Inlet	16.5, 20.4	0, 15	17, 23
Boeing 737-300 Engine Inlet	16.5, 20.4	0, 15	17, 23

Table 3 Test matrix for 1989 impingement tests (all tests were conducted at a freestream speed of 165-173 mph, each test condition was repeated 5 times, Ref. 7).

Geometry	MVD (μm)	α (deg.)	Mass Flow (lbm/sec)
Small Glaze Ice Shape on 2-in diameter cylinder	20.4	0	NA
Large Glaze Ice Shape on 2-in diameter cylinder	20.4	0	NA
NLF(1)-0414F airfoil (36 inch chord)	16.5, 20.4	0, 8	NA
MS(1)-0317 airfoil, 30 deg. infinite swept Wing (36 inch chord)	16.5, 20.4	0, 8	NA
NACA 0012, 30 deg. swept finite wing, (15 inch chord)	16.5, 20.4	0, 8	NA
Boeing 737-300 Engine Inlet	16.5, 20.4	0, 15	17, 23

Table 4 Survey participants by company.

AIRCRAFT COMPANIES	ENGINE AND INLET COMPANIES
Boeing Commercial Airplane Group - Seattle (8)	Allison Engine Company (2)
Boeing Commercial Airplane Group – Wichita Division (1)	GE Aircraft Engines (1)
Douglas Products Division -Long Beach (1)	Rohr, Inc. (1)
Lockheed Martin Aeronautical Systems (1)	**OTHER COMPANIES**
Cessna Aerospace Corporation (2)	AlliedSignal Aerospace (1)
Gulfstream Aerospace Corporation (1)	Chrysler Technologies Airborne Systems (2)
Learjet, Inc. (2)	Key Industries Corporation (1)
The New Piper Aircraft, Inc. (1)	**FAA/UNIVERSITIES**
HELICOPTER COMPANIES	FAA Technical Center - Atlantic City (1)
Bell Helicopter Textron, Inc. (1)	Univ. of Illinois at Urbana-Champaign (1)
Sikorsky Aircraft Corporation (1)	

The number in parentheses shows number of respondents

Table 5 Geometry requested by group.

ORGANIZATION	AIRFOIL SECTIONS	WINGS	TAILS	INLETS S-DUCTS	PROPS	OTHER
Large Aircraft Manufacturers	3/5/2	4/1/0/D	1/HV	2/0/1/2c		
Business Jet Manufacturers	1/2/1	3/0/1	2			I
Small Aircraft Manufacturers		5/0/0	1	1/0/1		
Helicopter Companies	3/1/1					
Aircraft Engine/Inlet Comp.				5/4/1/1c		II
Military Aircraft Companies				1/0/1		
FAA	1/2/0	2/0/0	1			
Universities	1/2/0				1	
Other	1/0/1			1/1/1		III
Total (Approx. 80 models)	**10/12/5**	**14/1/1/D**	**5/HV**	**10/5/5/3c**	**1**	

Airfoil Sections: Single/Multi-element/With Ice Shapes; **Wings:** Single/Multi-element/With Ice Shapes/Delta Wings; **Tails**: HV - Horizontal & Vertical; **Inlets S-Ducts:** Inlet/S-duct/With Ice Shapes/Cascade Configurations; **I** - Windshields, **II** - Spinners, Center bodies, **III** - Radomes, Antennas, Appendages.

Table 6 List of droplet trajectory parameters.

Parameter	Definition	Expression
Re_{MVD}	Reynolds number based on droplet diameter	$MVD \cdot V_\infty \cdot \frac{\rho_{air}}{\mu}$ where MVD represents Median Volumetric Diameter, ρ_{air} is the air density and μ is the absolute air viscosity
K	Droplet inertia parameter	$\rho_{droplet} \cdot V_\infty \cdot \frac{MVD^2}{18 \cdot \mu \cdot c}$ where $\rho_{droplet}$ is the droplet (water) density and c is the chord length of the airfoil model
$\frac{\lambda}{\lambda_s}$	Ratio of the true range of droplet as projectile injected into still air to the range of droplet as projectile following Stokes' law	$-0.022466 \cdot x^4 + 0.20109 \cdot x^3 - 0.59067 \cdot x^2 + 0.36072 \cdot x + 0.74544$ where $x = log(Re_{MVD})$ and $6 < Re_{MVD} < 1000$
K_0	Droplet modified inertia parameter	$K \cdot \frac{\lambda}{\lambda_s}$
ϕ	Deviation of the droplet drag force from Stokes' law	$\frac{(Re_{MVD})^2}{K}$
ψ		$\sqrt{\frac{\phi}{K}}$

Table 7 Pressure taps for 48-in NLF(1)-0414 airfoil.

Element	Chordwise Taps	Spanwise Taps
Main	58 taps at 33 inches above floor	12 taps (x/c=0.725) at 6 inch increments. 3 taps overlapping with chordwise ports.
Main	7 taps 43 inches above floor 7 taps 23 inches above floor	
Control	43 taps 33 inches above floor	

Table 8 Pressure taps for three-element high lift system airfoil.

Element	Chordwise Taps	Spanwise Taps Upper Surface
Slat	35	6 (row near LE)
Main	42	NA
Flap	33	6 (row near LE) 6 (row near TE)

Table 9 Summary of pressure transducer characteristics.

Transducer	Usage	Range (psig)	Error	Thermal Zero shift Error	Thermal Span shift Error
13 SETRA 206	Water lines	0-125	±0.13% FS	±1.0% FS/100°F	±1.5% FS/100°F
1 SETRA 204	Main air line	0-100	±0.11% FS	±0.4% FS/100°F	±0.3% FS/100°F
3 SETRA 206	Nozzle air lines	0-100	±0.13% FS	±1.0% FS/100°F	±1.5% FS/100°F

Note: all transducers were calibrated at temperature of 50°F

Table 10a Cloud MVD and corresponding spray system parameters from test measurements (1997 IRT tests).

FSSP+OAP MVD Range (μm)	Average Air Supply Pressure At Regulator (psig ± psi)	Average Tank Water Pressure (psig ± psi)	Average Water Pressure At Nozzle (psig ± psi)	Average Air Pressure At Nozzle (psig ± psi)	$\Delta P = P_{water}-P_{air}$ At Nozzle (psi)	Average Volume Flow Rate 12 Nozzles (GPM)	Spray Time (sec)
11.5	45.5 ± 0.6	68.0 ± 1.0	61.5 ± 1.0	40 ± 0.6	21.5	0.190	18
21	24.5 ± 0.9	76.5 ± 0.8	69.5 ± 0.8	21 ± 0.8	48.5	0.275	6
92	6.0 ± 0.3	40.5 ± 0.6	34.5 ± 0.6	4.5 ± 0.3	30.0	0.205	3

Pressures, flow rates and errors have been calculated from 100 randomly selected tests for each MVD case.

Table 10b Cloud MVD and corresponding spray system parameters from test measurements (1999 IRT tests).

FSSP+OAP MVD Range (μm)	Average Air Supply Pressure At Regulator (psig ± psi)	Average Tank Water Pressure (psig ± psi)	Average Water Pressure At Nozzle (psig ± psi)	Average Air Pressure At Nozzle (psig ± psi)	$\Delta P = P_{water}-P_{air}$ At Nozzle (psi)	Average Volume Flow Rate 12 Nozzles (GPM)	Spray Time (sec)
11	43.0 ± 0.7	67.0 ± 0.4	62.8 ± 0.5	38.2 ± 0.4	24.6	0.226	9.0
21	22.0 ± 0.4	77.0 ± 0.4	72.5 ± 0.5	18.9 ± 0.4	53.6	0.329	3.8
92	6.0 ± 0.6	37.0 ± 0.4	32.4 ± 0.5	4.7 ± 0.5	27.2	0.185	2.2

Pressures, flow rates and errors have been calculated from 45 randomly selected tests for each MVD case.

Table 11 Collector theoretical efficiency and King probe LWC measurements for 1997 and 1999 test MVDs.

Year	MVD Range (FSSP+OAP) (μm)	Average MVD (μm)	Average LWC[1,2] (g/m^3)	Collector Efficiency (%)
1997	11-12	11.5	0.04	82
	20-22	21	0.15	89
	90-94	92	0.22	97
1999	11-12	11	0.05	82
	20-22	21	0.19	89
	90-94	94	0.22	97

1. 1997 LWC King Probe data were obtained at the center of the tunnel test section (relative humidity ranged from 70% to 80%). IRT spray bar air was used to enhance cloud uniformity.
2. 1999 King Probe LWC data were obtained at the center of the tunnel test section (relative humidity ranged from 70% to 75%). IRT spray bar air was not used. Automatic feedback was used to control air and water pressures.

Table 12a Test models and conditions (1997 Impingement tests).

Test Model	Number of Surface Pressure Taps	Angle of Attack (α) Flap deflection (δ) (degrees)	MVD (μm)	Average Air Speed	Number of Runs per MVD	Total Number of Runs
MS(1)-0317 (c = 36 in) Strip Location: Midspan	49	α = 0, 8	11.5, 21, 92	176 mph	4	24
NACA 65_2-415 (c = 36 in) Strip Location: Midspan	100	α = 0, 8	11.5, 21, 92	176 mph	4 to 11	53
Commercial transport tail section (c = 36 in) Strip Location: Midspan	44	α = 0, 4	11.5, 21, 92	176 mph	4-10	19
GLC 305 (c = 36 in) Strip Location: Midspan	44	α = 1.5, 6	11.5, 21, 92	176 mph	4	24
NACA 64A008 tail (Λ_{LE} = 29.1°, Λ_{TE} = 11.1°, c_r = 45.48 in, c_t = 28.16 in) See figure 14d for locations	60	α = 0, 6	11.5, 21, 92	176 mph	4	24
Three-element high lift system airfoil (36 in nested chord) Strip Location: Midspan	128	α = 0, 4 δ = Landing Configuration	11.5, 21, 92	176 mph	4	24
Collector Mechanism	NA	α = 0, 3 locations	11.5, 21, 92	176 mph	4 to 6	133
Uniformity 6ft x 6ft Grid	NA	NA	11.5, 21, 92	175 mph	43	140
MVD, LWC measurements	NA	NA	10-130	176 mph	2-4	53
Humidity studies, Blotter penetration tests, Other	NA	NA	11.5, 21, 92	176 mph	1-3	24

Table 12b Test models and conditions (1999 impingement tests).

Test Model	Number of Surface Pressure Taps	Angle of Attack (α) Flap deflection (δ) (degrees)	MVD (μm)	True Air Speed & Inlet Mass Flow	Number of Runs per MVD	Total Number of Runs
MS(1)-0317 (c = 36 in) Strip Location: Midspan	49	α = 0	11, 21, 94	176 mph	3	9
NLF(1)-0414 (c = 36 in) Strip Location: Midspan	5	α = 0, 8	11, 21, 94	176 mph	3	21
NLF(1)-0414 (c = 48 in) Strip Location: Midspan	124	α = 0, 4, 8 δ = 0	11, 21, 94	175 mph	3 to 4	46
NLF(1)-0414 (c = 48 in) Strip Location: Midspan	124	α = 0 δ = 15	11, 21, 94	175 mph	3 to 4	46
25%-scale Business Jet Empennage See figure 15e for location.	126	α = 1, 6 δ = 0	11, 21, 94	176 mph	3	21
Full-scale Business Jet Tail Section See figure 16e for locations	NA	α = 1, 2, 6 δ = 0, 3	11, 21, 94	176 mph	3	18
S-duct Engine Inlet See figure 22h for blotter strip locations	30	NA	11, 21, 94	130 mph MIF= 23 lb/s SF = 1.57 lb/s CAR = 0.84 170 mph MIF = 23 lb/s SF = 2.08 lb/s CAR = 0.65	2-3	17
Collector Mechanism	NA	α = 0 (3 locations)	11, 21, 94	175 – 176mph	1 to 6	54
Uniformity Test (include 6ft x 6ft grid and laser sheet technique)	NA	NA	11, 21, 94	170 – 177 mph	1 to 24	176
MVD, LWC measurements	NA	NA	11, 21, 94	175 – 176 mph	3 to 4	67
Humidity studies, Droplet break-up tests, Blotter penetration tests, Other	NA	NA	11, 21, 94, 270	40 – 200 mph	1 to 3	46

1. MIF = Main Inlet Flow
2. SF = Scavenge Flow
3. CAR = Capture Area Ratio

Table 13 Summary of model geometry and impingement parameters (All dimensions are in English Units (inch, mph); Values inside parenthesis are in SI Units (meter, m/s) (Continued).

Geometry (test year)	Chord (in)	t_{max} (in)	x/c at t_{max}	V_∞ mph	Re_c Million	AOA (deg.)	MVD (μm)	Re_{MVD}	K	K_0	φ
MS(1)-0317 (1997 & 1999)	36 (0.914)	6.12 (0.155)	0.376	176 (78.66)	4.83	0.0	11.5	60	0.036	0.015	101,845
							21.0	110	0.119	0.041	
							92.0	483	2.286	0.413	
						8.0	11.5	60	0.036	0.015	
							21.0	110	0.119	0.041	
							92.0	483	2.286	0.413	
GLC-305 (1997)	36 (0.914)	3.12 (0.079)	0.398	176 (78.66)	4.83	1.5	11.5	60	0.036	0.015	101,846
							21.0	110	0.119	0.041	
							92.0	483	2.286	0.413	
						6.0	11.5	60	0.036	0.015	
							21.0	110	0.119	0.041	
							92.0	483	2.286	0.413	
NACA 65_2-415 (1997)	36.53 (0.928)	5.49 (0.139)	0.402	176 (78.66)	4.85	0.0	11.5	60	0.035	0.015	103,345
							21.0	110	0.117	0.040	
							92.0	483	2.253	0.407	
						8.0	11.5	60	0.035	0.015	
							21.0	110	0.117	0.040	
							92.0	483	2.253	0.407	
Commercial transport tail section (1997)	36 (0.914)	3.23 (0.082)	0.338	176 (78.66)	4.84	0.0	11.5	60	0.036	0.015	101,846
							21.0	110	0.119	0.041	
							92.0	483	2.286	0.413	
						4.0	11.5	60	0.036	0.015	
							21.0	110	0.119	0.041	
							92.0	483	2.286	0.413	

Table 13 Summary of model geometry and impingement parameters (All dimensions are in English Units (inch, mph); Values inside parenthesis are in SI Units (meter, m/s) (Continued).

Geometry (test year)	Chord (in)	t_{max} (in)	x/c at t_{max}	V_∞ mph	Re_c Million	AOA (deg.)	MVD (μm)	Re_{MVD}	K	K_0	φ
36-inch NLF(1)-0414 (1999)	36 (0.914)	5.14 (0.131)	0.467+	176 (78.66)	4.84	0.0	11.0	58	0.033	0.014	101,846
							21.0	110	0.119	0.041	
							94.0	493	2.386	0.427	
						8.0	11.0	58	0.033	0.014	
							21.0	110	0.119	0.041	
							94.0	493	2.386	0.427	
48-inch NLF(1)-0414 (with 25% chord flap) (1999)	48 (1.219)	6.85 (0.1744)	0.467+	175 (78.22)	6.53	0.0	11.0	58	0.025	0.011	135,794
							21.0	110	0.089	0.030	
							94.0	493	1.790	0.320	
						4.0	11.0	58	0.025	0.011	
							21.0	110	0.089	0.030	
							94.0	493	1.790	0.320	
						8.0	11.0	58	0.025	0.011	
							21.0	110	0.089	0.030	
							94.0	493	1.790	0.320	
NACA 64A008 Swept finite span tail (1997)	37.65* (0.956*)	3.01* (0.077*)	0.39	176 (78.66)	5.03*	0.0	11.5	60	0.034*	0.014*	106,514*
							21.0	110	0.114*	0.039*	
							92.0	483	2.186*	0.395*	
						6.0	11.5	60	0.034*	0.014*	
							21.0	110	0.114*	0.039*	
							92.0	483	2.186*	0.395*	

Table 13 Summary of model geometry and impingement parameters (All dimensions are in English Units (inch, mph); Values inside parenthesis are in SI Units (meter, m/s)

Geometry (test year)	Chord (in)	t_{max} (in)	x/c at t_{max}	V_∞ mph	Re_c Million	AOA (deg.)	MVD (μm)	Re_{MVD}	K	K_0	φ
25%-scale Business jet empennage (1999)	12.31* (0.313*)	0.9*	0.39	176 (78.66)	1.493*	-1.0	11.0	58	0.105	0.045	31,764*
							21.0	110	0.383	0.130	
							94.0	494	7.671	1.371	
						-6.0	11.0	58	0.105	0.045	
							21.0	110	0.383	0.130	
							94.0	494	7.671	1.371	
Full-scale Business jet tail section (1999)	32.18* (0.82)	2.57* (0.065)	0.39	176 (78.66)	4.312*	1.0	11.0	58	0.034	0.015	99,824*
							21.0	111	0.123	0.042	
							94.0	496	2.463	0.440	
						6.0	21.0	111	0.123	0.042	

* Data based on MAC; + Average value

Table 14 Effect of relative humidity on droplet distribution and LWC (FSSP measurements) – MVD = 11-12 μm.

Droplet Size (μm)	Droplet Counts (60% Relative Humidity)	Droplet Counts (70% Relative Humidity)	Droplet Counts (70% Relative Humidity)	Droplet Counts (80% Relative Humidity)
3.5	875.84	1202.65	1306.98	2702.63
6.5	781.12	1151.86	1208.51	1984.2
9.5	571.82	821.65	888.41	1464.71
12.5	186.71	223.73	254.35	468.61
15.5	67.22	74.92	85.43	158.39
18.5	31.63	29.27	34.55	64.98
21.5	10.69	6.51	8.35	16.55
24.5	2.31	1	1.39	2.63
27.5	0.2	0.06	0.12	0.1
30.5	0	0.04	0.02	0.06
MVD (μm)	12	11	11	11.3
LWC (g/m^3)	0.030	0.044	0.049	0.098

Table 15 Summary of test repeatability results.

Test Case	AOA deg	MVD = 11, 11.5 μm	MVD = 21 μm	MVD =92, 94 μm
MS(1)-0317 (1997)	0	±12%	± 3%	± 9.1%
MS(1)-0317 (1997)	8	± 8.8%	± 7.1%	± 3.6%
MS(1)-0317 (1999)	0	± 5.7%	± 3.1%	± 11%
GLC-305 (1997)	1.5	± 8.7%	± 8.8%	± 8.7%
GLC-305 (1997)	6	± 16%	± 6%	± 4.9%
NACA 65_2-415 (1997)	0	± 14%	± 8.1%	± 7%
NACA 65_2-415 (1997)	8	± 13%	± 11%	± 17%
Transport Tail (1997)	0	± 9.6%	± 4.8%	± 9.2%
Transport Tail (1997)	4	± 1.7%	± 7%	± 9.8%
NLF-0414 36-in (1999)	0	± 5.3%	± 0.24%	± 14%
NLF-0414 36-in (1999)	8	± 3.8%	± 2.3%	± 11%
NLF-0414f 48-in (1999) δ=0	0	± 2.9%	± 7.3%	± 8.1%
NLF-0414f 48-in (1999) δ=0	4	± 4.6%	± 8%	± 0.8%
NLF-0414f 48-in (1999) δ=0	8	± 3.8%	± 9.7%	± 6.2%
NLF-0414f 48-in (1999)δ=15	0	± 5.9%	± 7.9%	± 11%
NACA 64A008 (1997)	0	± 4.9%	± 7.4%	± 3.9%
NACA 64A008 (1997)	6	± 12%	± 8.2%	± 3.2%
25%-Scale BJE (1999) Inboard	-1	± 4%	± 6.2%	± 5.9%
25%-Scale BJE (1999) Inboard	-6	± 4.9%	± 5.7%	± 7.1%
25%-Scale BJE (1999) Outboard	-1	± 4.8%	± 14%	± 3.7%
25%-Scale BJE (1999) Outboard	-6	± 3.4%	± 4.6%	± 3.2%
BJ Horizontal Tail (1999) Inboard	1	± 4.4%	± 1.9%	± 8.5%
BJ Horizontal Tail (1999) Inboard	6	-	± 8.7%	-
BJ Horizontal Tail (1999) Outboard	1	± 1.6%	± 2.4%	± 8.2%
BJ Horizontal Tail (1999)Outboard	6	-	± 6.7%	-
High Lift System (1997) Slat	0	±7.7%	±11%	±9.2%
High Lift System (1997) Main	0	±17%	±17%	-
High Lift System (1997) Flap	0	±10%	±10%	±8.6%
High Lift System (1997) Slat	4	±11%	±9.4%	±16%
High Lift System (1997) Main	4	±11%	±5.6%	±9.5%
High Lift System (1997) Flap	4	±7.5%	±8.5%	±15%
S-Duct Inlet car=0.6 A	0	±6.8%	±4.6%	±11%
S-Duct Inlet car=0.6 B	0	-	±13%	±12%

Table 16 Summary of impingement efficiency data for both 1997 and 1999 IRT tests (Continued).

Model (Test Year)	Test Conditions			β_{max}	$S_{\beta_{max}}$ (mm)	S_u (mm)	S_l (mm)	x_u/c	x_l/c	$A_{\bar{\beta}}$ (mm)	A_f (mm)	$\bar{E}$
	α	MVD	δ									
MS(1)-0317 (1997)	0	11.5	NA	0.32	-6	-71	30	0.048	0.016	11.09	155.50	0.0713
		21.0	NA	0.50	-1	-90	45	0.068	0.031	26.43	155.50	0.1699
		92.0	NA	0.68	-4	-240	149	0.229	0.142	49.53	155.50	0.3186
	8.0	11.5	NA	0.25	+16	-15	66	0.004	0.053	7.690	186.91	0.0411
		21.0	NA	0.51	+12	-34	185	0.016	0.181	33.43	186.91	0.1788
		92.0	NA	0.76	+8	-60	300	0.038	0.307	67.41	186.91	0.3607
MS(1)-0317 (1999)	0	11.0	NA	0.33	-6	-62	30	0.048	0.016	12.08	155.50	0.0777
		21.0	NA	0.50	0	-89	63	0.078	0.047	29.84	155.50	0.1919
		94.0	NA	0.68	-2	-164	117	0.147	0.107	50.17	155.50	0.3224
GLC-305 (1997)	1.5	11.5	NA	0.47	+1	-26	34	0.017	0.041	9.248	79.321	0.1166
		21.0	NA	0.66	+2	-42	55	0.026	0.069	16.34	79.321	0.2060
		92.0	NA	0.76	+2	-153‡	229‡	0.145	0.264	26.08	79.321	0.3288
	6.0	11.5	NA	0.43	+6	-14	60	0.007	0.075	8.956	115.18	0.0778
		21.0	NA	0.60	+6	-22	322	0.015	0.365	25.81	115.18	0.2241
		92.0	NA	0.72	+4	-25	526‡	0.168	0.588	46.75	115.18	0.4059
NACA 65_2-415 (1997)	0	11.5	NA	0.45	+1	-48	40	0.037	0.035	8.255	139.34	0.0592
		21.0	NA	0.62	0	-140	75	0.132	0.072	19.51	139.34	0.1400
		92.0	NA	0.73	-2	-195	150	0.192	0.200	36.48	139.34	0.2618
	8.0	11.5	NA	0.30	+11	-15	135	0.005	0.136	7.896	175.83	0.0449
		21.0	NA	0.52	+11	-20	227	0.010	0.234	22.04	175.83	0.1254
		92.0	NA	0.69	+8	-100‡	407‡	0.090	0.556	61.63	175.83	0.3505
Commercial transport tail section (1997)	0	11.5	NA	0.47	-1	-41	25	0.038	0.016	9.051	82.035	0.1103
		21.0	NA	0.60	-1	-82	52	0.082	0.043	17.76	82.035	0.2165
		92.0	NA	0.76	-1	-130	100	0.135	0.094	29.81	82.035	0.3634
	4.0	11.5	NA	0.41	+4	-23	55	0.019	0.046	8.959	98.976	0.0905
		21.0	NA	0.54	+4	-40	175	0.037	0.176	19.03	98.976	0.1923
		92.0	NA	0.74	+2	-80	371‡	0.080	0.390	42.06	98.976	0.4249

Table 16 Summary of impingement efficiency data for both 1997 and 1999 IRT tests (Continued).

Model (Test Year)	Test Conditions α	MVD	δ	β_{max}	$S_{\beta_{max}}$ (mm)	S_u (mm)	S_l (mm)	x_u/c	x_l/c	$A_{\bar{\beta}}$ (mm)	A_f (mm)	$\bar{E}$
36-inch NLF(1)-0414 (1999)	0	11.0	NA	0.45	-3	-35	33	0.023	0.028	9.705	130.48	0.0744
		21.0	NA	0.60	-2	-76	79	0.065	0.077	20.45	130.48	0.1567
		94.0	NA	0.77	-2	-230**	180	0.231	0.187	35.26	130.48	0.2702
	8.0	11.0	NA	0.37	+5	-22	100	0.011	0.010	10.79	189.49	0.0569
		21.0	NA	0.57	+8	-20	400	0.009	0.427	36.85	189.49	0.1945
		94.0	NA	0.75	+8	-30	465**	0.018	0.498	61.48	189.49	0.3244
48-inch NLF(1)-0414 with 25%-chord flap (1999)	0	11.0	0	0.40	-2	-35	45	0.015	0.029	10.32	173.97	0.0593
		21.0	0	0.55	-2	-95	84	0.060	0.060	22.81	173.97	0.1312
		94.0	0	0.75	-2	-200	180	0.144	0.138	44.98	173.97	0.2586
	4.0	11.0	0	0.38	+10	-25	65	0.008	0.045	10.19	193.66	0.0526
		21.0	0	0.52	+8	-40	340	0.018	0.268	31.46	193.66	0.1624
		94.0	0	0.72	+7	-60	446	0.033	0.355	55.71	193.66	0.2877
	8.0	11.0	0	0.36	+16	-10	98	0.001	0.071	11.22	252.65	0.0444
		21.0	0	0.51	+11	-28	370	0.010	0.293	36.87	252.65	0.1459
		94.0	0	0.70	+7	-42	750	0.020	0.604	78.30	252.65	0.3099
	0	11.0	15	0.41	+7	-33*	70*	0.013	0.049	12.13*	212.09	0.0572*
		21.0	15	0.55	+8	-50*	180*	0.026	0.138	27.29*	212.09	0.1287*
		94.0	15	0.75	+6	-110*	300*	0.072	0.236	51.81*	212.09	0.2443*
NACA 64A008 Swept finite span tail (1997)	0	11.5	NA	0.45	0	-25	25	0.023	0.022	5.974	76.514	0.0781
		21.0	NA	0.61	+2	-80	80	0.082	0.082	13.86	76.514	0.1811
		92.0	NA	0.71	0	-180	180	0.191	0.190	23.08	76.514	0.3016
	6.0	11.5	NA	0.45	+6	-5	80	0.017	0.082	8.789	116.07	0.0757
		21.0	NA	0.61	+5	-10	310	0.020	0.332	26.23	116.07	0.2260
		92.0	NA	0.70	+3	-20	400‡	0.018	0.431	41.69	116.07	0.3592

Table 16 Summary of impingement efficiency data for both 1997 and 1999 IRT tests.

Model (Test Year)	Test Conditions α	MVD	δ	β_{max}	$S_{\beta_{max}}$ (mm)	S_u (mm)	S_l (mm)	x_u/c	x_l/c	$A_{\bar{\beta}}$ (mm)	A_f (mm)	$\bar{E}$
25%-scale Business jet empennage (1999) <Inboard>	-1.0	11.0	0	0.60	0	-20^s	20^p	0.049^s	0.050^p	7.467	29.037	0.2571
		21.0	0	0.70	0	-40^s	50^p	0.105^s	0.134^p	11.74	29.037	0.4043
		94.0	0	0.80	+1	-40^s	50^p	0.105^s	0.134^p	13.33	29.037	0.4592
	-6.0	11.0	0	0.59	+3	-10^s	80^p	0.022^s	0.219^p	10.13	45.292	0.2237
		21.0	0	0.68	+3	-15^s	150^p	0.036^s	0.416^p	15.42	45.292	0.3405
		94.0	0	0.77	+3	-20^s	150^p	0.049^s	0.416^p	15.94	45.292	0.3519
25%-scale Business jet empennage (1999) <Outboard>	-1.0	11.0	0	0.62	0	-20^s	25^p	0.063^s	0.082^p	6.794	23.242	0.2923
		21.0	0	0.73	0	-35^s	40^p	0.119^s	0.131^p	11.87	23.242	0.5106
		94.0	0	0.81	+1	-40^s	45^p	0.133^s	0.152^p	13.03	23.242	0.5606
	-6.0	11.0	0	0.62	+2	-10^s	70^p	0.029^s	0.240^p	10.27	36.253	0.2833
		21.0	0	0.71	+3	-15^s	150^p	0.046^s	0.521^p	17.48	36.253	0.4822
		94.0	0	0.77	+2	-20^s	150^p	0.063^s	0.521^p	13.19	36.253	0.3638
Full-scale business jet horizontal tail (1999) <Inboard>	1.0	11.0	0	0.44	-1	-35	30	0.033	0.028	7.714	71.202	0.1083
		21.0	0	0.58	0	-70	45	0.071	0.045	16.30	71.202	0.2289
		94.0	0	0.72	-1	-120	$110^‡$	0.127	0.118	21.21	71.202	0.2979
	6.0	21.0	0	0.57	+5	-35	305	0.033	0.344	18.57	118.88	0.1562
Full-scale business jet horizontal tail (1999) <Outboard>	1.0	11.0	0	0.46	0	-35	30	0.036	0.031	8.661	65.682	0.1319
		21.0	0	0.61	-1	-70	45	0.078	0.049	15.87	65.682	0.2417
		94.0	0	0.75	0	-120	110	0.139	0.128	23.66	65.682	0.3602
	6.0	21.0	0	0.61	+3	-35	305	0.036	0.373	22.78	122.82	0.1855

Nomenclature for Table 16

1. $S_{\beta_{max}}$ represents the surface distance from the reference point to the location of the maximum impingement efficiency. S_u and S_l represent the surface distances of impingement limits on the upper and lower surfaces. x_u/c and x_l/c represent the stations of the impingement limits on upper and lower surfaces with respect to the chord.
2. $A_{\bar{\beta}}$ represents the total area under the local impingement efficiency curve, which is defined as $\int \beta \, ds$; where *ds* is the infinitesimal surface distance.
3. A_f represents the projected frontal area of the airfoil.
4. $\bar{E}$ represents the total impingement efficiency, which is defined as $\bar{E} = \frac{A_{\bar{\beta}}}{A_f}$
5. * impingement characteristics on the main-element only, do not include the flap-element (for 48 in NLF(1)-0414 airfoil)
6. ‡ end of blotter strip
7. s = suction surface, p = pressure surface

Table 17 Summary of impingement efficiency data for three-element high lift system.

Element (test year)	Test Condition α	MVD	δ	β_{max}	$S_{\beta_{max}}$ (mm)	S_u (mm)	S_l (mm)	x_u/c	x_l/c	$A_{\bar{\beta}}$ (mm)	A_f (mm)	$\bar{E}$
Leading Edge Slat (1997)	0	11.5	30	0.35	-5	-71	15	-0.048	-0.080	9.294	231.42	0.0402
		21.0	30	0.60	-7	-142^{++}	20	0.001	-0.076	27.46	231.42	0.1187
		92.0	30	0.84	-7	-142^{++}	25	0.001	-0.072	60.23	231.42	0.2603
	4.0	11.5	30	0.35	+2	-35	30	-0.071	-0.067	7.696	292.45	0.0263
		21.0	30	0.64	+2	-142^{++}	37	0.001	-0.061	22.12	292.45	0.0756
		92.0	30	0.82	+1	-142^{++}	40	0.001	-0.058	43.62	292.45	0.1492
Main Element (1997)	0	11.5	NA	0.05	+35	0	110	0	0.134	1.459	231.42	0.0063
		21.0	NA	0.04	+21	0	275	0	0.281	4.763	231.42	0.0206
		92.0	NA	0.04	+204	NA	160 ~ $370^{(+)}$	NA	0.178 ~ 0.367	1.176	231.42	0.0051
	4.0	11.5	NA	0.40	+20	NA	8 ~ $130^{(+)}$	NA	0.046 ~ 0.152	14.94	292.45	0.0511
		21.0	NA	0.38	+24	0	300	0	0.304	33.41	292.45	0.1142
		92.0	NA	0.30	+85	NA	10 ~ $420^{(+)}$	NA	0.047 ~ 0.411	42.47	292.45	0.1452
Trailing Edge Flap (1997)	0	11.5	30	0.29	+14	-4	286^{++}	0.872	1.092	11.81	231.42	0.0510
		21.0	30	0.51	+24	-4	286^{++}	0.872	1.092	47.96	231.42	0.2072
		92.0	30	0.74	+24	-4	286^{++}	0.872	1.092	96.72	231.42	0.4179
	4.0	11.5	30	0.23	+15	-4	286^{++}	0.872	1.092	9.424	292.45	0.0322
		21.0	30	0.53	+16	-4	286^{++}	0.872	1.092	51.37	292.45	0.1757
		92.0	30	0.78	+22	-4	286^{++}	0.872	1.092	110.9	292.45	0.3793

Nomenclature for Table 17

1. The frontal area, A_f of the three-element high lift system is defined as follows:

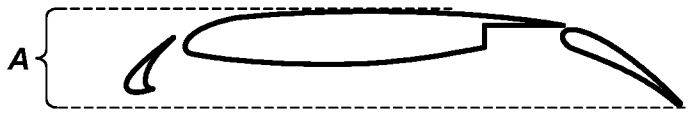

(frontal area for 0 degree of angle of attack)

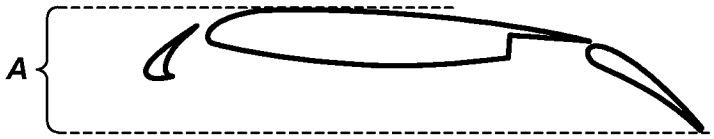

(frontal area for 4 degrees of angle of attack)

2. ‡ end of blotter strip,
3. Certain regions of leading edge slat are located in negative x-axis.
4. (+) traced impingement starts and ends at lower surface

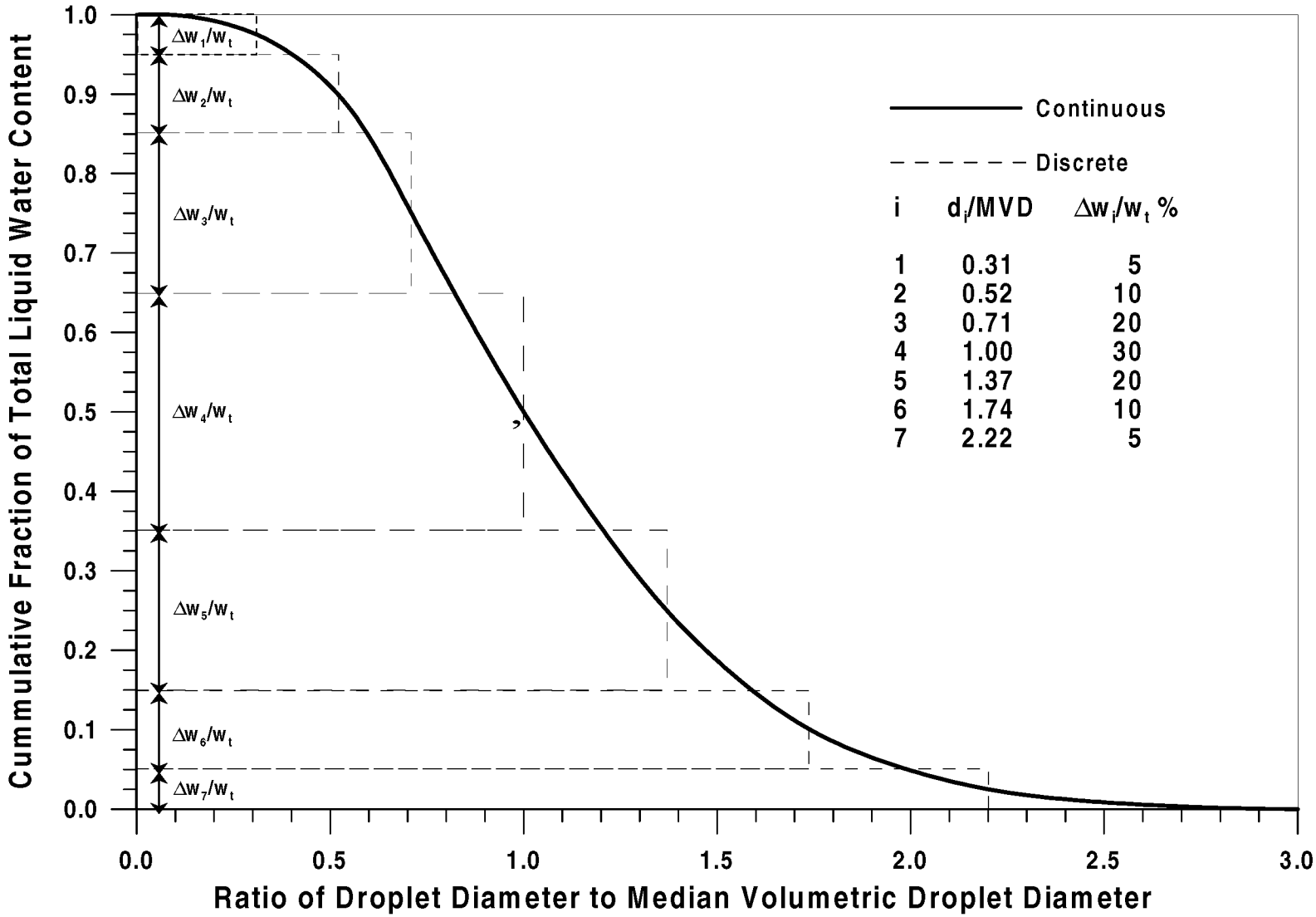

Fig. 1a Langmuir “D” dimensionless distribution of droplet sizes.

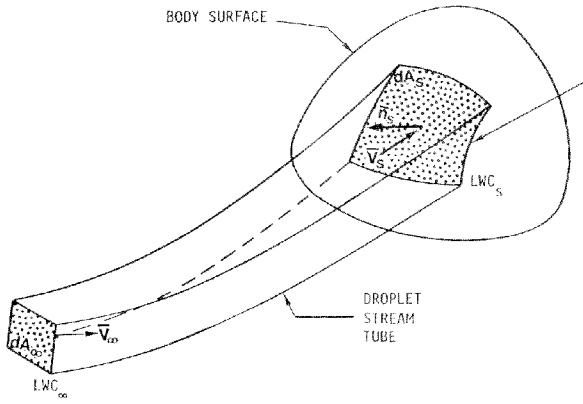

$$\overline{n}_\infty \,//\, \overline{V}_\infty$$

$$\overline{dA_s} = \overline{n}_s dA_s$$

$$\overline{dA_\infty} = \overline{n}_\infty dA_\infty$$

$$LWC_\infty \overline{V}_\infty \cdot \overline{dA_\infty} = LWC_s \overline{V}_s \cdot \overline{dA_s}$$

$$LWC_\infty \overline{V}_\infty \cdot \overline{dA_\infty} = LWC_s \left(-\overline{n}_s \cdot \overline{V}_s\right) dA_s$$

$$\beta = \frac{dA_\infty}{dA_s} = \frac{LWC_s \left(-\overline{n}_s \cdot \overline{V}_s\right)}{LWC_\infty V_\infty}$$

Fig. 1b Definition of local impingement efficiency for a body in a cloud of uniform droplet size.

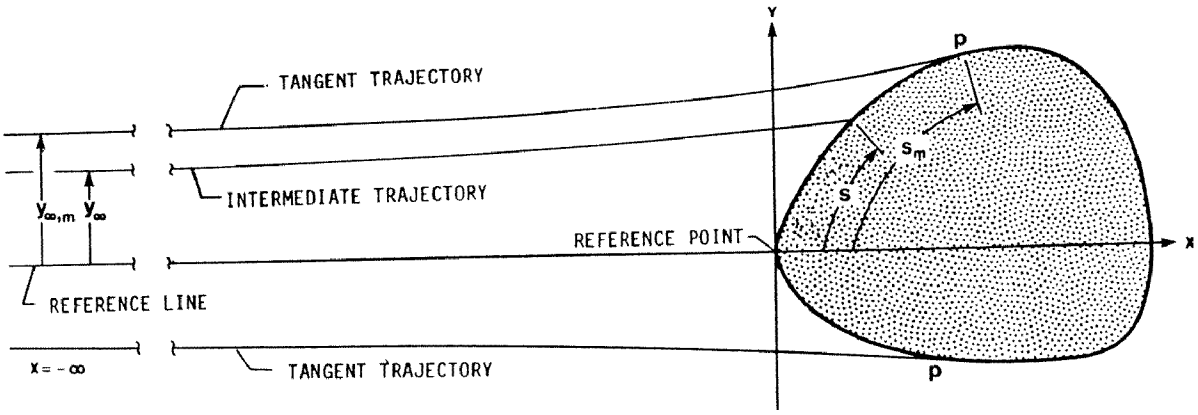

Fig. 1c Two-dimensional droplet trajectories for a body in a cloud of uniform droplet size.

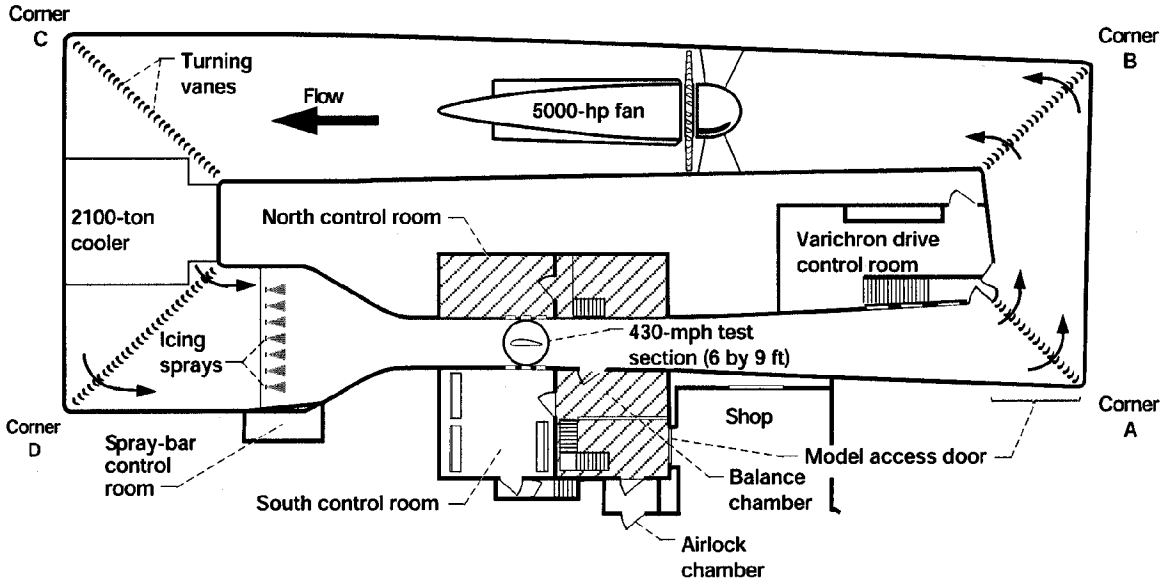

Fig. 2 Plan view of NASA Glenn Icing Research Tunnel (IRT).

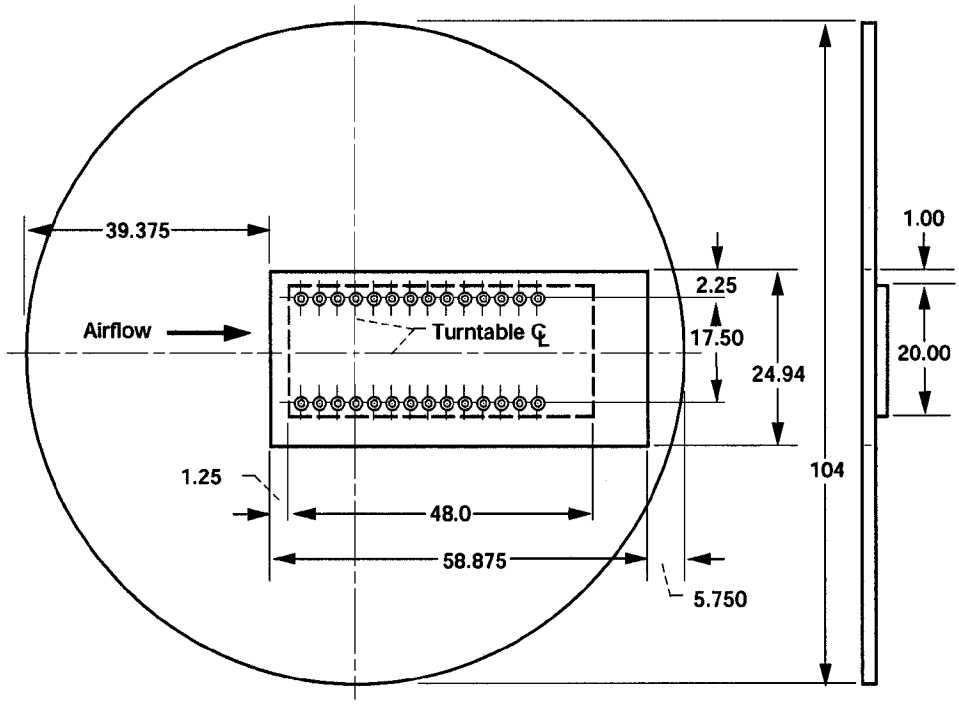

Fig. 3 Icing Research Tunnel turntable and model mounting plate (all dimensions are given in inches).

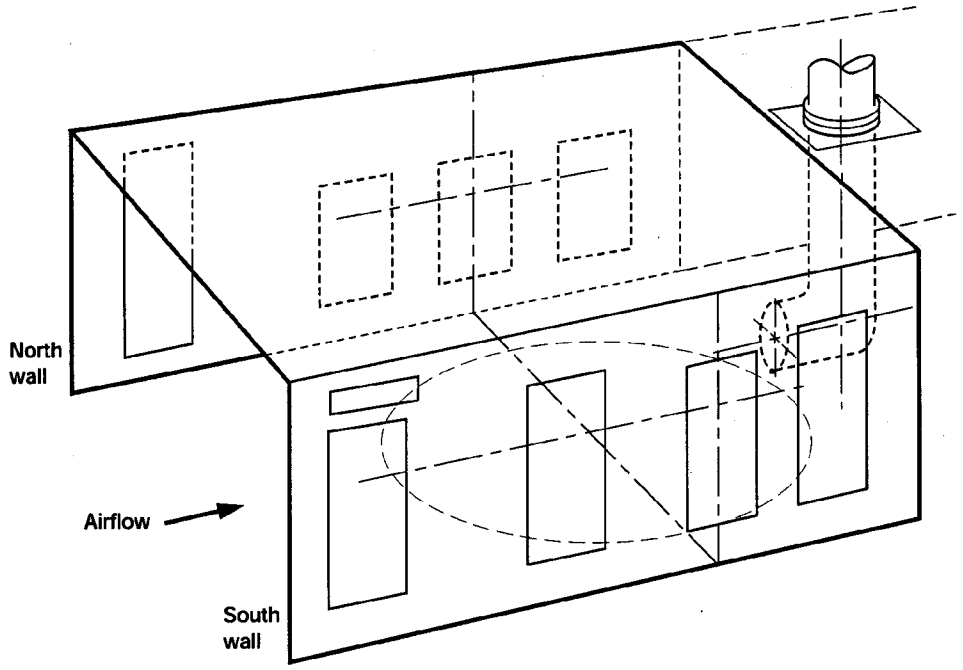

Fig. 4 IRT test section north and south walls showing visual access windows, turntable, and altitude exhaust piping.

Water tube diameter of an IRT nozzle:
Standard Nozzle – 0.025 inches
Mod-1 Nozzle – 0.015 inches

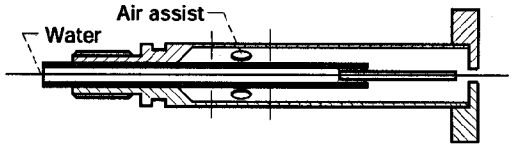

Fig. 5 Schematic of an IRT spray nozzle.

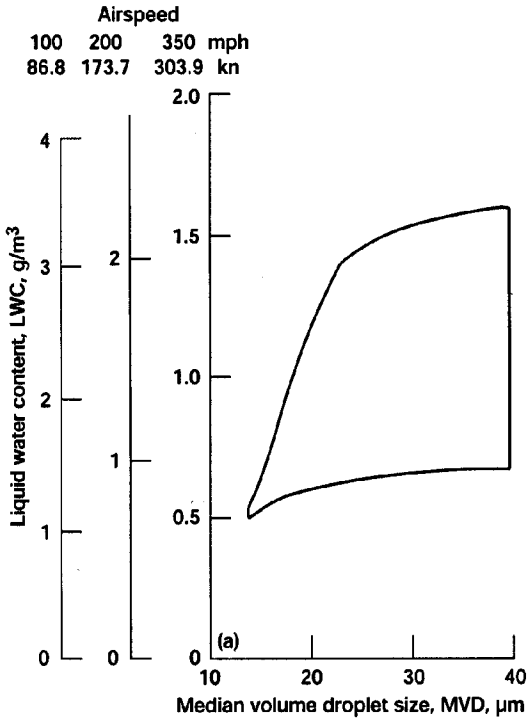

Fig. 6 IRT icing cloud operating envelopes for standard nozzles.

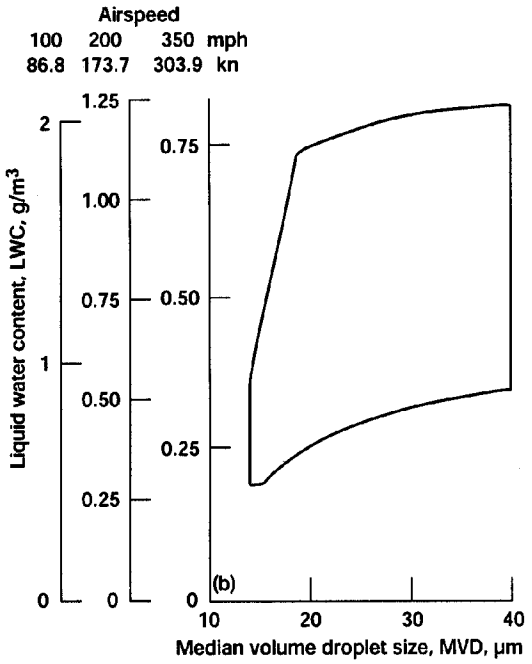

Fig. 7 IRT icing cloud operating envelopes for MOD-1 type nozzles.

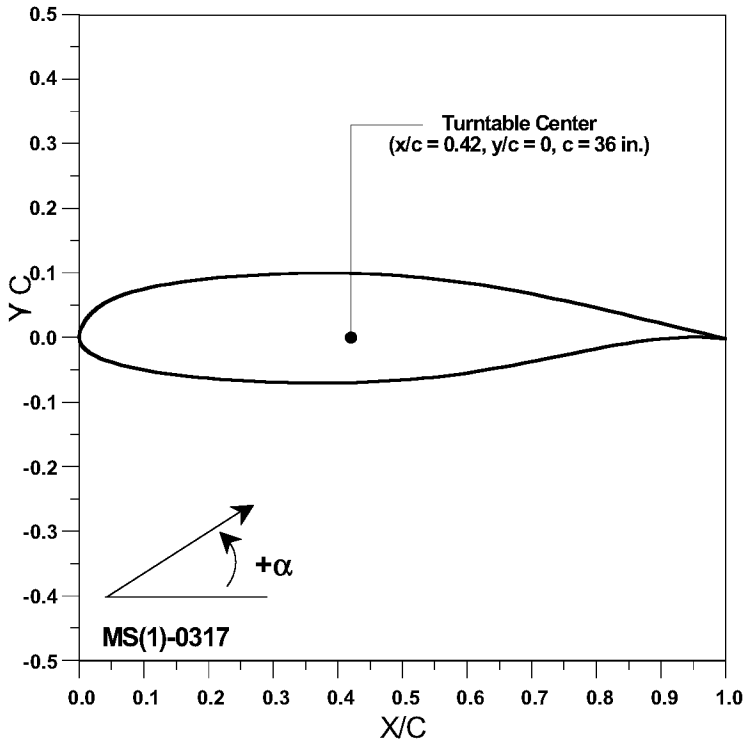

Fig. 8a MS(1)-0317 medium speed airfoil section.

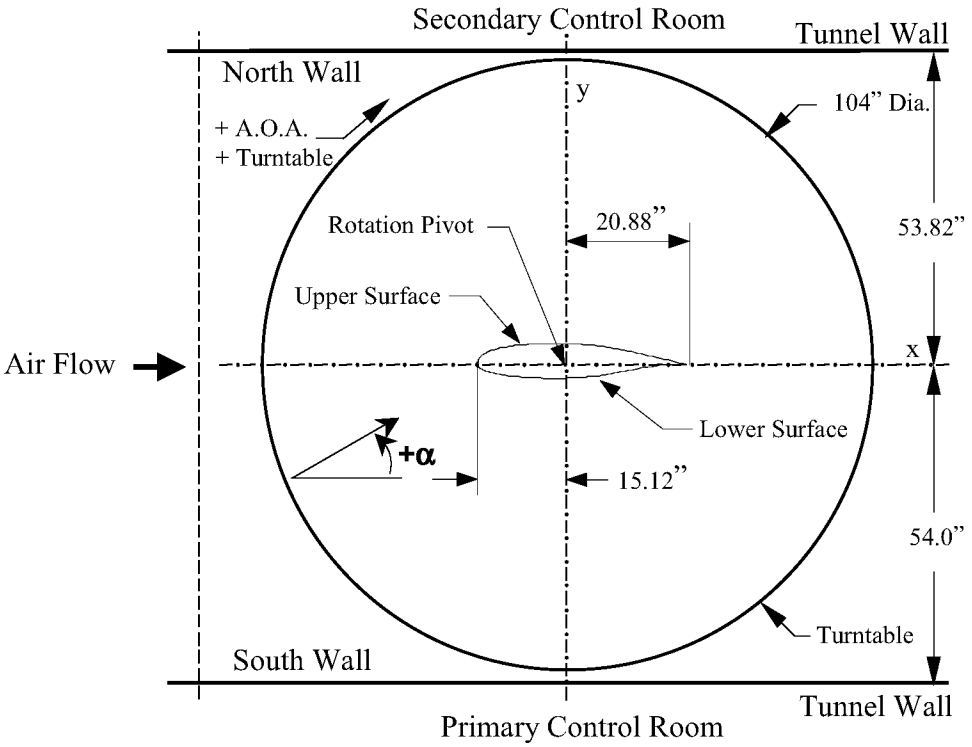

Fig. 8b MS(1)-0317 airfoil installation in IRT test section (top view).

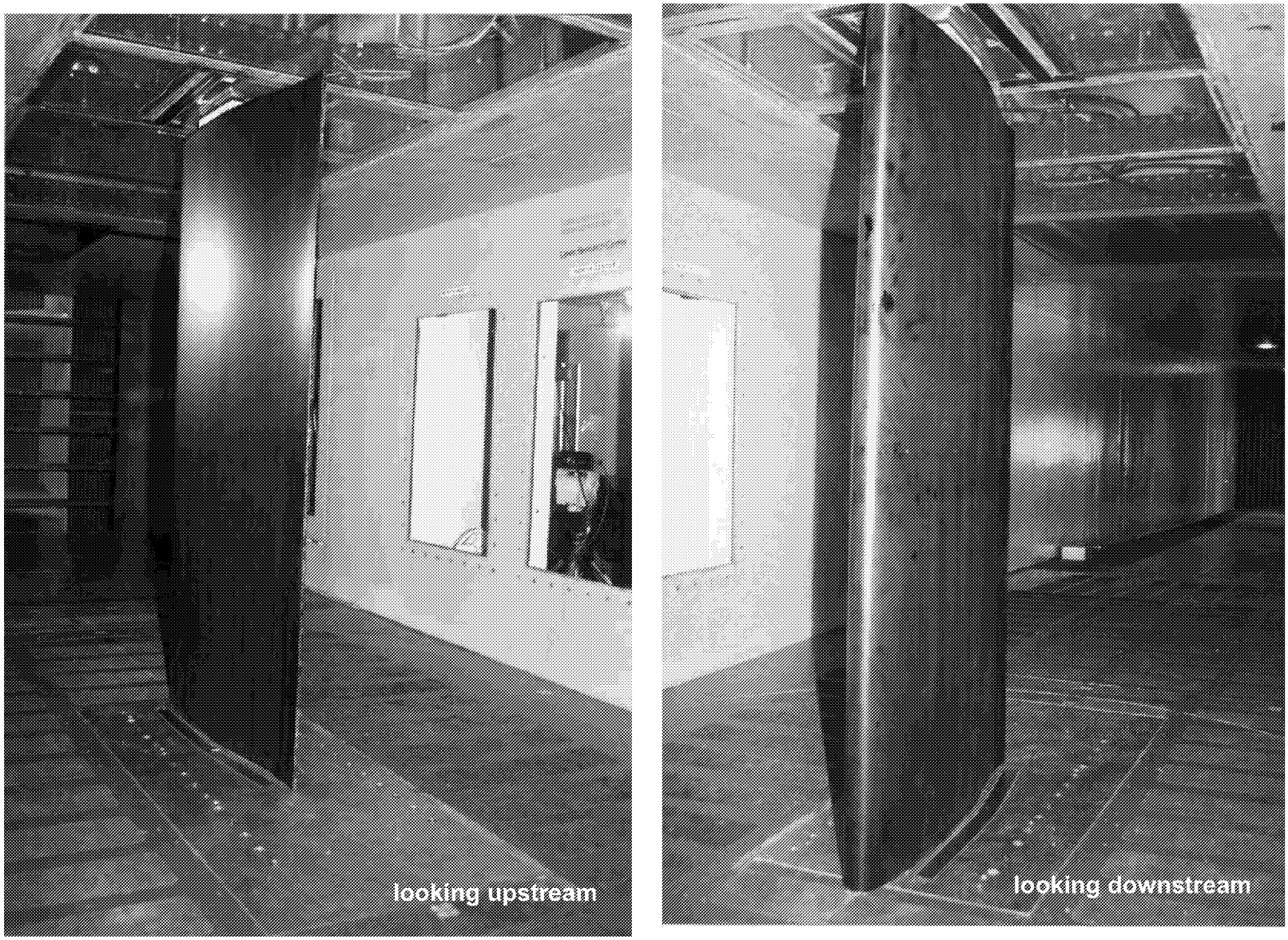

Fig. 8c MS(1)-0317 airfoil installed in IRT test section.

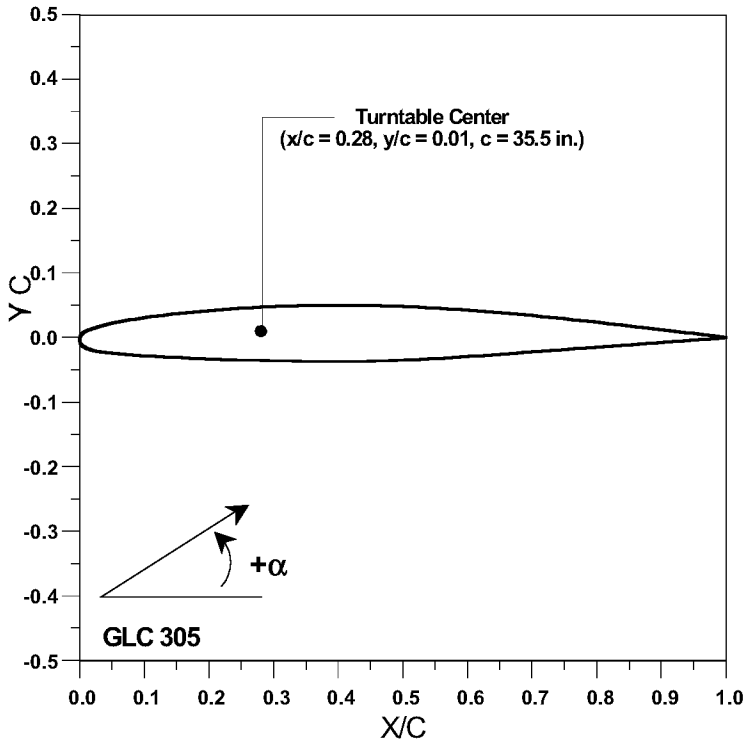

Fig. 9a GLC-305 airfoil section.

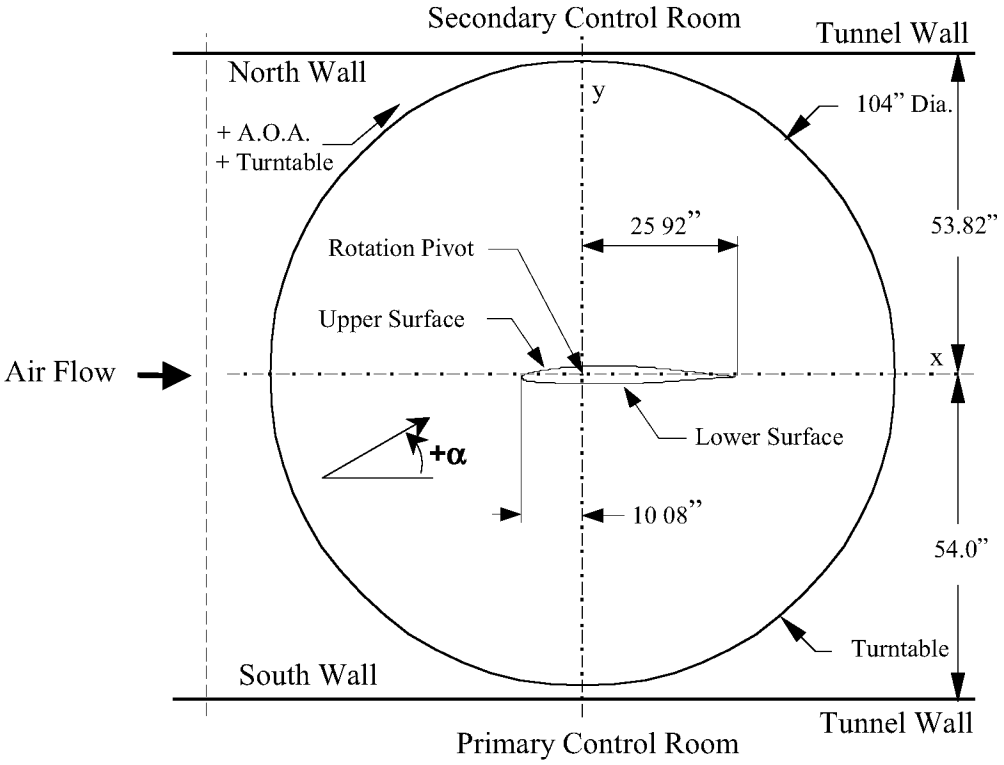

Fig. 9b GLC-305 airfoil installation in IRT test section (top view).

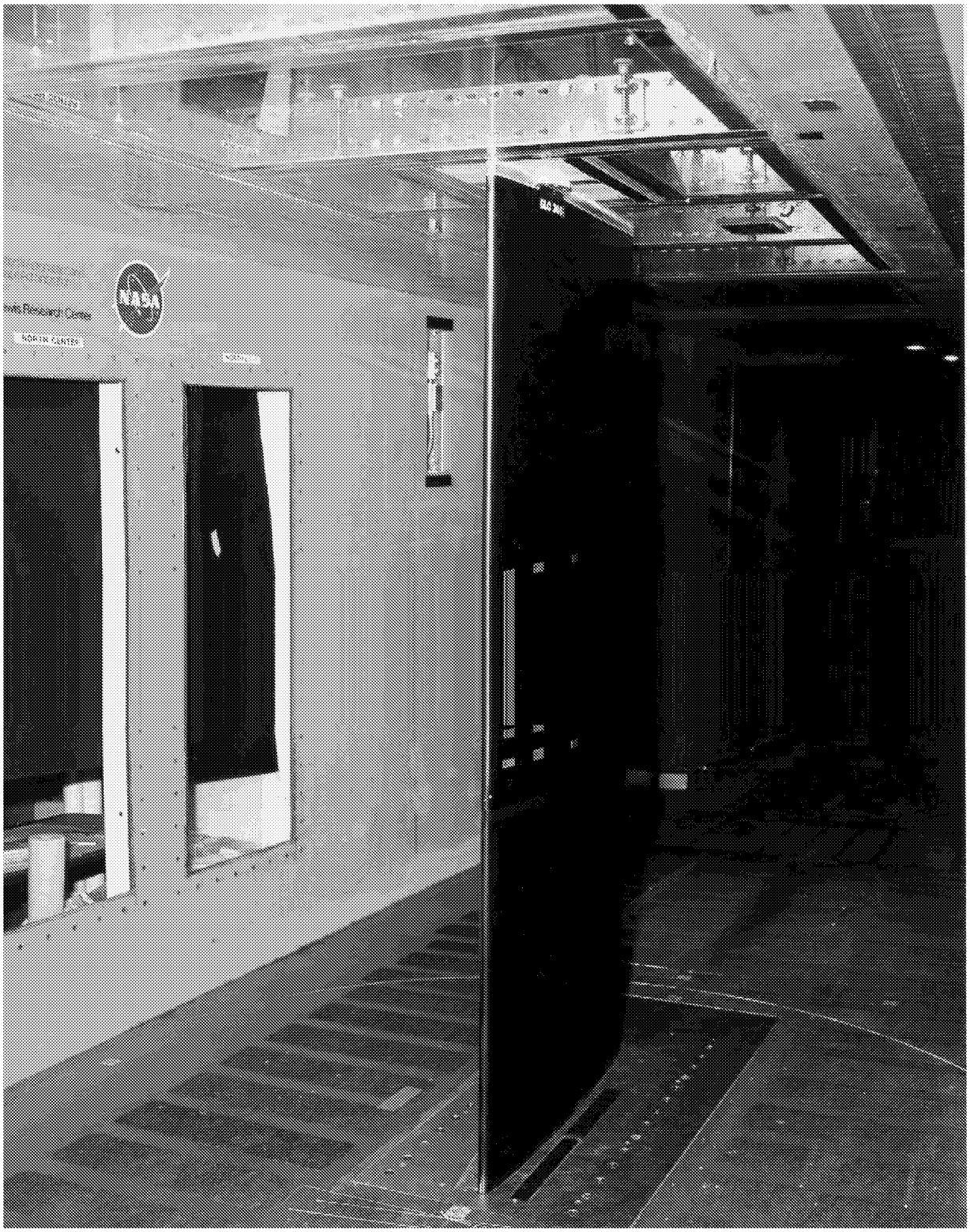

Fig. 9c GLC-305 airfoil installed in IRT test section (looking downstream).

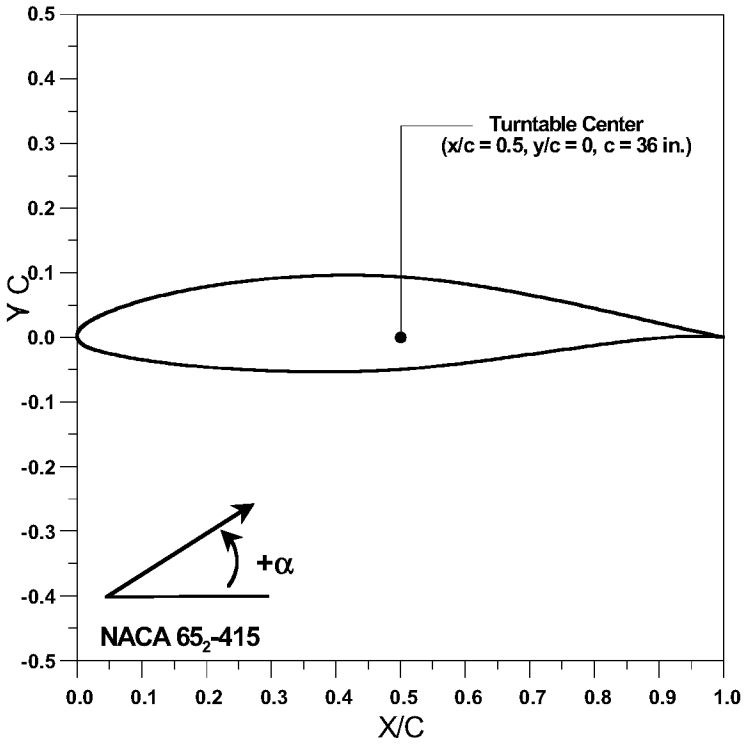

Fig. 10a NACA 65_2-415 airfoil section.

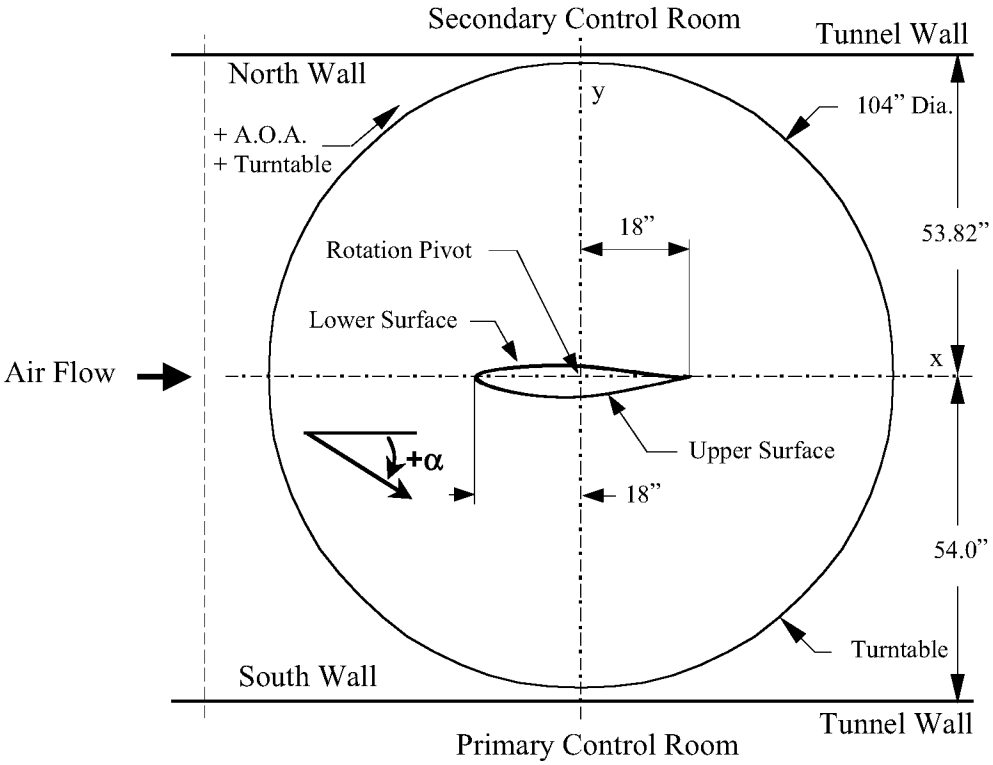

Fig. 10b NACA 65_2-415 airfoil installation in IRT test section (top view).

Fig. 10c NACA 65_2-415 airfoil installed IRT test section (looking downstream).

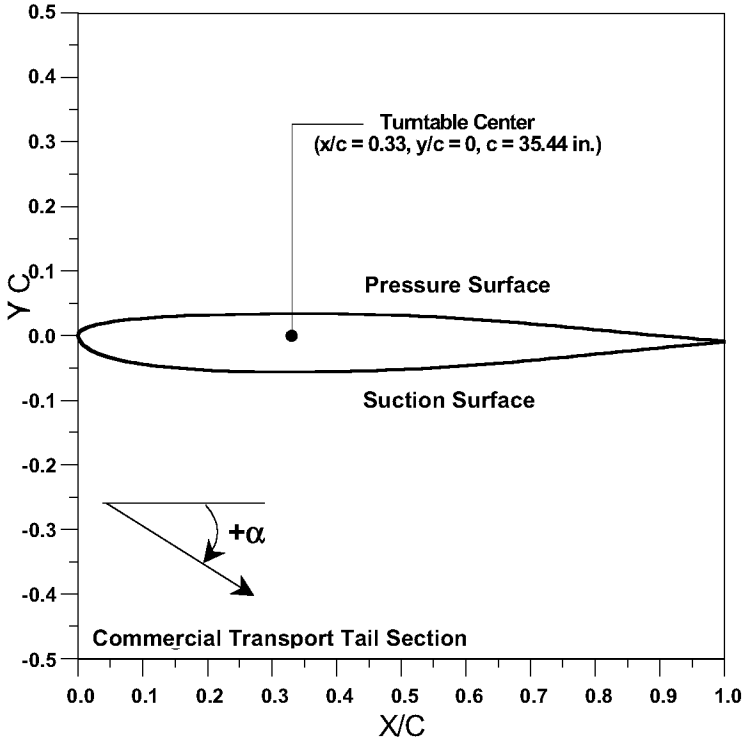

Fig. 11a Commercial transport horizontal tail section.

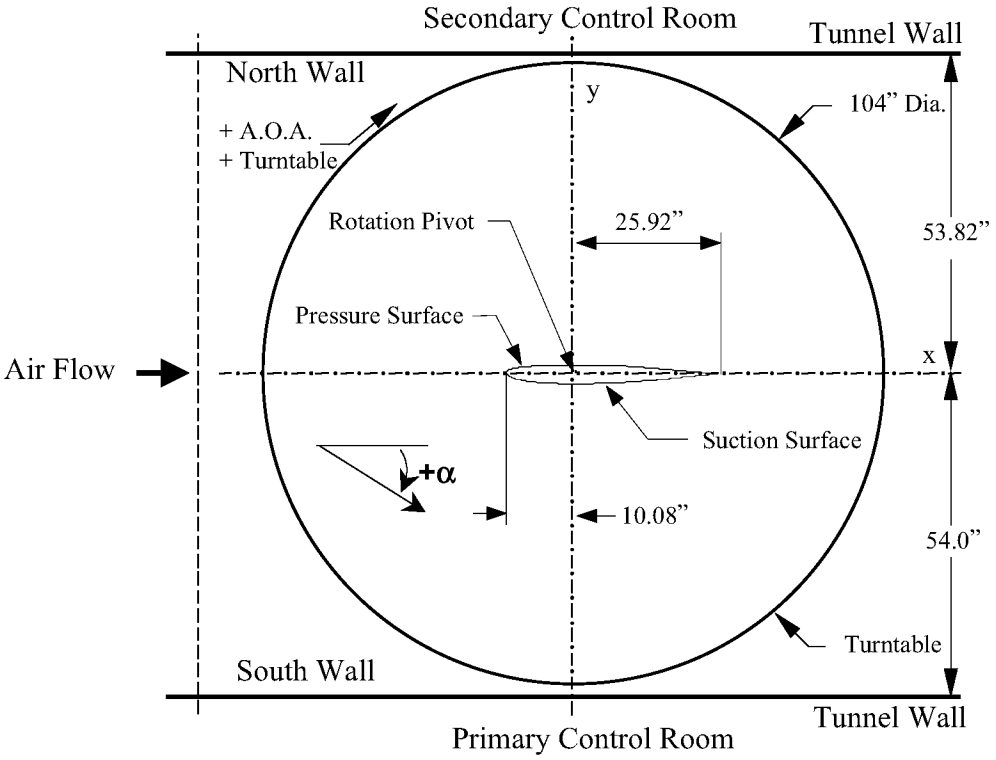

Fig. 11b Commercial transport horizontal tail installation in IRT test section (top view).

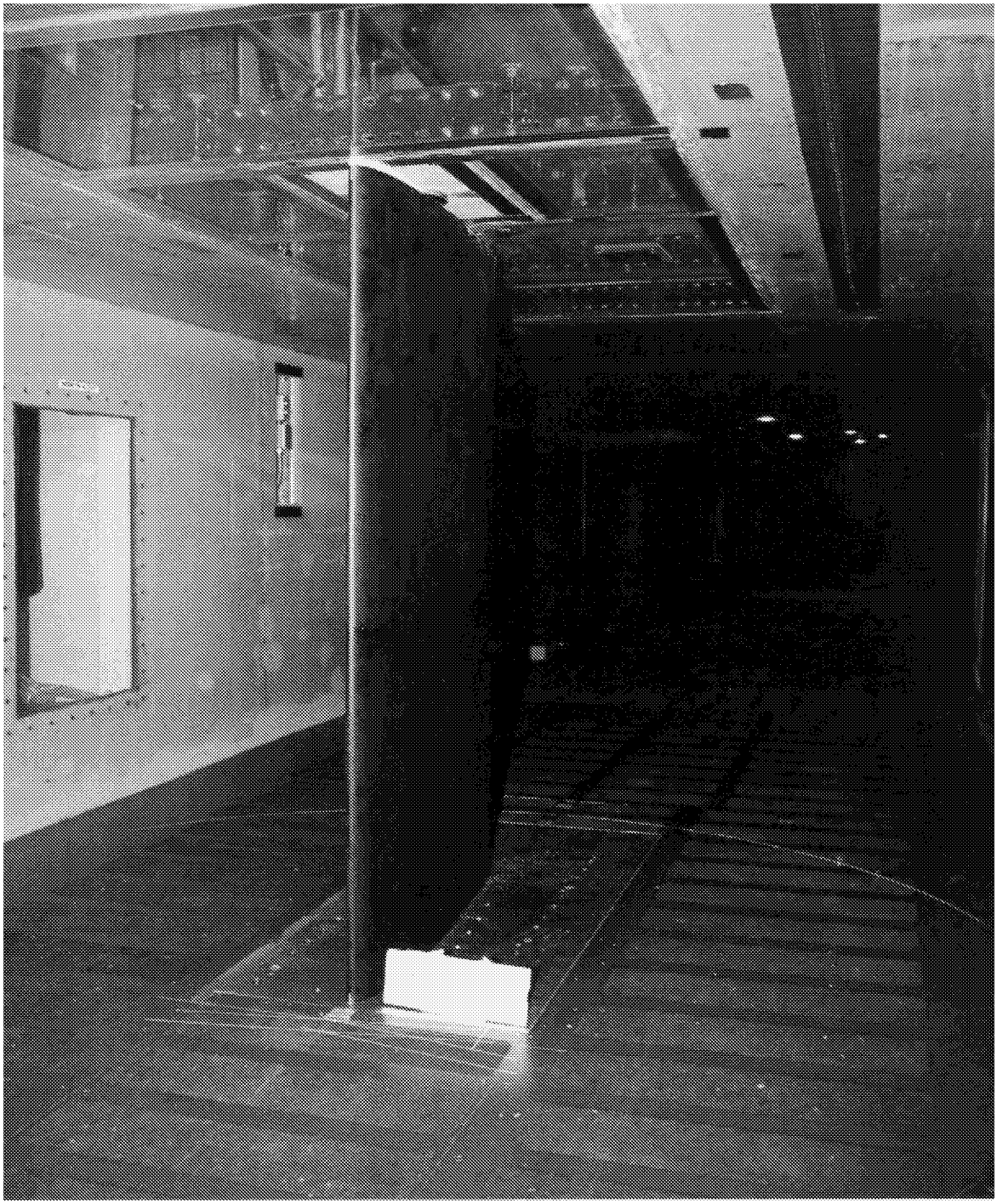

Fig. 11c Commercial transport horizontal tail installed in IRT test section (looking downstream).

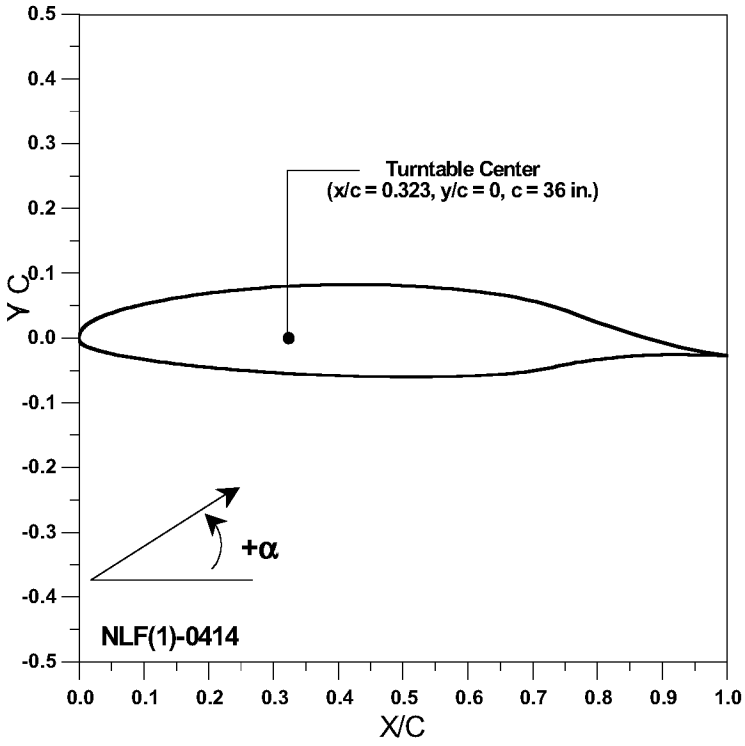

Fig. 12a NLF(1)-0414 36-in airfoil section.

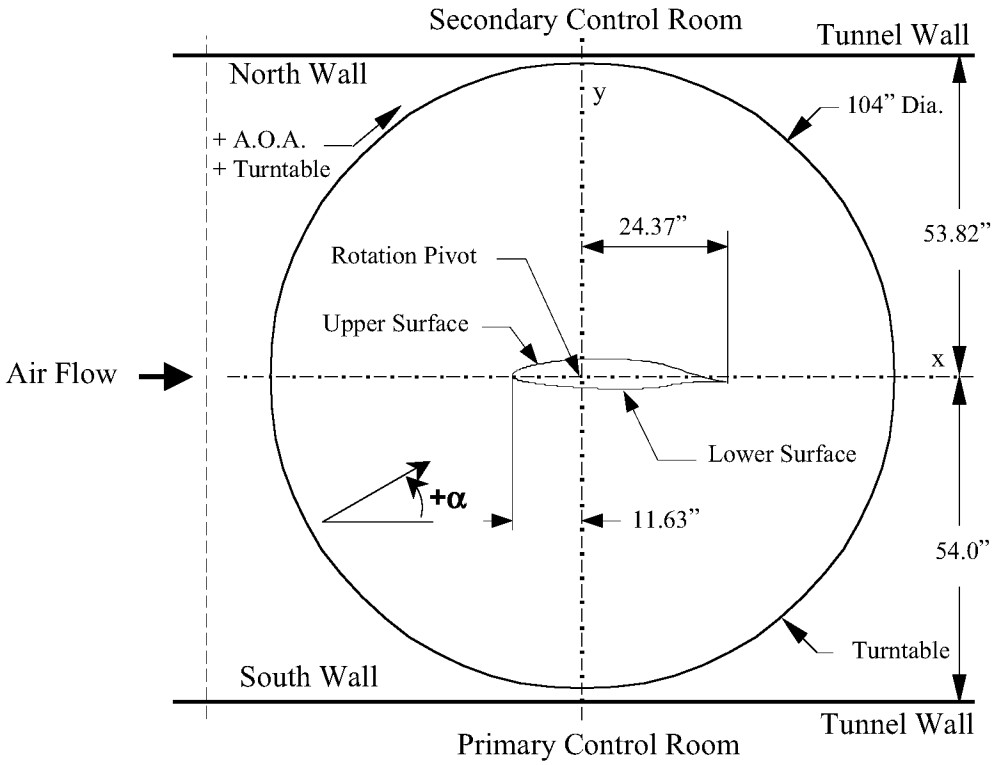

Fig. 12b NLF(1)-0414 36-in airfoil installation in IRT test section (top view).

Fig. 12c NLF(1)-0414 36-in airfoil installed in IRT test section (looking downstream).

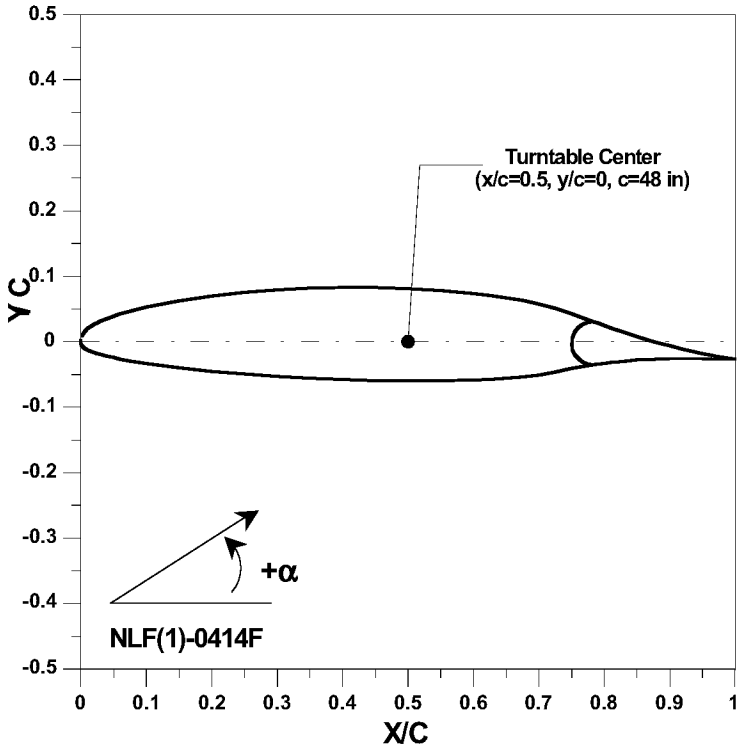

Fig. 13a NLF(1)-0414 48-in airfoil section.

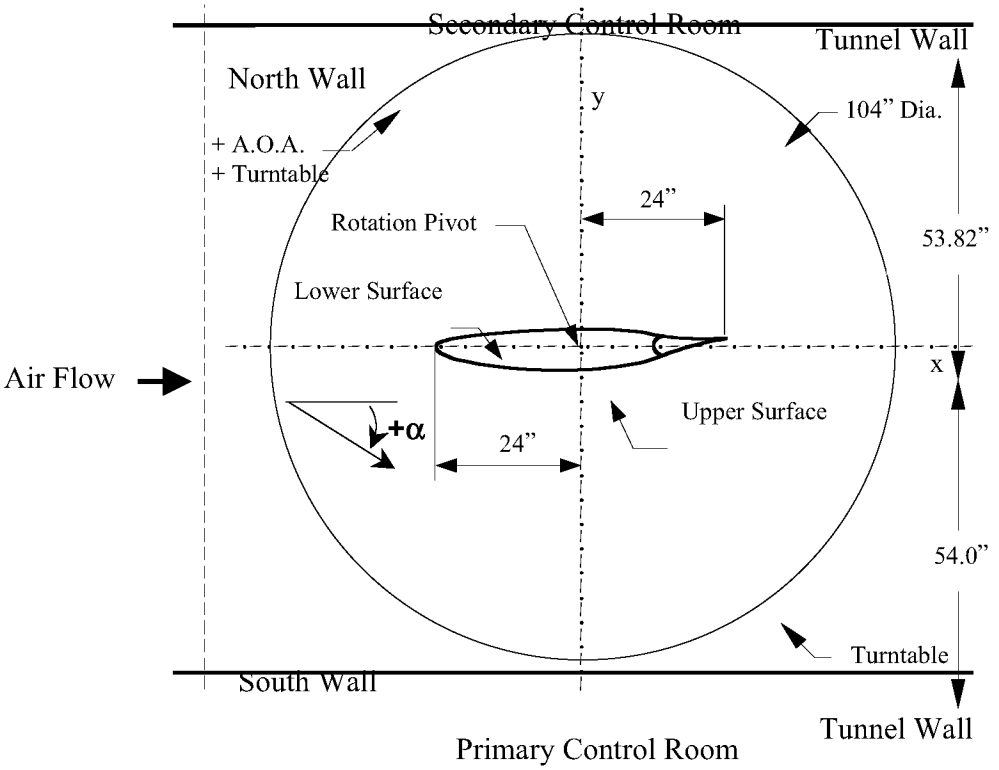

Fig. 13b NLF(1)-0414 48-in airfoil installation in IRT test section (top view).

Fig. 13c NLF(1)-0414 48-in airfoil installed in IRT test section.

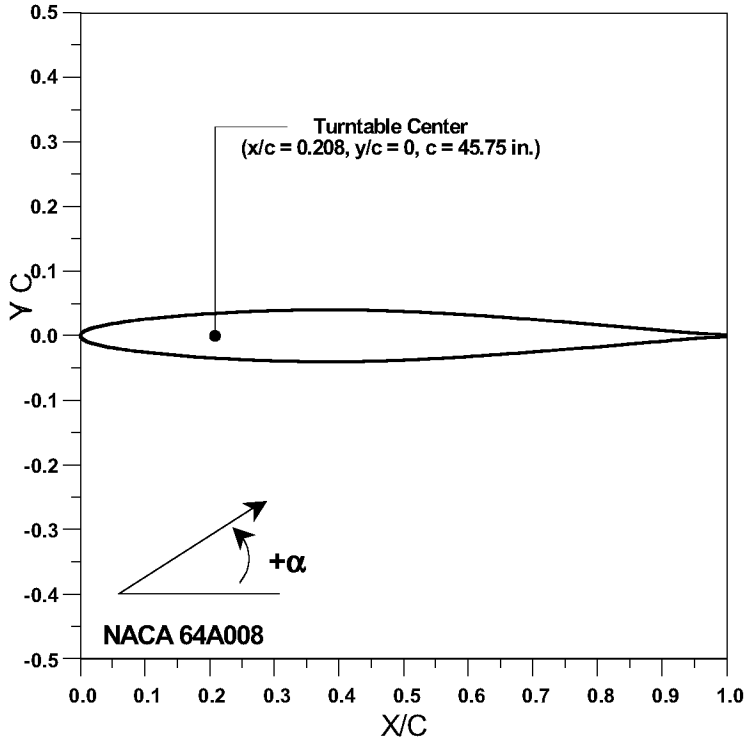

Fig. 14a NACA 64A008 swept tail.

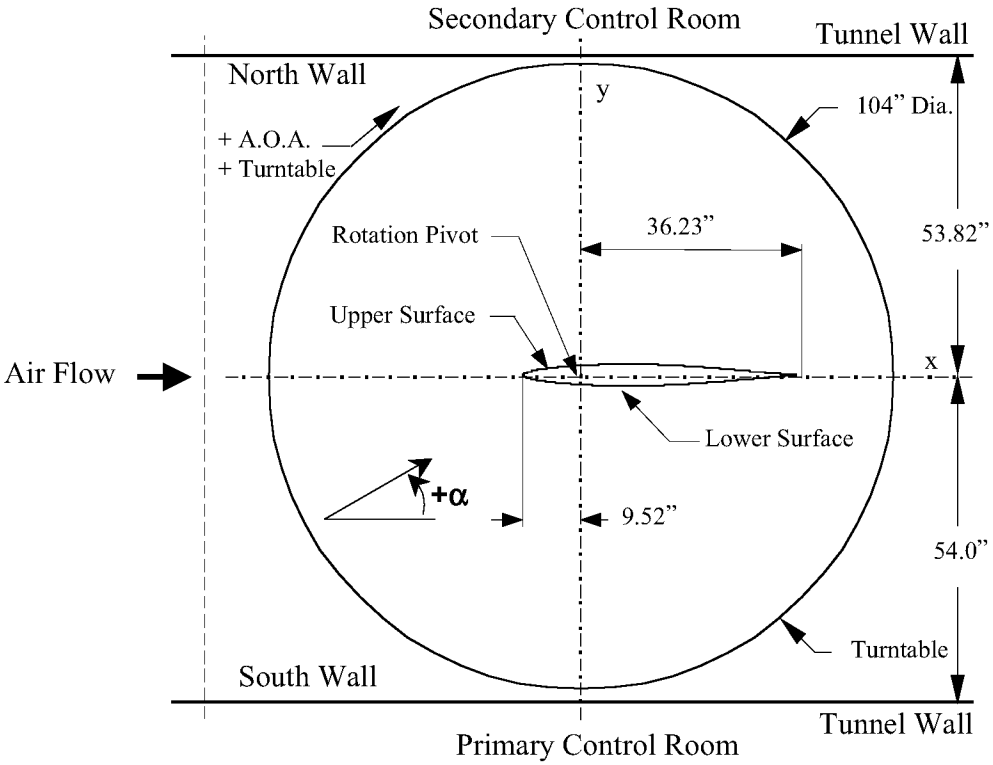

Fig. 14b NACA 64A008 swept tail installation in IRT test section (top view).

NACA 64A008 Airfoil
Taper Ration = 0.62
Wing Area = 1767.6 in^2
Aspect Ration = 2.6
Leading Edge Sweep Angle = 29.1°
Trailing Edge Sweep Angle = 11.1°

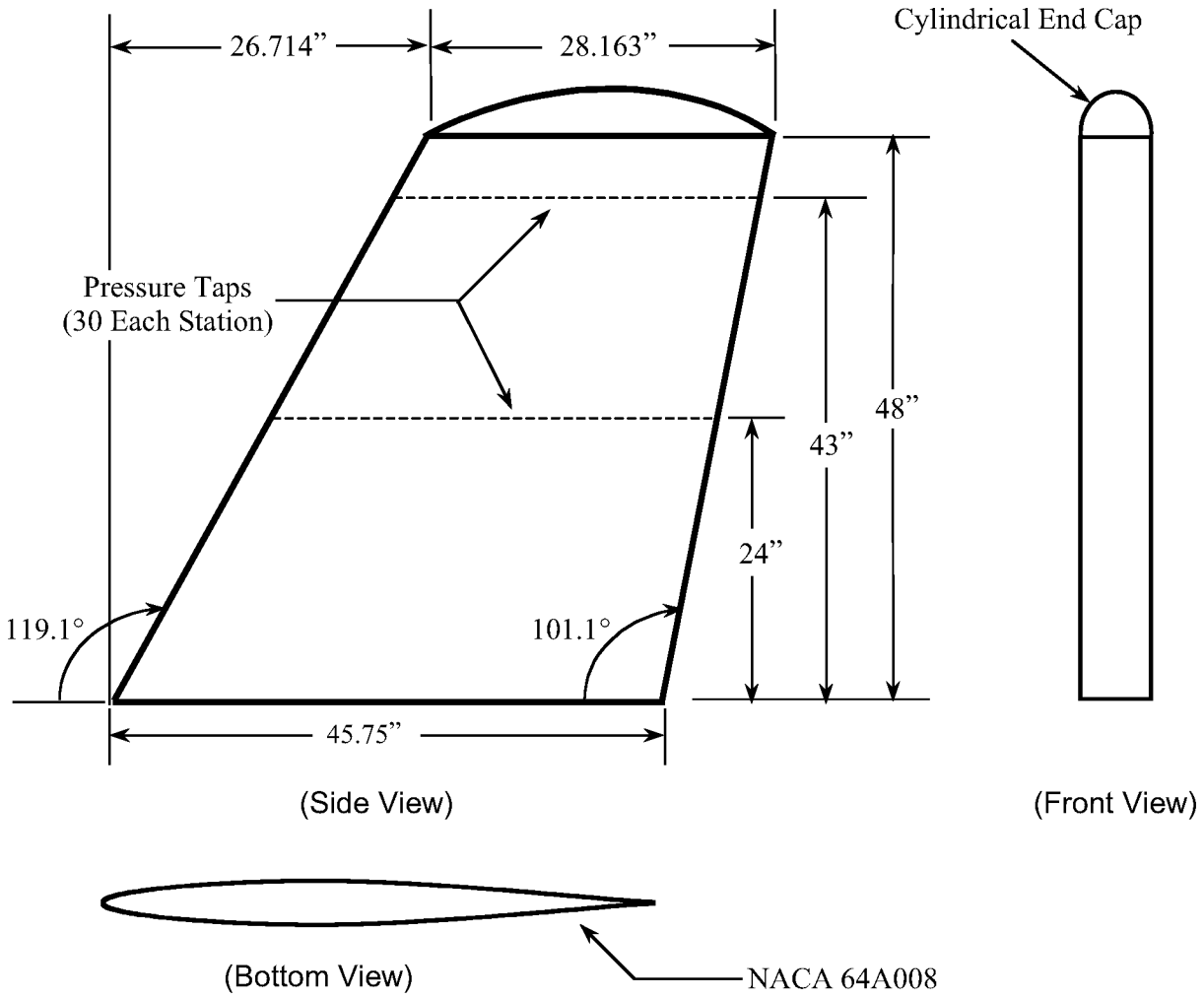

Fig. 14c NACA 64A008 swept tail (3-View Plot).

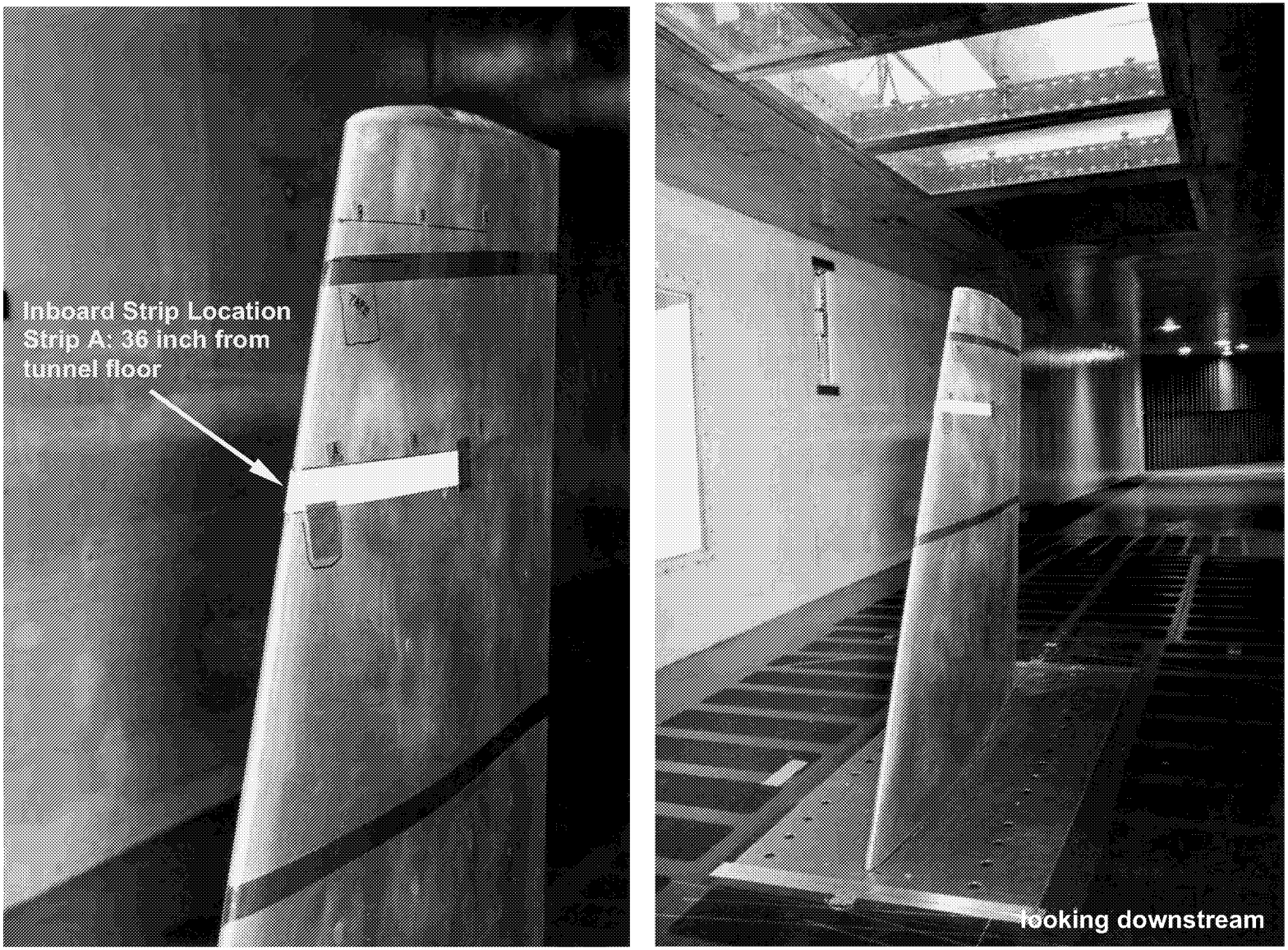

Fig. 14d NACA 64A008 swept tail installed in IRT test section (looking downstream).

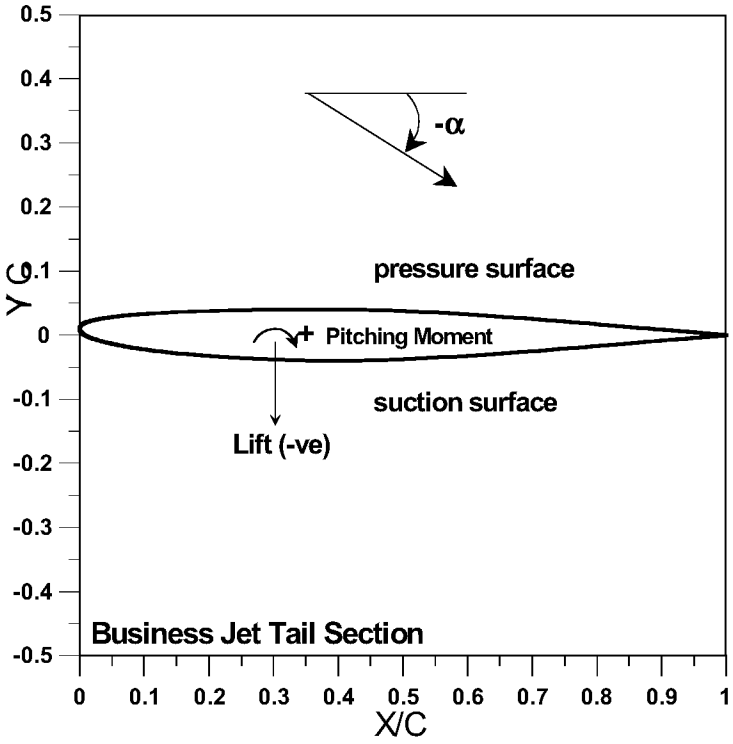

Fig. 15a 25%-scale business jet empennage horizontal tail section.

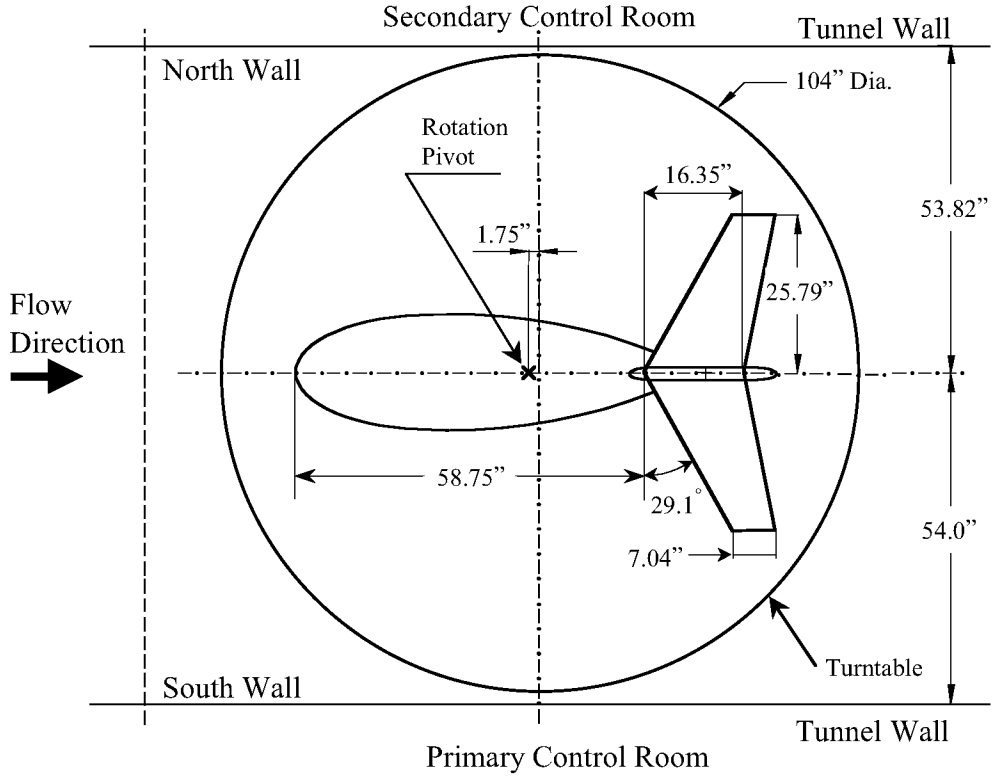

Fig. 15b 25%-scale business jet empennage installation in IRT test section (top view).

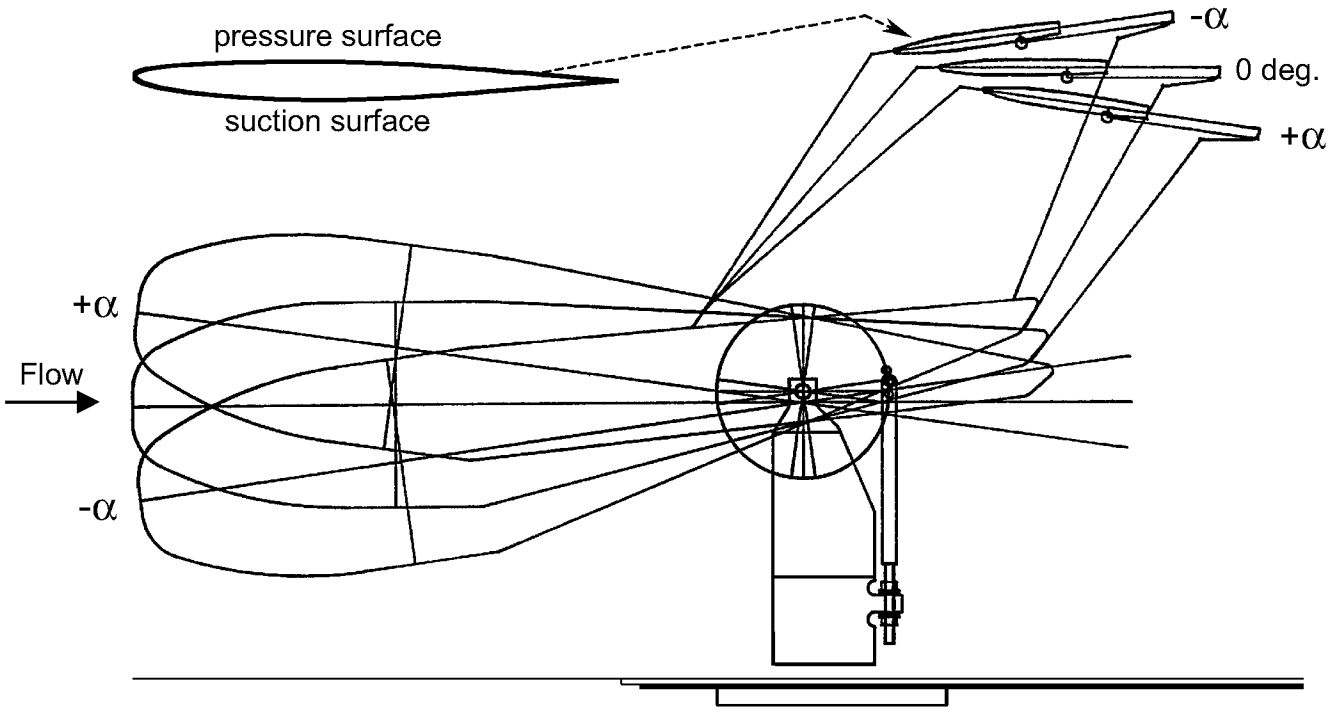

Fig. 15c Business jet empennage and mounting device (side view).

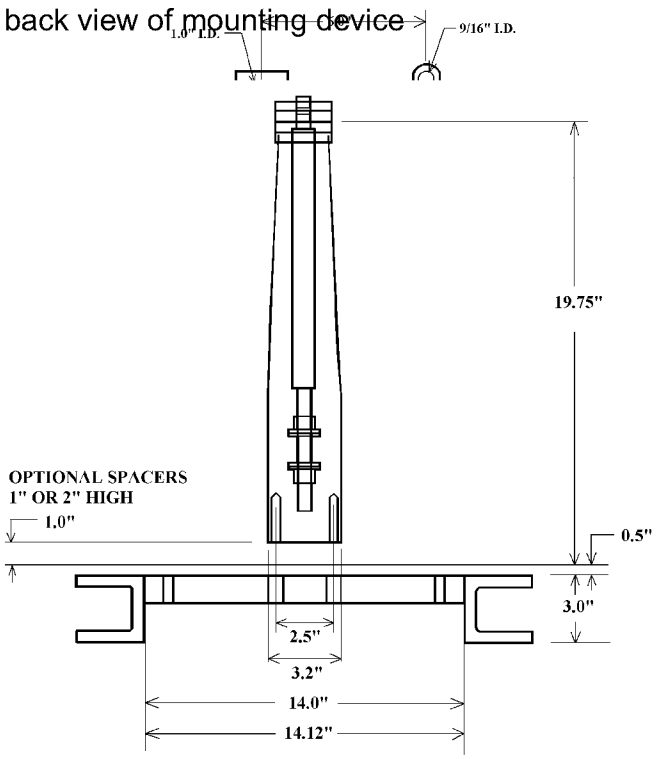

Fig. 15d Business jet empennage mounting device.

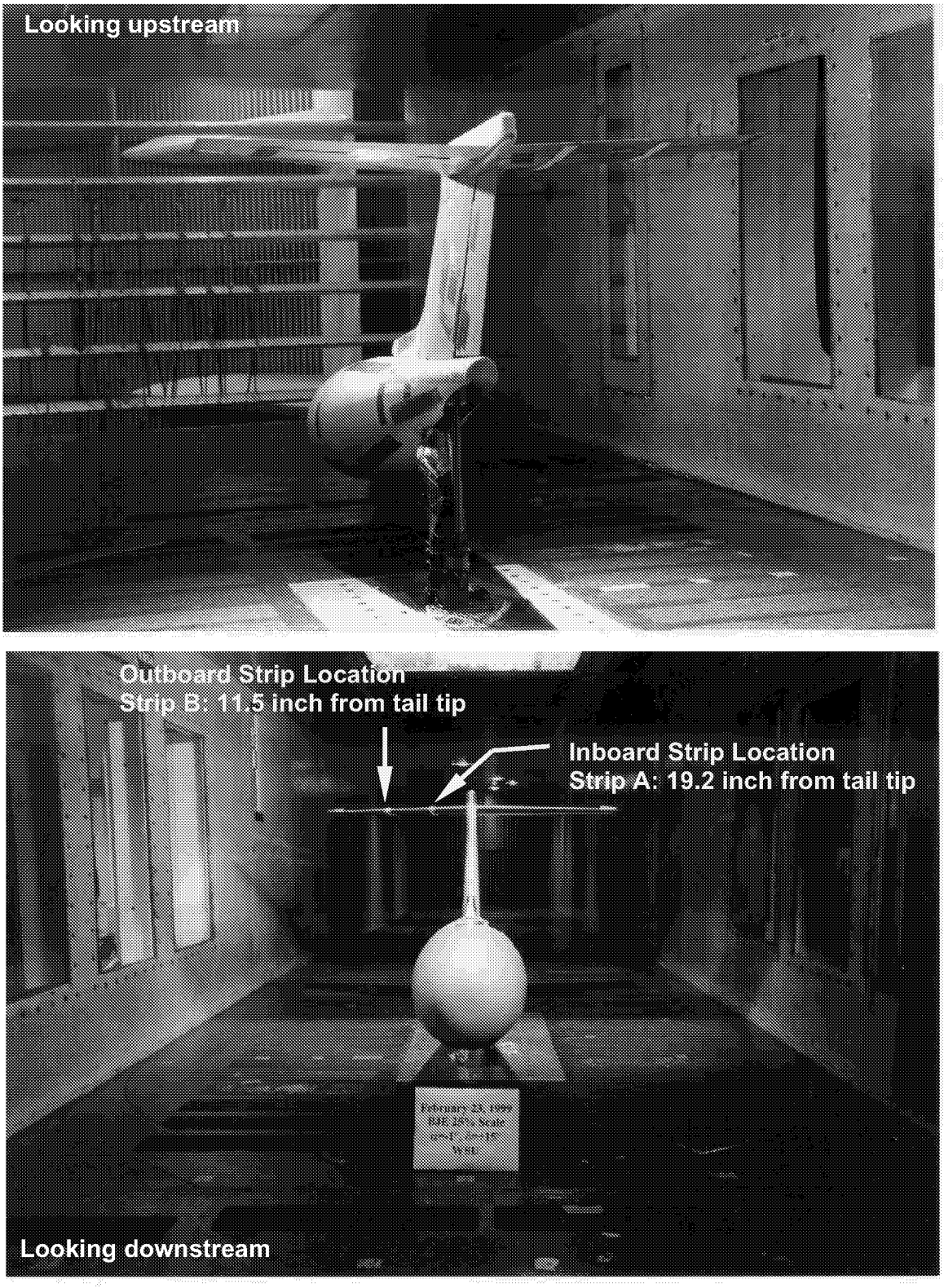

Fig. 15e 25%-scale business jet empennage installed in IRT test section.

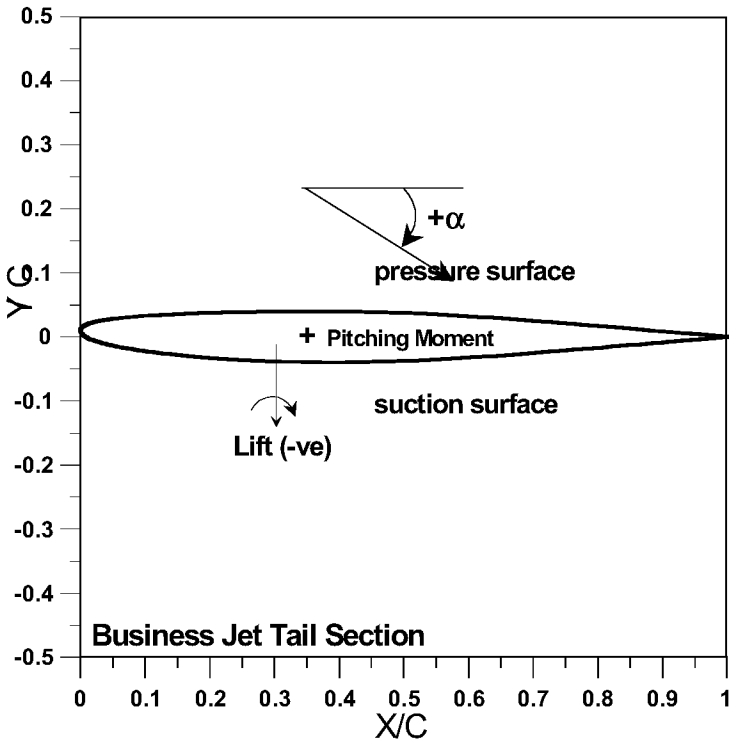

Fig. 16a Full-scale business jet horizontal tail section.

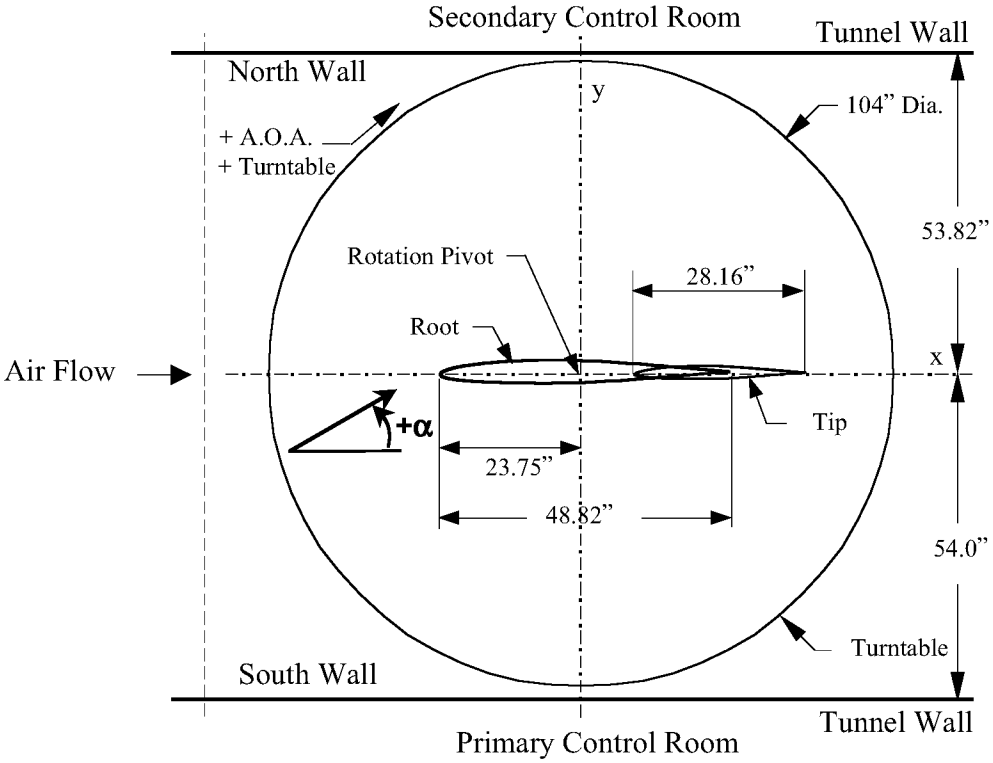

Fig. 16b Full-scale business jet horizontal tail installation in IRT test section (top view).

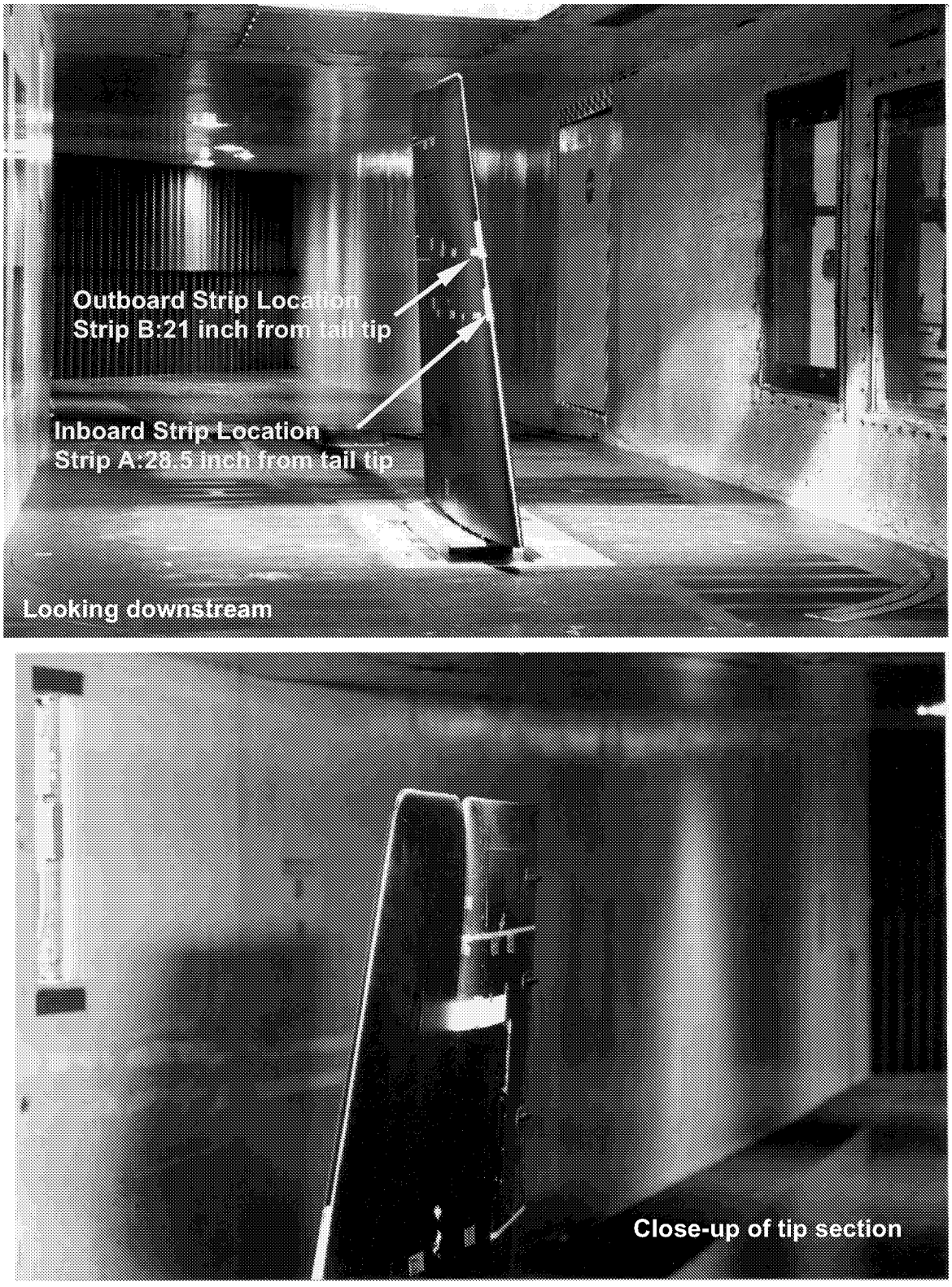

Fig. 16c Full-scale business jet horizontal tail installed in IRT test section.

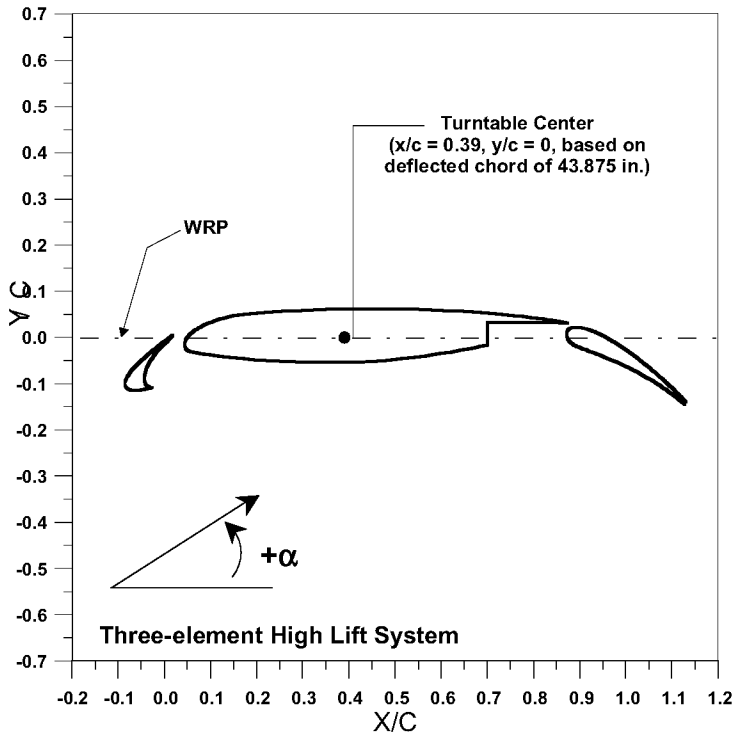

Fig. 17a Three-element high lift system.

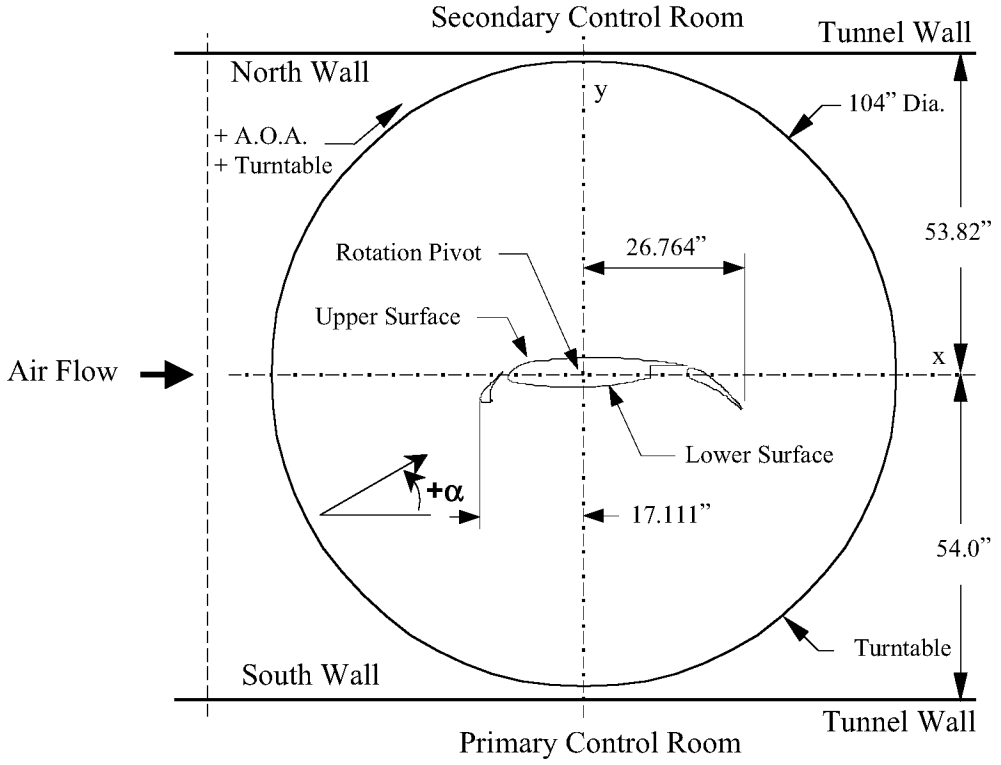

Fig. 17b Three-element high lift system installation in IRT test section (top view).

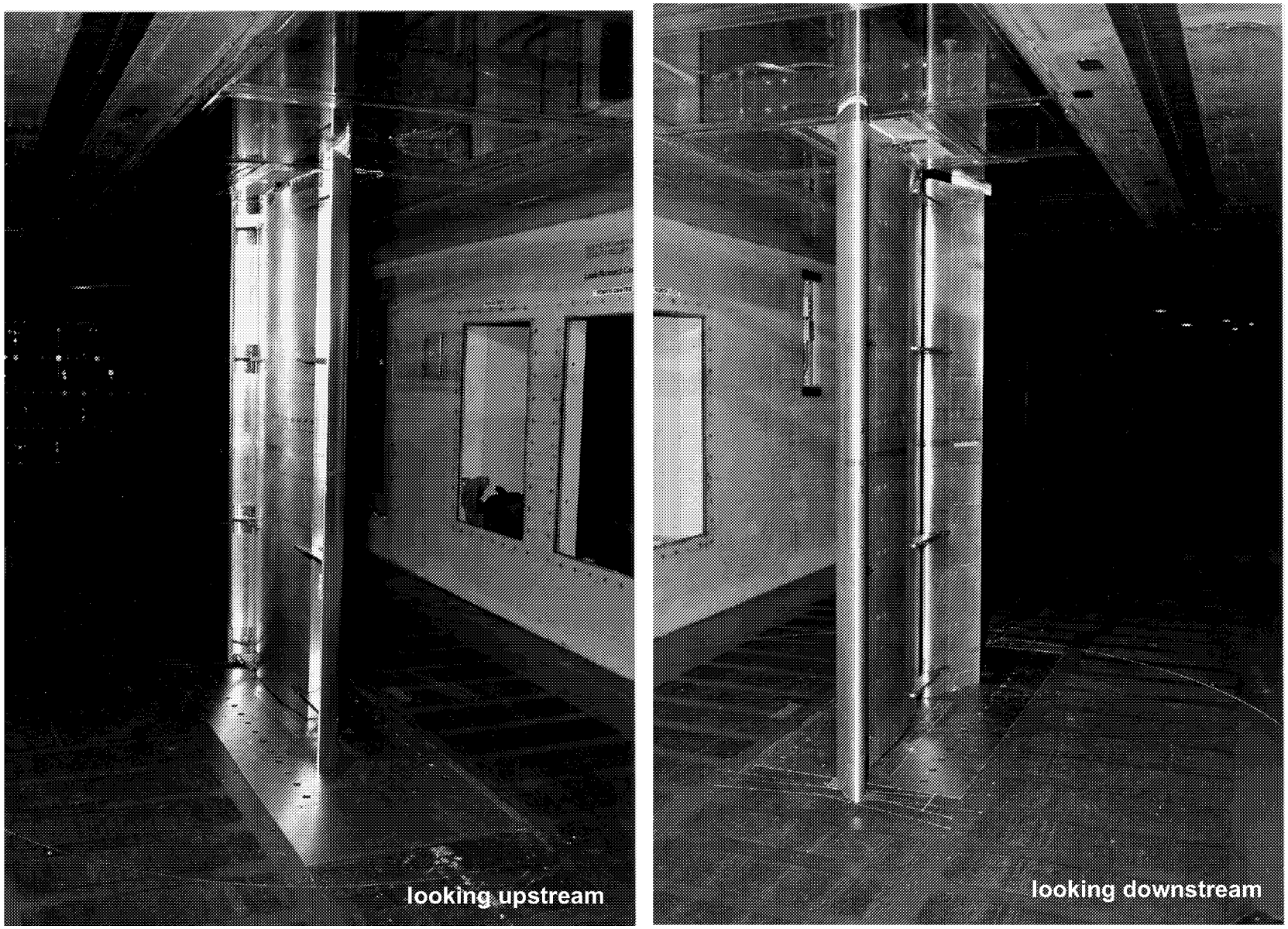

Fig. 17c Three-element high lift system installed in IRT test section (looking downstream).

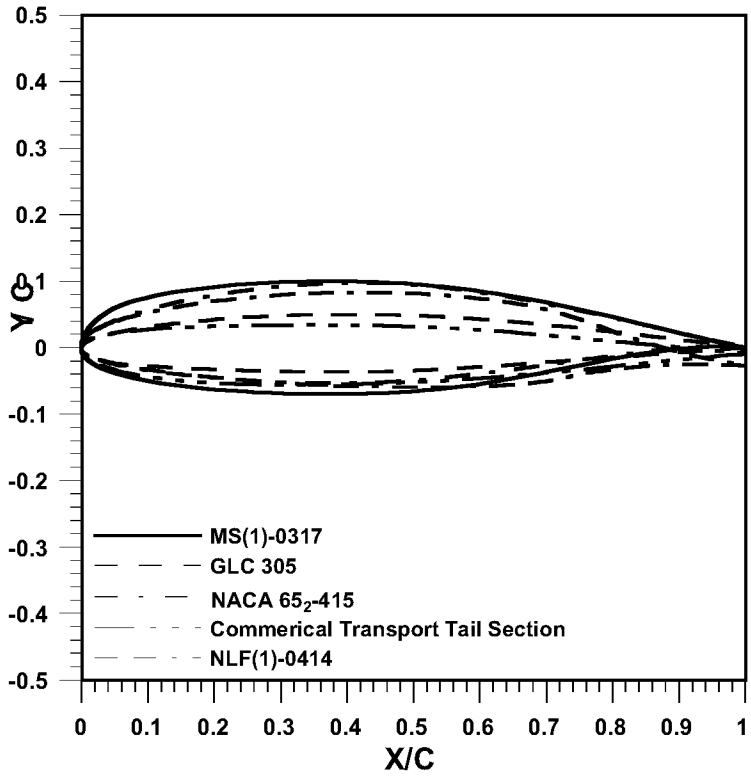

Fig. 18 Comparison of airfoil sections for 2-D models.

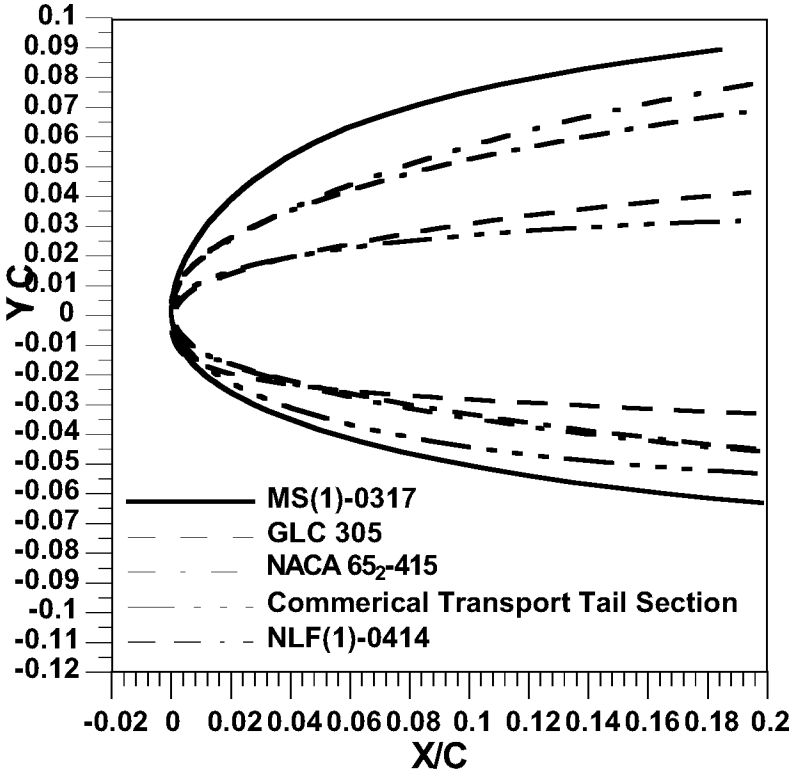

Fig. 19 Close up of leading edge geometry 2-D models.

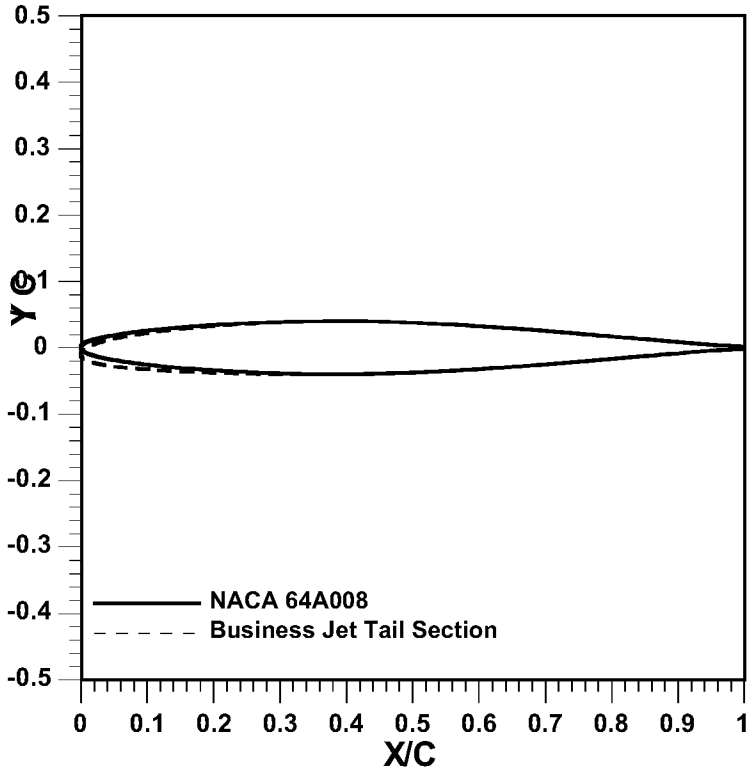

Fig. 20 Comparison of airfoil sections for 3-D models.

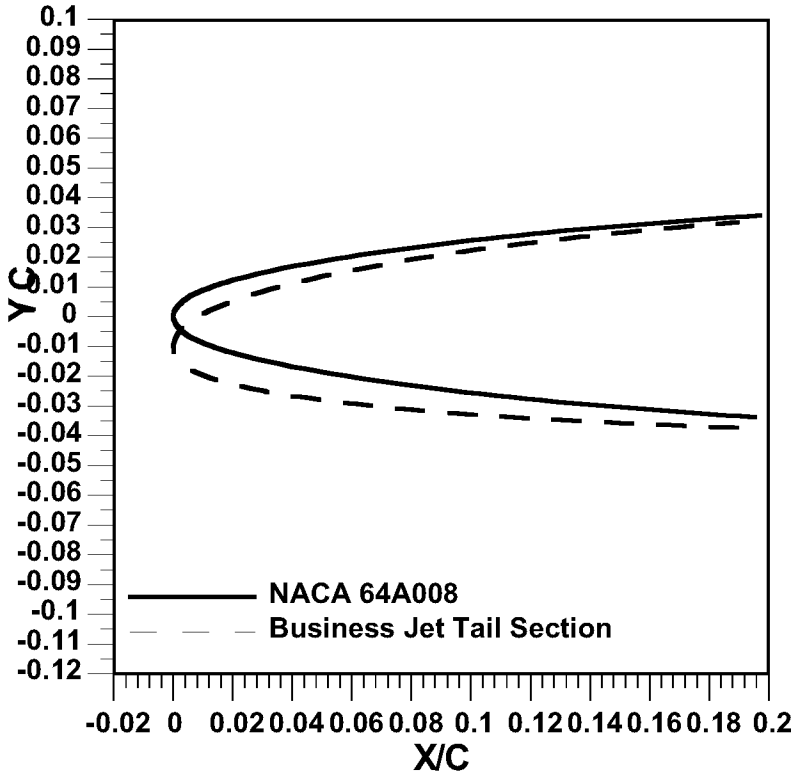

Fig. 21 Close up of leading edge geometry 3-D models.

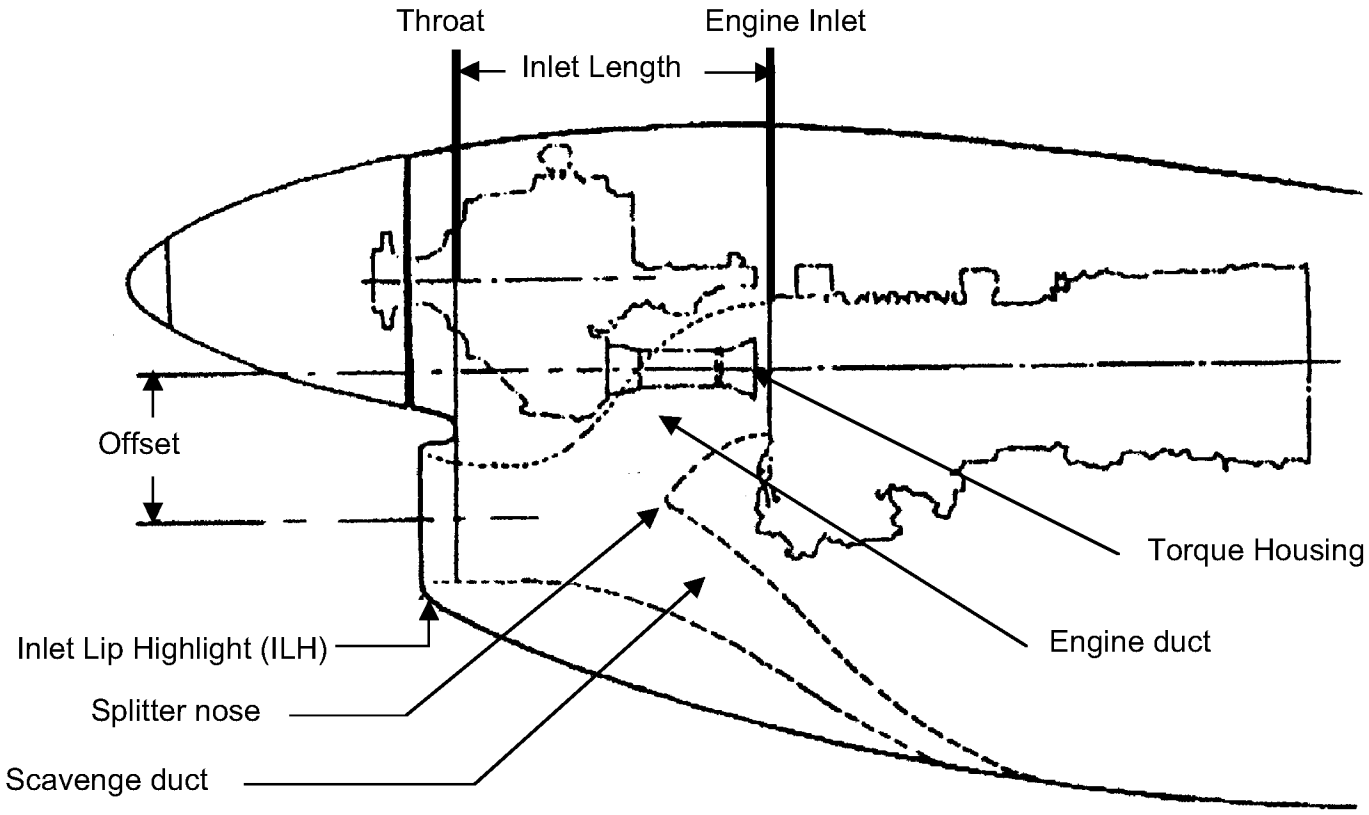

Fig. 22a S-duct engine inlet configuration.

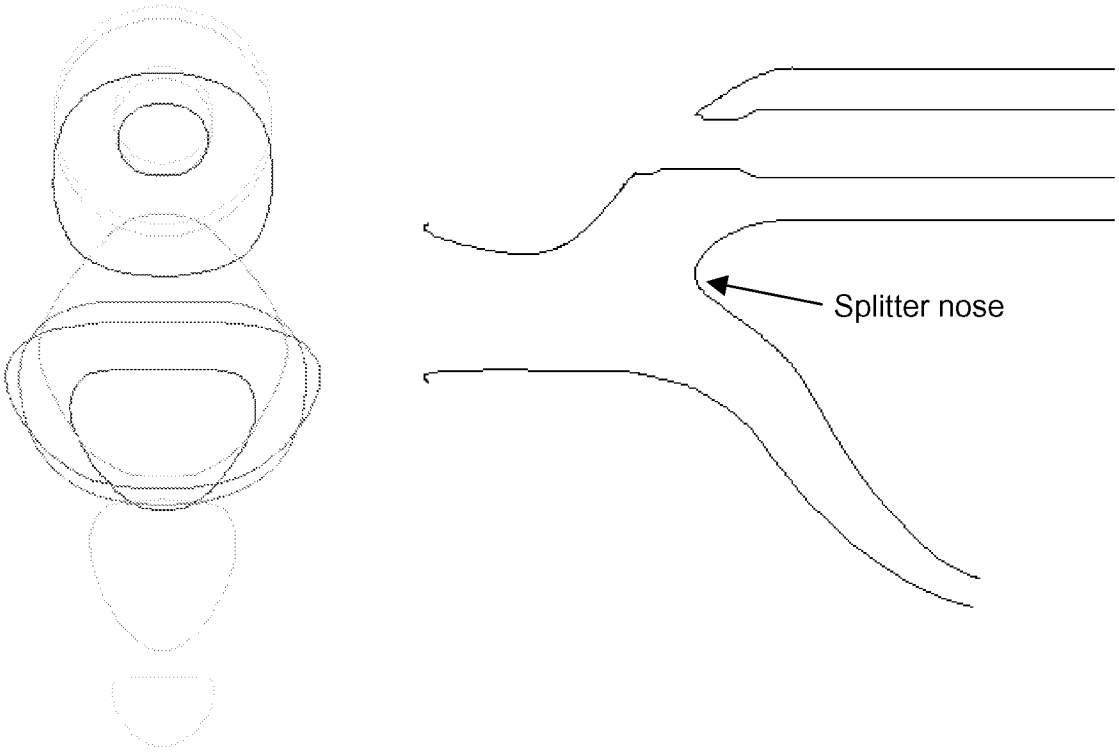

Fig. 22b S-duct engine inlet section views (front and side).

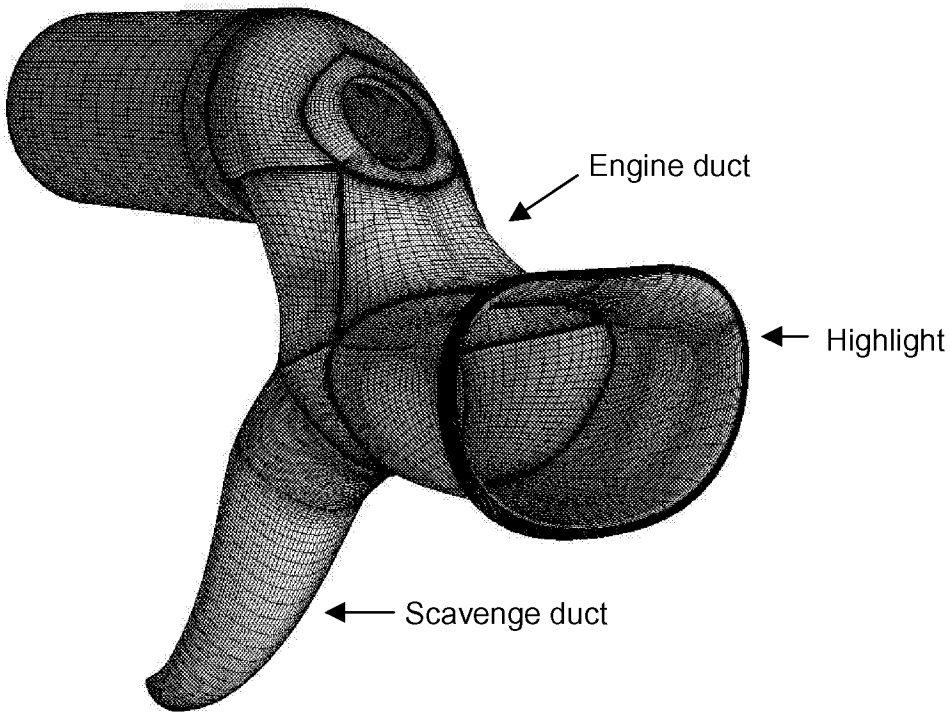

Fig. 22c S-duct engine inlet.

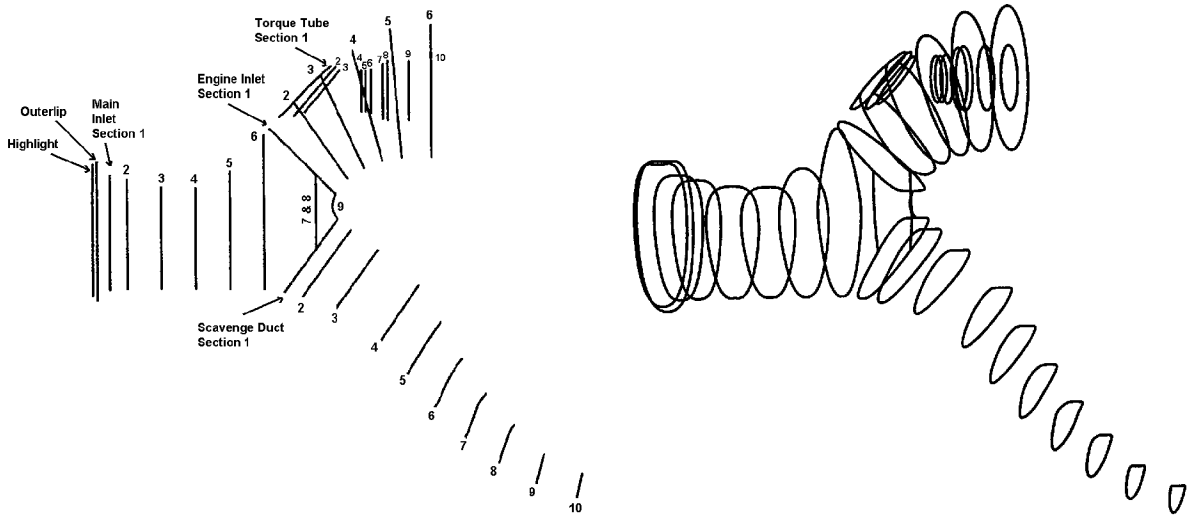

Fig. 22d S-duct engine inlet geometry definition (side view).

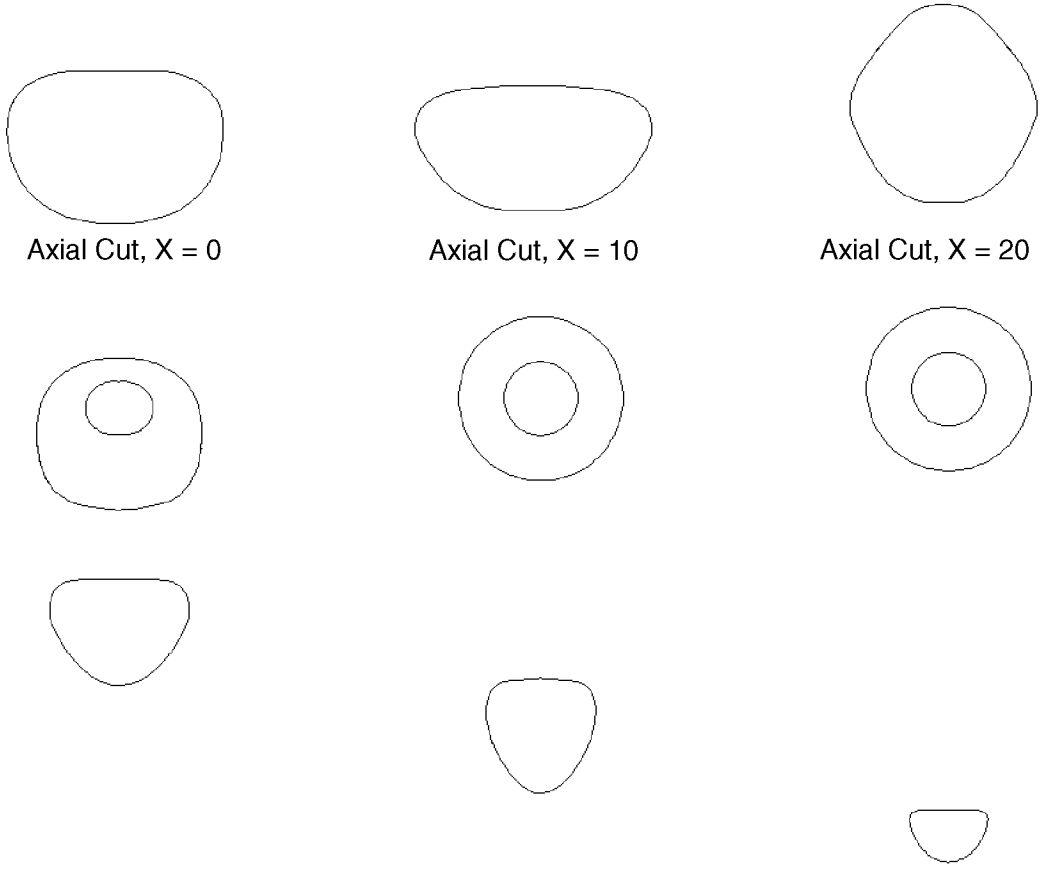

Fig. 22e S-duct engine inlet axial cuts (front view, looking downstream).

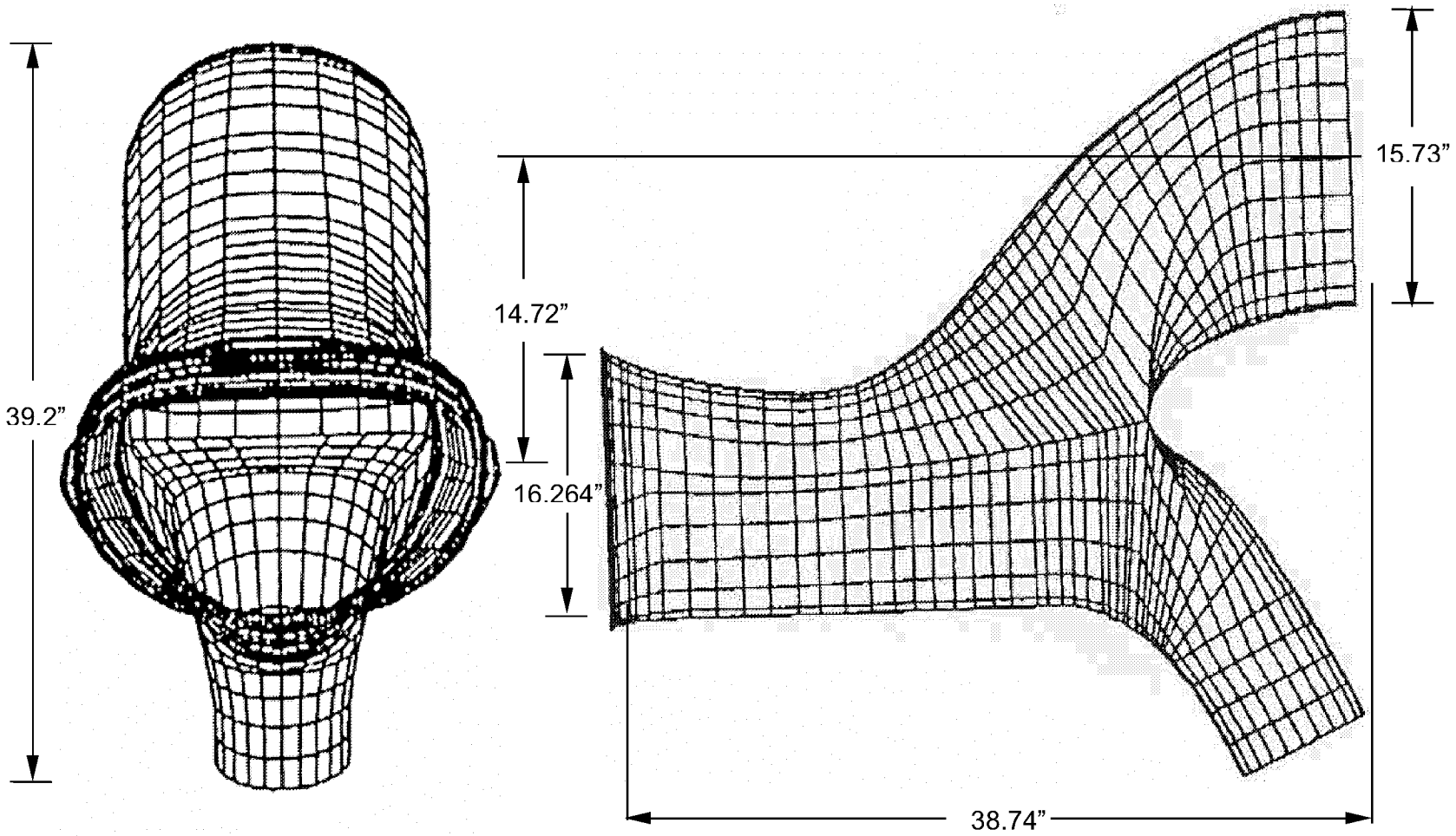

Fig. 22f Dimension of S-duct engine inlet (in inches).

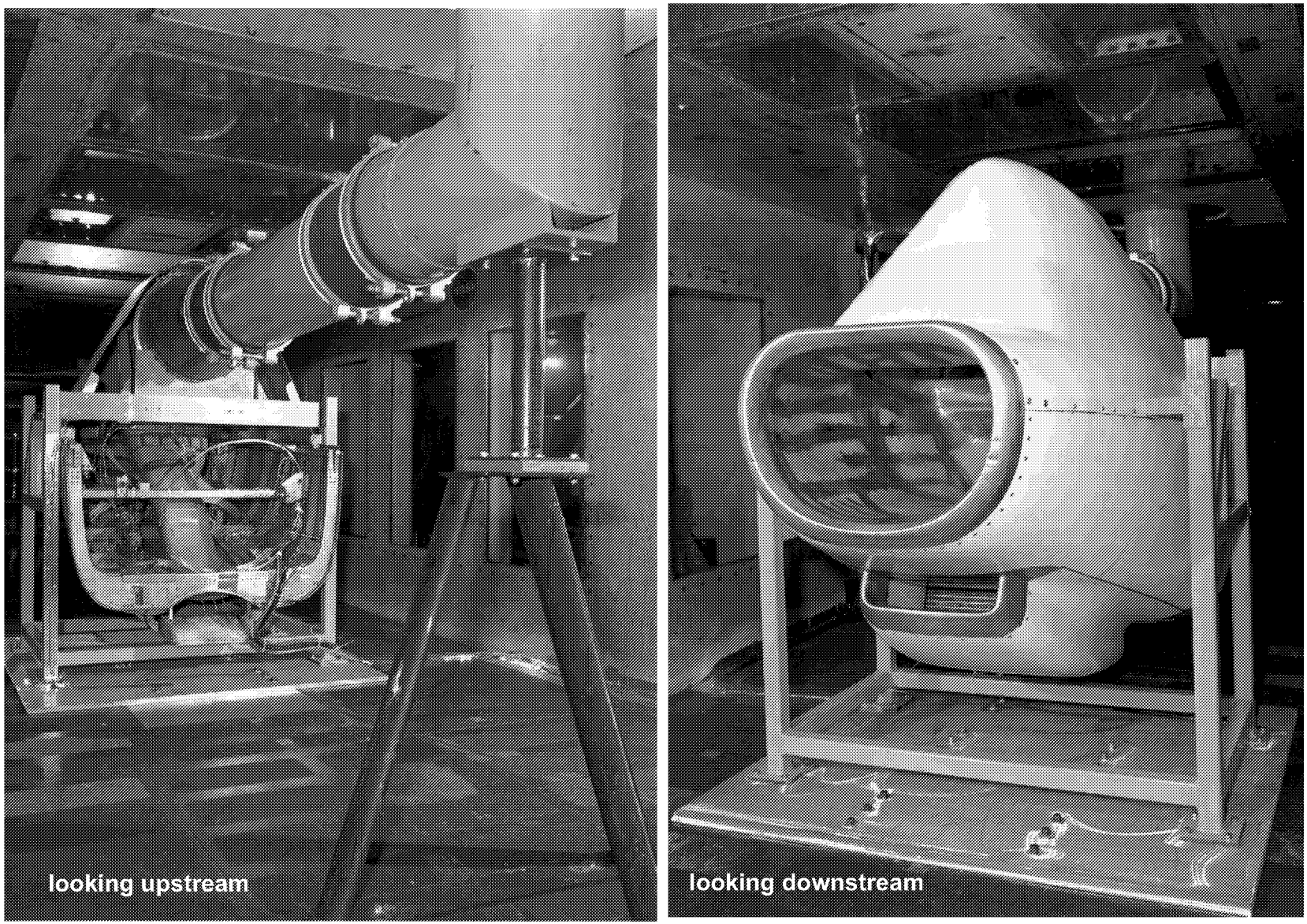

Fig. 22g S-duct engine inlet installed in IRT test section (looking downstream).

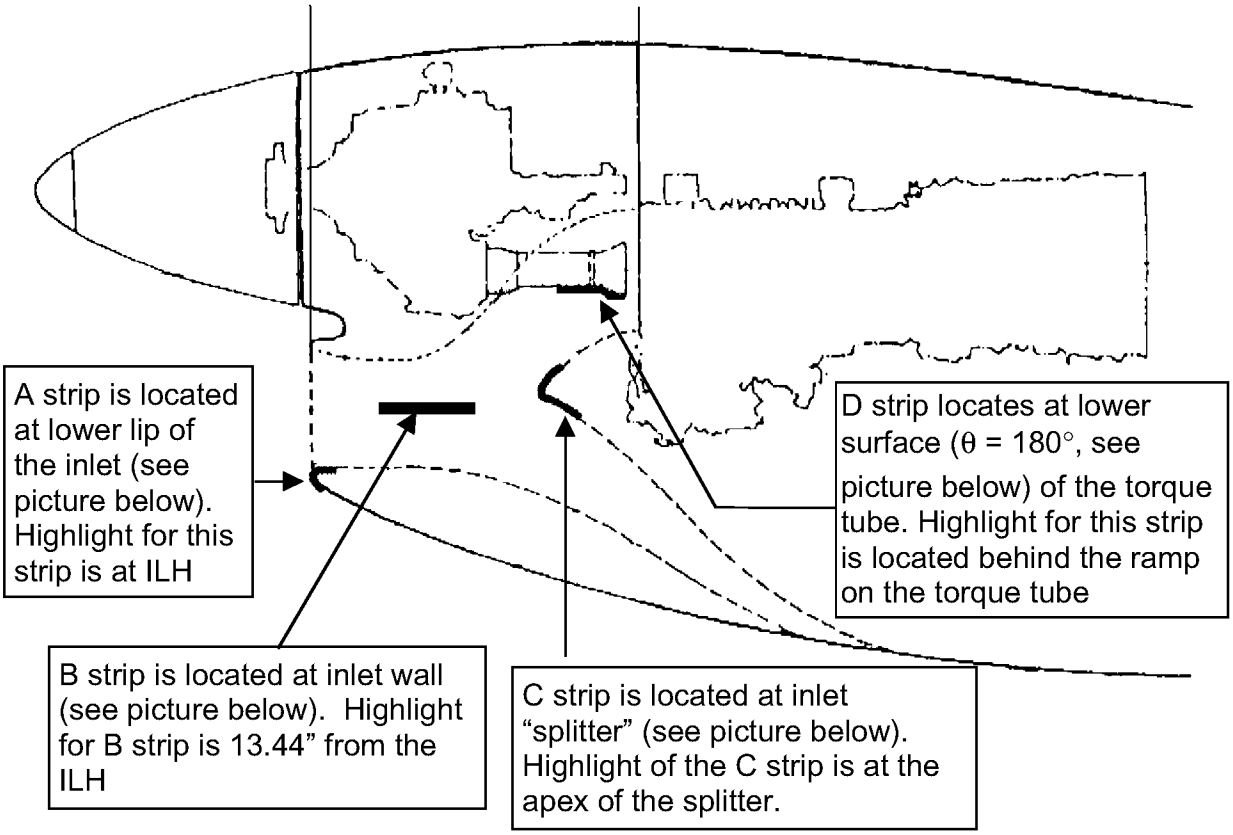

ILH = Inlet Lip Highlight, most forward point on the Inlet Lip (see Figure 22a)

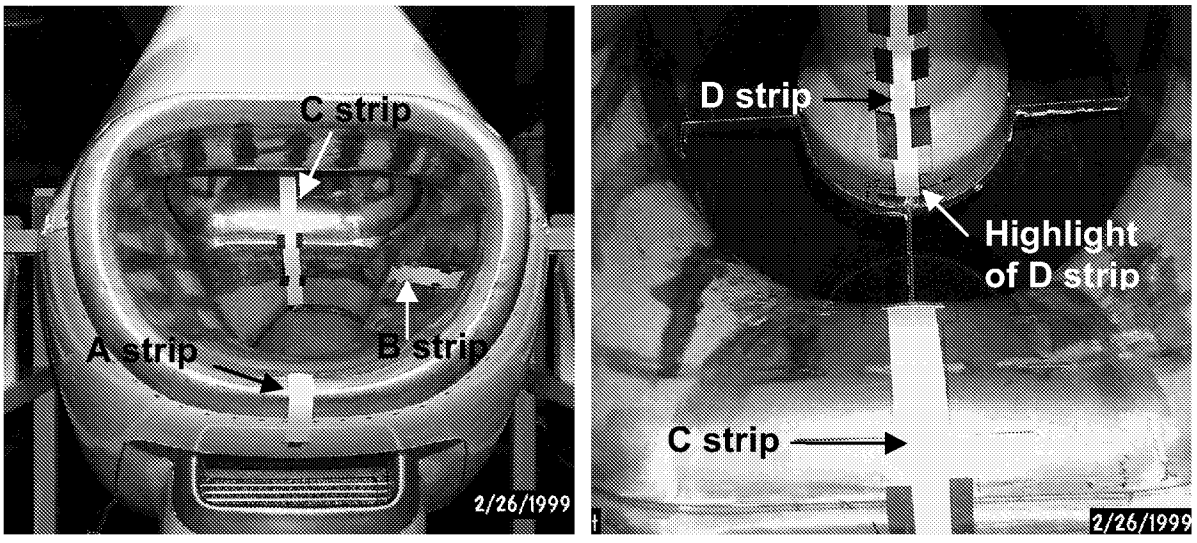

Fig. 22h Blotter strip locations for S-duct engine inlet geometry (looking downstream, 1999 IRT tests.

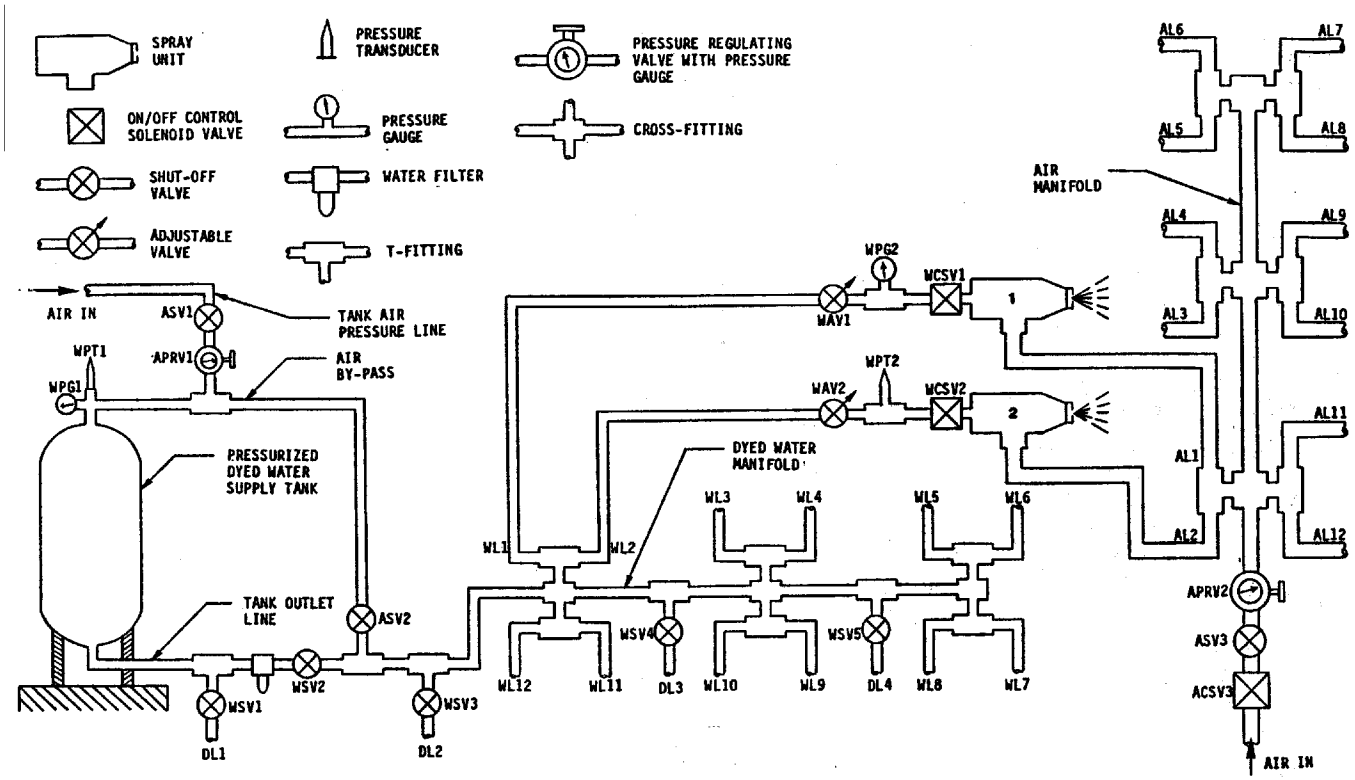

Fig. 23 Schematic of Original WSU 12–nozzle spray system used during the 1985 and 1989 impingement tests.

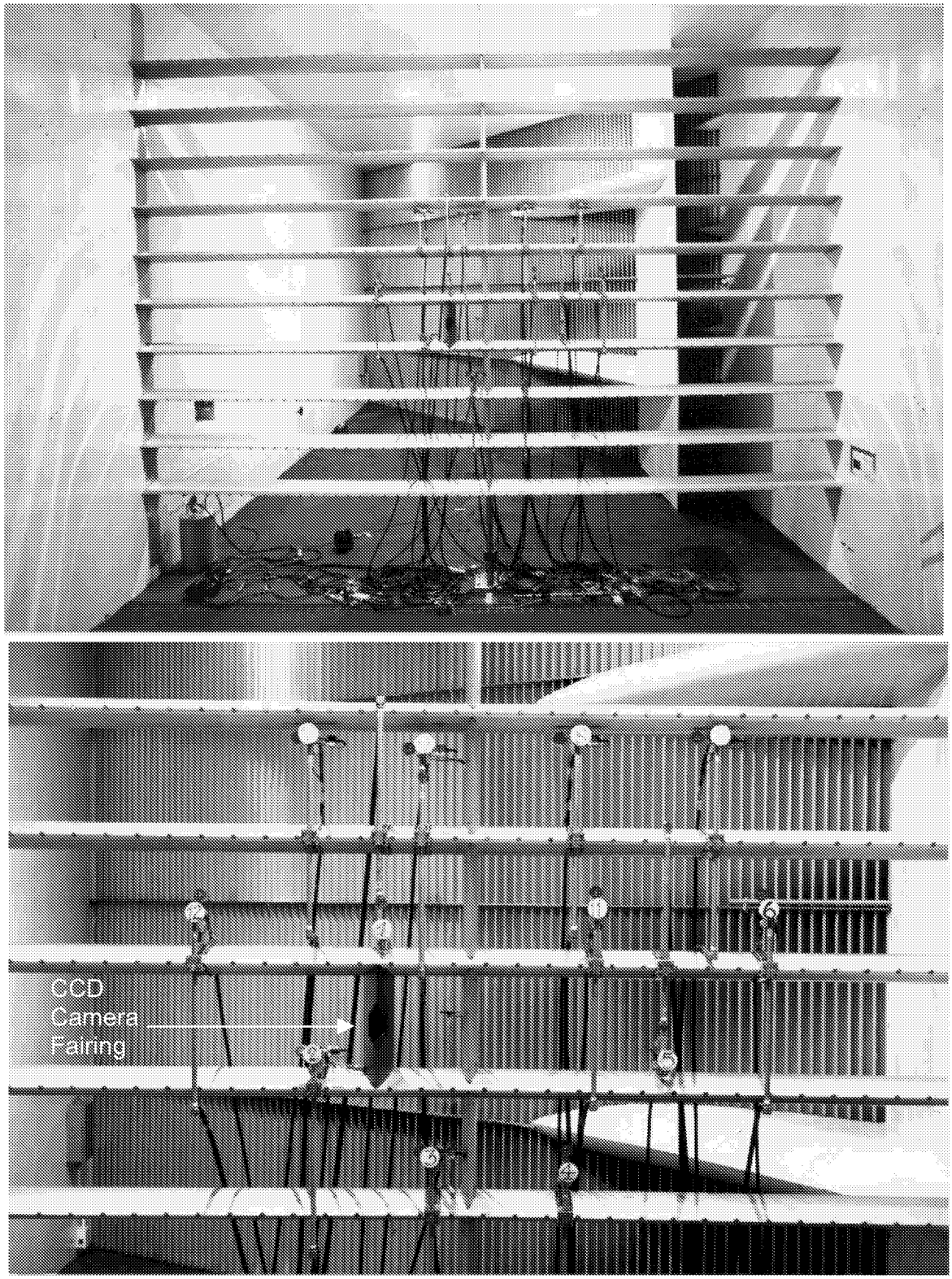

Fig. 24 WSU spray system installed in IRT plenum chamber (1997 IRT entry).

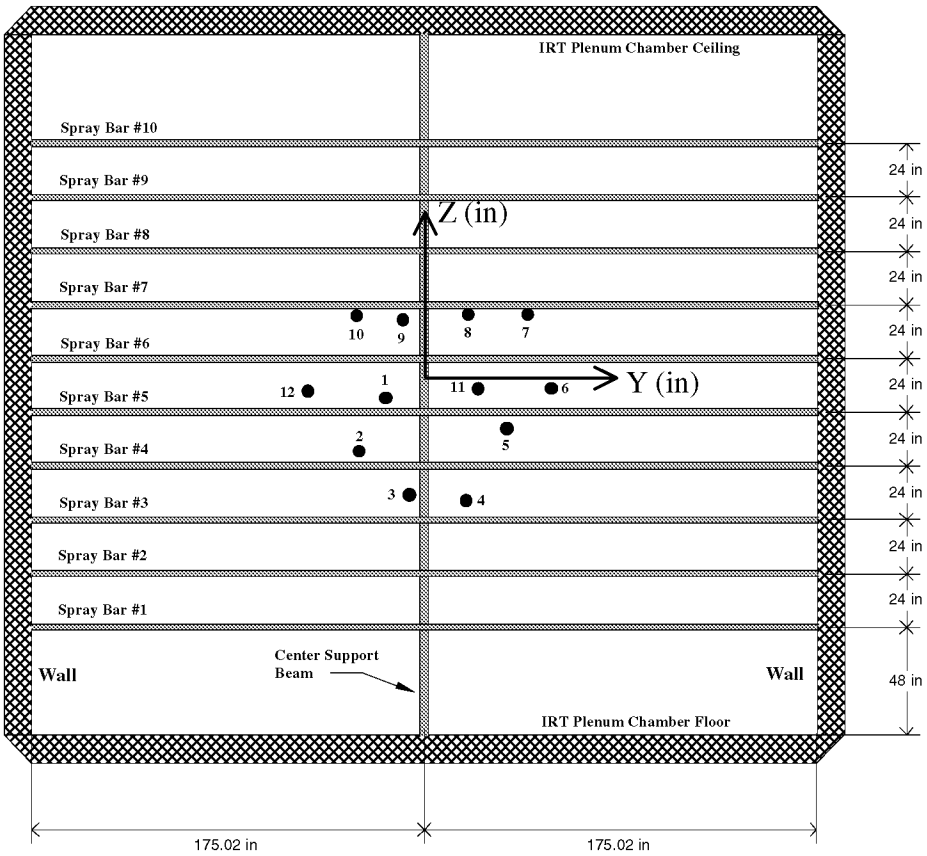

(1997 WSU spray system; all dimensions in inches)

WSU Nozzle Assembly #	NASA MOD-1 Nozzle #	C_f	Y-Coordinate (in) (Notes:1,2)	Z-Coordinates (in) (Note:1)
1	277	0.00400	-17.250	+6.750/SP5
2	306	0.00399	-29.375	+6.750/SP4
3	279	0.00399	-6.750	+11.250/SP3
4	217	0.00398	+18.500	+8.750/SP3
5	308	0.00401	+37.000	+17.125/SP4
6	311	0.00406	+56.500	+11.000/SP5
7	210	0.00402	+46.250	-4.000/SP7
8	233	0.00400	+19.750	-4.250/SP7
9	242	0.00401	-9.500	-6.500/SP7
10	243	0.00401	-30.250	-4.750/SP7
11	249	0.00401	+23.750	+10.750/SP5
12	252	0.00403	-52.000	+9.500/SP5

1. Positive Y to the right looking upstream measured from trailing edge of center beam.
2. Example: WSU Nozzle Assembly # 11. Y = 23.750 inches to the right of center beam, looking upstream. Z = +10.750/SP5, i.e., 10.75 inches above trailing edge (upstream edge) of spray bar #5 (SP5).

Fig. 25 WSU spray system nozzle locations with respect to the IRT spray bars (1997 IRT Entry).

Fig. 26 WSU spray system installed in IRT plenum chamber (1999 IRT entry).

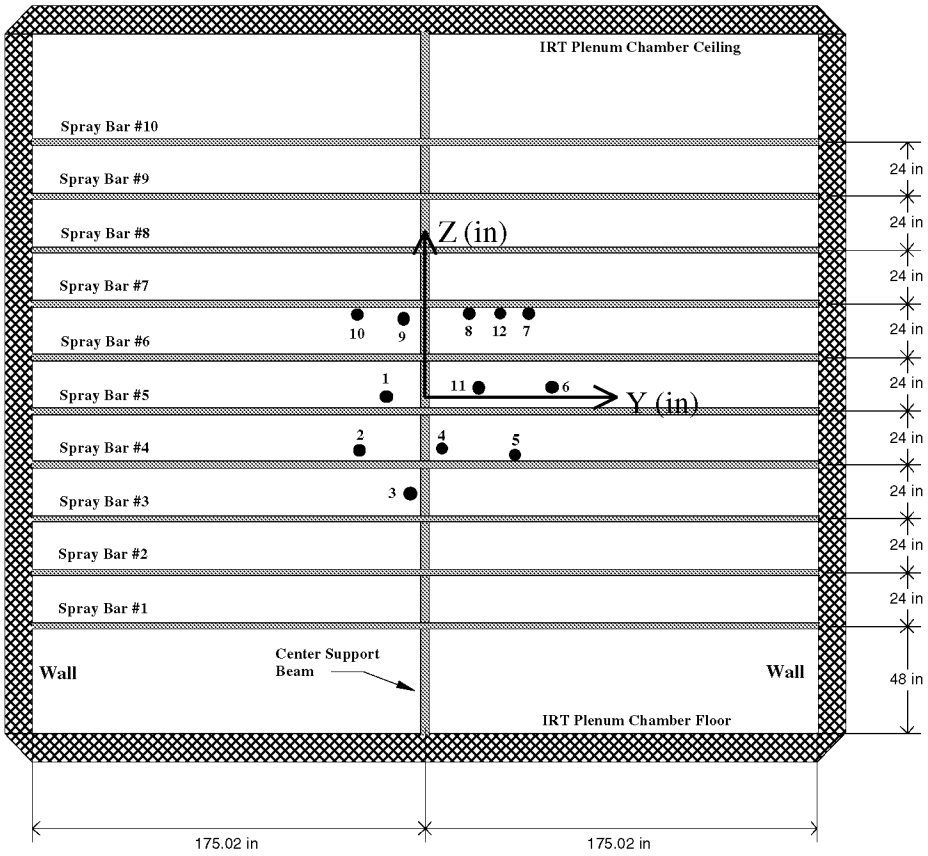

(1999 WSU spray system; all dimensions in inches)

WSU Nozzle Assembly #	NASA MOD-1 Nozzle #	C_f	Y-Coordinate (in) (Notes:1,2)	Z-Coordinates (in) (Note:1)
1	277	0.00400	-17.375	-17.375/SP6
2	306	0.00399	-31.750	+8.250/SP4
3	234	0.00399	-6.750	+11.250/SP3
4	217	0.00398	+7.750	+7.500/SP4
5	308	0.00401	+37.000	-17.375/SP5
6	243	0.00406	+56.500	+11.125/SP5
7	210	0.00402	+46.125	+20.250/SP6
8	233	0.00400	+9.000	+18.000/SP6
9	242	0.00401	-9.250	+17.500/SP6
10	311	0.00401	-37.500	+17.125/SP6
11	249	0.00401	+24.000	+11.000/SP5
12	252	0.00403	+26.000	+17.000/SP6

Fig. 27 WSU spray system nozzle locations with respect to the IRT spray bars (1999 IRT entry).

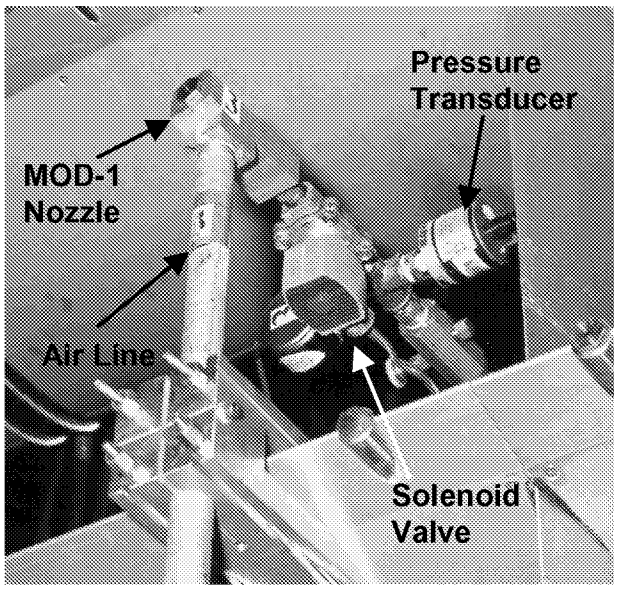

Fig. 28 Close up of WSU nozzle assembly.

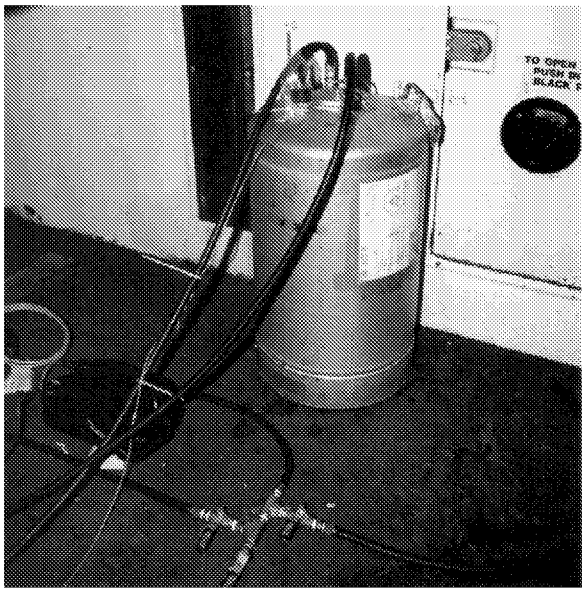

Fig. 29 Stainless steel pressure tank.

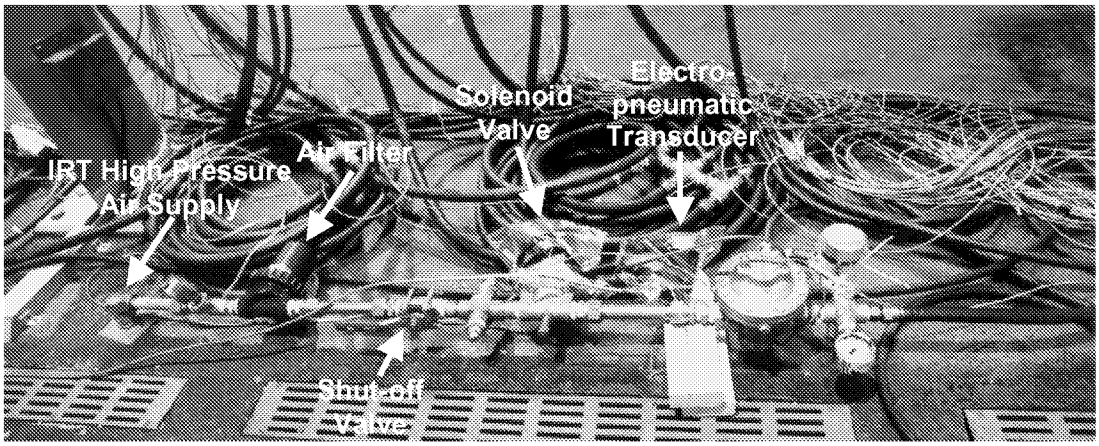

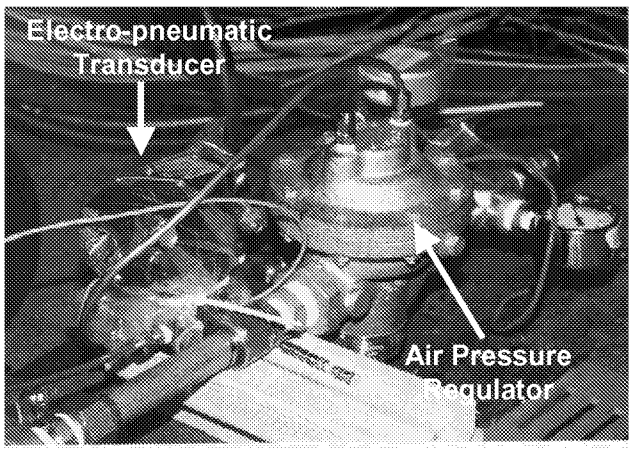

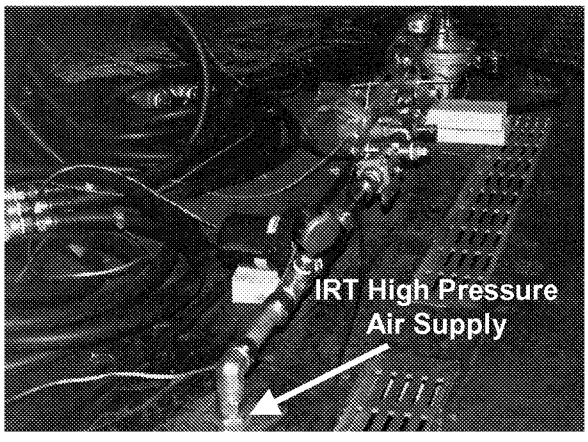

Fig. 30 Main air supply control system for WSU spray nozzles.

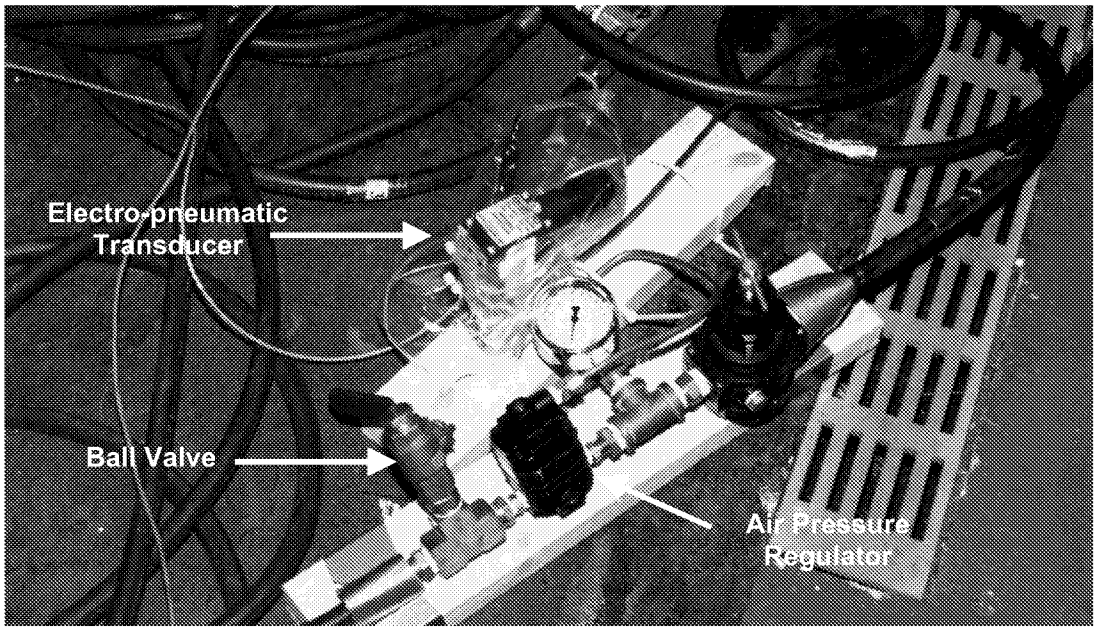

Fig. 31a Main water supply control system for WSU spray nozzles.

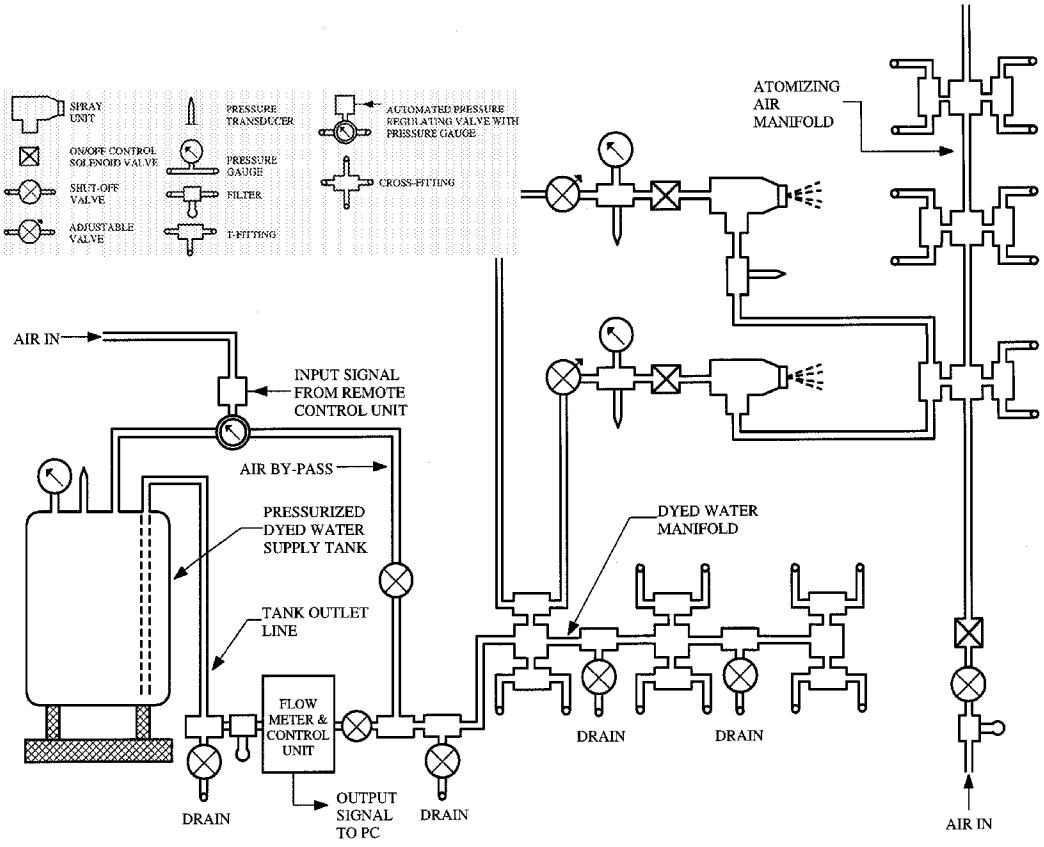

Fig. 31b Schematic of Improved WSU 12–nozzle spray system used during the 1997 and 1999 impingement tests.

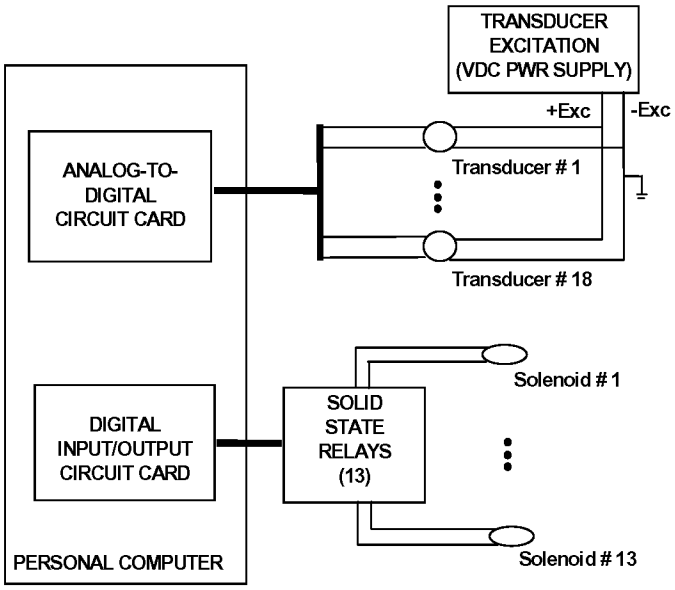

Fig. 32 Simplified data acquisition system block diagram.

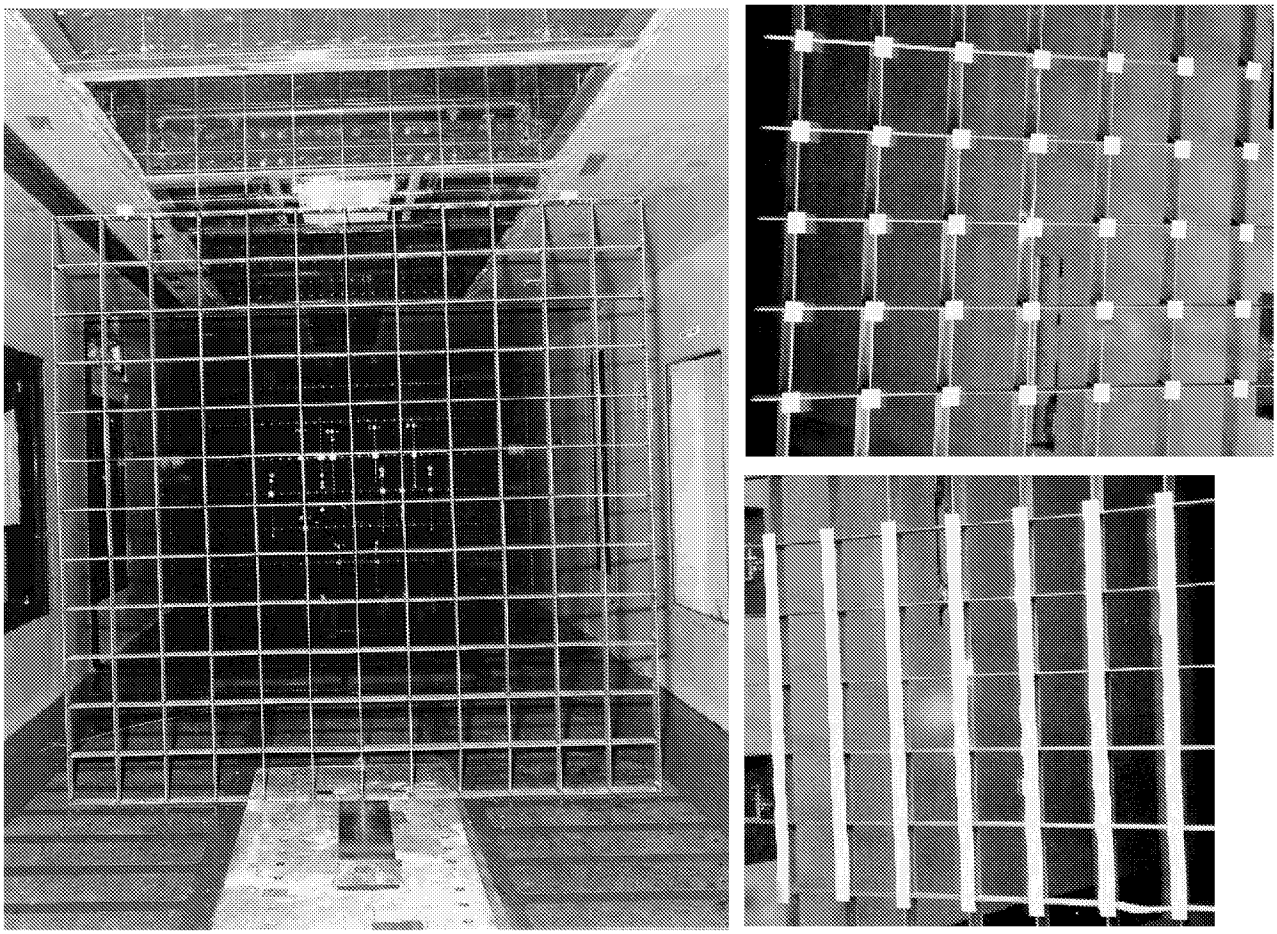

Fig. 33 6-ft by 6-ft uniformity grid with/without blotter squares or strips.

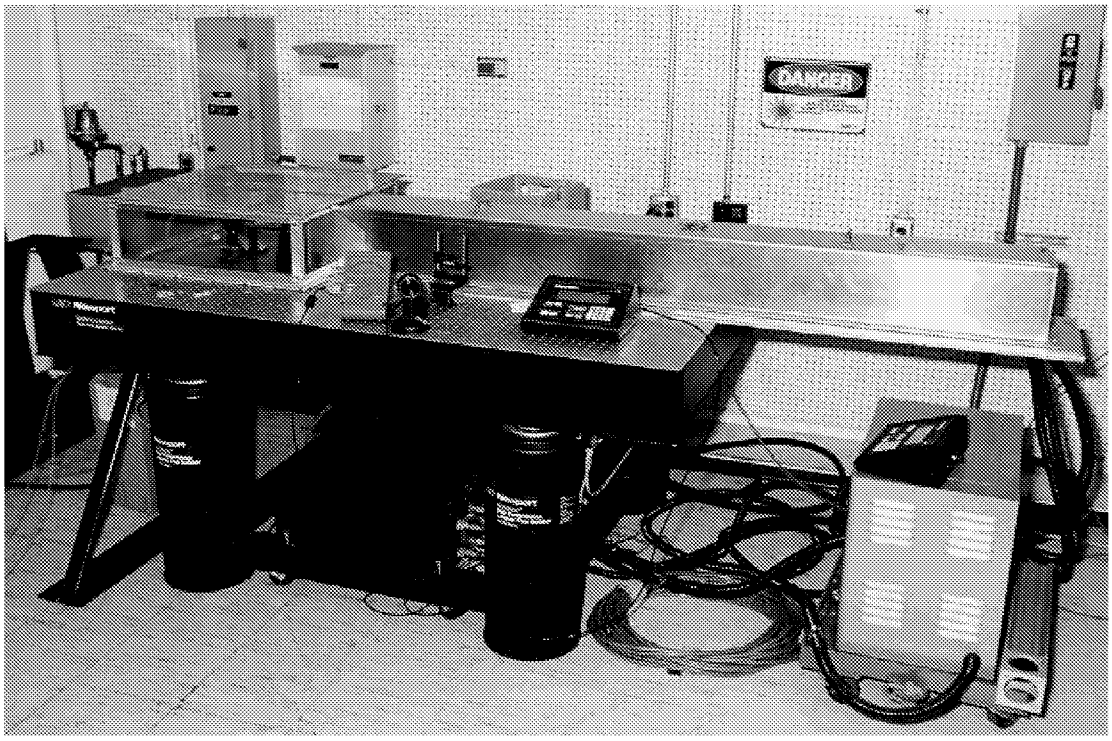

Fig. 34 Argon-Ion laser emission.

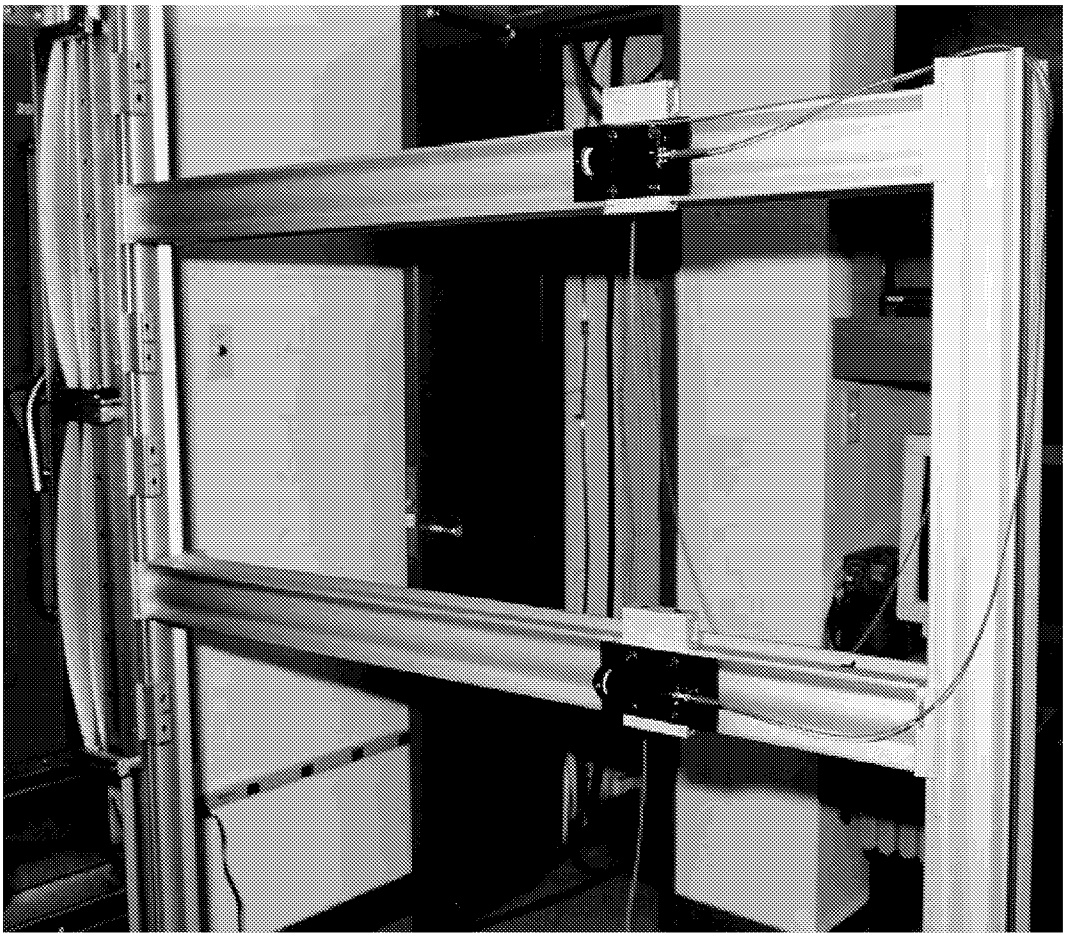

Fig. 35 Laser sheet set up.

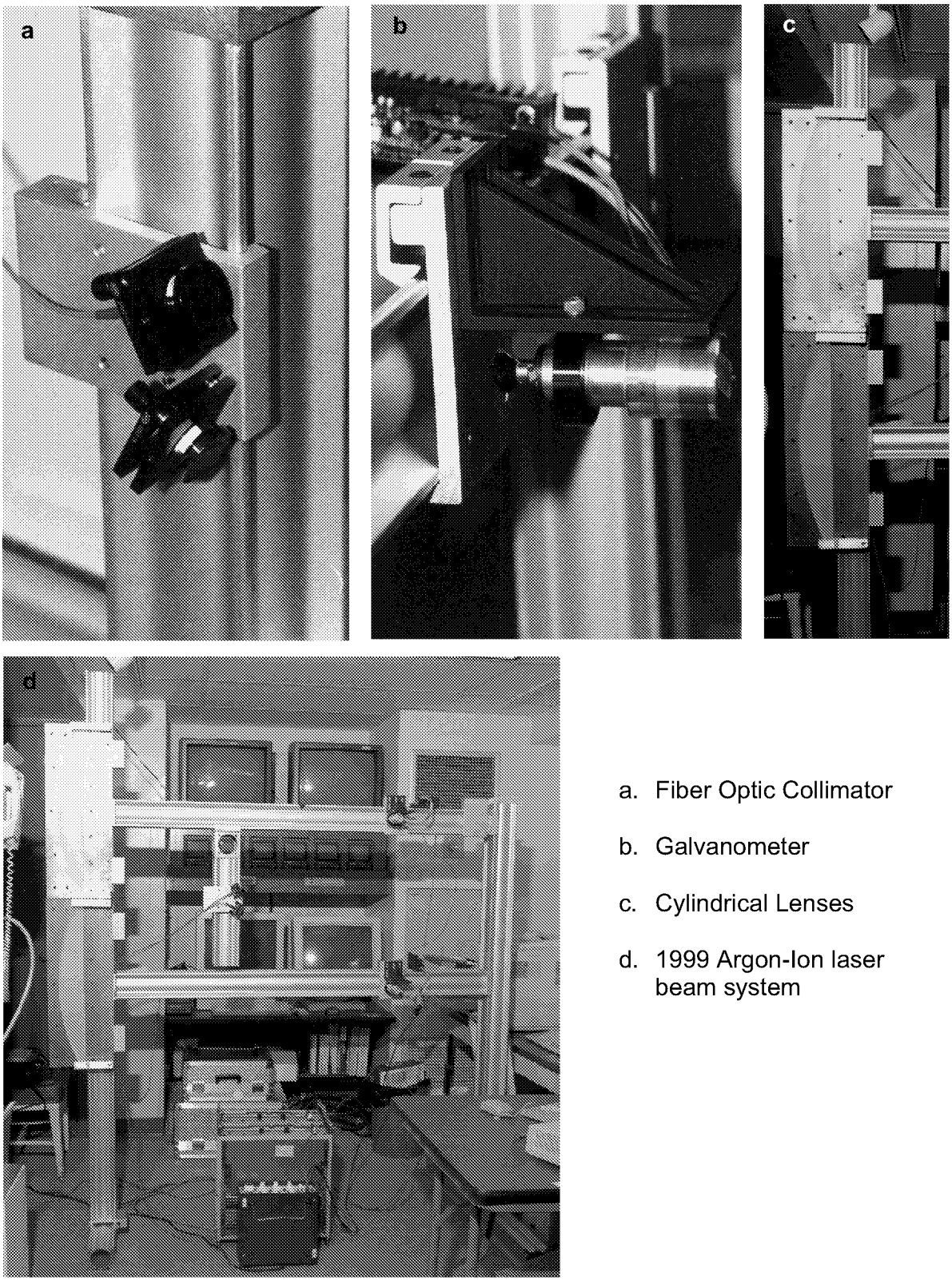

a. Fiber Optic Collimator

b. Galvanometer

c. Cylindrical Lenses

d. 1999 Argon-Ion laser beam system

Fig. 36 Key components of Argon-Ion laser beam system (1999 IRT entry).

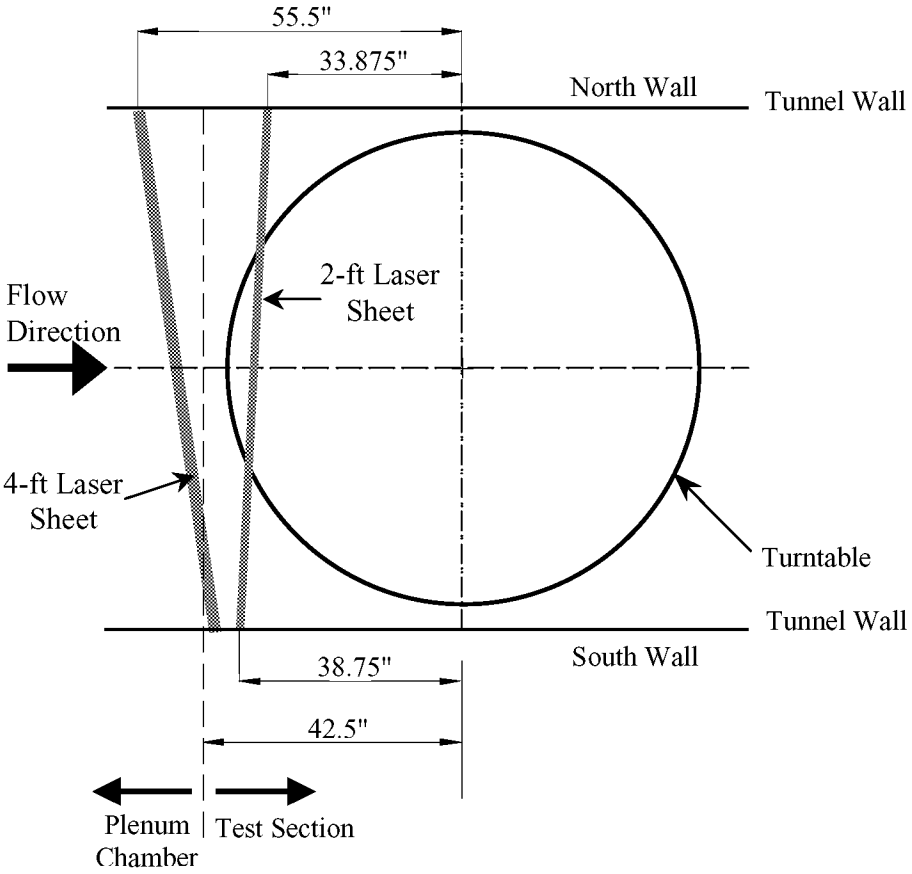

Fig. 37 Laser sheets axial locations in IRT test section.

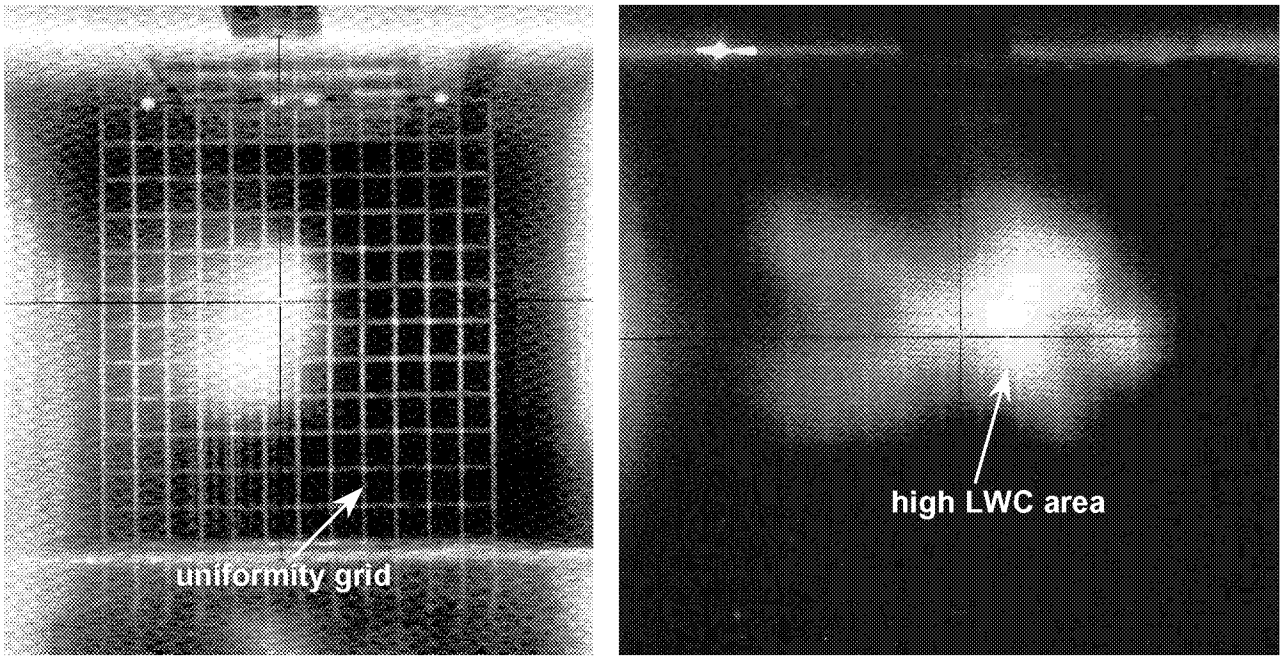

Fig. 38 CCD cloud images in IRT test section.

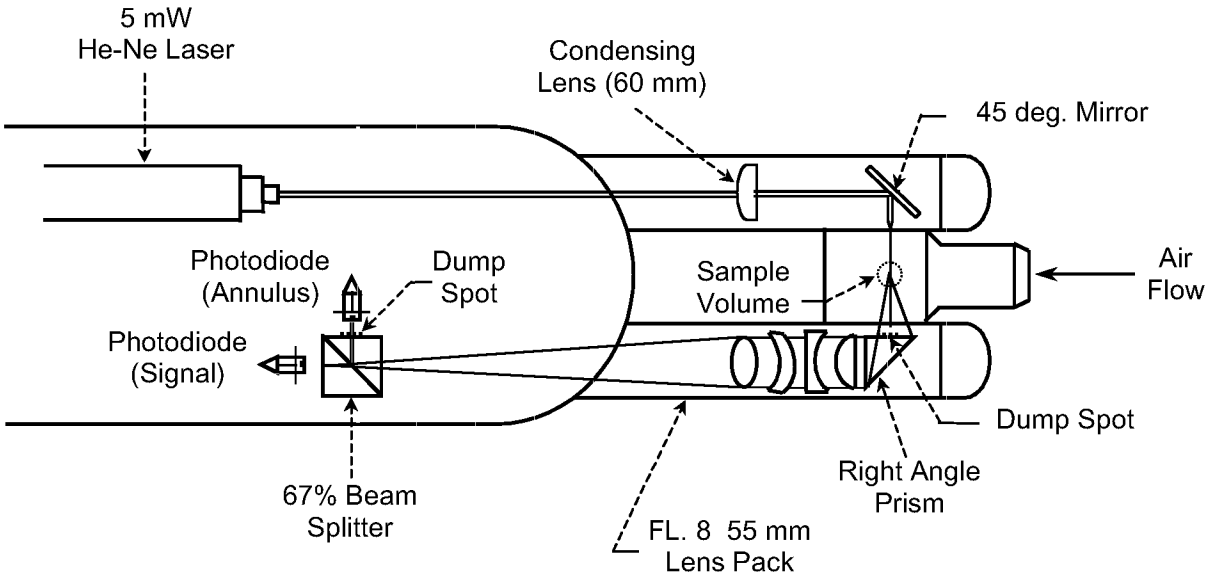

a. Forward Scattering Spectrometer Probe (FSSP) optical configuration.

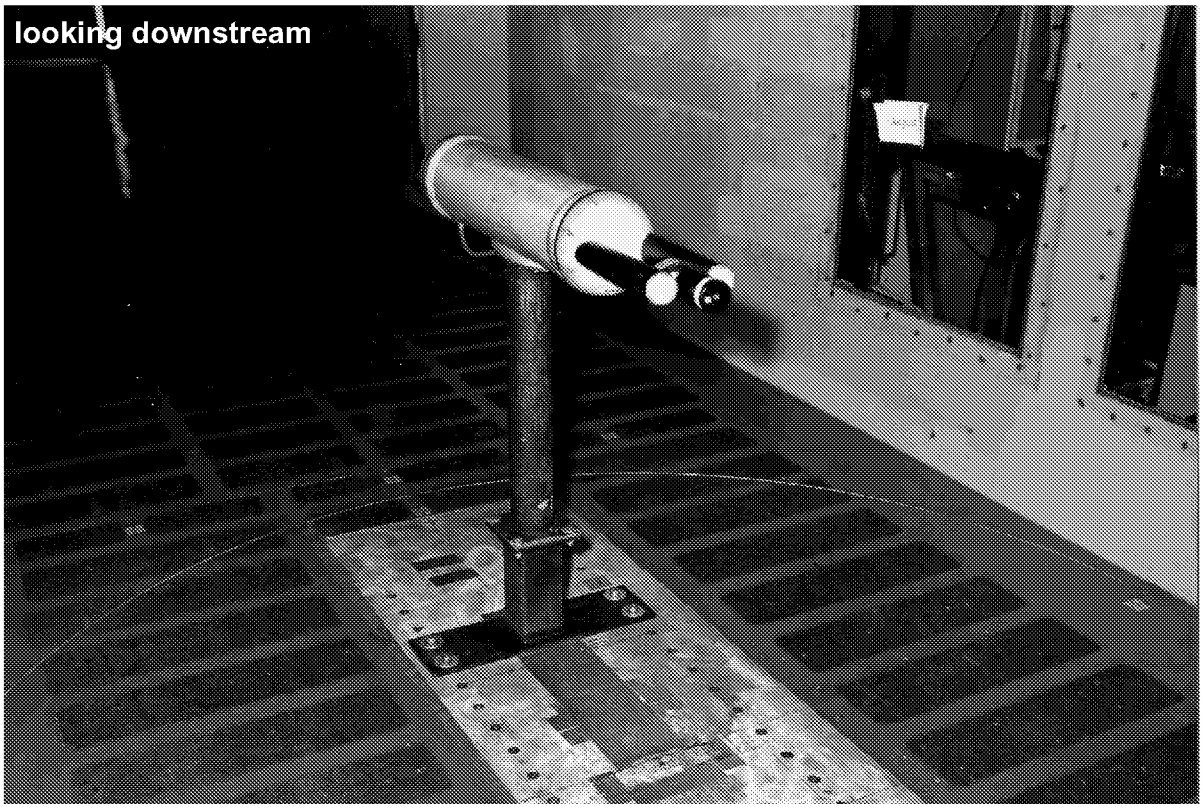

b. FSSP installed in IRT test section

Fig. 39 Forward Scattering Spectrometer Probe (FSSP).

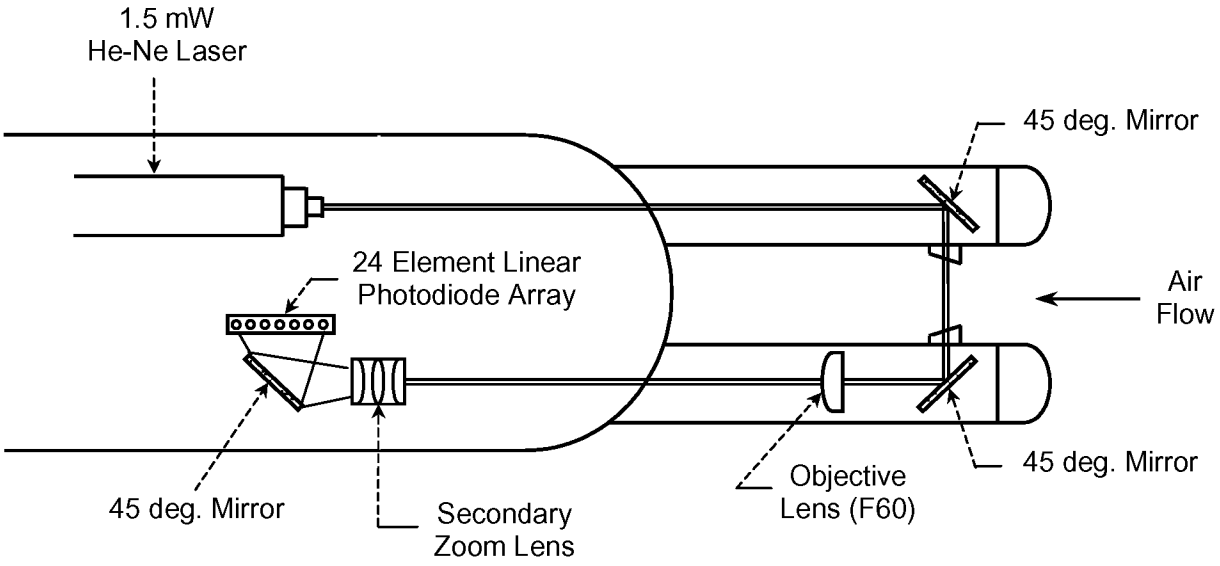

Fig. 40 Optical Array Probe (OAP).

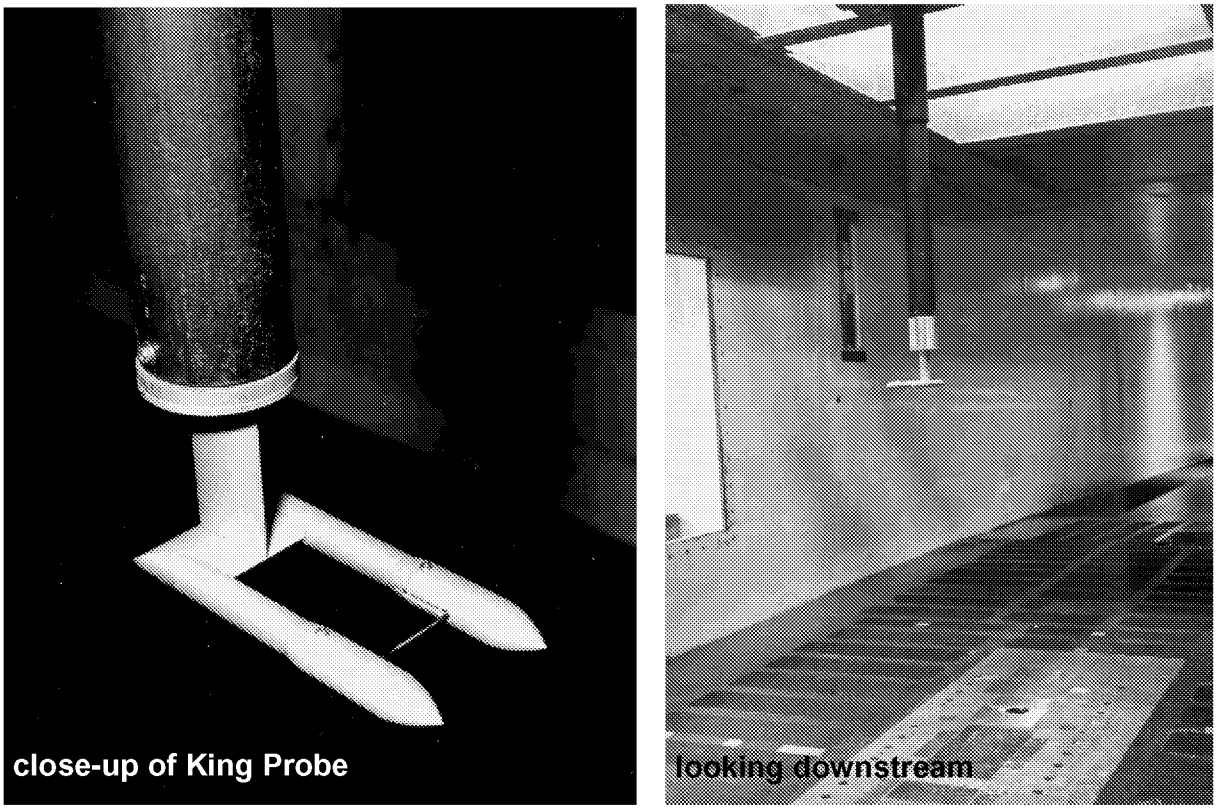

Fig. 41 King Probe installed in IRT test section.

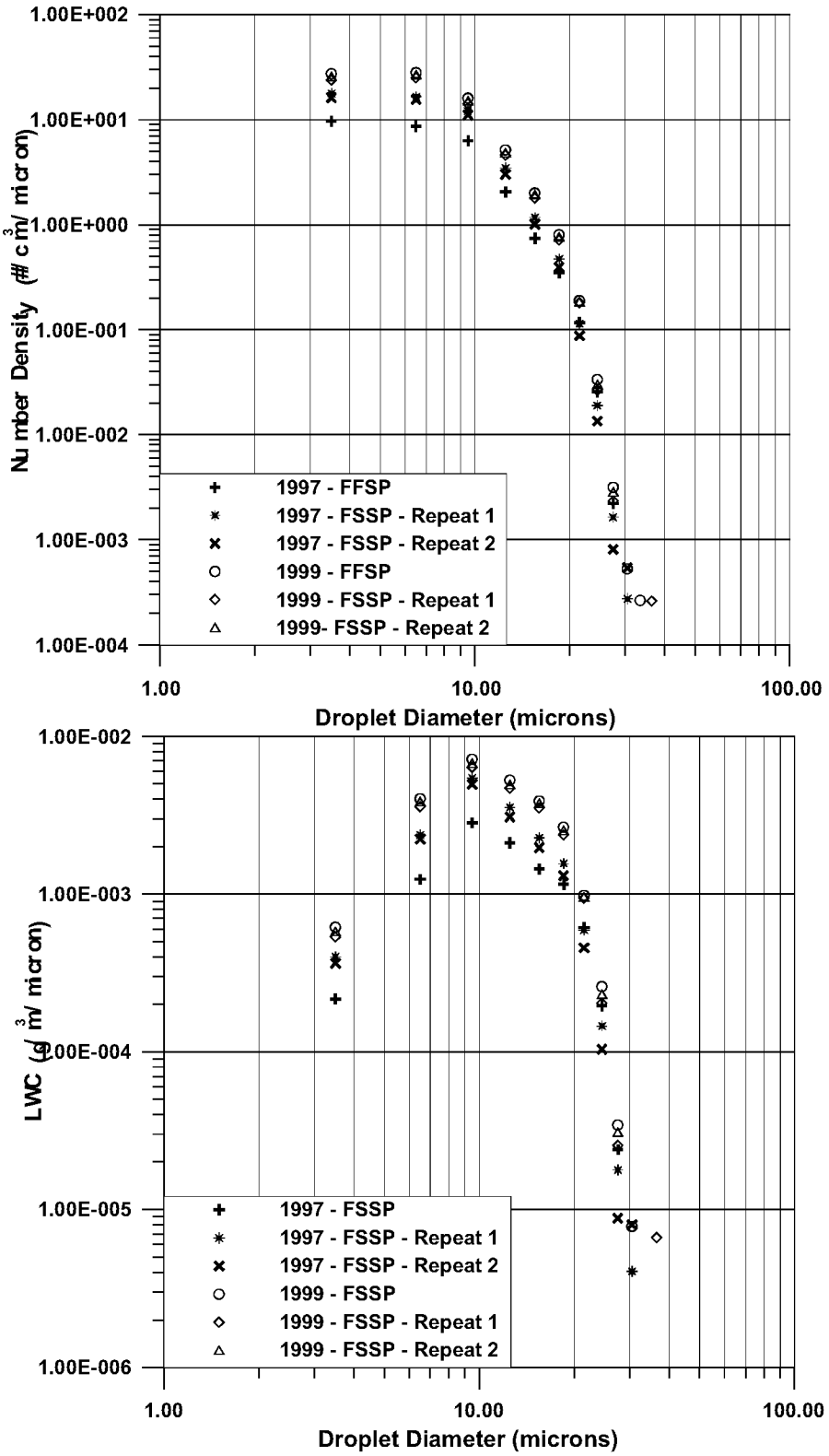

Fig. 42a Measured MVD and LWC distributions for 1997 and 1999 IRT tests (MVD = 11, 11.5 μm) (Continued).

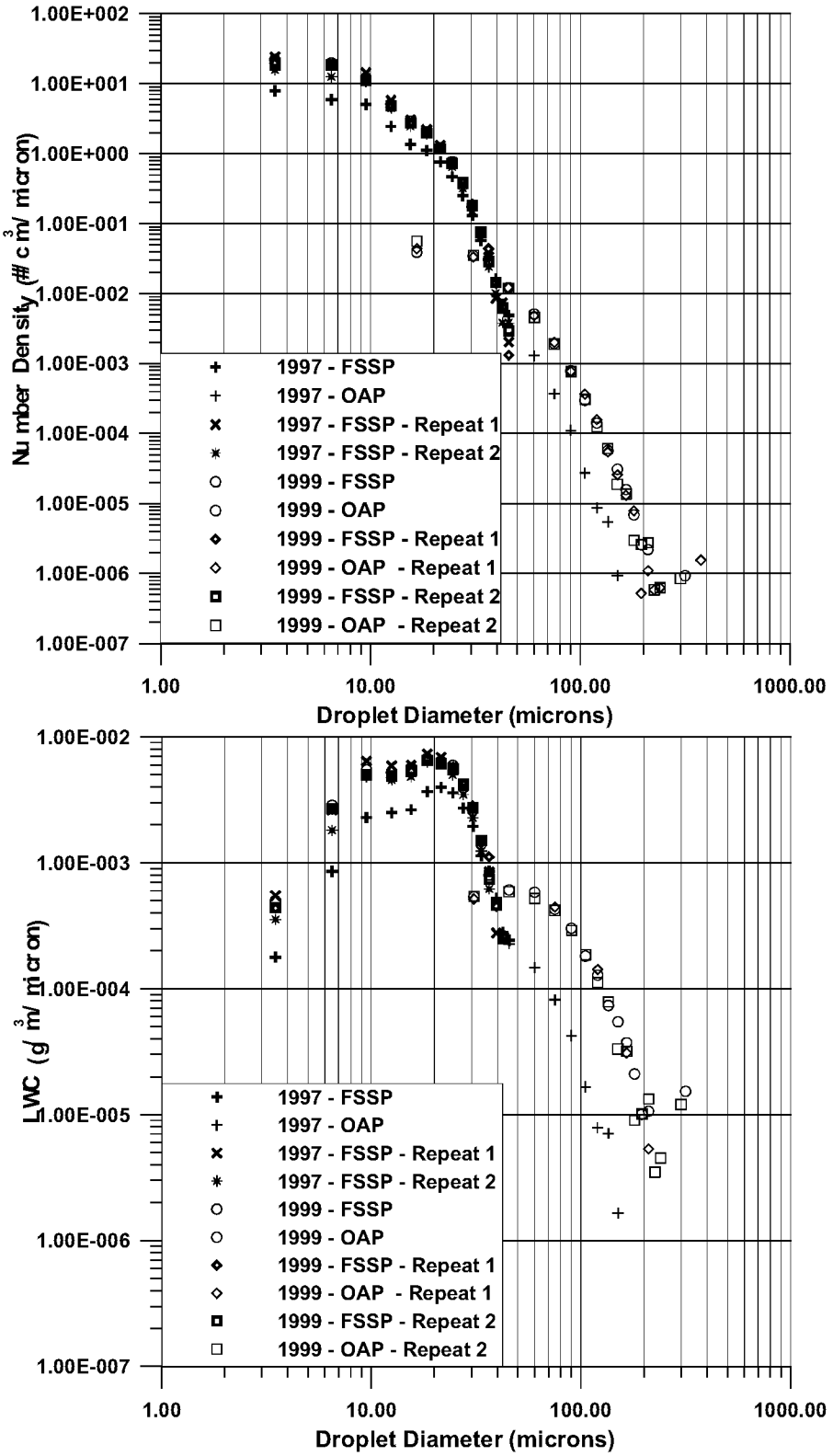

Fig. 42b Measured MVD and LWC distributions for 1997 and 1999 IRT tests (MVD = 21 μm) (Continued).

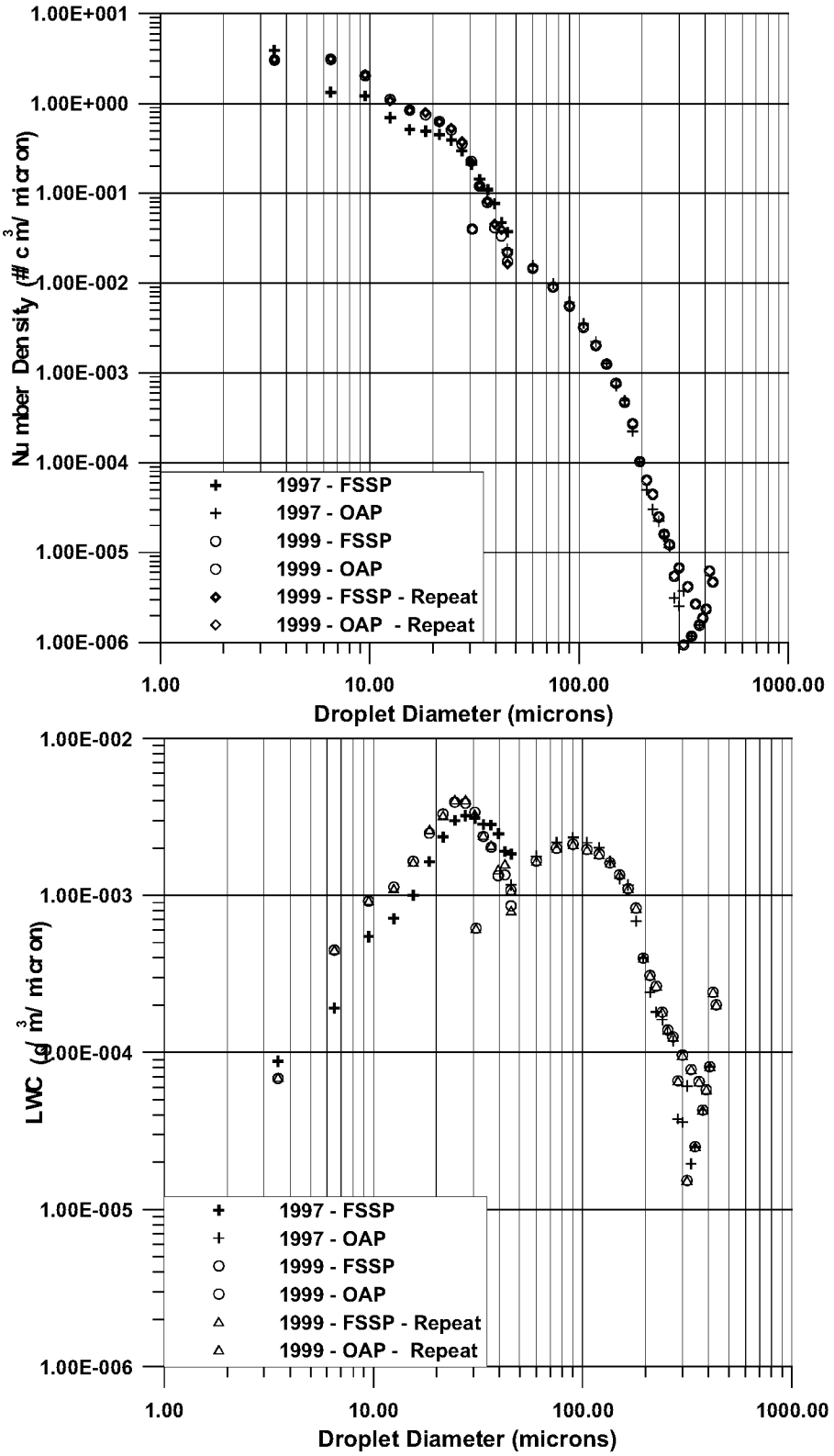

Fig. 42c Measured MVD and LWC distributions for 1997 and 1999 IRT tests (MVD = 92, 94 μm).

Fig. 43 Collector mechanism installed in IRT test section.

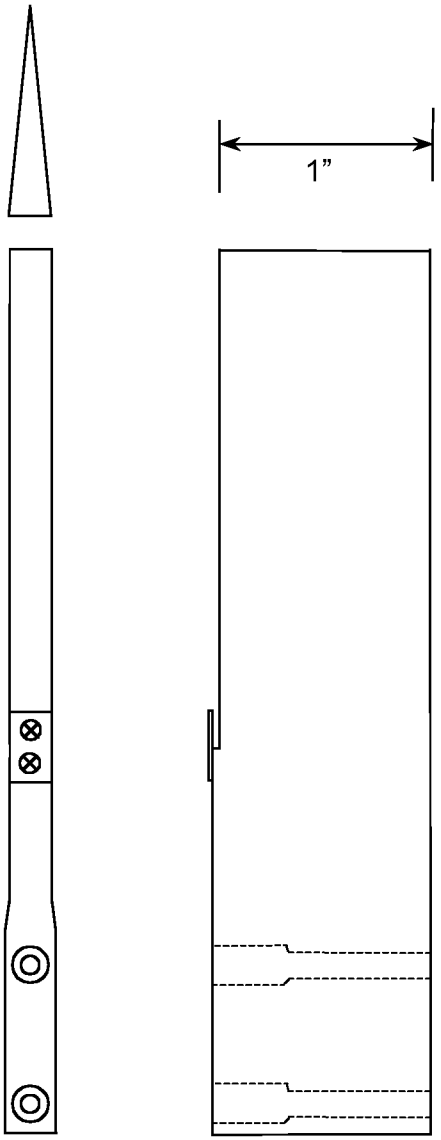

Fig. 44 Collector blade geometry (not to scale).

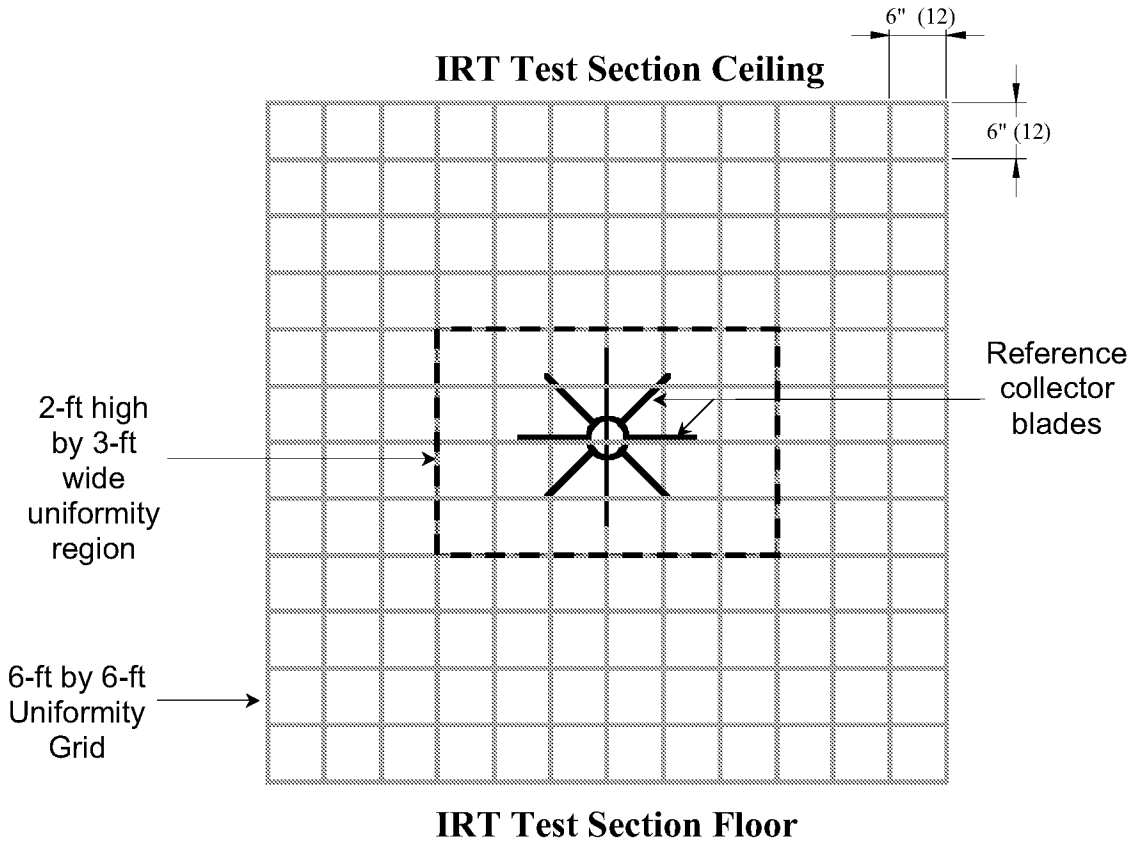

Fig. 45 Location of the collector mechanism with respect to the uniformity grid.

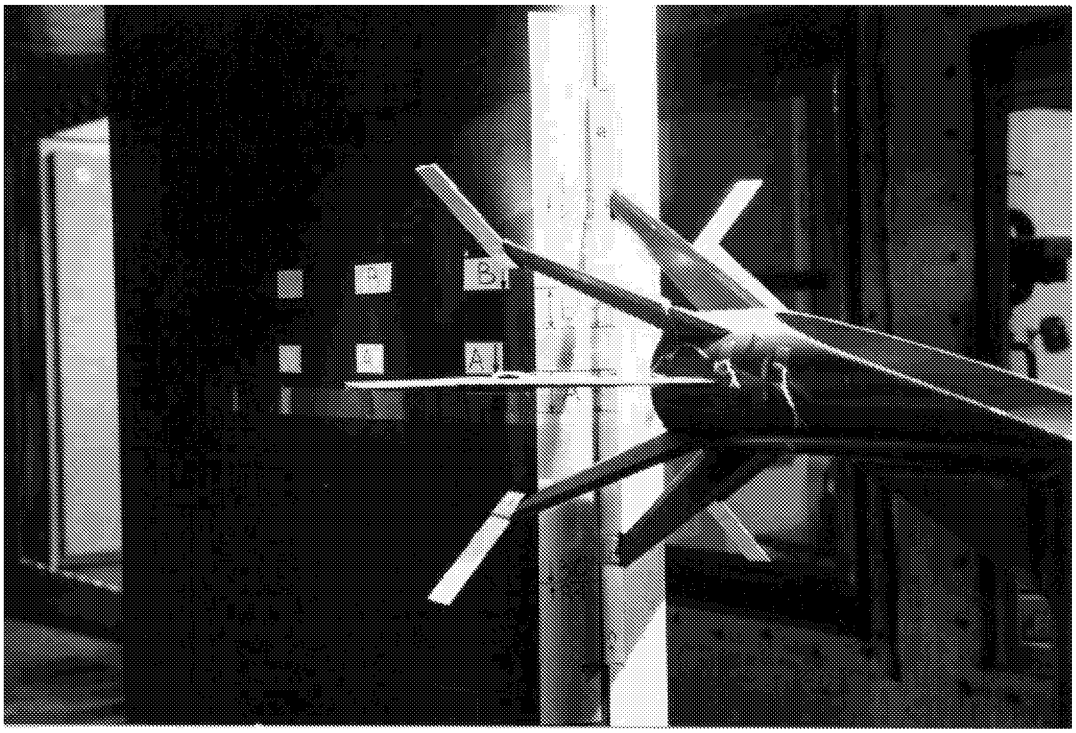

Fig. 46 Close up of the reference collector matching the blotter strips locations on a MS(1)-0317 airfoil.

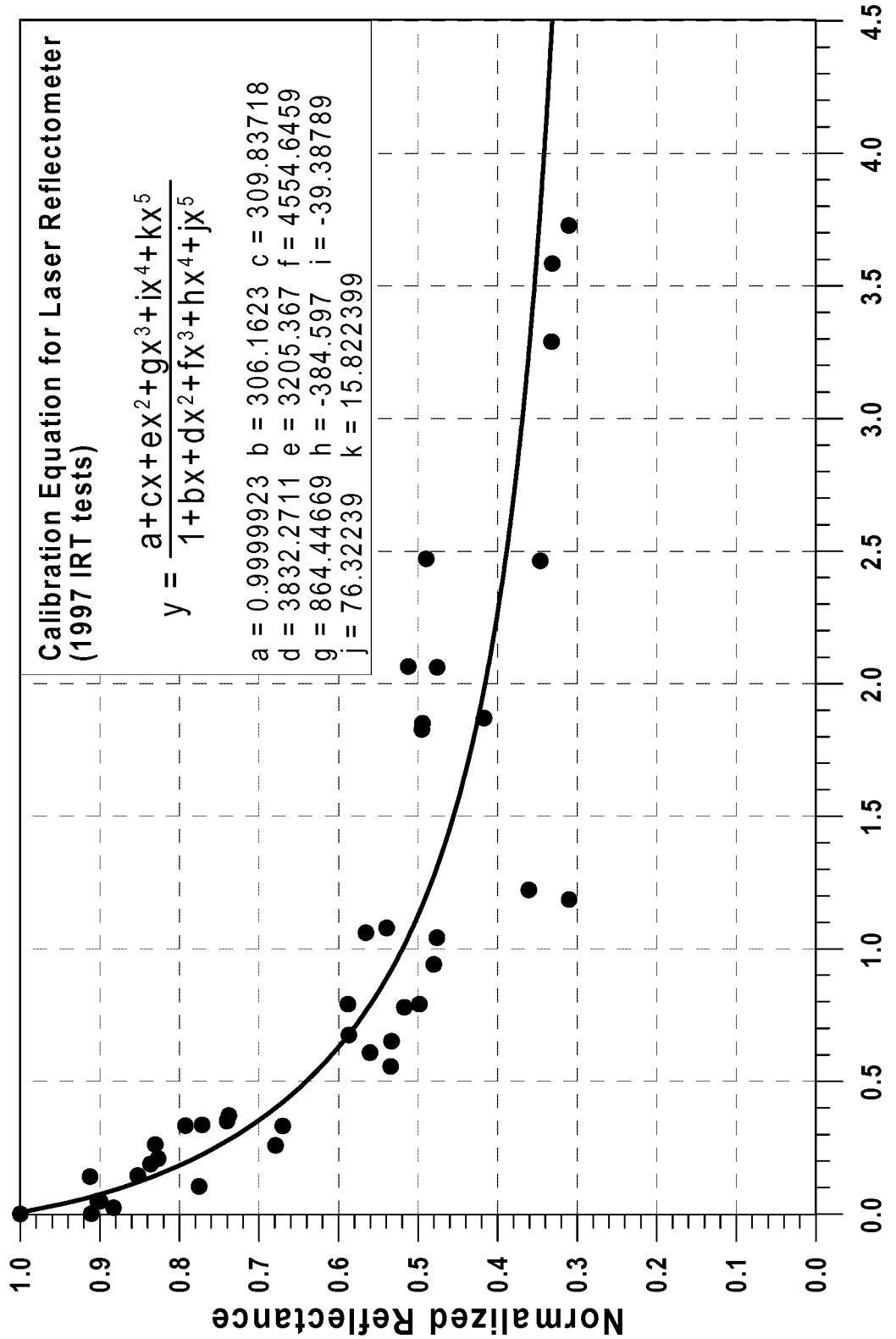

Fig. 47 Laser Reflectometer calibration curve (Verigood 100# paper, 1997 IRT tests).

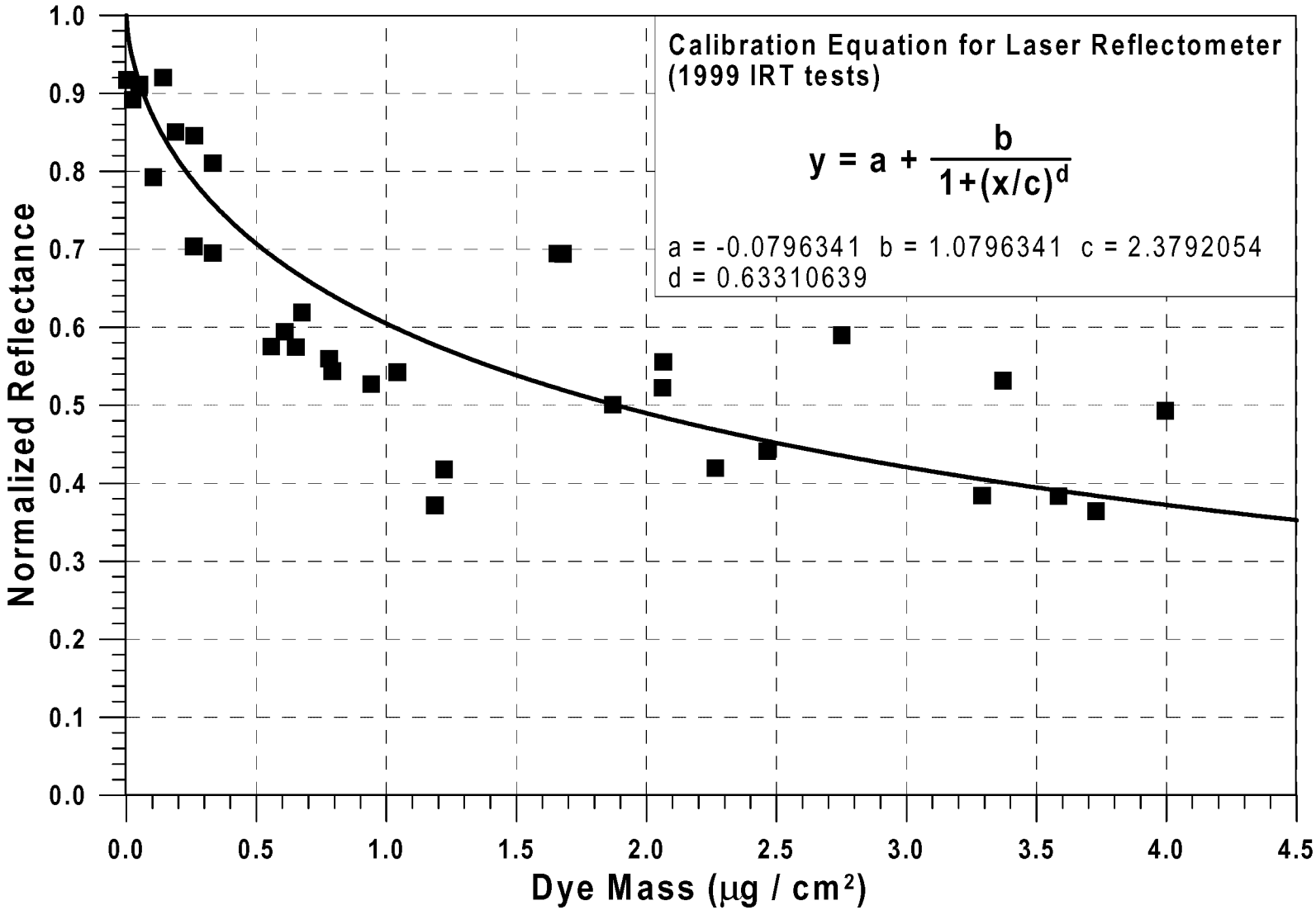

Fig. 48 Laser Reflectometer calibration curve (Verigood 100# blotter paper, 1999 IRT tests).

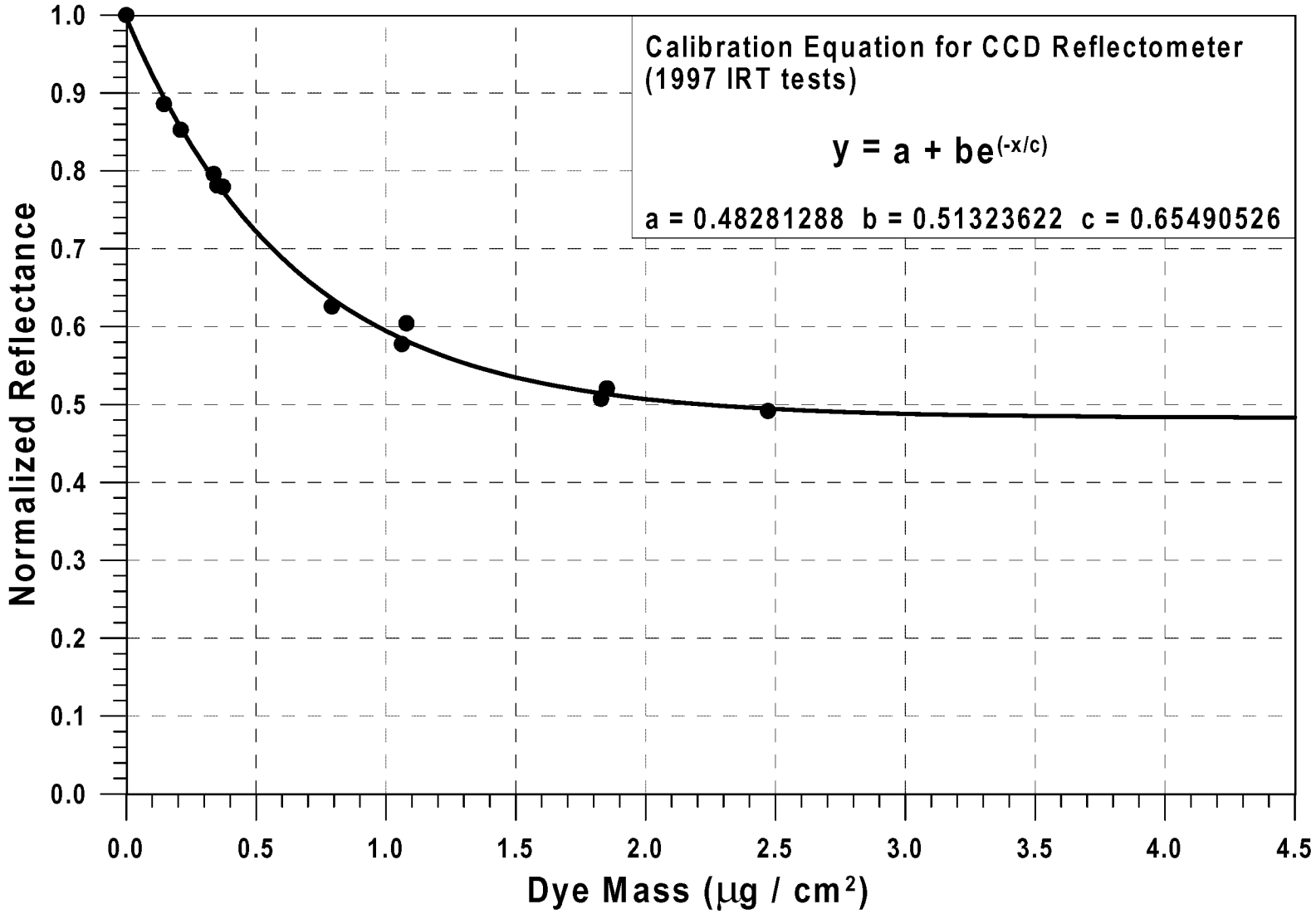

Fig. 49 CCD Reflectometer calibration curve (Verigood 100# blotter paper, 1997 IRT tests).

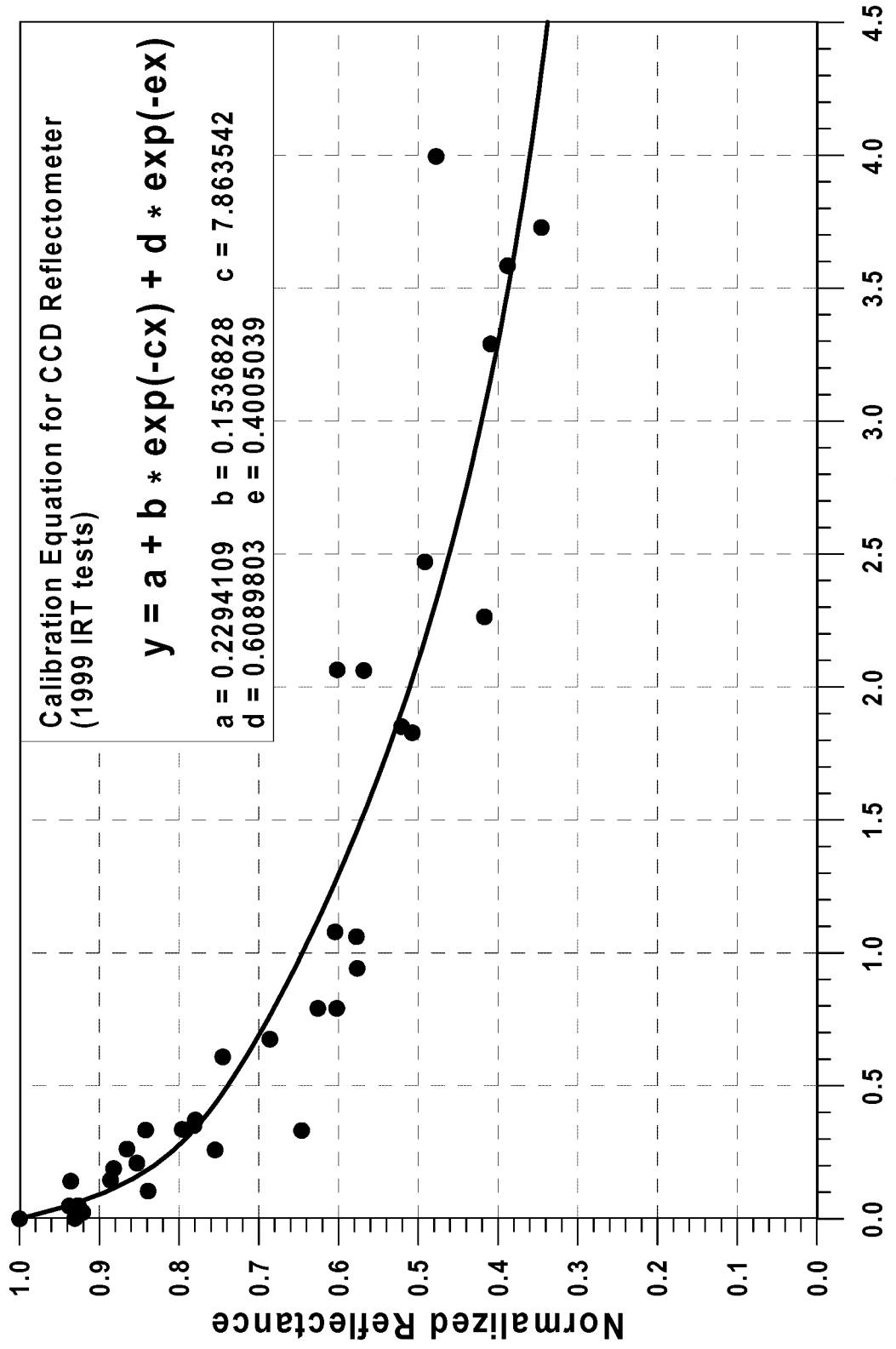

Fig. 50 CCD Reflectometer calibration curve (Verigood 100# blotter paper, 1999 IRT tests).

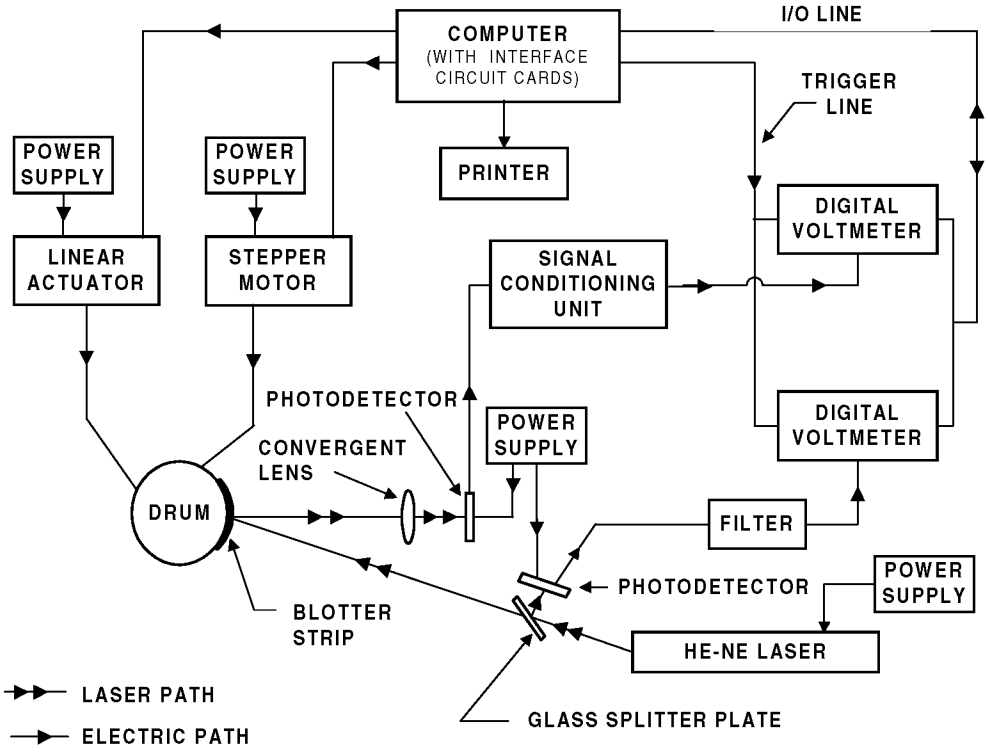

a. Schematic of automated laser reflectometer and digital data acquisition system.

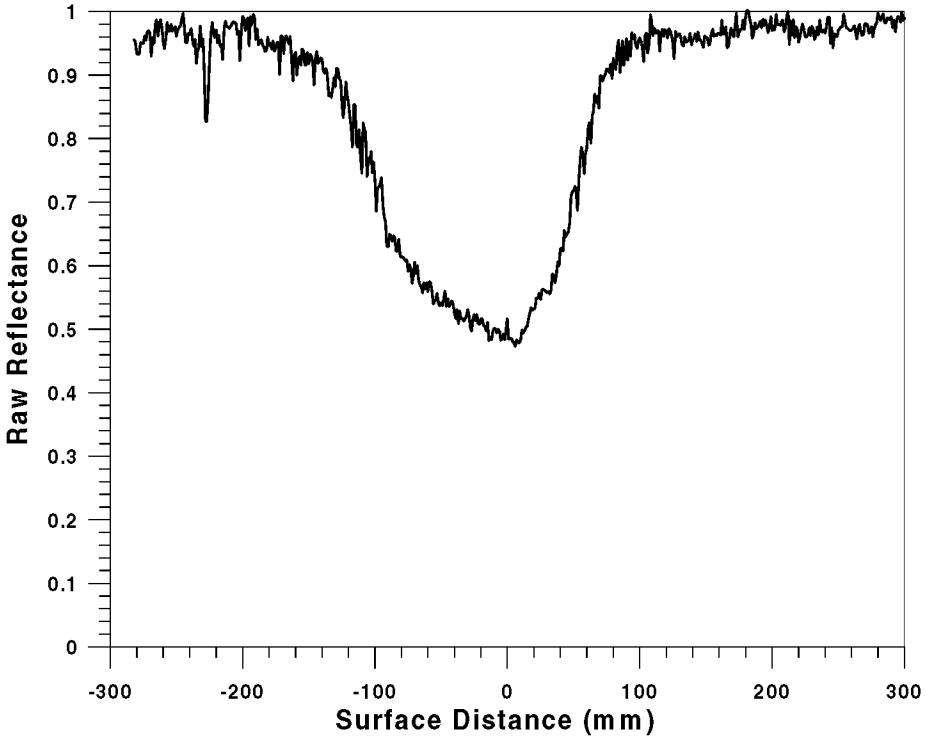

b. Typical raw surface reflectance distribution for a dyed blotter strip

Fig. 51 Automated Laser Reflectometer data reduction system.

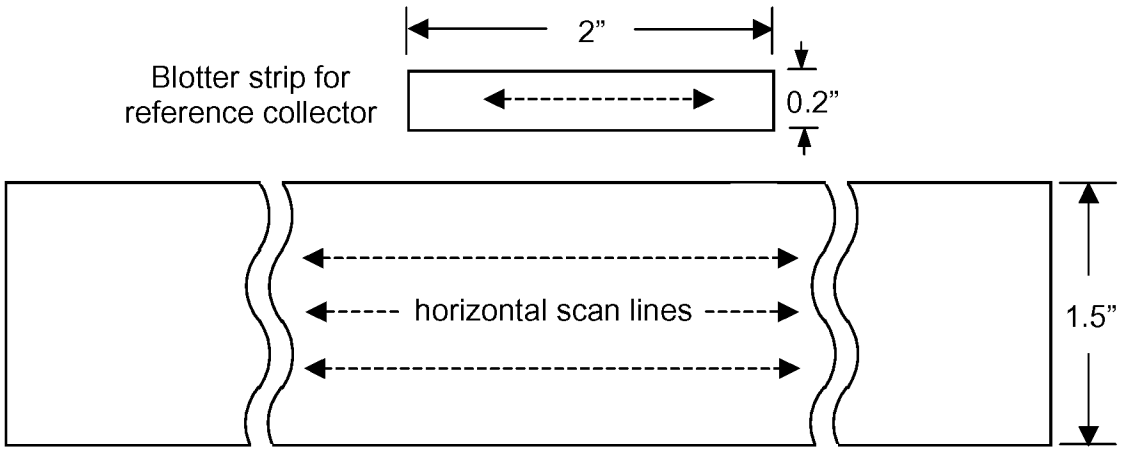

a. Scan locations for test model and reference collector strips (laser reflectometer)

b. Blotter strip image analysis region for CCD data reduction system

- V-shape blotter strips for 3D models
- Sectional scan required

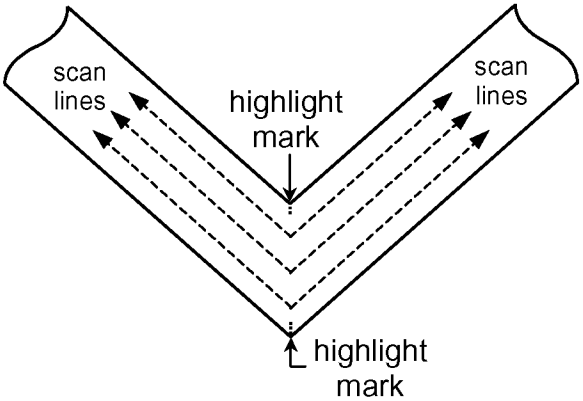

c. Scan locations for 3D models (laser reflectometer)

- User specifies the locations of A, B, C, and D
- Program determines the locations of E, F, G, and corresponding region

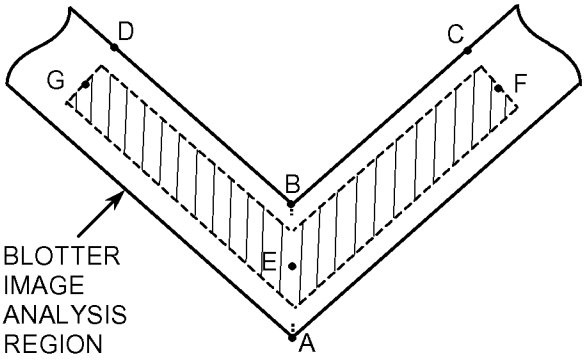

d. V-strip image analysis region for CCD data reduction system

Fig. 52 Blotter strip analysis with laser reflectometer and CCD data reduction systems.

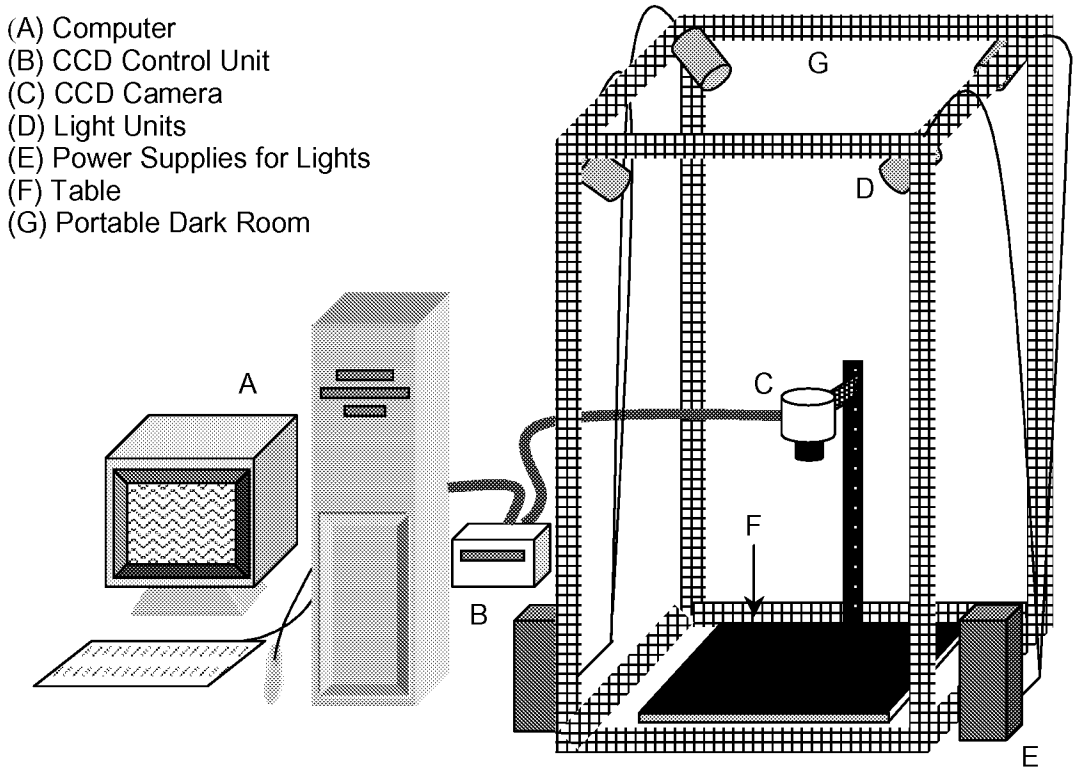

a. Schematic diagram of the CCD Reflectometer

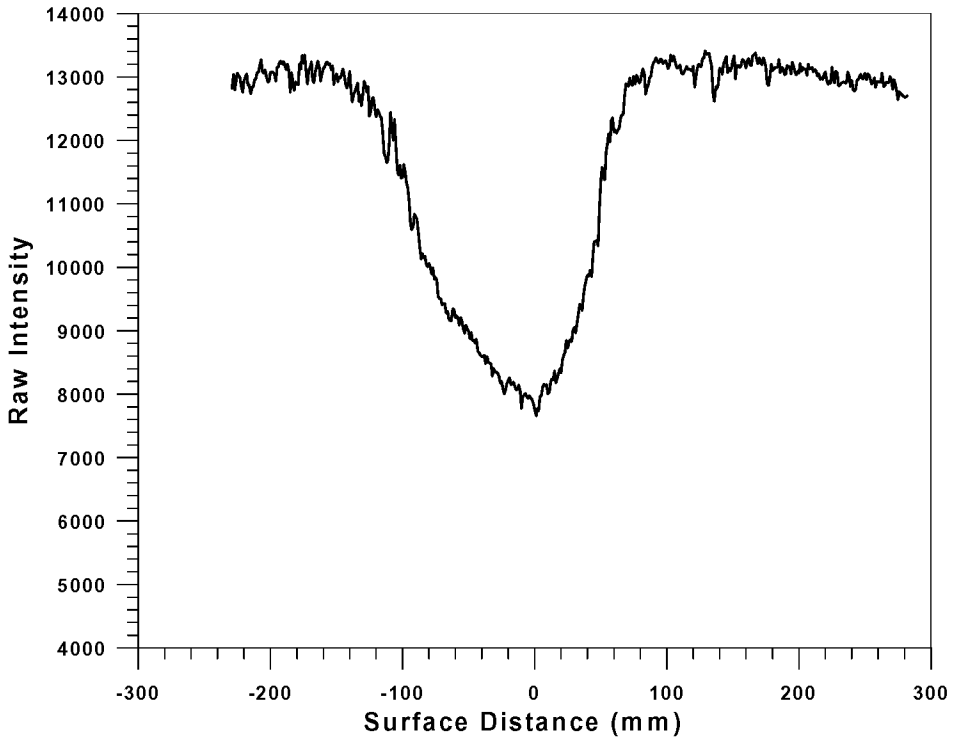

b. Typical raw intensity (reflectance) distribution for a dyed blotter strip

Fig. 53 CCD Reflectometer data reduction system.

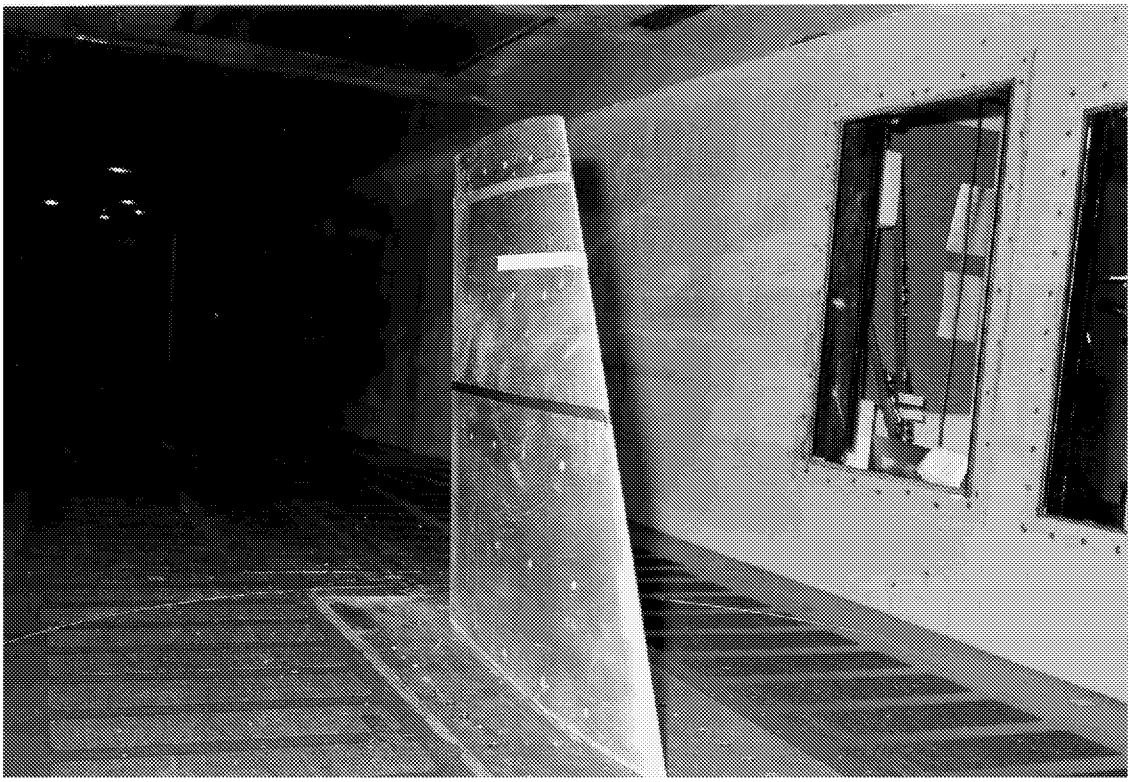

a. NACA 64A008 swept horizontal tail section installation in IRT test section

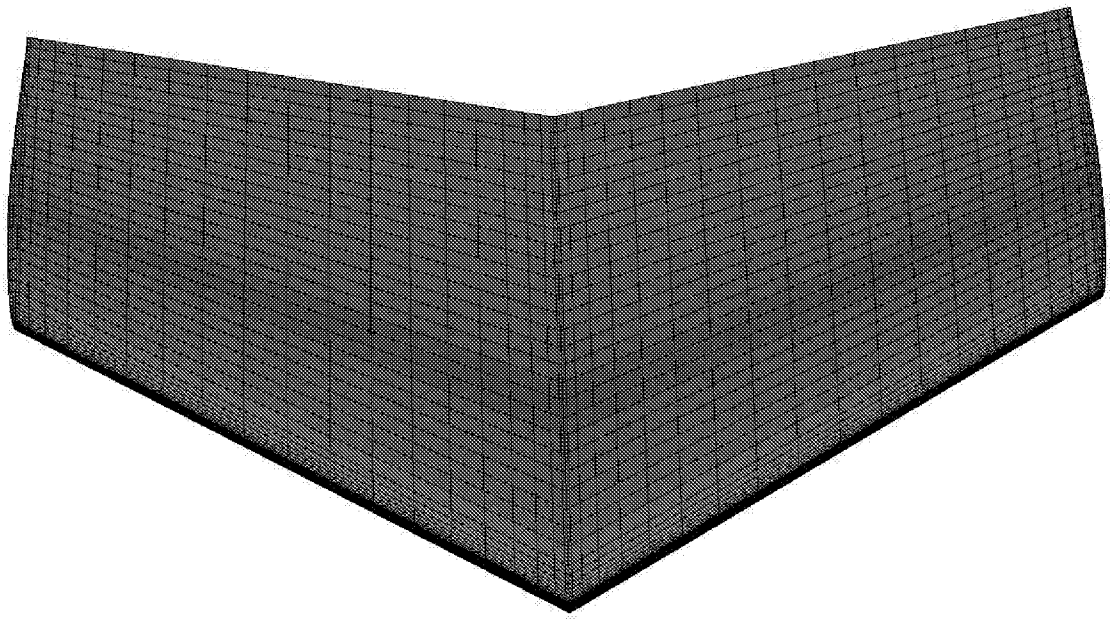

b. PMARC panel model for NACA 64A008 swept finite tail

Fig. 54 NACA 64A008 swept horizontal tail wind tunnel and analytical flow models (Continued).

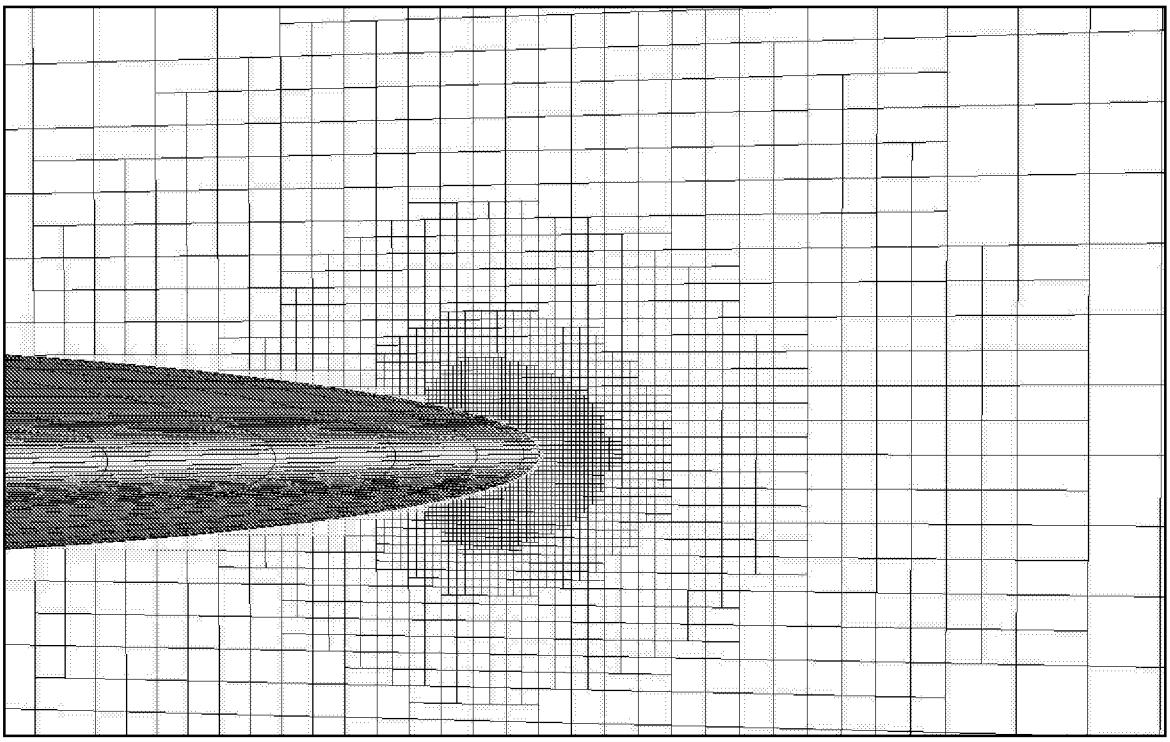

c. Grid at Y = 0 plane

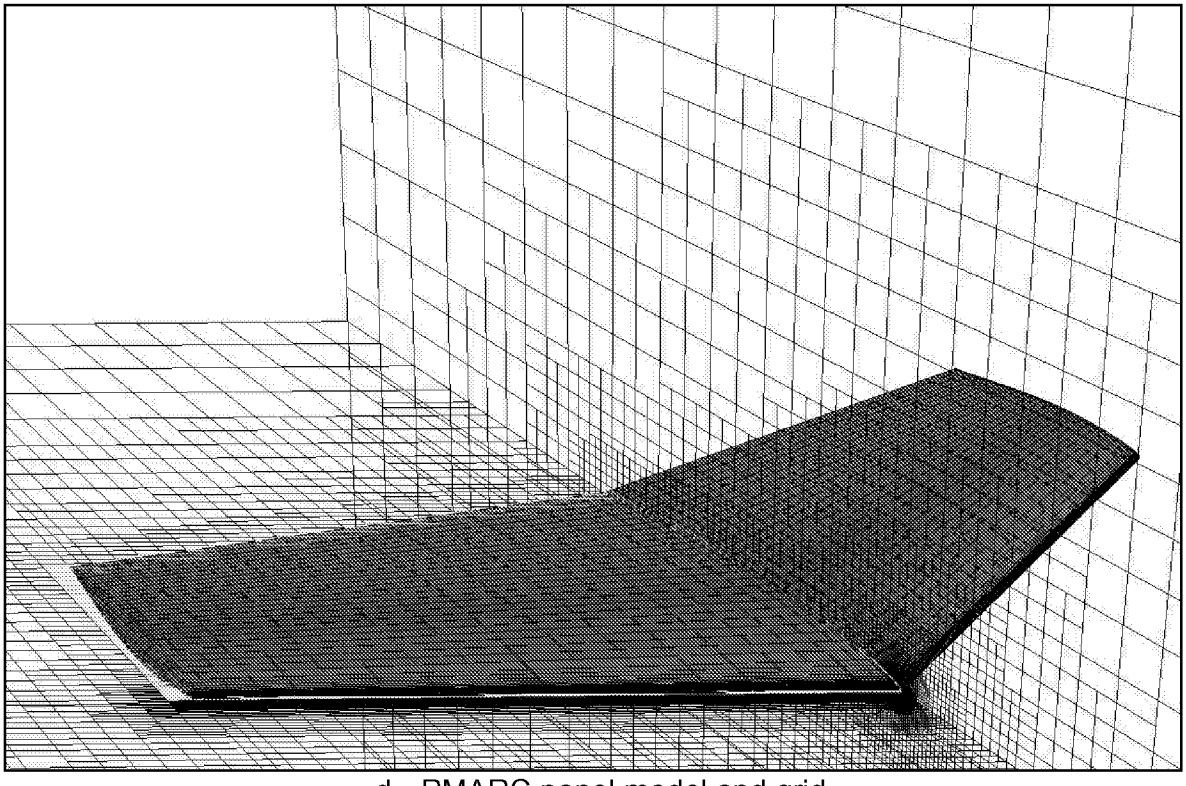

d. PMARC panel model and grid

Fig. 54 NACA 64A008 swept horizontal tail wind tunnel model and analytical flow

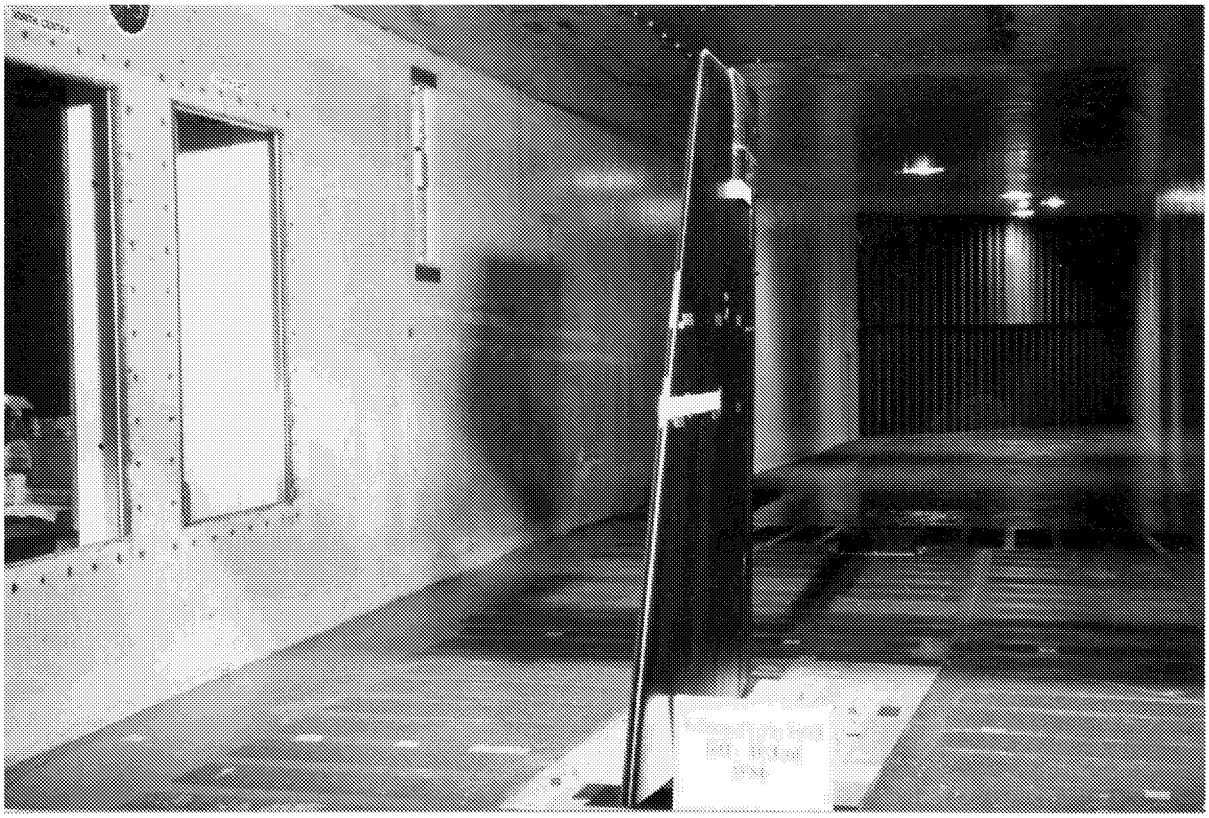

a. Full-scale business jet horizontal tail installation in IRT test section

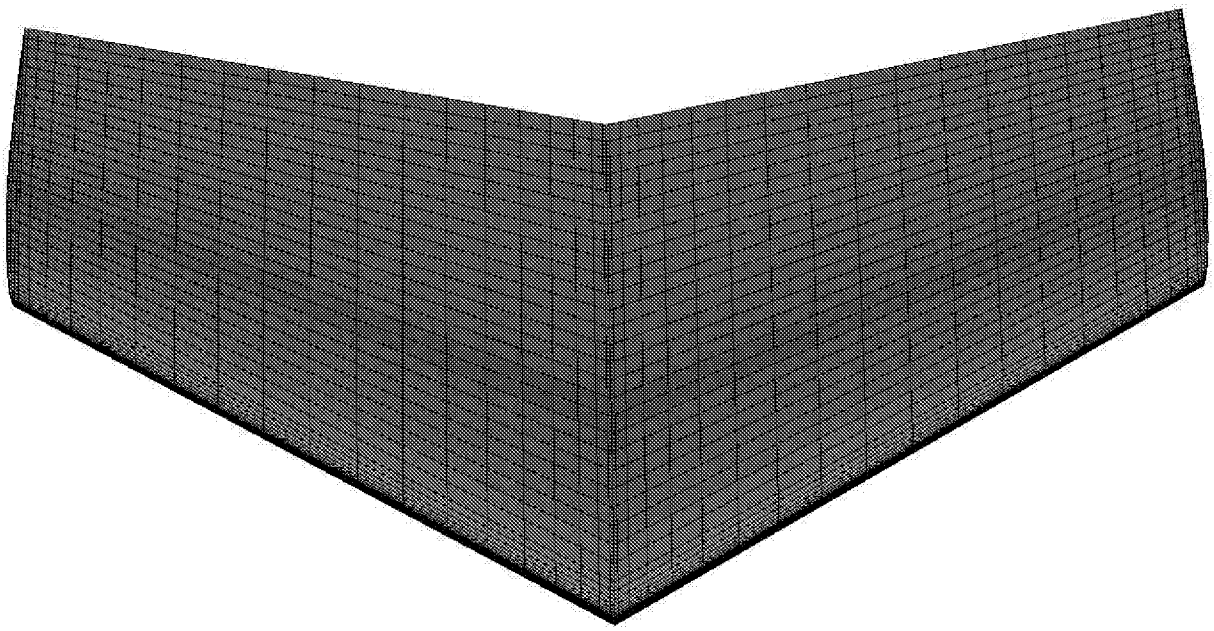

b. PMARC panel model

Fig. 55 Wind tunnel and analytical flow model for full-scale business jet horizontal tail (Continued).

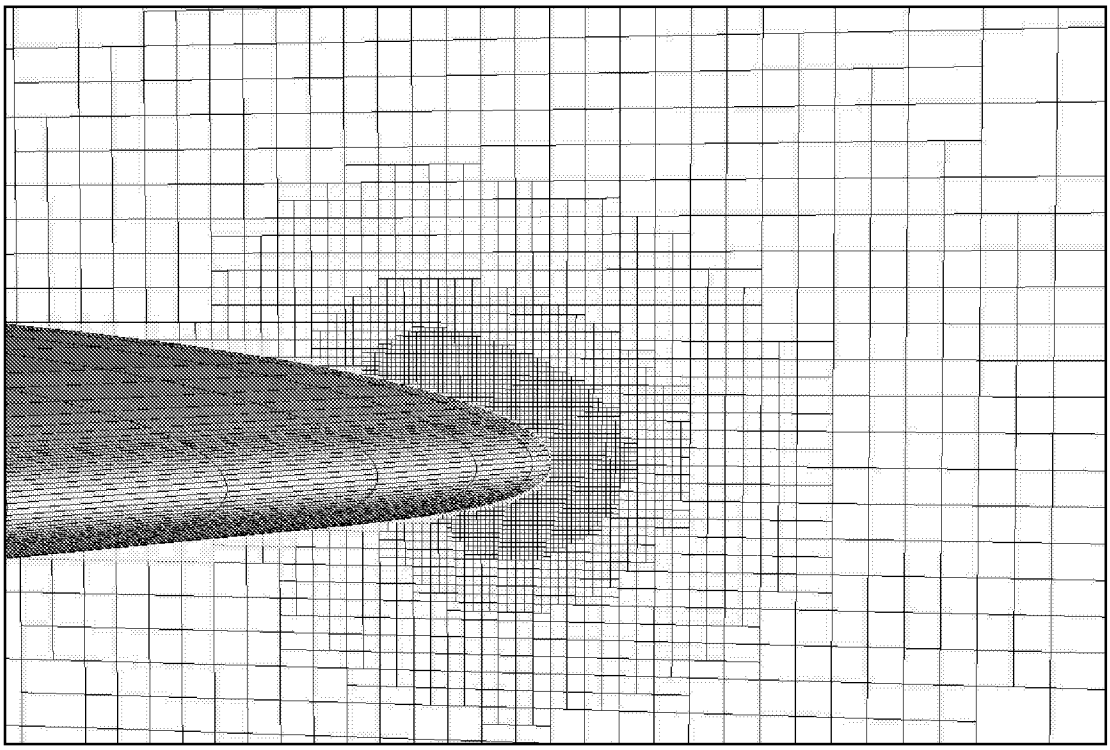

c. Grid at Y = 0 plane

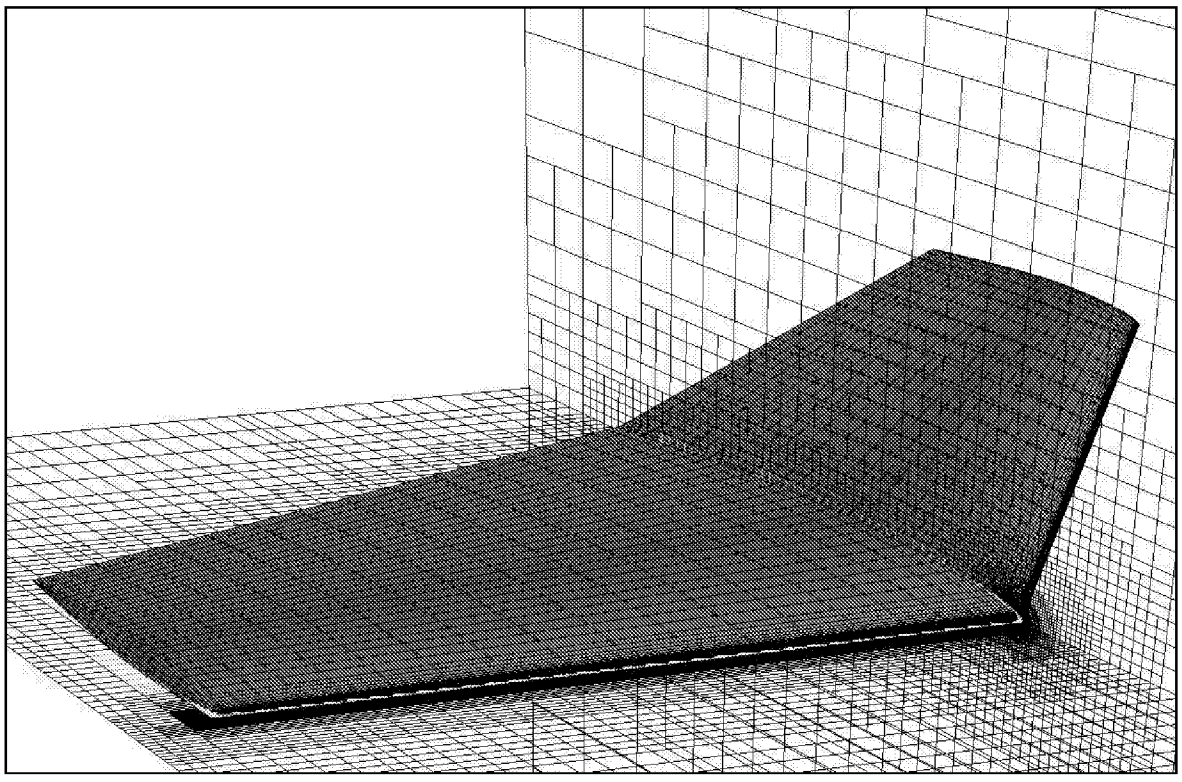

d. PMARC panel model and grid

Fig. 55 Wind tunnel and analytical flow model for full-scale business jet horizontal tail.

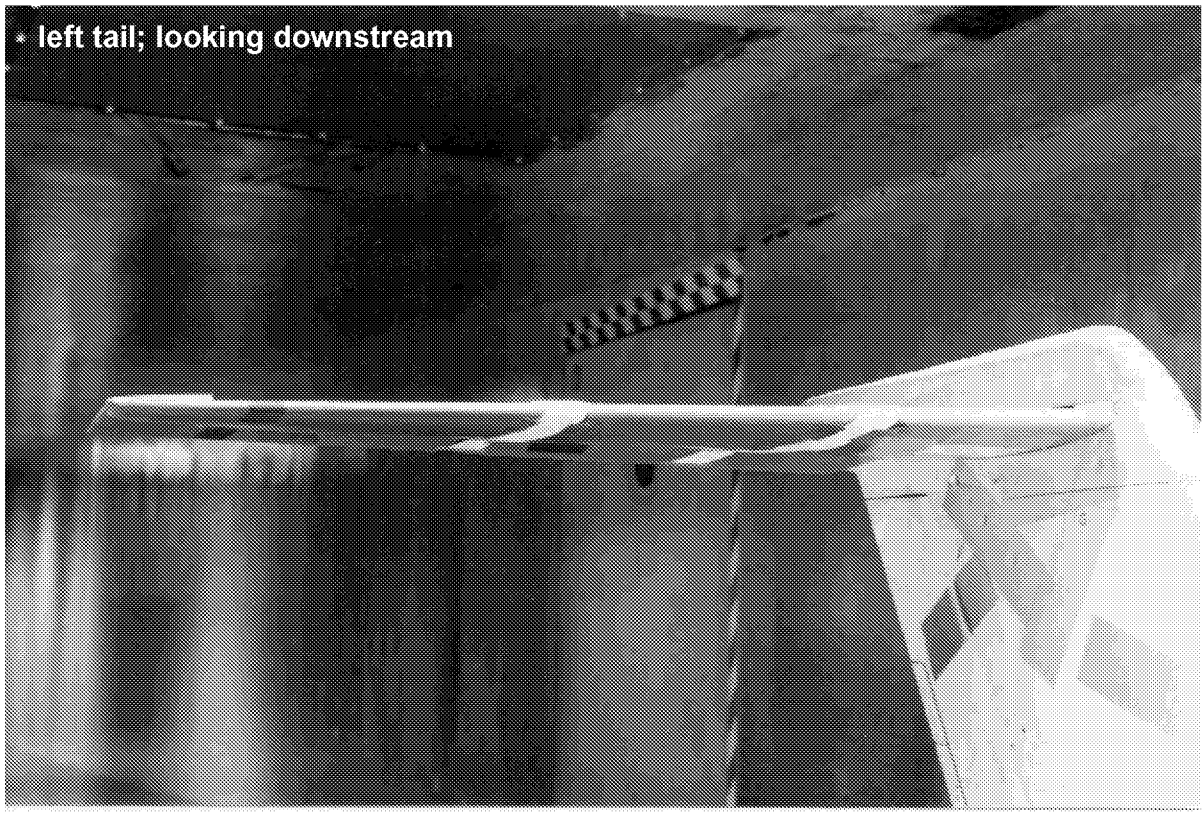

a. 25%-scale business jet empennage installation in IRT test section

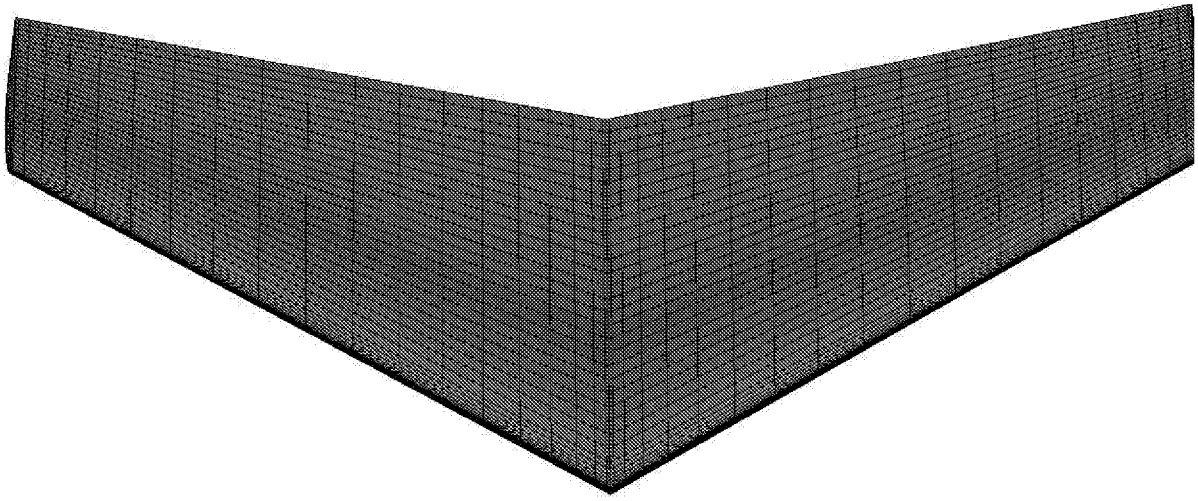

b. PMARC panel model

Fig. 56 Wind tunnel and analytical flow model for 25%-scale business Empennage (Continued).

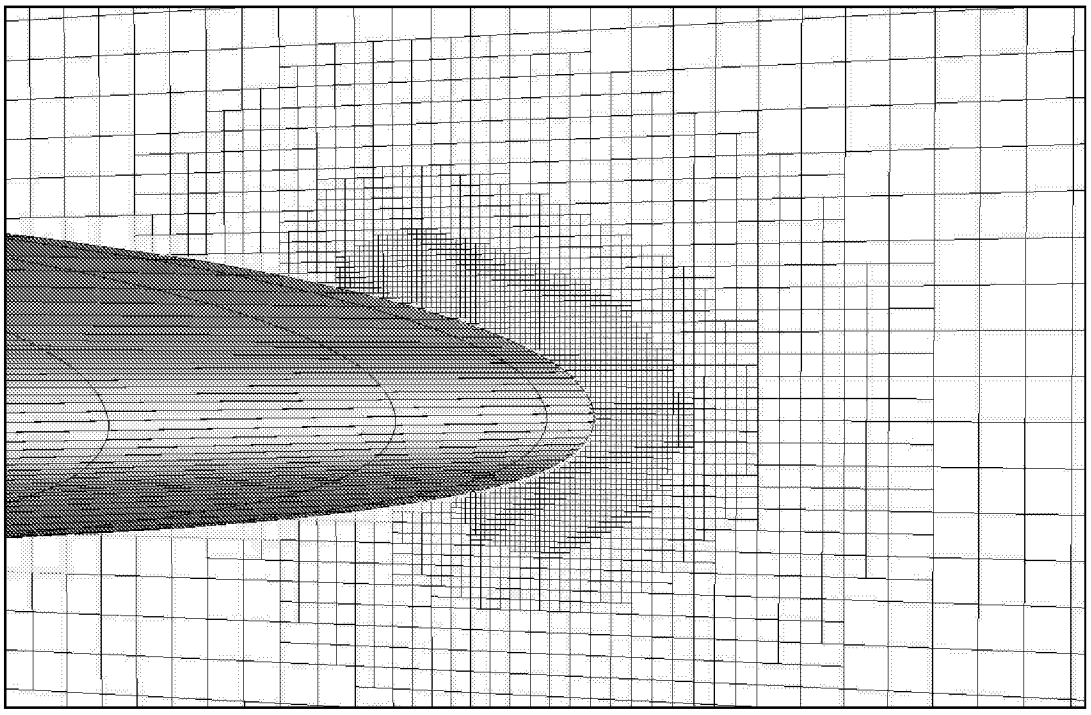

c. Grid at Y = 0 plane

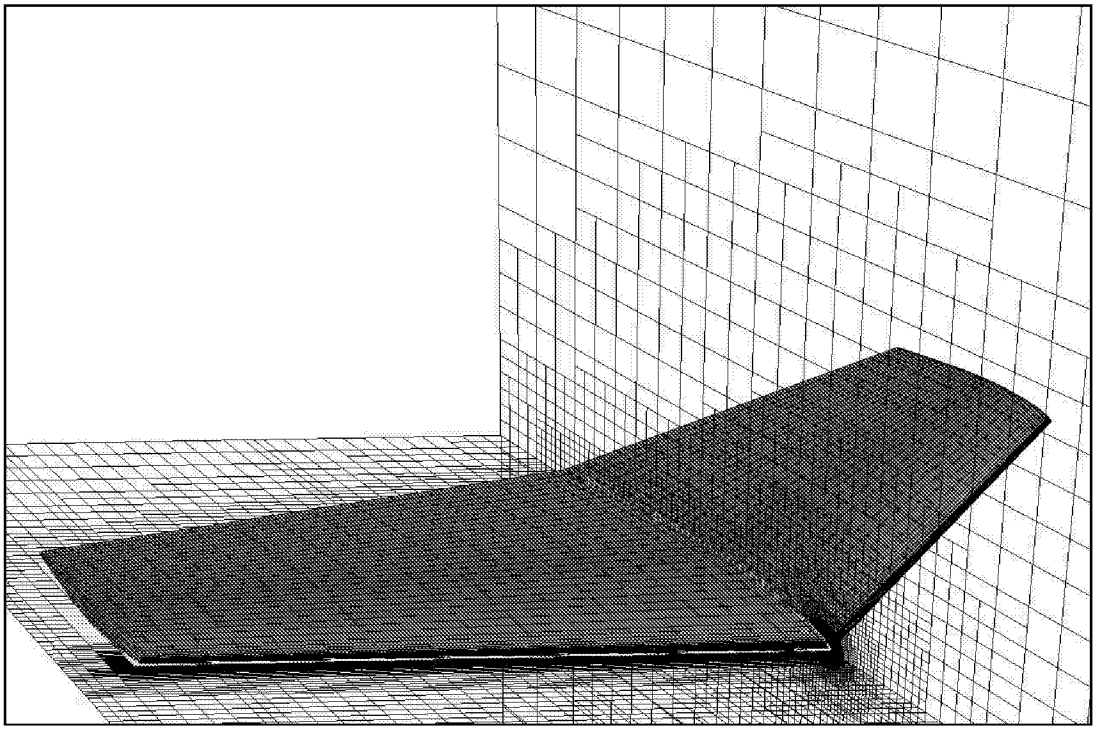

d. PMARC panel model and grid

Fig. 56 Wind tunnel and analytical flow models for 25%-scale business jet empennage.

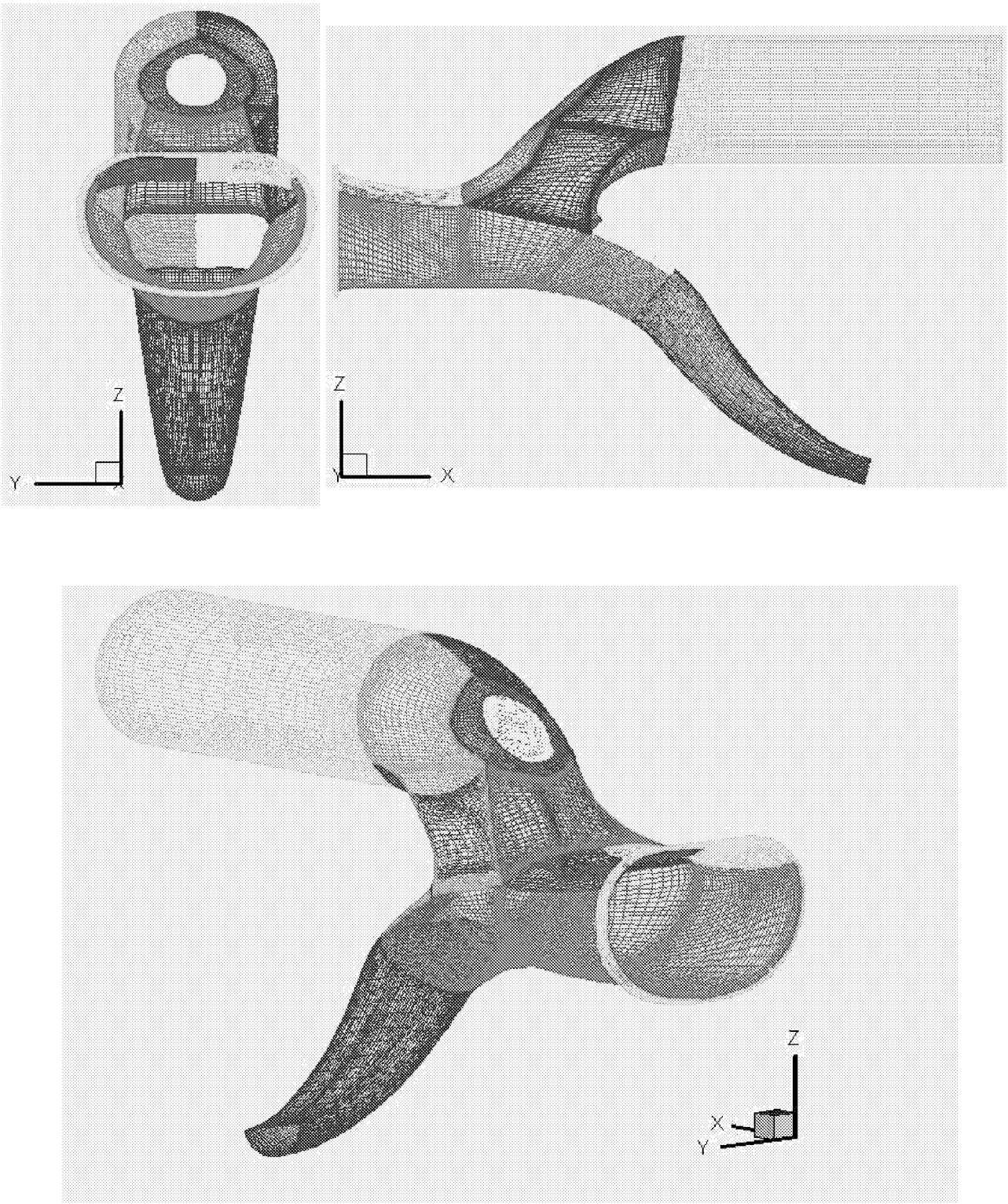

Fig. 57 Computational grid system (997,450 grid points) for the S-duct engine inlet.

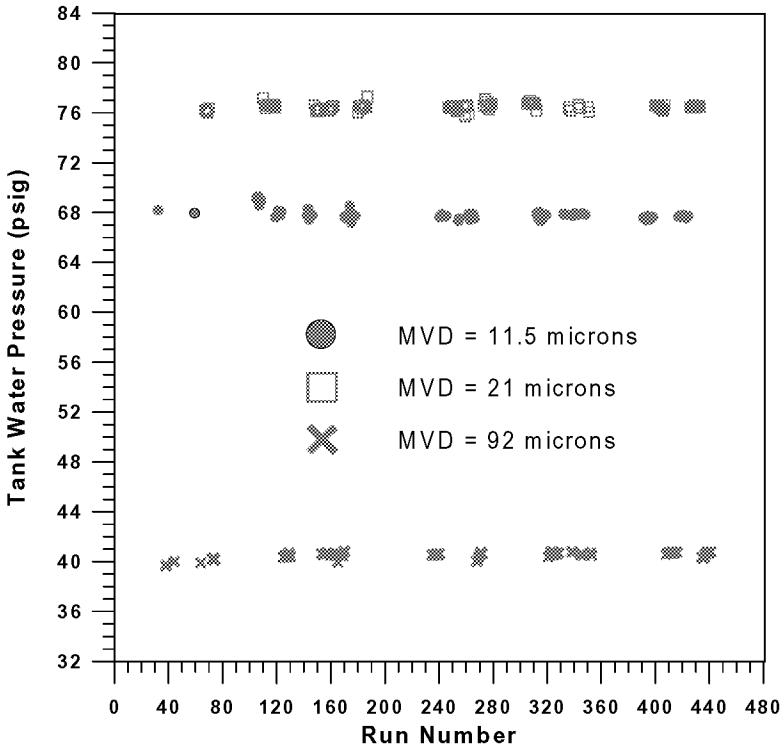

a. Variation in average tank water pressure.

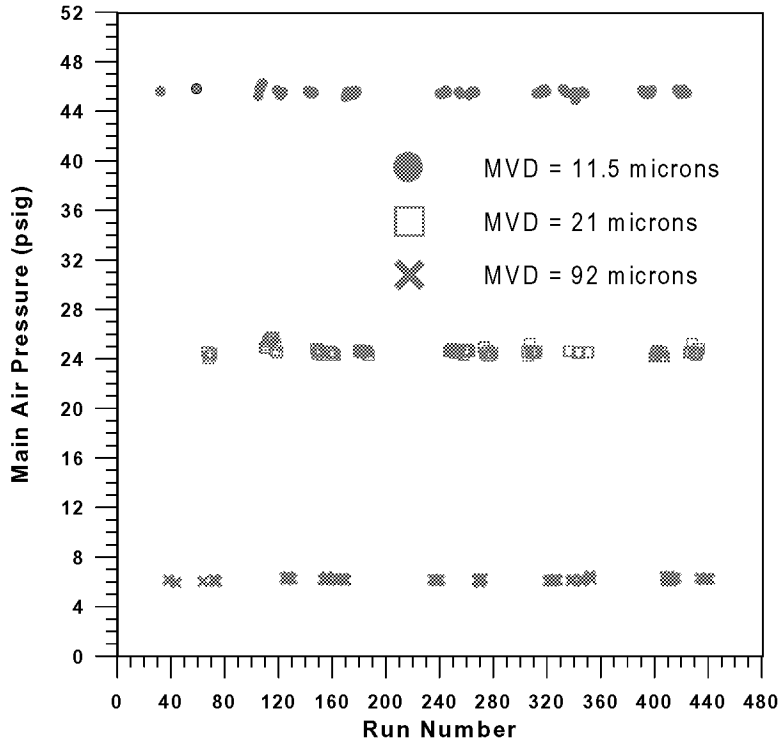

b. Variation in average air supply pressure.

Fig. 58 Repeatability of average spray system air and water pressures (1997 tests).

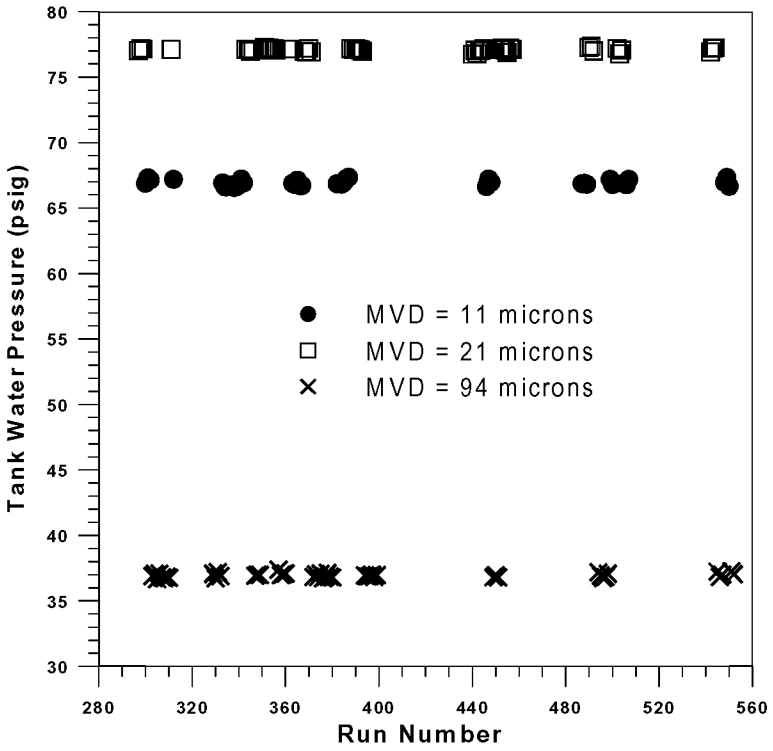

a. Variation in average tank water pressure.

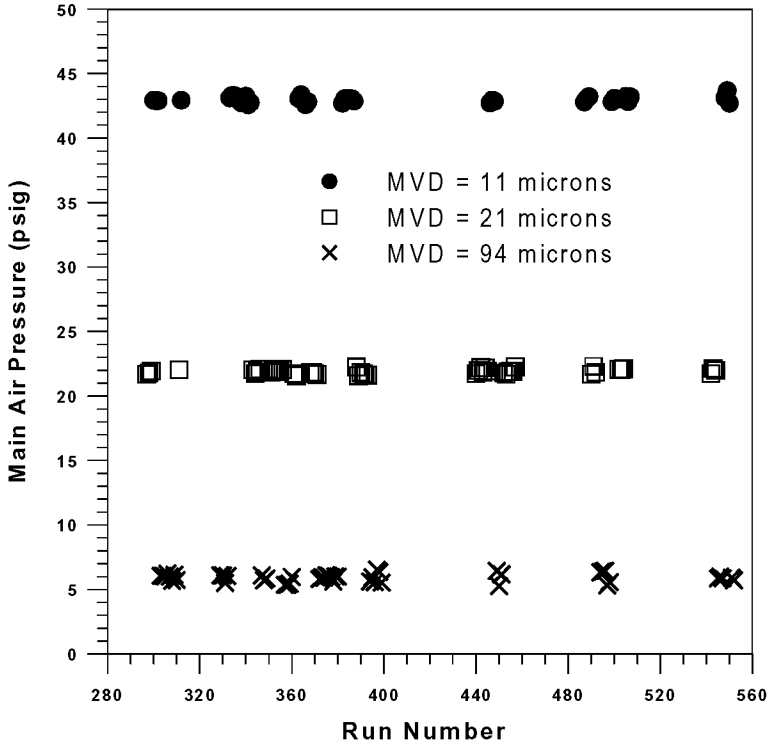

b. Variation in average air supply pressure.

Fig. 59 Repeatability of average spray system air and water pressures (1999 tests).

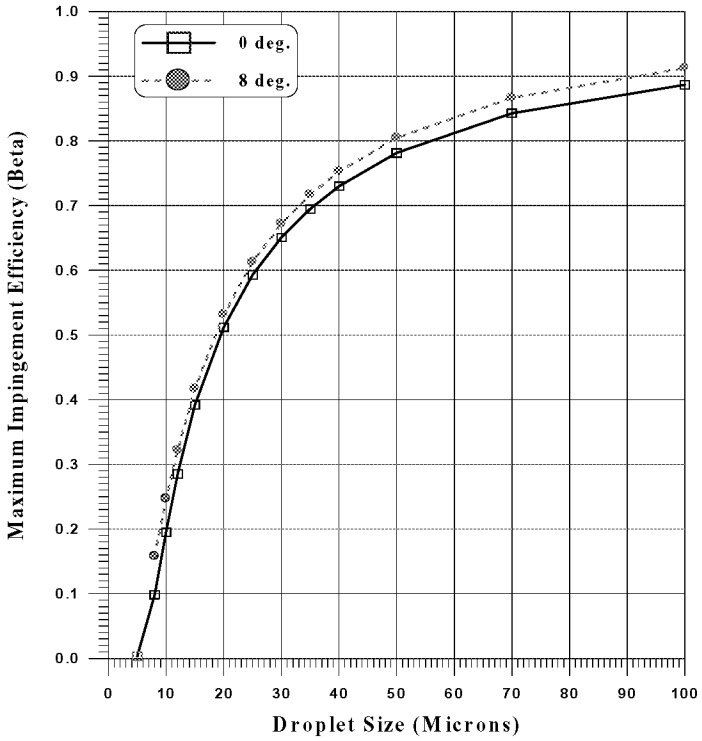

a. Variation in β_{max} with MVD

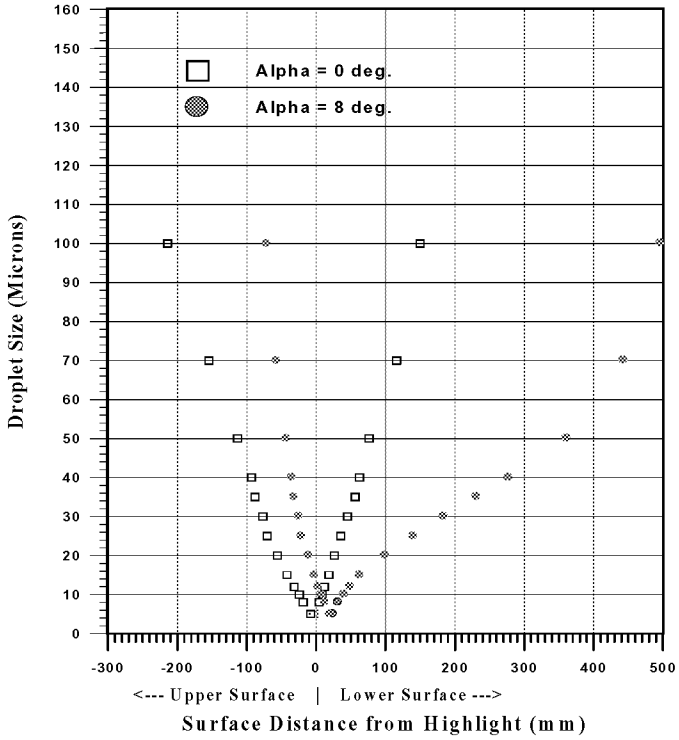

b. Variation in impingement limits with MVD

Fig. 60 Variation in maximum impingement efficiency and impingement limits with MVD for MS(1)-0317 airfoil; computational results obtained with monodispersed droplet distribution.

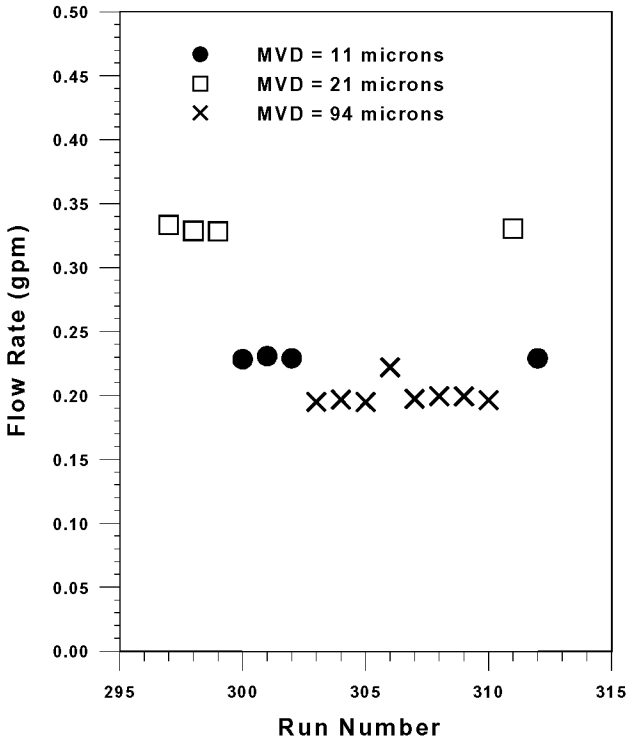

a. MS(1)-0317 airfoil

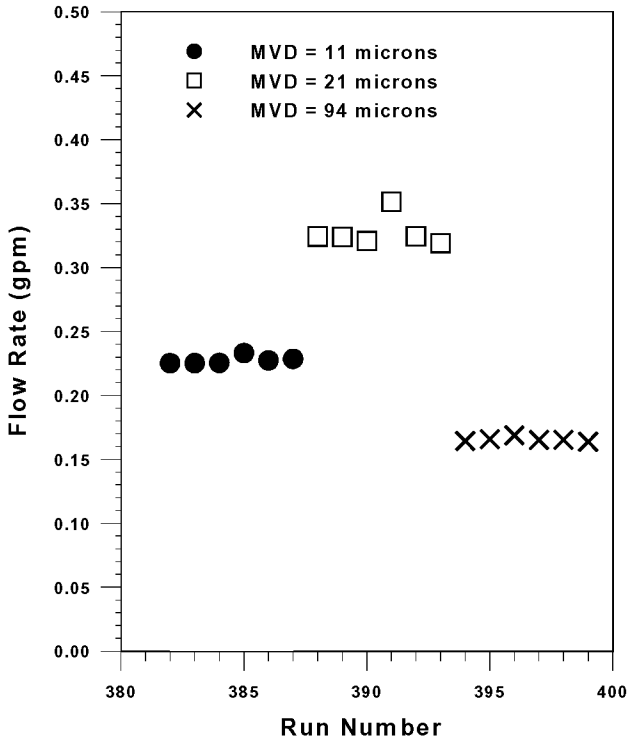

b. NLF(1)-0414 airfoil

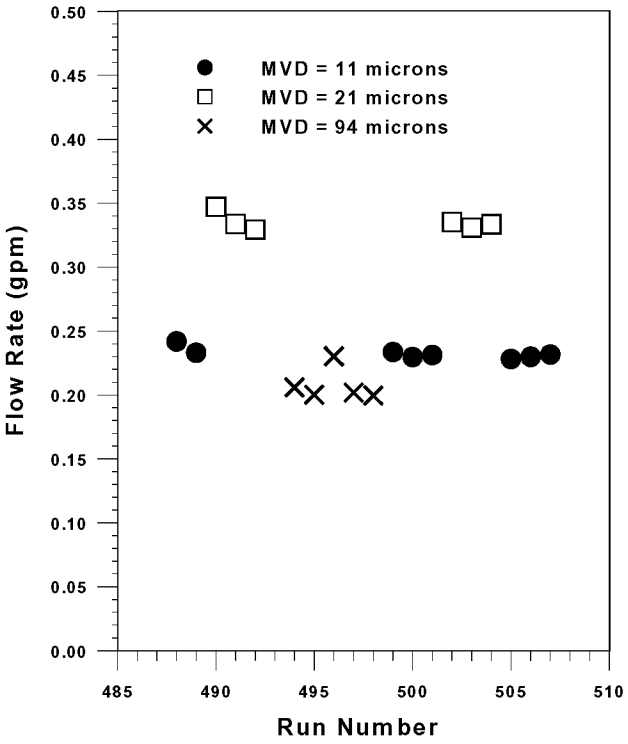

c. 25%-scale business jet empennage

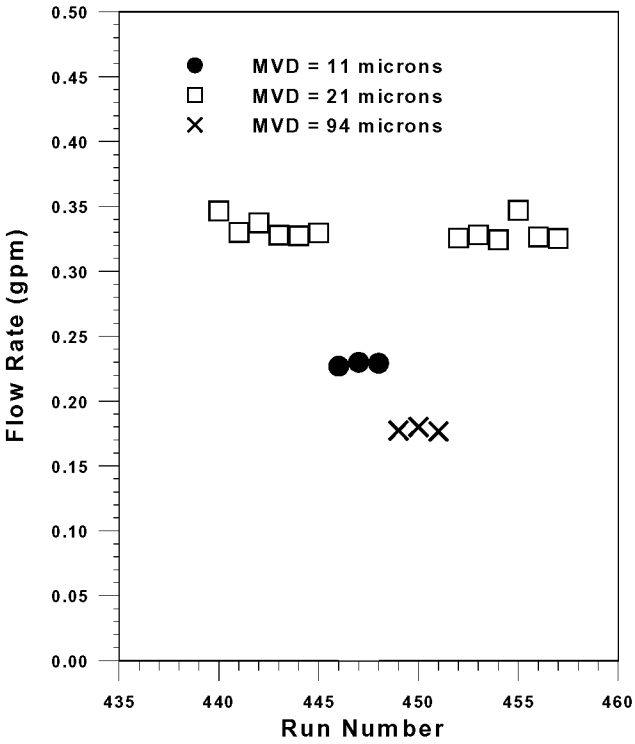

d. Full-scale business jet tail section

Fig. 61 Variation in WSU 12-nozzle spray system water flow rate (1999 tests).

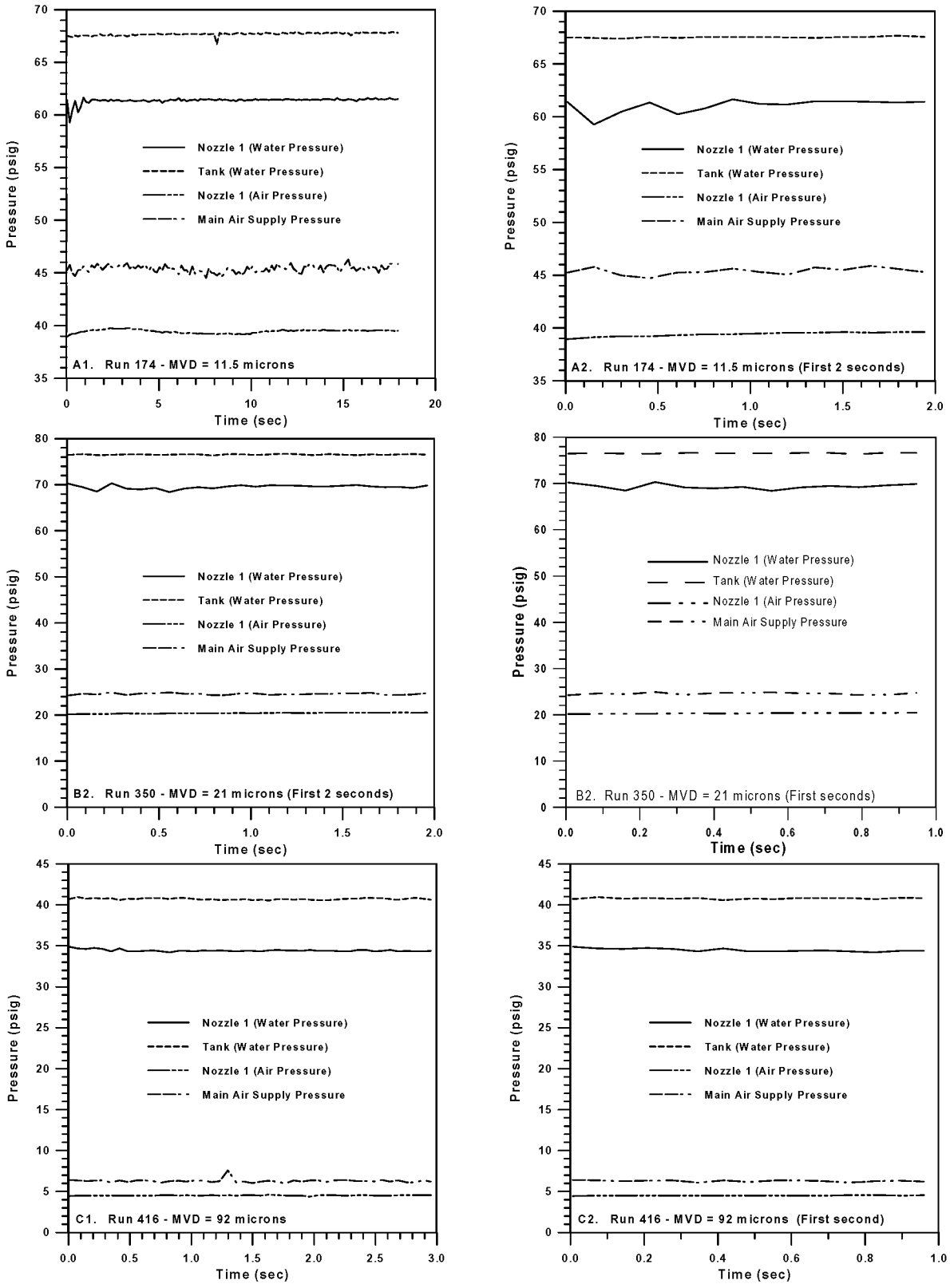

Fig. 62 Spray system pressures versus spray time for all MVD cases (1997 tests).

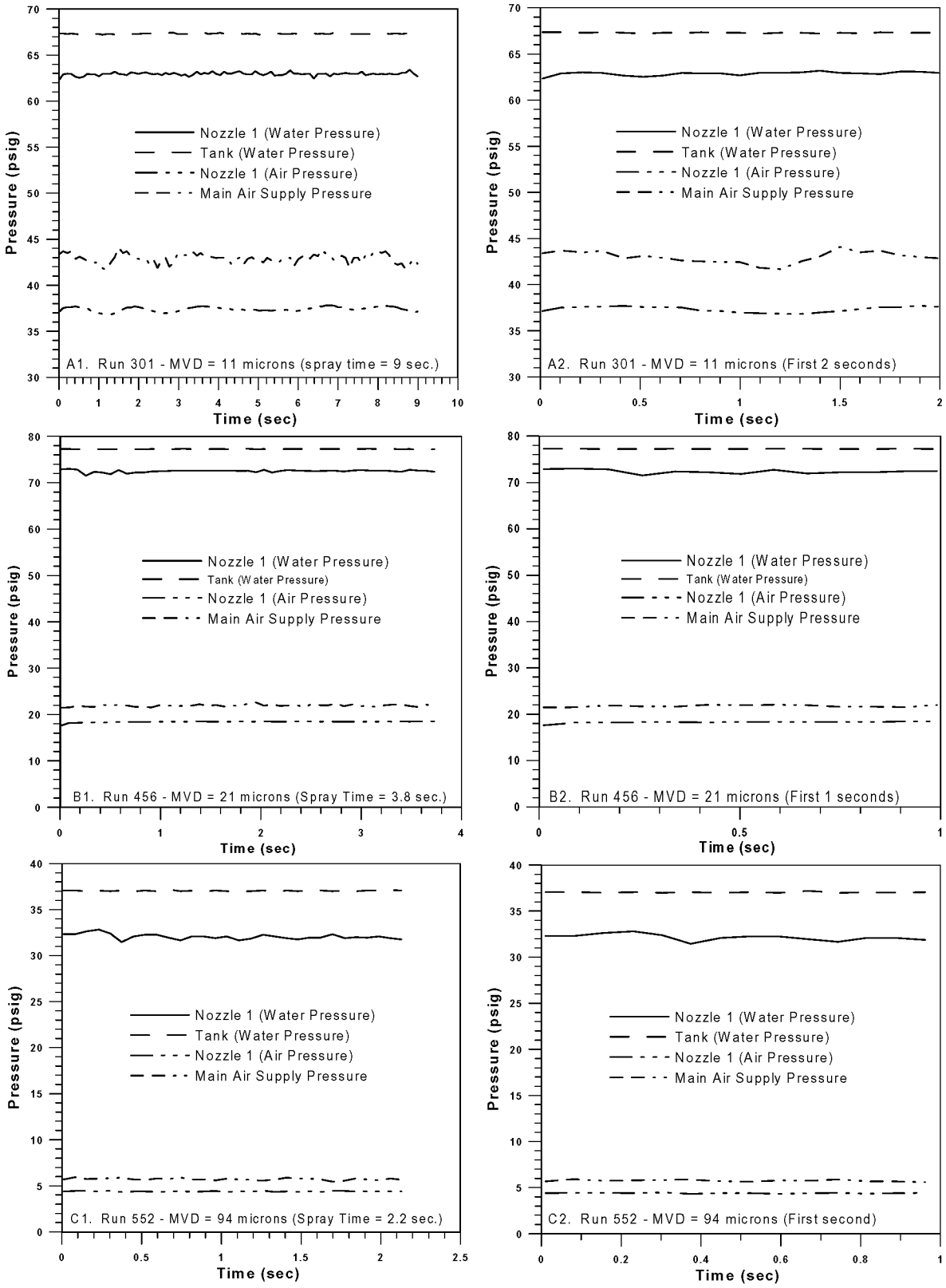

Fig. 63 Spray system pressures versus spray time for all MVD cases (1999 tests).

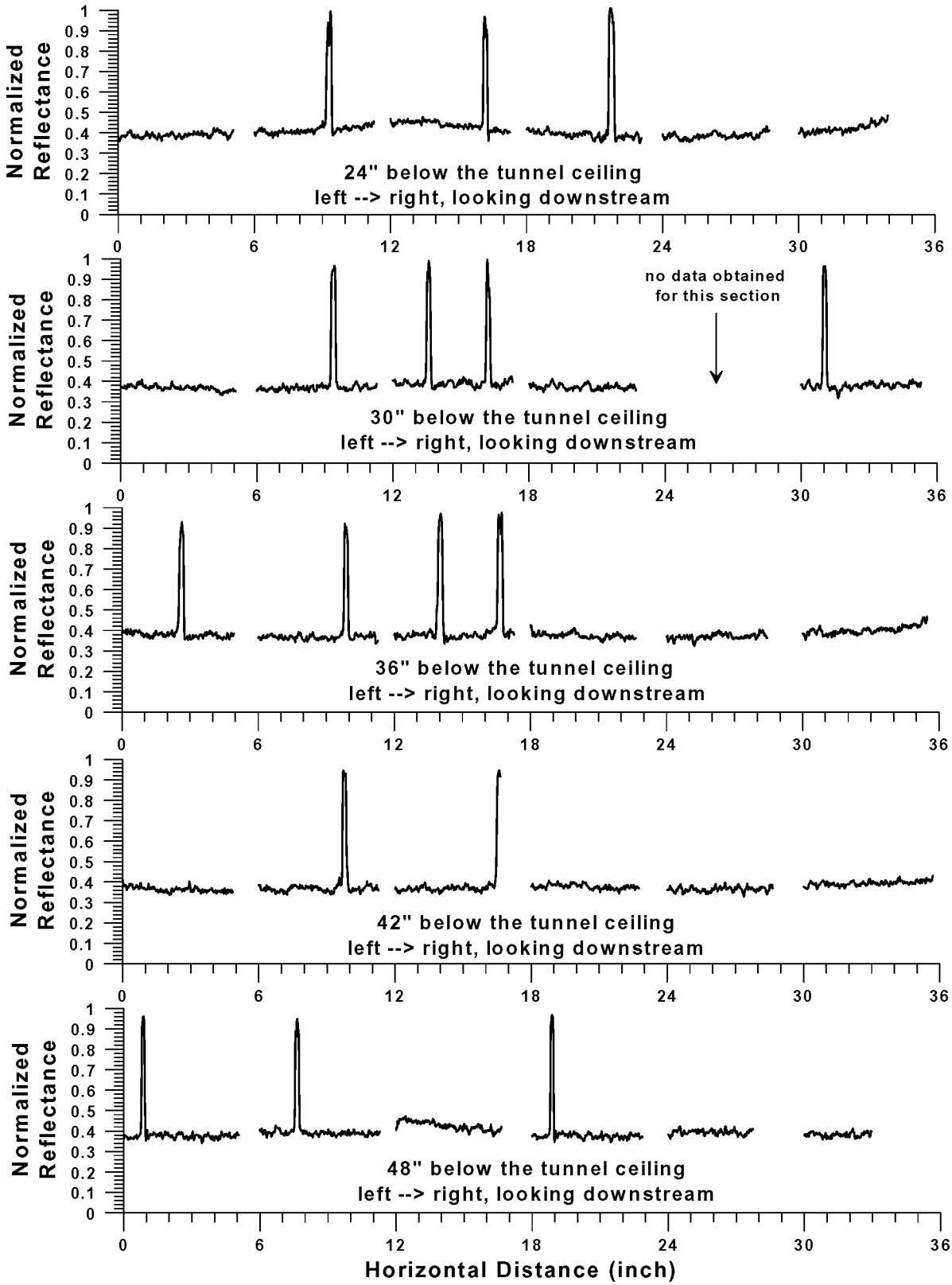

Fig. 64 Cloud uniformity tests using IRT uniformity grid;
1999 impingement tests, MVD = 11 microns.

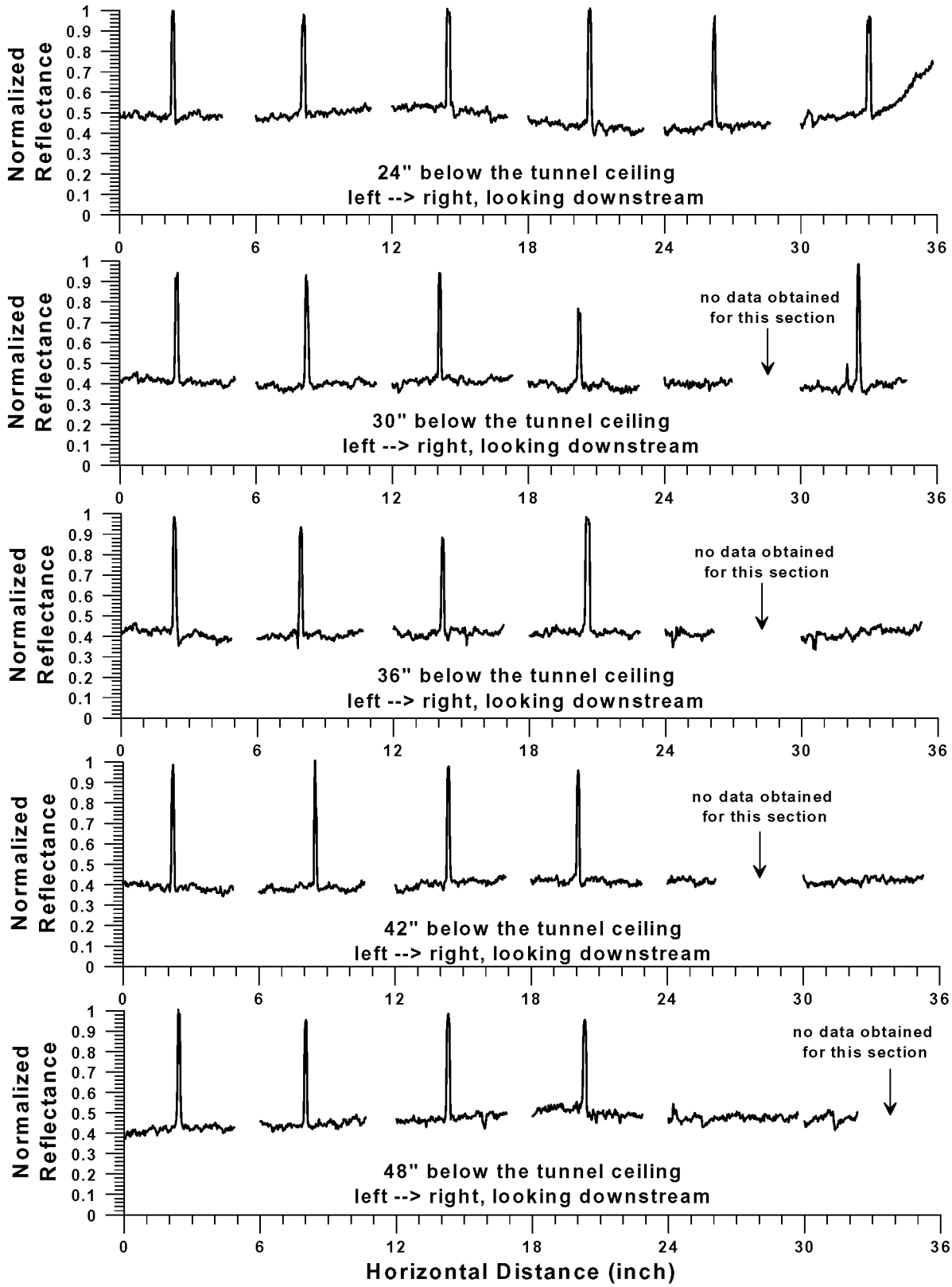

Fig. 65 Cloud uniformity tests using IRT uniformity grid;
1999 impingement tests, MVD = 21 microns.

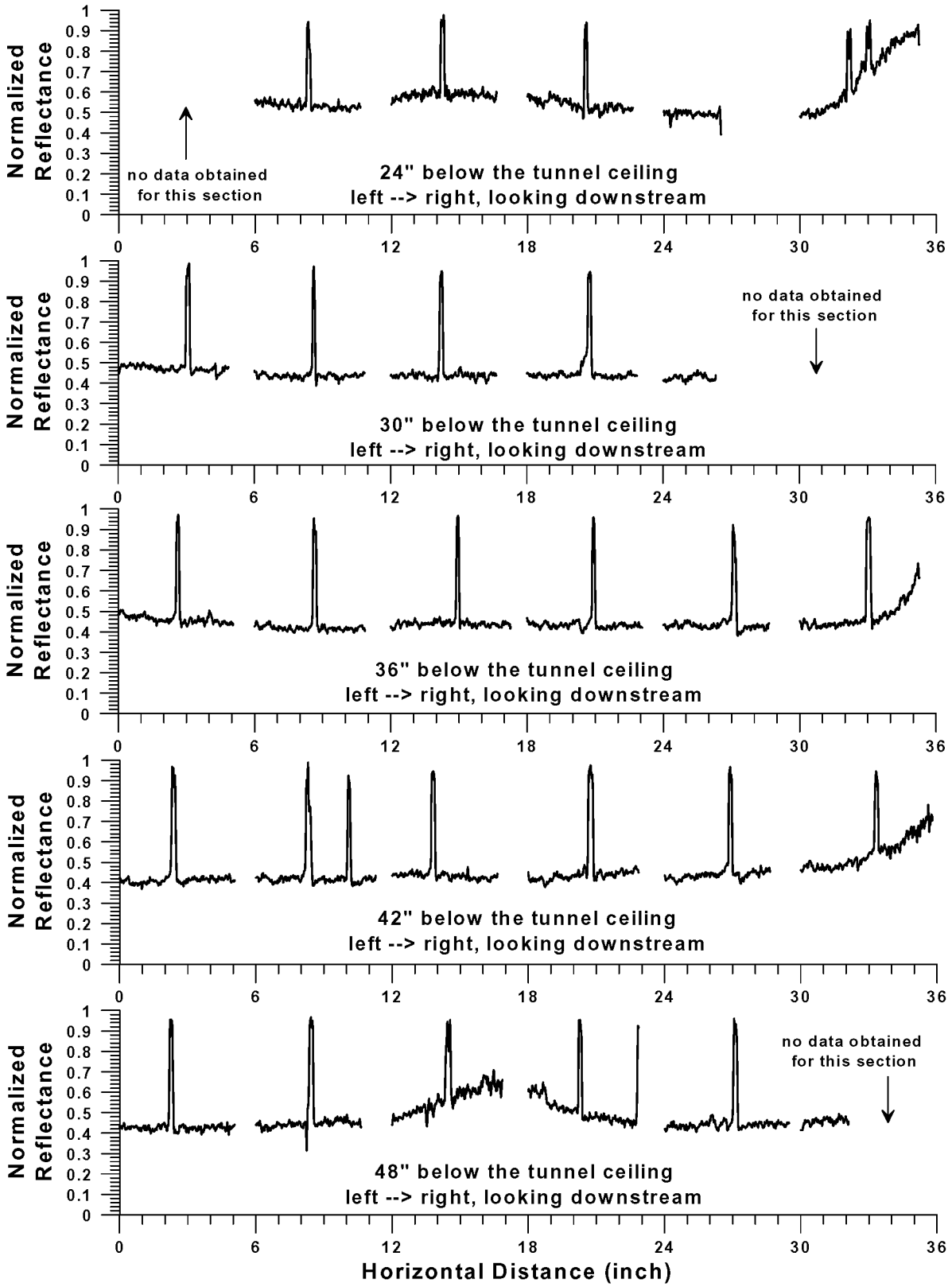

Fig. 66 Cloud uniformity tests using IRT uniformity grid; 1999 impingement tests, MVD = 94 microns.

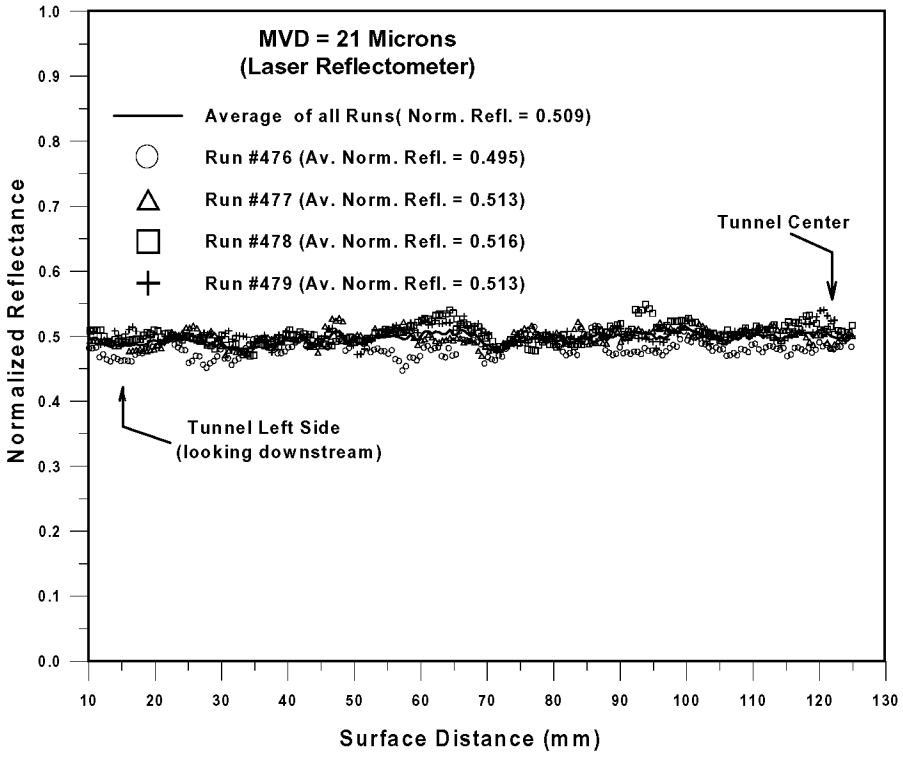

a. 9-inch hrizontal blade (1997 IRT tests)

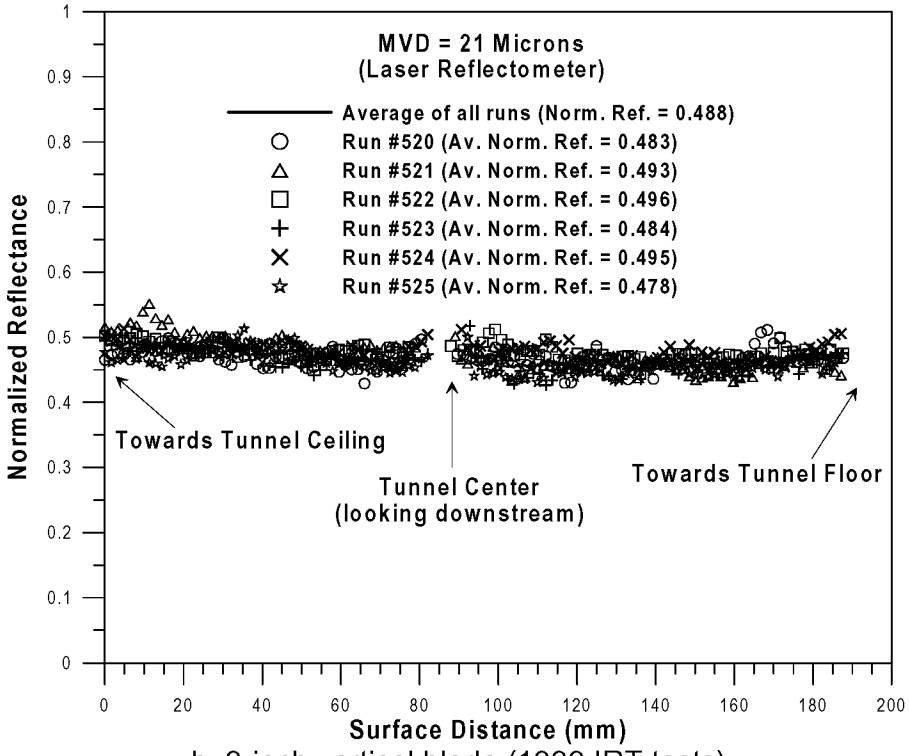

b. 9-inch vertical blade (1999 IRT tests)

Fig. 67 Test repeatability for reference collector mechanism.

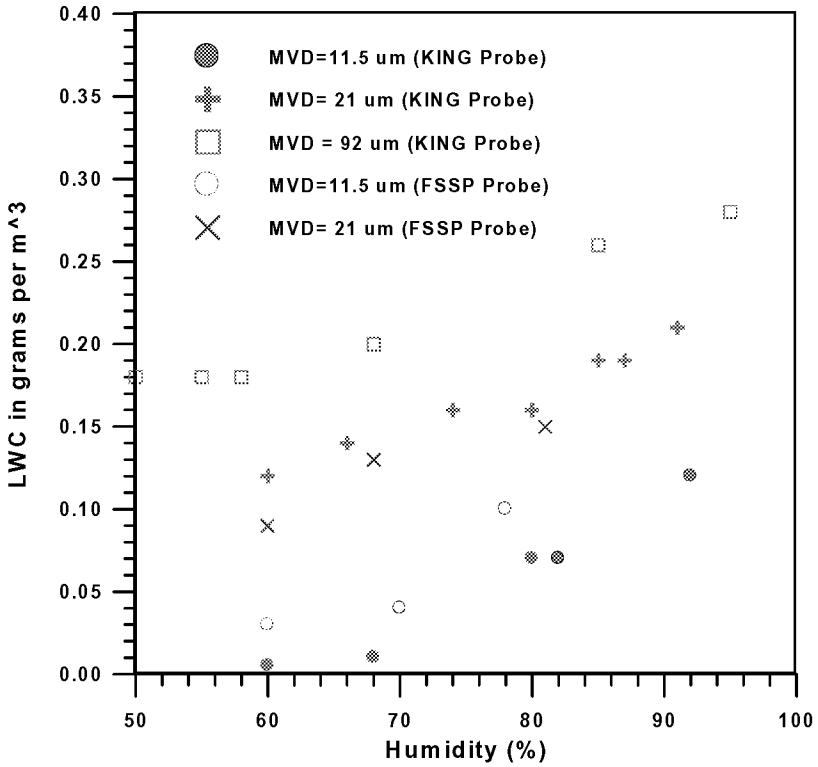

a. 1997 IRT tests

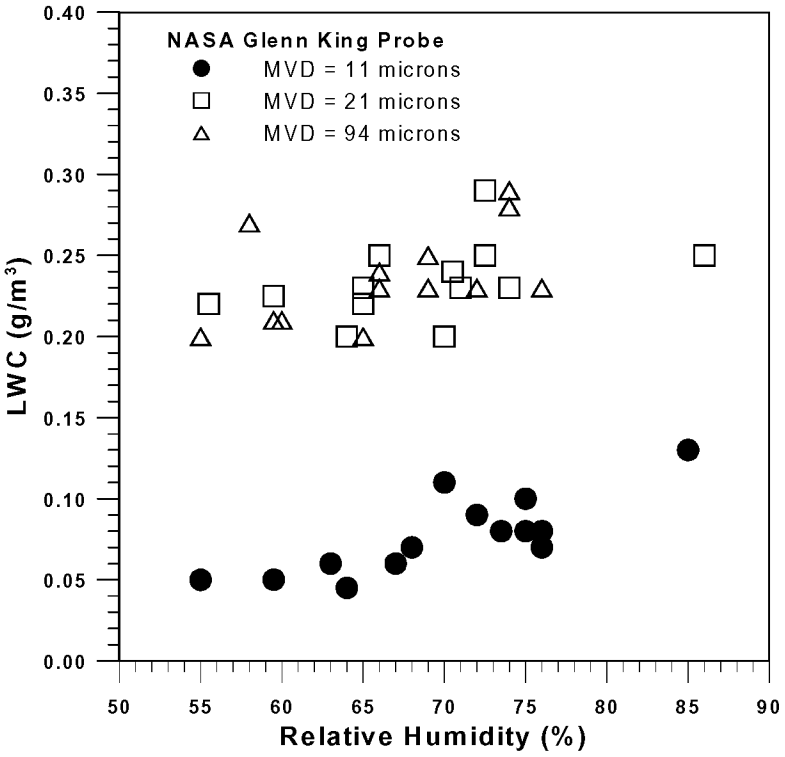

b. 1999 IRT tests

Fig. 68 Effect of relative humidity on LWC.

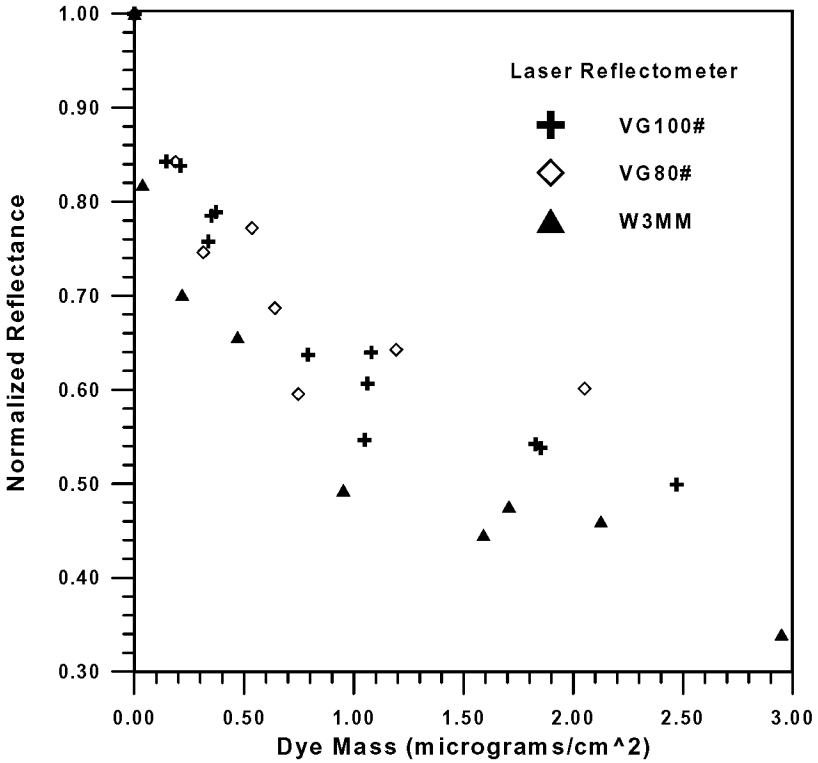

Fig. 69 Normalized reflectance obtained with the laser reflectometer versus dye mass for three types of blotter paper.

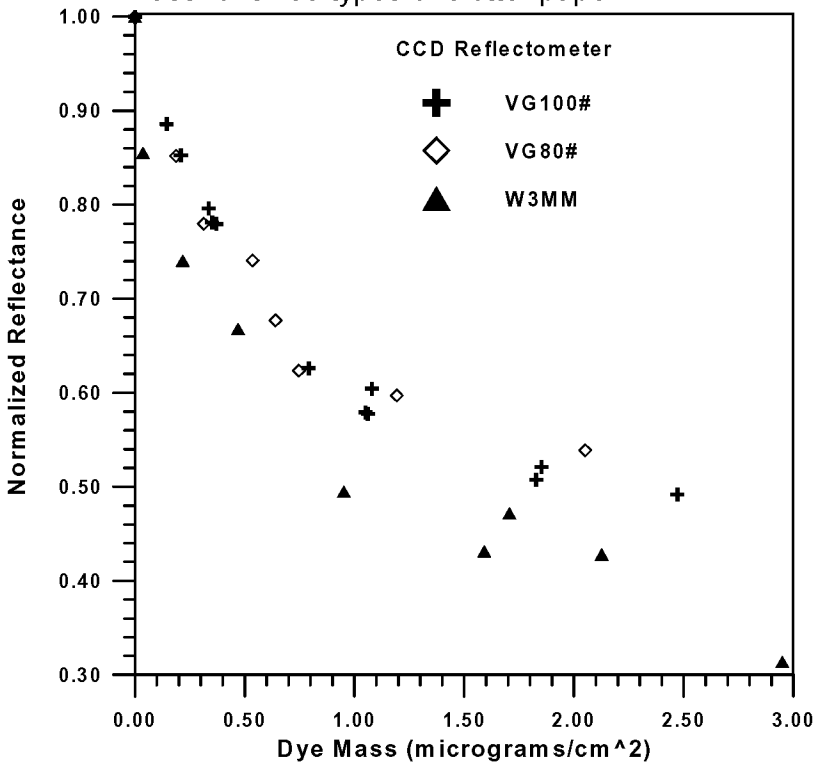

Fig. 70 Normalized reflectance obtained with the CCD reflectometer versus dye mass for three types of blotter paper.

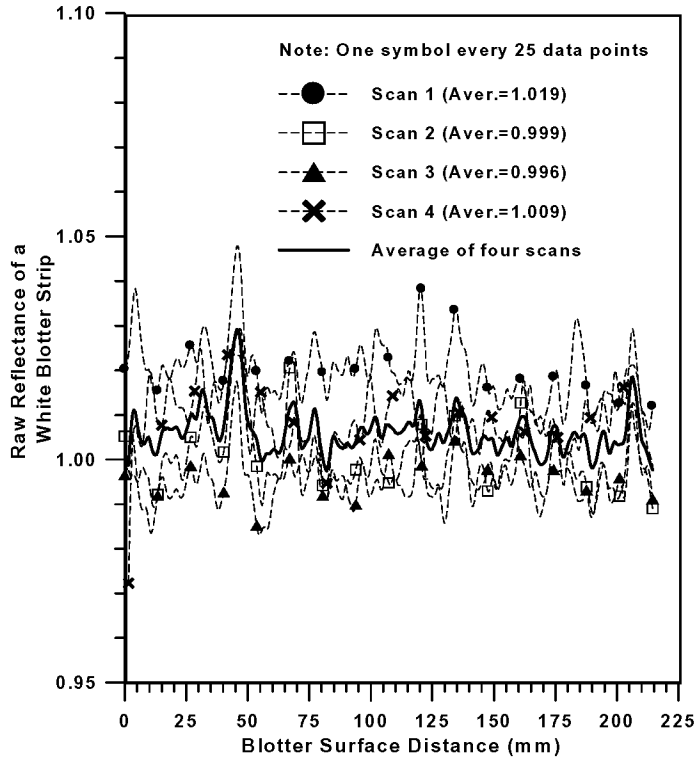

a. Laser Reflectometer

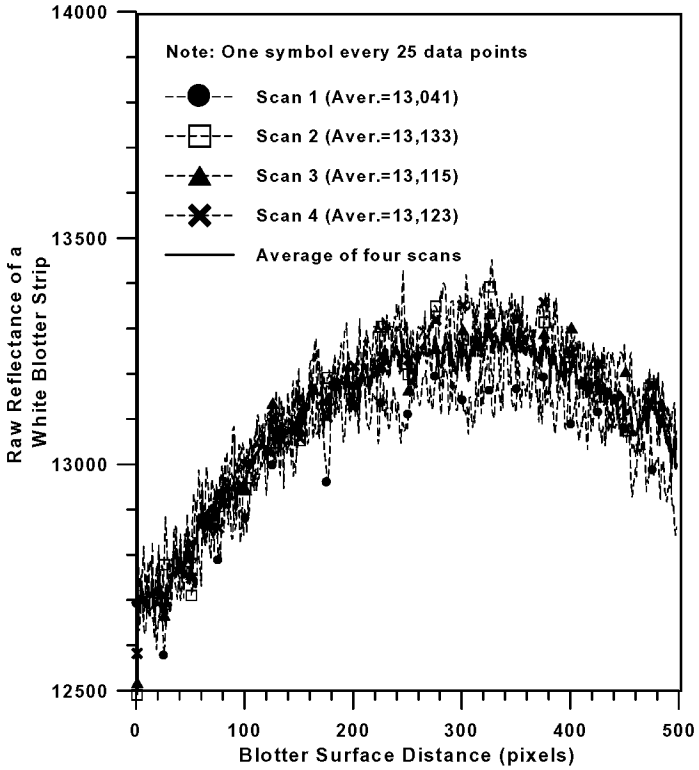

b. CCD Reflectometer

Fig. 71 Repeatability of data reduction systems (1997 tests).

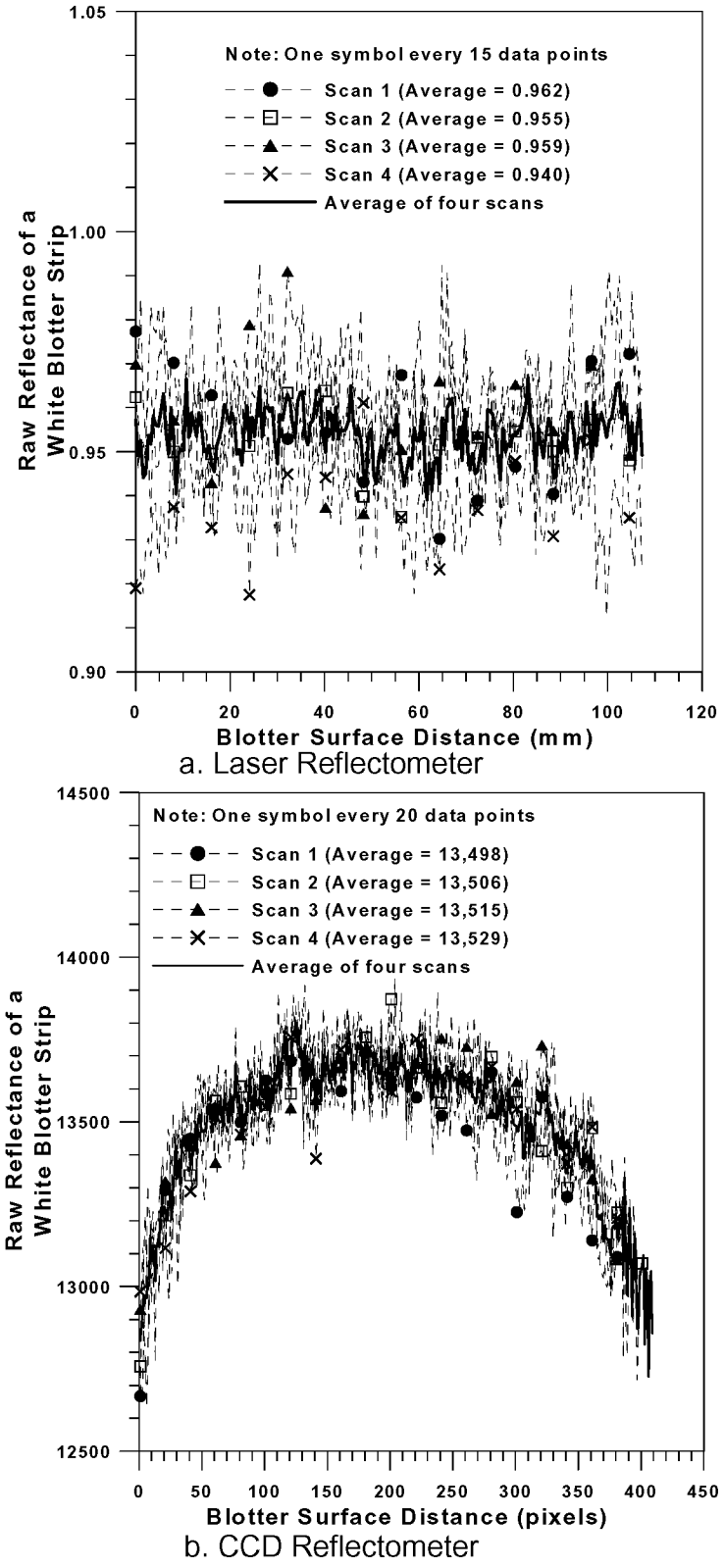

Fig. 72 Repeatability of data reduction systems (1999 tests).

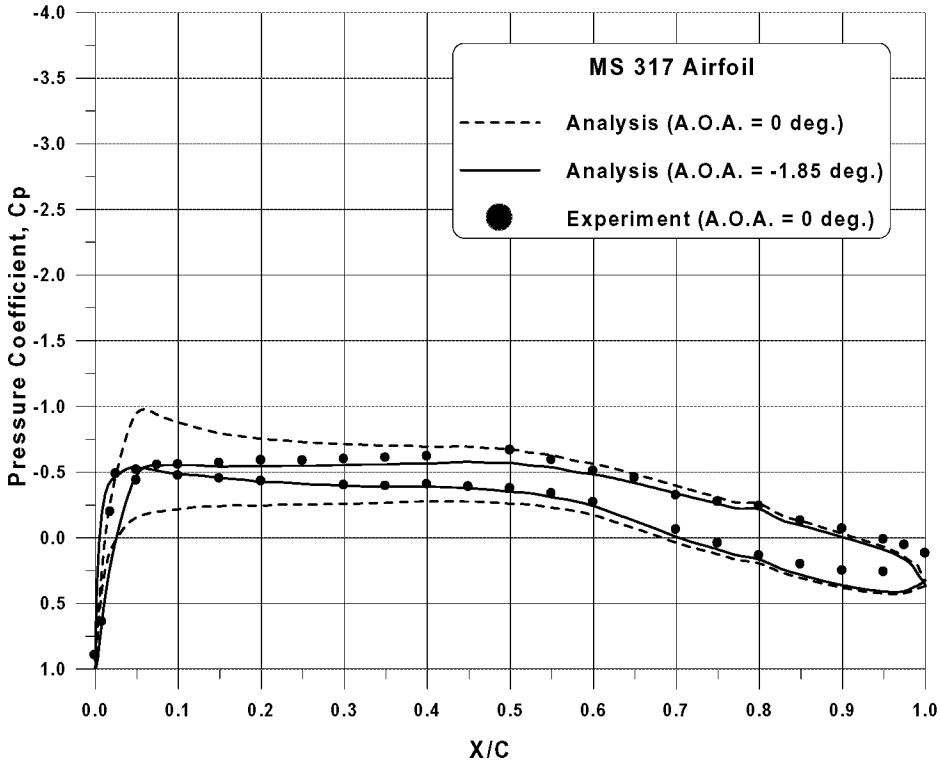

a. $\alpha = 0°$, M = 0.23, Re = 4.9 million

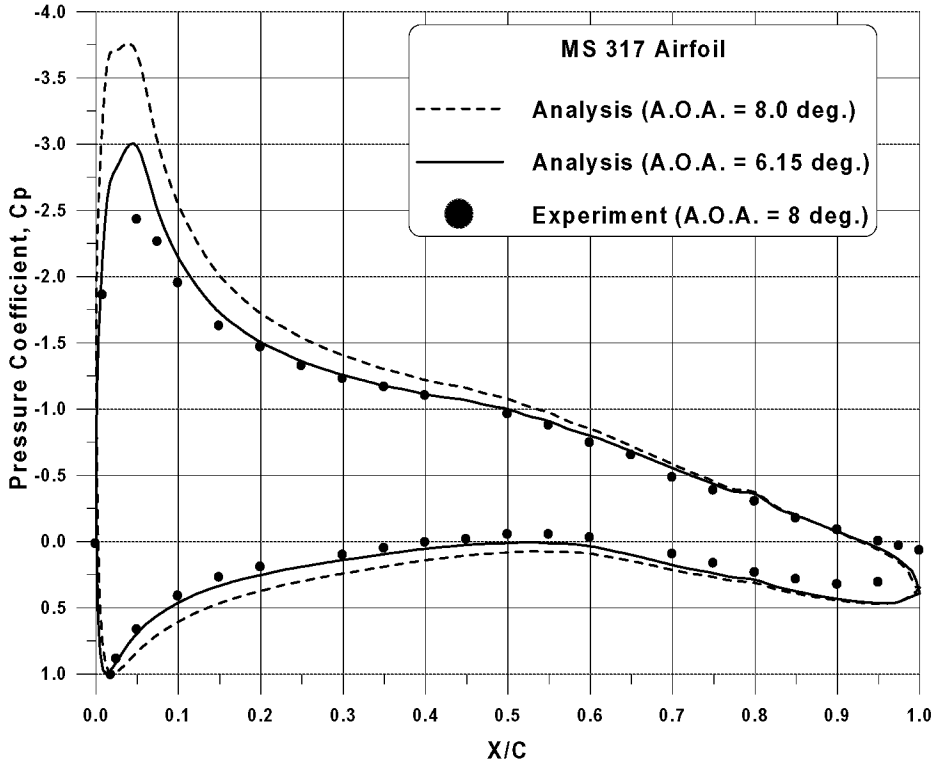

b. $\alpha = 8°$, M = 0.23, Re = 4.9 million

Fig. 73 Comparison of pressure distributions for MS(1)-0317 airfoil.

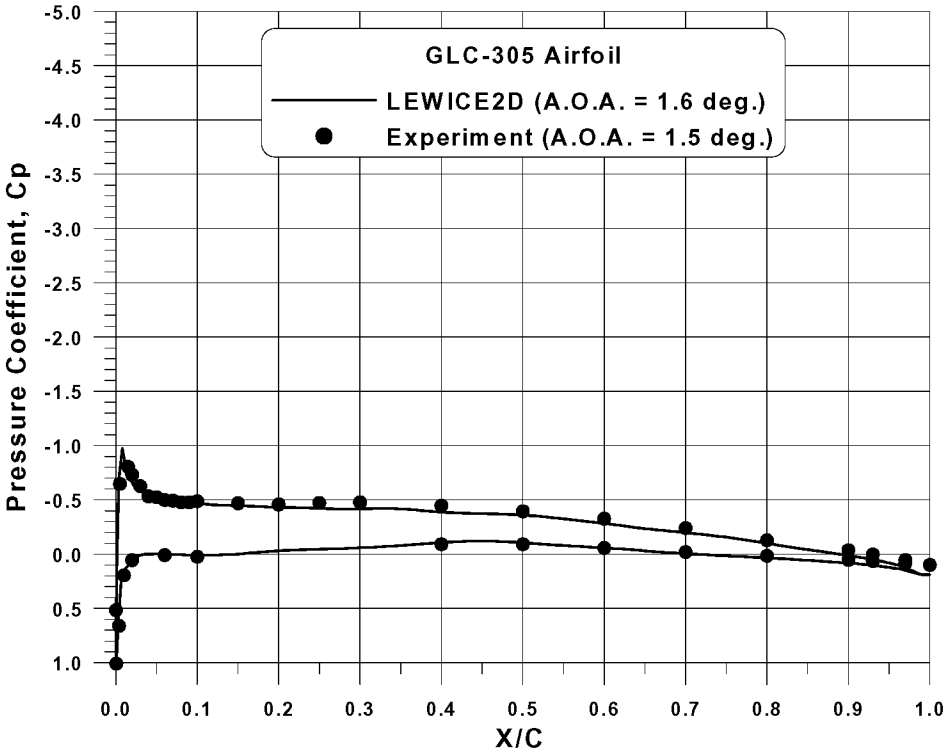

a. α = 1.5°, M = 0.23, Re = 4.83 million

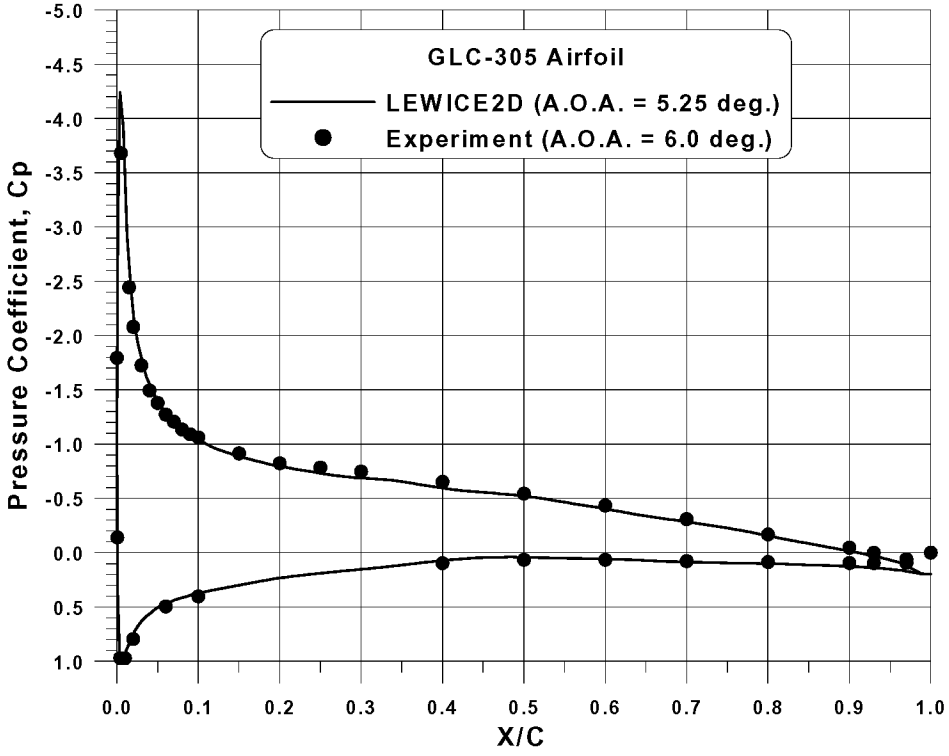

b. α = 6°, M = 0.23, Re = 4.83 million

Fig. 74 Comparison of pressure distributions for GLC-305 airfoil.

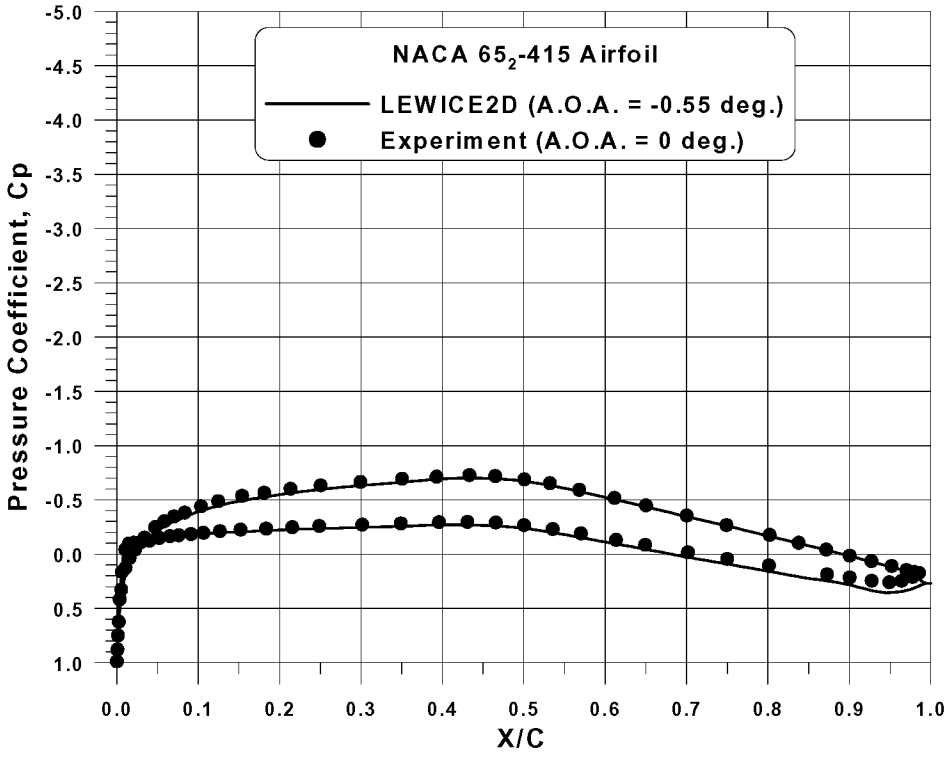

a. $\alpha = 0°$, M = 0.23, Re = 4.85 million

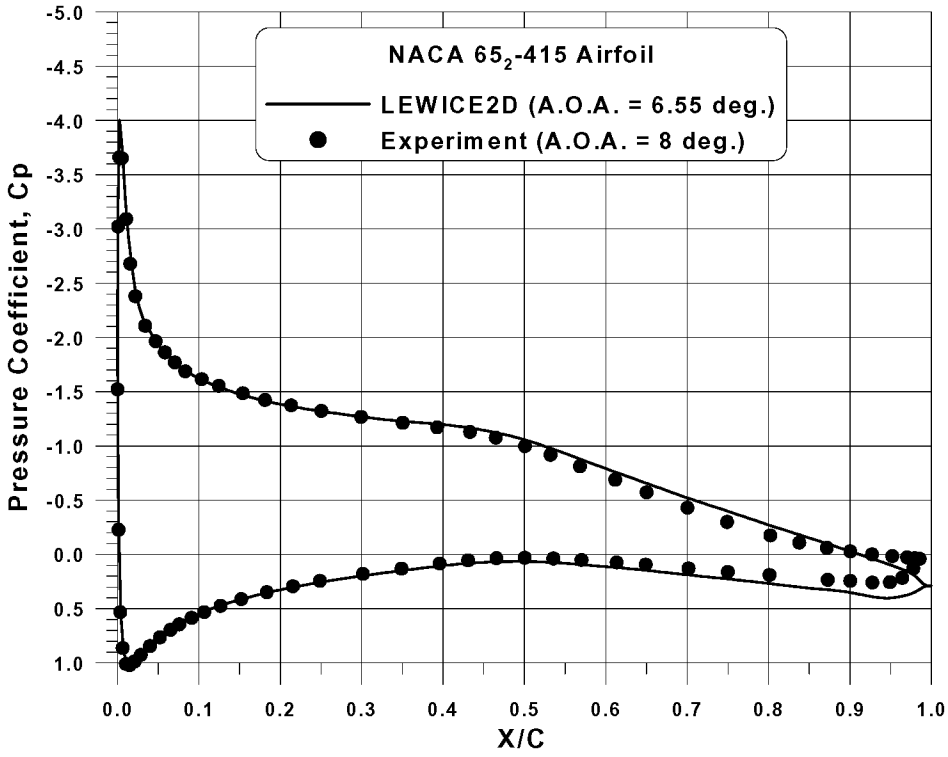

b. $\alpha = 8°$, M = 0.23, Re = 4.85 million

Fig. 75 Comparison of pressure distributions for NACA 65$_2$-415 airfoil.

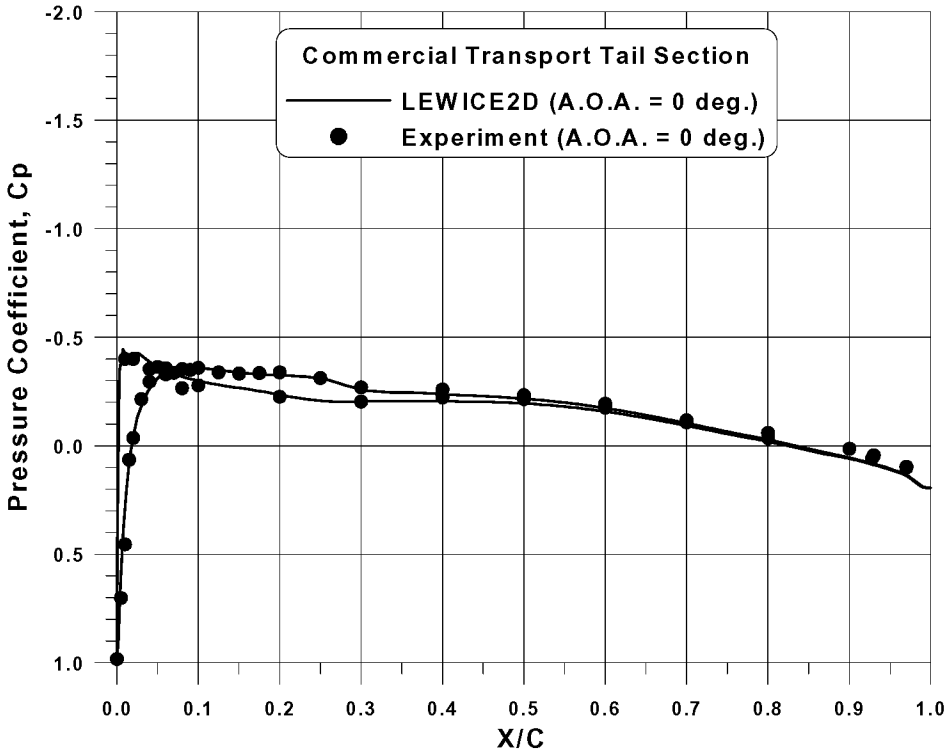

a. $\alpha = 0°$, M = 0.23, Re = 4.84 million

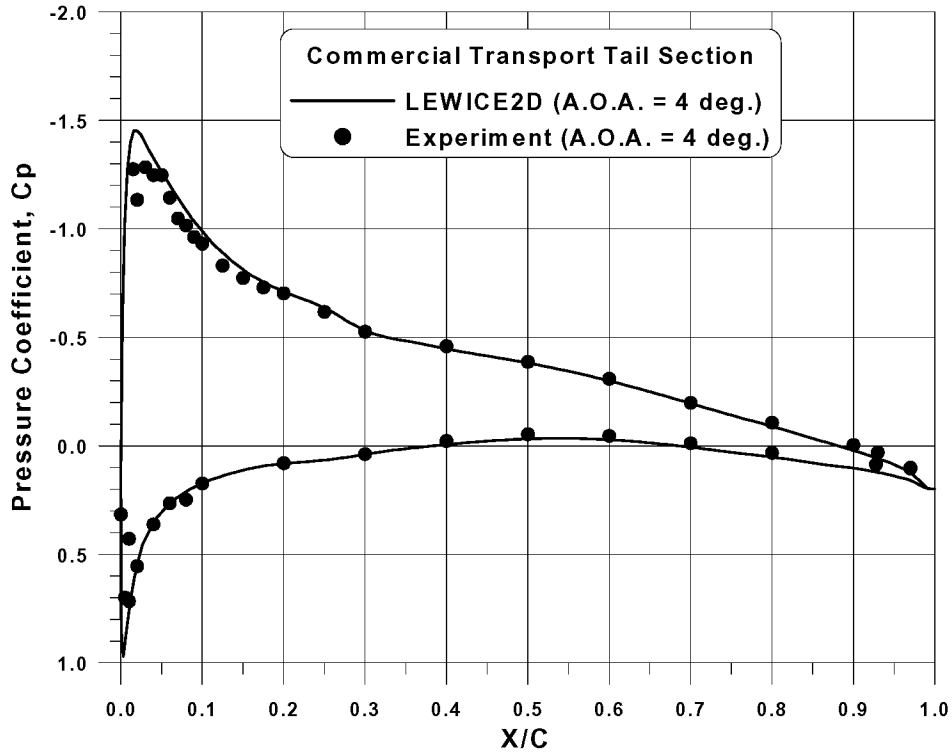

b. $\alpha = 4°$, M = 0.23, Re = 4.84 million

Fig. 76 Comparison of pressure distributions for commercial transport horizontal tail.

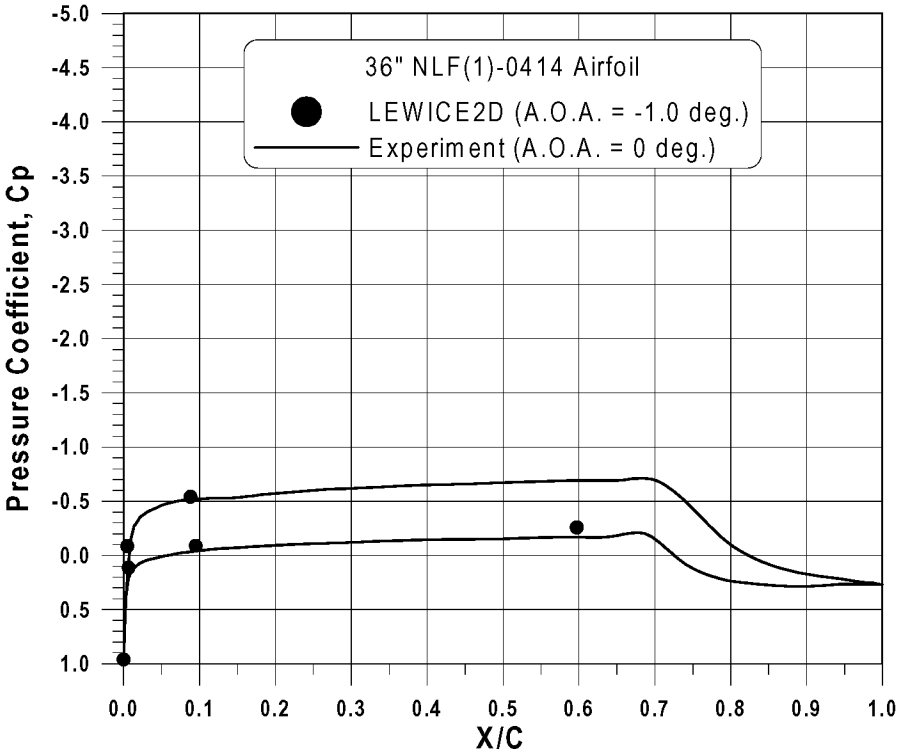

a. $\alpha = 0°$, M = 0.23, Re = 4.84 million

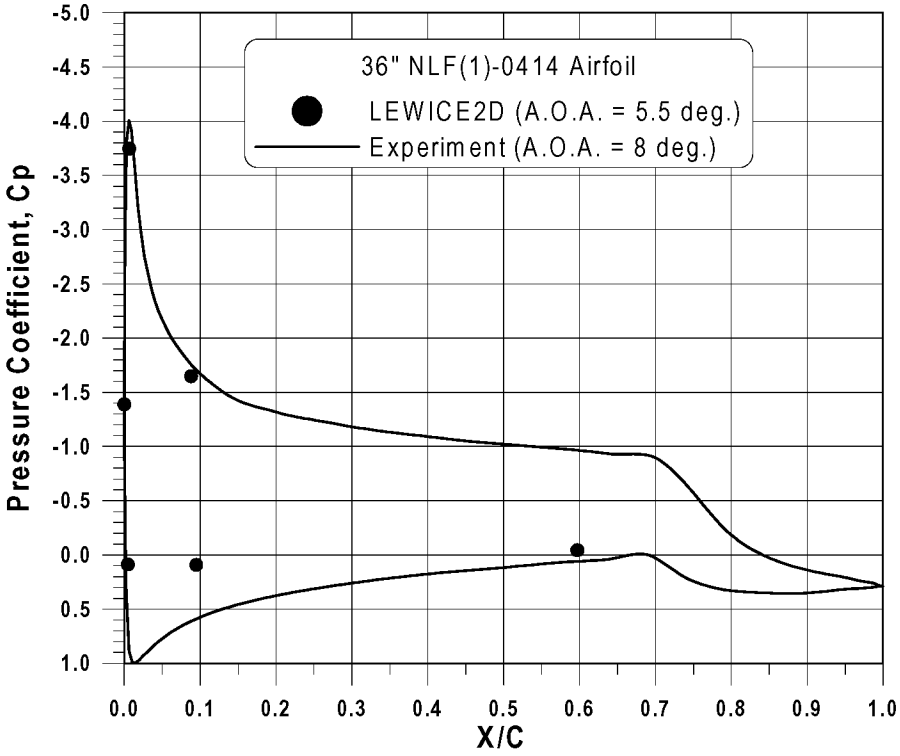

b. $\alpha = 8°$, M = 0.23, Re = 4.84 million

Fig. 77 Comparison of pressure distributions for 36-inch NLF(1)-0414 airfoil.

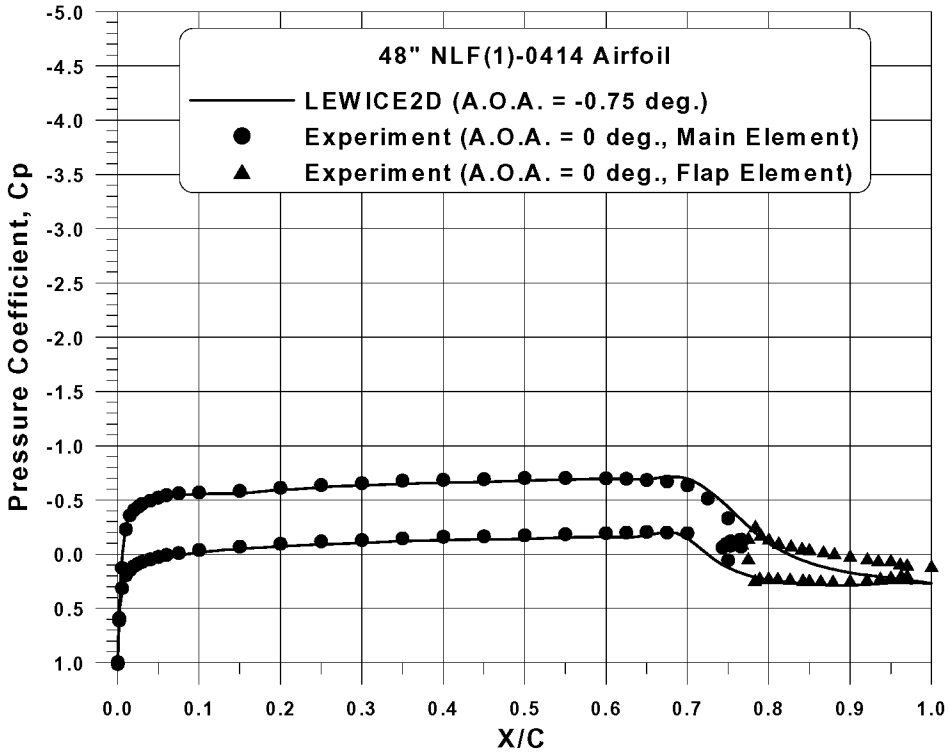

a. $\alpha = 0°$, M = 0.23, Re = 6.53 million

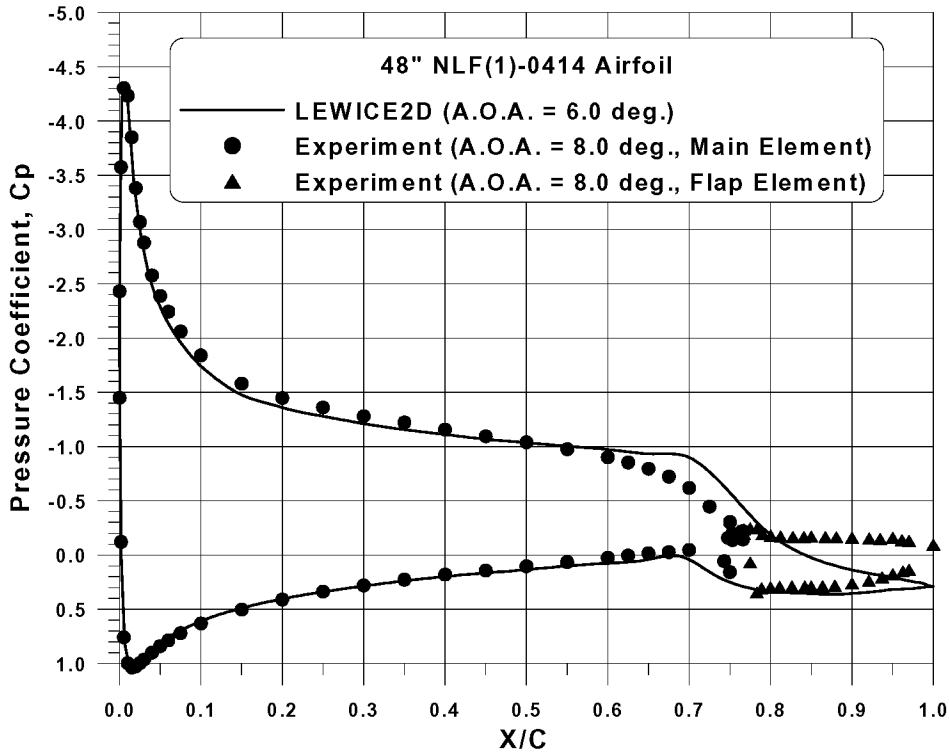

b. $\alpha = 8°$, M = 0.23, Re = 6.53 million

Fig. 78 Comparison of pressure distributions for 48-inch NLF(1)-0414 airfoil.

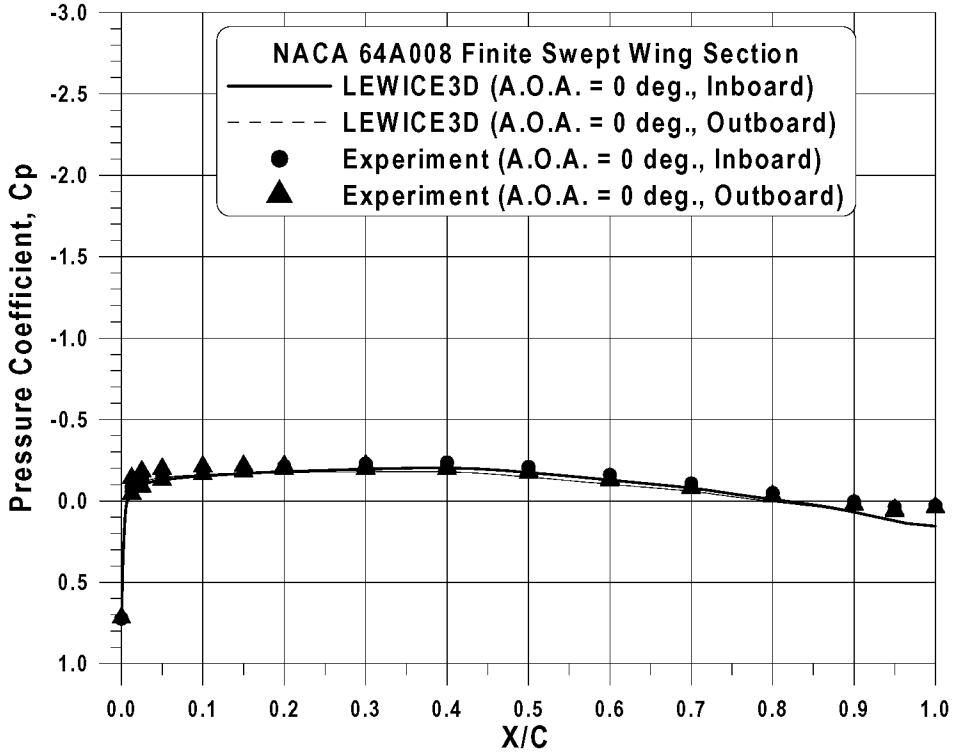

a. $\alpha = 0°$, M = 0.23, Re = 5.03 million

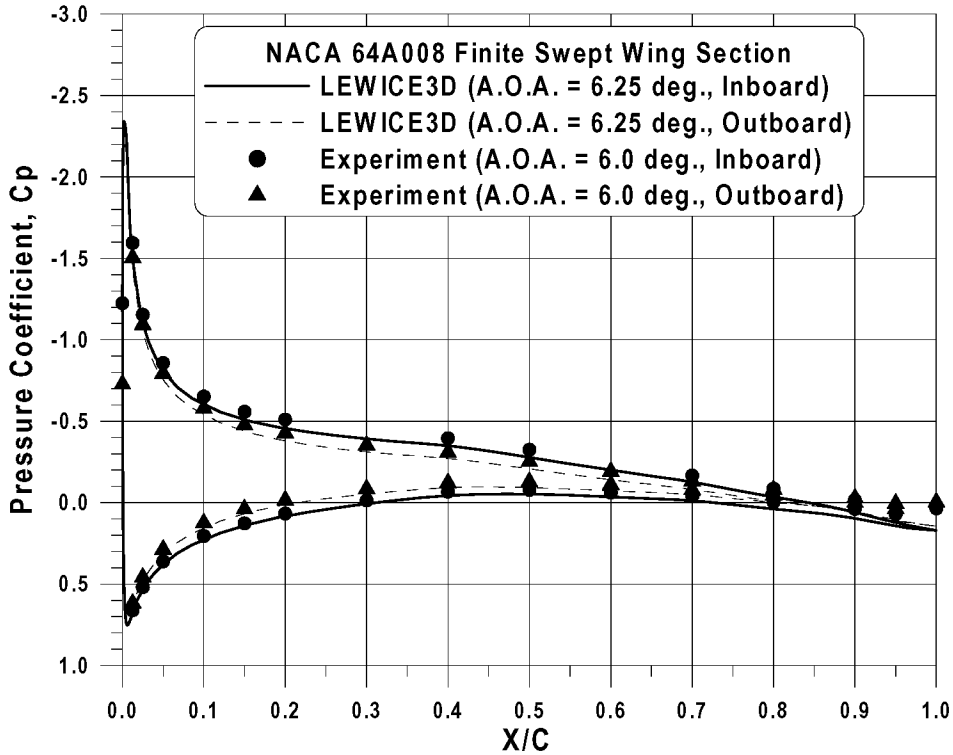

b. $\alpha = 6°$, M = 0.23, Re = 5.03 million

Fig. 79 Comparison of pressure distributions for NACA 64A008 finite swept tail.

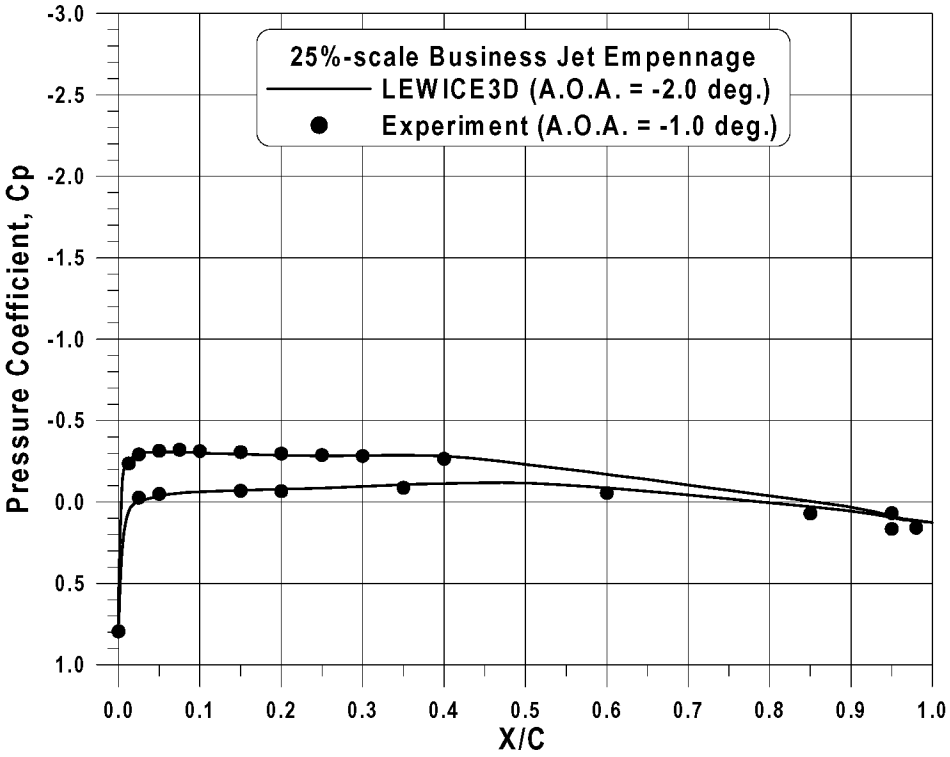

a. α = -1°, M = 0.23, Re = 1.49 million

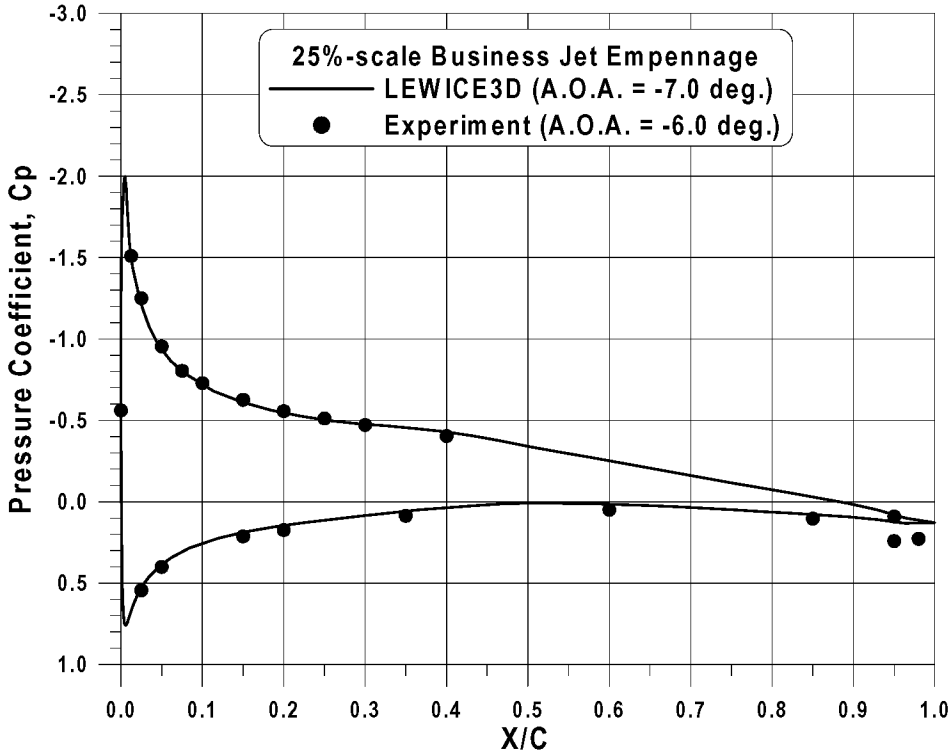

b. α = -6°, M = 0.23, Re = 1.49 million

Fig. 80 Comparison of pressure distributions for 25%-scale Business Jet Empennage.

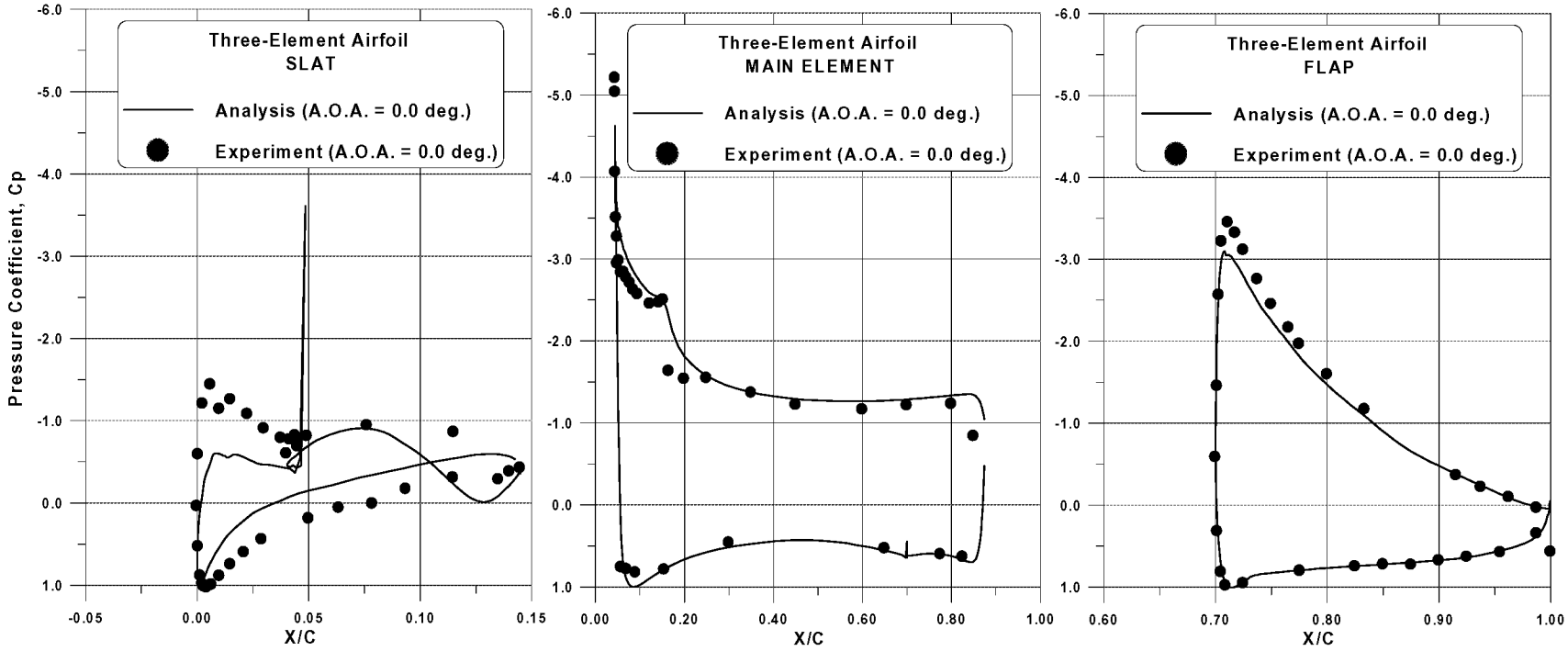

Fig. 81 Comparison of experimental and INS2D pressure distributions for the three-element high lift system; $\alpha = 0°$, M = 0.23, Re = 4.9 million, landing configuration, slat deflection 30 deg., flap deflection 30 deg.

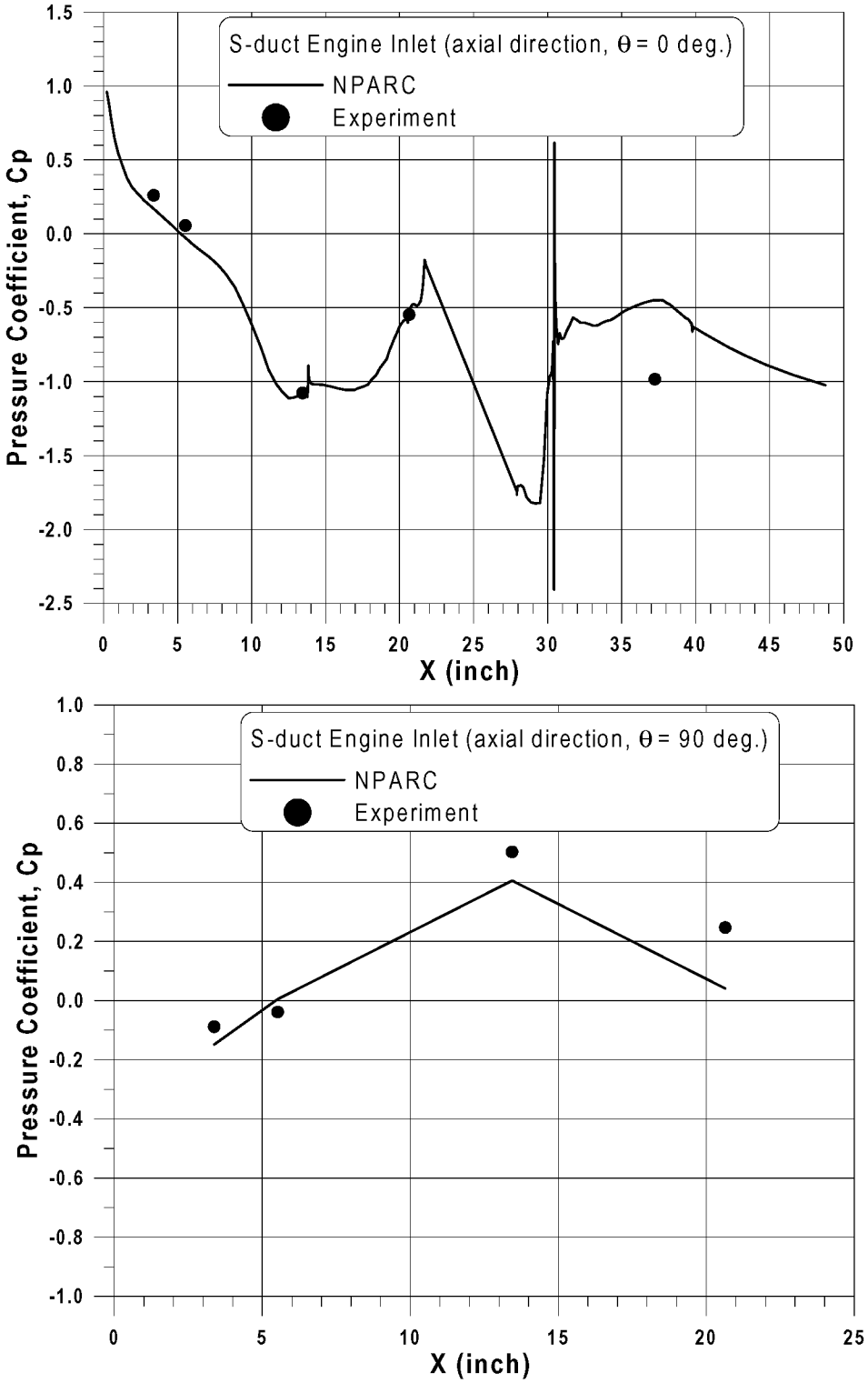

Fig. 82a Comparison of experimental and NPARC pressure distributions for the S-duct engine inlet; V_∞ = 170 mph, mass flow rate = 23 lbm/sec (Continued).

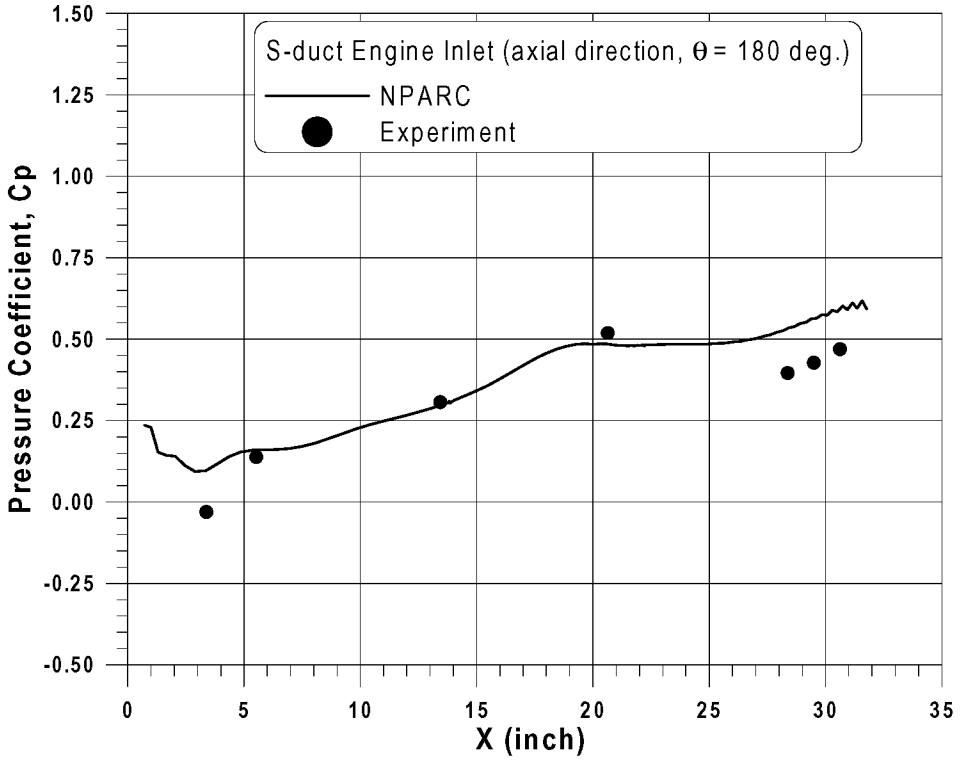

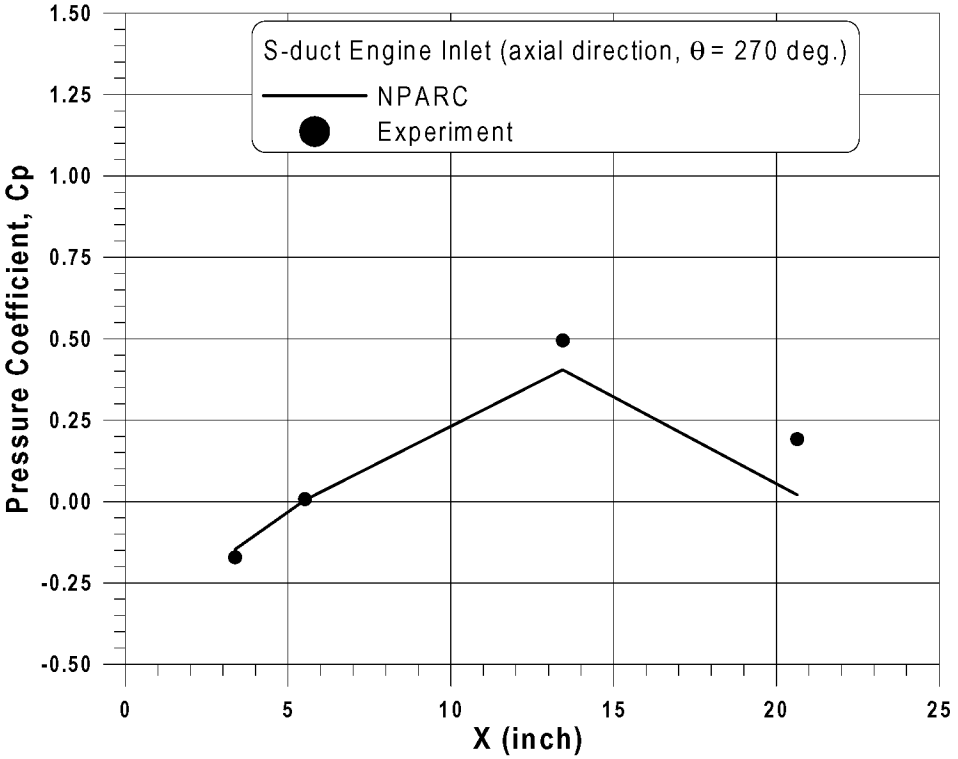

Fig. 82b Comparison of experimental and NPARC pressure distributions for the S-duct engine inlet; V_∞ = 170 mph, mass flow rate = 23 lbm/sec (Continued).

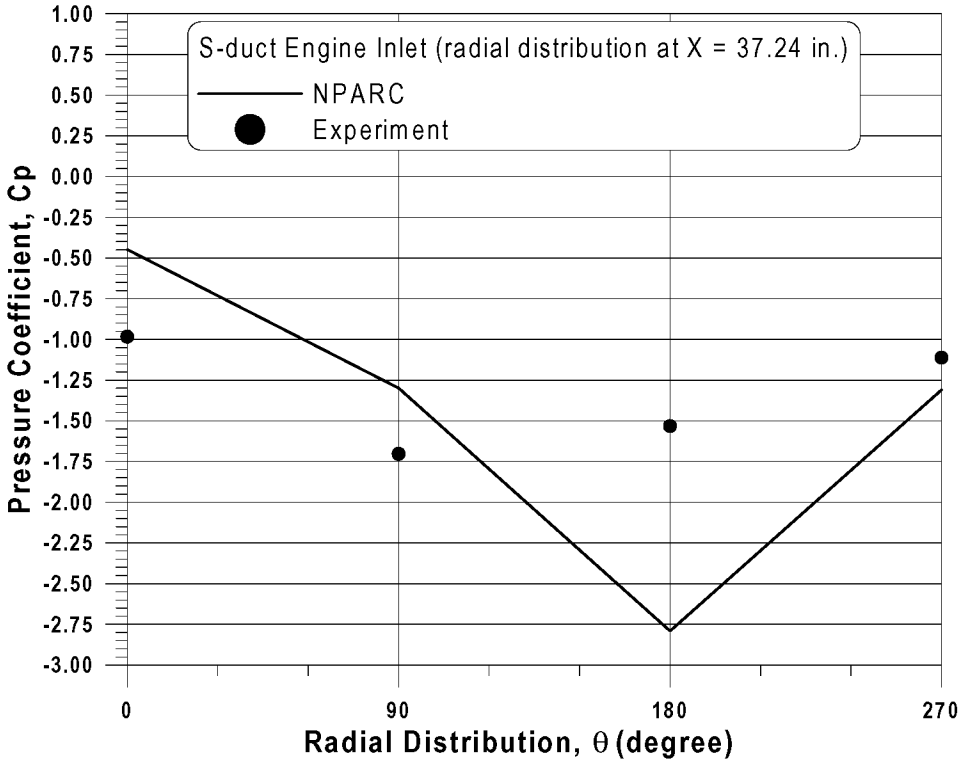

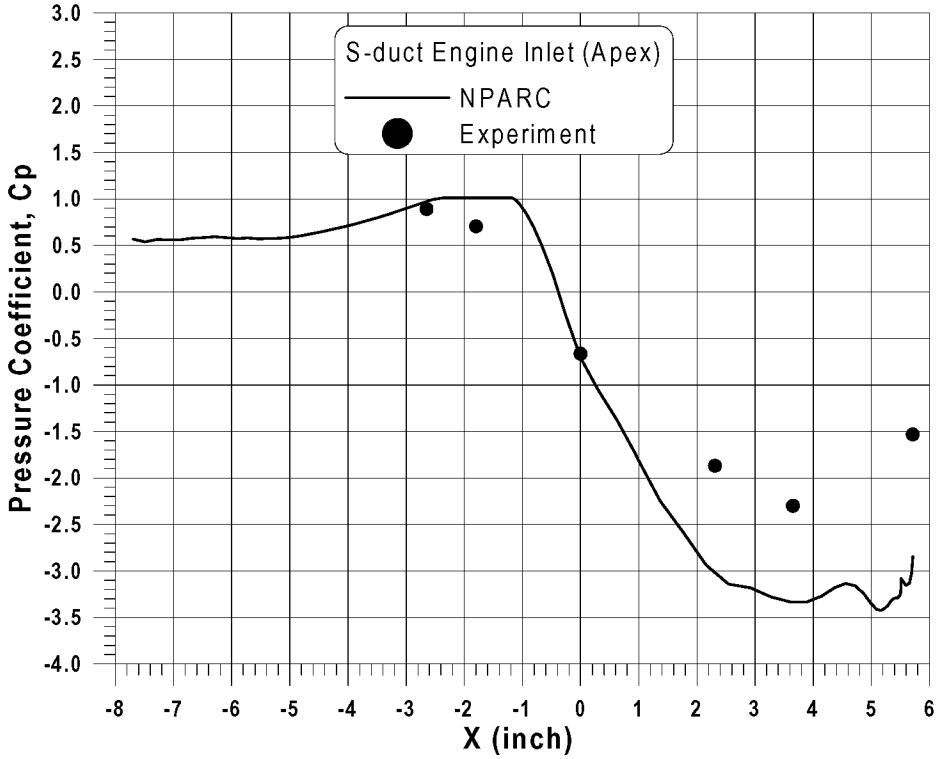

Fig. 82c Comparison of experimental and NPARC pressure distributions for the S-duct engine inlet; V_∞ = 170 mph, mass flow rate = 23 lbm/sec.

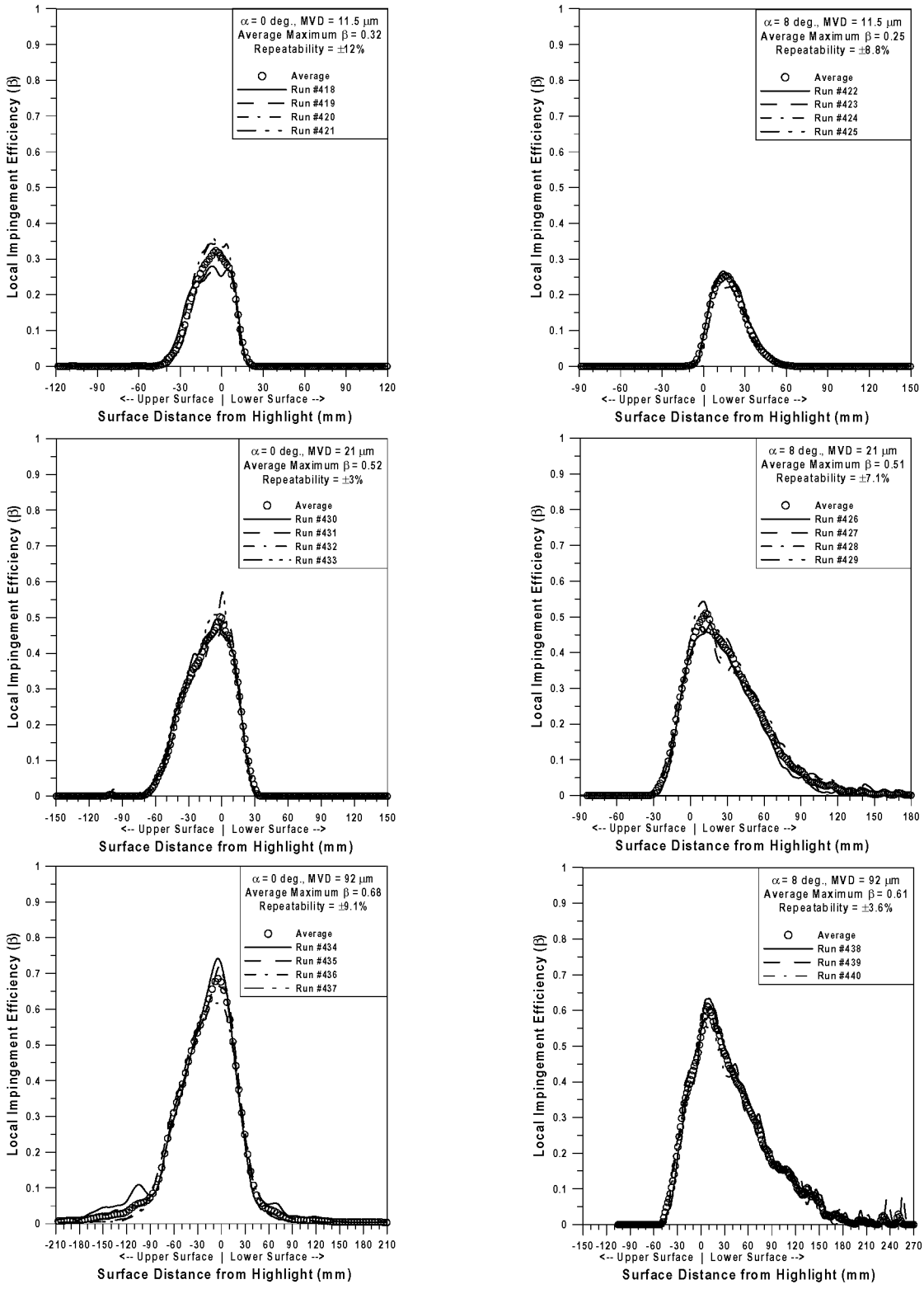

Fig. 83 Test repeatability for MS-317 airfoil -1997 IRT tests.

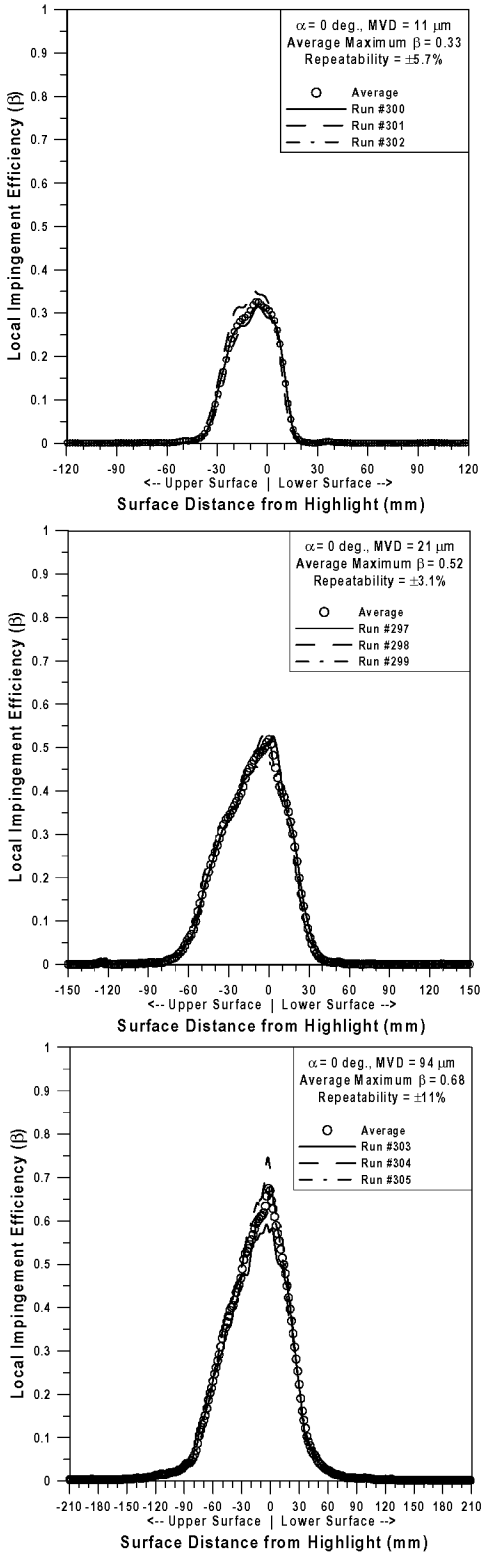

Fig. 84 Test repeatability for MS-317 airfoil -1999 IRT tests.

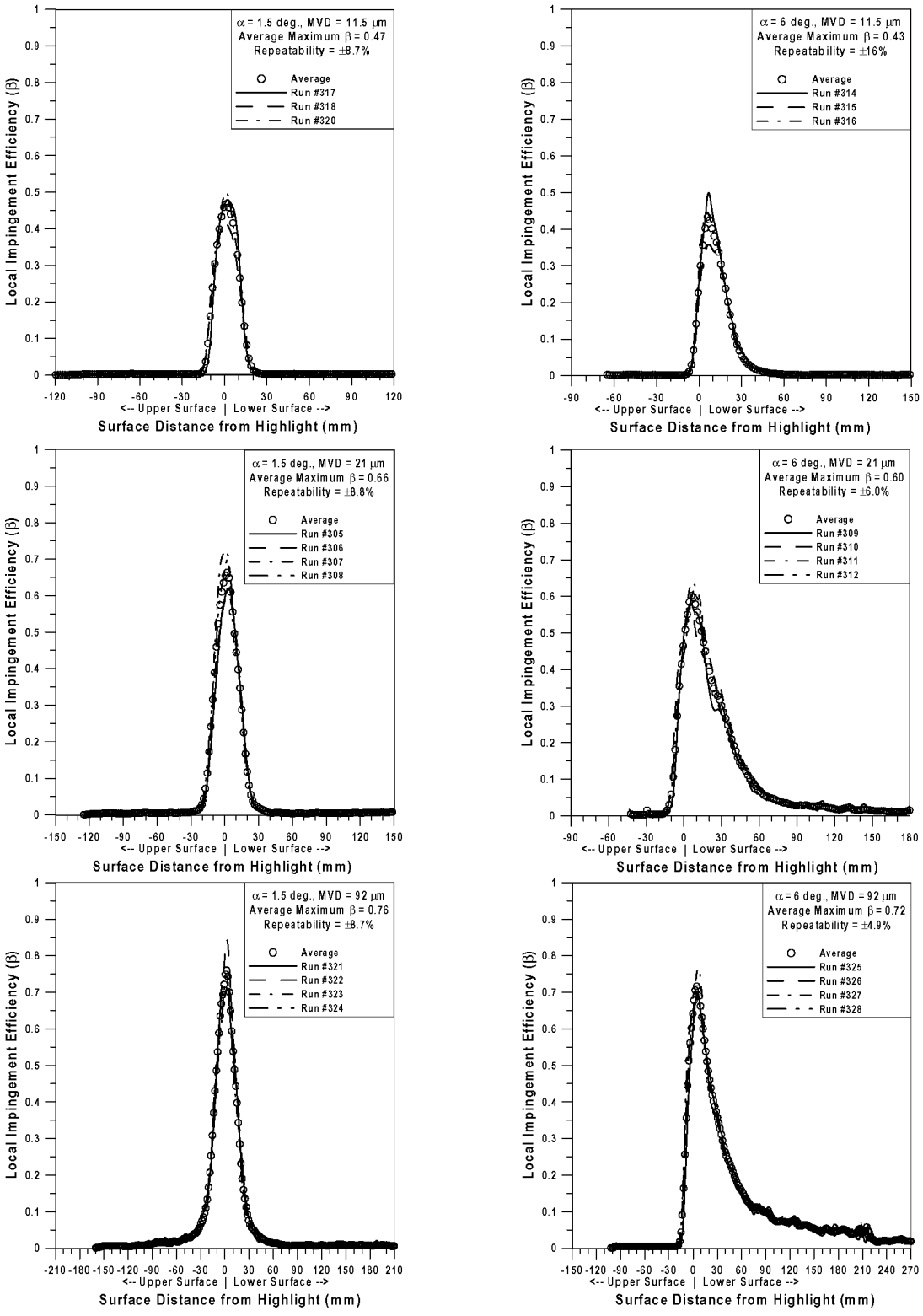

Fig. 85 Test repeatability for GLC-305 airfoil - 1997 IRT tests.

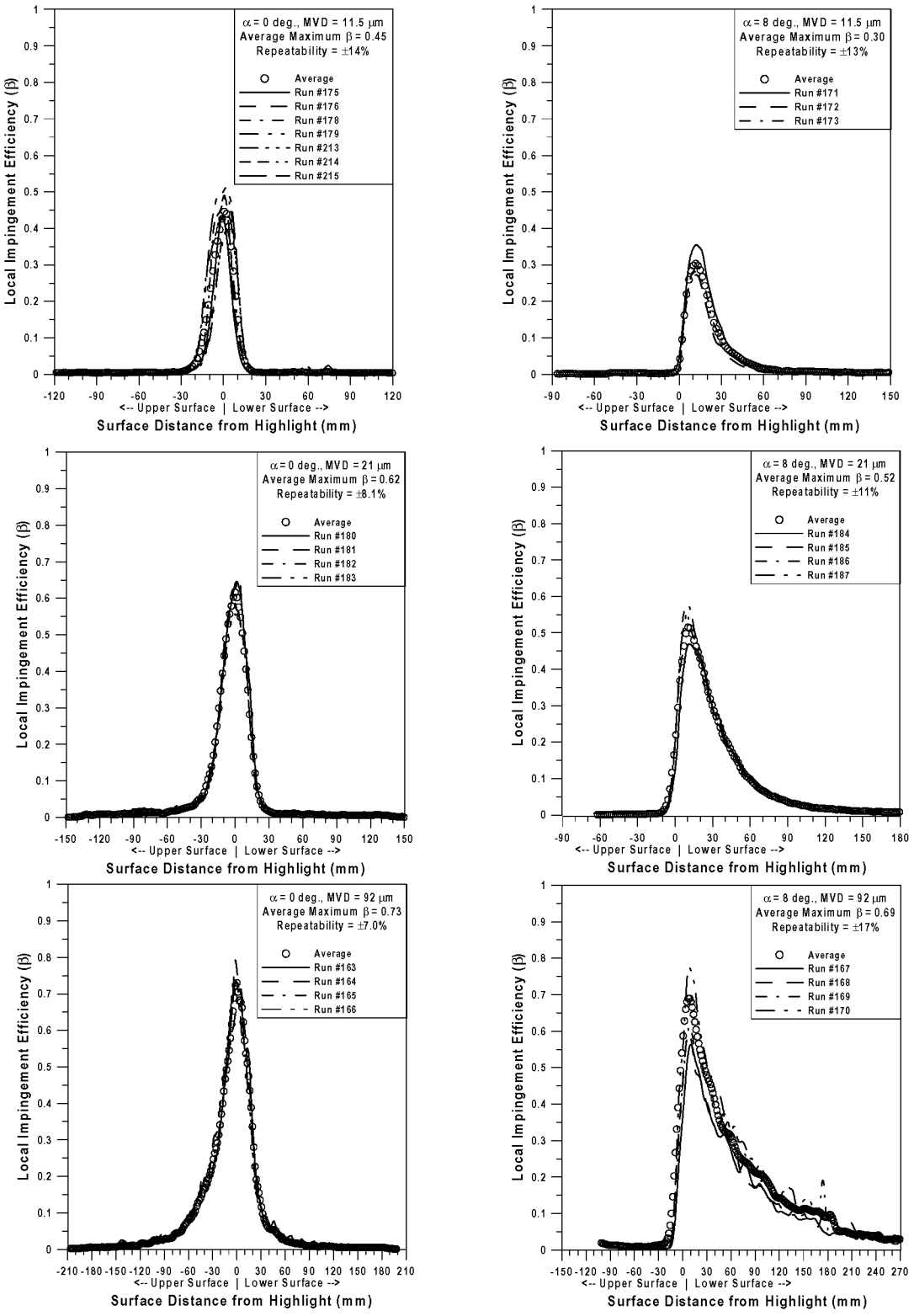

Fig. 86 Test repeatability for NACA 65_2-415 airfoil -1997 IRT tests.

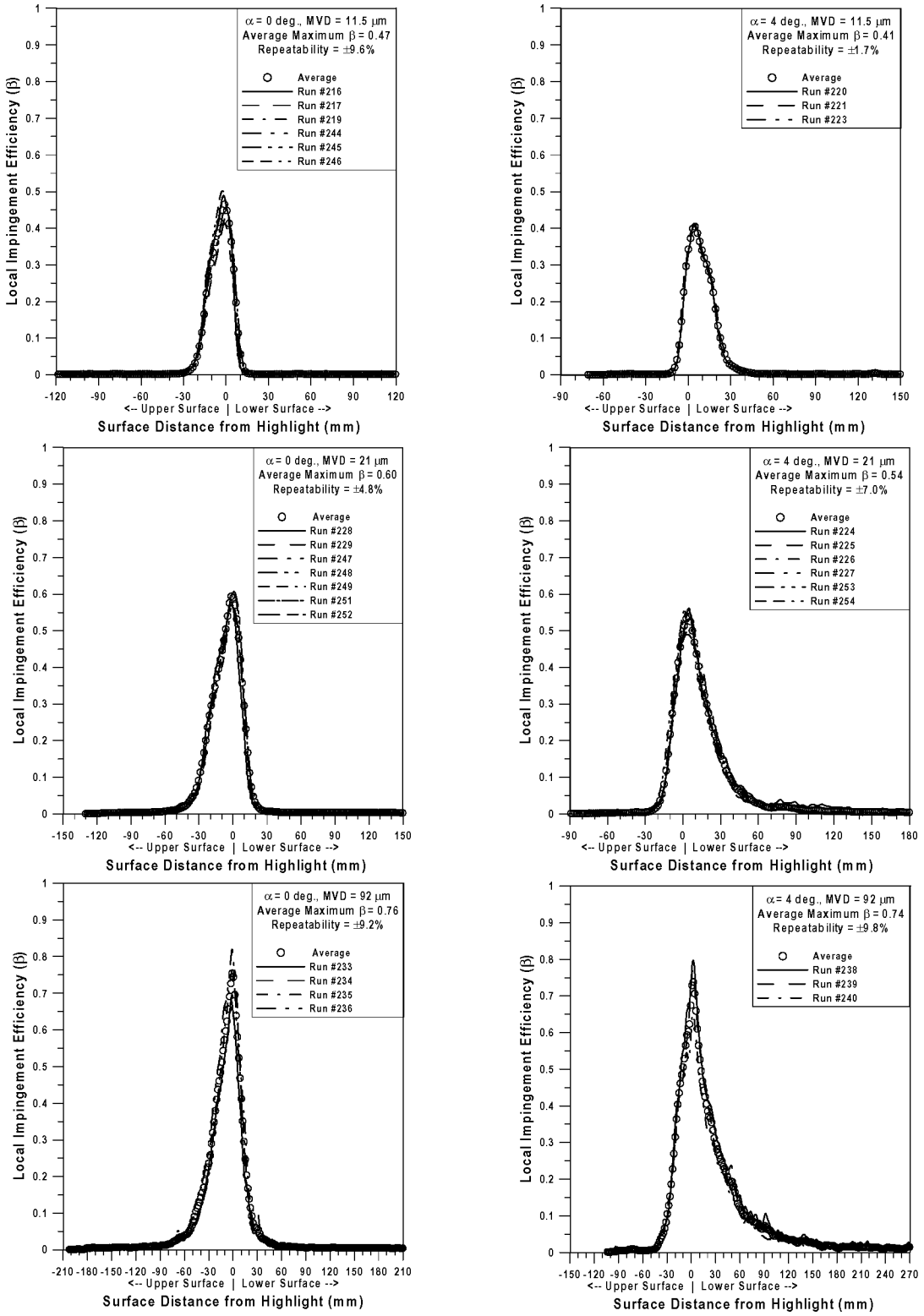

Fig. 87 Test repeatability for commercial transport tail section - 1997 IRT tests.

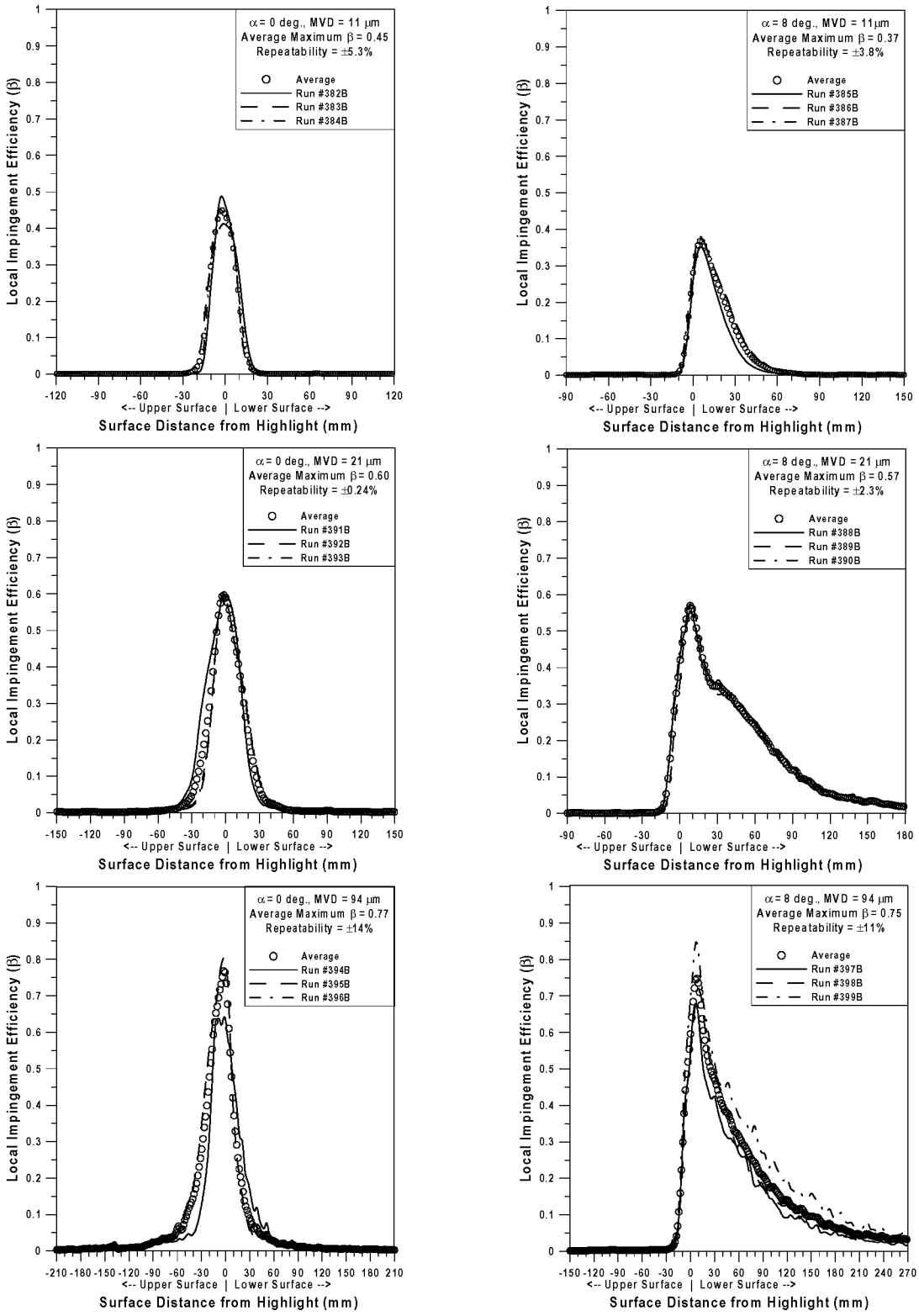

Fig. 88 Test repeatability for 36-in NLF(1)-0414 airfoil -1999 IRT tests.

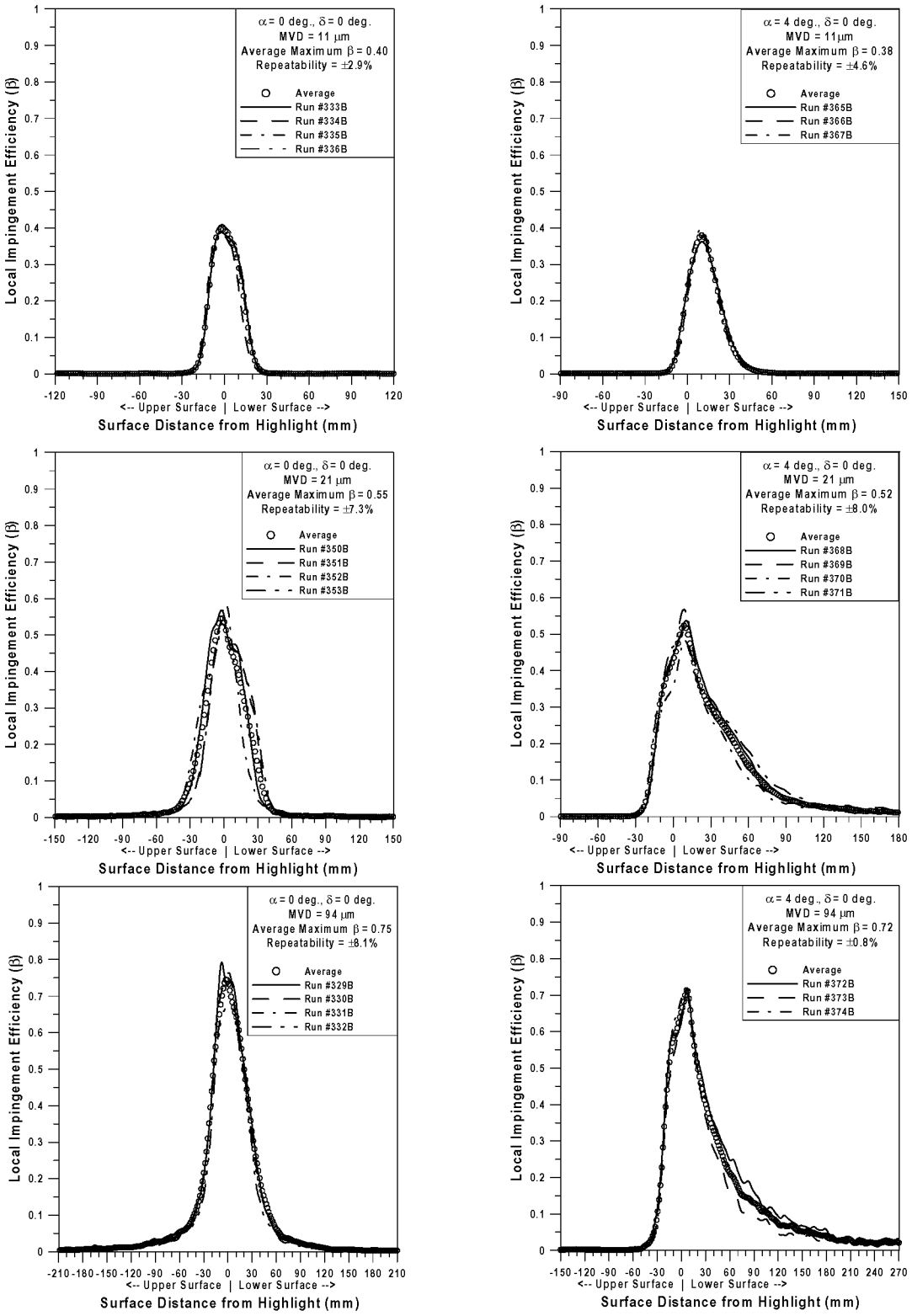

Fig. 89a Test repeatability for 48-in NLF(1)-0414 airfoil -1999 IRT tests (Continued).

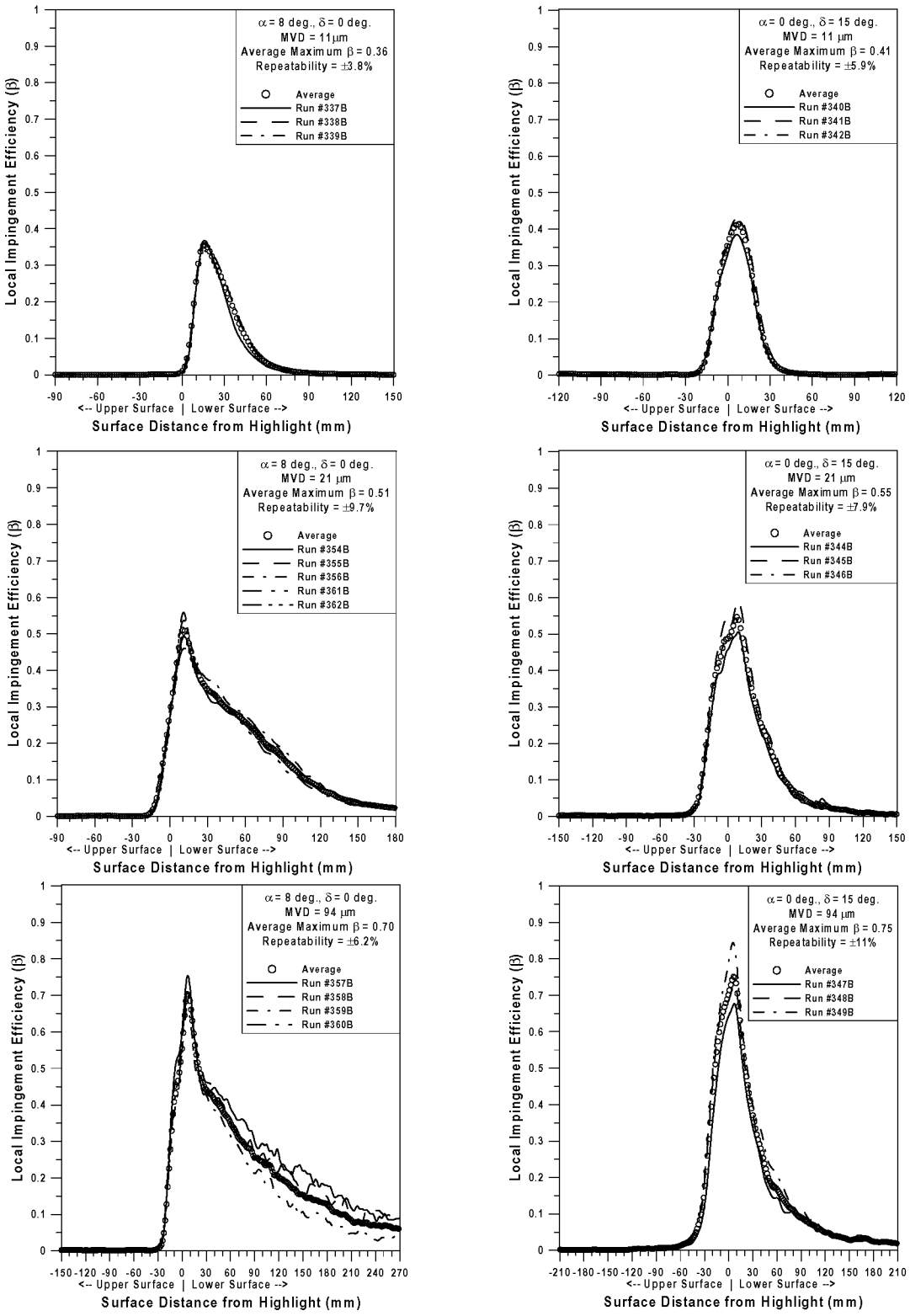

Fig. 89b Test repeatability for 48-in NLF(1)-0414 airfoil -1999 IRT tests.

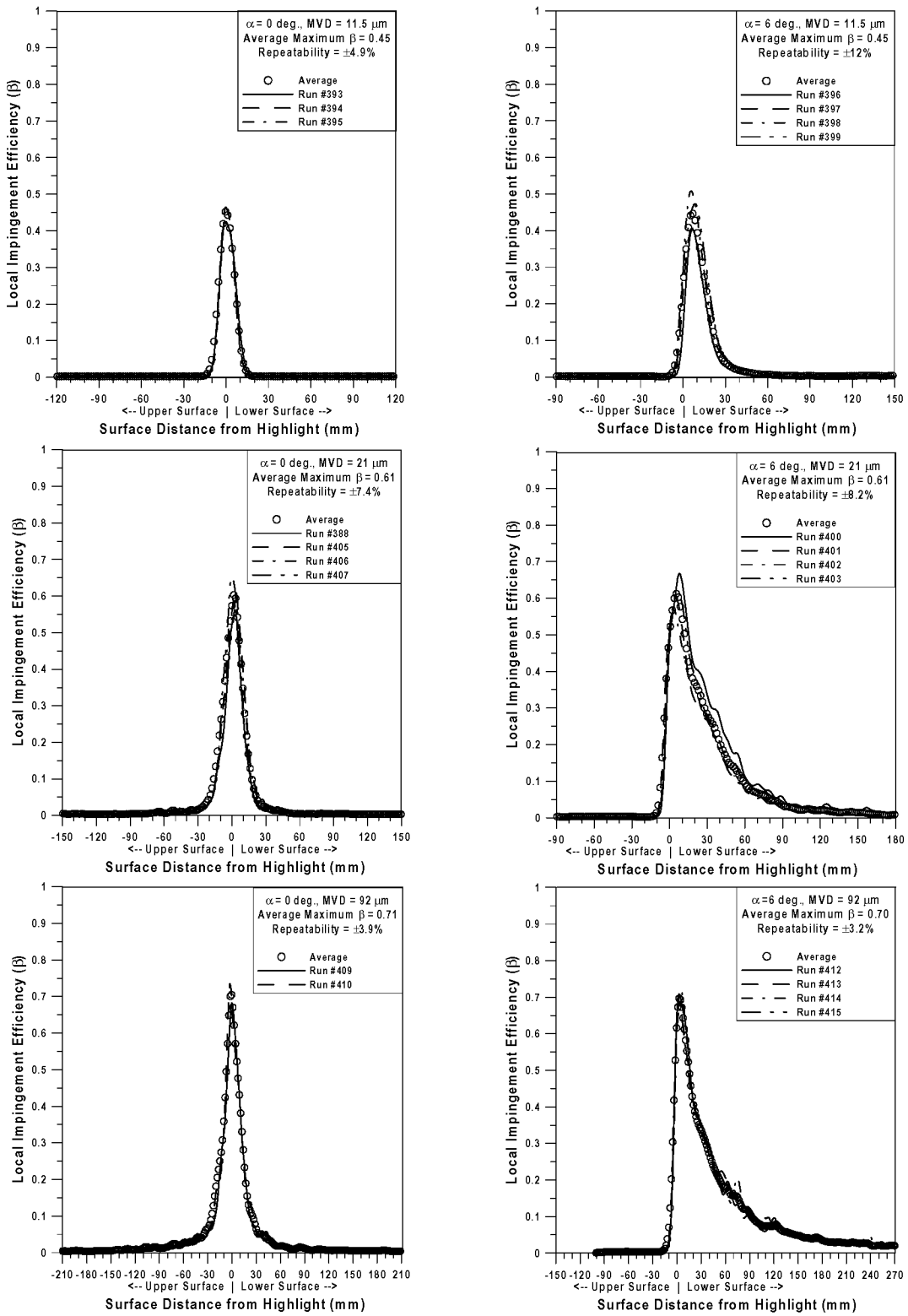

Fig. 90 Test repeatability for NACA 64A008 swept tail -1997 IRT tests.

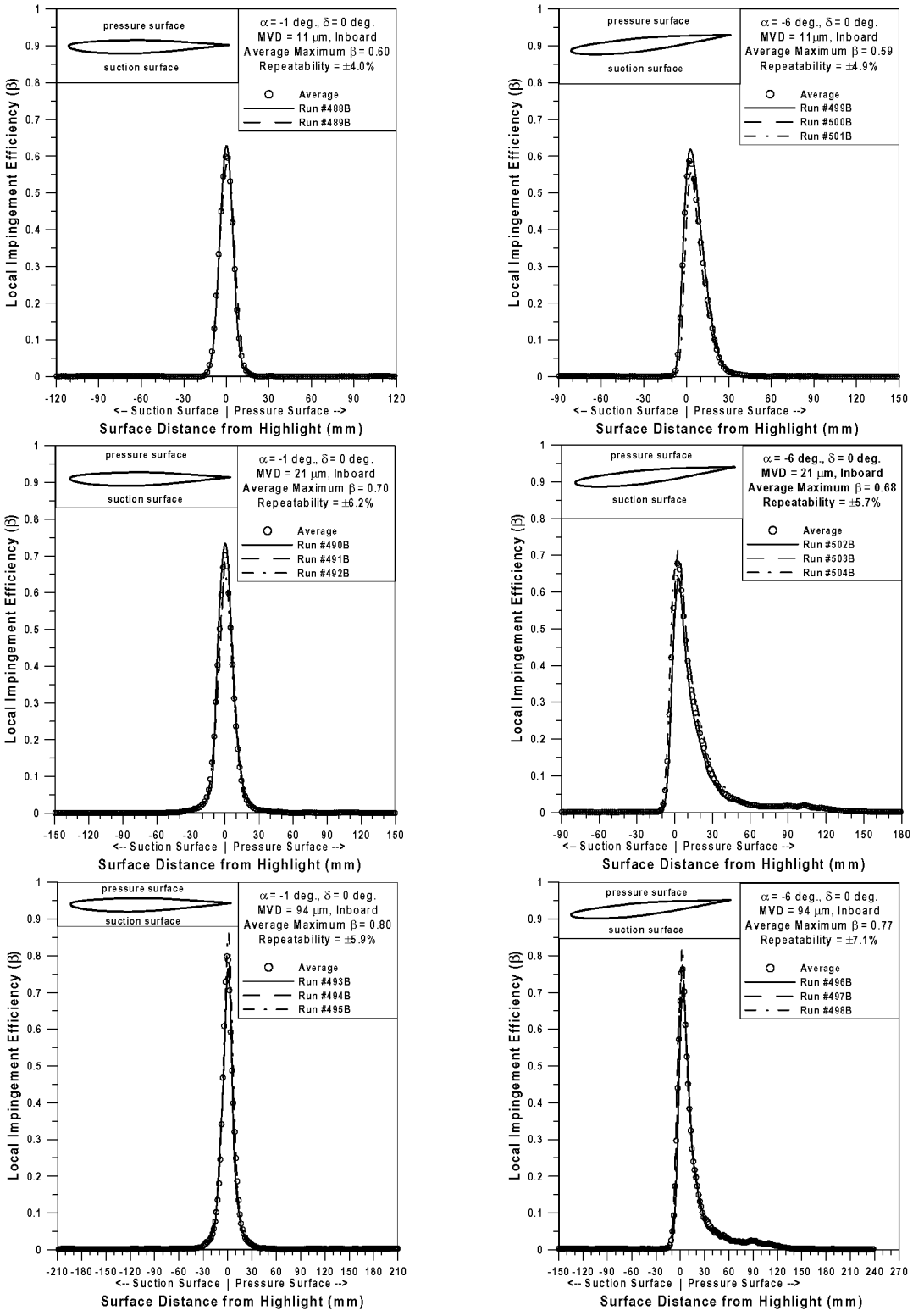

Fig. 91a Test repeatability for 25%-scale Business Jet Empennage 1999 IRT tests; Inboard (Continued).

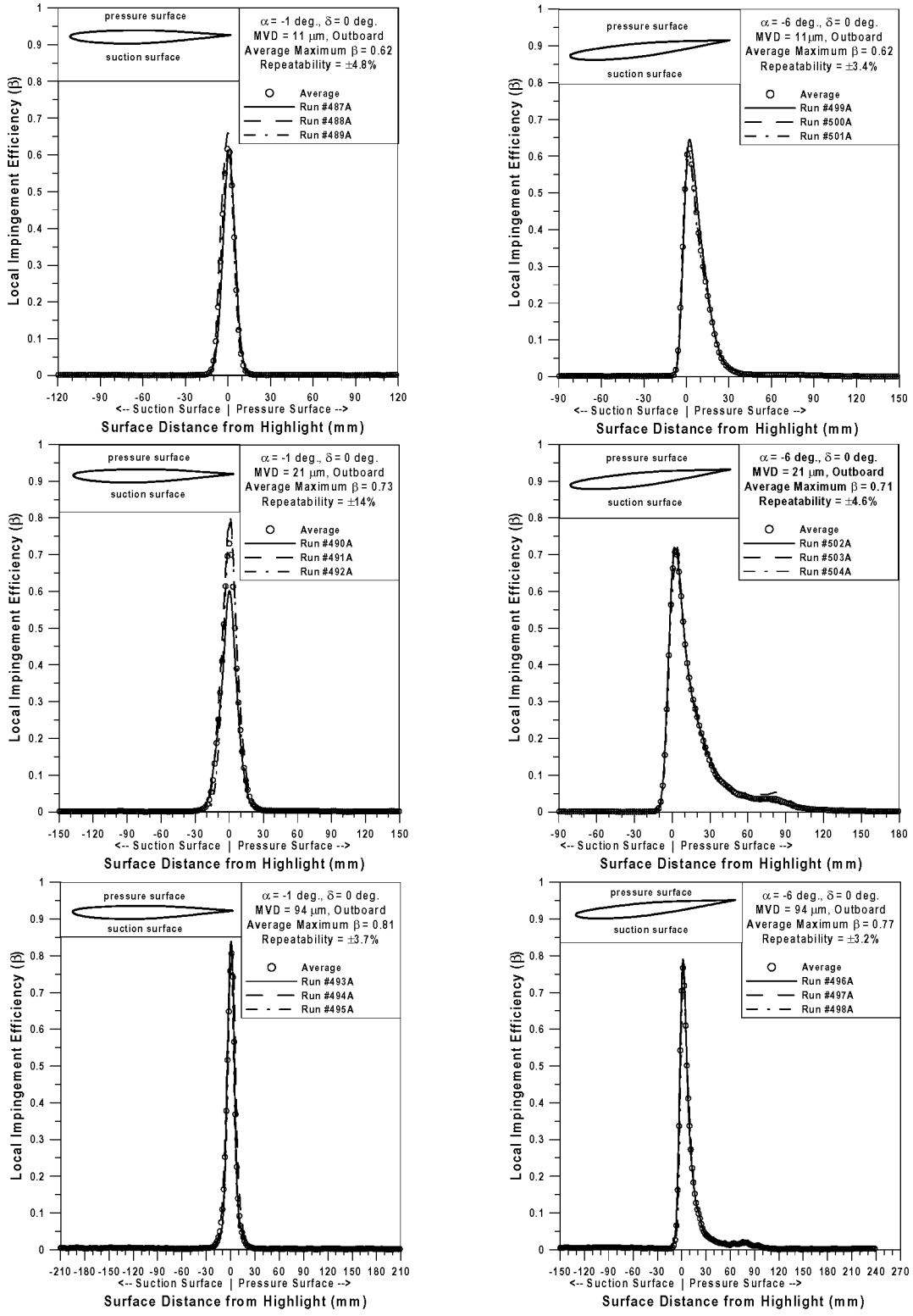

Fig. 91b Test repeatability for 25%-scale Business Jet Empennage
1999 IRT tests; Outboard

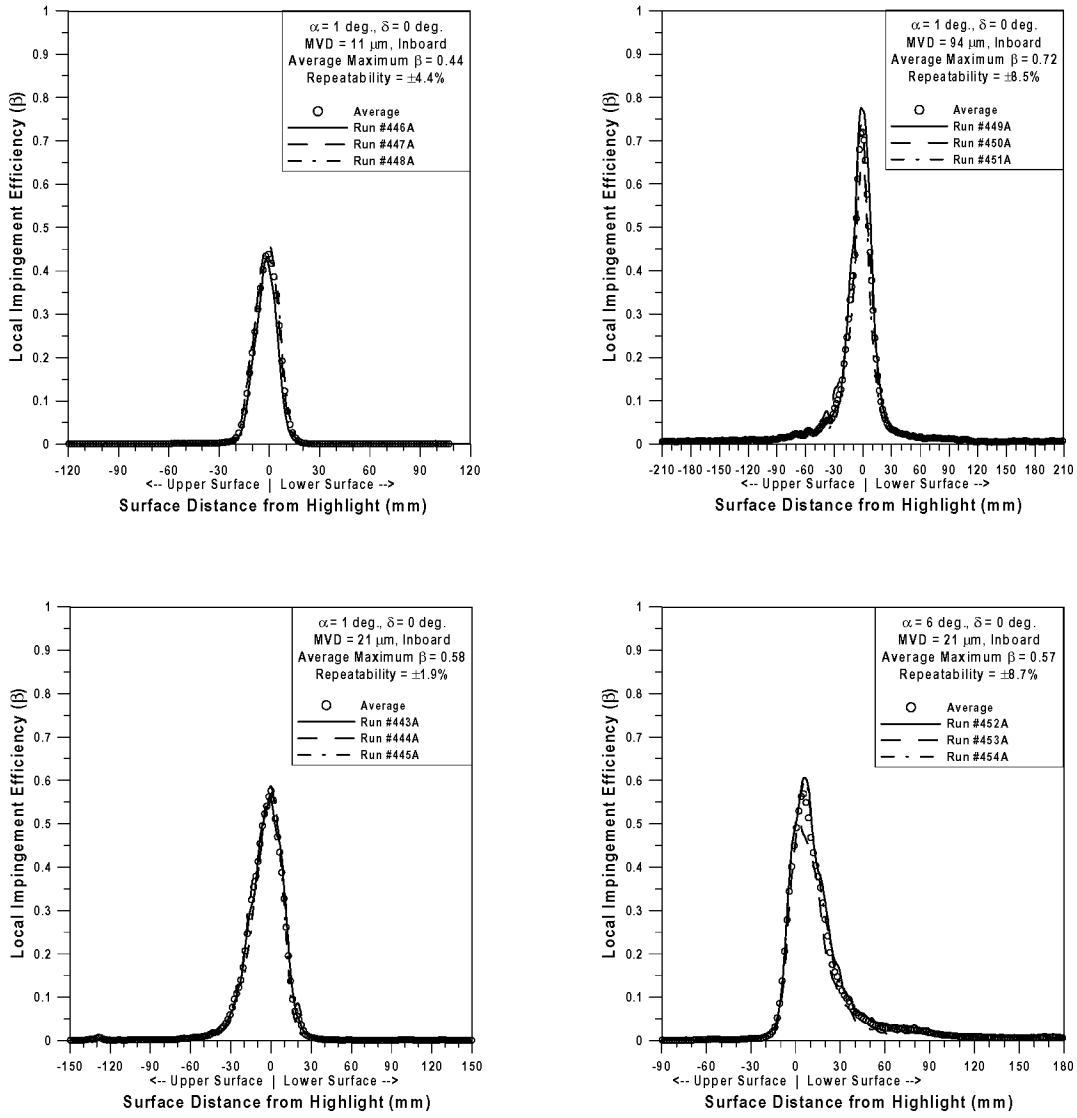

Fig. 92a Test repeatability for full-scale Business Jet horizontal tail - 1999 IRT tests; Inboard (Continued).

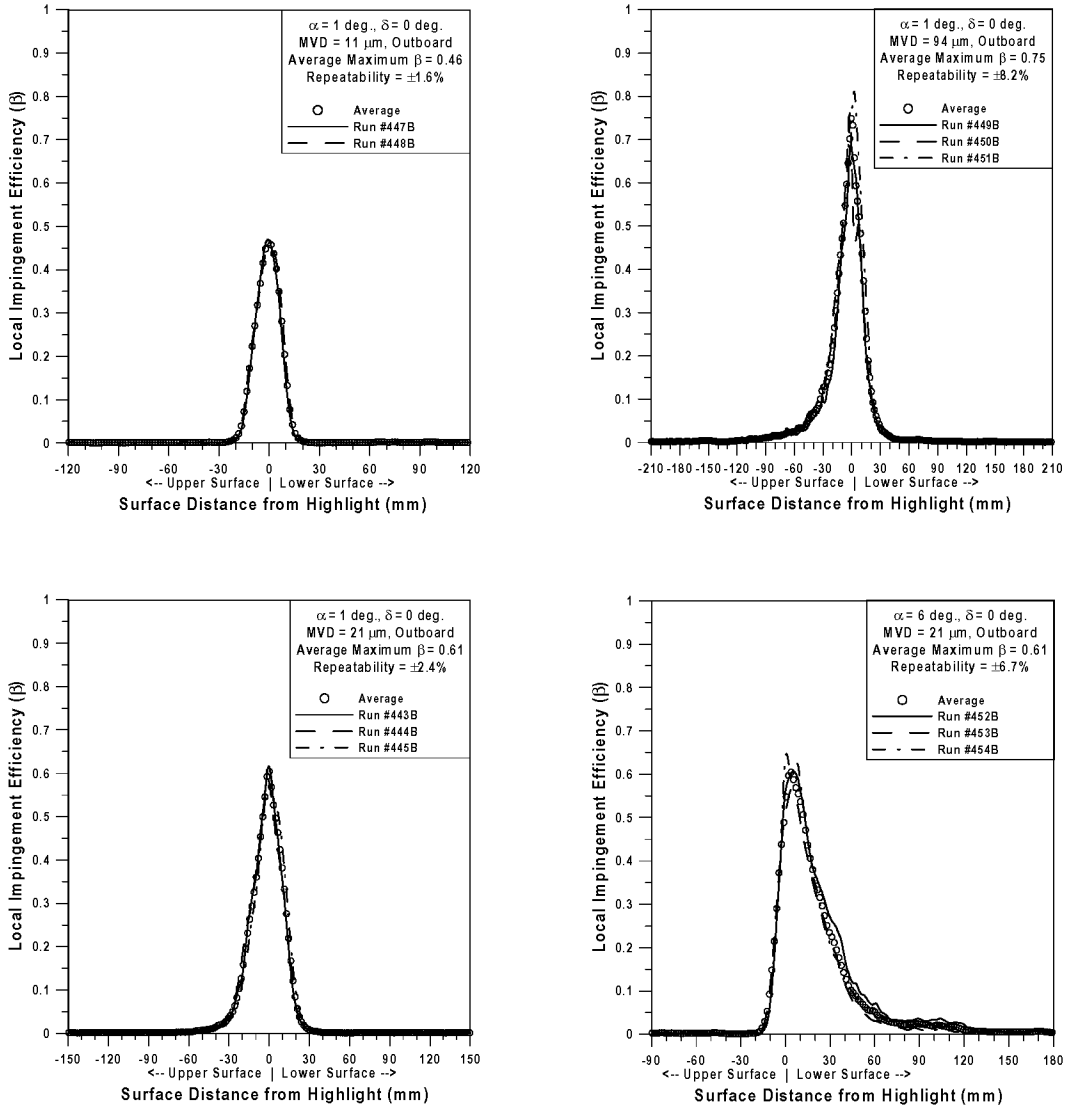

Fig. 92b Test repeatability for full-scale Business Jet horizontal tail - 1999 IRT tests; Outboard.

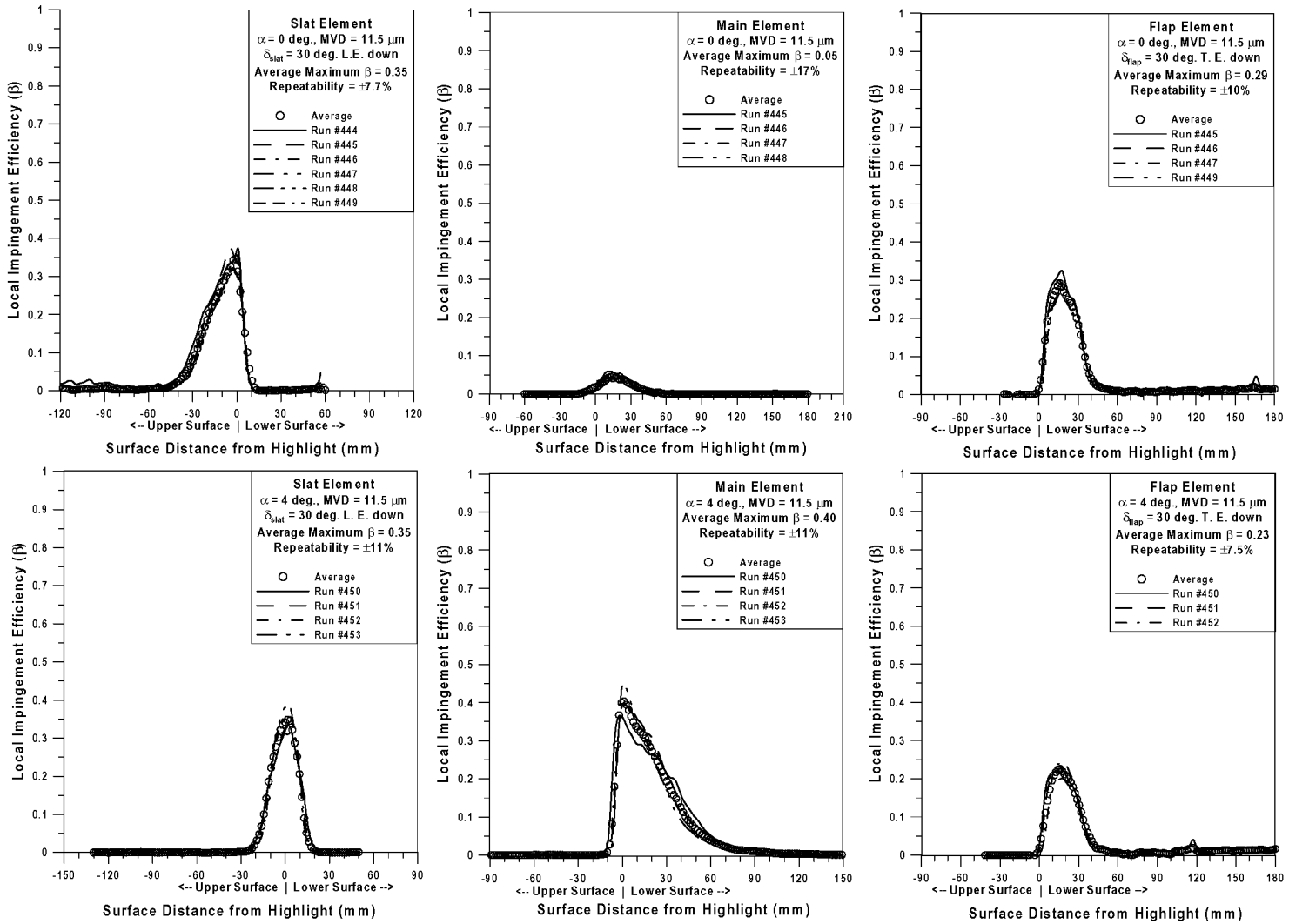

Fig. 93a Test repeatability for three-element high lift system airfoil - 1997 IRT tests; MVD = 11.5 μm (Continued).

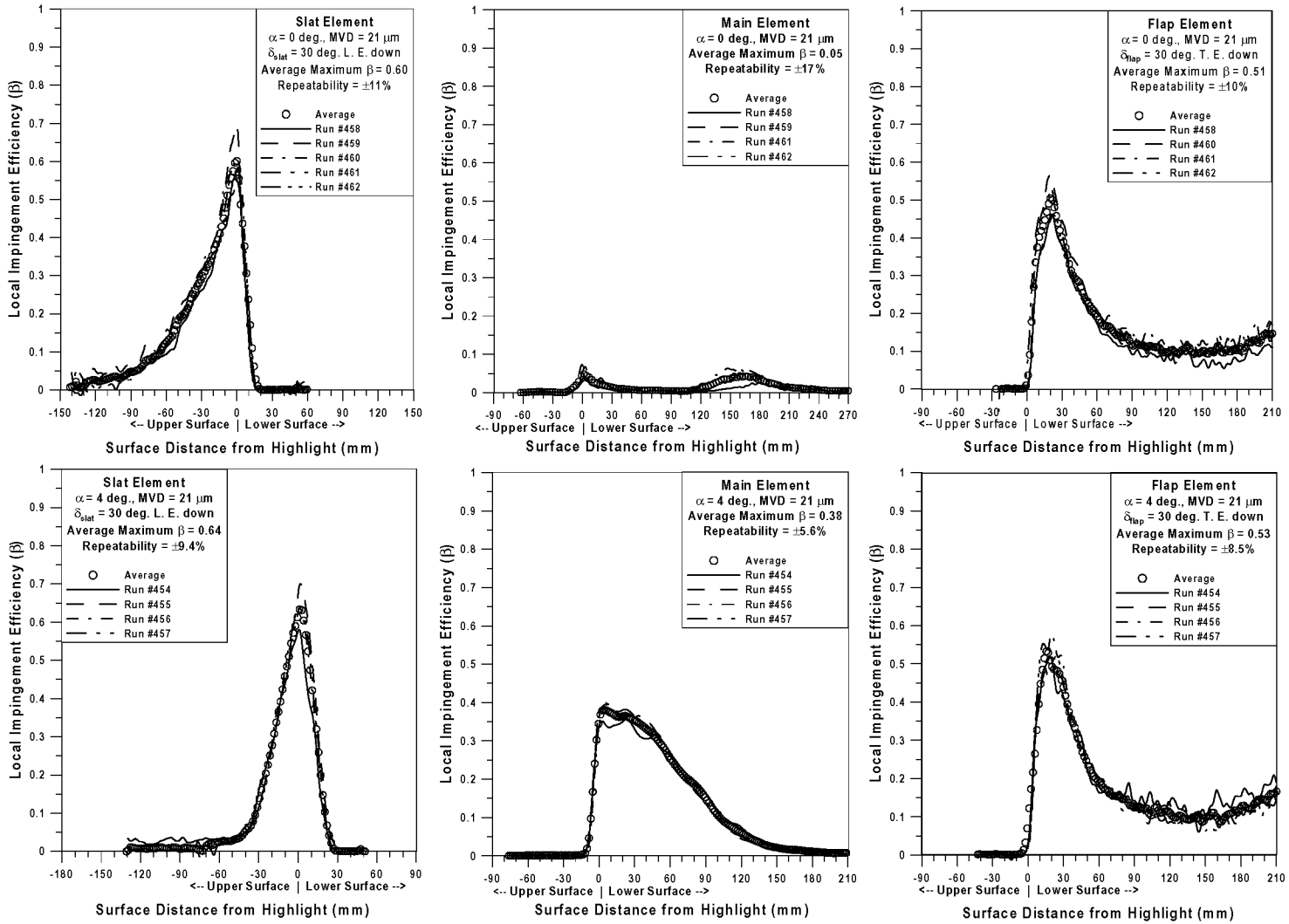

Fig. 93b Test repeatability for three-element high lift system airfoil - 1997 IRT tests; MVD = 21 μm (Continued).

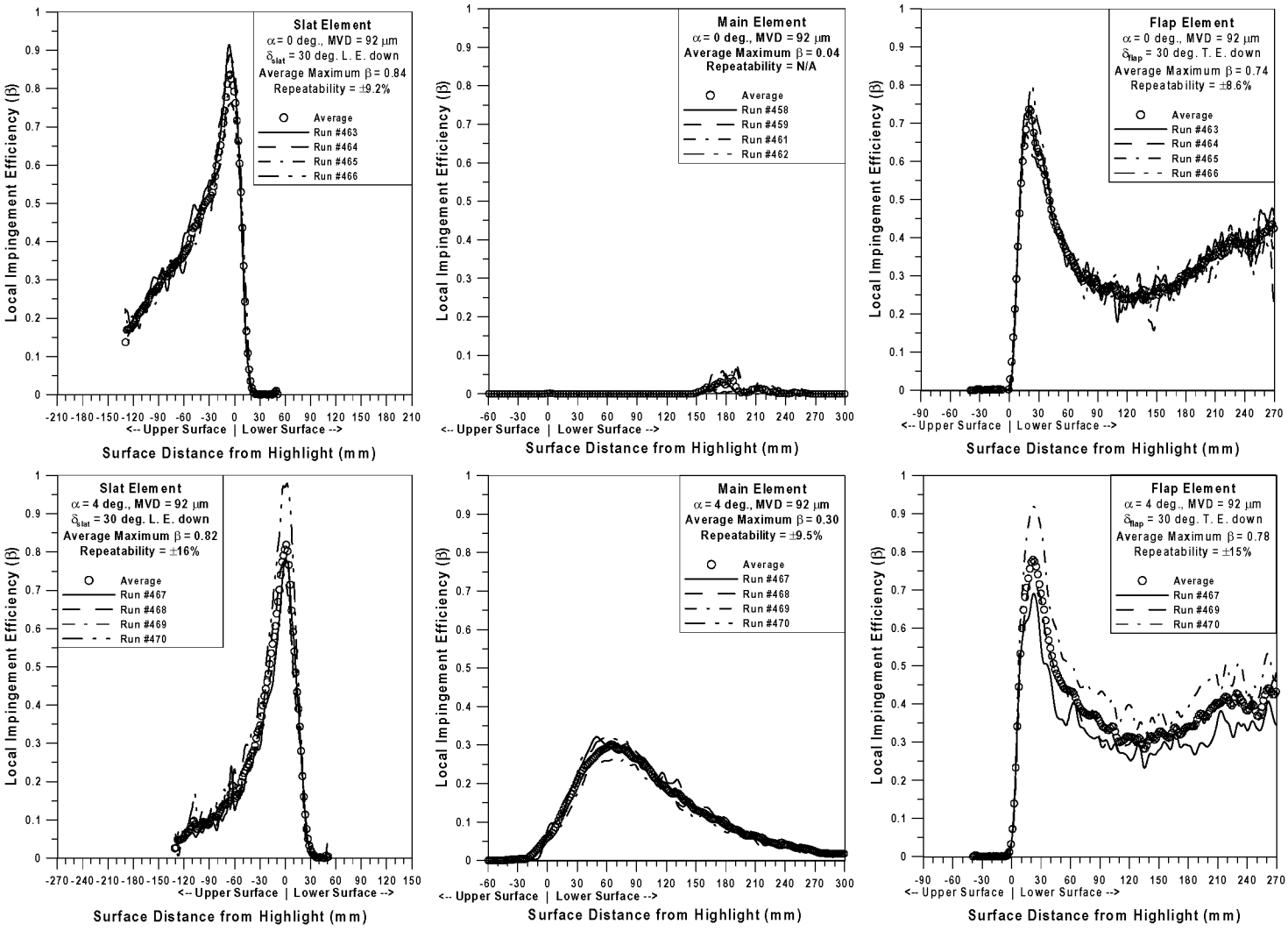

Fig. 93c Test repeatability for three-element high lift system airfoil - 1997 IRT tests; MVD = 92 μm.

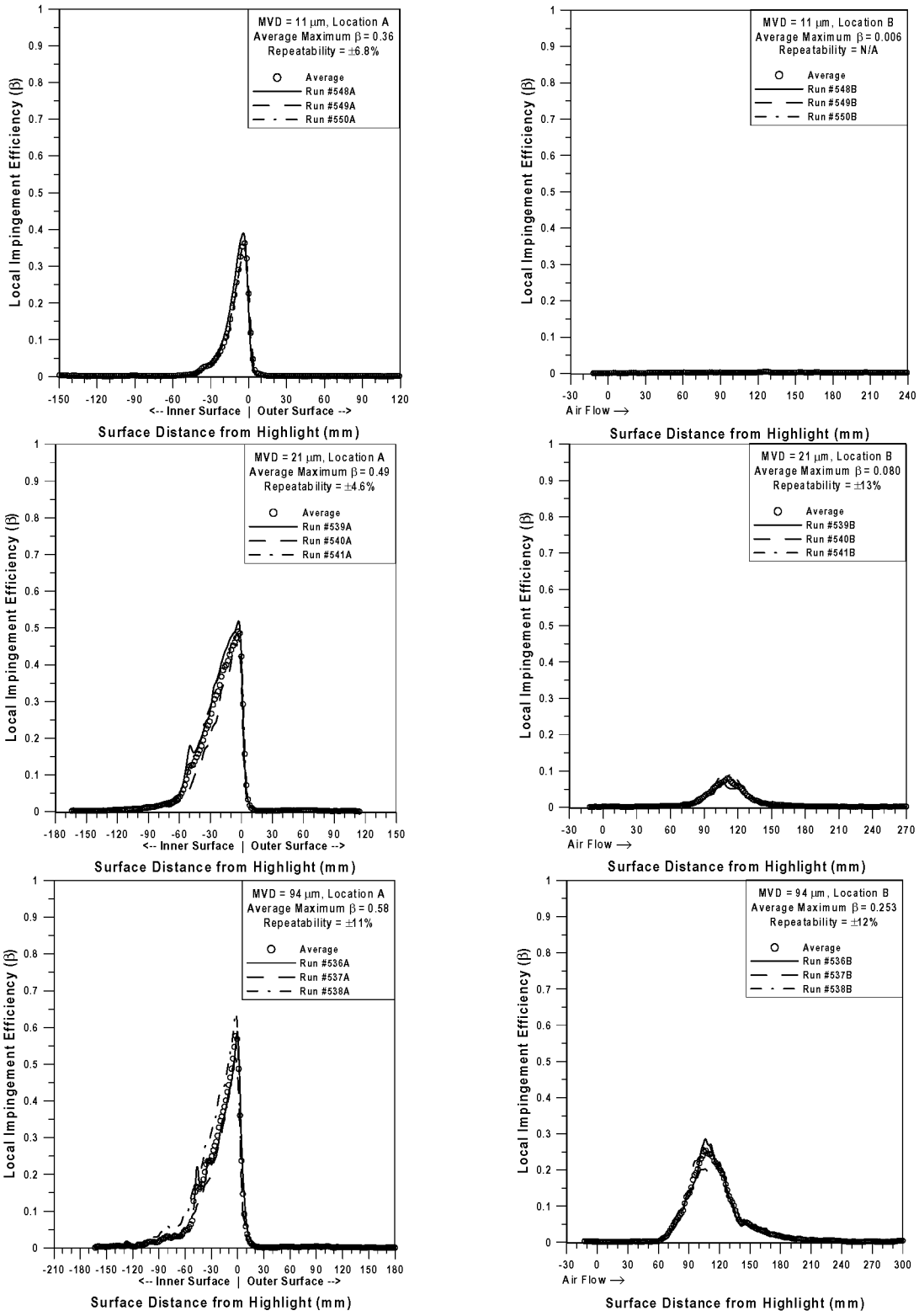

Fig. 94 Test repeatability for S-duct engine inlet - 1999 IRT tests; V_∞ = 170 mph, capture area ratio = 0.65, mass flow rate = 23 lbm/sec.

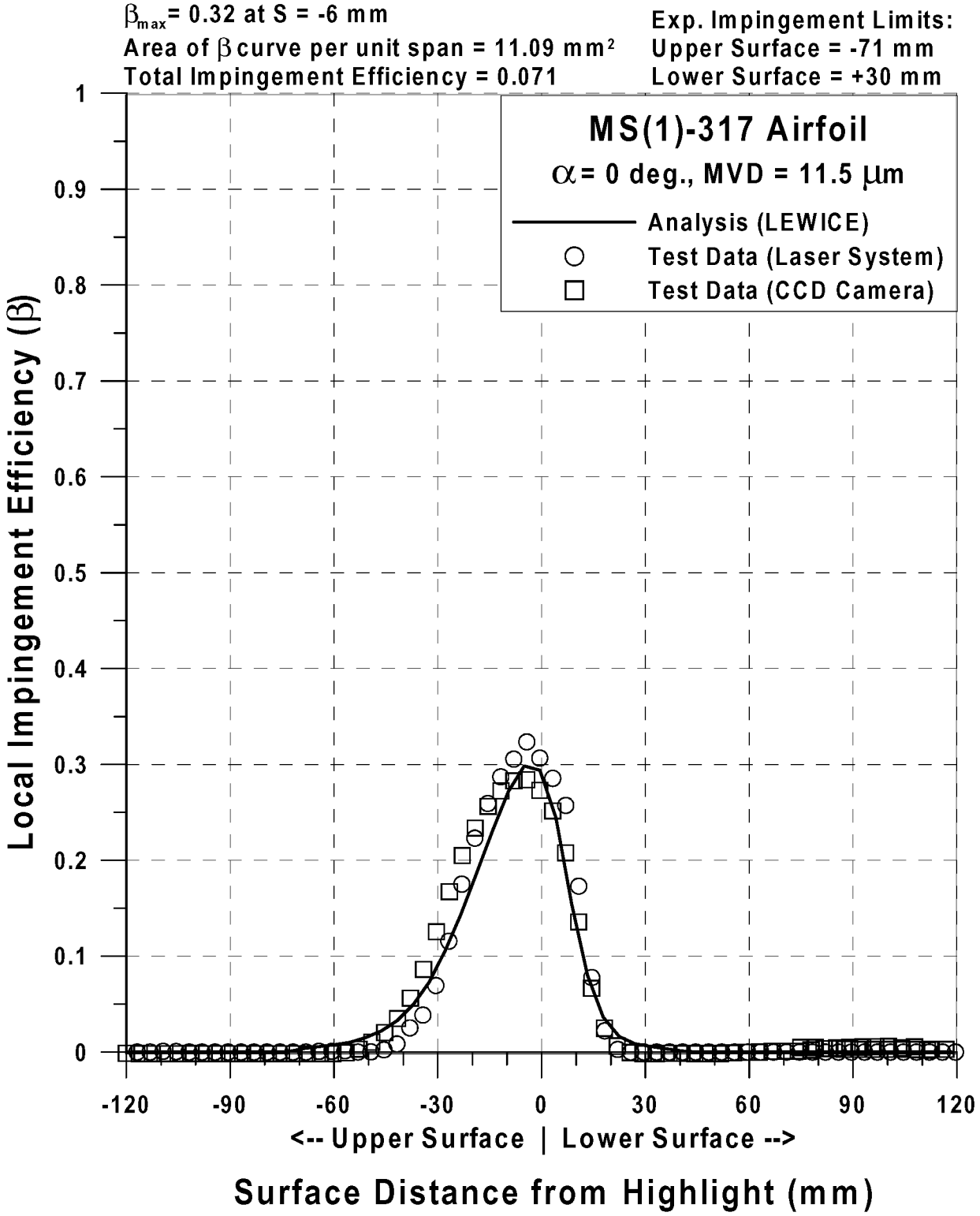

Fig. 95a Impingement efficiency distribution for MS(1)-0317 airfoil;
1997 IRT tests, c = 36-in, V_∞ = 176 mph, α=0°, MVD =11.5 μm (Continued).

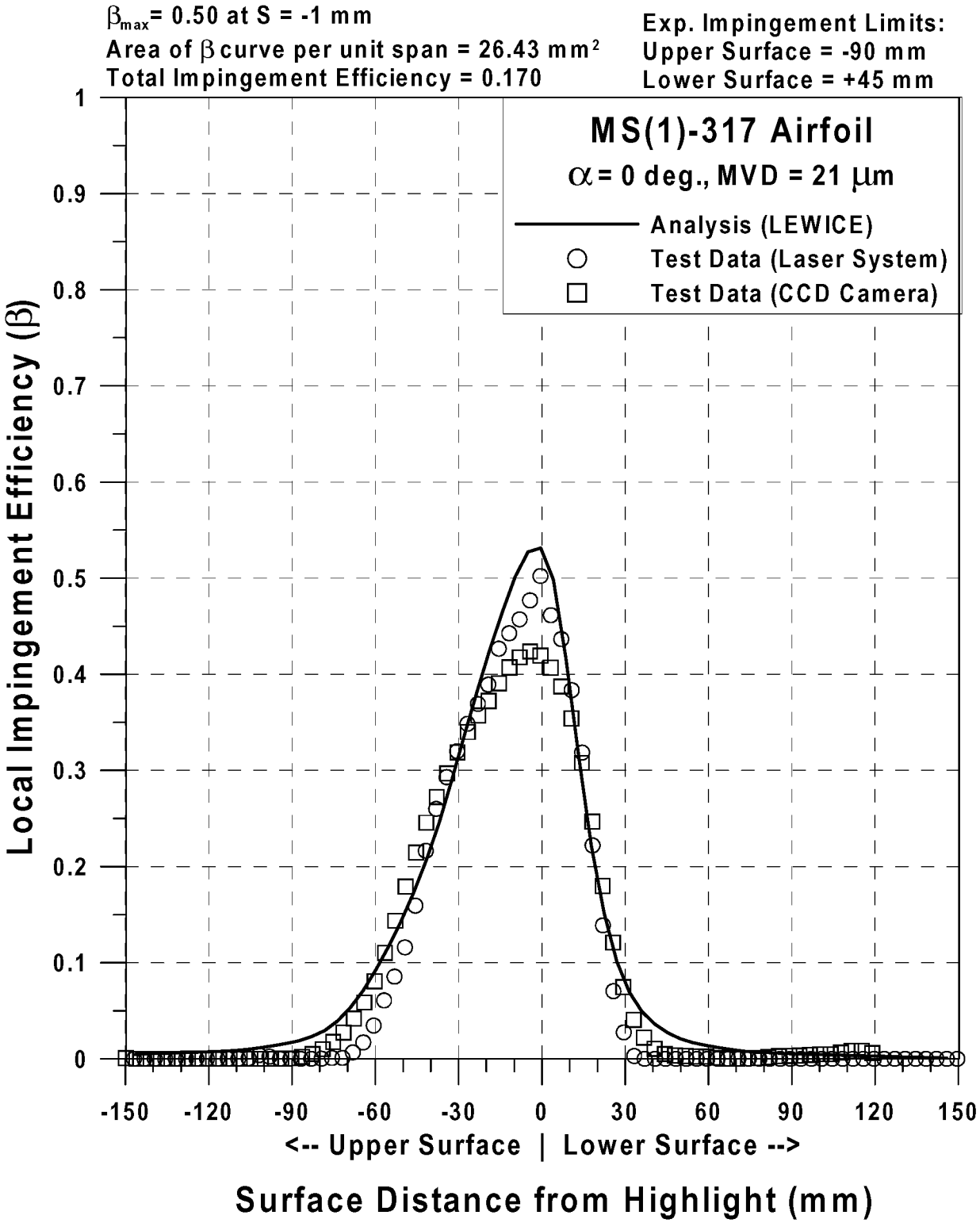

Fig. 95b Impingement efficiency distribution for MS(1)-0317 airfoil; 1997 IRT tests, c = 36-in, V_∞ = 176 mph, $\alpha=0^\circ$, MVD =21 μm (Continued).

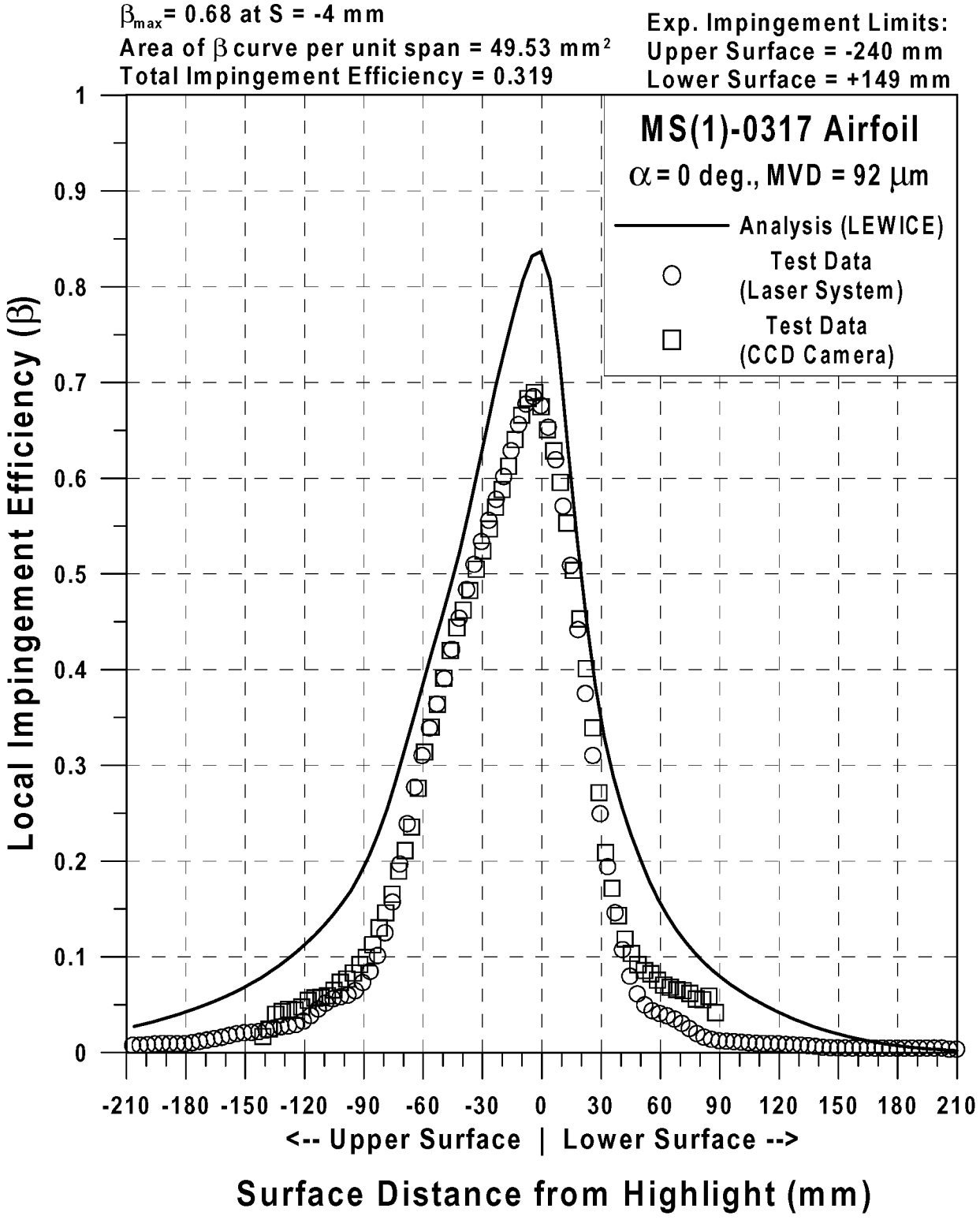

Fig. 95c Impingement efficiency distribution for MS(1)-0317 airfoil; 1997 IRT tests, c = 36-in, V_∞ = 176 mph, $\alpha=0^\circ$, MVD =92 μm (Continued).

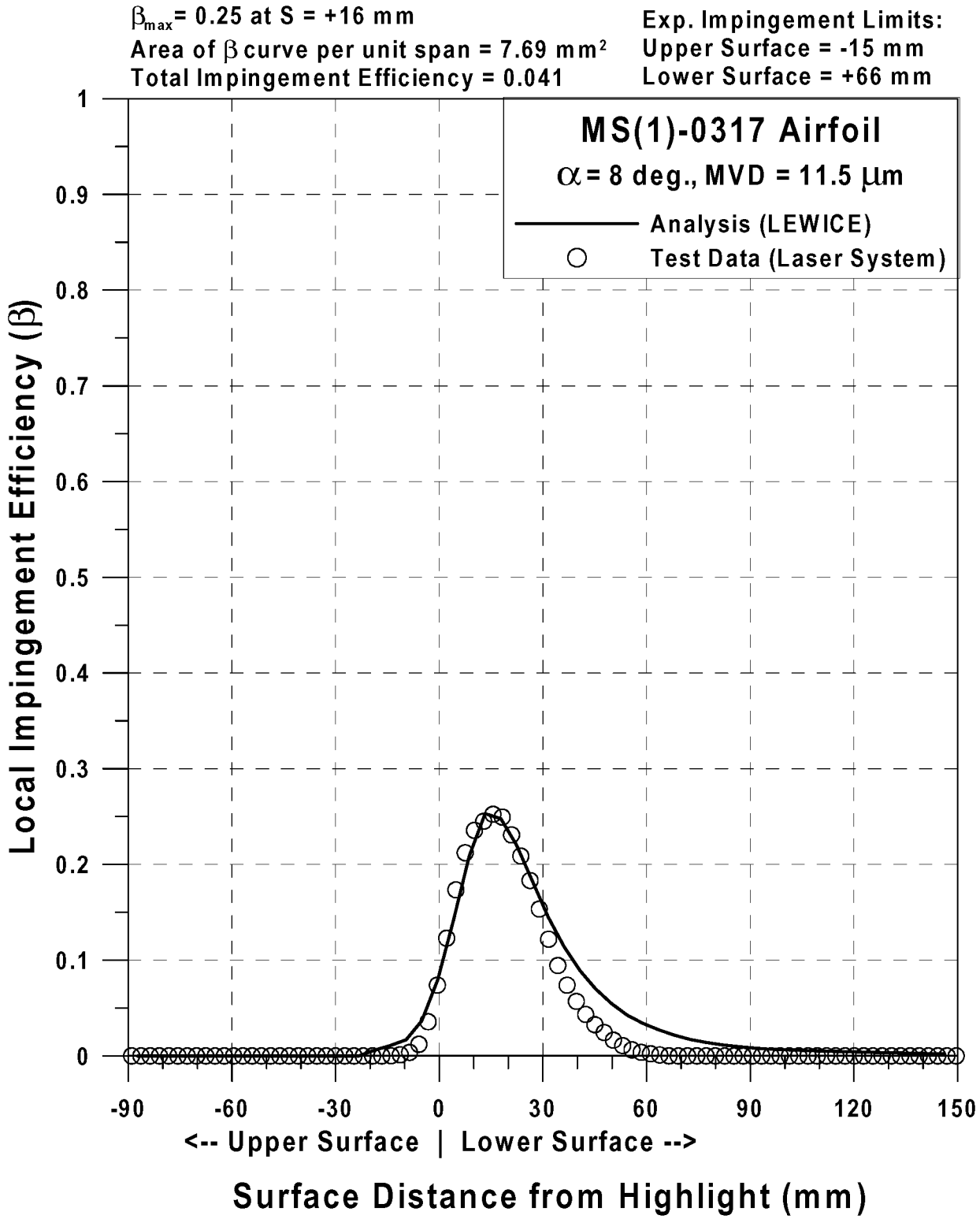

Fig. 95d Impingement efficiency distribution for MS(1)-0317 airfoil;
1997 IRT tests, c = 36-in, V_∞ = 176 mph, α=8°, MVD =11.5 μm (Continued).

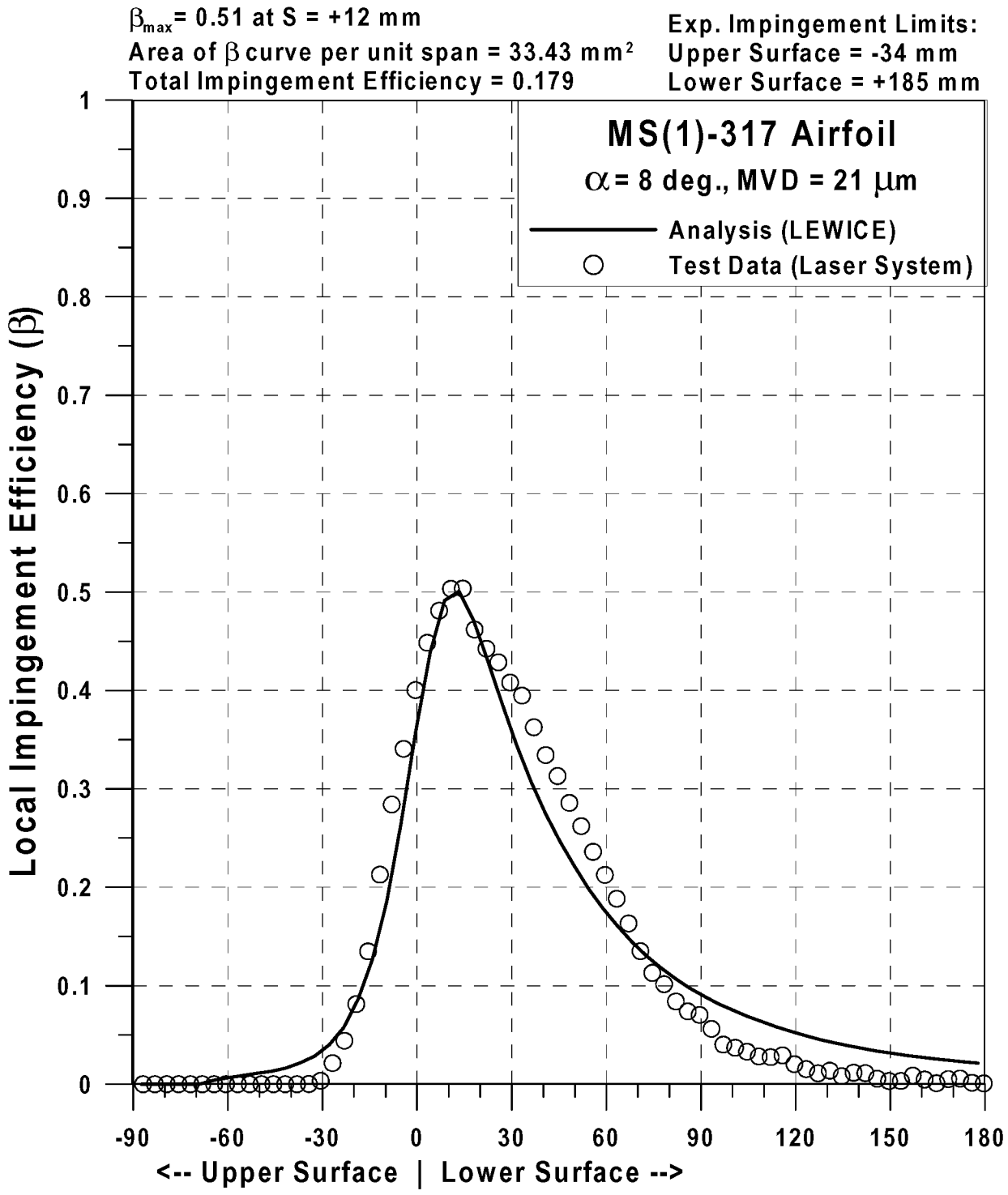

Fig. 95e Impingement efficiency distribution for MS(1)-0317 airfoil; 1997 IRT tests, c = 36-in, V_∞ = 176 mph, α=8°, MVD =21 μm (Continued).

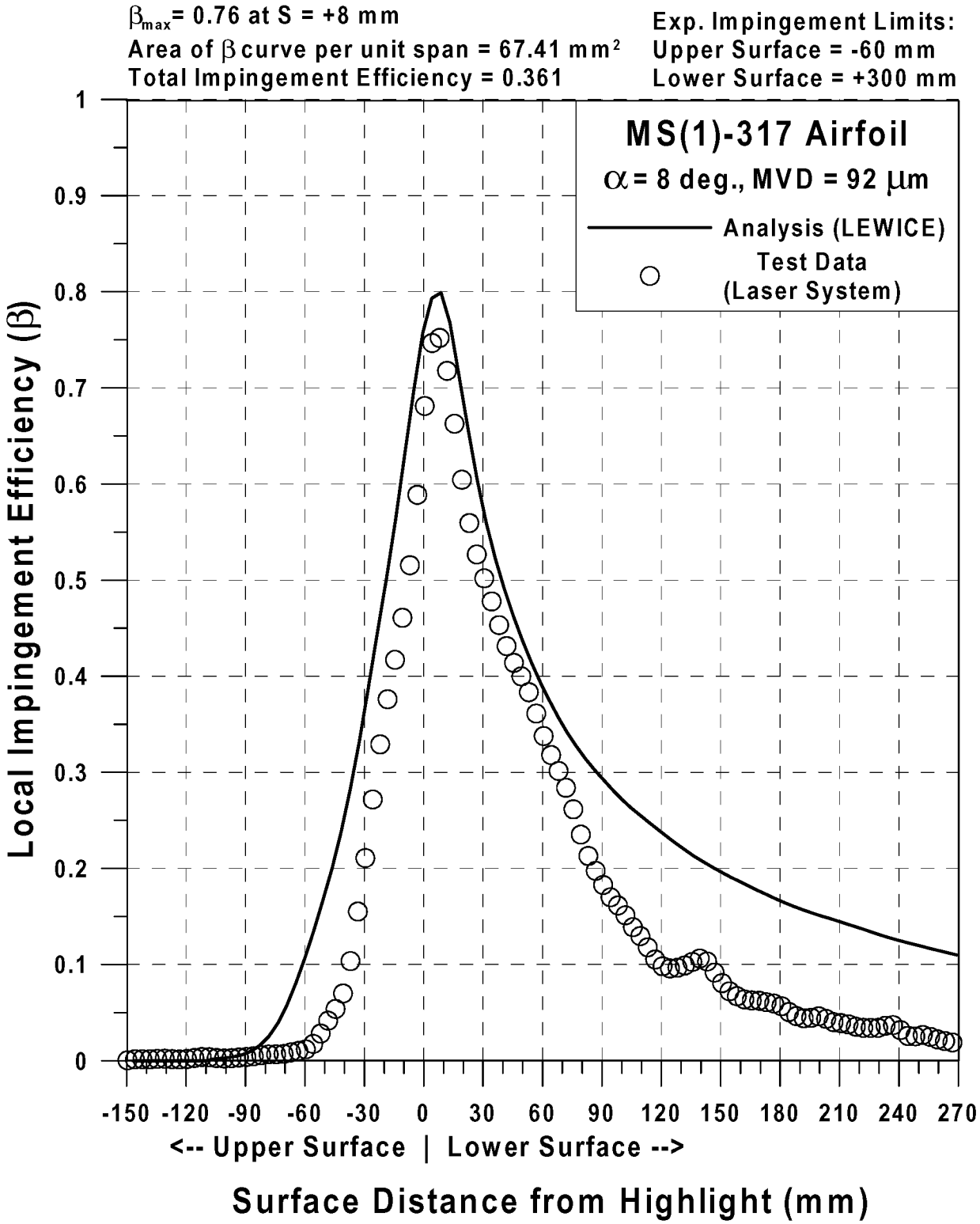

Fig. 95f Impingement efficiency distribution for MS(1)-0317 airfoil; 1997 IRT tests, c = 36-in, V_∞ = 176 mph, α=8°, MVD =92 μm.

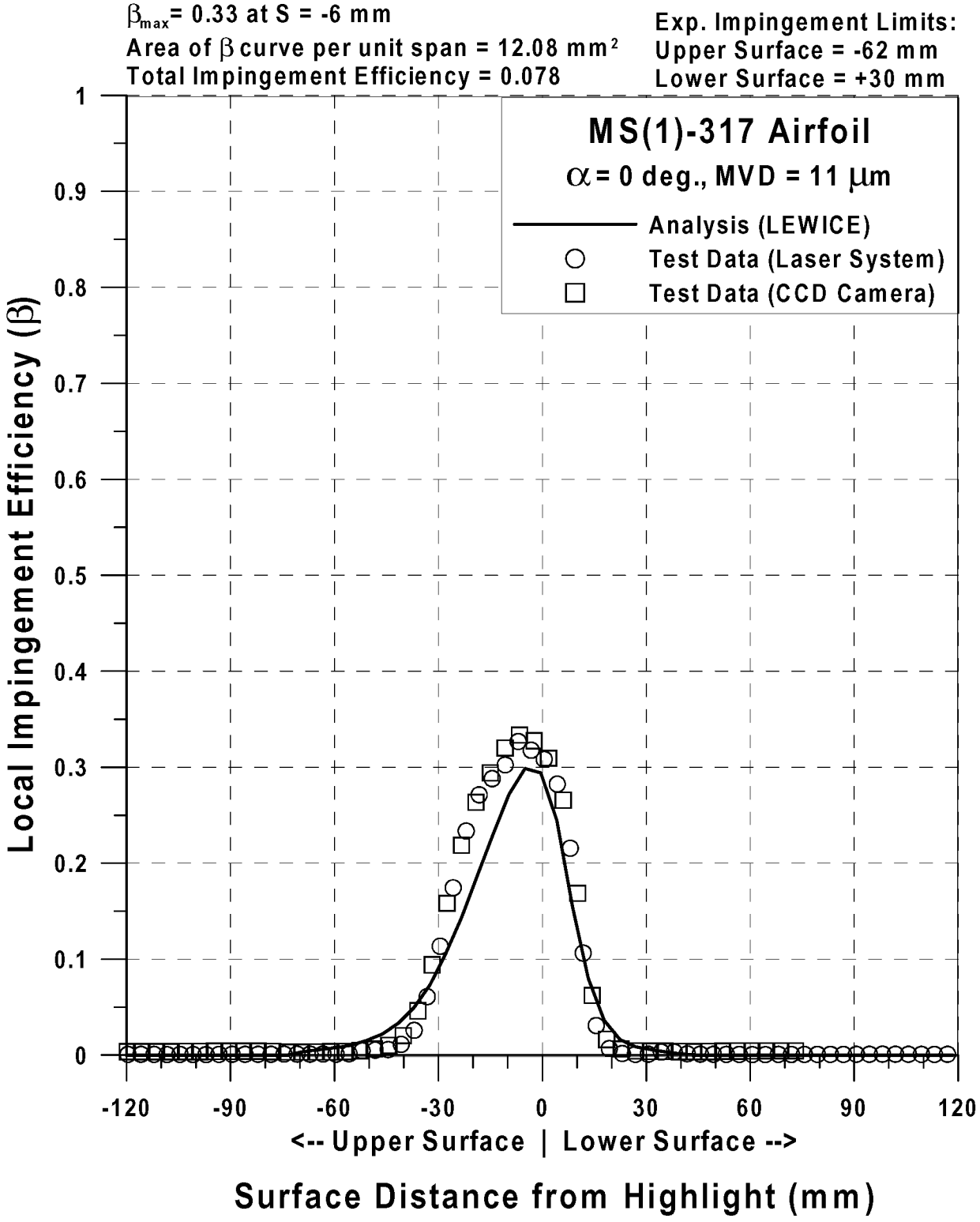

Fig. 96a Impingement efficiency distribution for MS(1)-0317 airfoil; 1999 IRT tests, c = 36-in, V_∞ = 176 mph, α=0°, MVD =11 μm (Continued).

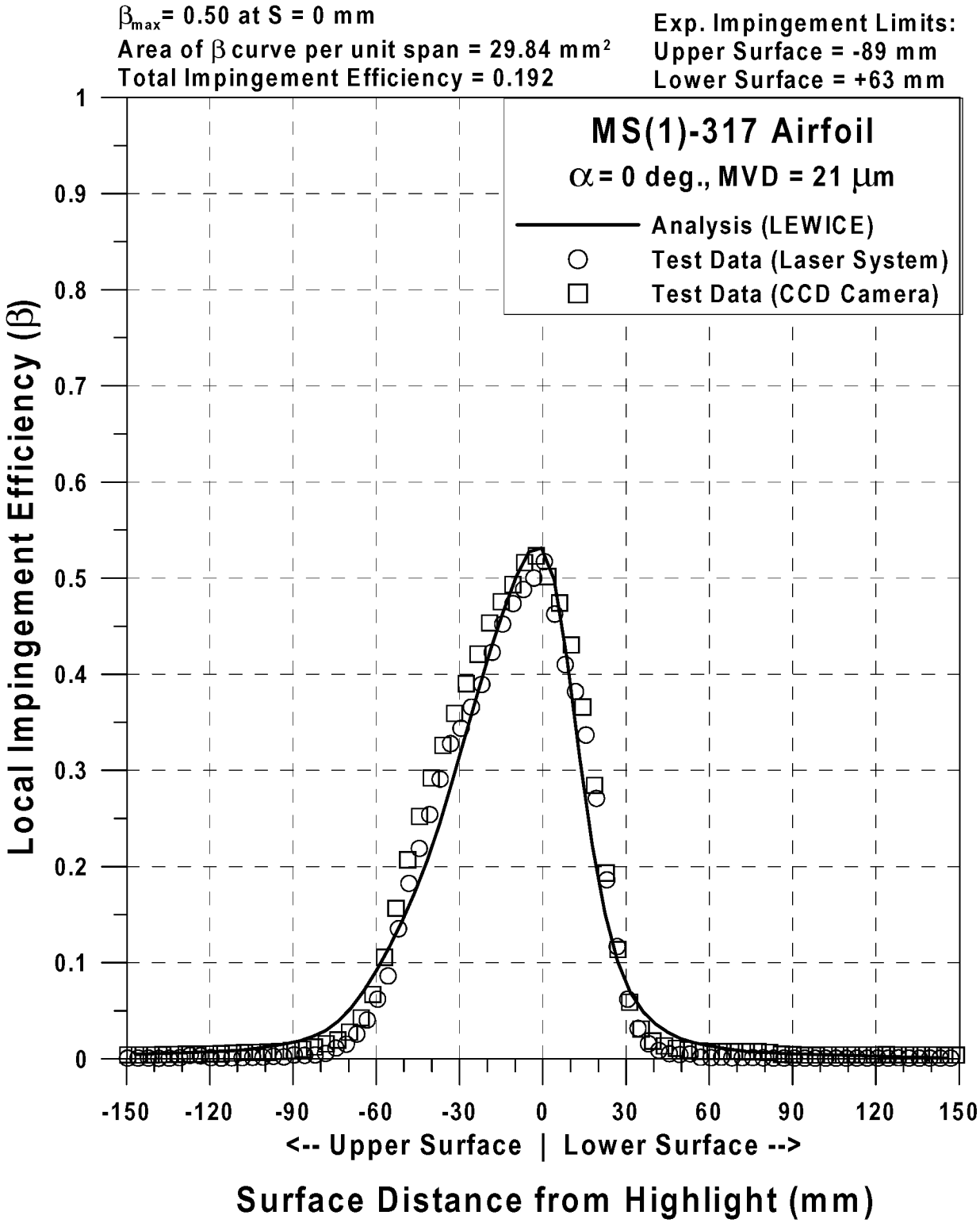

Fig. 96b Impingement efficiency distribution for MS(1)-0317 airfoil; 1999 IRT tests, c = 36-in, V_∞ = 176 mph, $\alpha=0^\circ$, MVD =21 μm (Continued).

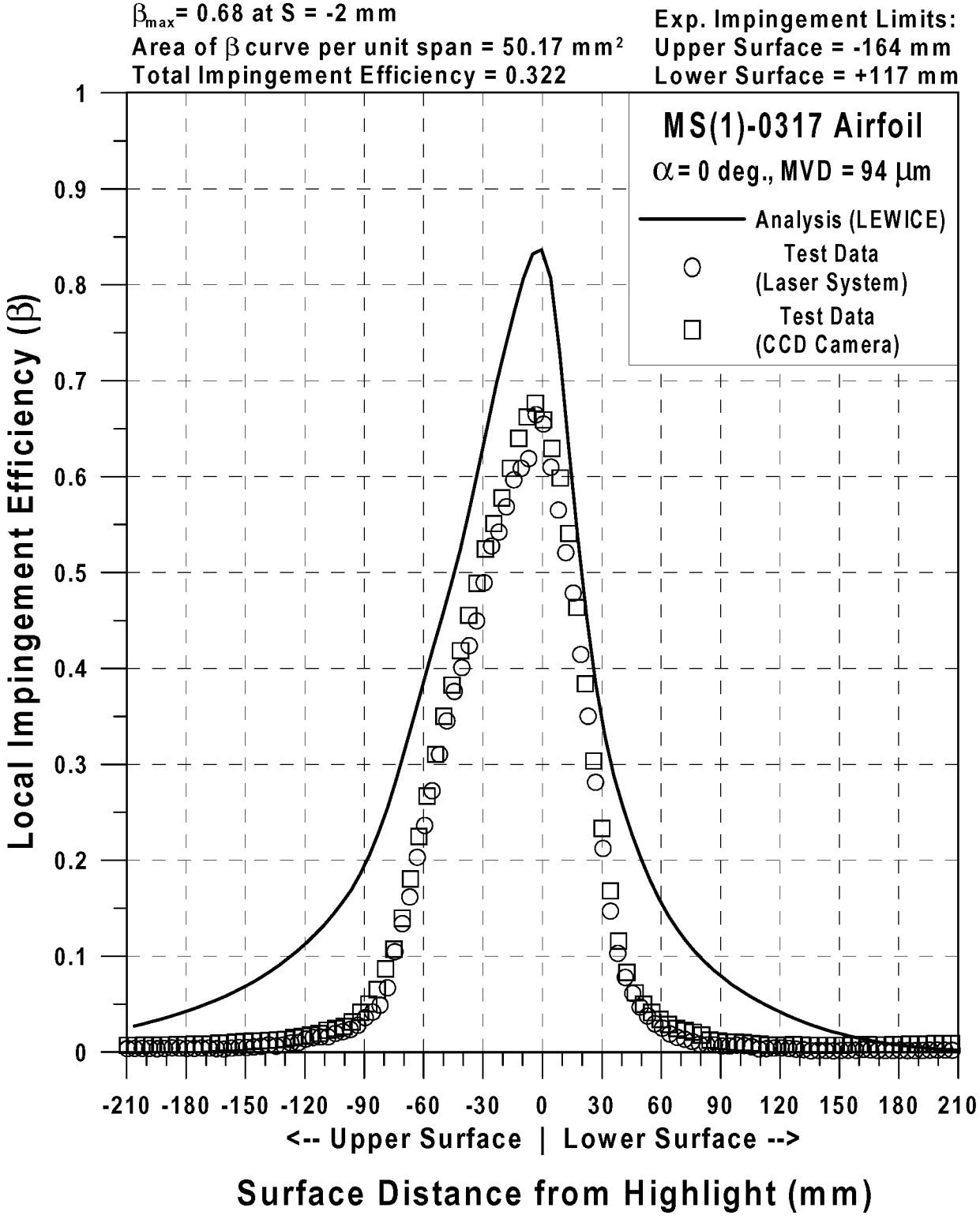

Fig. 96c Impingement efficiency distribution for MS(1)-0317 airfoil; 1999 IRT tests, c = 36-in, V_∞ = 176 mph, $\alpha=0^\circ$, MVD =94 μm.

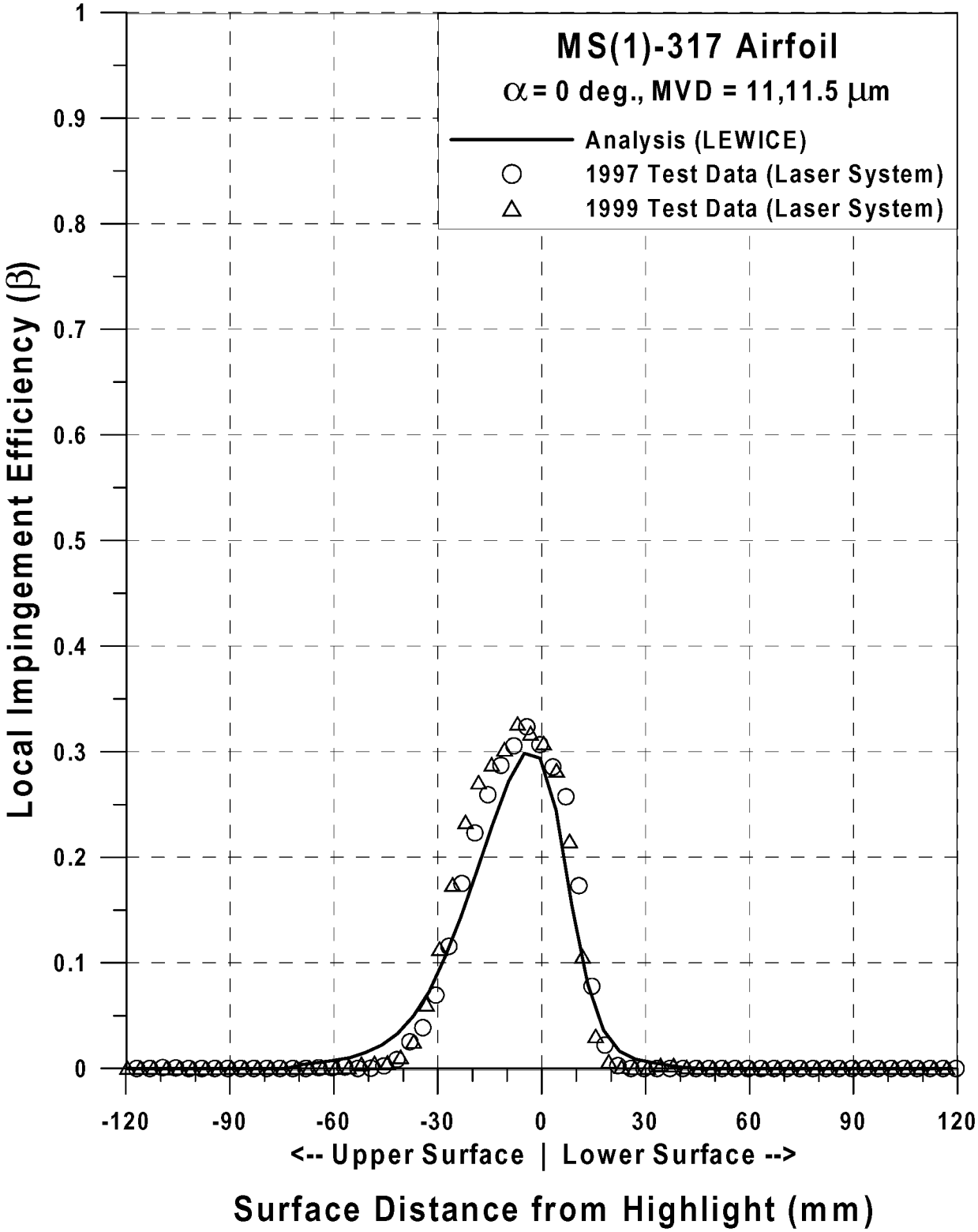

Fig. 97a Comparison of 1997 and 1999 impingement efficiency test results for MS(1)-0317 airfoil; c = 36-in, V_∞ = 176 mph, $\alpha=0^\circ$, MVD =11, 11.5 μm. (Continued).

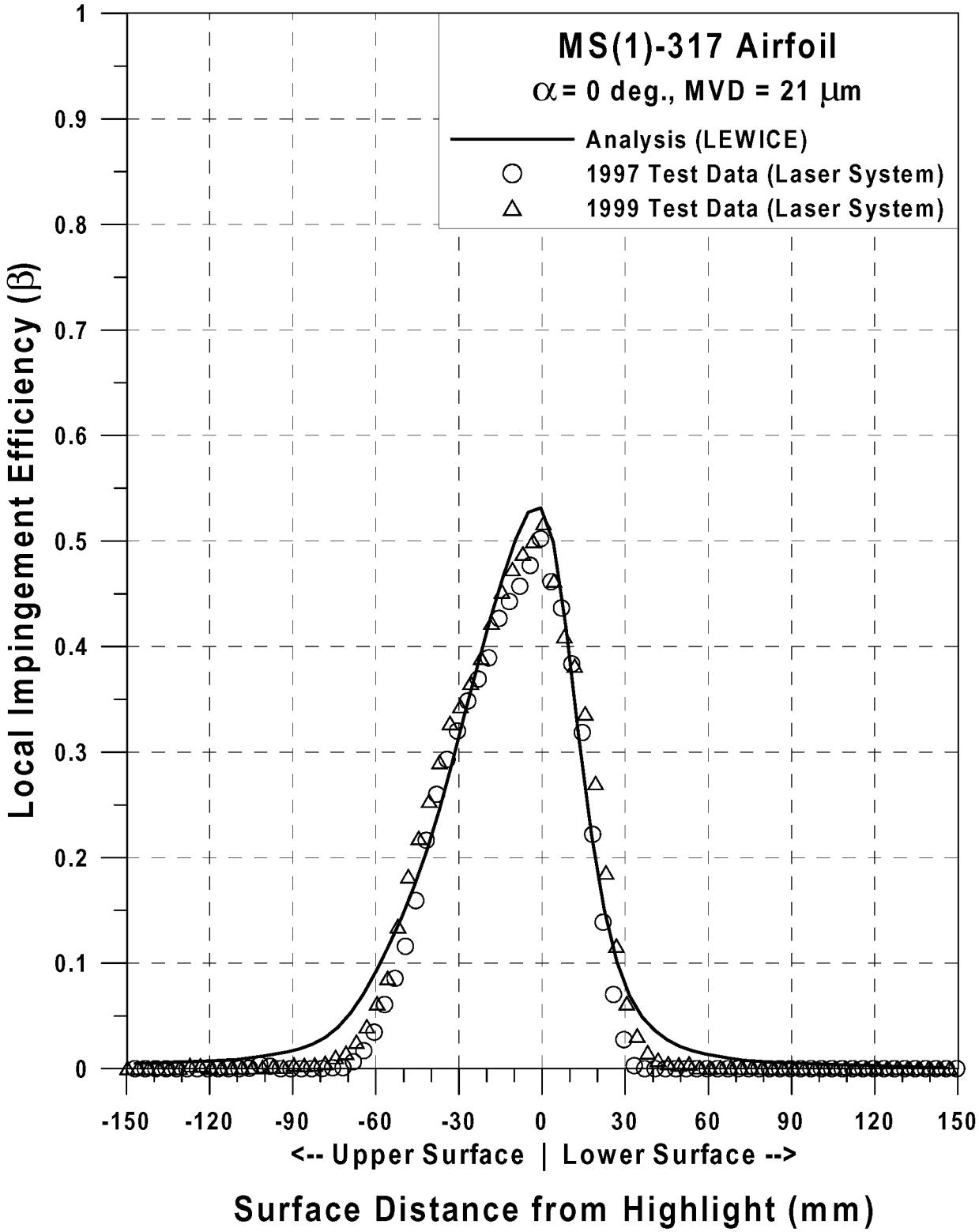

Fig. 97b Comparison of 1997 and 1999 impingement efficiency test results for MS(1)-0317 airfoil; c = 36-in, V_∞ = 176 mph, $\alpha=0^\circ$, MVD =21 μm (Continued).

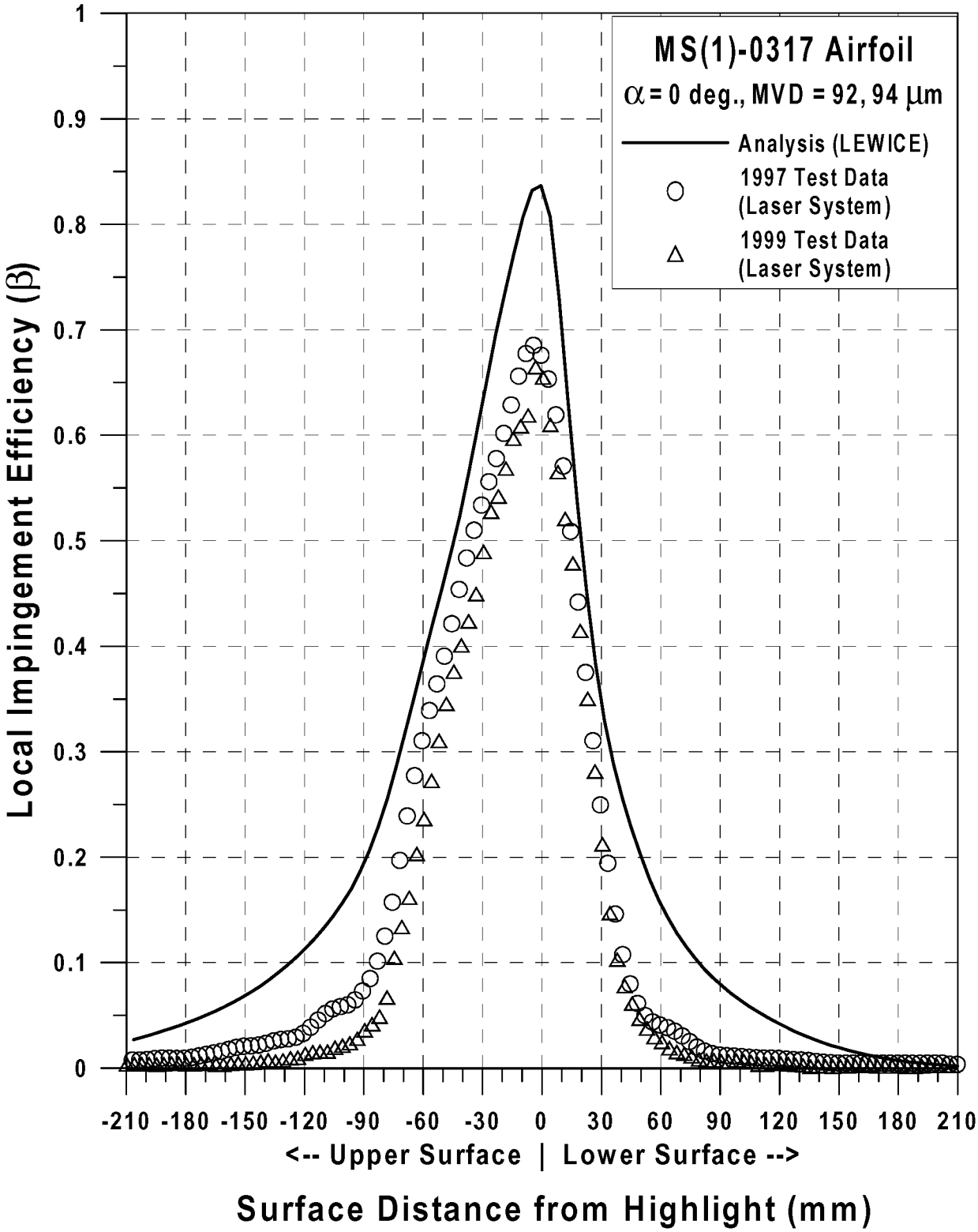

Fig. 97c Comparison of 1997 and 1999 impingement efficiency test results for MS(1)-0317 airfoil; c = 36-in, V_∞ = 176 mph, α=0°, MVD =92, 94 μm.

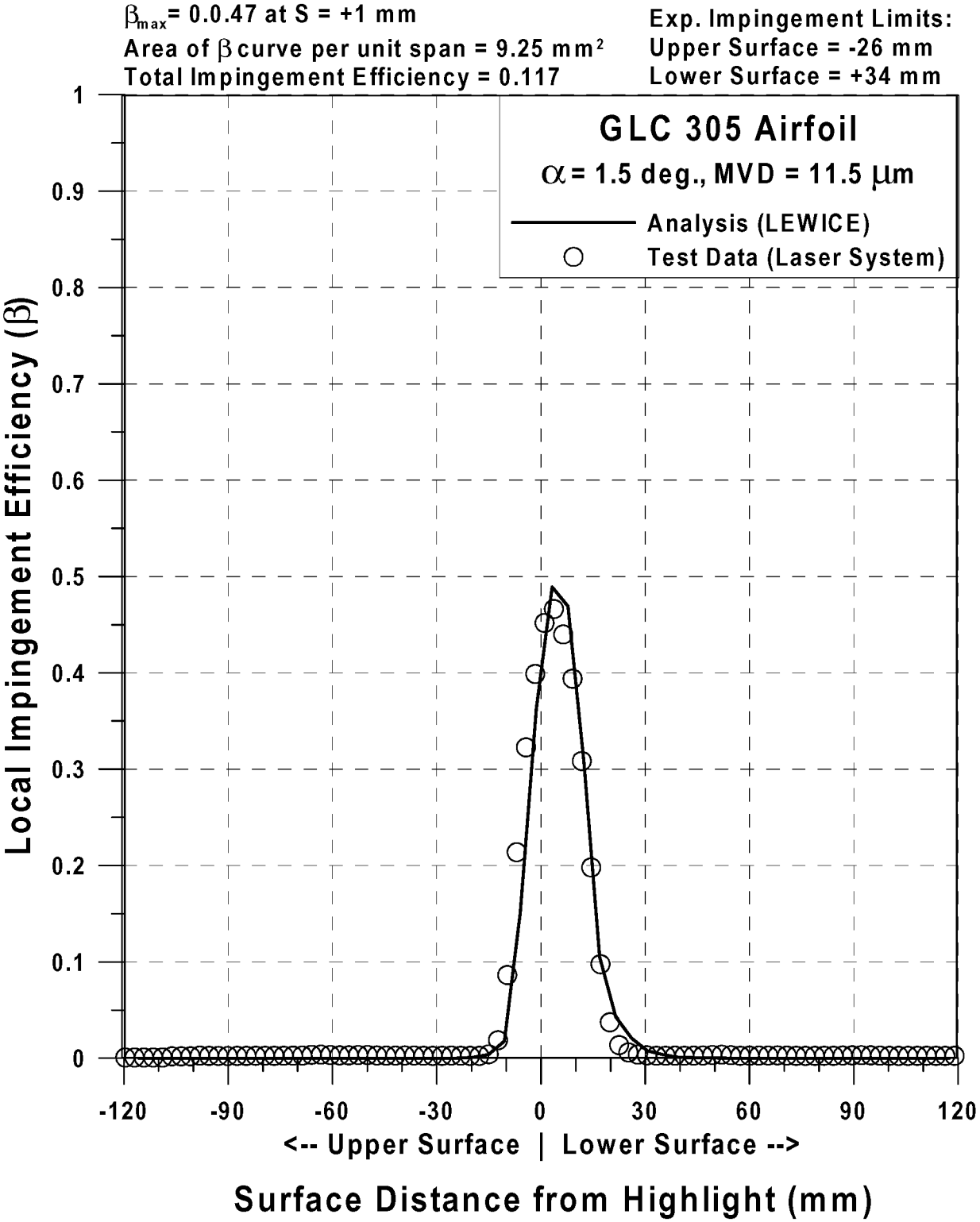

Fig. 98a Impingement efficiency distribution for GLC-305 airfoil;
c = 36-in, V_∞ = 176 mph, α=1.5°, MVD =11.5 μm (Continued).

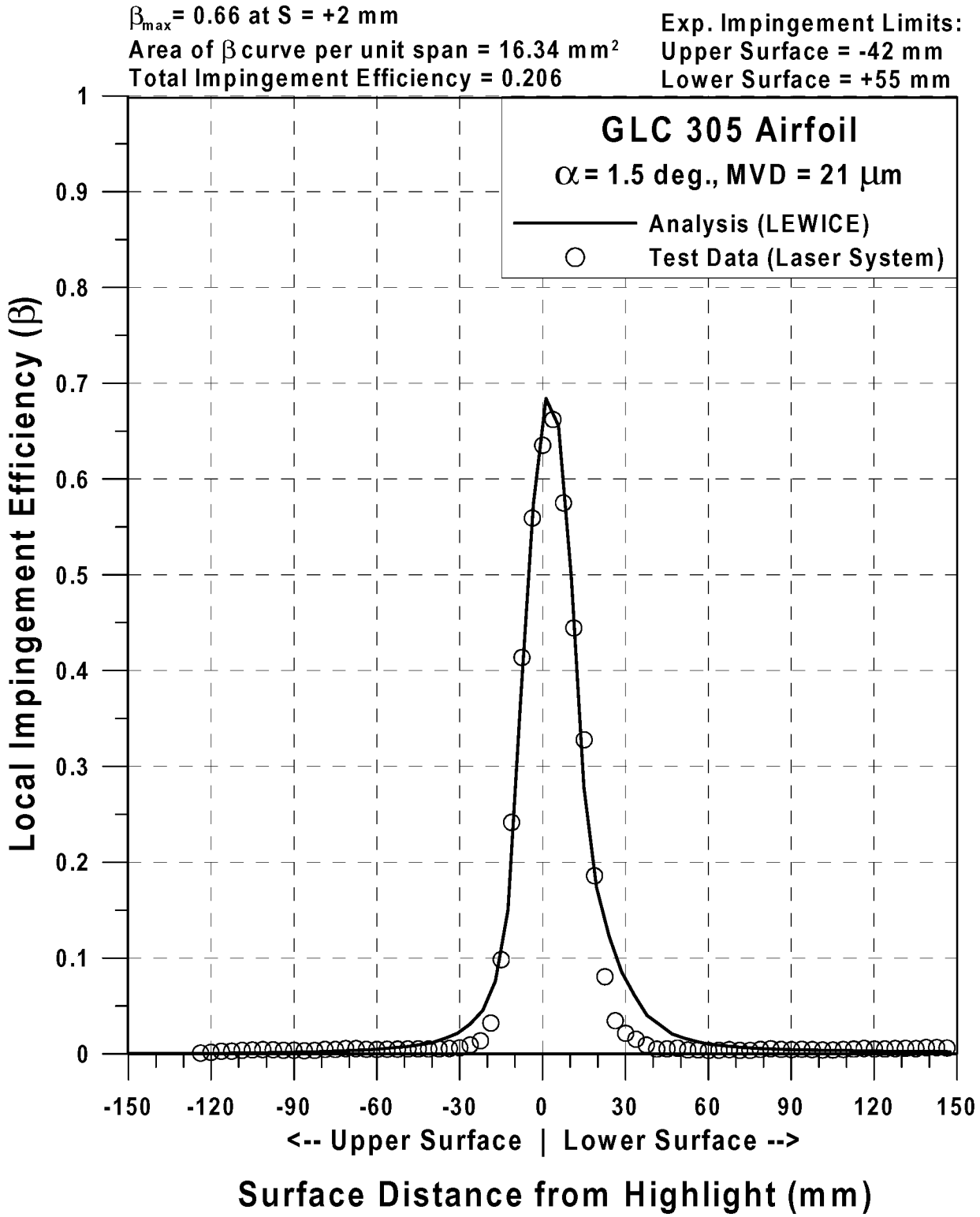

Fig. 98b Impingement efficiency distribution for GLC-305 airfoil;
c = 36-in, V_∞ = 176 mph, α=1.5°, MVD =21 μm (Continued).

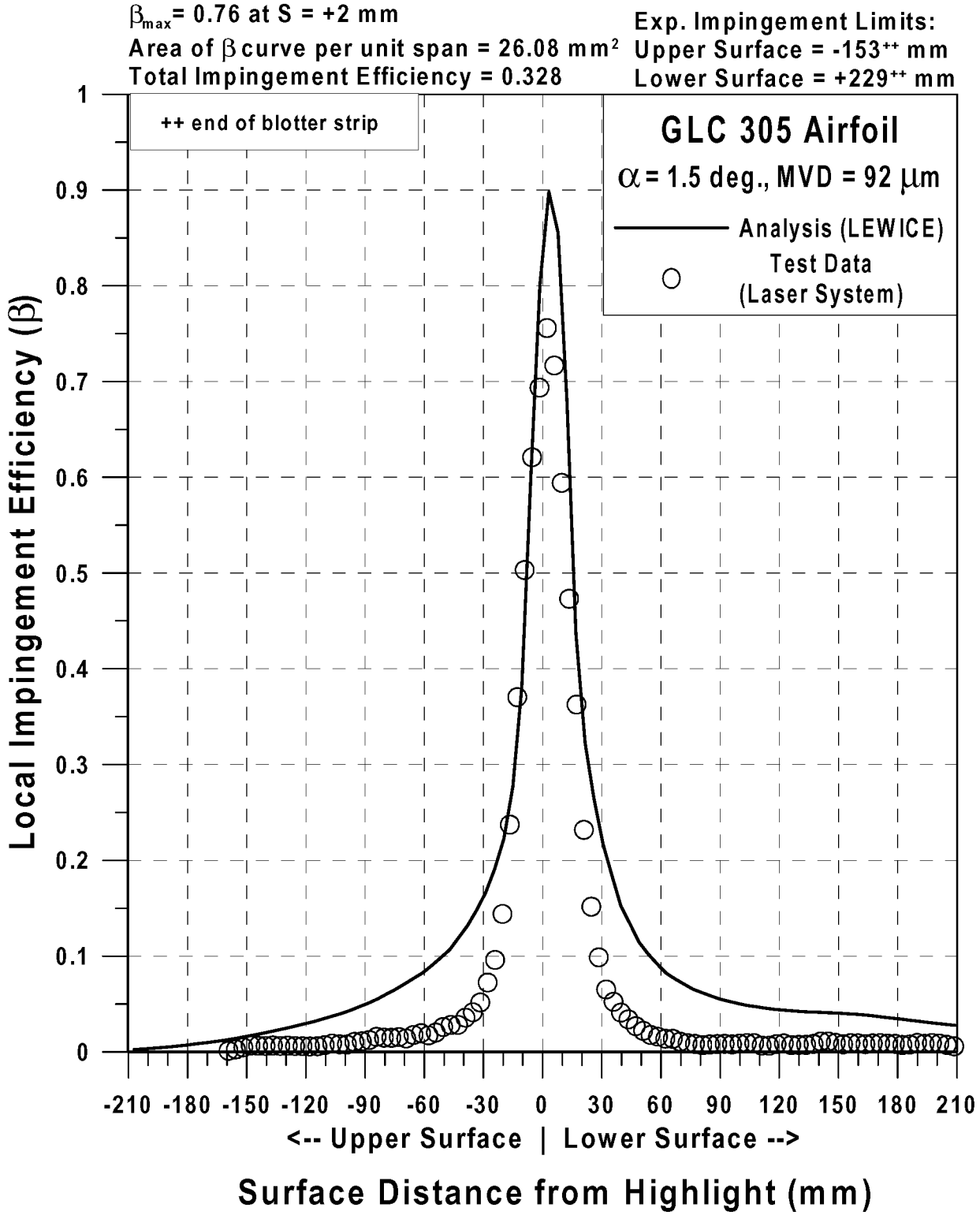

Fig. 98c Impingement efficiency distribution for GLC-305 airfoil;
c = 36-in, V_∞ = 176 mph, α=1.5°, MVD =92 μm (Continued).

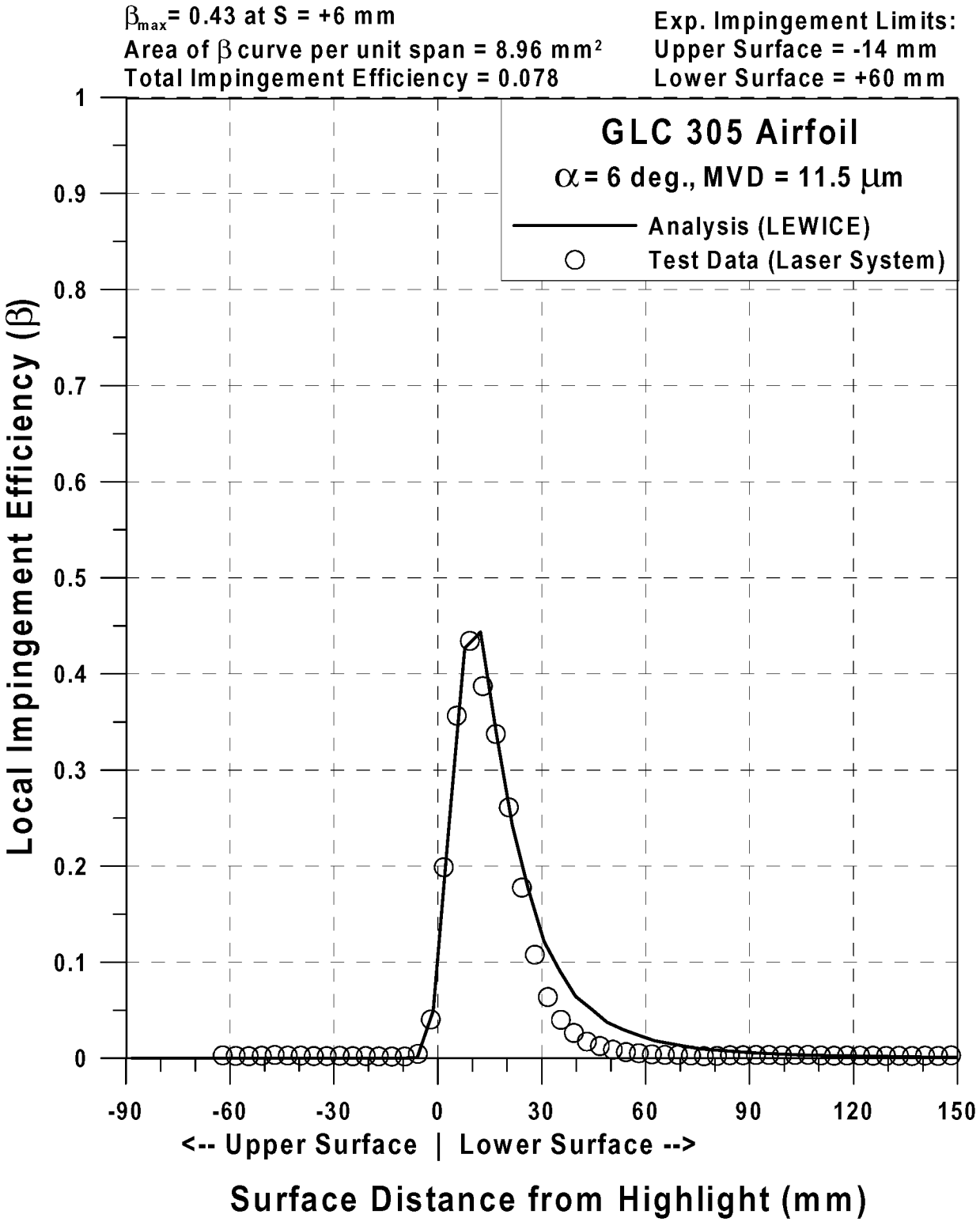

Fig. 98d Impingement efficiency distribution for GLC-305 airfoil;
c = 36-in, V_∞ = 176 mph, α=6°, MVD =11.5 μm (Continued).

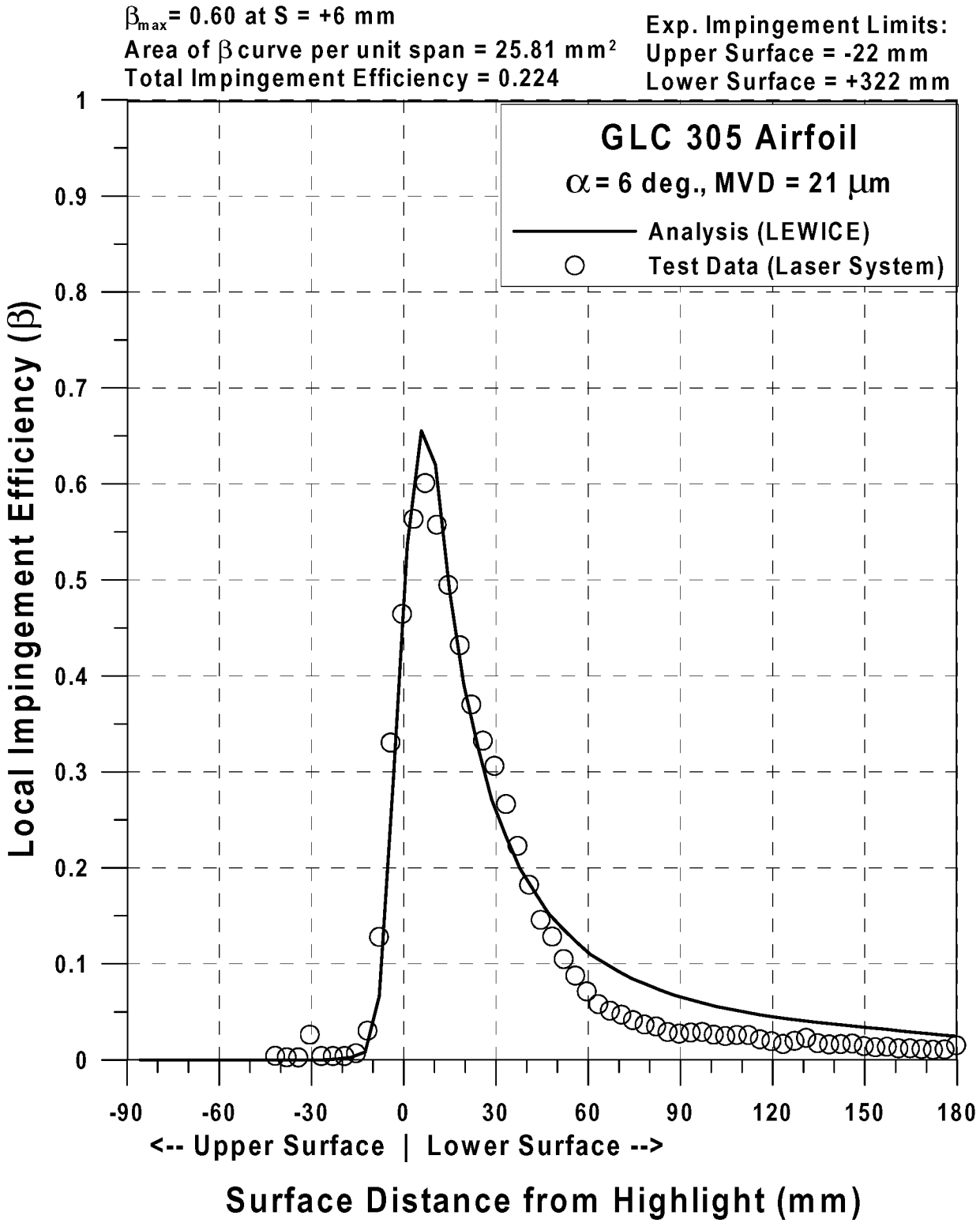

Fig. 98e Impingement efficiency distribution for GLC-305 airfoil;
c = 36-in, V_∞ = 176 mph, α=6°, MVD =21 μm (Continued).

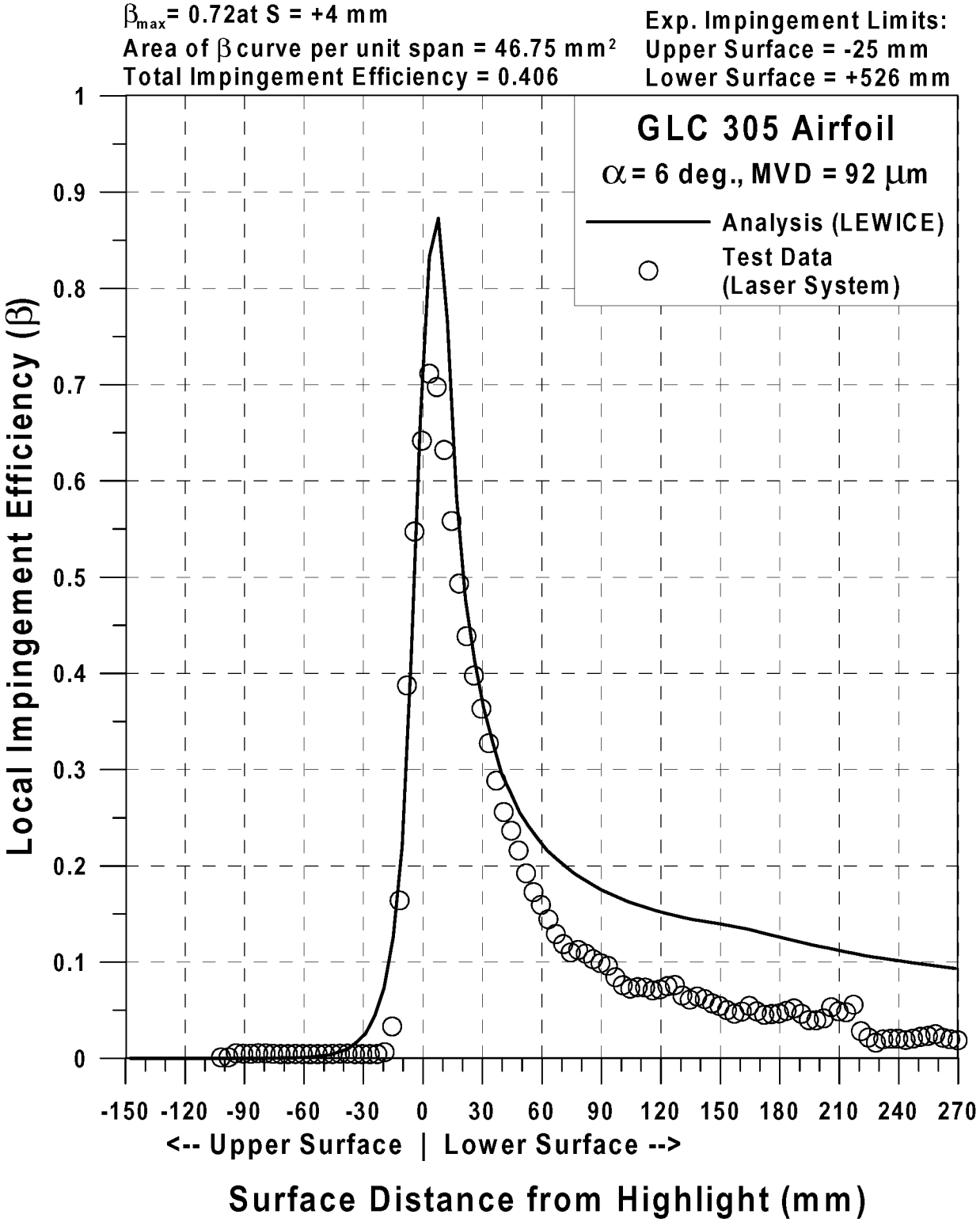

Fig. 98f Impingement efficiency distribution for GLC-305 airfoil;
c = 36-in, V_∞ = 176 mph, α=6°, MVD =92 μm.

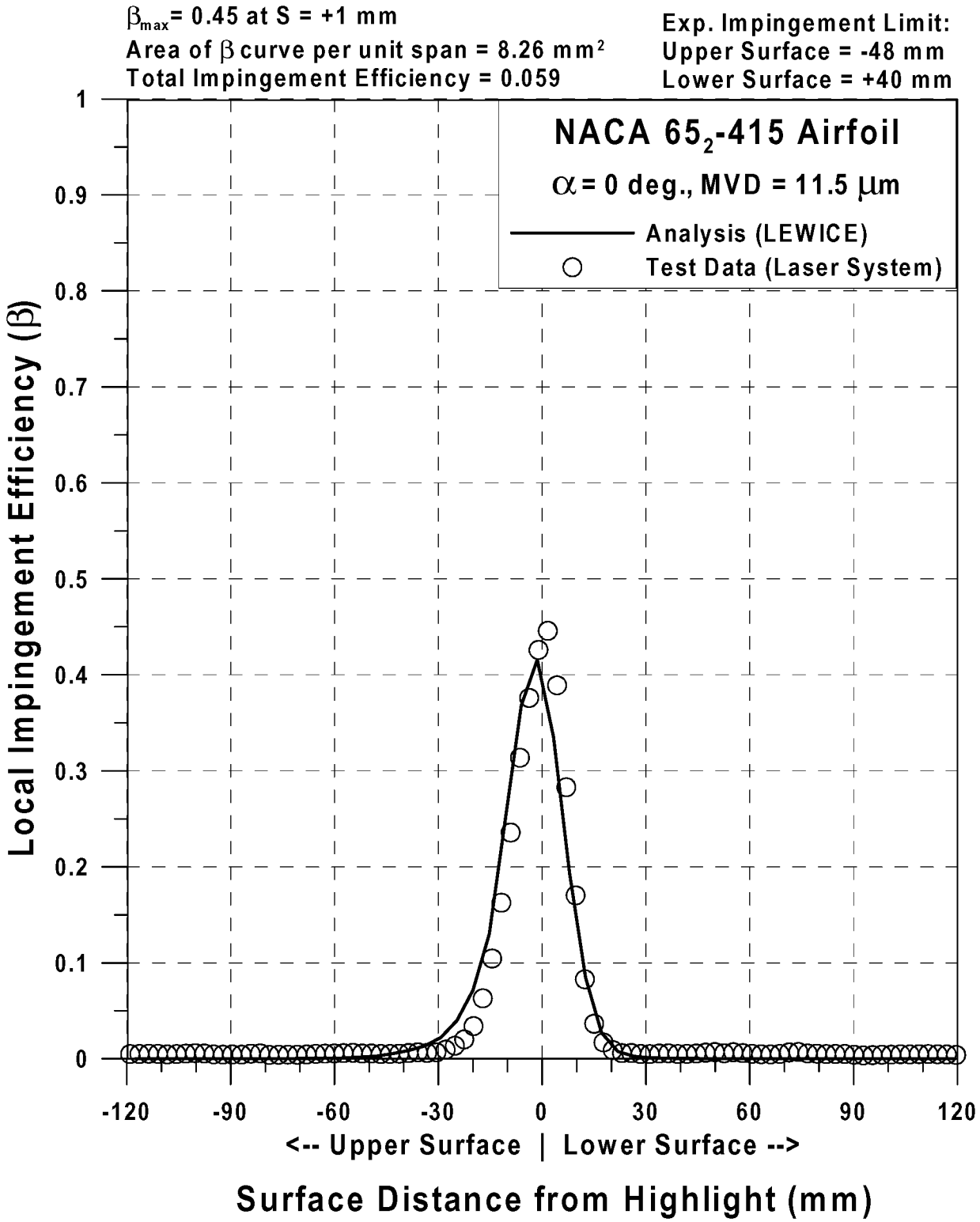

Fig. 99a Impingement efficiency distribution for NACA 65_2-415 airfoil; c = 36-in, V_∞ = 176 mph, $\alpha=0^\circ$, MVD =11.5 μm (Continued).

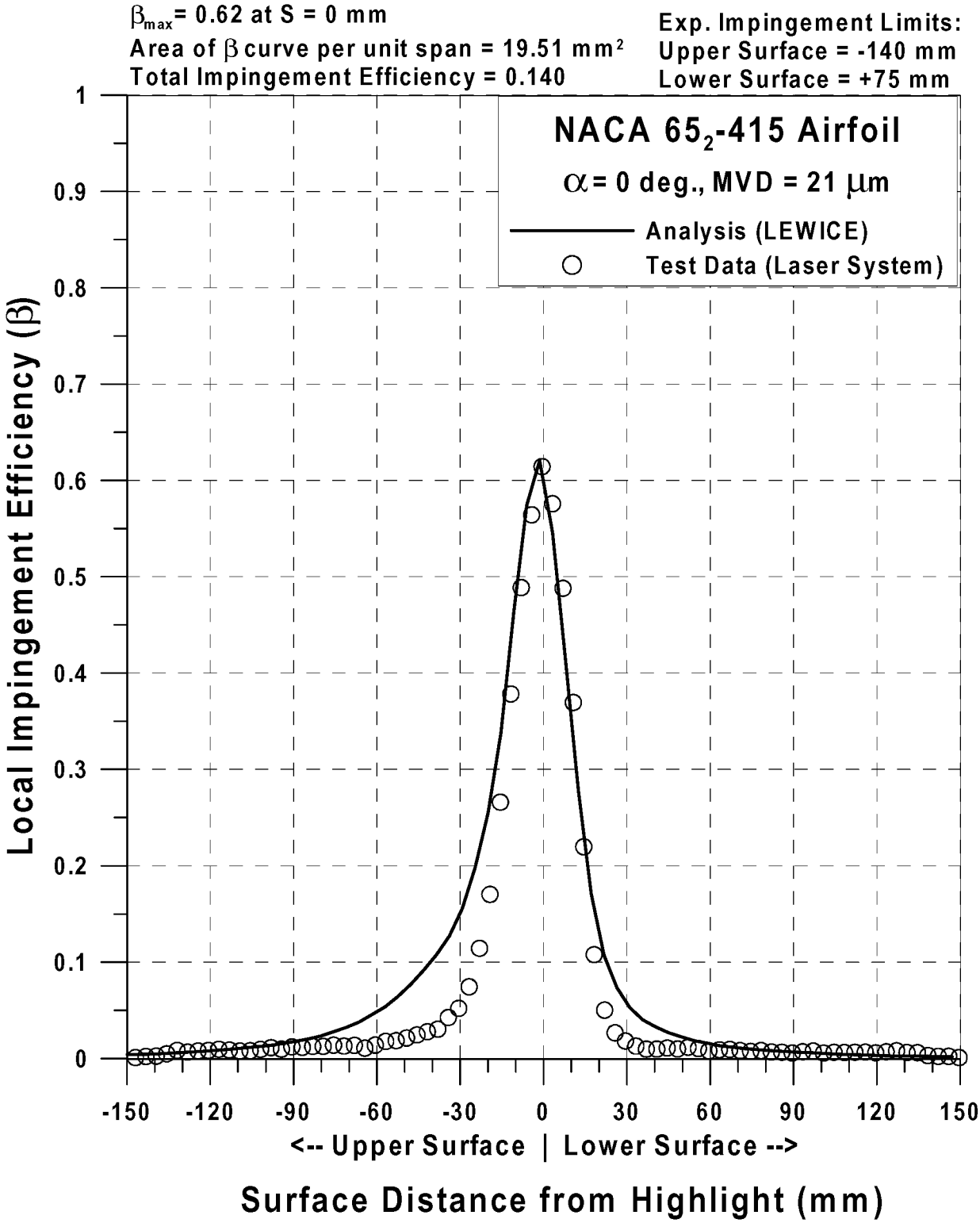

Fig. 99b Impingement efficiency distribution for NACA 65_2-415 airfoil; c = 36-in, V_∞ = 176 mph, α=0°, MVD =21 μm (Continued).

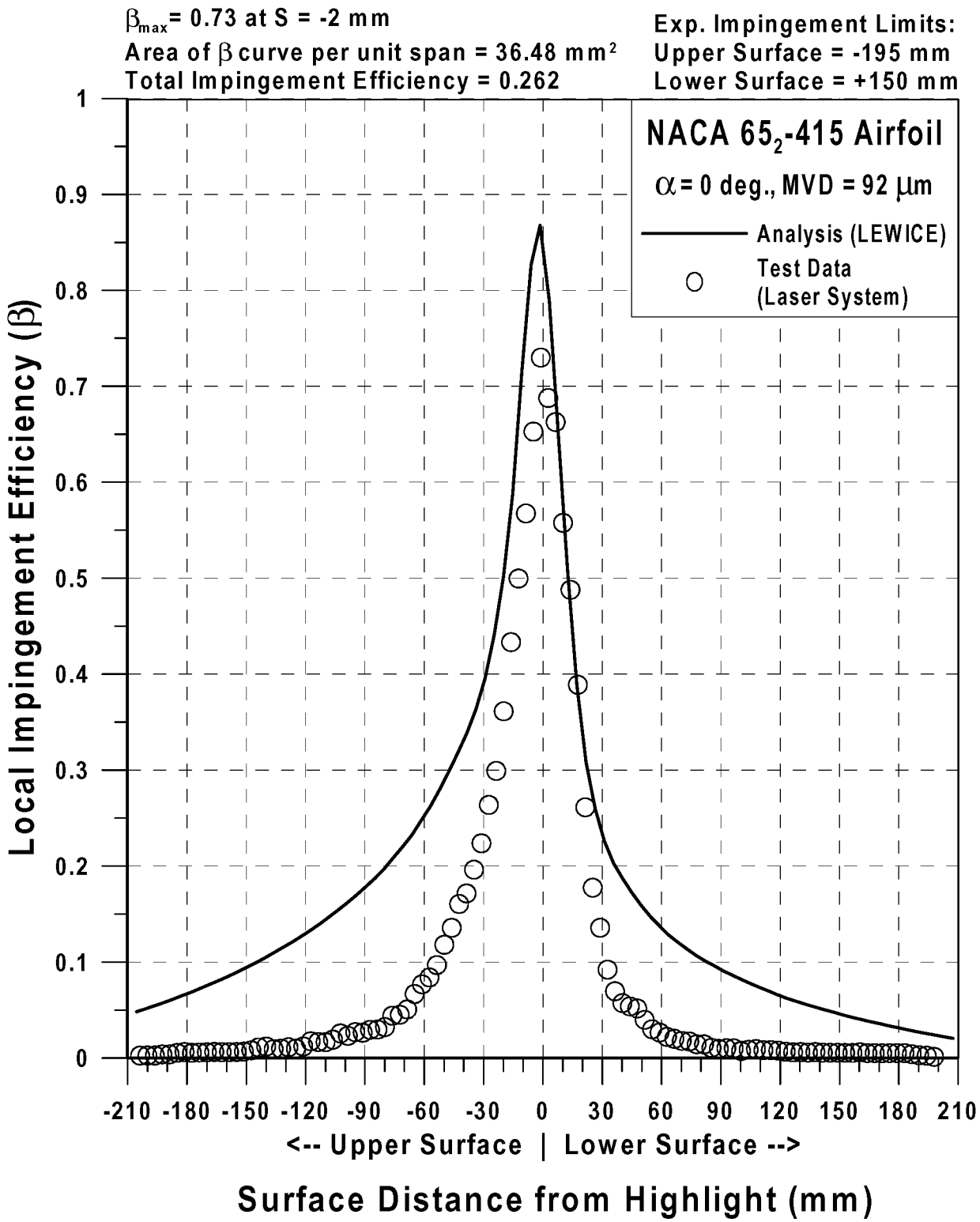

Fig. 99c Impingement efficiency distribution for NACA 65_2-415 airfoil; c = 36-in, V_∞ = 176 mph, α=0°, MVD =92 μm (Continued).

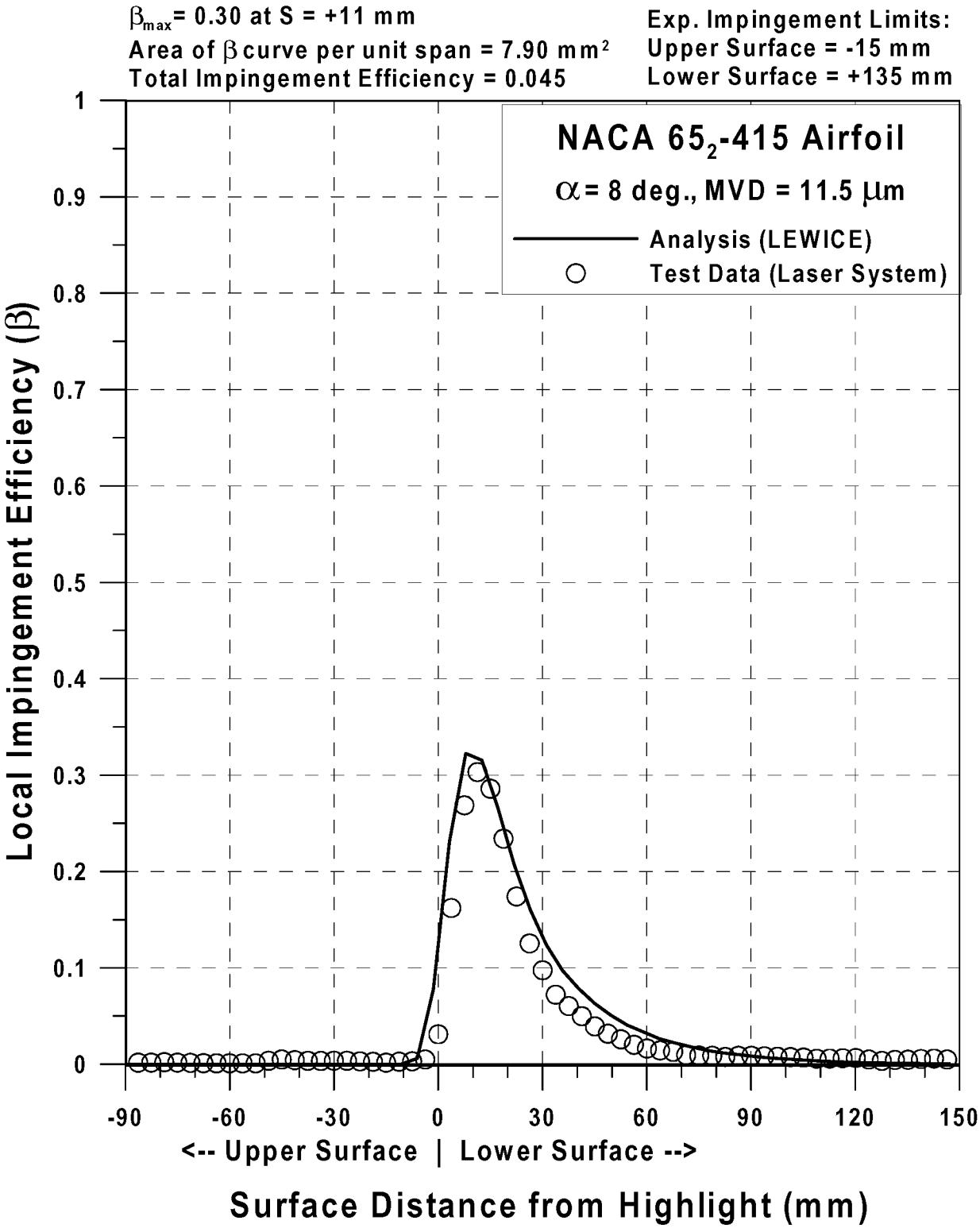

Fig. 99d Impingement efficiency distribution for NACA 65_2-415 airfoil; c = 36-in, V_∞ = 176 mph, α=8°, MVD =11.5 μm (Continued).

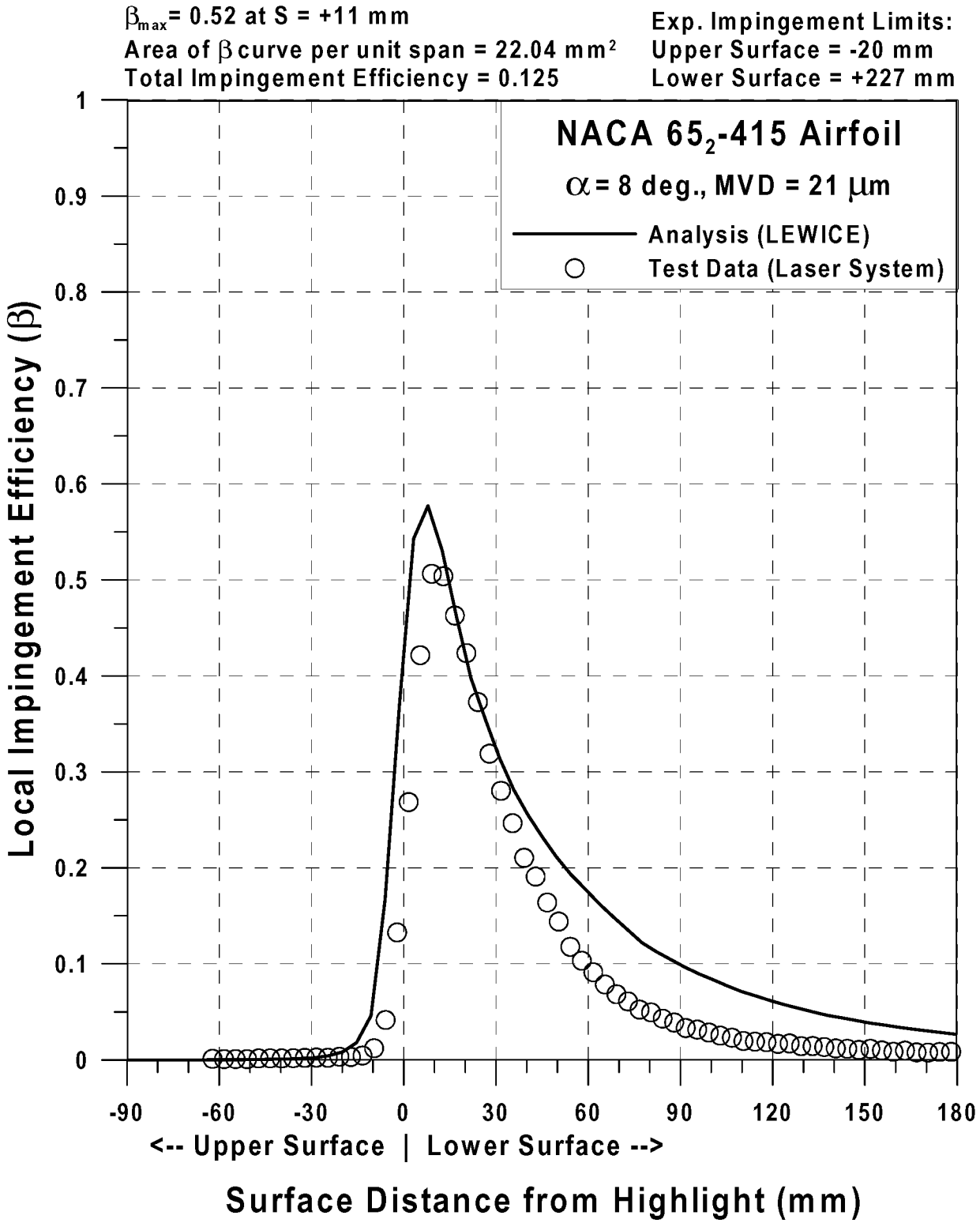

Fig. 99e Impingement efficiency distribution for NACA 65_2-415 airfoil; c = 36-in, V_∞ = 176 mph, α=8°, MVD =21 μm (Continued).

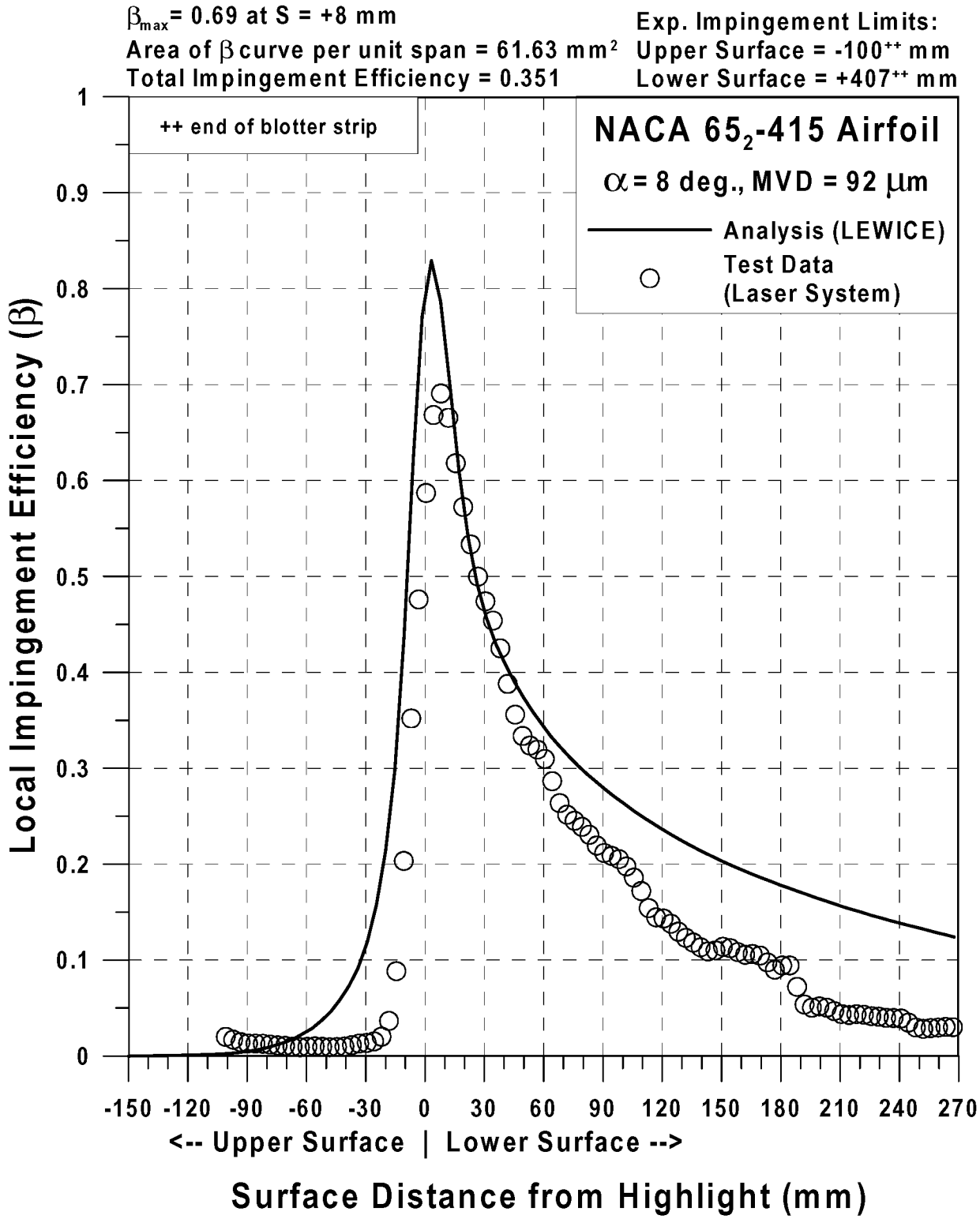

Fig. 99f Impingement efficiency distribution for NACA 65_2-415 airfoil;
c = 36-in, V_∞ = 176 mph, α=8°, MVD =92 μm.

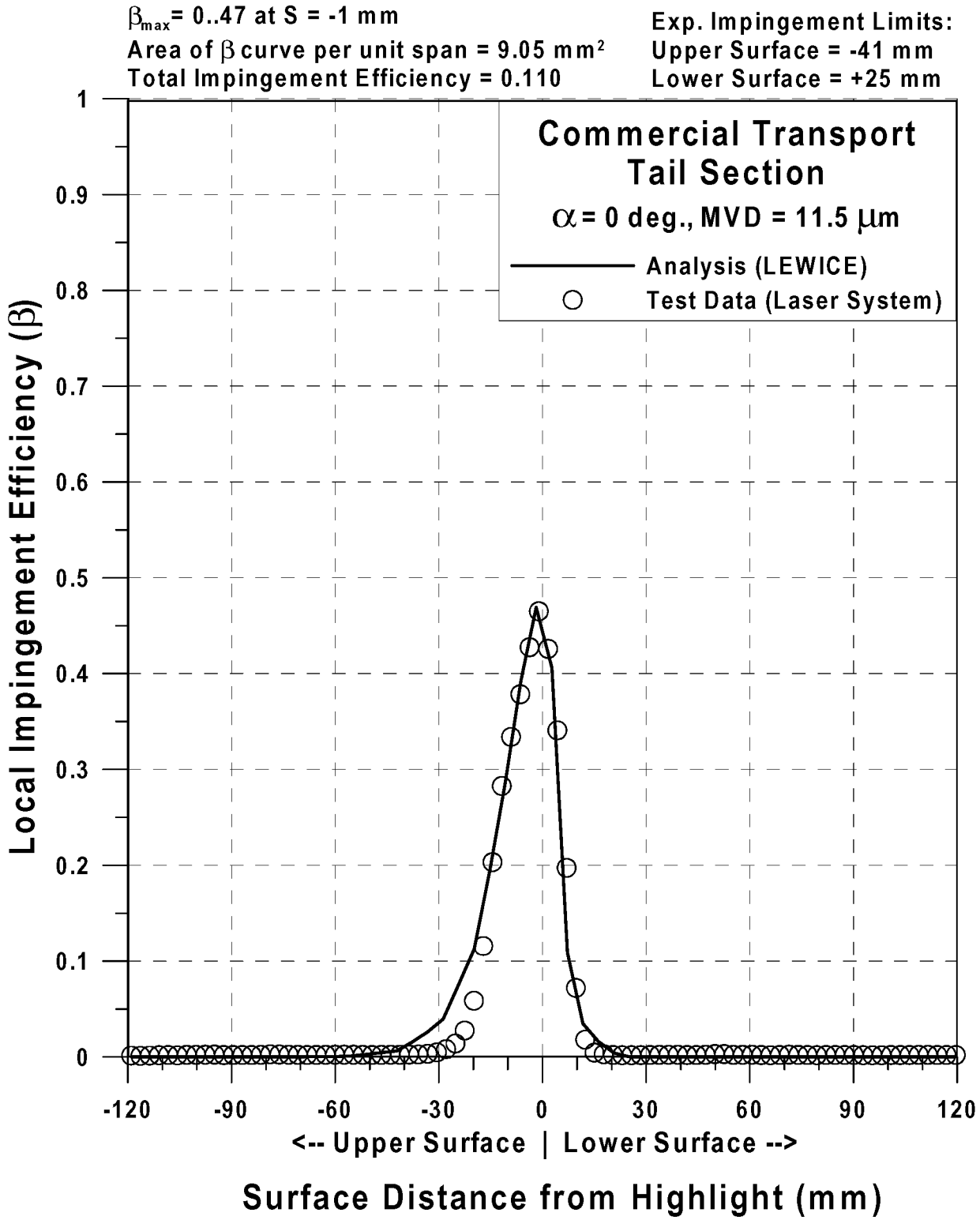

Fig. 100a Impingement efficiency distribution for commercial transport tail section; c = 36-in, V_∞ = 176 mph, α=0°, MVD =11.5 μm (Continued).

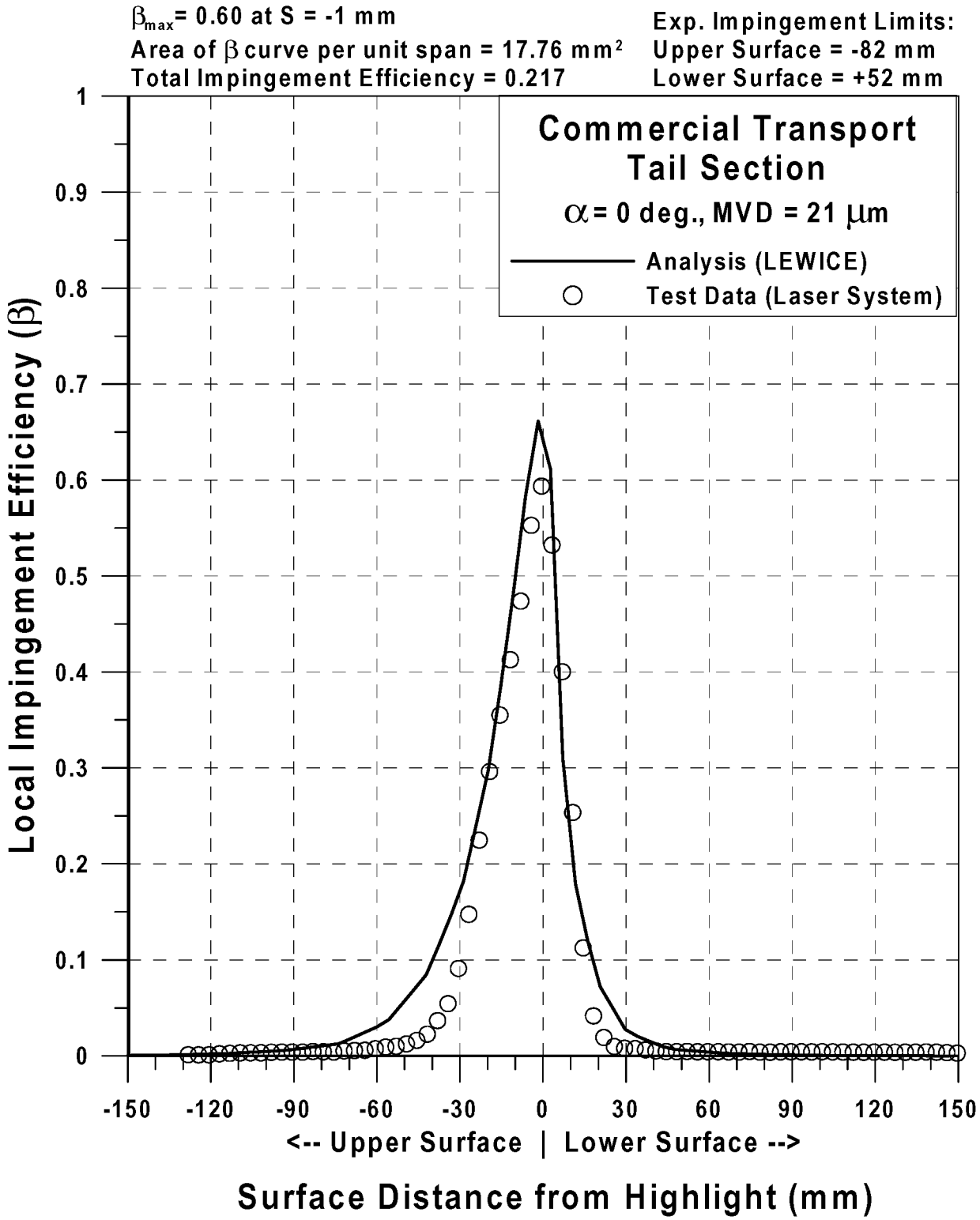

Fig. 100b Impingement efficiency distribution for commercial transport tail section; c = 36-in, V_∞ = 176 mph, α=0°, MVD =21 μm (Continued).

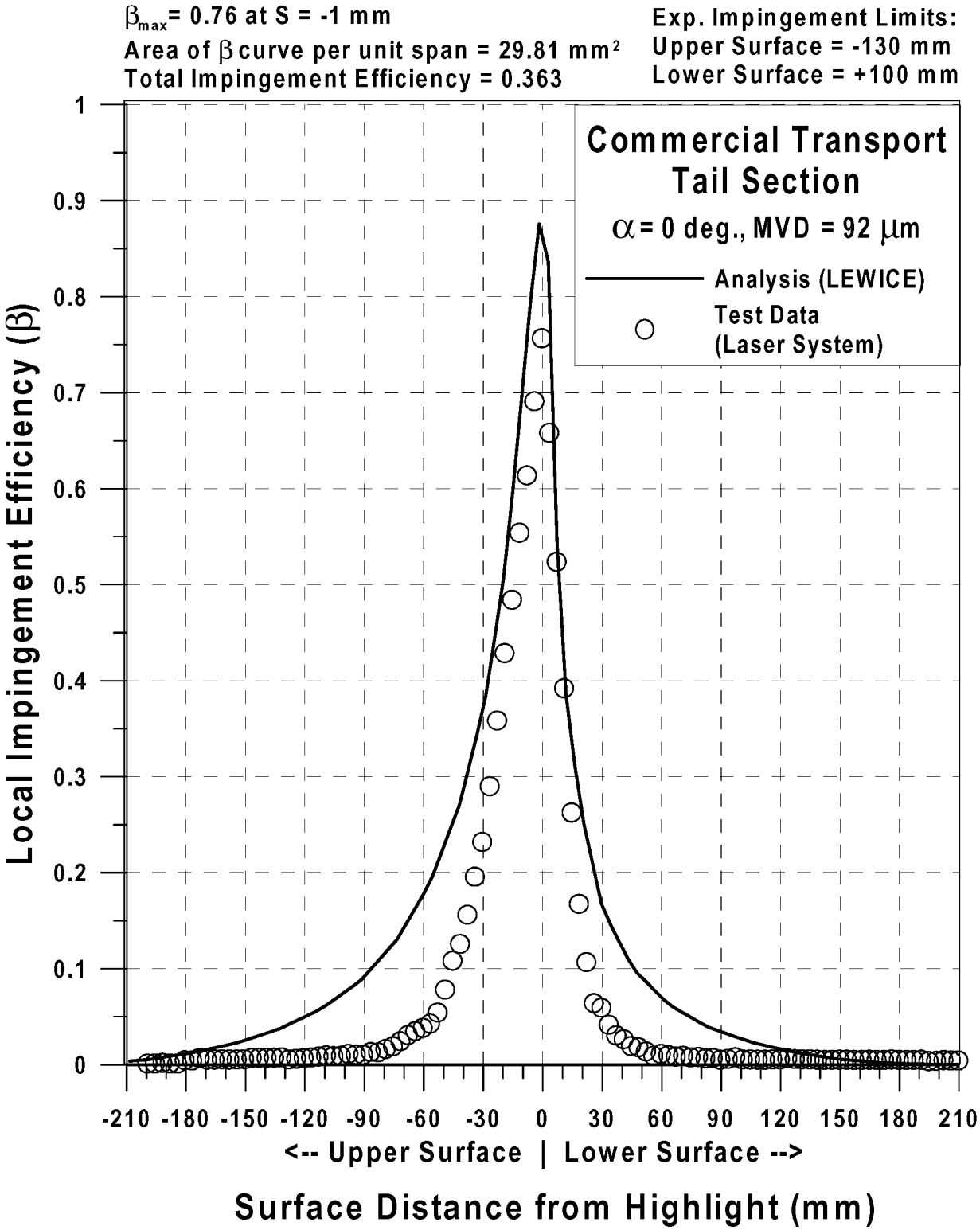

Fig. 100c Impingement efficiency distribution for commercial transport tail section; c = 36-in, V_∞ = 176 mph, α=0°, MVD =92 μm (Continued).

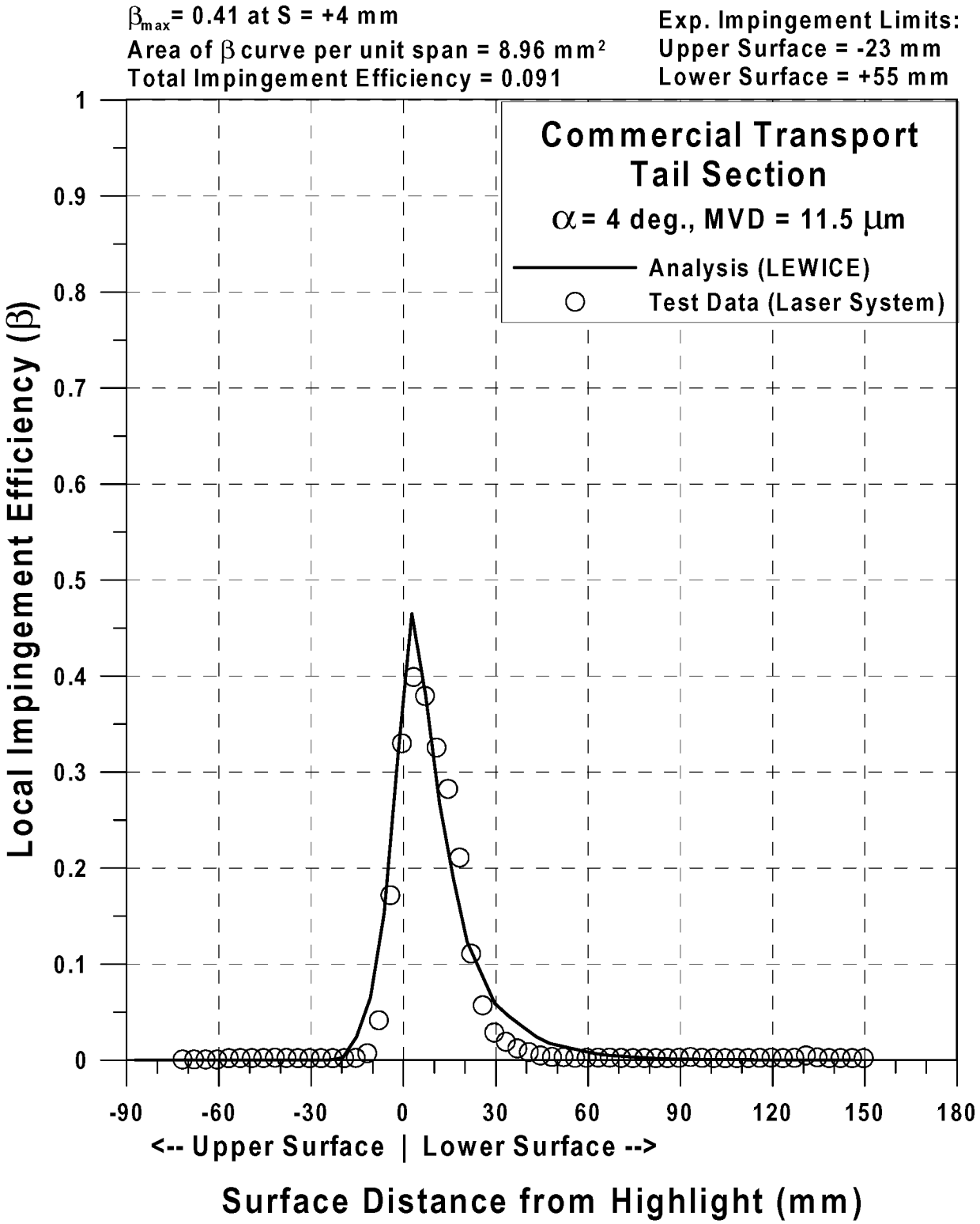

Fig. 100d Impingement efficiency distribution for commercial transport tail section; c = 36-in, V_∞ = 176 mph, α=4°, MVD =11.5 μm (Continued).

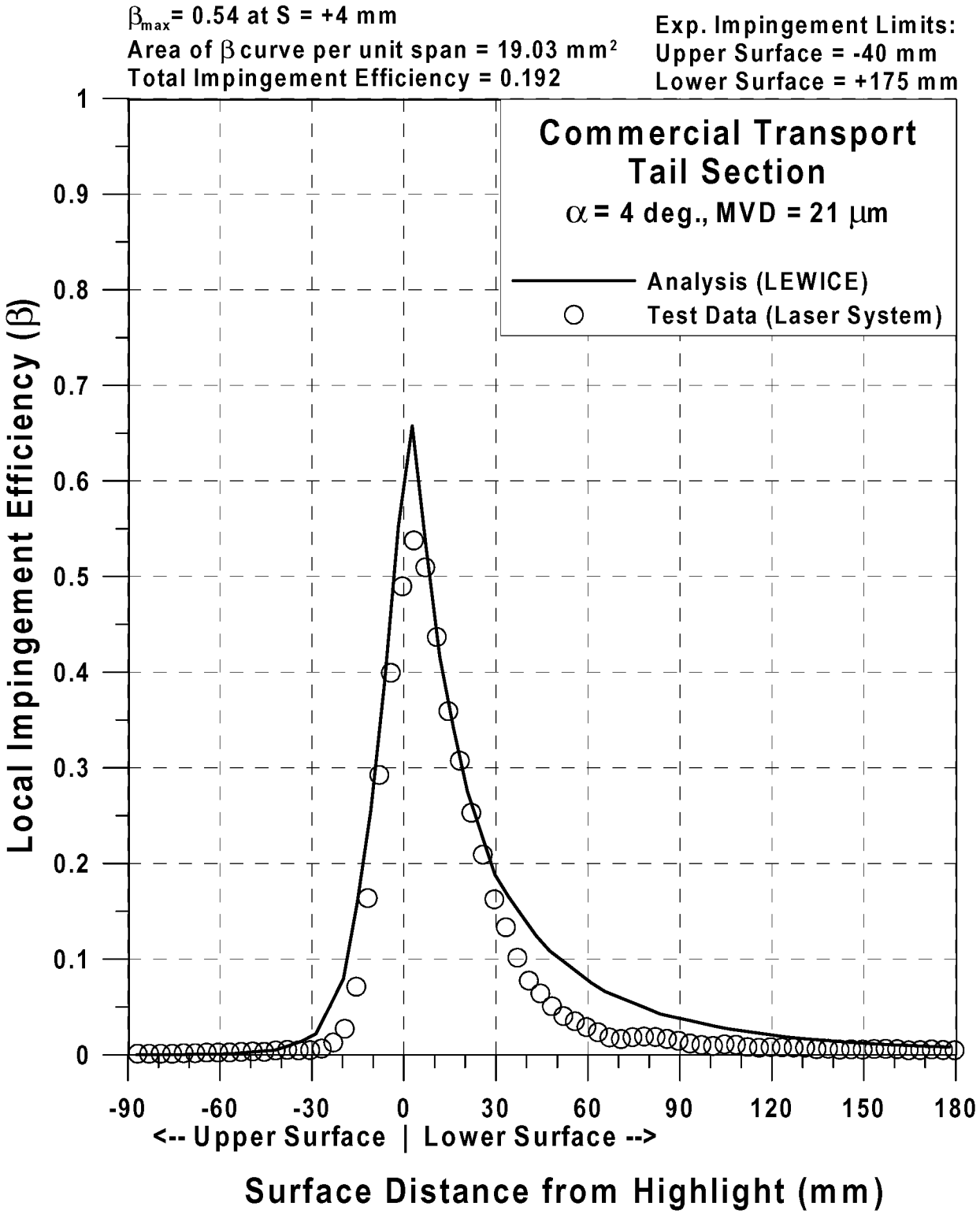

Fig. 100e Impingement efficiency distribution for commercial transport tail section; c = 36-in, V_∞ = 176 mph, α=4°, MVD =21 μm (Continued).

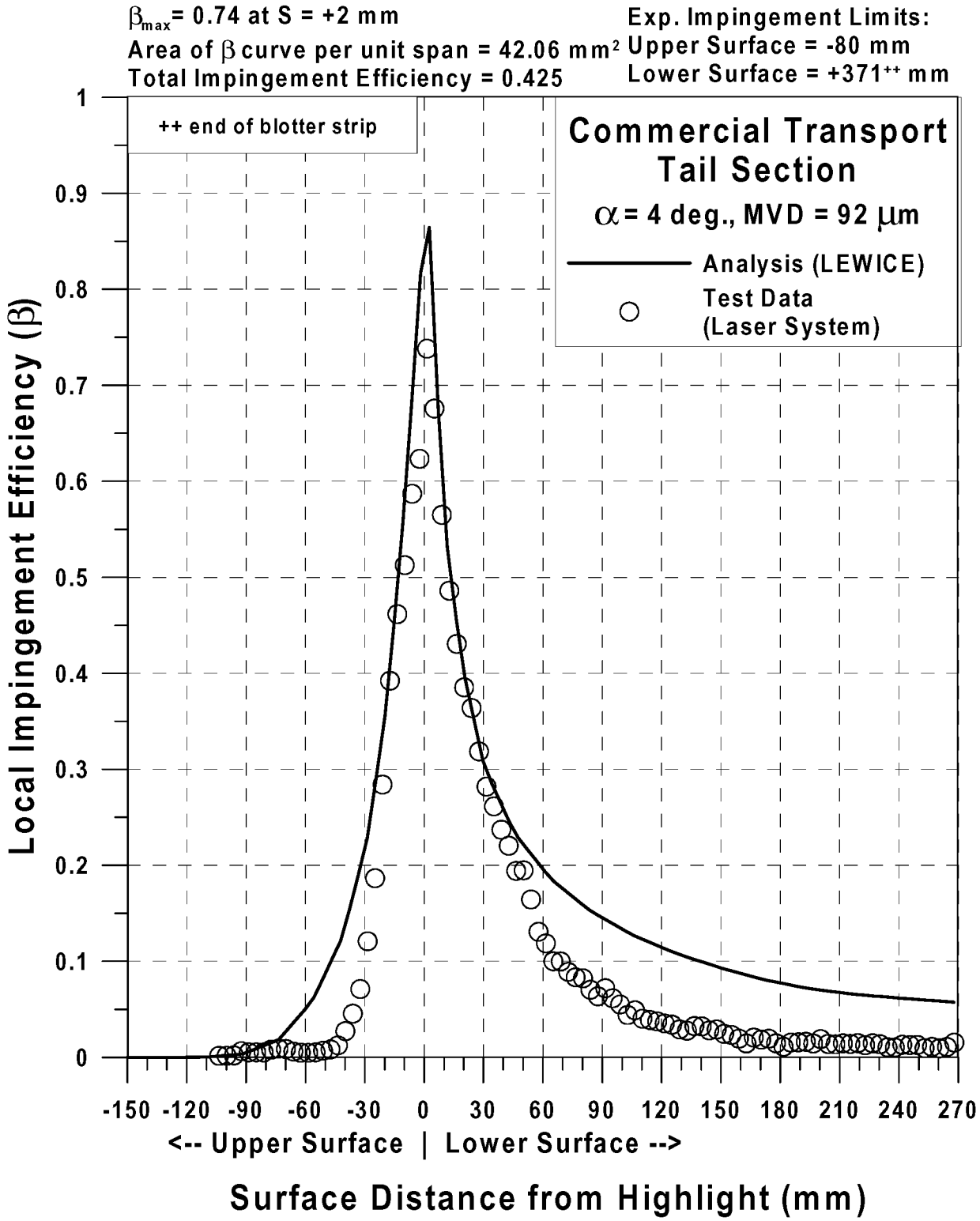

Fig. 100f Impingement efficiency distribution for commercial transport tail section; c = 36-in, V_∞ = 176 mph, α=4°, MVD =92 μm.

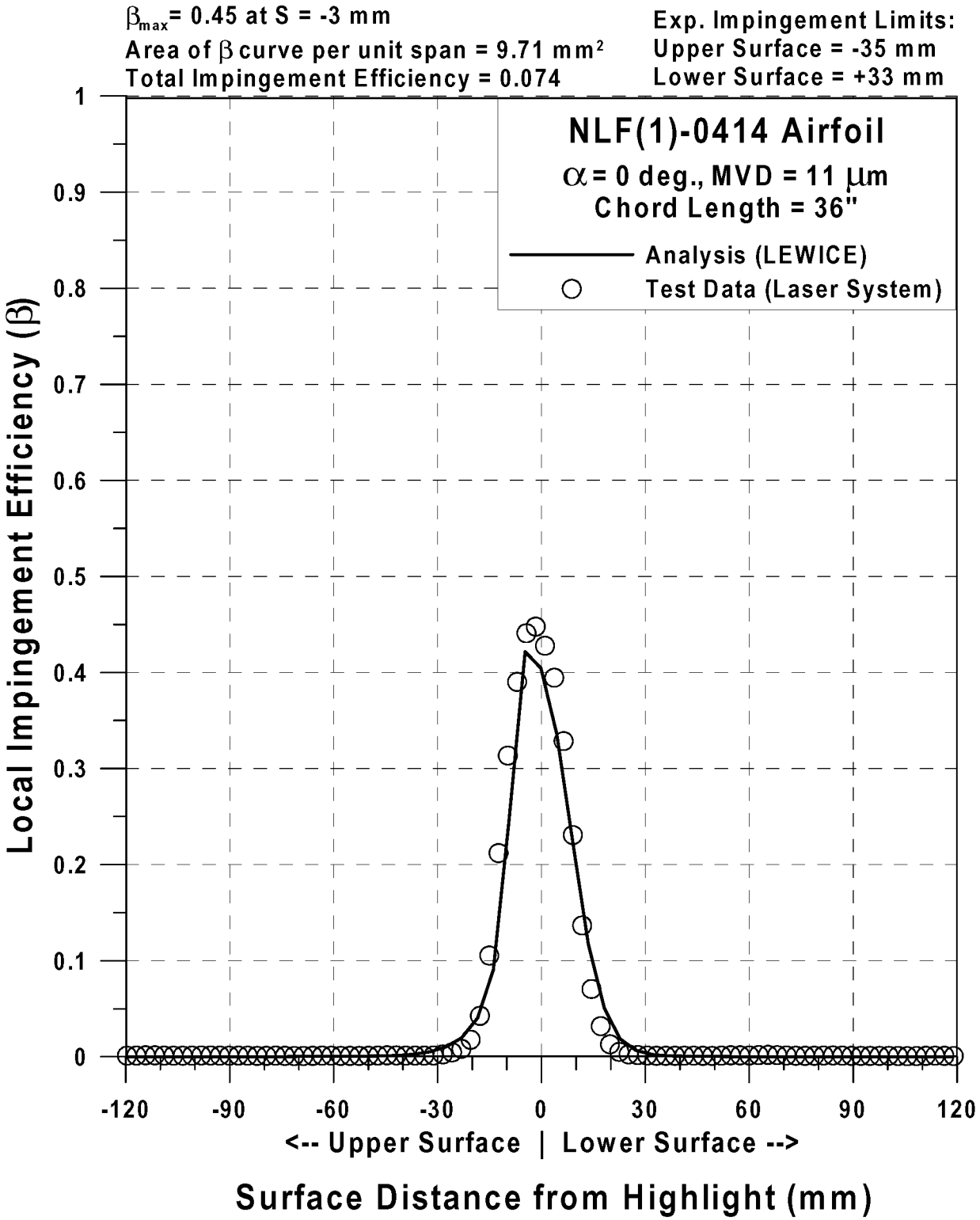

Fig. 101a Impingement efficiency distribution for NLF(1)-0414 airfoil; c = 36-in, V_∞ = 176 mph, α=0°, MVD =11 μm (Continued).

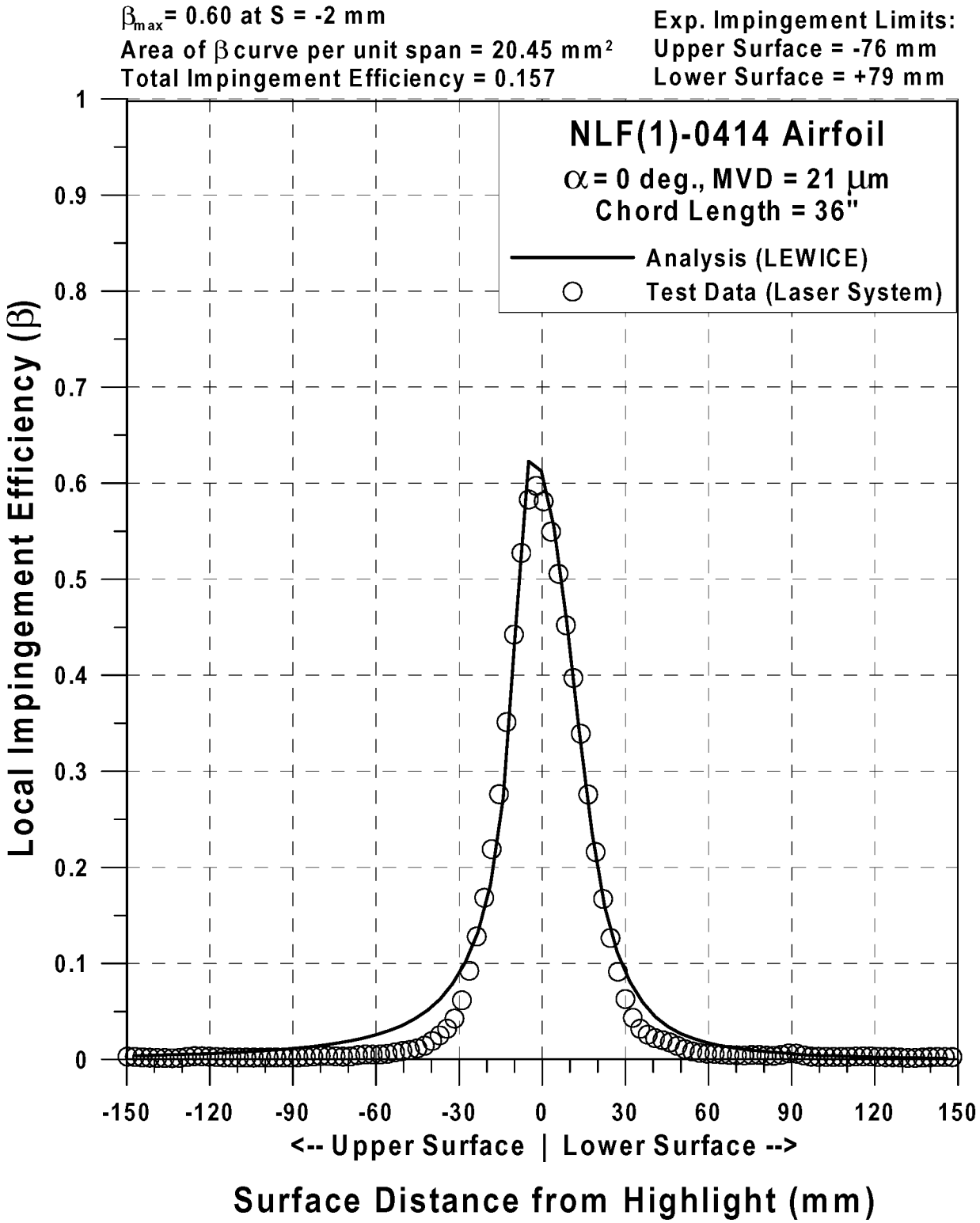

Fig. 101b Impingement efficiency distribution for NLF(1)-0414 airfoil; c = 36-in, V_∞ = 176 mph, α=0°, MVD =21 μm (Continued).

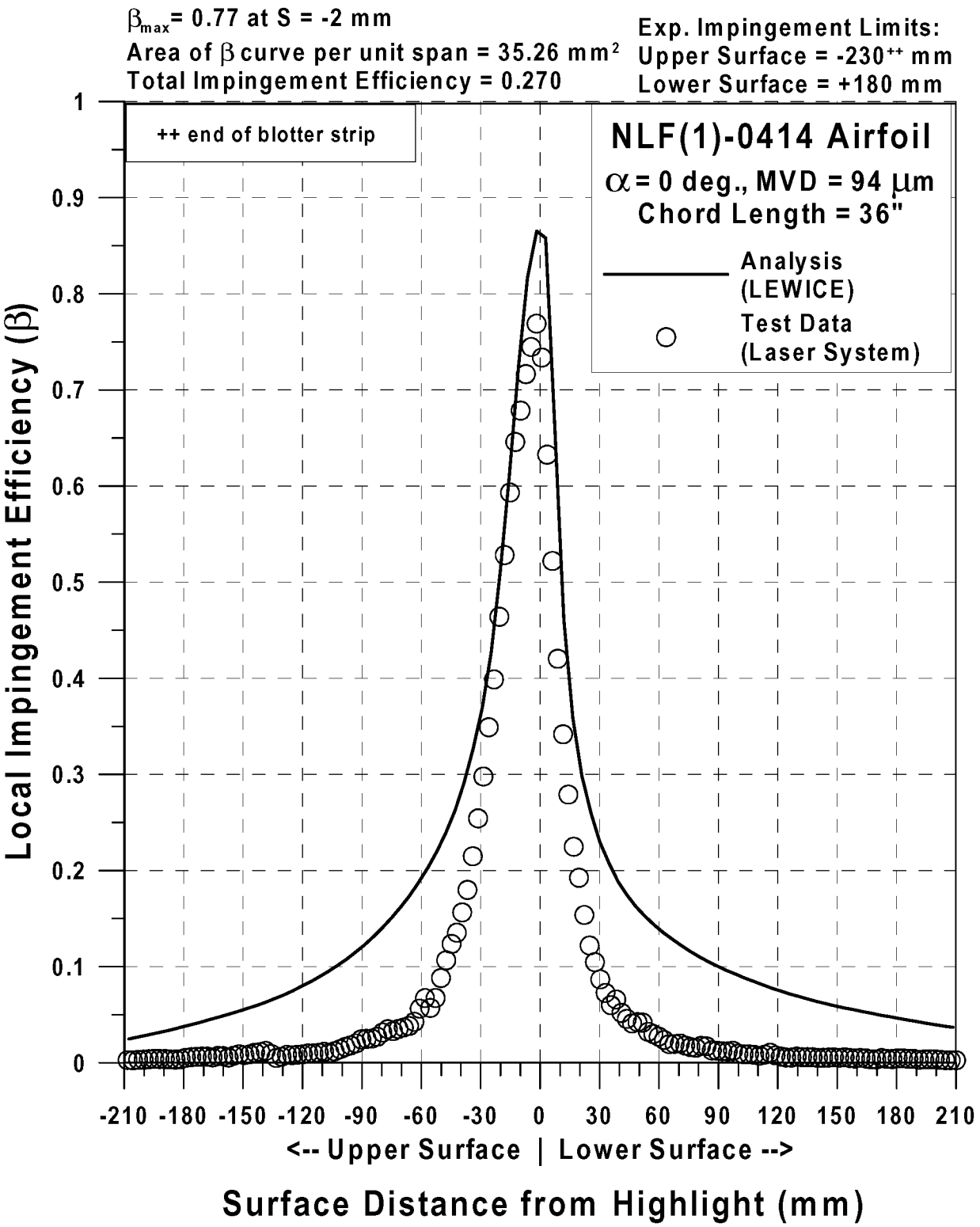

Fig. 101c Impingement efficiency distribution for NLF(1)-0414 airfoil; c = 36-in, V_∞ = 176 mph, α=0°, MVD =94 μm (Continued).

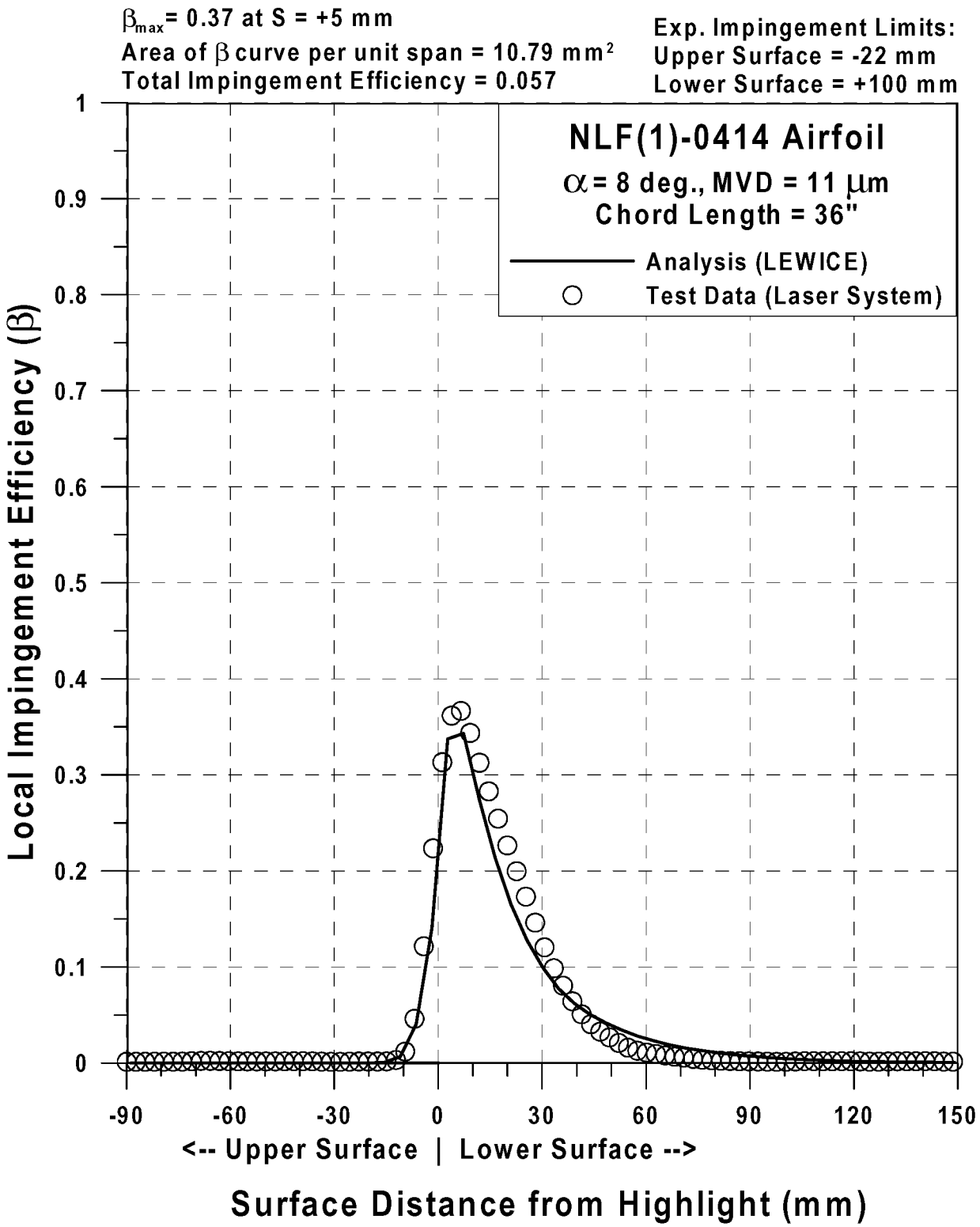

Fig. 101d Impingement efficiency distribution for NLF(1)-0414 airfoil; c = 36-in, V_∞ = 176 mph, α=8°, MVD =11 μm (Continued).

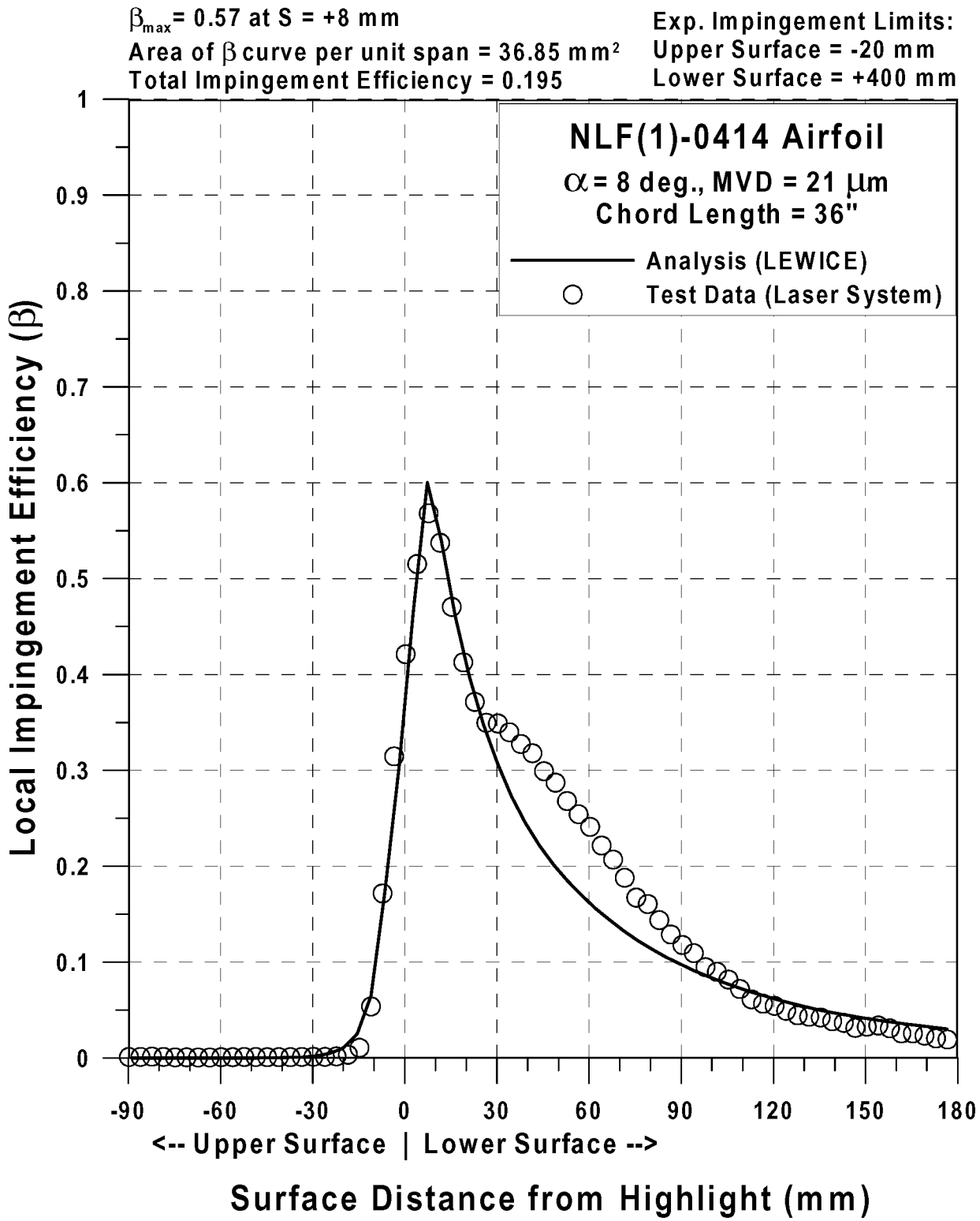

Fig. 101e Impingement efficiency distribution for NLF(1)-0414 airfoil; c = 36-in, V_∞ = 176 mph, α=8°, MVD =21 μm (Continued).

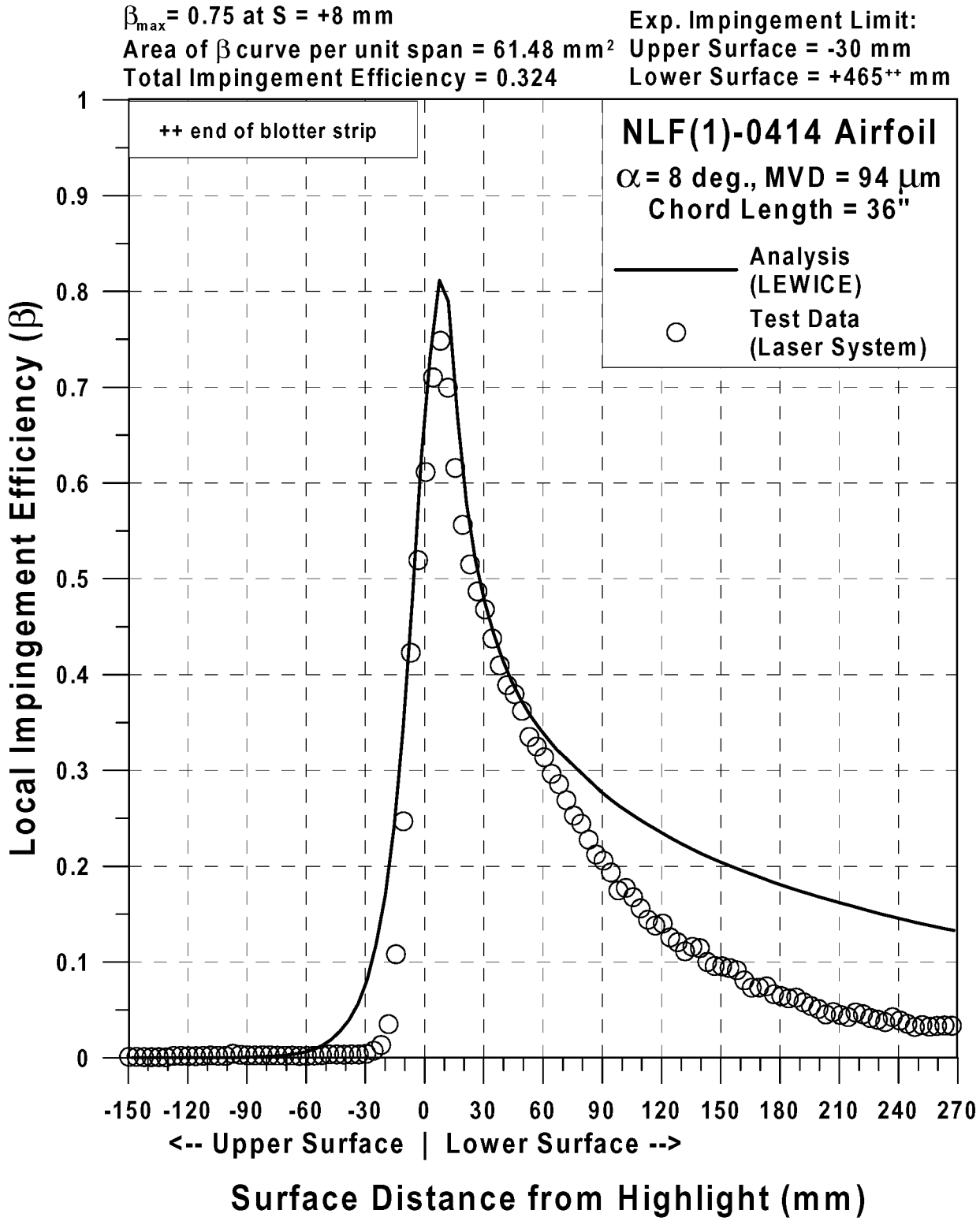

Fig. 101f Impingement efficiency distribution for NLF(1)-0414 airfoil;
c = 36-in, V_∞ = 176 mph, α=8°, MVD =94 μm.

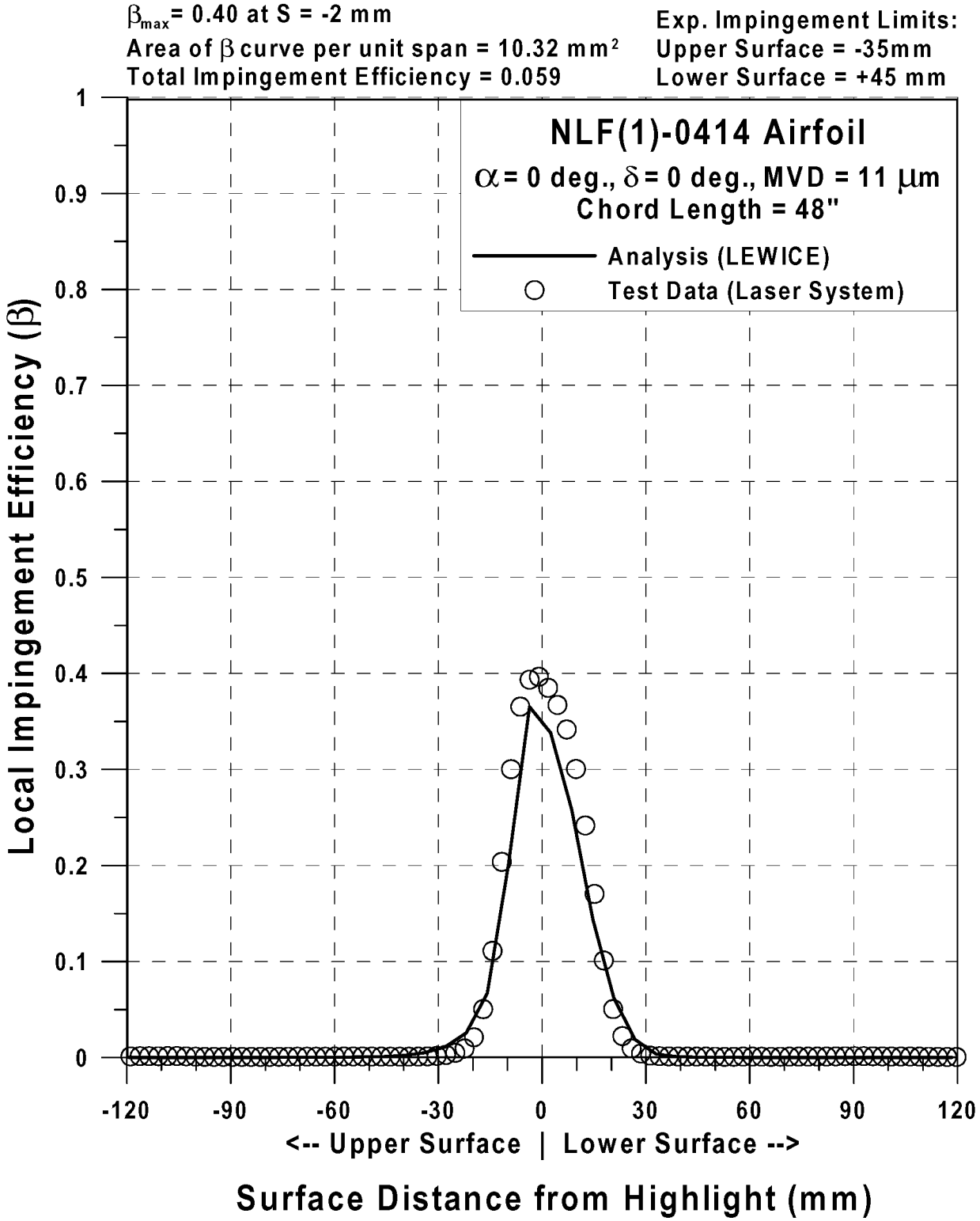

Fig. 102a Impingement efficiency distribution for NLF(1)-0414 airfoil; c = 48-in, 25%-chord full-span flap, V_∞ = 176 mph, $\alpha=0^\circ$, $\delta=0^\circ$, MVD =11 μm (Continued).

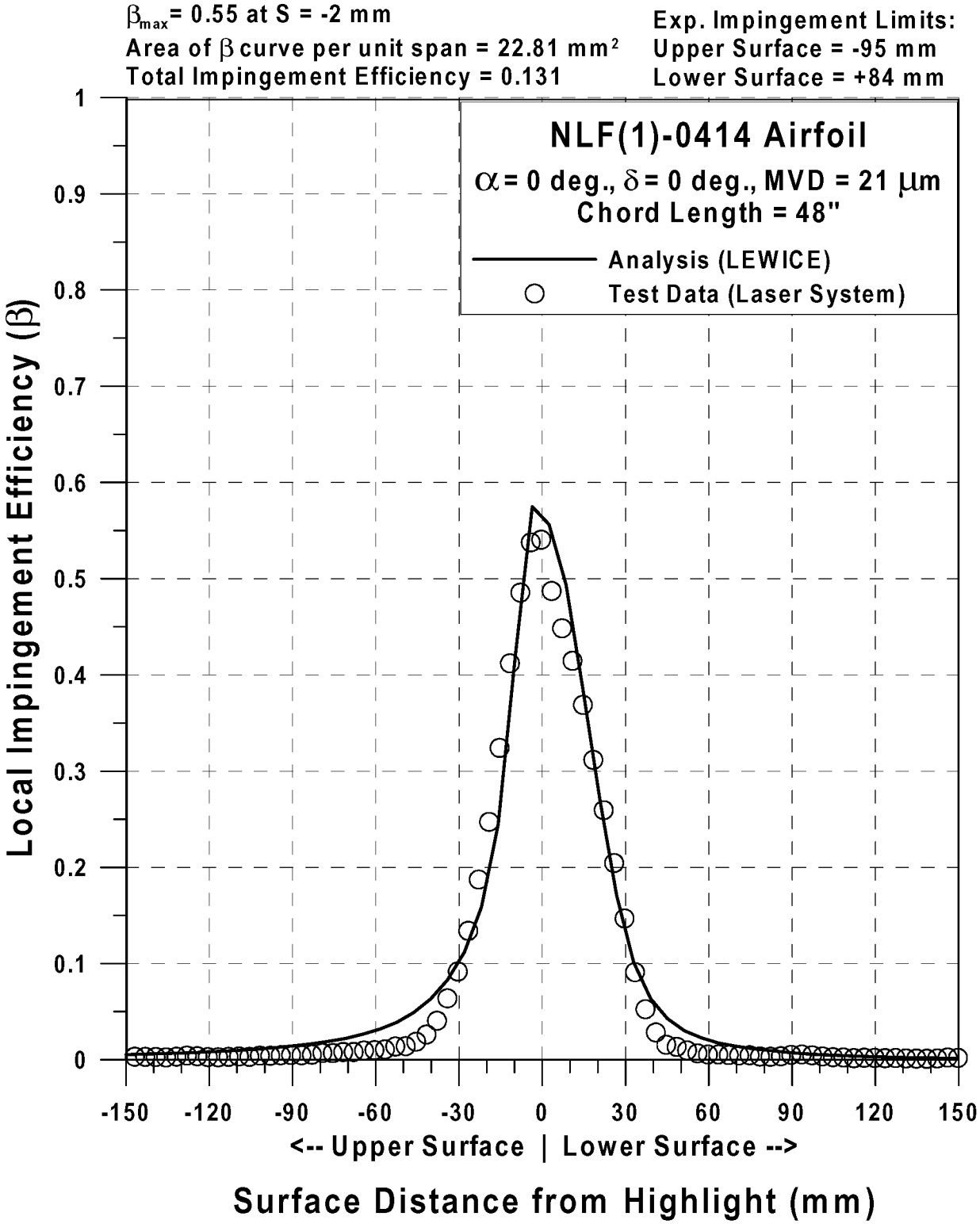

Fig. 102b Impingement efficiency distribution for NLF(1)-0414 airfoil; c = 48-in, 25%-chord full-span flap, V_∞ = 176 mph, $\alpha=0^\circ$, $\delta=0^\circ$, MVD =21 μm (Continued).

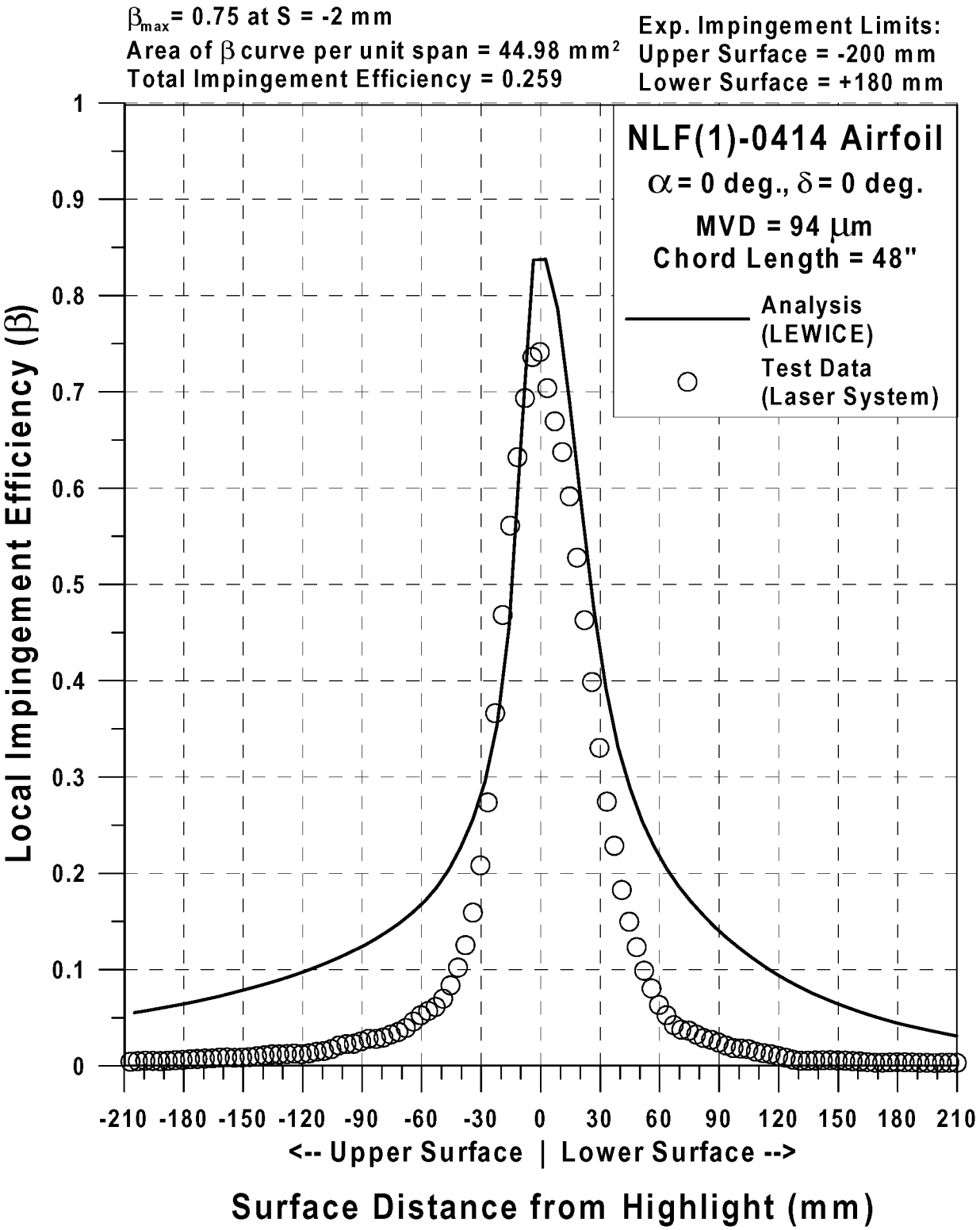

Fig. 102c Impingement efficiency distribution for NLF(1)-0414 airfoil; c = 48-in, 25%-chord full-span flap, V_∞ = 176 mph, α=0°, δ=0°, MVD =94 μm (Continued).

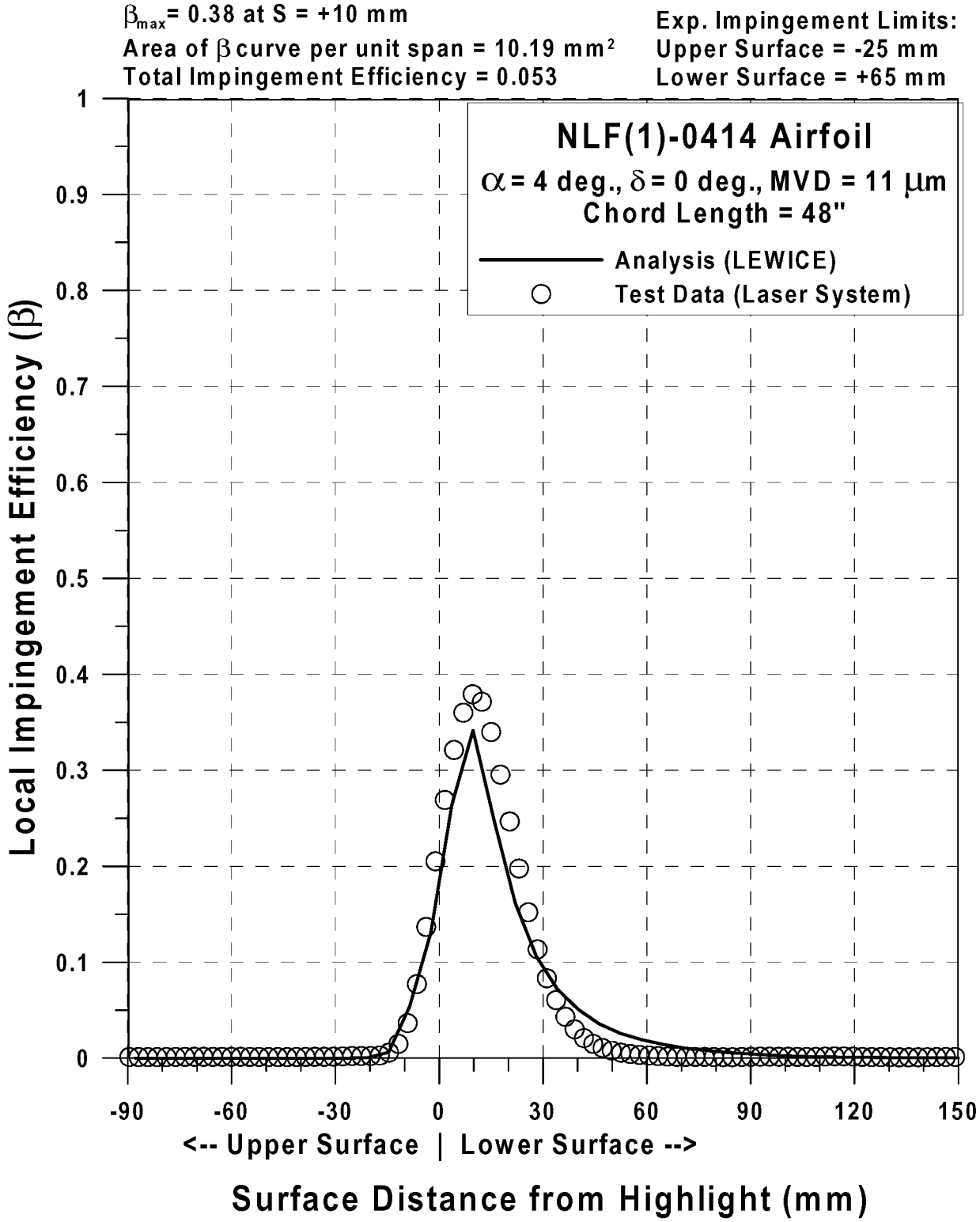

Fig. 102d Impingement efficiency distribution for NLF(1)-0414 airfoil; c = 48-in, 25%-chord full-span flap, V_∞ = 176 mph, α=4°, δ=0°, MVD =11 μm (Continued).

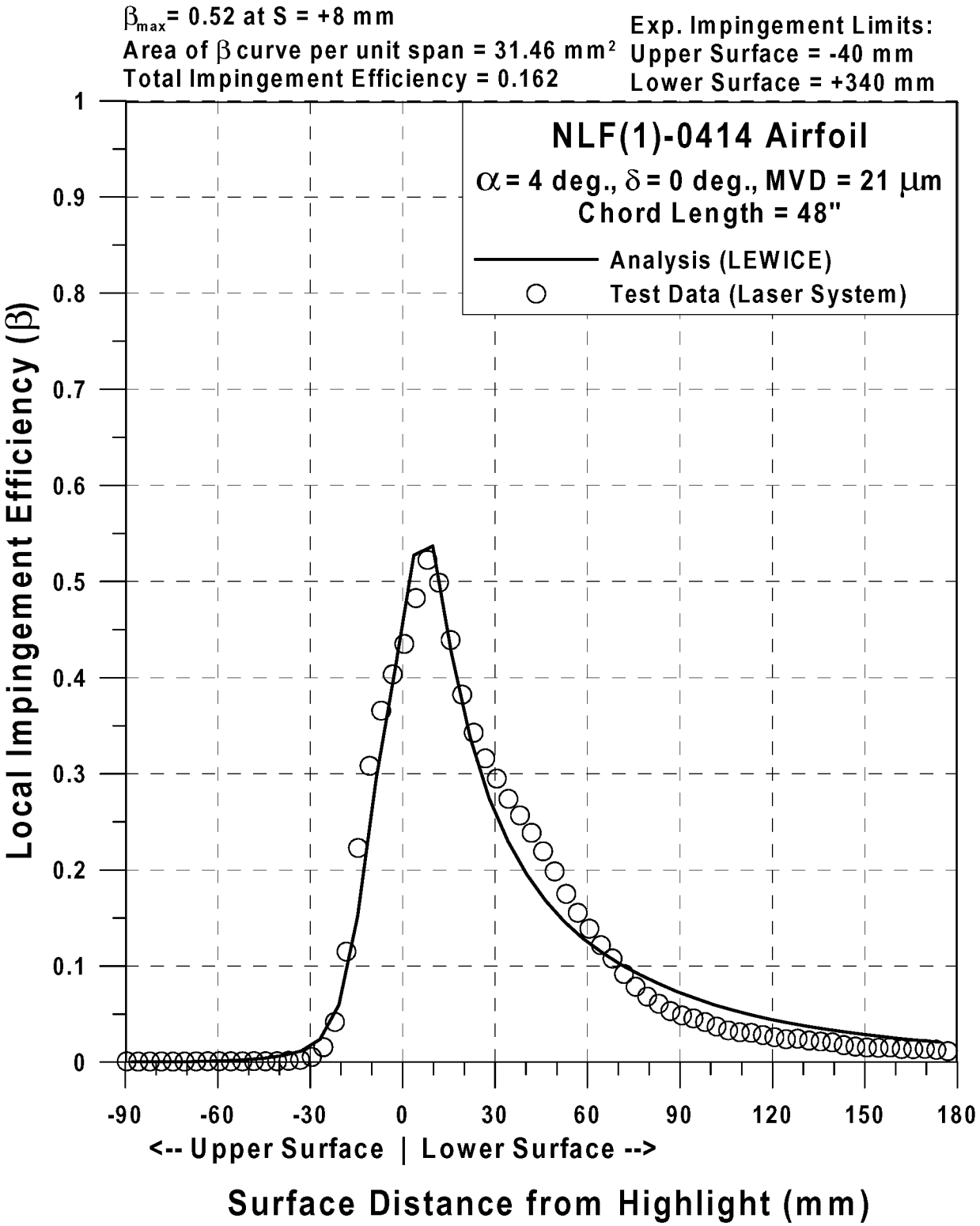

Fig. 102e Impingement efficiency distribution for NLF(1)-0414 airfoil; c = 48-in, 25%-chord full-span flap, V_∞ = 176 mph, α=4°, δ=0°, MVD =21 μm (Continued).

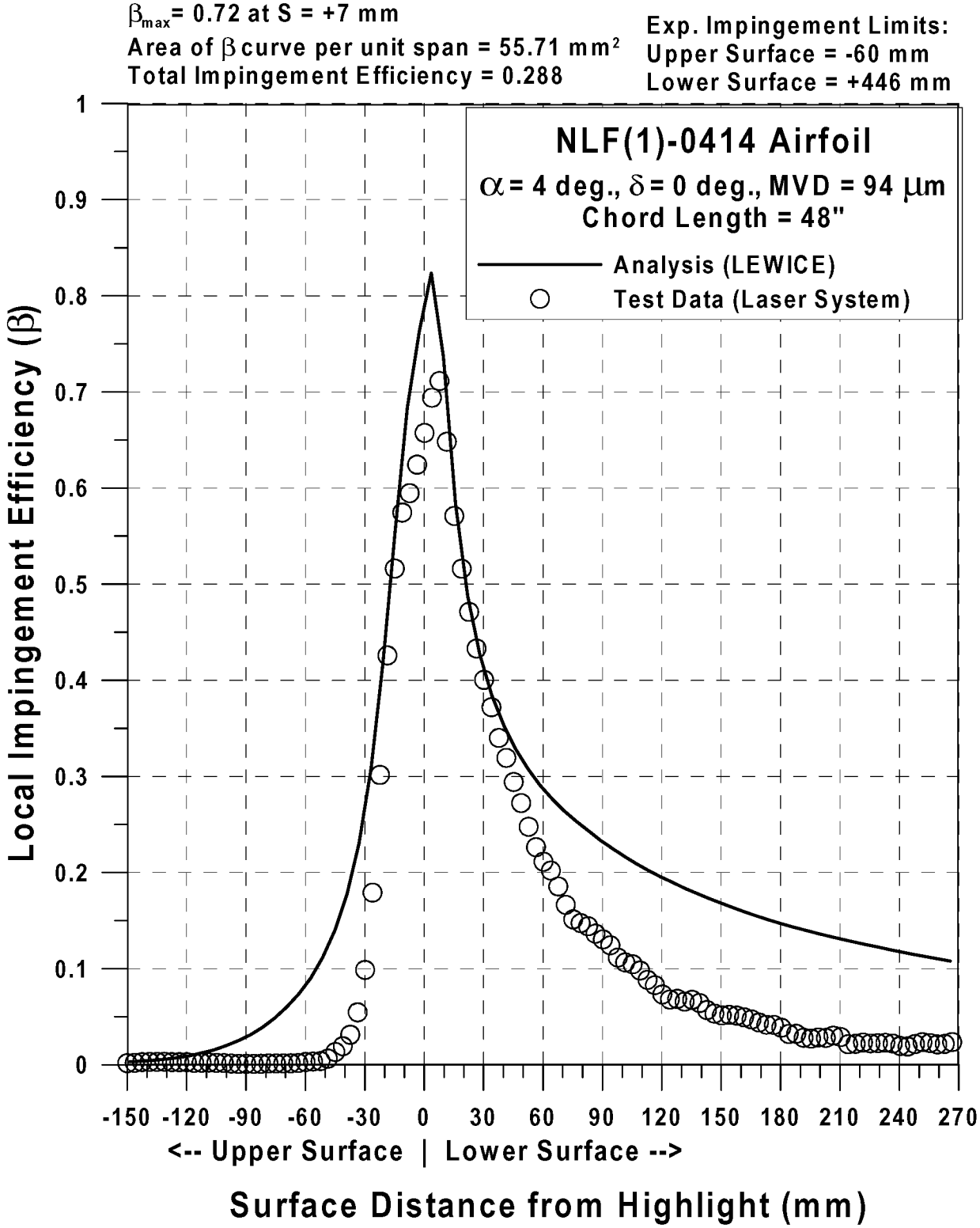

Fig. 102f Impingement efficiency distribution for NLF(1)-0414 airfoil; c = 48-in, 25%-chord full-span flap, V_∞ = 176 mph, α=4°, δ=0°, MVD =94 μm (Continued).

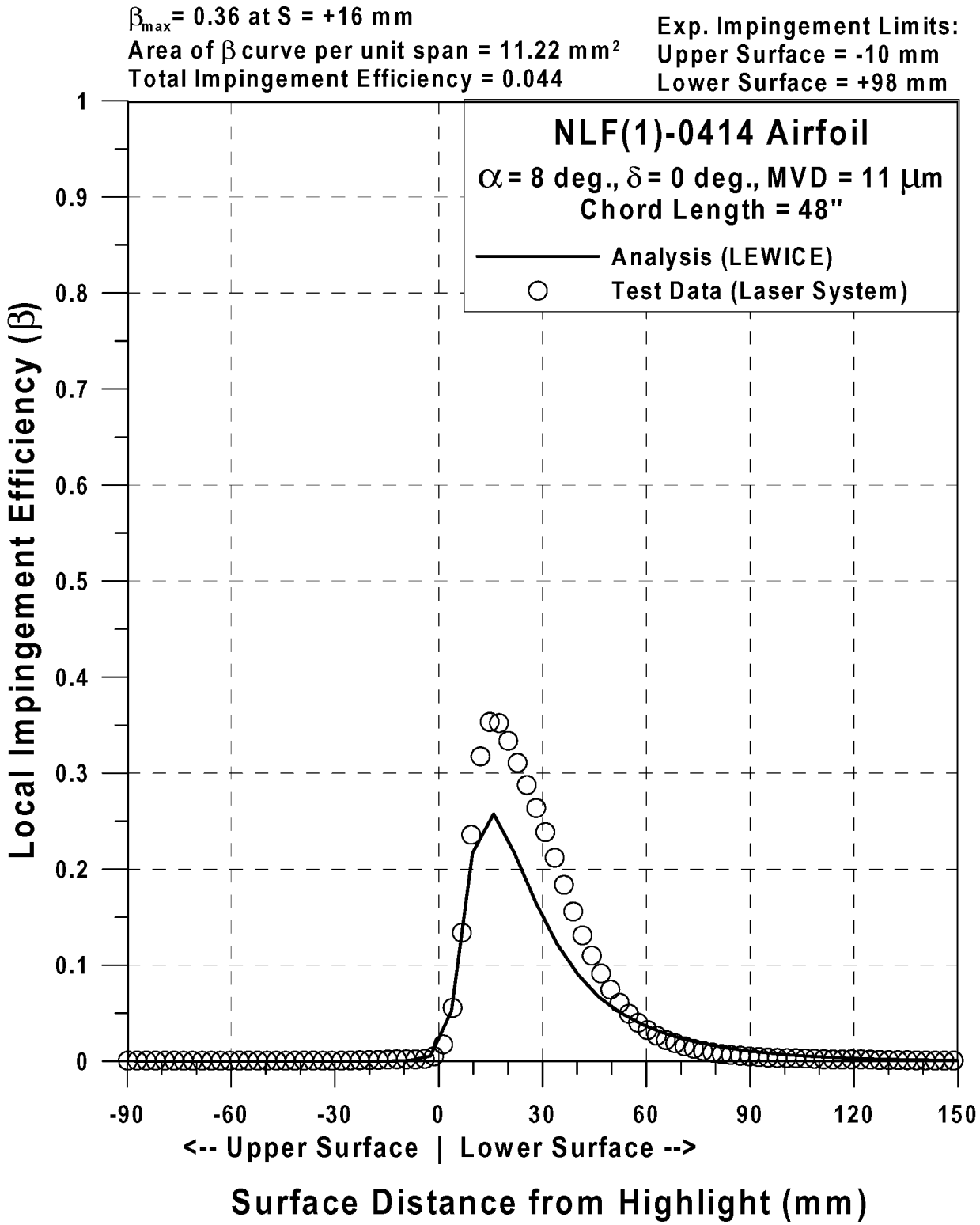

Fig. 102g Impingement efficiency distribution for NLF(1)-0414 airfoil; c = 48-in, 25%-chord full-span flap, V_∞ = 176 mph, α=8°, δ=0°, MVD =11 μm (Continued).

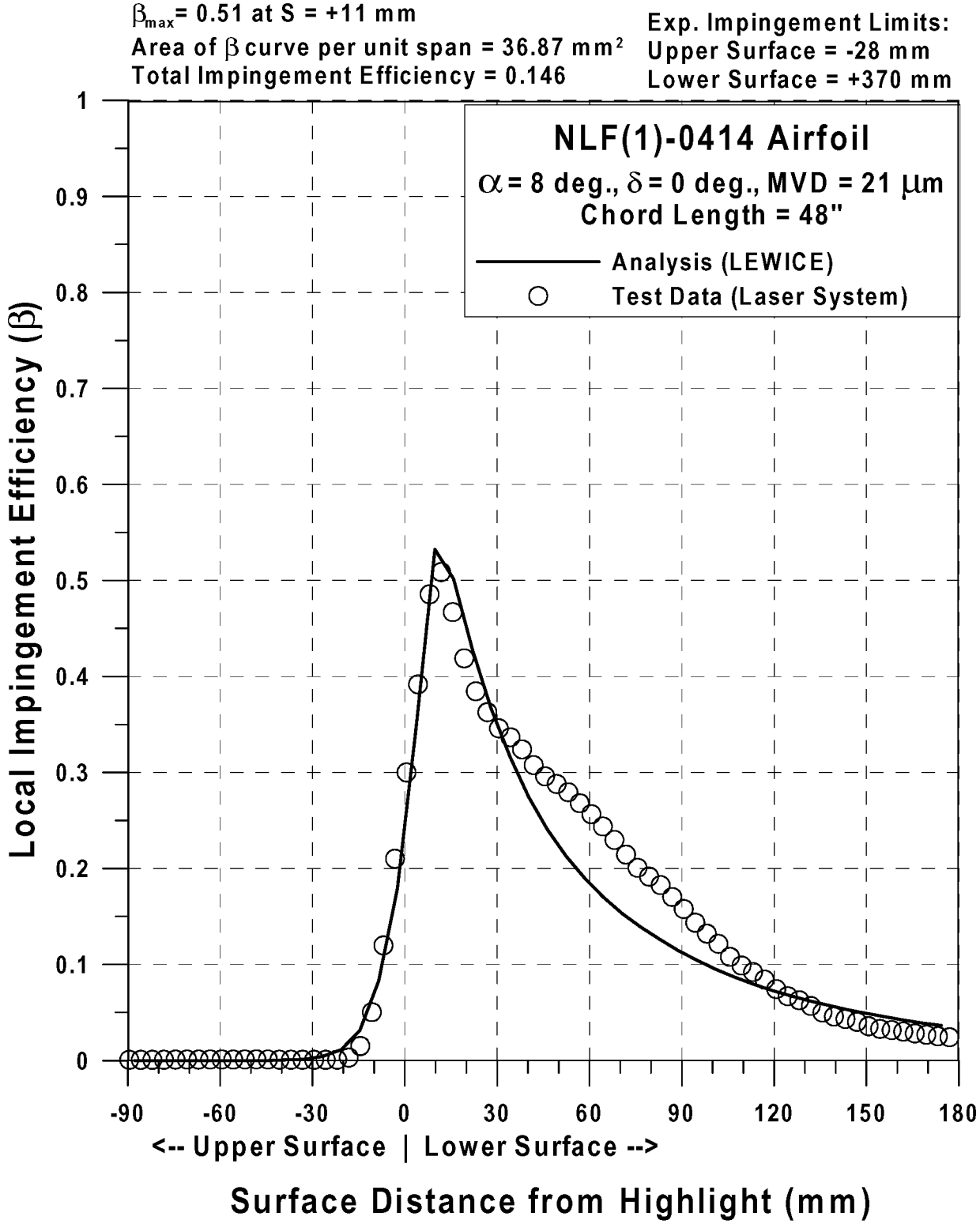

Fig. 102h Impingement efficiency distribution for NLF(1)-0414 airfoil; c = 48-in, 25%-chord full-span flap, V_∞ = 176 mph, α=8°, δ=0°, MVD =21 μm (Continued).

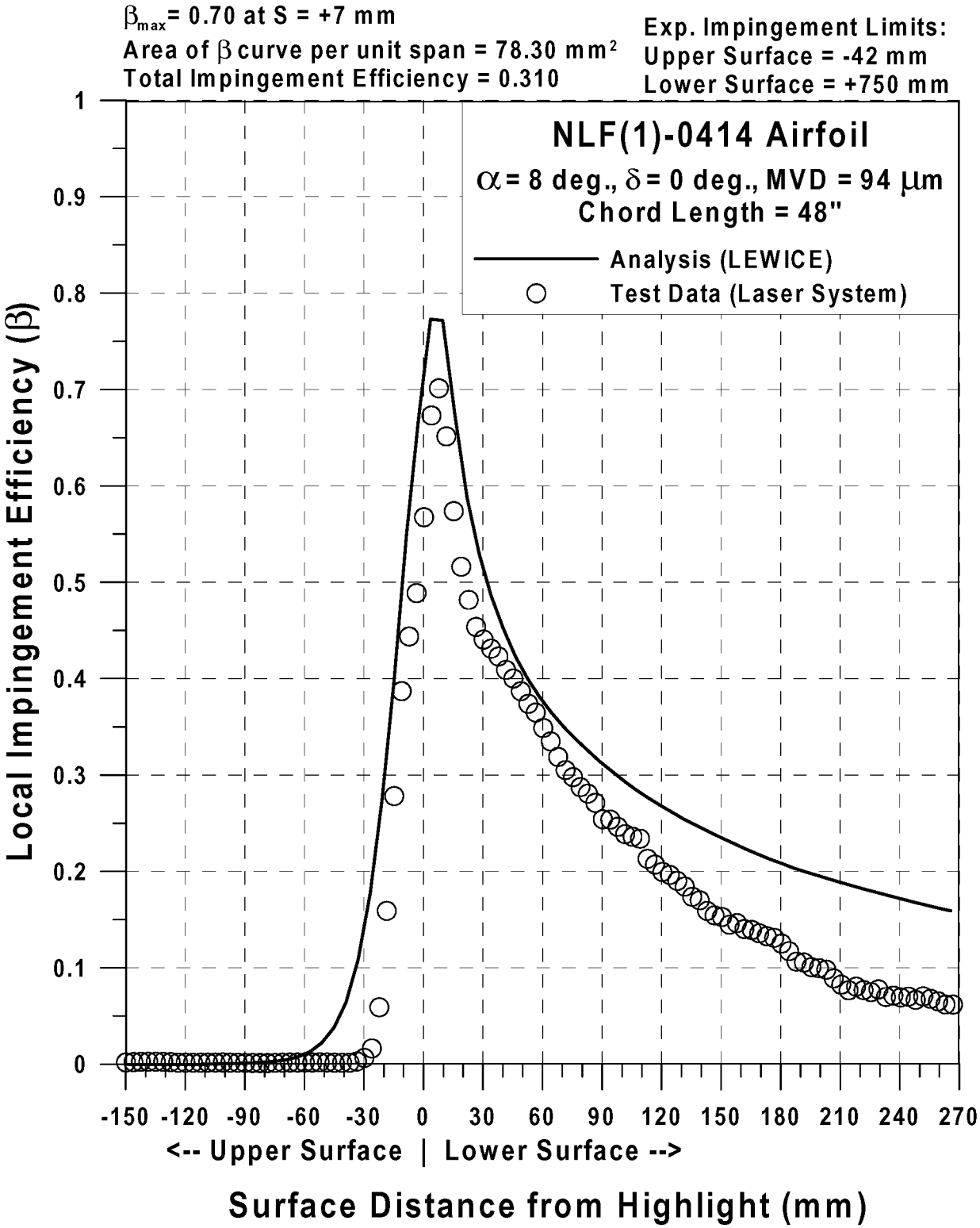

Fig. 102i Impingement efficiency distribution for NLF(1)-0414 airfoil; c = 48-in, 25%-chord full-span flap, V_∞ = 176 mph, α=8°, δ=0°, MVD =94 μm (Continued).

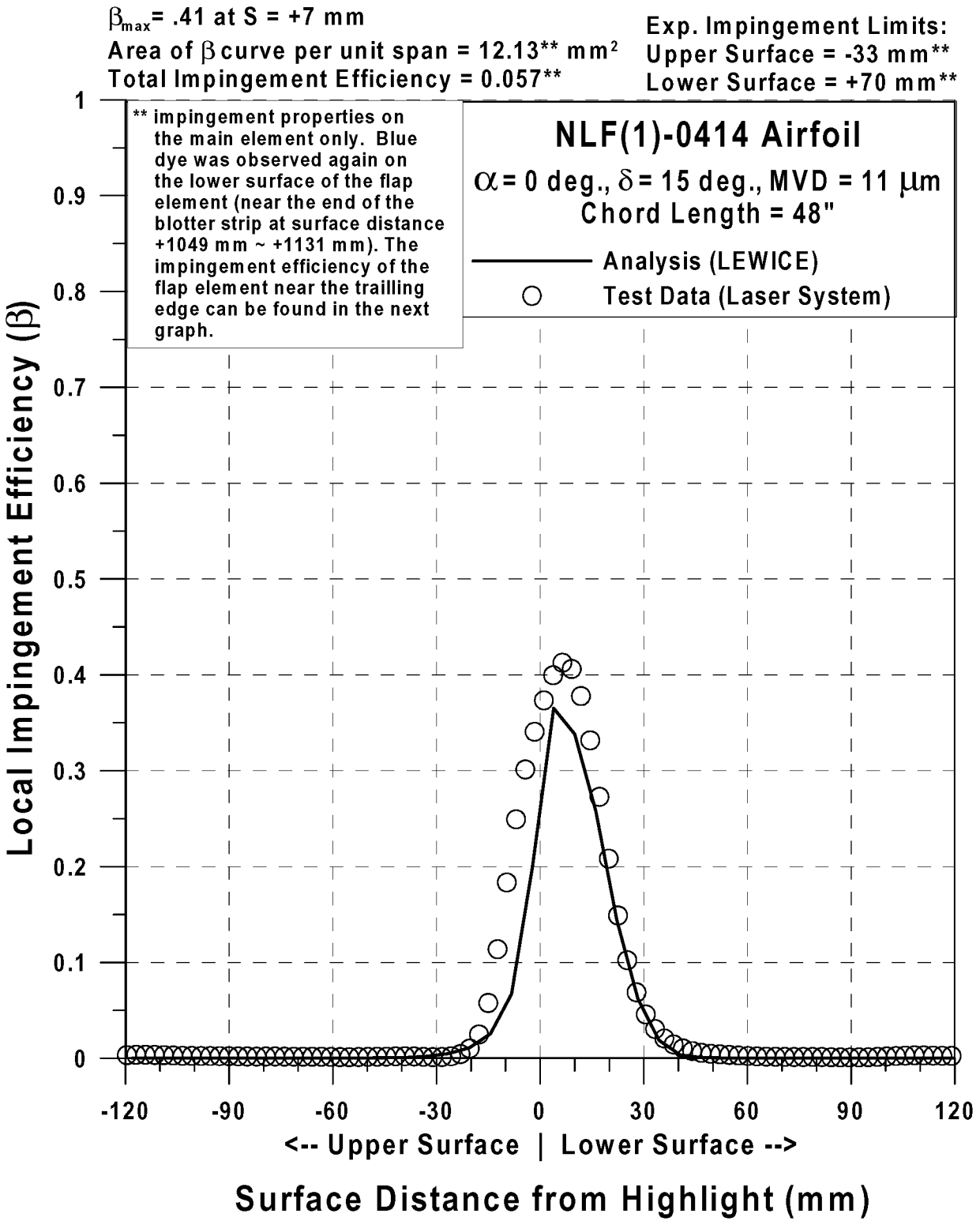

Fig. 102j Impingement efficiency distribution for NLF(1)-0414 airfoil; c =48-in, 25%-chord full-span flap, V_∞ = 176 mph, α=0°, δ=15°, MVD =11 μm (Continued).

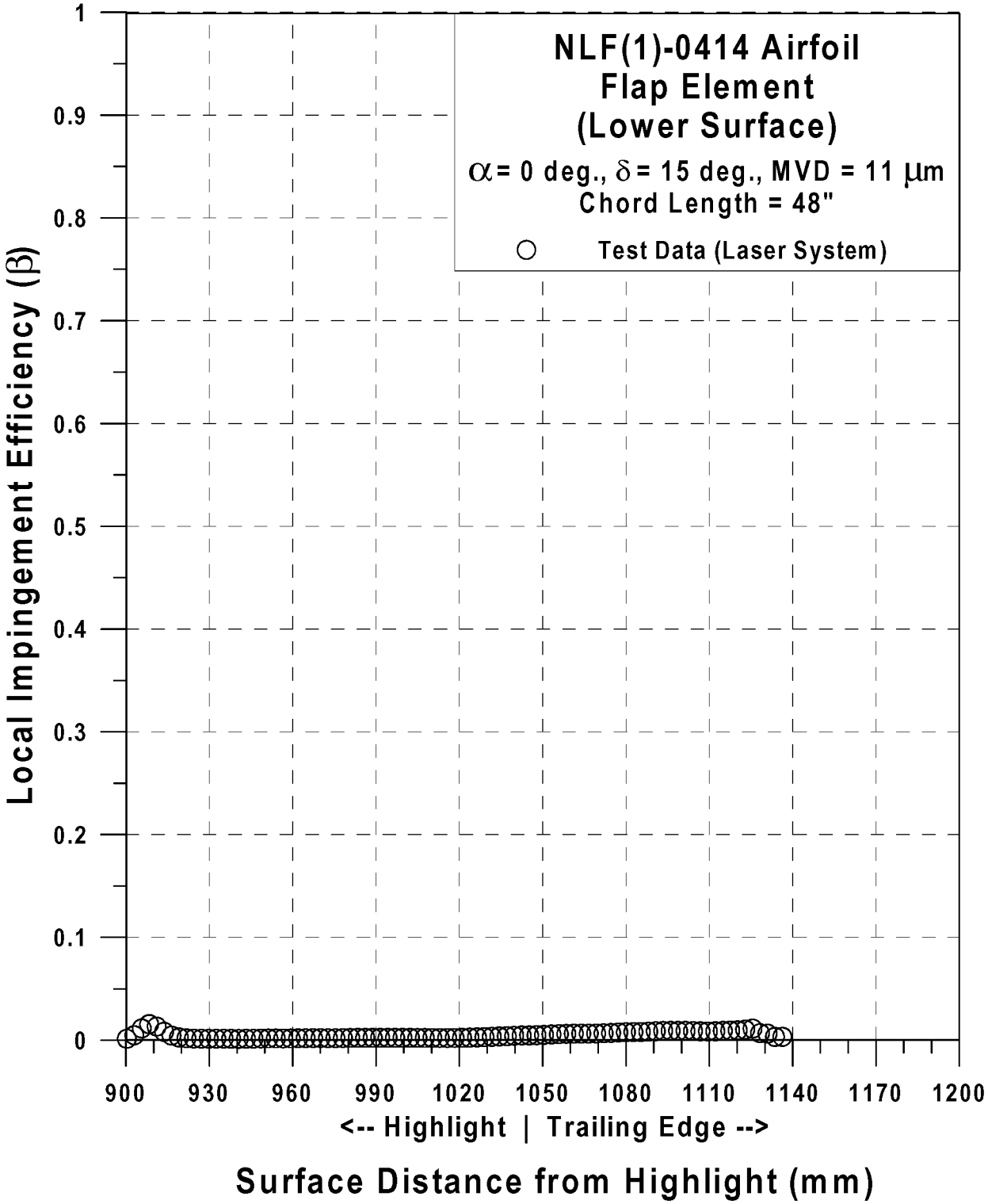

Fig. 102k Impingement efficiency distribution for NLF(1)-0414 flap element; c =48-in, 25%-chord full-span flap, V_∞ = 176 mph, $\alpha=0^\circ$, $\delta=15^\circ$, MVD =11 μm (Continued).

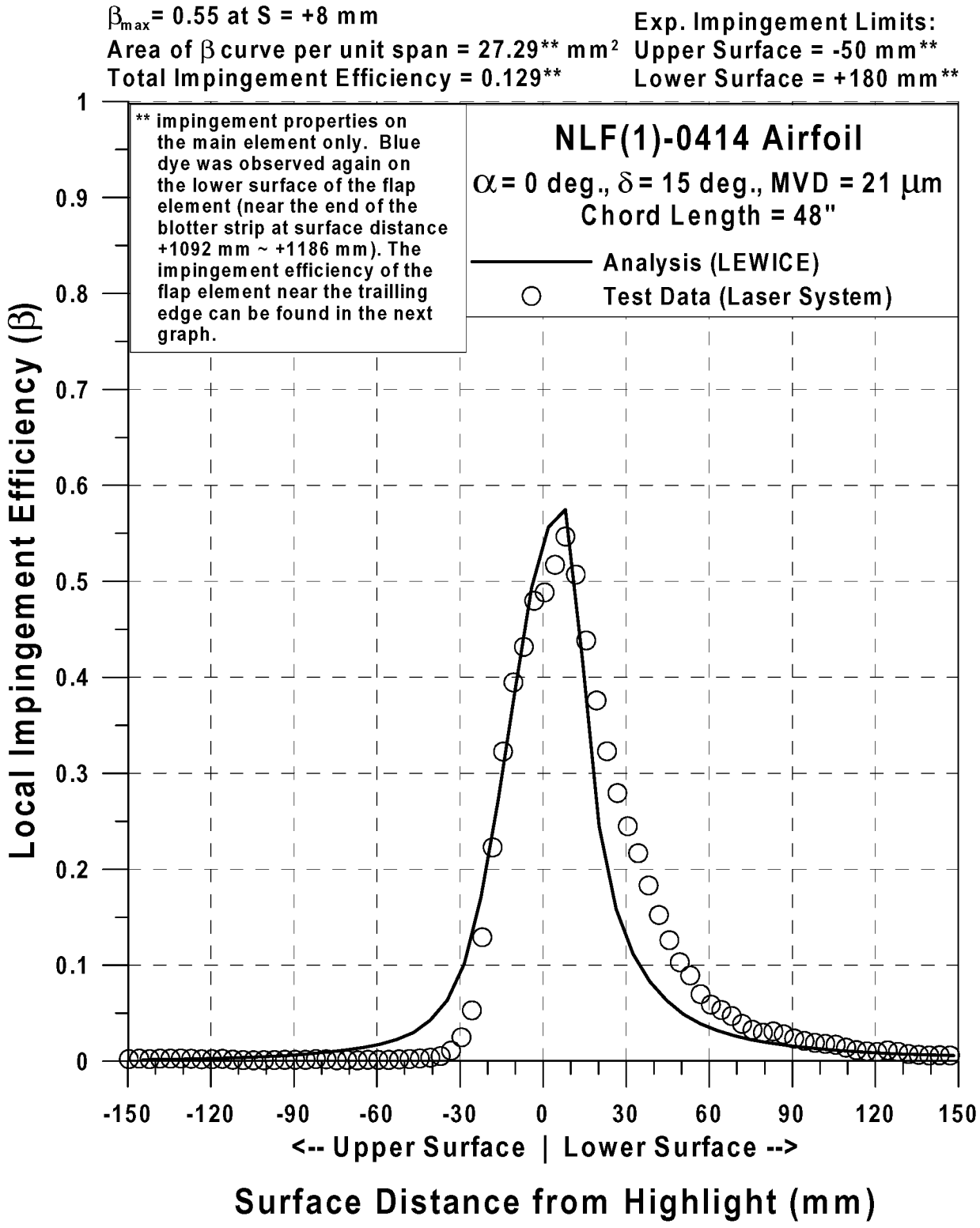

Fig. 102l Impingement efficiency distribution for NLF(1)-0414 airfoil; c =48-in, 25%-chord full-span flap, V_∞ = 176 mph, α=0°, δ=15°, MVD =21 μm (Continued).

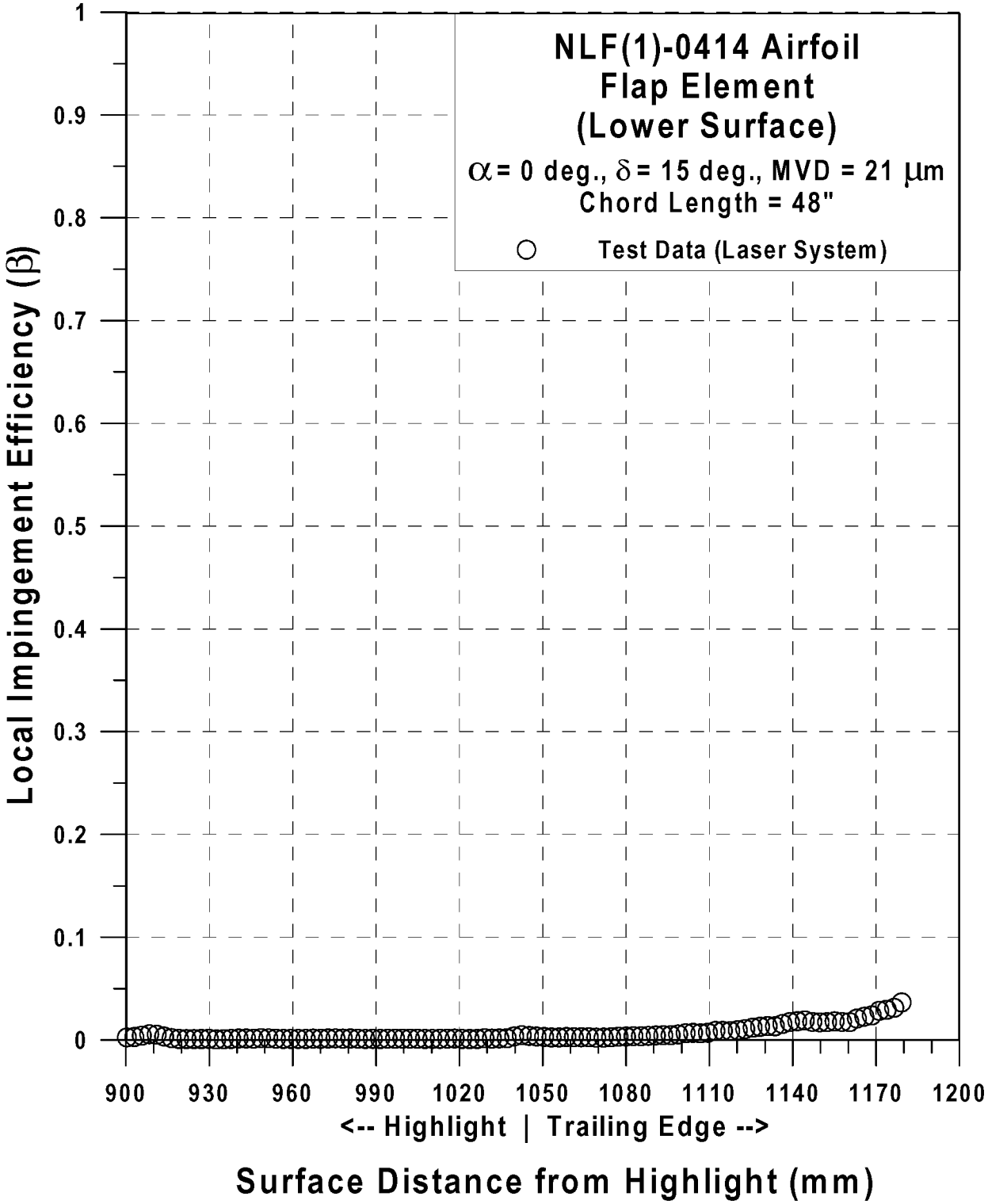

Fig. 102m Impingement efficiency distribution for NLF(1)-0414 flap element; c =48-in, 25%-chord full-span flap, V_∞ = 176 mph, $\alpha=0^\circ$, $\delta=15^\circ$, MVD =21 μm (Continued).

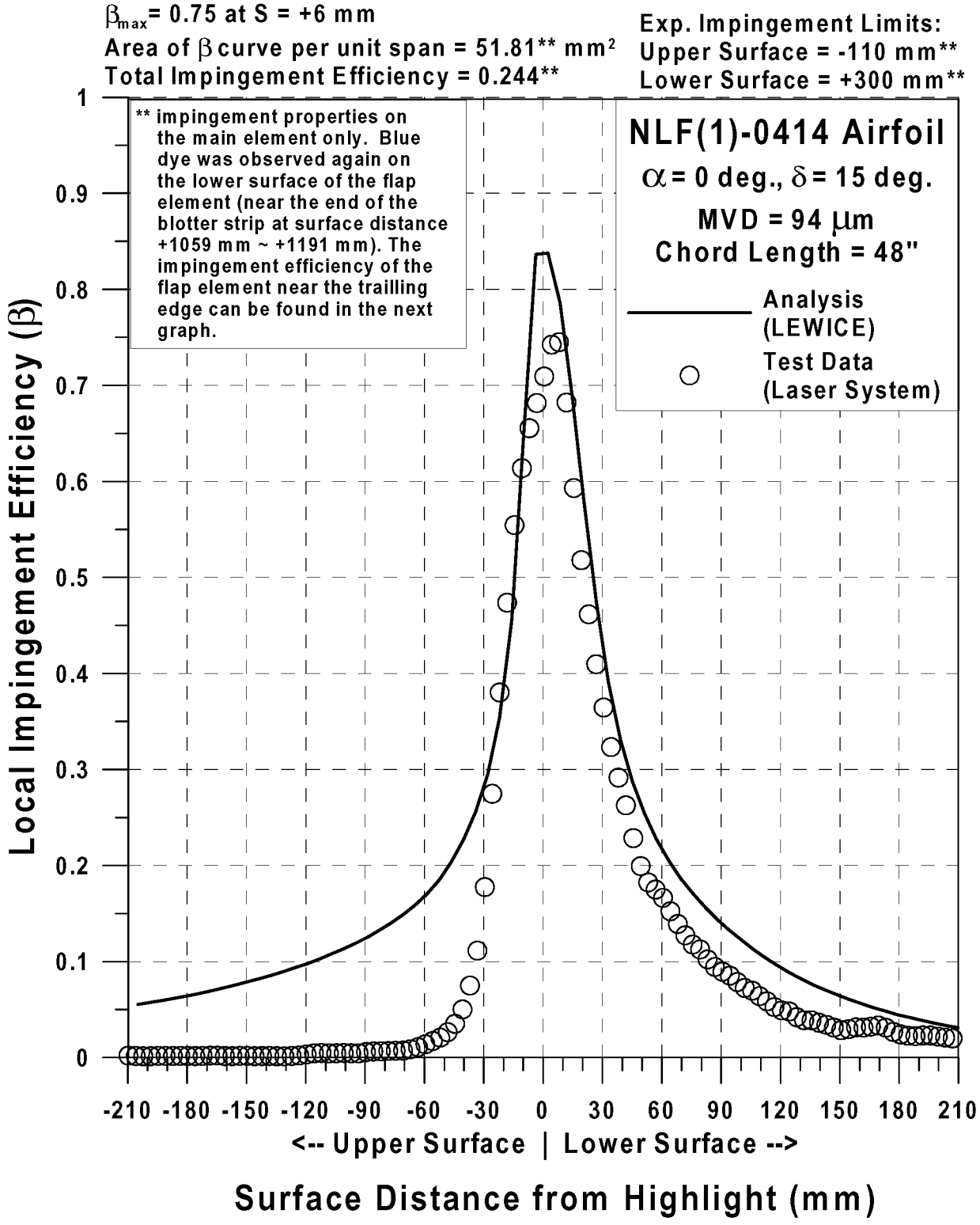

Fig. 102n Impingement efficiency distribution for NLF(1)-0414 airfoil; c =48-in, 25%-chord full-span flap, V_∞ = 176 mph, α=0°, δ=15°, MVD =94 μm (Continued).

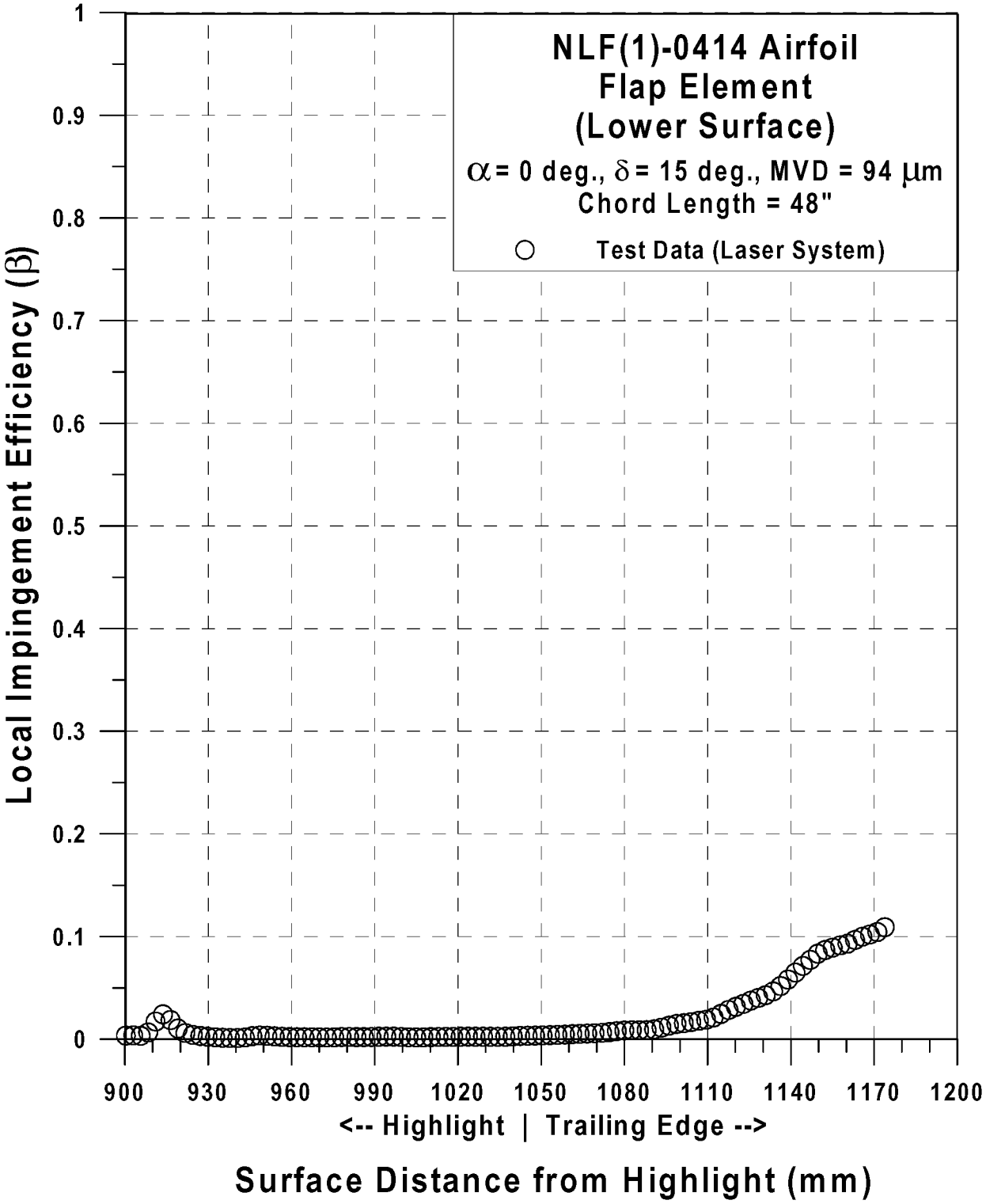

Fig. 102o Impingement efficiency distribution for NLF(1)-0414 flap element; c =48-in, 25%-chord full-span flap, V_∞ = 176 mph, $\alpha=0^\circ$, $\delta=15^\circ$, MVD =94 μm.

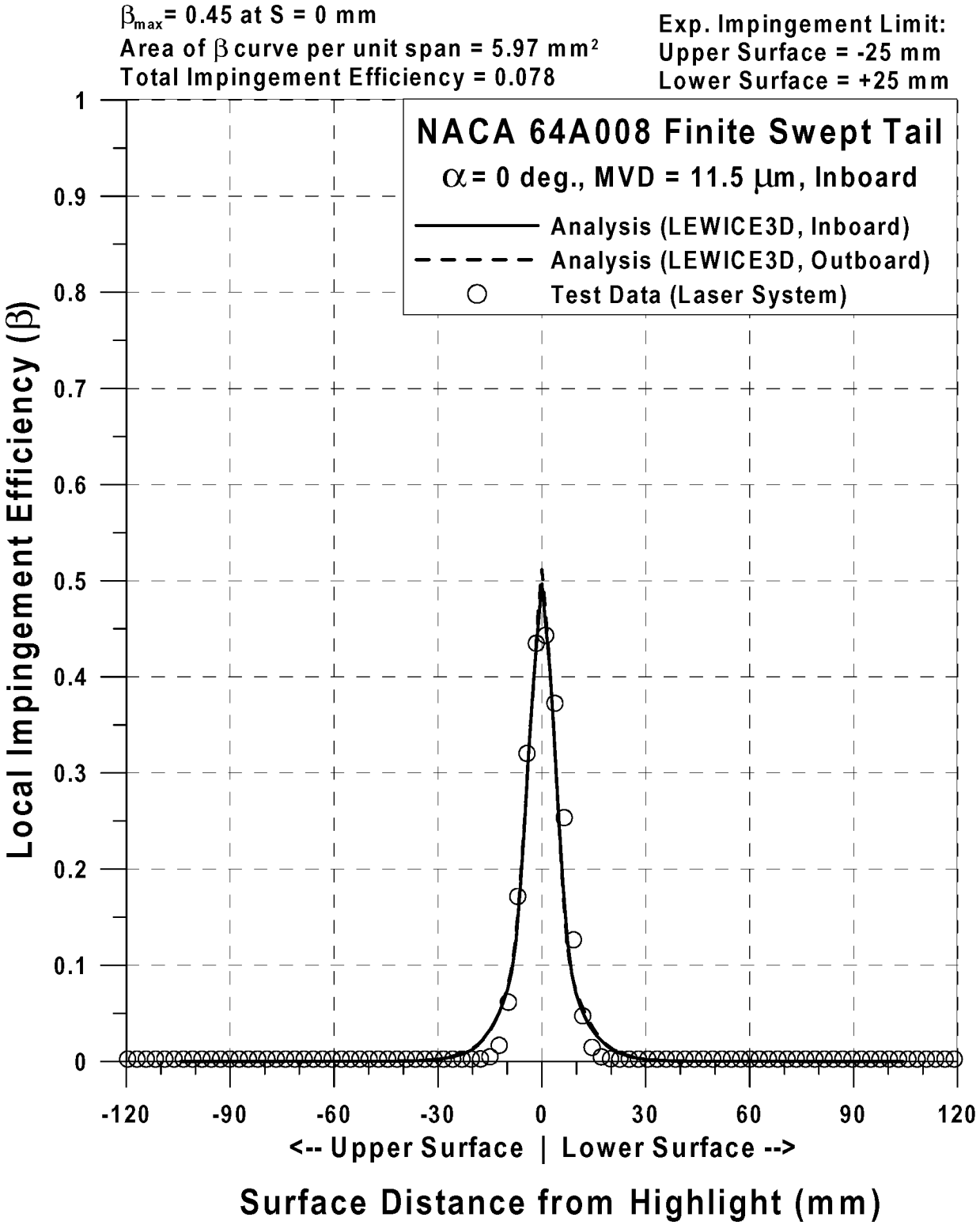

Fig. 103a Impingement efficiency distribution for NACA 64A008 finite swept tail; c = 45.75-in, V_∞ = 176 mph, α=0°, MVD =11.5 μm (Continued).

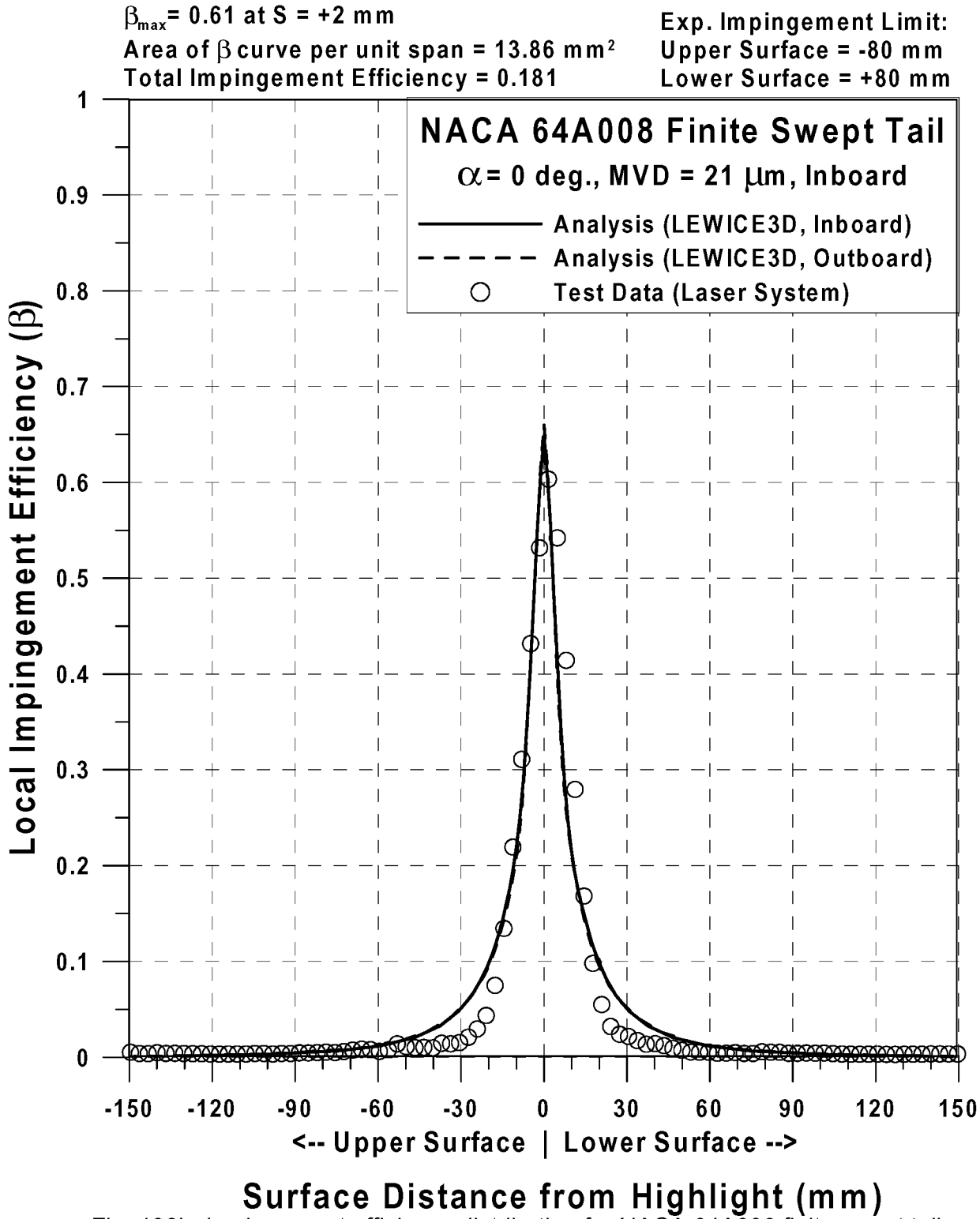

Fig. 103b Impingement efficiency distribution for NACA 64A008 finite swept tail; c = 45.75-in, V_∞ = 176 mph, α=0°, MVD =21 μm (Continued).

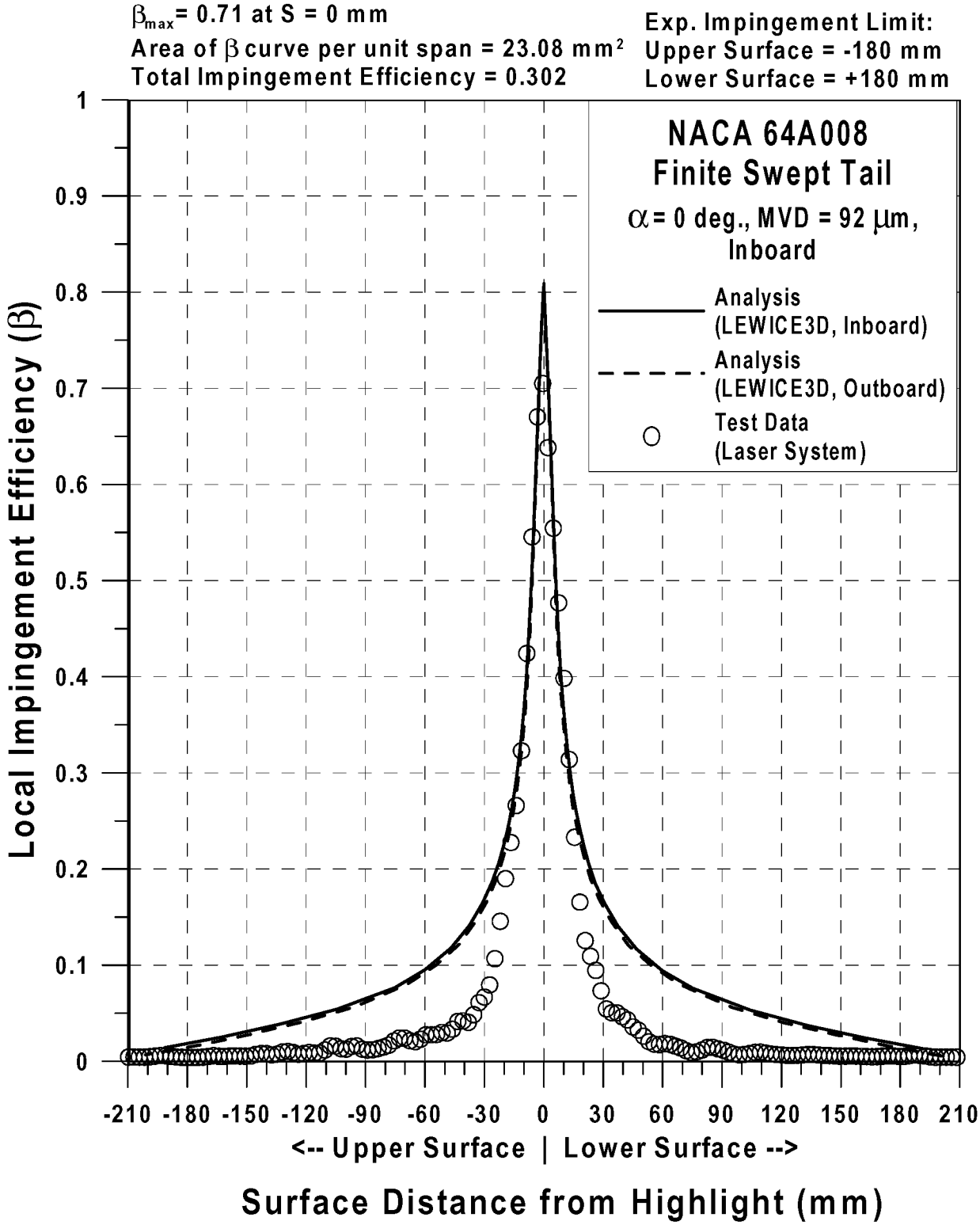

Fig. 103c Impingement efficiency distribution for NACA 64A008 finite swept tail; c = 45.75-in, V_∞ = 176 mph, α=0°, MVD =92 μm (Continued).

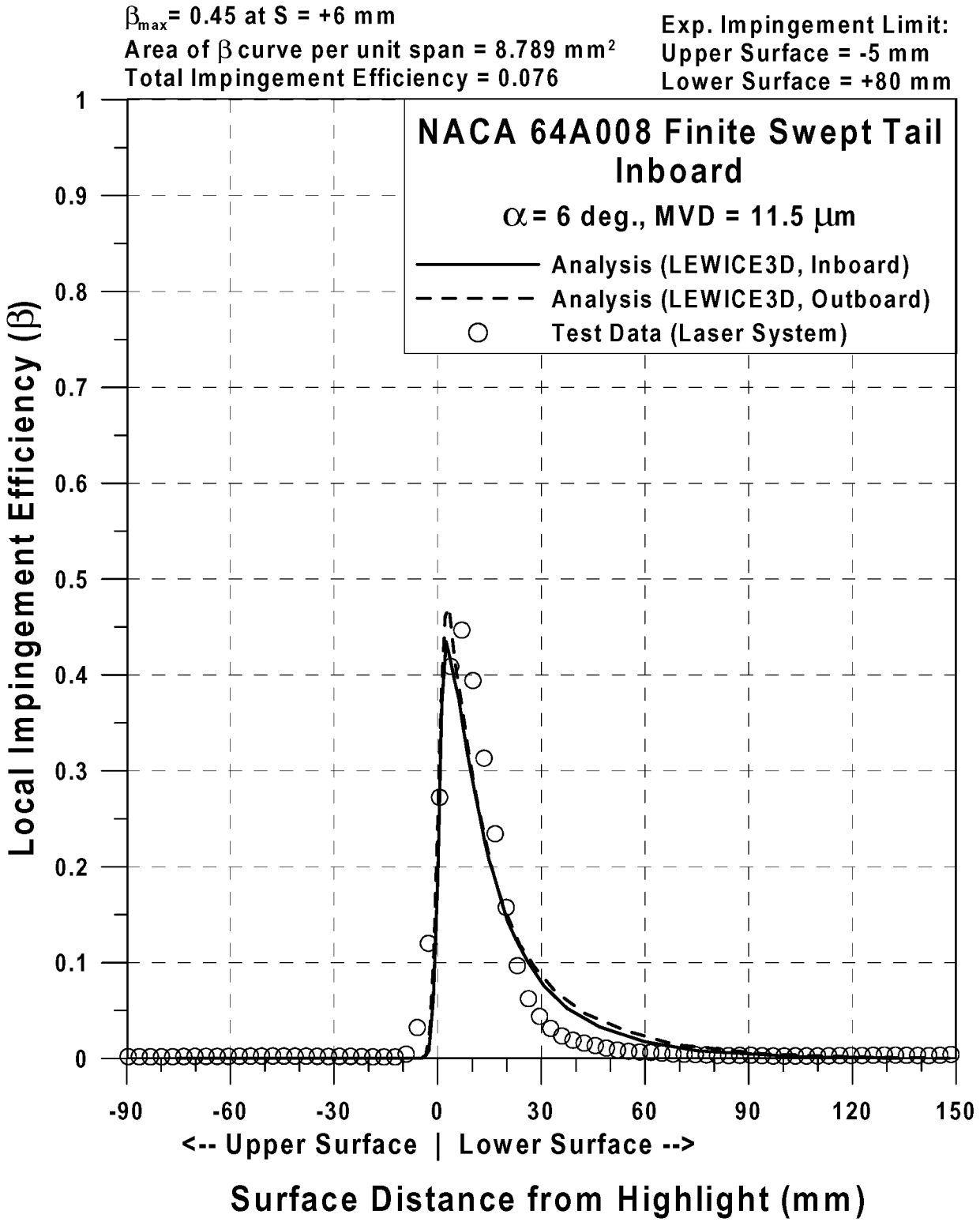

Fig. 103d Impingement efficiency distribution for NACA 64A008 finite swept tail; c = 45.75-in, V_∞ = 176 mph, α=6°, MVD =11.5 μm (Continued).

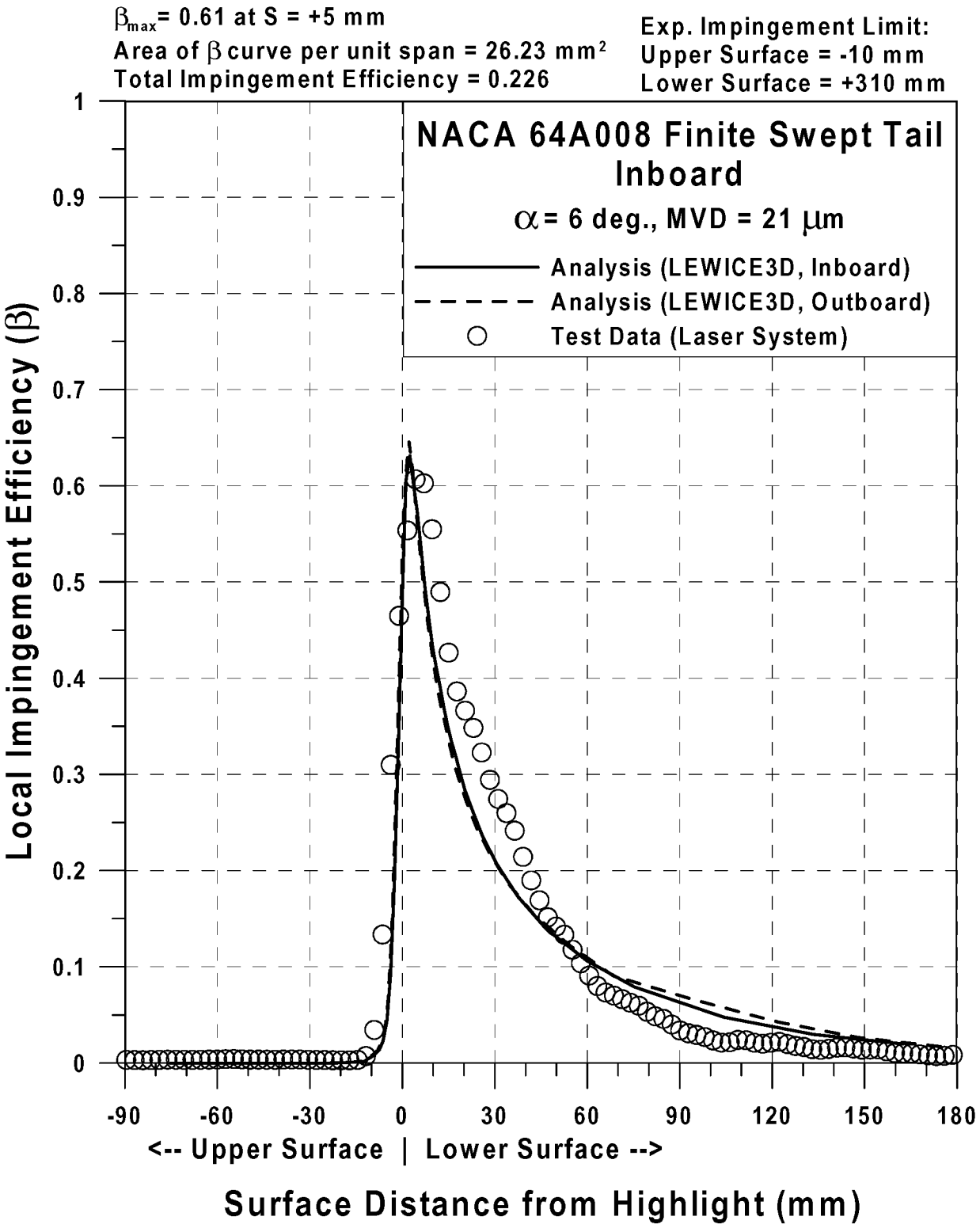

Fig. 103e Impingement efficiency distribution for NACA 64A008 finite swept tail; c = 45.75-in, V_∞ = 176 mph, α=6°, MVD =21 μm (Continued).

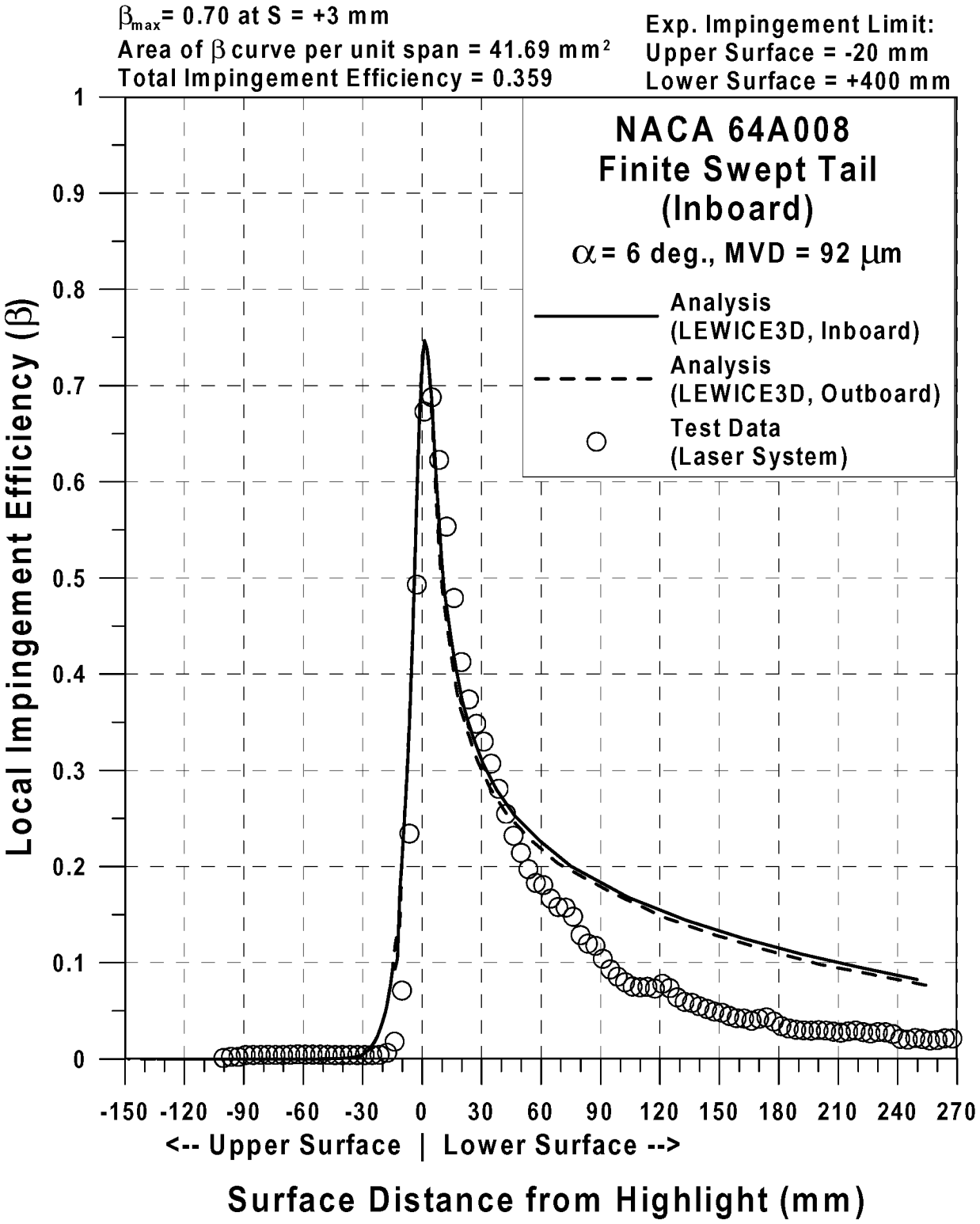

Fig. 103f Impingement efficiency distribution for NACA 64A008 finite swept tail; c = 45.75-in, V_∞ = 176 mph, α=6°, MVD =92 μm.

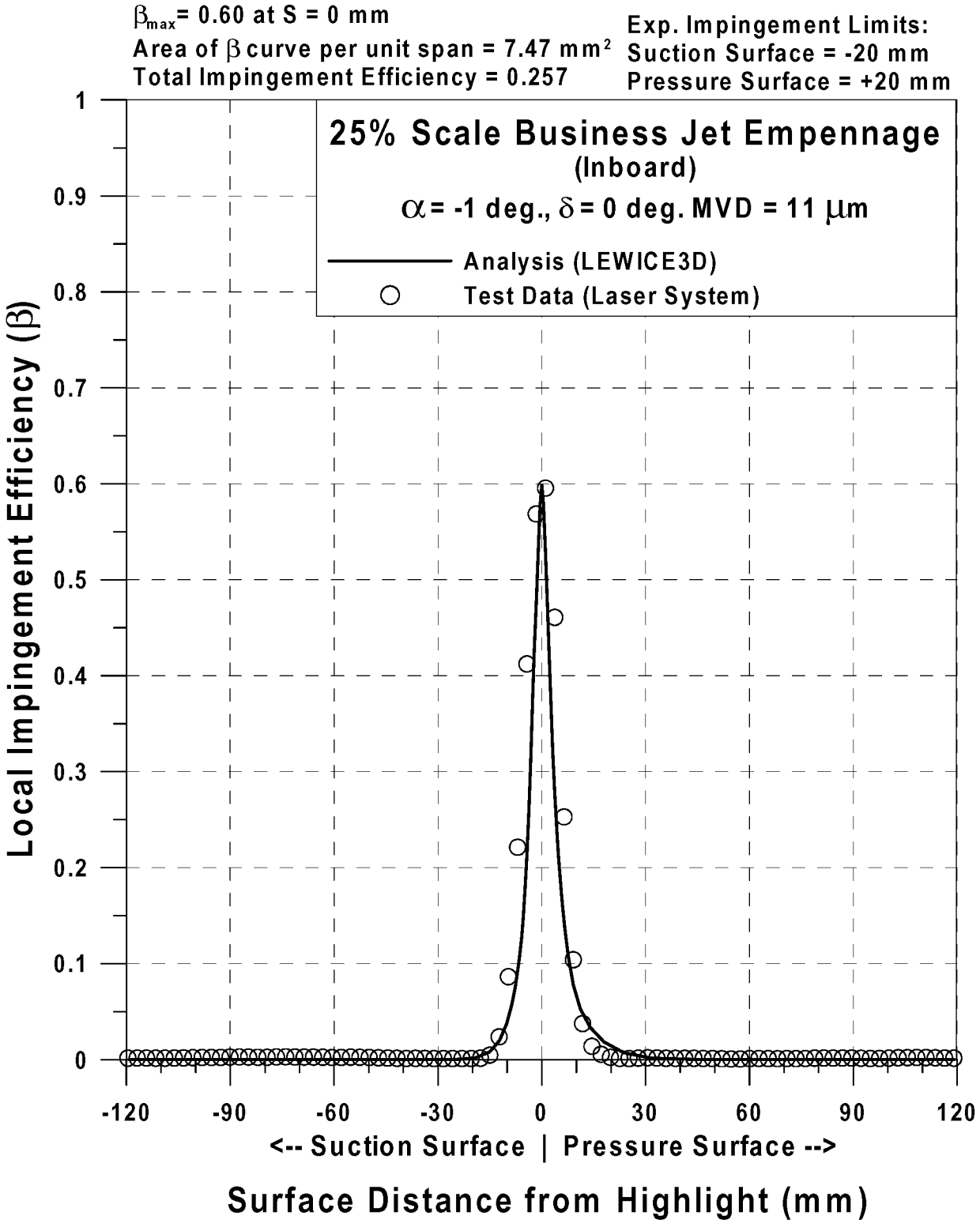

Fig. 104a Impingement efficiency distribution for 25%-scale Business Jet Empennage; Inboard, V_∞ = 176 mph, α= -1°, δ=0°, MVD =11 μm (Continued).

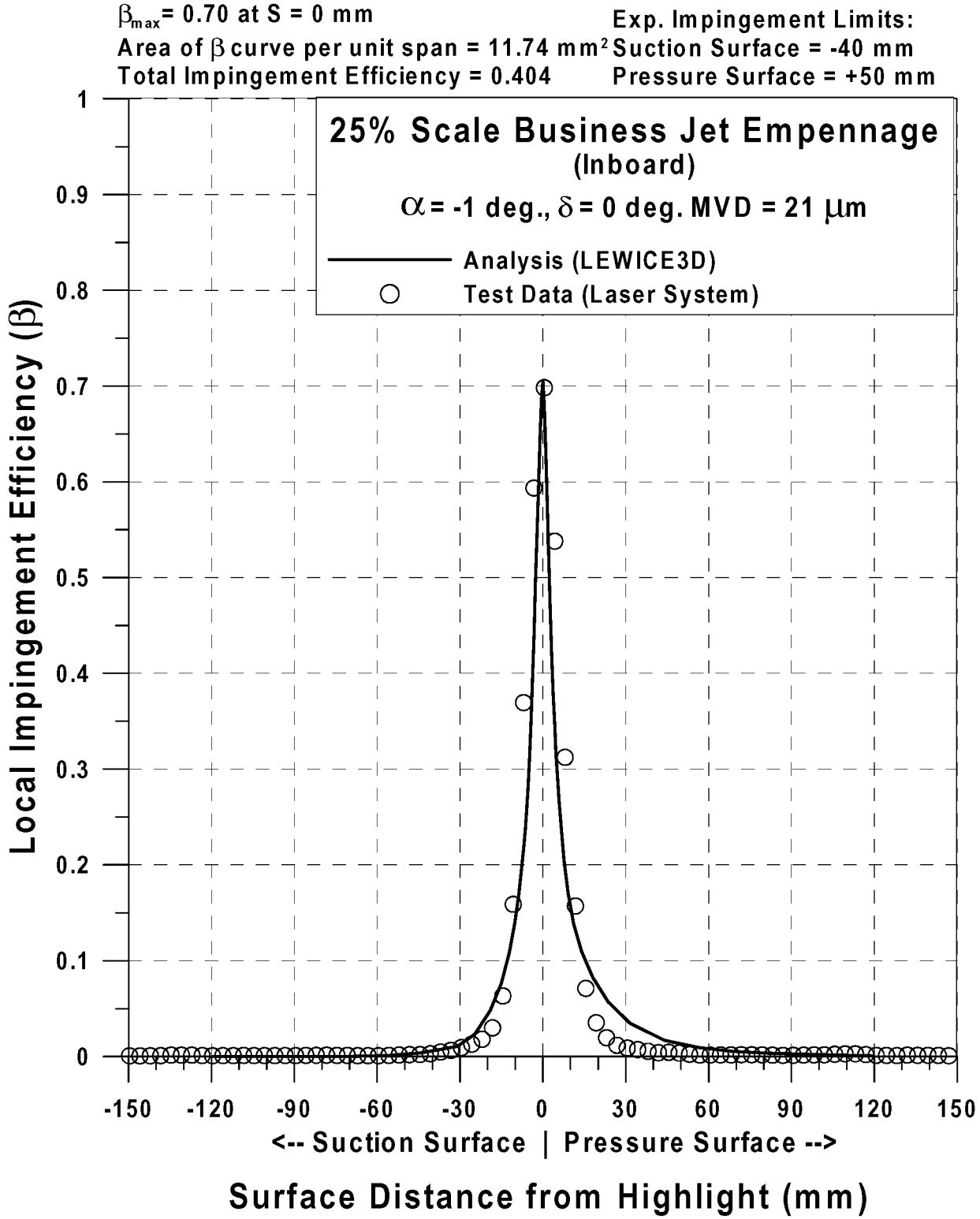

Fig. 104b Impingement efficiency distribution for 25%-scale Business Jet Empennage; Inboard, V_∞ = 176 mph, α= -1°, δ=0°, MVD =21 μm (Continued).

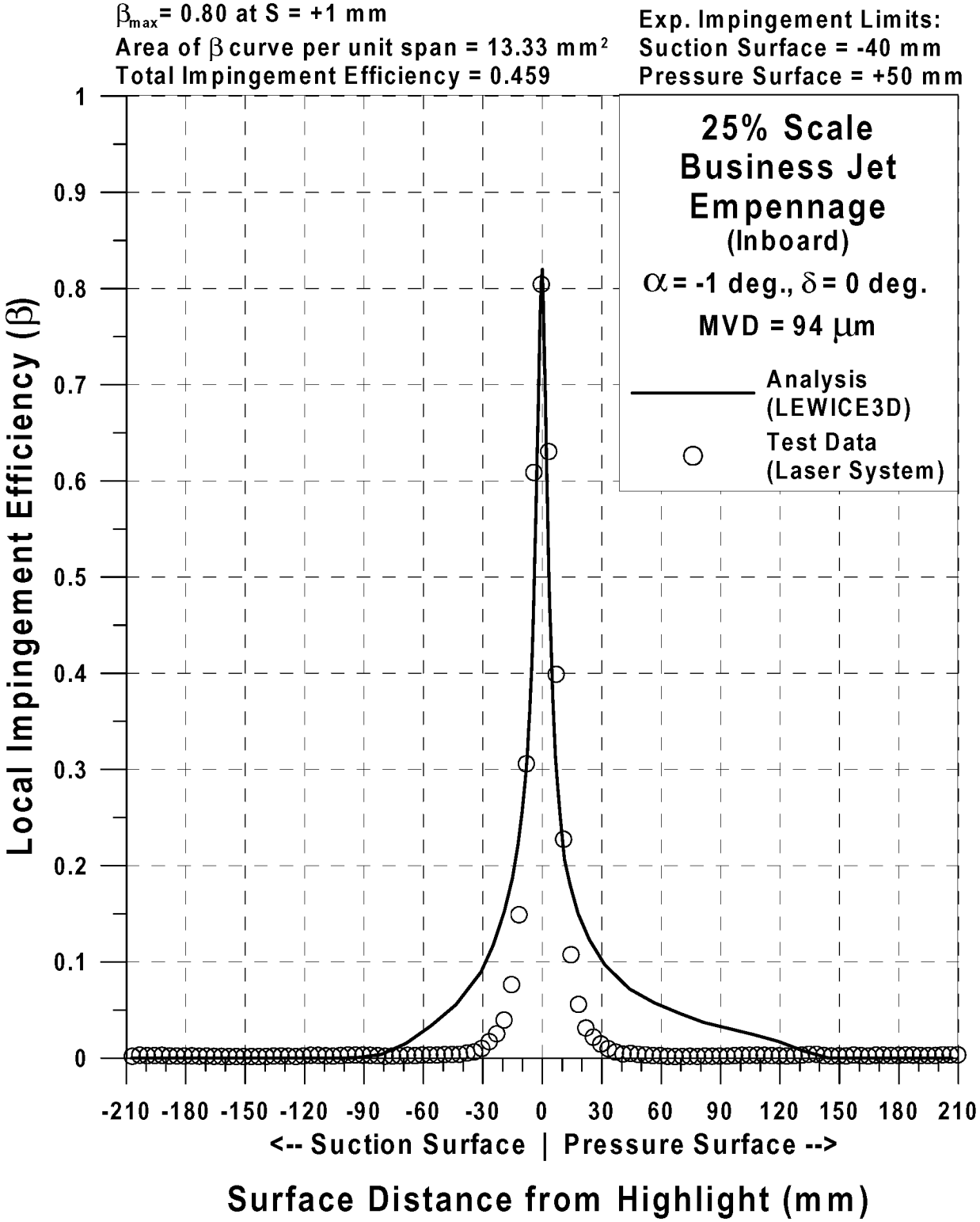

Fig. 104c Impingement efficiency distribution for 25%-scale Business Jet Empennage; Inboard, V_∞ = 176 mph, α= -1°, δ=0°, MVD =94 μm (Continued).

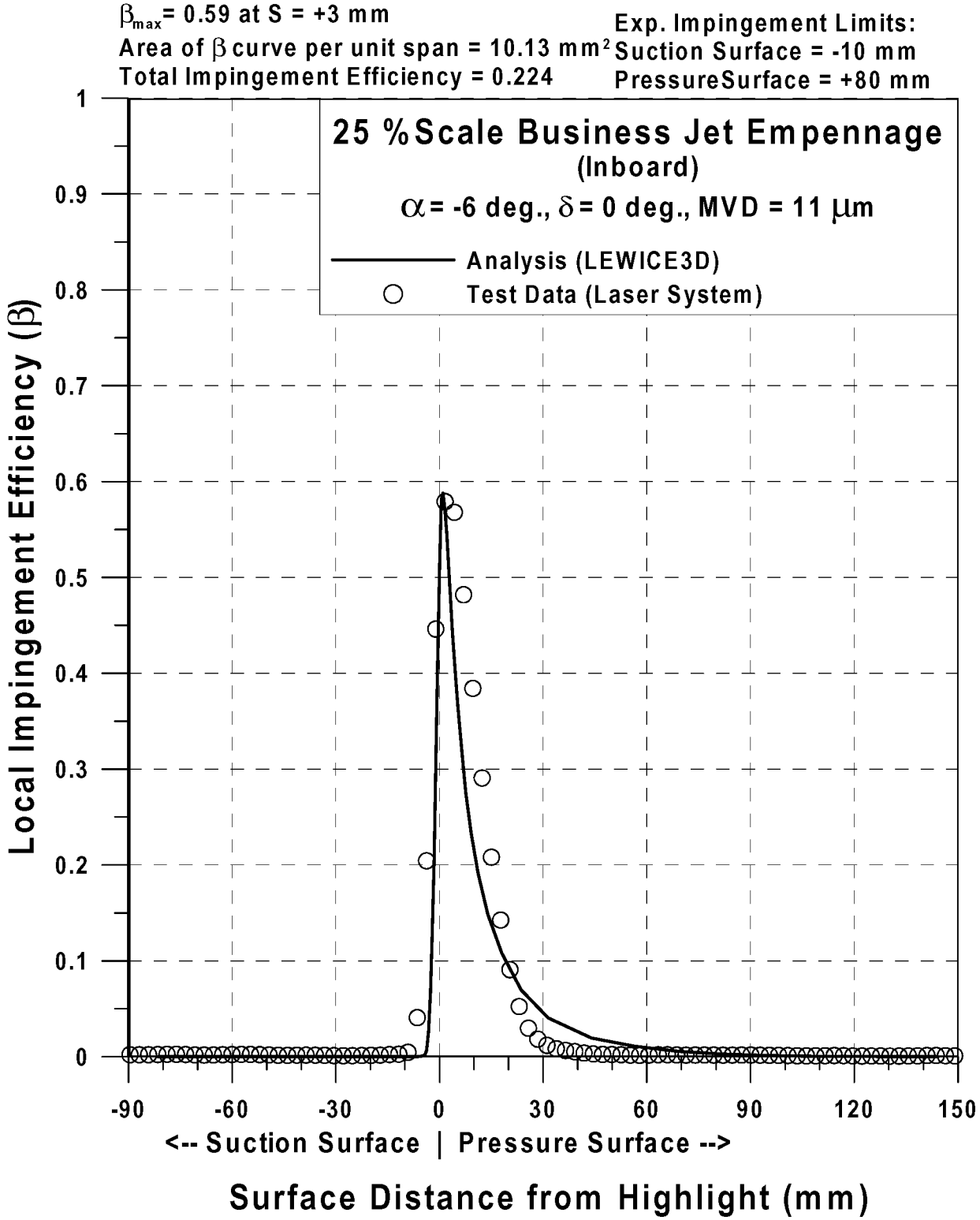

Fig. 104d Impingement efficiency distribution for 25%-scale Business Jet Empennage; Inboard, V_∞ = 176 mph, α= -6°, δ=0°, MVD =11 μm (Continued).

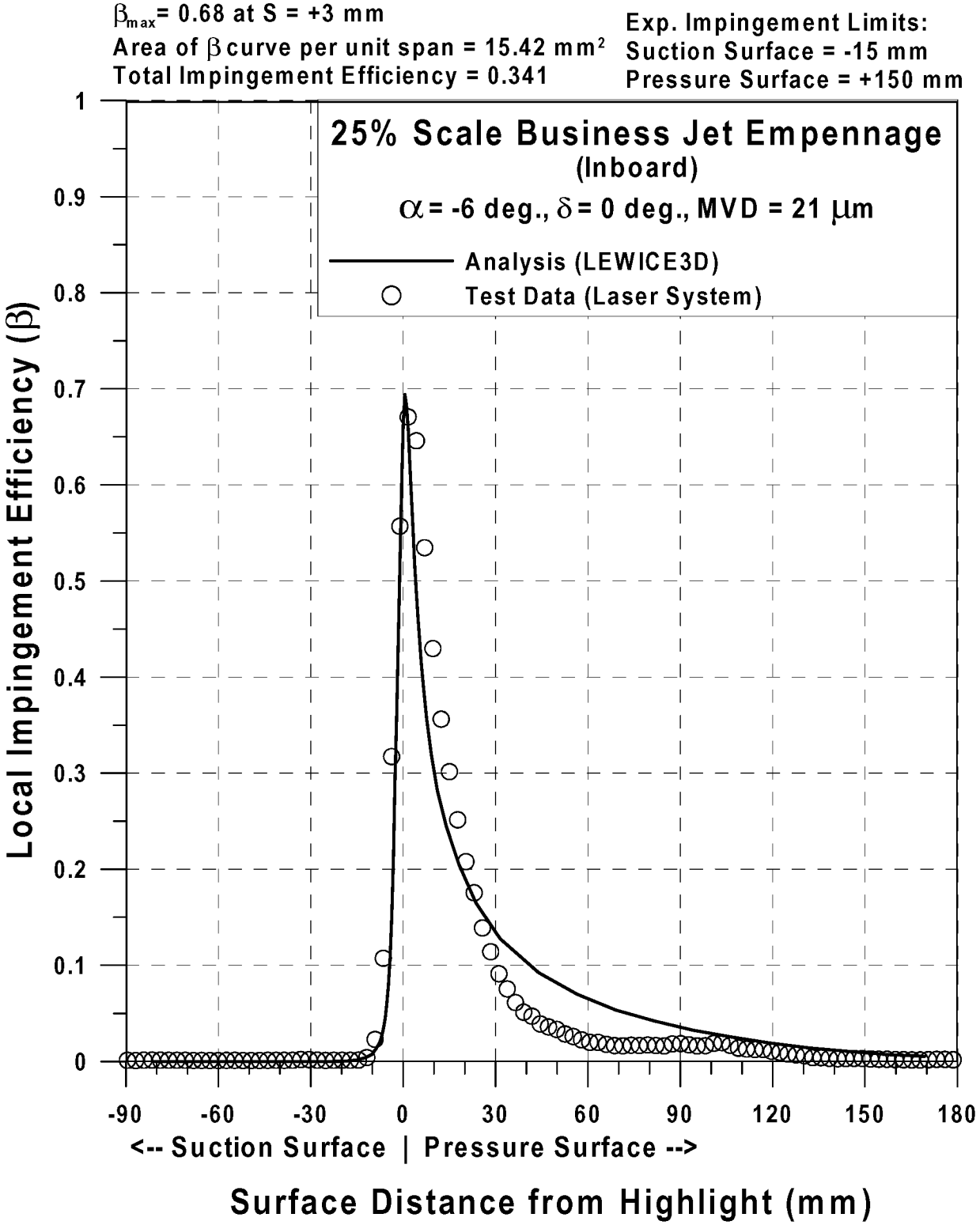

Fig. 104e Impingement efficiency distribution for 25%-scale Business Jet Empennage; Inboard, V_∞ = 176 mph, α= -6°, δ=0°, MVD =21 μm (Continued).

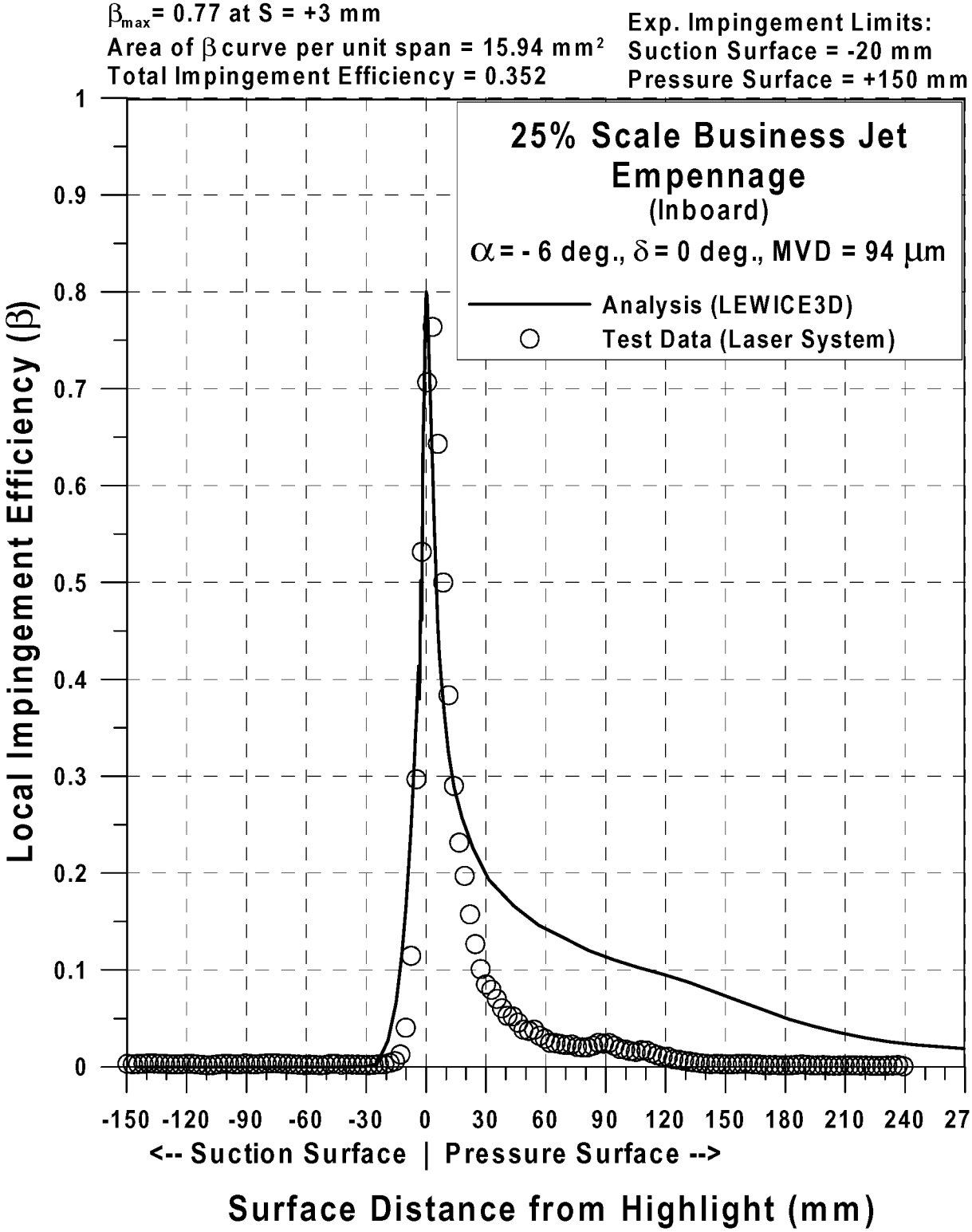

Fig. 104f Impingement efficiency distribution for 25%-scale Business Jet Empennage; Inboard, V_∞ = 176 mph, α= -6°, δ=0°, MVD =94 μm (Continued).

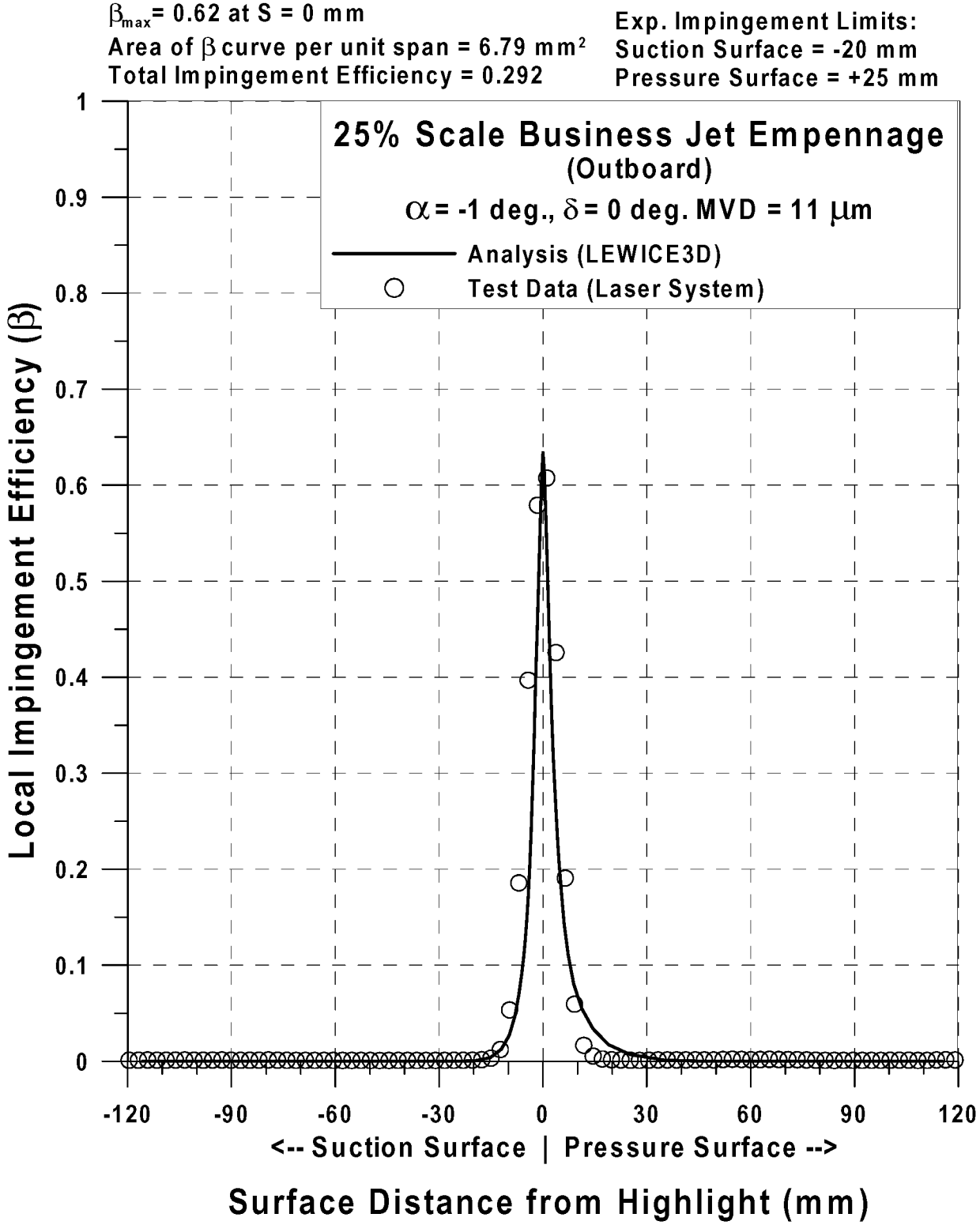

Fig. 104g Impingement efficiency distribution for 25%-scale Business Jet Empennage; Outboard, V_∞ = 176 mph, α= -1°, δ=0°, MVD =11 μm (Continued).

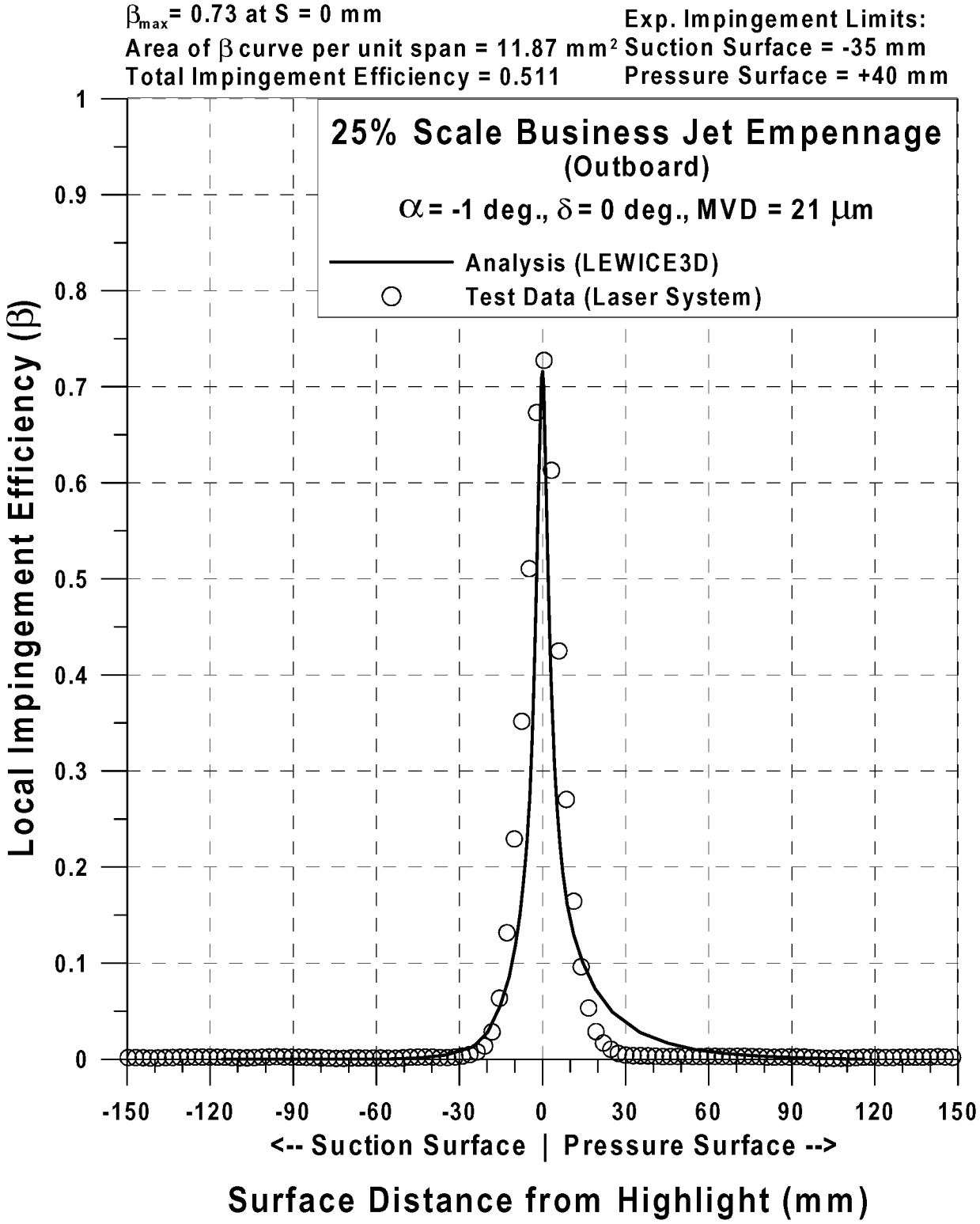

Fig. 104h Impingement efficiency distribution for 25%-scale Business Jet Empennage; Outboard, V_∞ = 176 mph, α= -1°, δ=0°, MVD =21 μm (Continued).

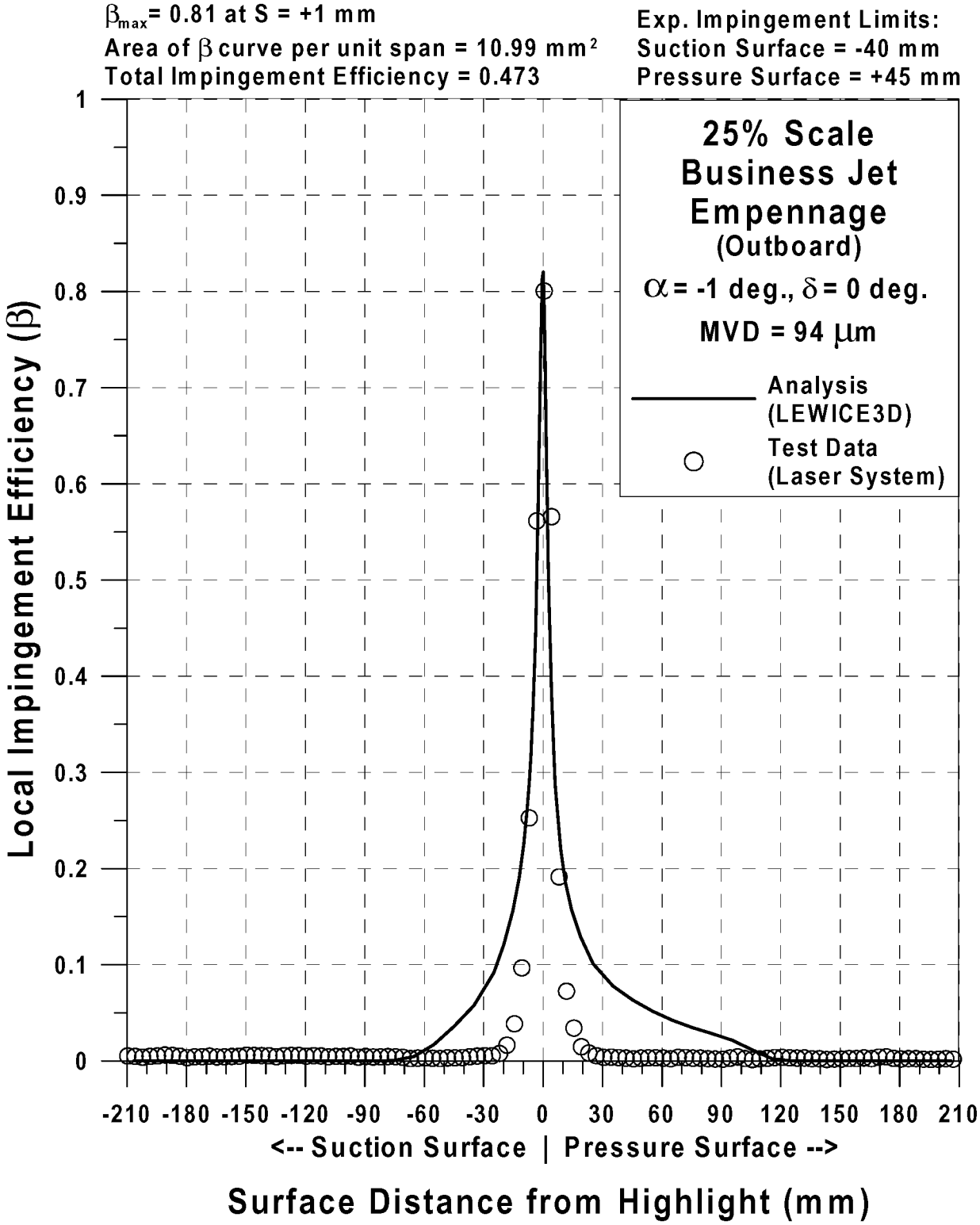

Fig. 104i Impingement efficiency distribution for 25%-scale Business Jet Empennage; Outboard, V_∞ = 176 mph, α= -1°, δ=0°, MVD =94 μm (Continued).

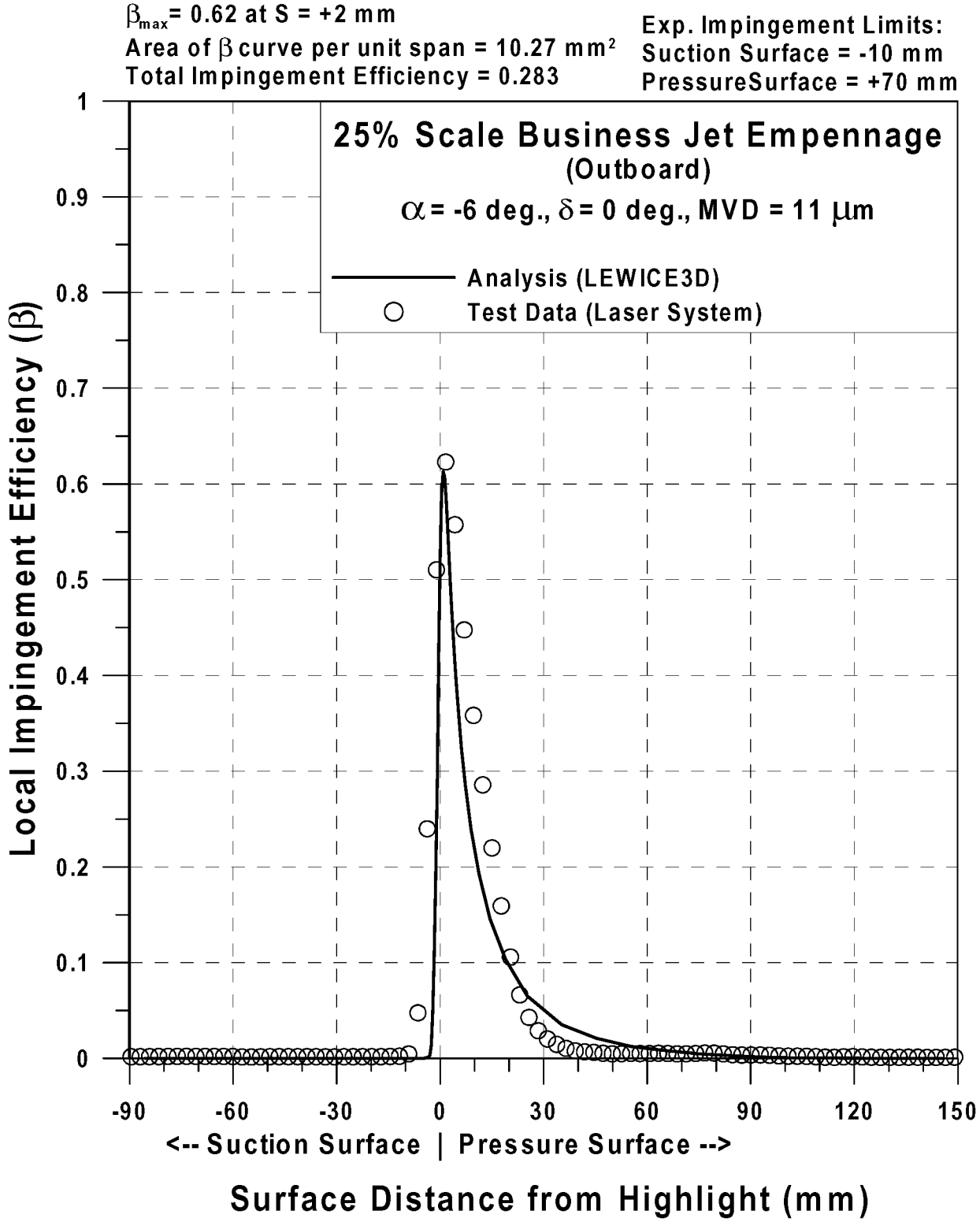

Fig. 104j Impingement efficiency distribution for 25%-scale Business Jet Empennage; Outboard, V_∞ = 176 mph, α=-6°, δ=0°, MVD =11 μm (Continued).

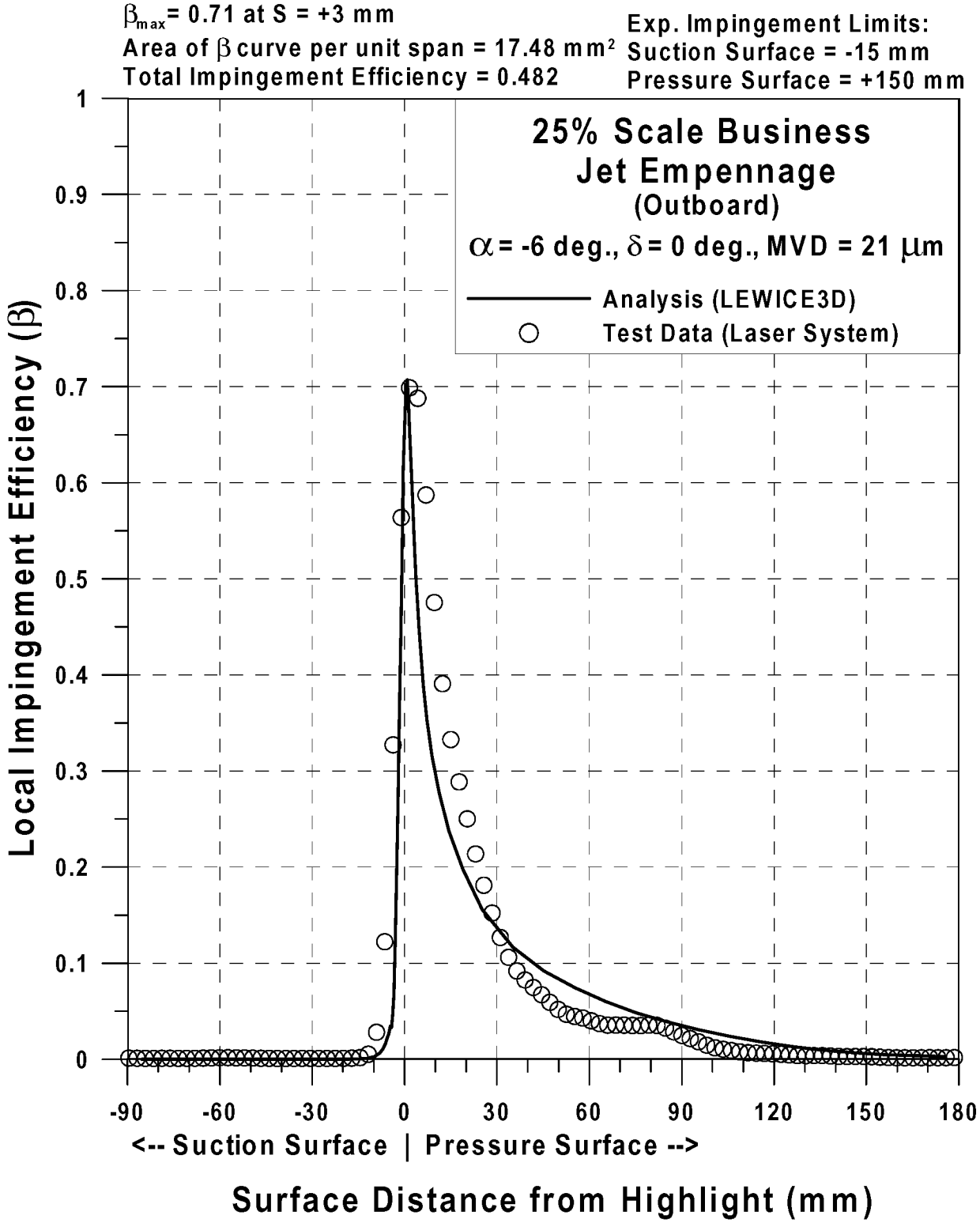

Fig. 104k Impingement efficiency distribution for 25%-scale Business Jet Empennage; Outboard, V_∞ = 176 mph, α=-6°, δ=0°, MVD =21 μm (Continued).

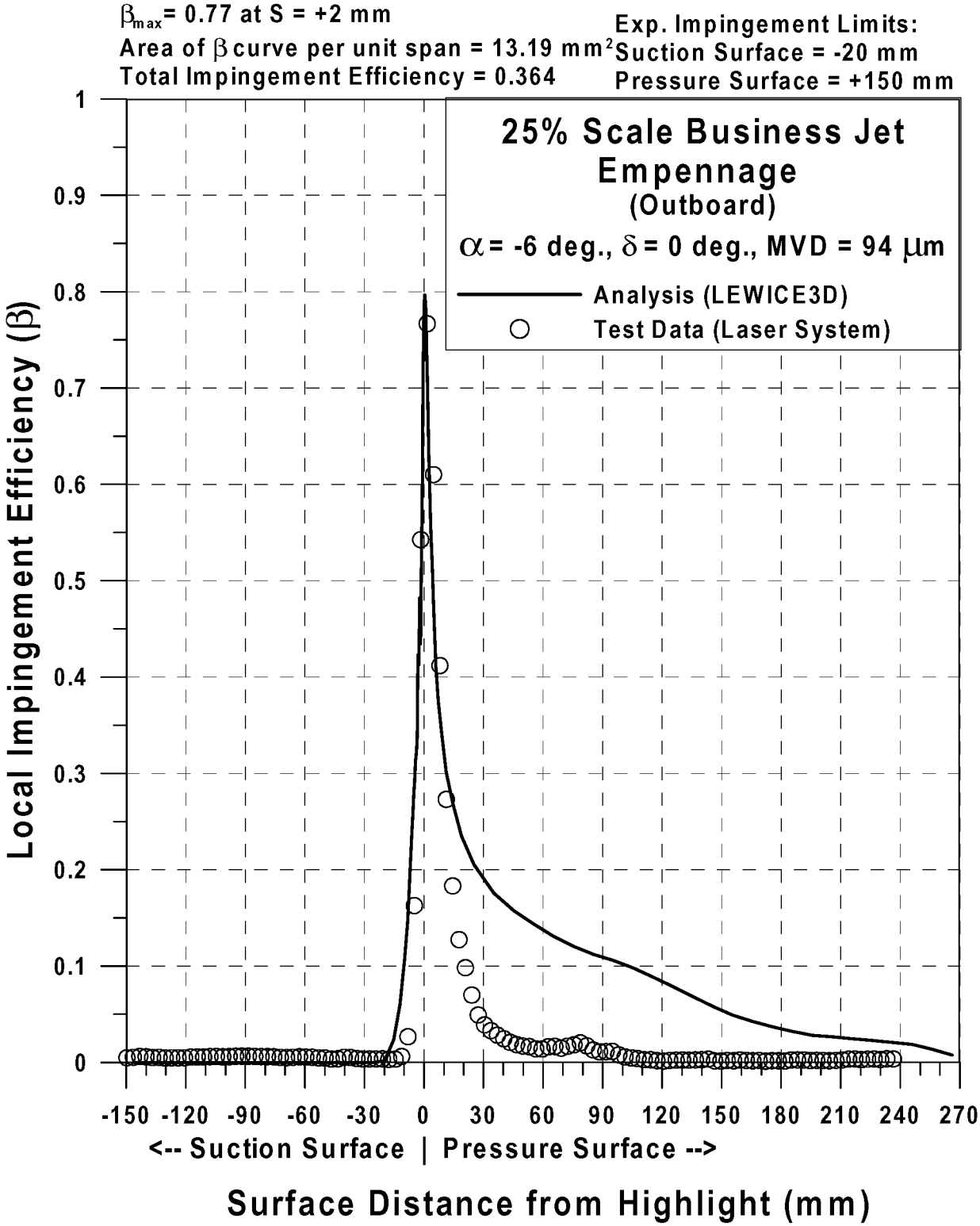

Fig. 104l Impingement efficiency distribution for 25%-scale Business Jet Empennage; Outboard, V_∞ = 176 mph, α=-6°, δ=0°, MVD =94 μm.

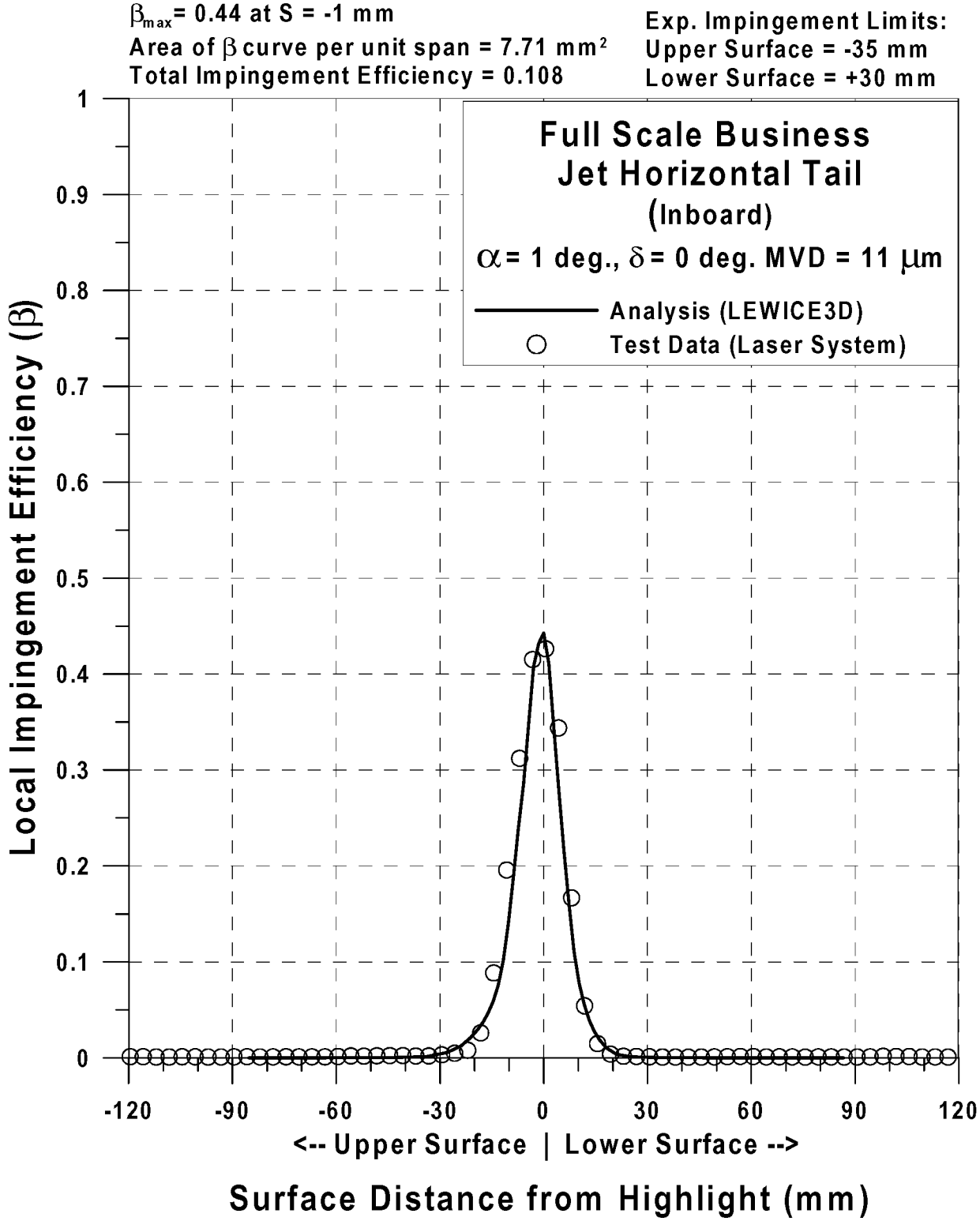

Fig. 105a Impingement efficiency distribution for full-scale Business Jet horizontal tail; Inboard, V_∞ = 176 mph, α=1°, δ=0°, MVD =11 μm (Continued).

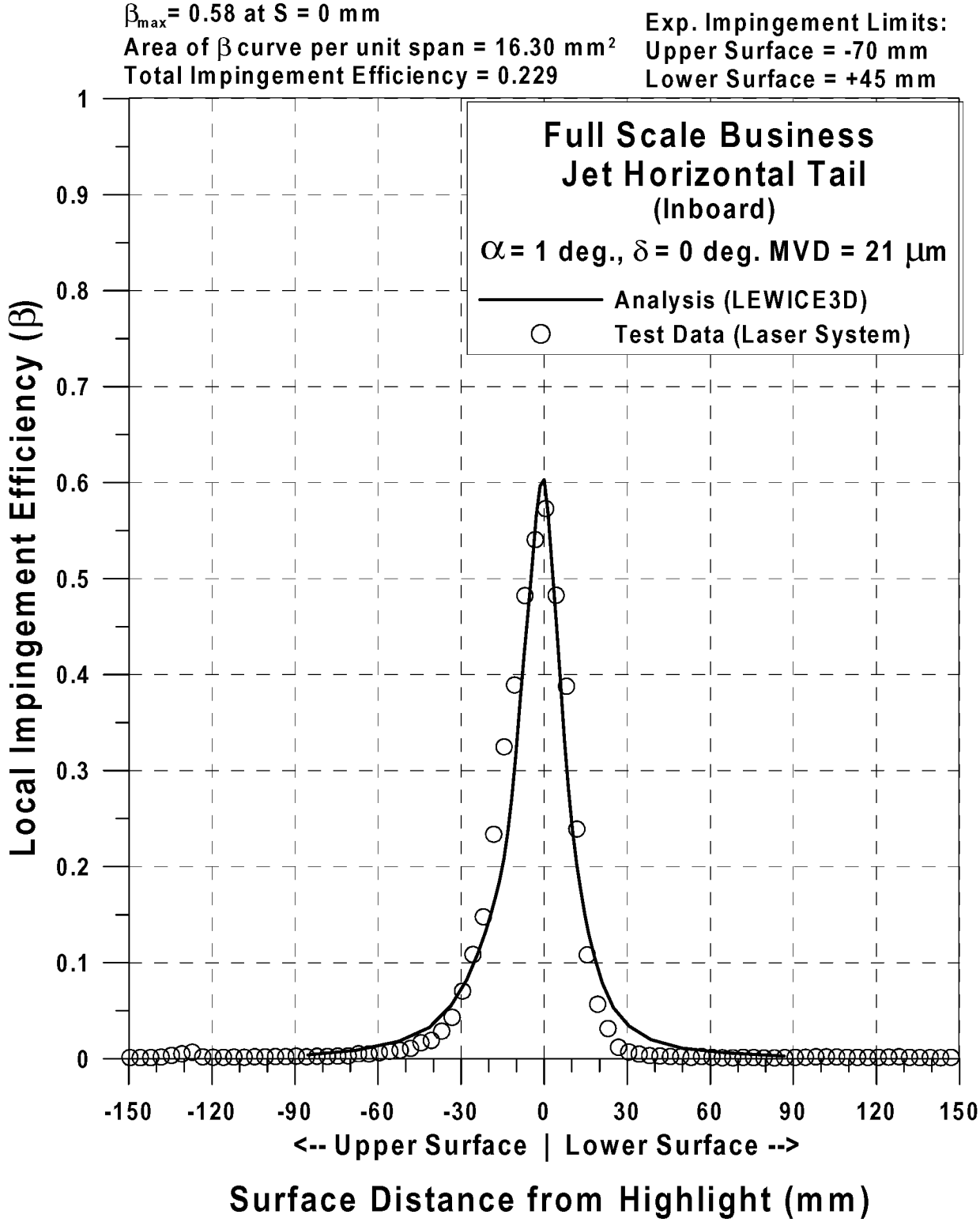

Fig. 105b Impingement efficiency distribution for full-scale Business Jet horizontal tail; Inboard, V_∞ = 176 mph, α=1°, δ=0°, MVD =21 μm (Continued).

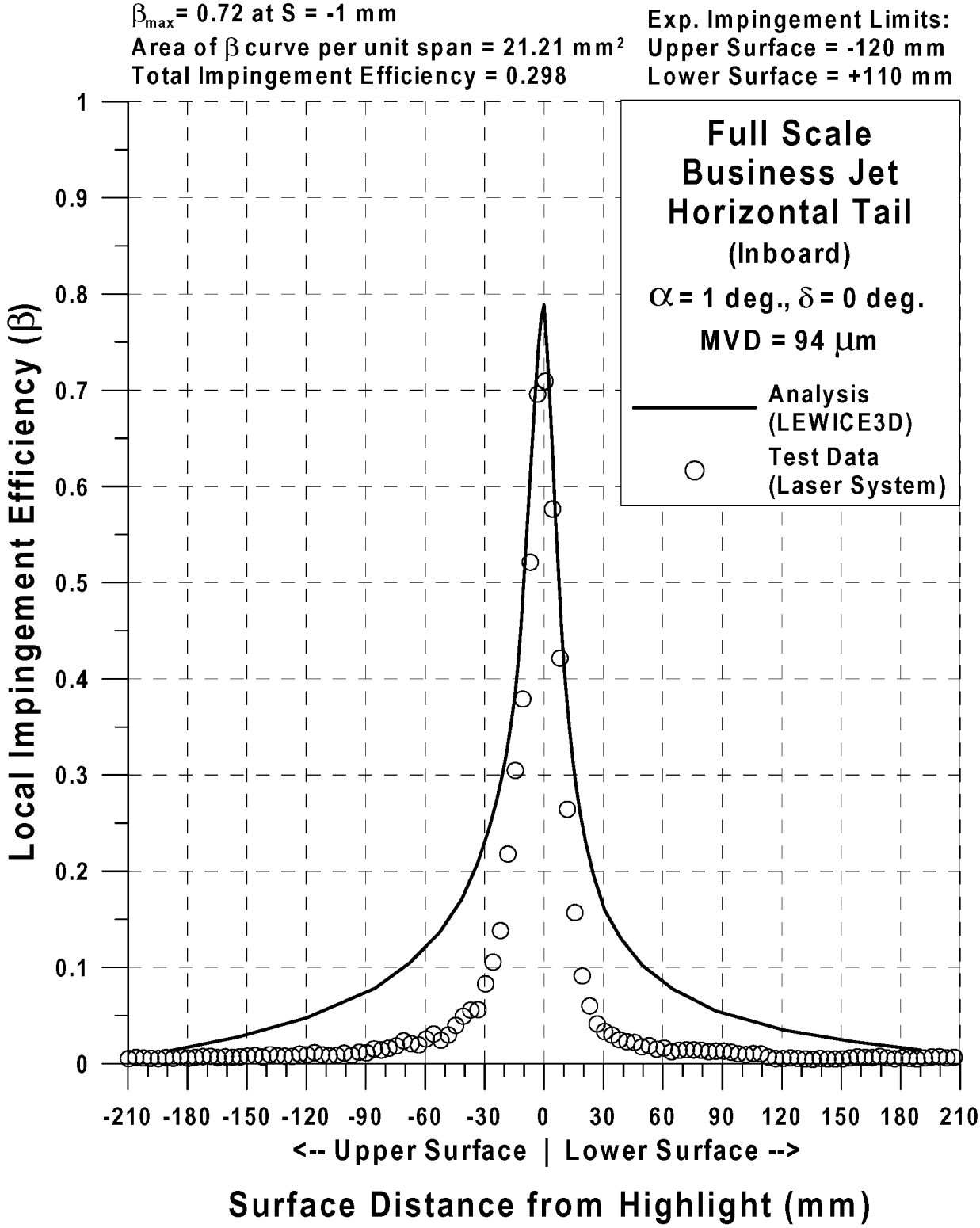

Fig. 105c Impingement efficiency distribution for full-scale Business Jet horizontal tail; Inboard, V_∞ = 176 mph, α=1°, δ=0°, MVD =94 μm (Continued).

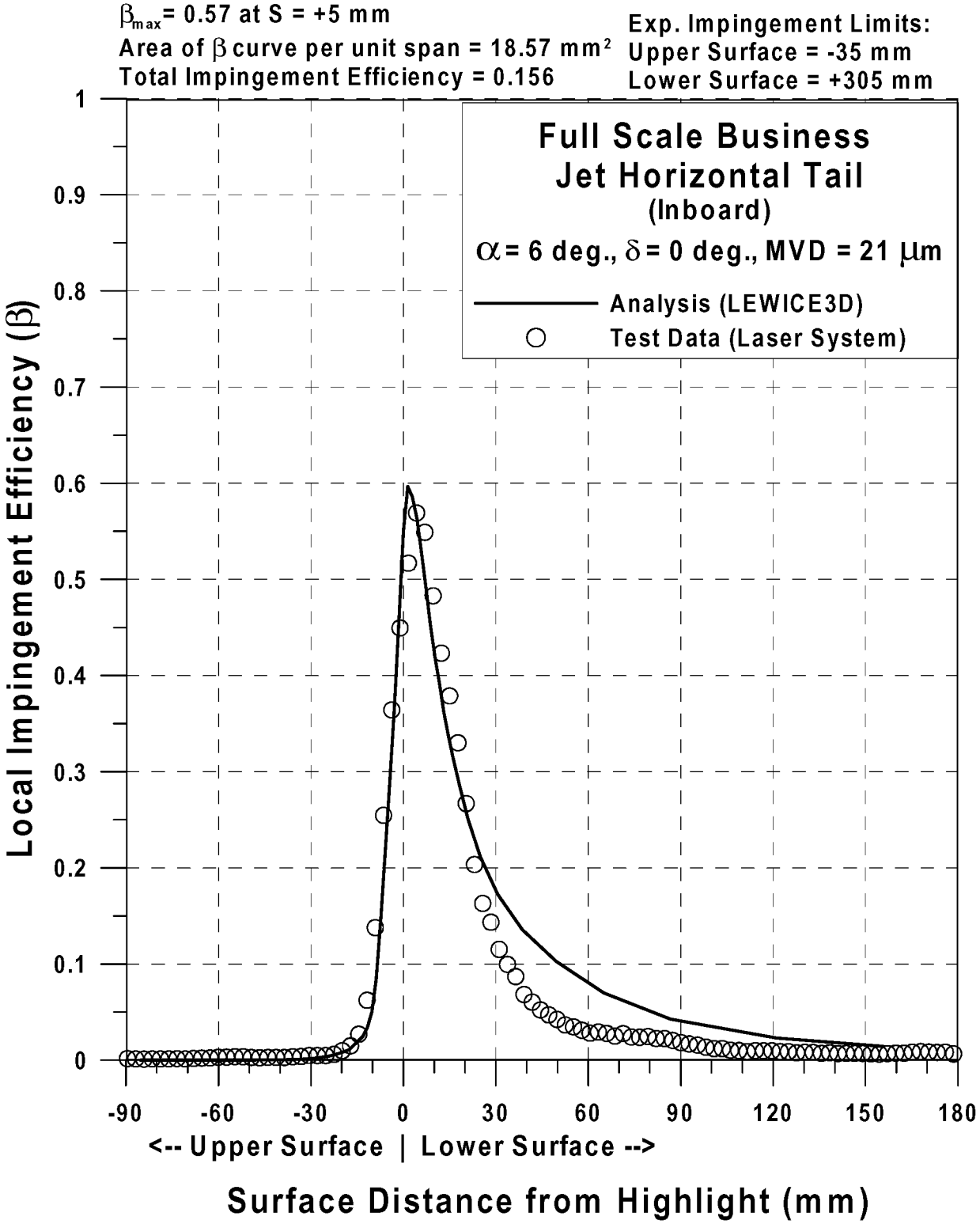

Fig. 105d Impingement efficiency distribution for full-scale Business Jet horizontal tail; Inboard, V_∞ = 176 mph, α=6°, δ=0°, MVD =21 μm (Continued).

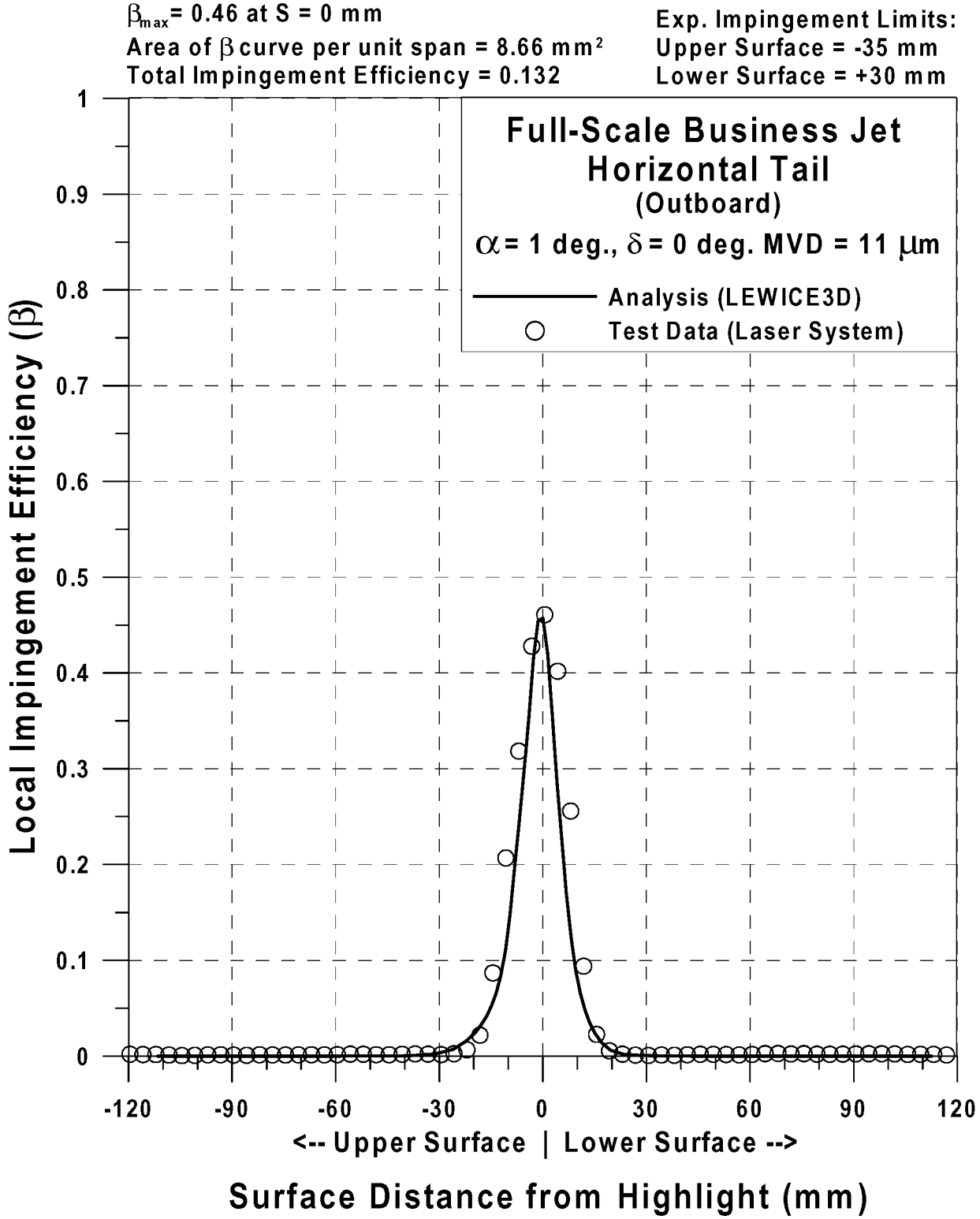

Fig. 105e Impingement efficiency distribution for full-scale Business Jet horizontal tail; Outboard, V_∞ = 176 mph, α=1°, δ=0°, MVD =11 μm (Continued).

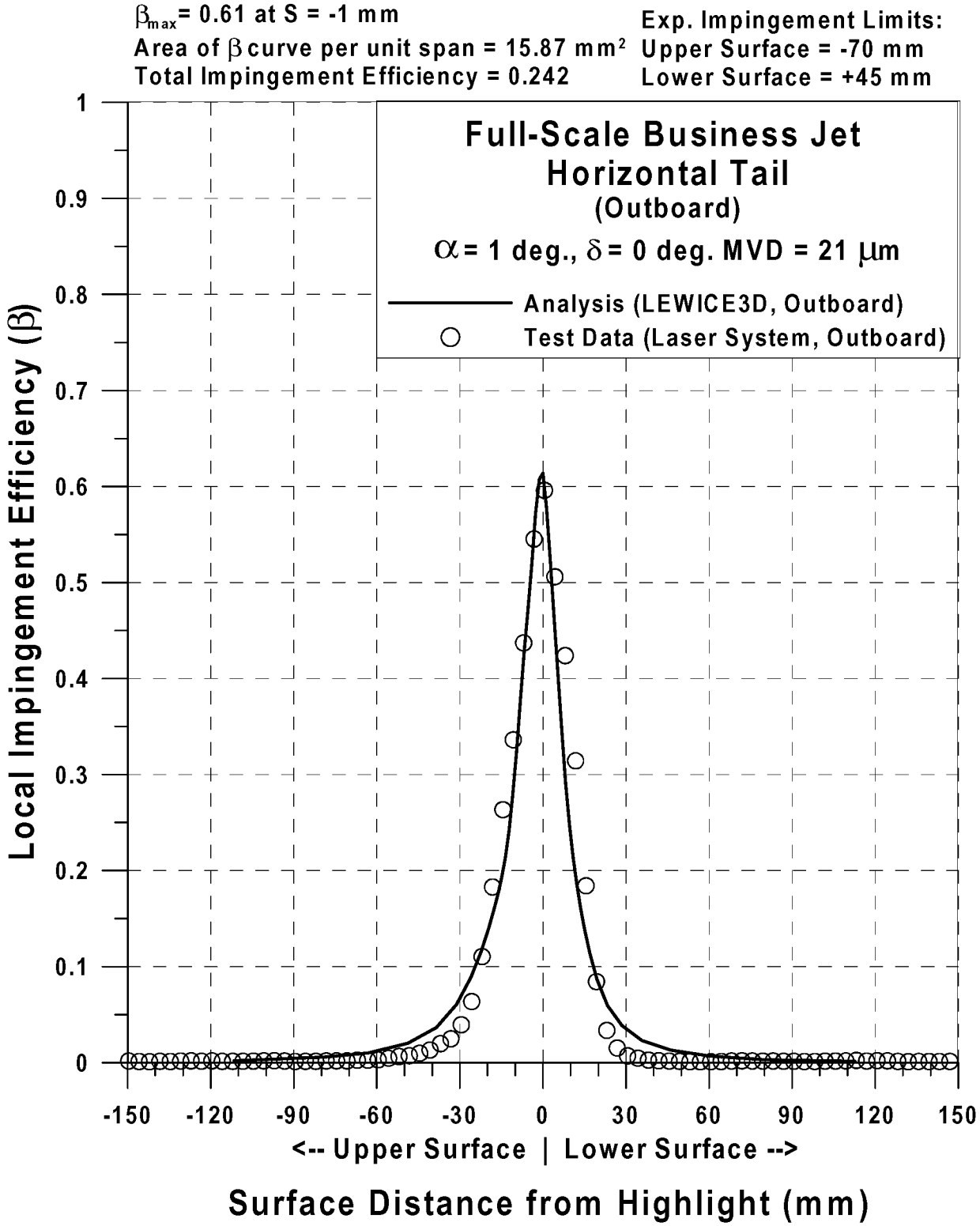

Fig. 105f Impingement efficiency distribution for full-scale Business Jet horizontal tail; Outboard, V_∞ = 176 mph, α=1°, δ=0°, MVD =21 μm (Continued).

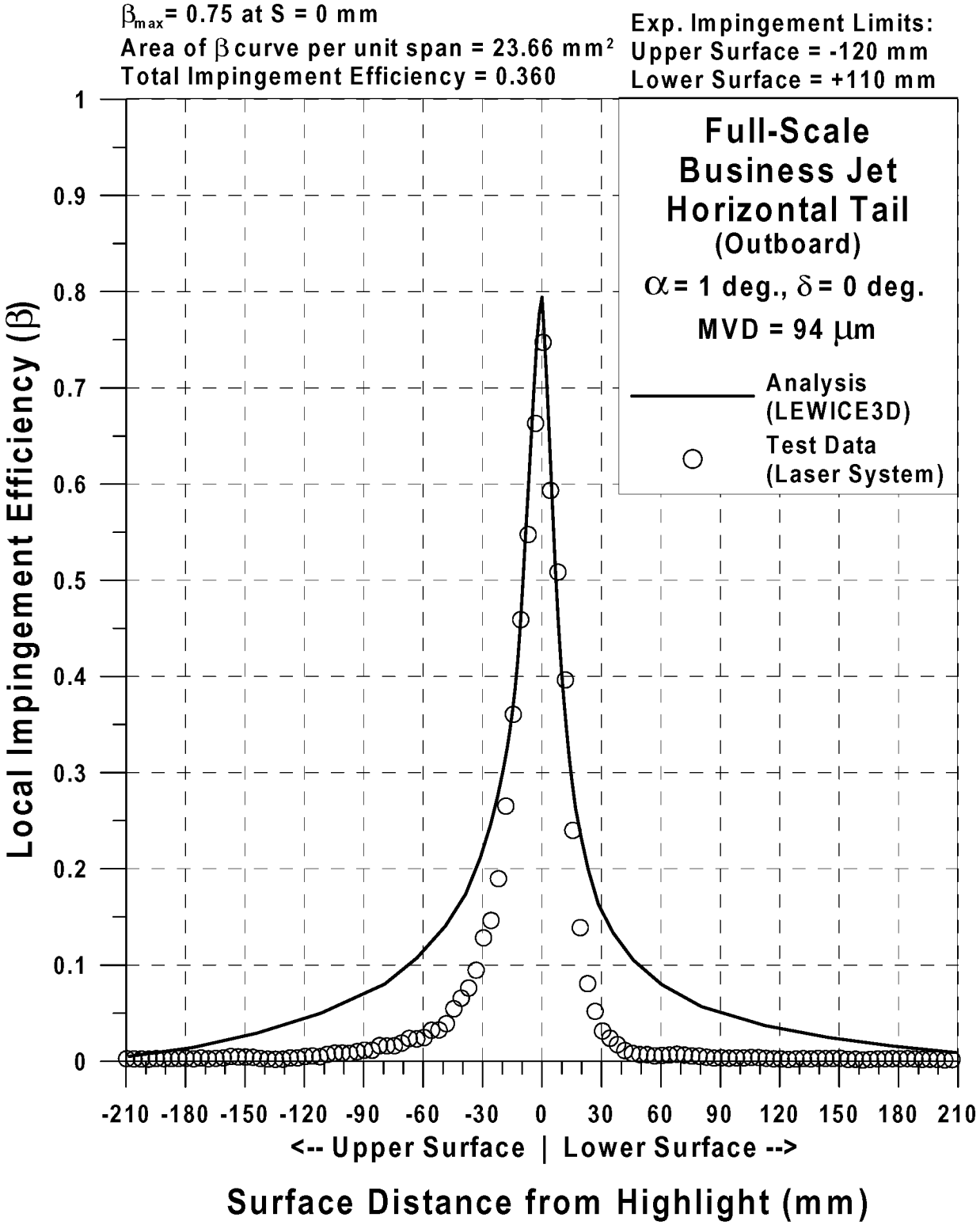

Fig. 105g Impingement efficiency distribution for full-scale Business Jet horizontal tail; Outboard, V_∞ = 176 mph, α=1°, δ=0°, MVD =94 μm (Continued).

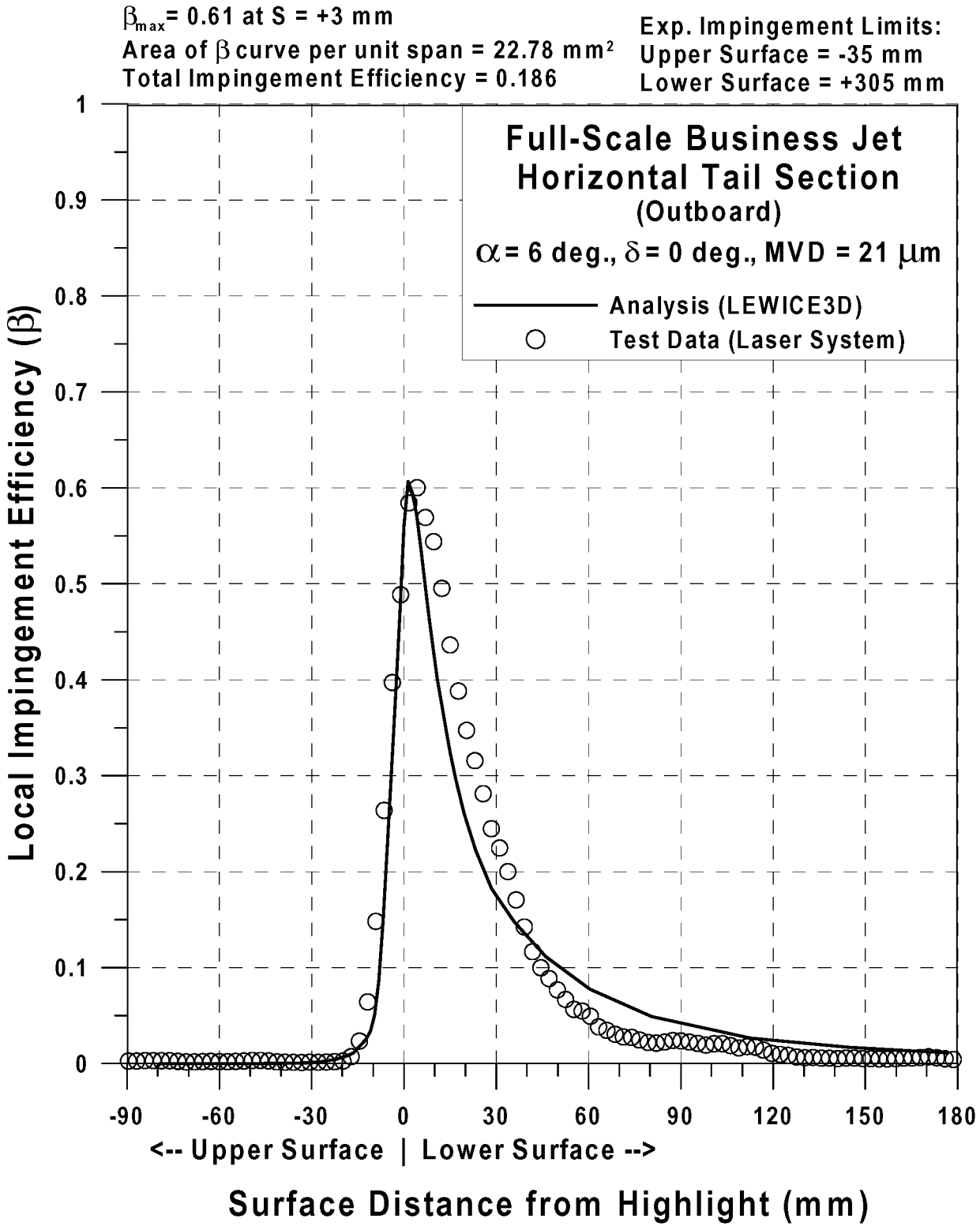

Fig. 105h Impingement efficiency distribution for full-scale Business Jet horizontal tail; Outboard, V_∞ = 176 mph, α=6°, δ=0°, MVD =21 μm.

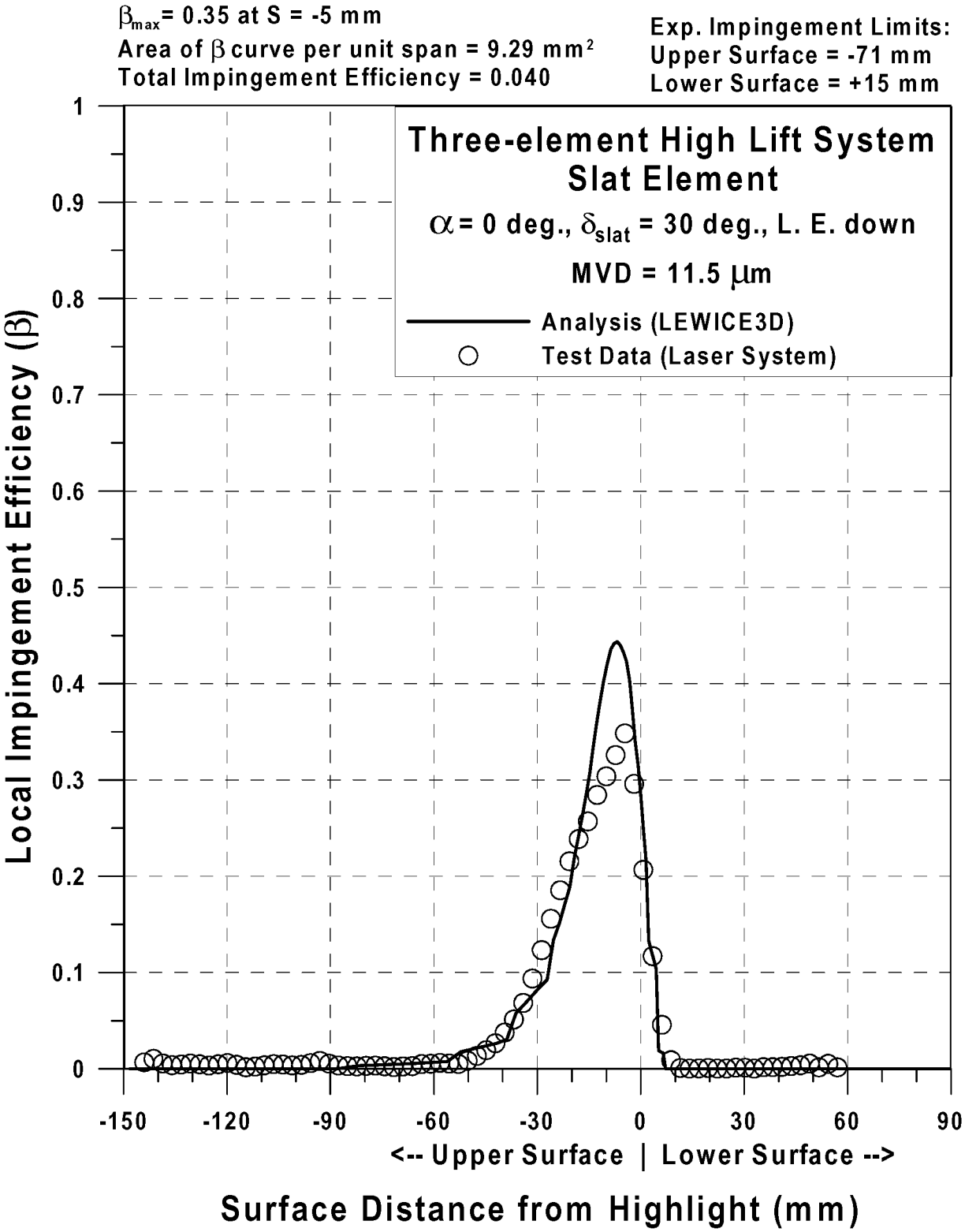

Fig. 106a Impingement efficiency distribution for three-element high lift system; slat element, LE down, V_∞ = 176 mph, α=0°, δ_{slat}=30°, MVD =11.5 μm (Continued).

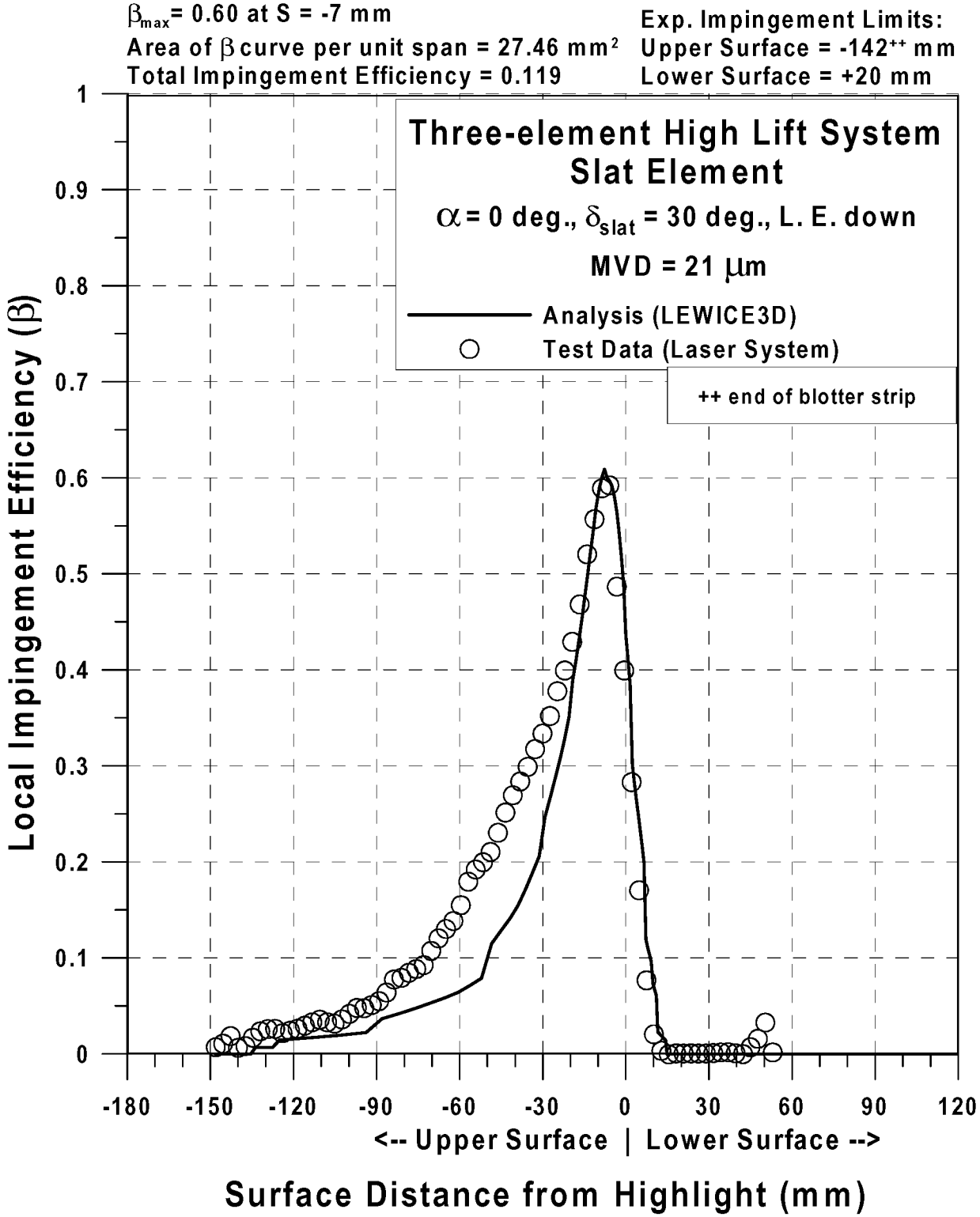

Fig. 106b Impingement efficiency distribution for three-element high lift system; slat element, LE down, V_∞ = 176 mph, α=0°, δ_{slat}=30°, MVD =21 μm (Continued).

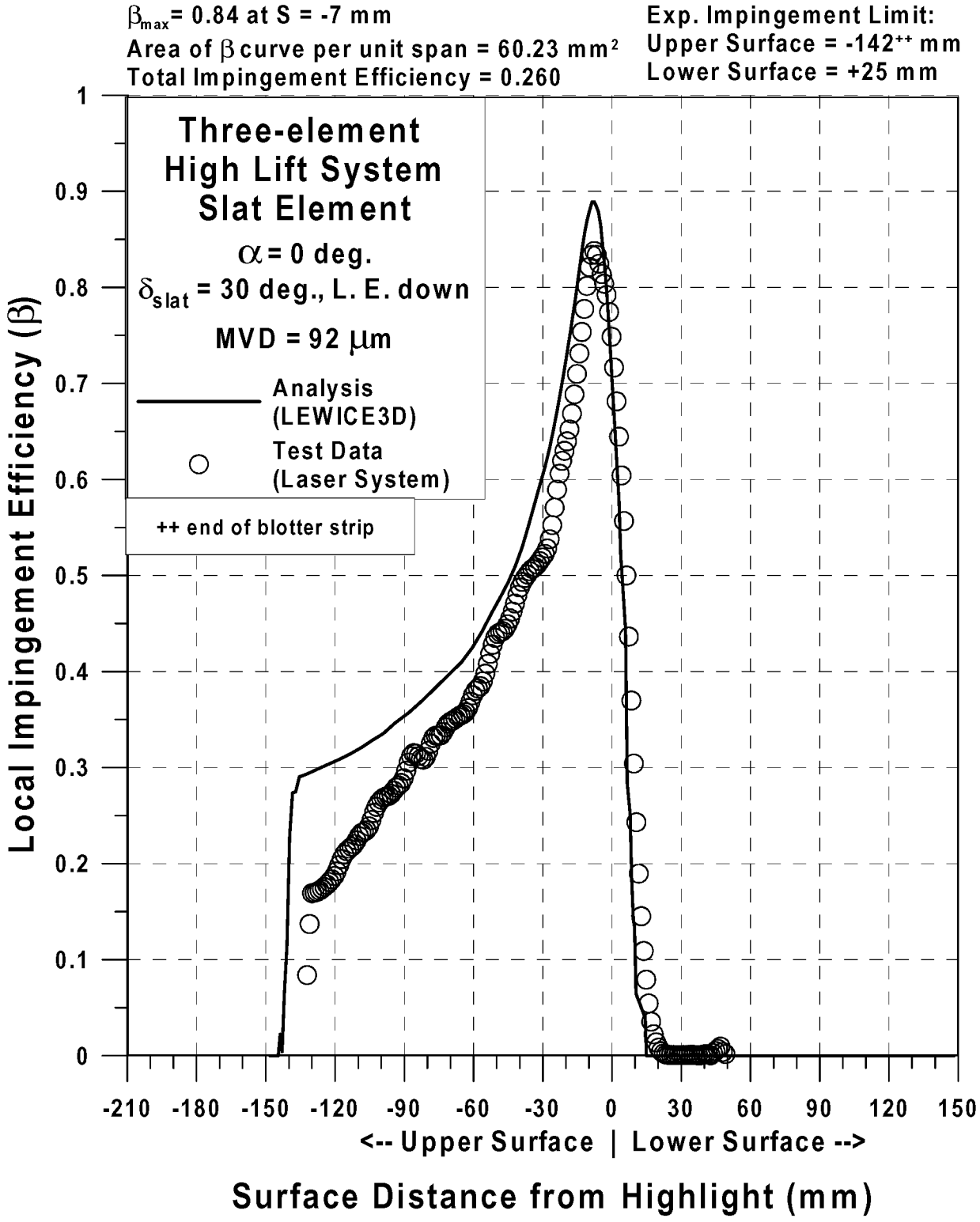

Fig. 106c Impingement efficiency distribution for three-element high lift system; slat element, LE down, V_∞ = 176 mph, $\alpha=0^\circ$, $\delta_{slat}=30^\circ$, MVD =92 μm (Continued).

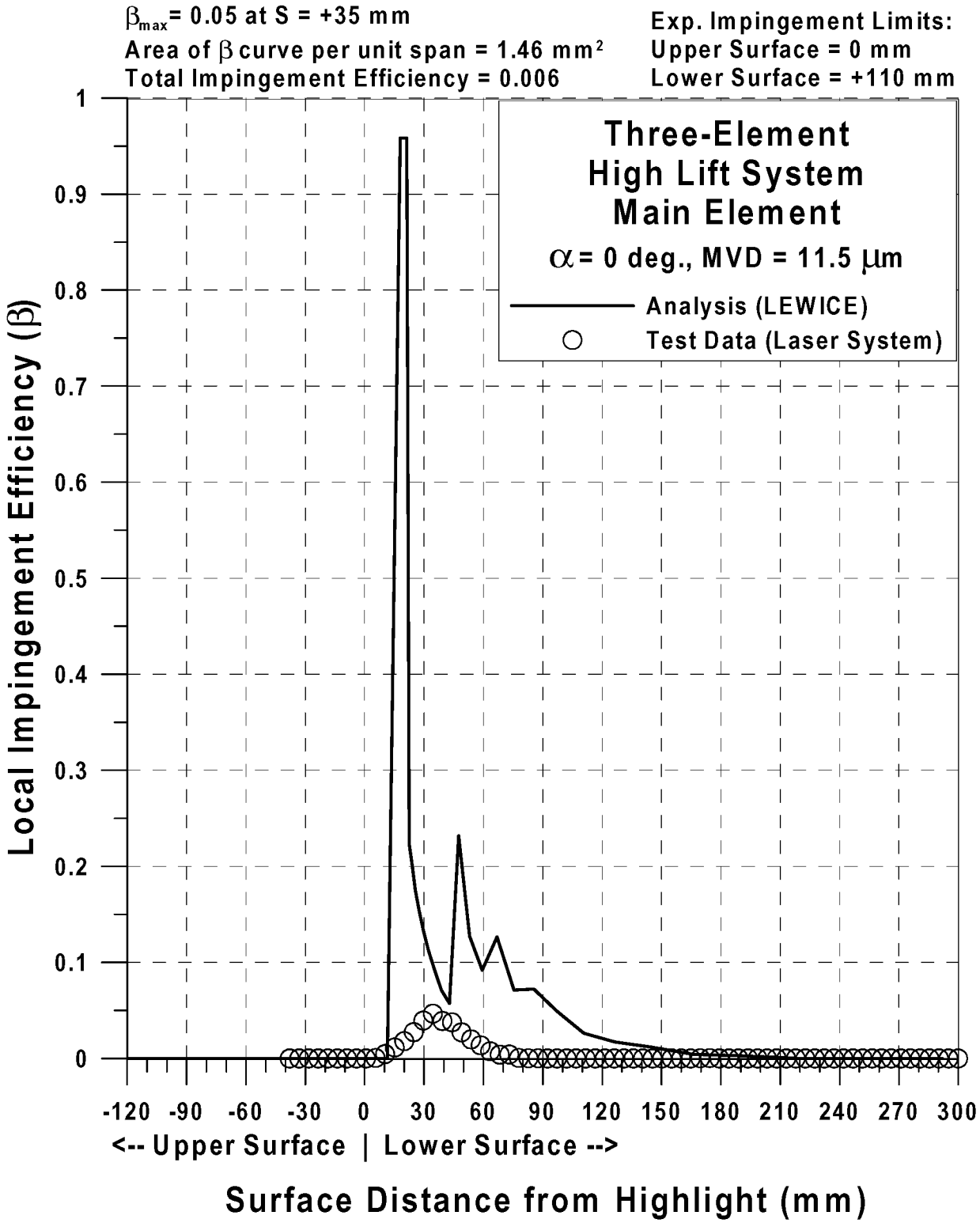

Fig. 106d Impingement efficiency distribution for three-element high lift system; main element, V_∞ = 176 mph, $\alpha=0^\circ$, MVD =11.5 μm (Continued).

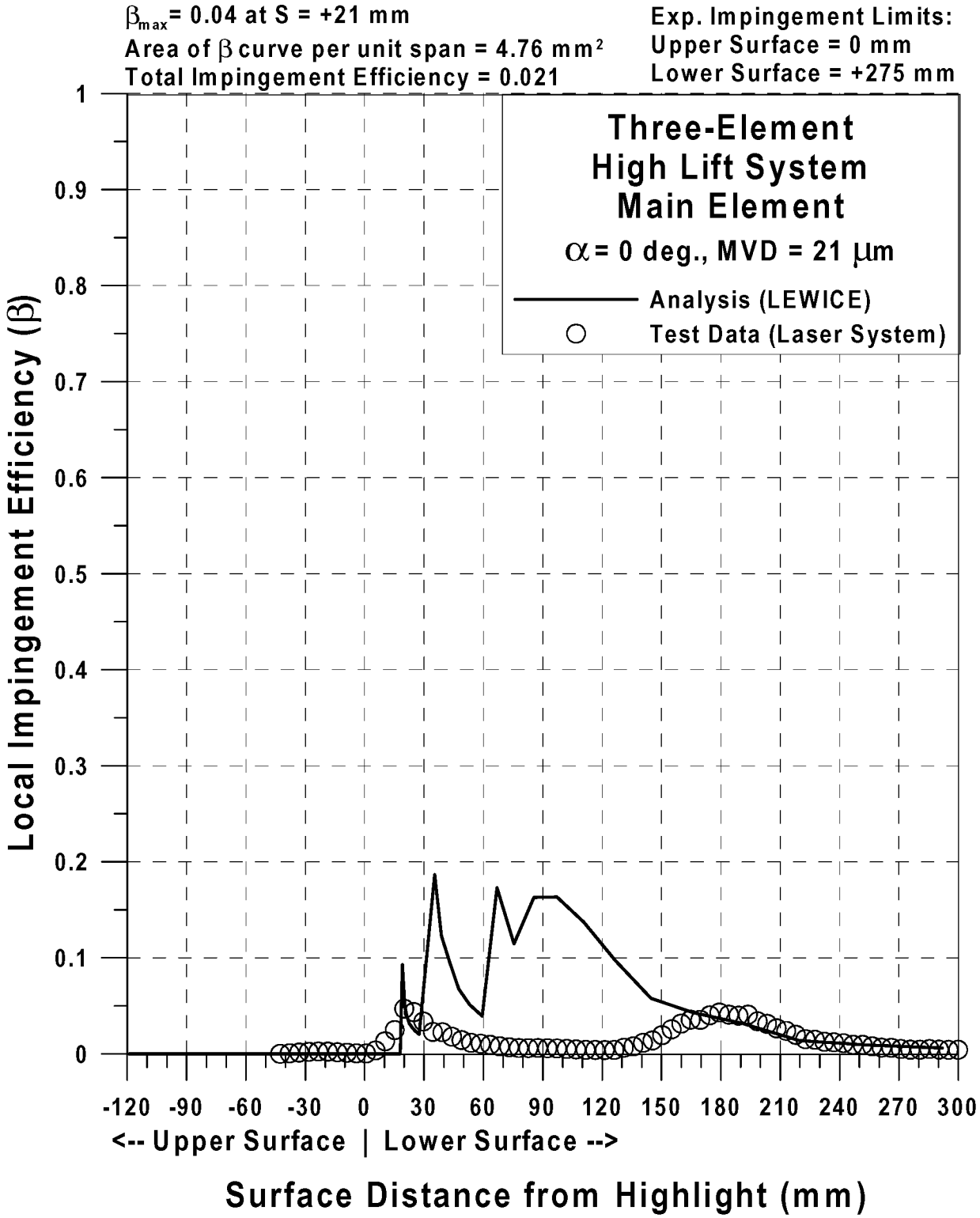

Fig. 106e Impingement efficiency distribution for three-element high lift system; main element, V_∞ = 176 mph, α=0°, MVD =21 μm (Continued).

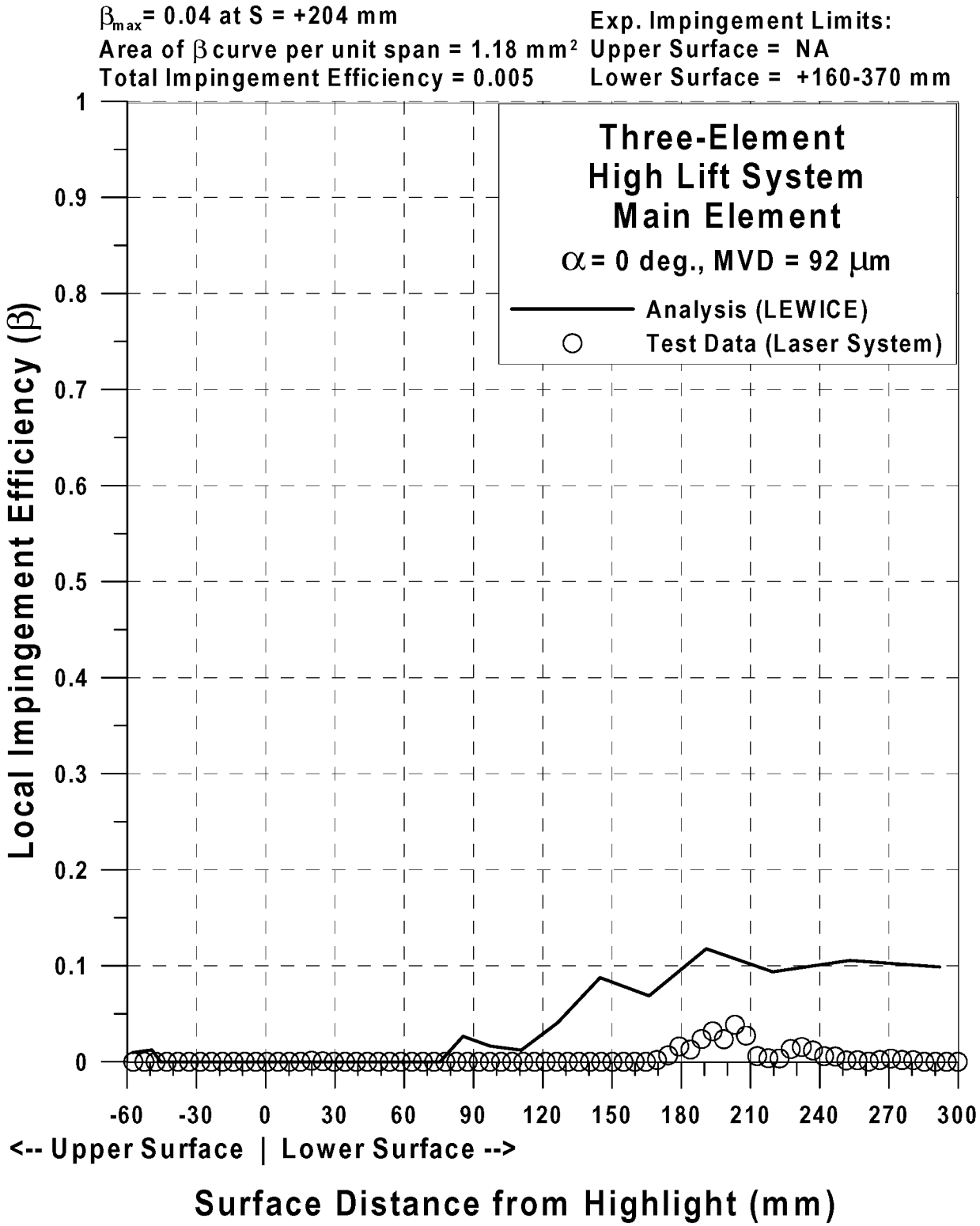

Fig. 106f Impingement efficiency distribution for three-element high lift system; main element, V_∞ = 176 mph, α=0°, MVD =92 μm (Continued).

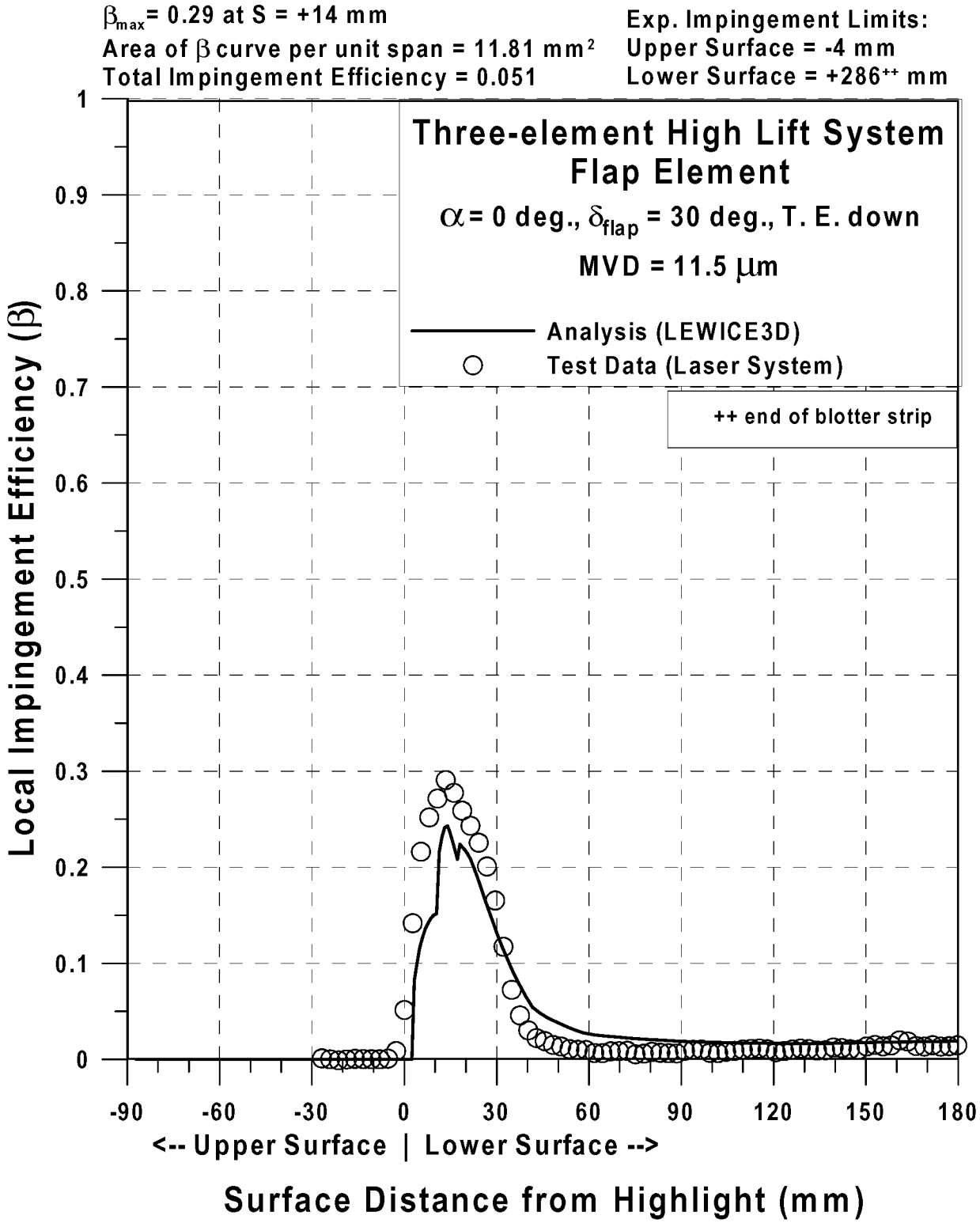

Fig. 106g Impingement efficiency distribution for three-element high lift system; flap element, TE down, V_∞ = 176 mph, α=0°, δ_{flap}=30°, MVD =11.5 μm (Continued).

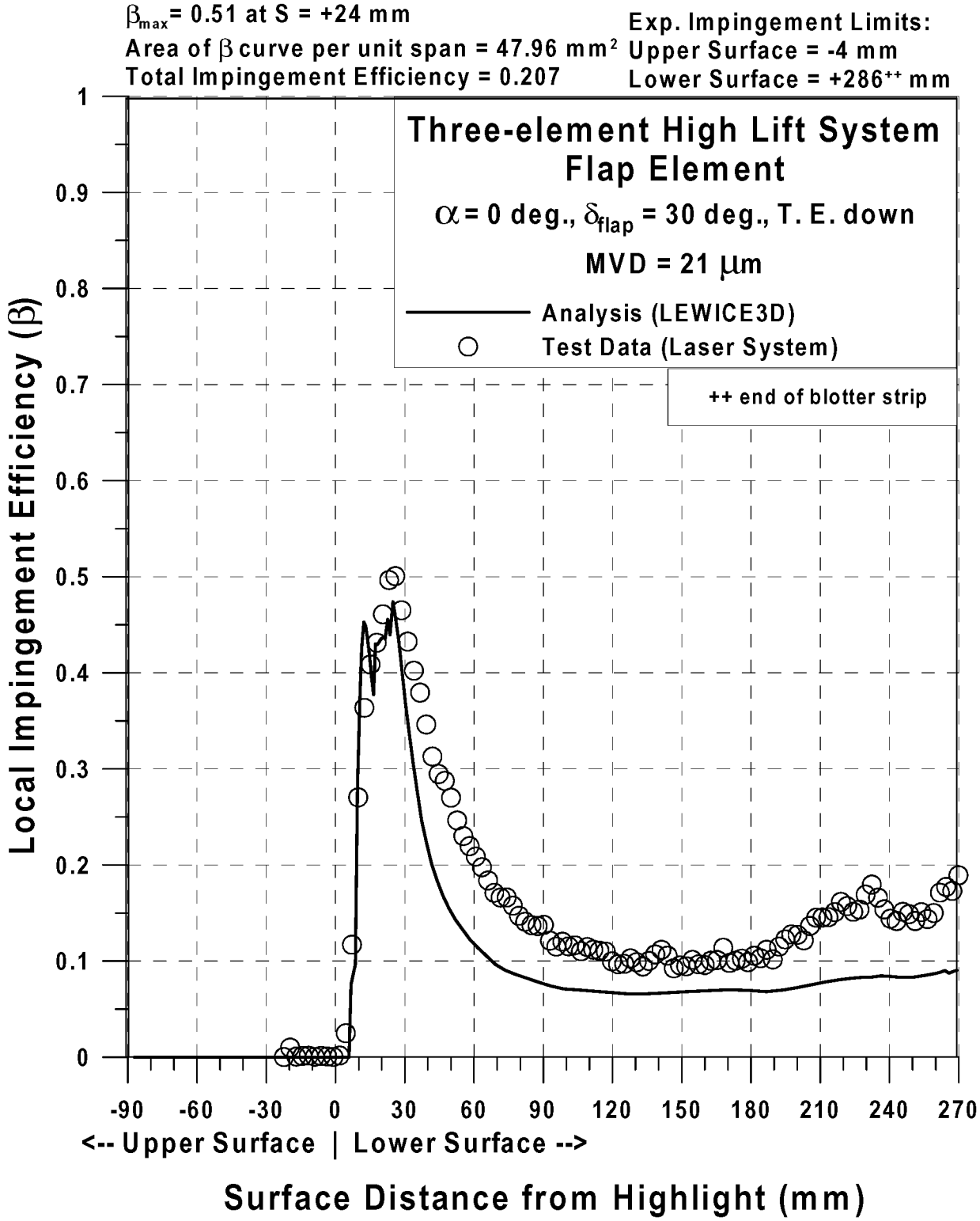

Fig. 106h Impingement efficiency distribution for three-element high lift system; flap element, TE down, V_∞ = 176 mph, α=0°, δ_{flap}=30°, MVD =21 μm (Continued).

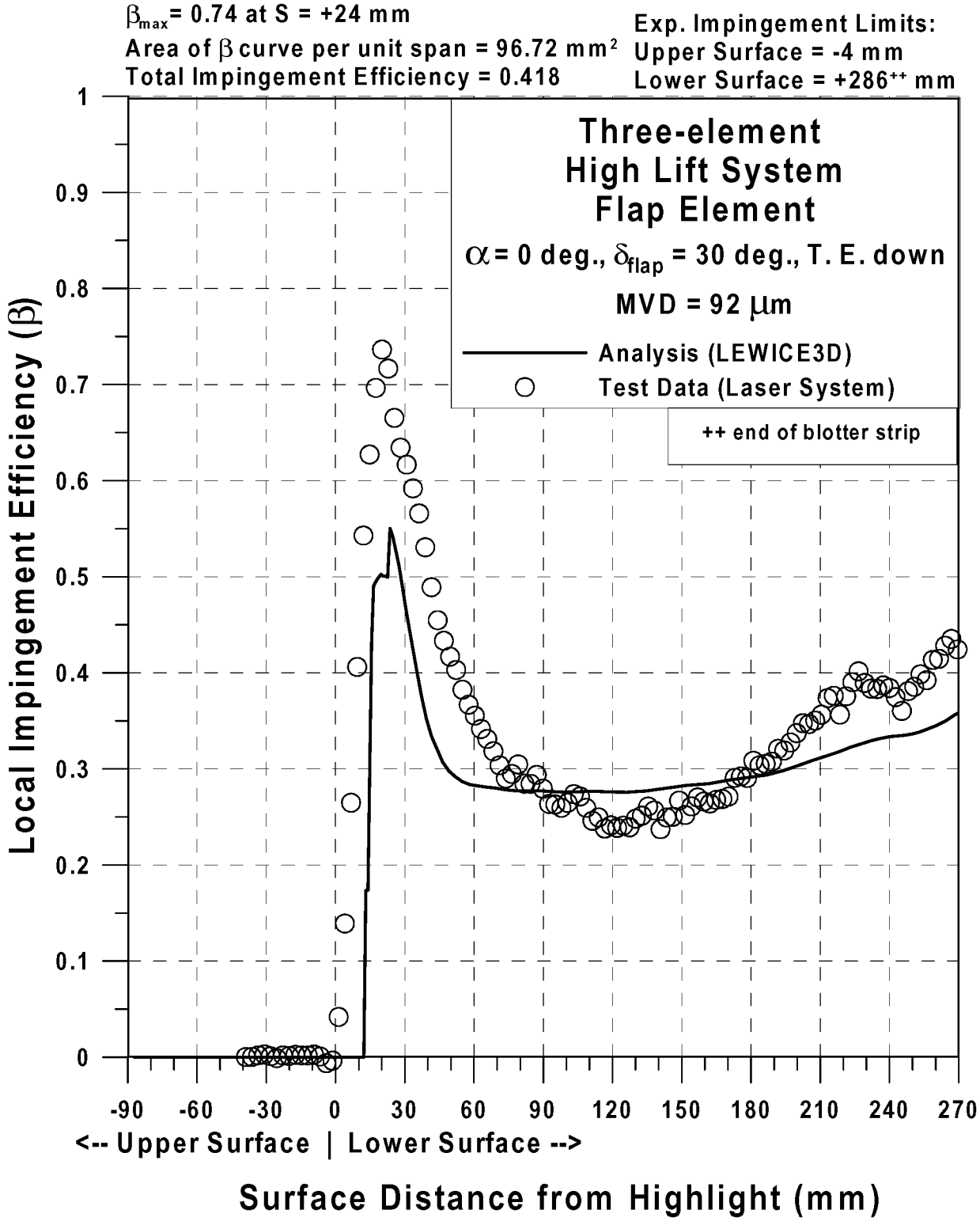

Fig. 106i Impingement efficiency distribution for three-element high lift system; flap element, TE down, V_∞ = 176 mph, α=0°, δ_{flap}=30°, MVD =92 μm (Continued).

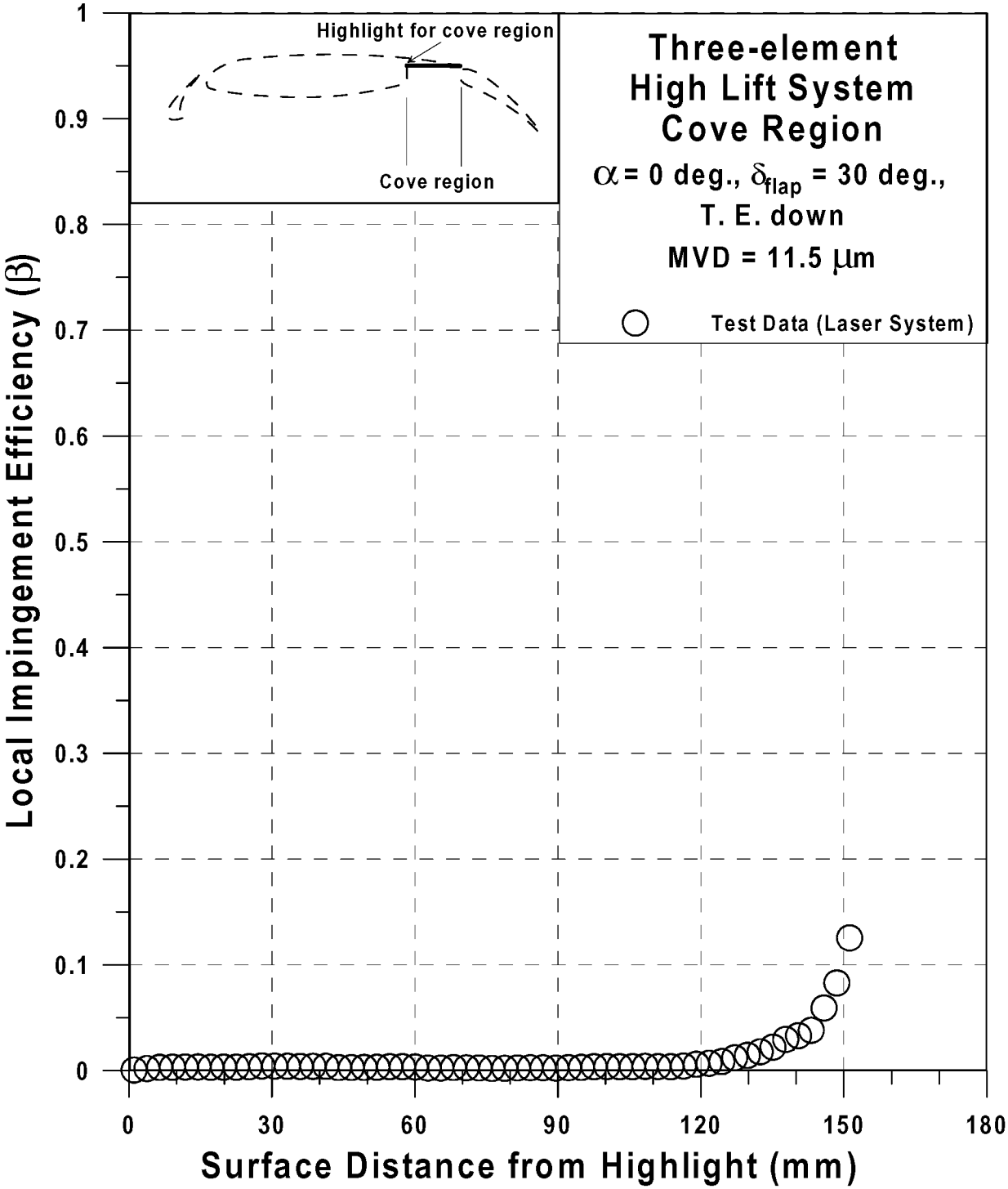

Fig. 106j Impingement efficiency distribution for three-element high lift system; cove region, TE down, V_∞ = 176 mph, α=0°, δ_{flap}=30°, MVD =11.5 μm (Continued).

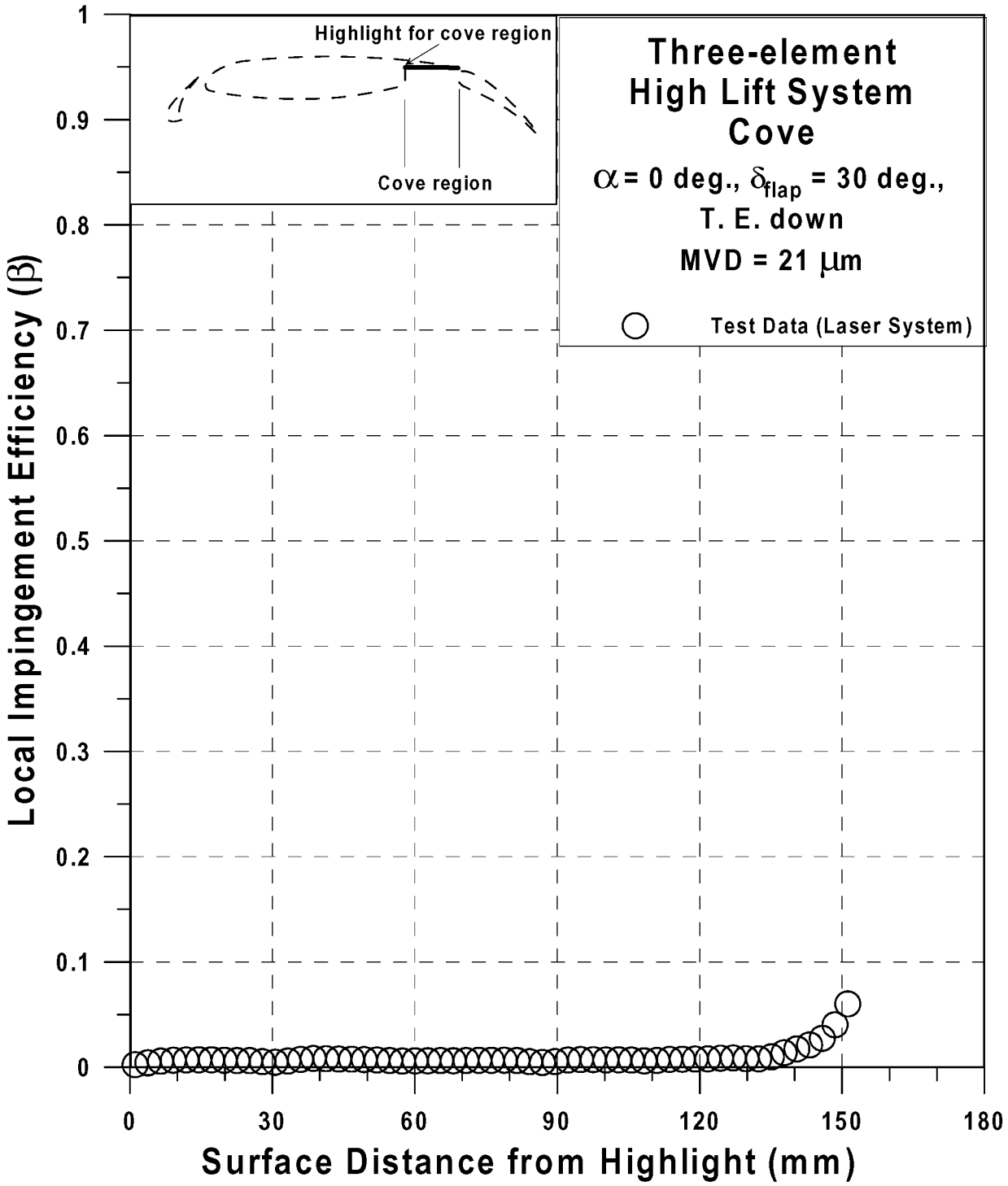

Fig. 106k Impingement efficiency distribution for three-element high lift system; cove region, TE down, V_∞ = 176 mph, α=0°, δ_{flap}=30°, MVD =21 μm (Continued).

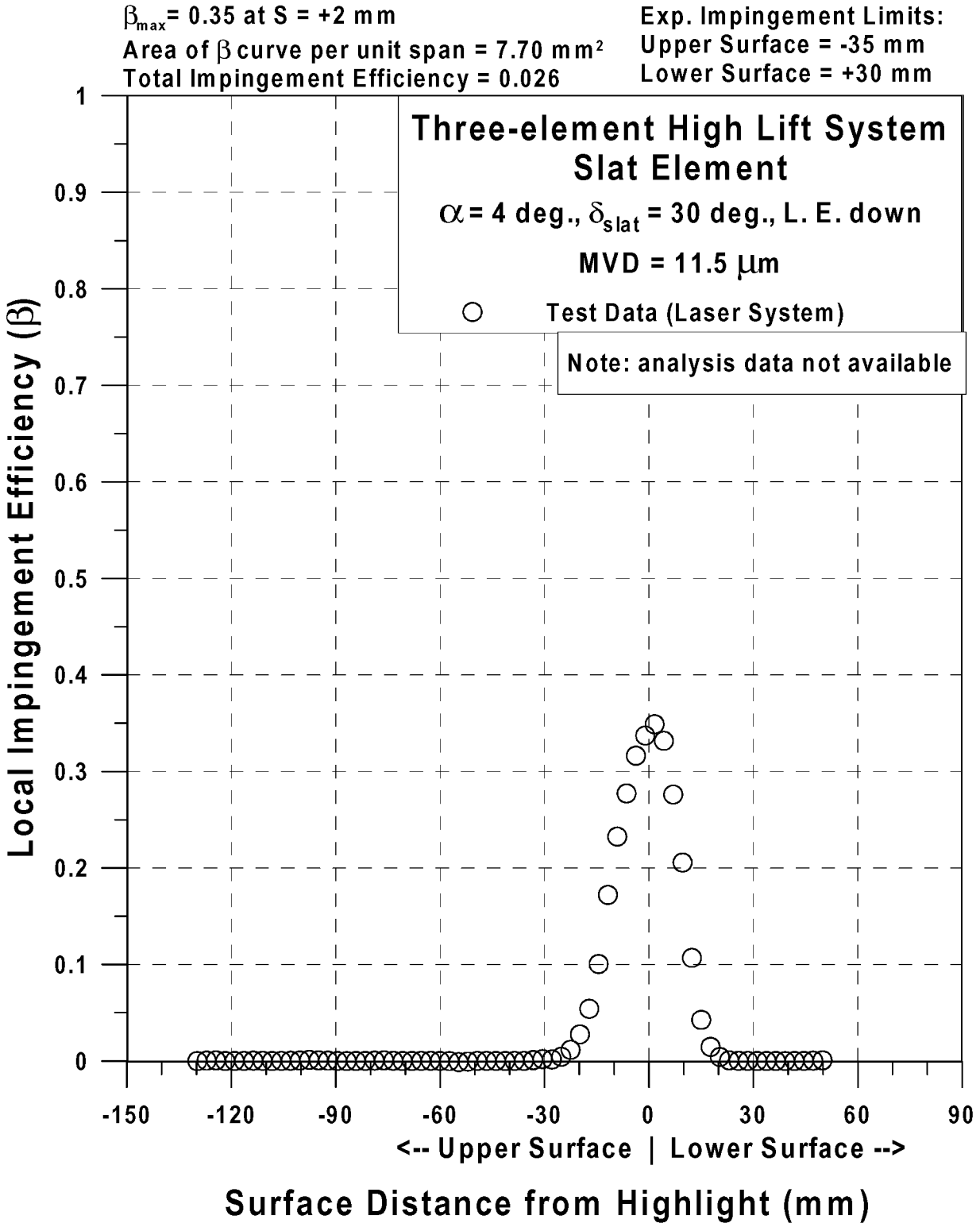

Fig. 106l Impingement efficiency distribution for three-element high lift system; slat element, LE down, V_∞ = 176 mph, α=4°, δ_{slat}=30°, MVD =11.5 μm (Continued).

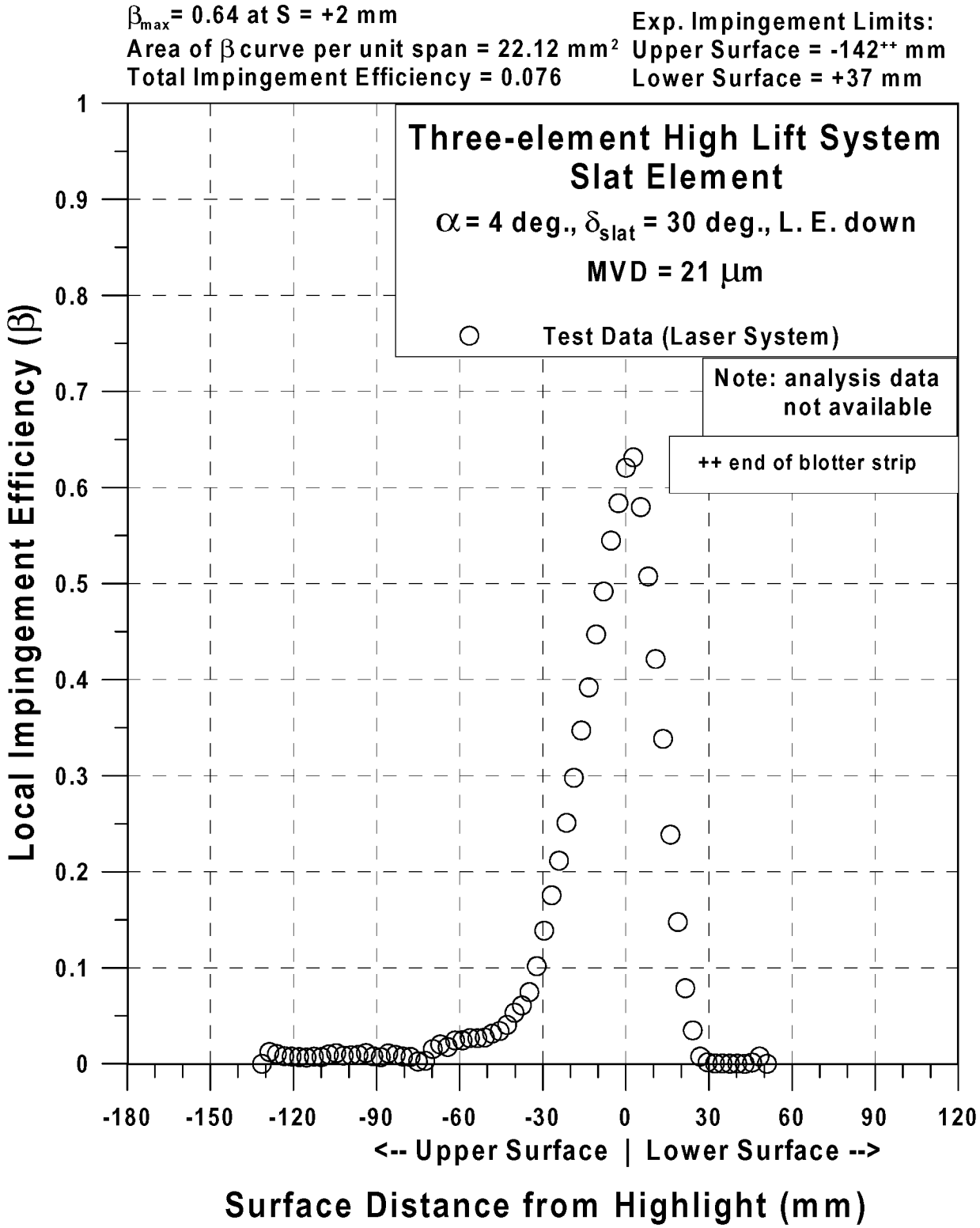

Fig. 106m Impingement efficiency distribution for three-element high lift system; slat element, LE down, V_∞ = 176 mph, α=4°, δ_{slat}=30°, MVD =21 μm (Continued).

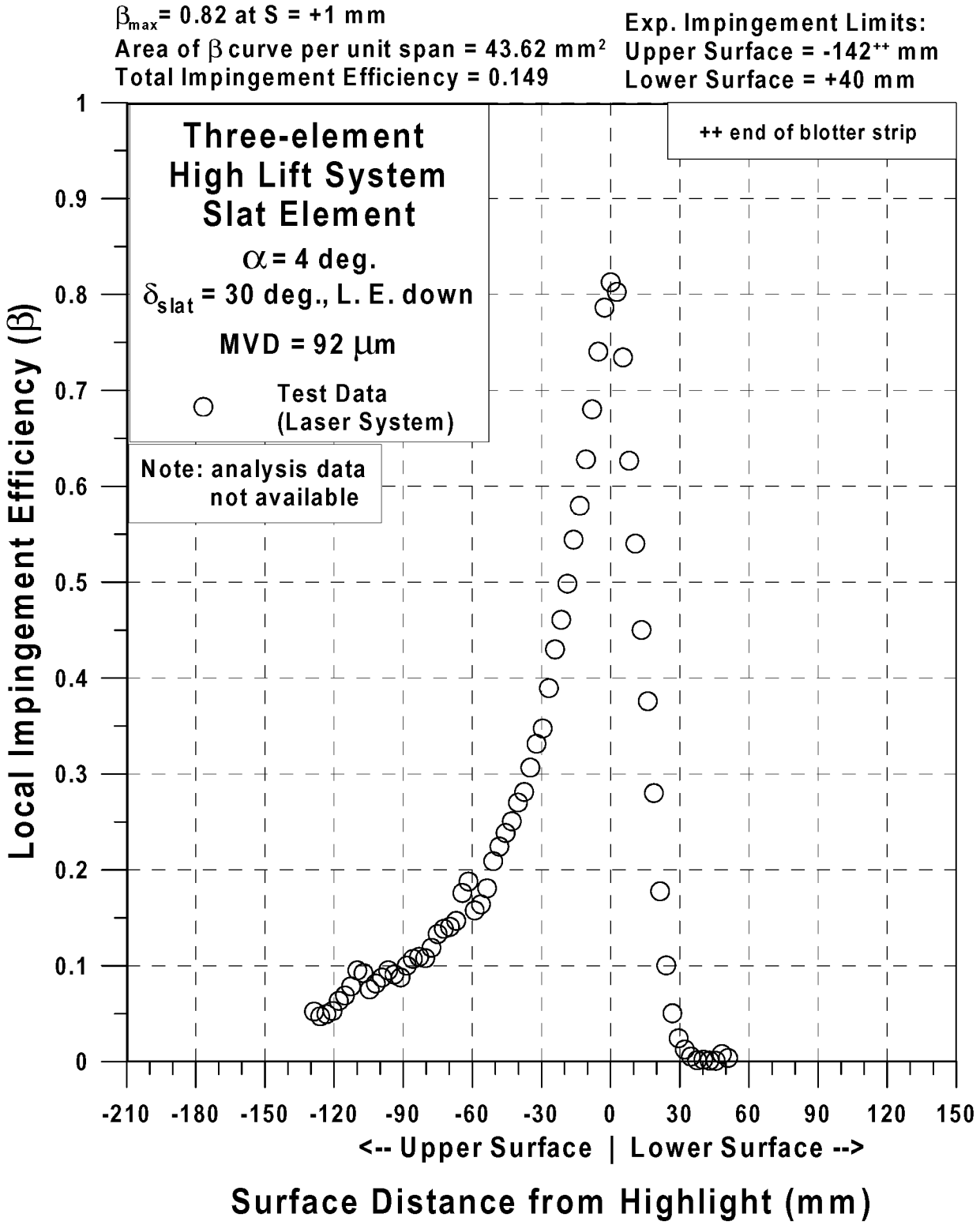

Fig. 106n Impingement efficiency distribution for three-element high lift system; slat element, LE down, V_∞ = 176 mph, α=4°, δ_{slat}=30°, MVD =92 μm (Continued).

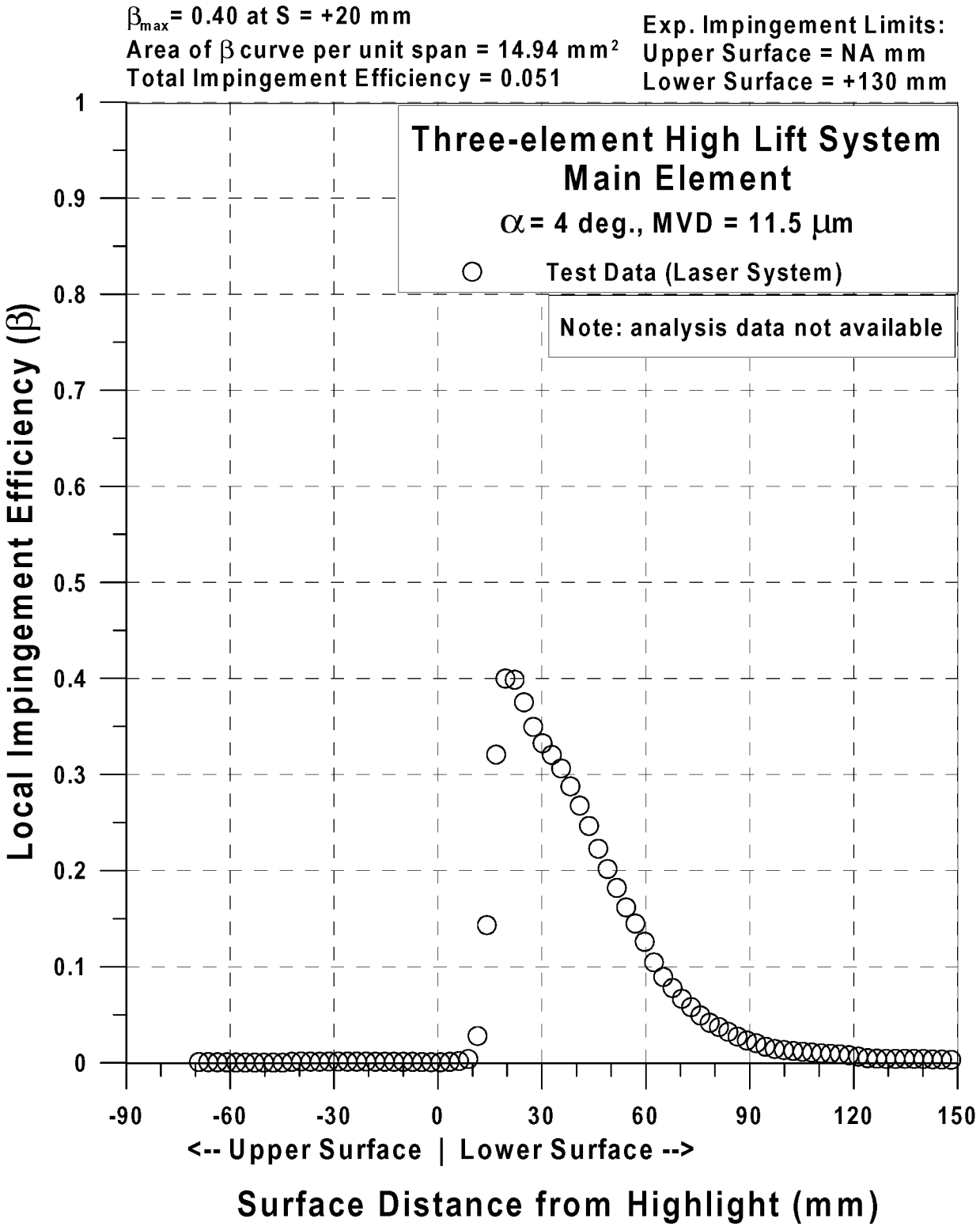

Fig. 106o Impingement efficiency distribution for three-element high lift system; main element, V_∞ = 176 mph, α=4°, MVD =11.5 μm (Continued).

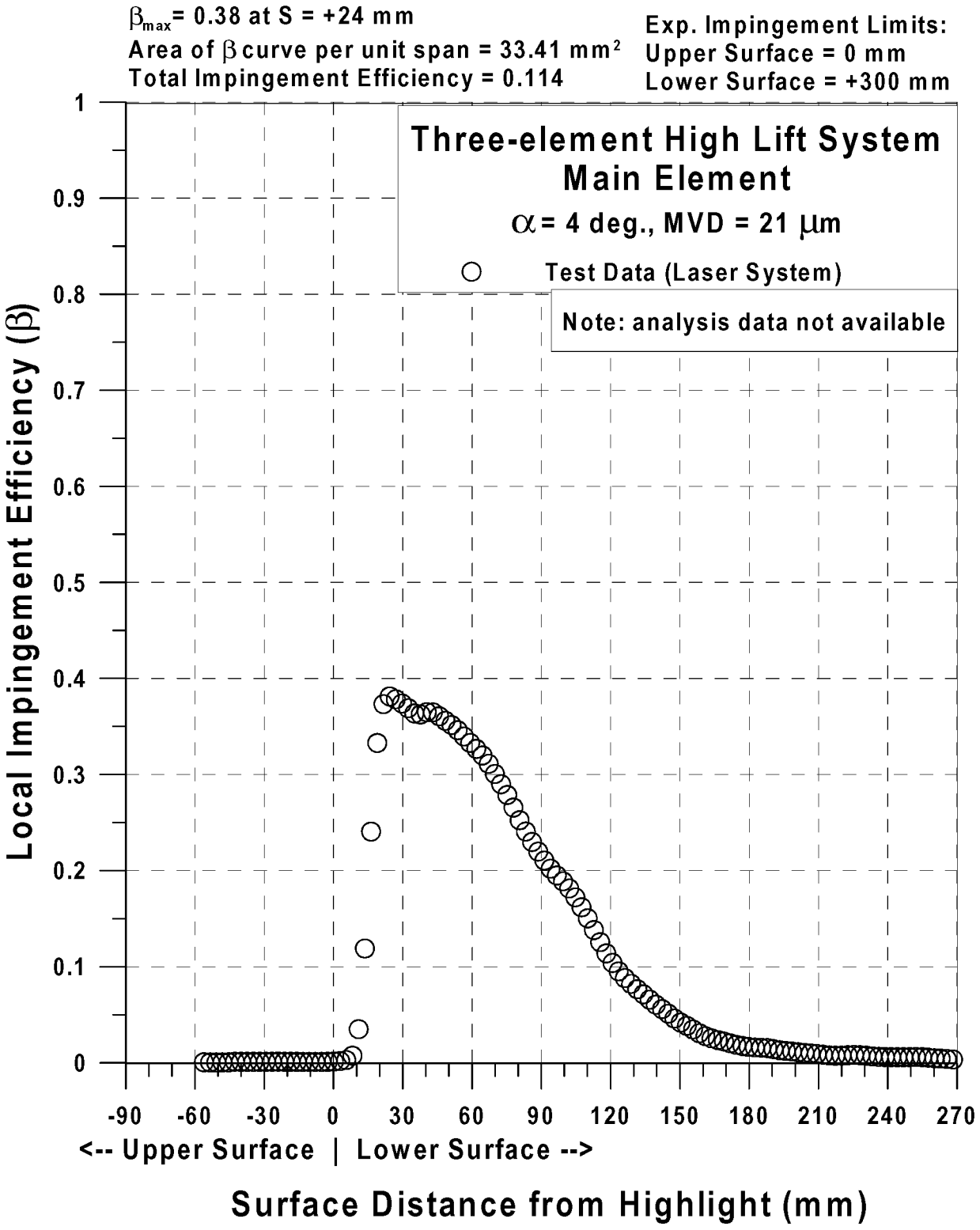

Fig. 106p Impingement efficiency distribution for three-element high lift system; main element, V_∞ = 176 mph, α=4°, MVD =21 μm (Continued).

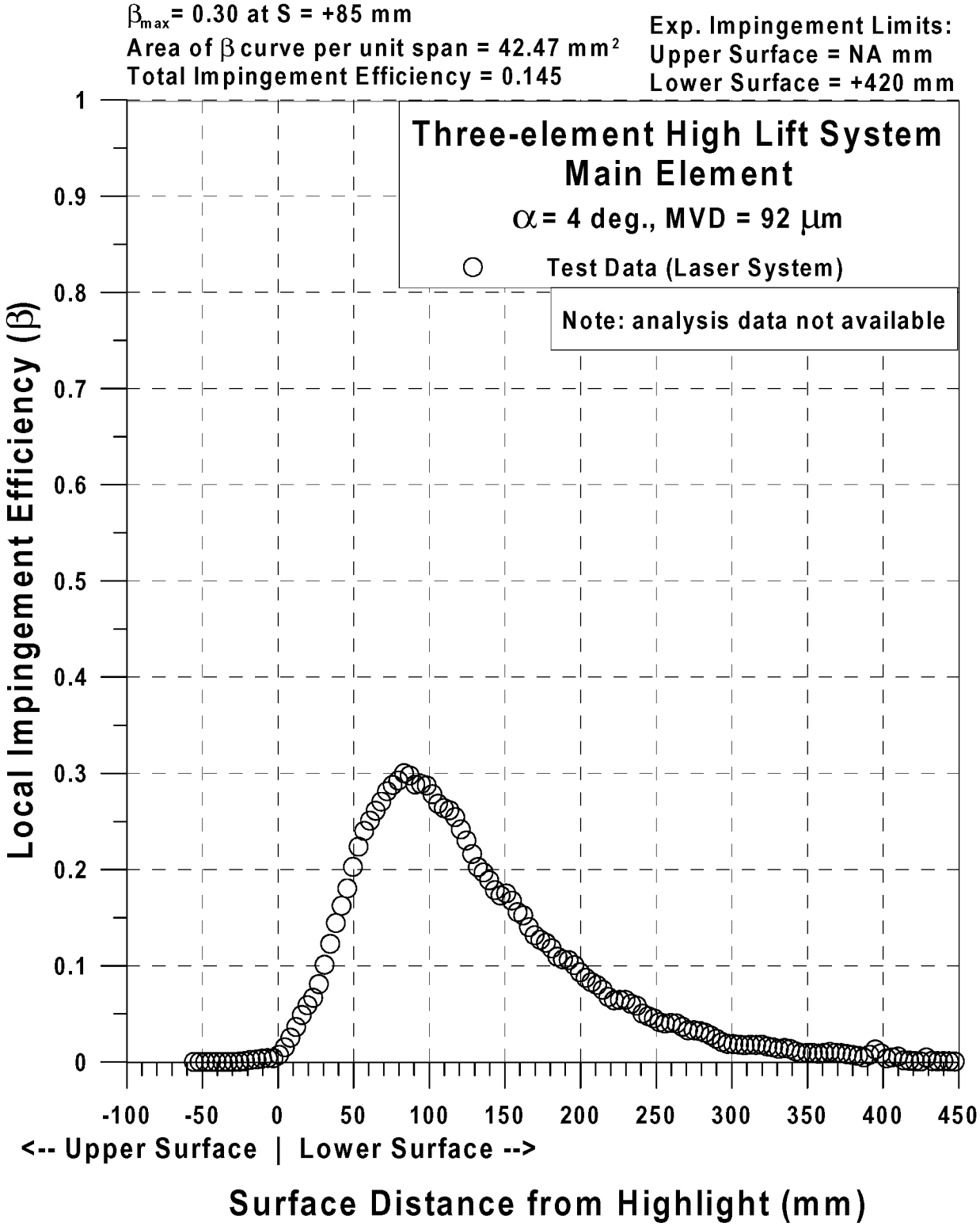

Fig. 106q Impingement efficiency distribution for three-element high lift system; main element, V_∞ = 176 mph, α=4°, MVD =92 μm (Continued).

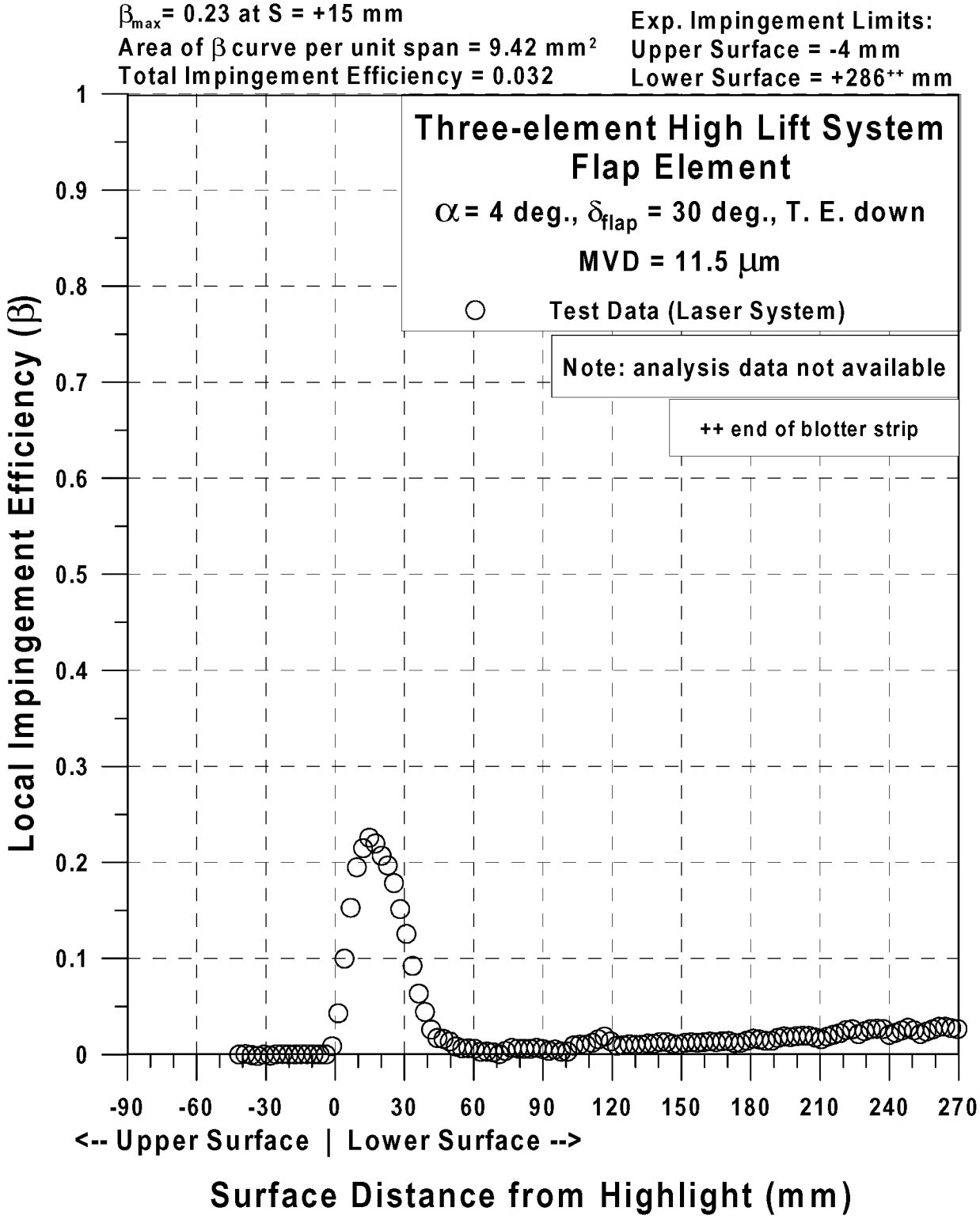

Fig. 106r Impingement efficiency distribution for three-element high lift system; flap element, TE down, V_∞ = 176 mph, α=4°, δ_{flap}=30°, MVD =11.5 μm (Continued).

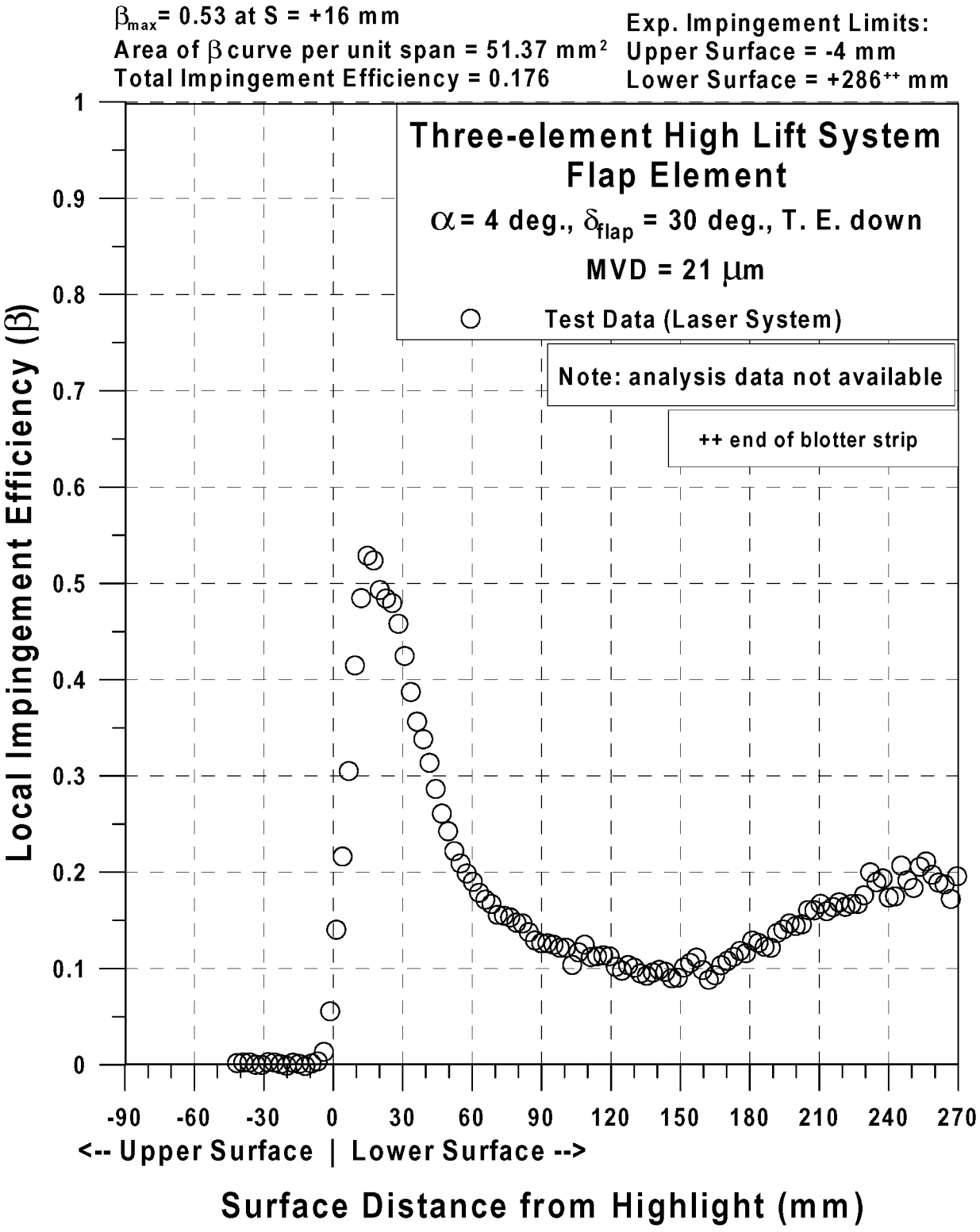

Fig. 106s Impingement efficiency distribution for three-element high lift system; flap element, TE down, V_∞ = 176 mph, α=4°, δ_{flap}=30°, MVD =21 μm (Continued).

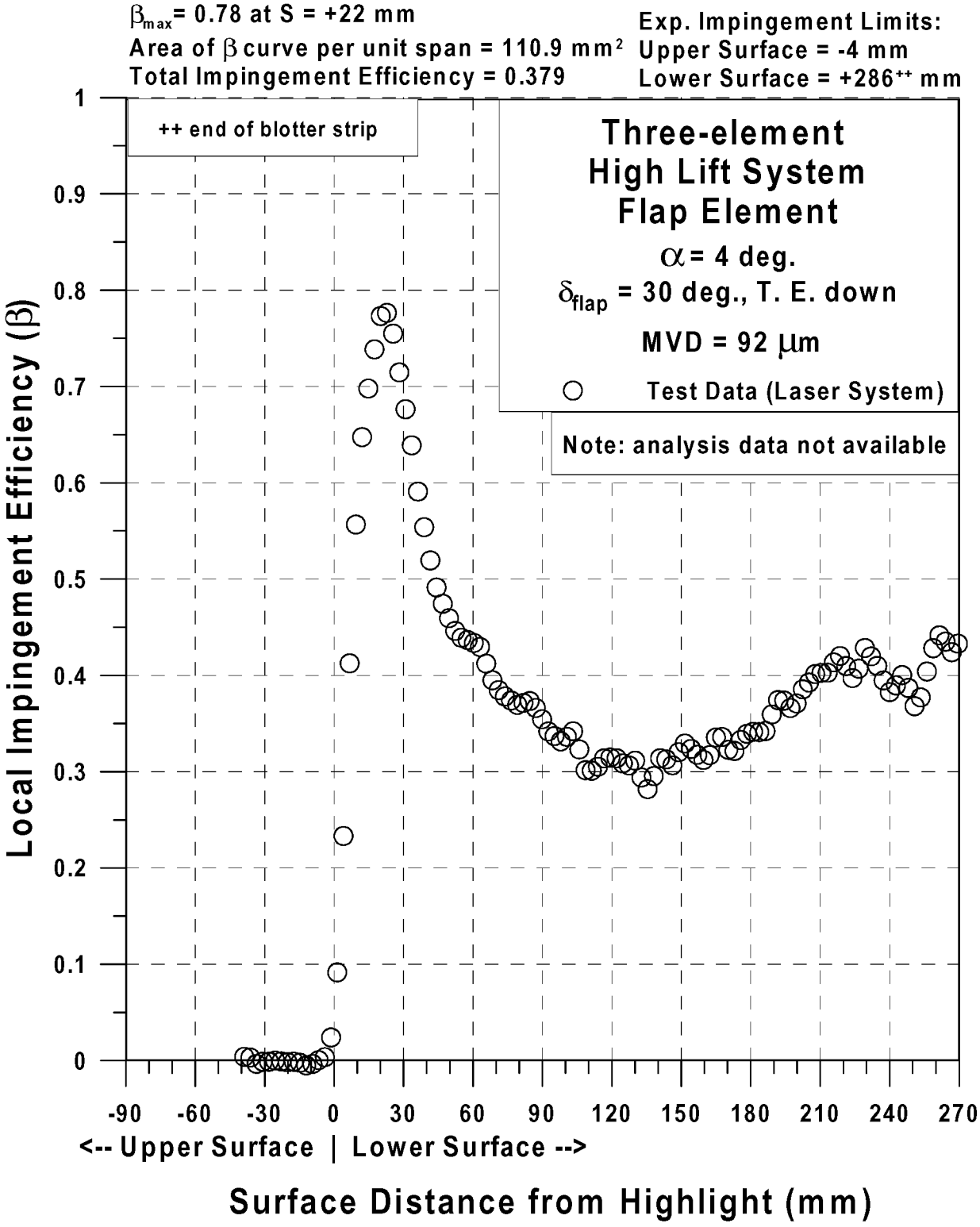

Fig. 106t Impingement efficiency distribution for three-element high lift system; flap element, TE down, V_∞ = 176 mph, α=4°, δ_{flap}=30°, MVD =92 μm (Continued).

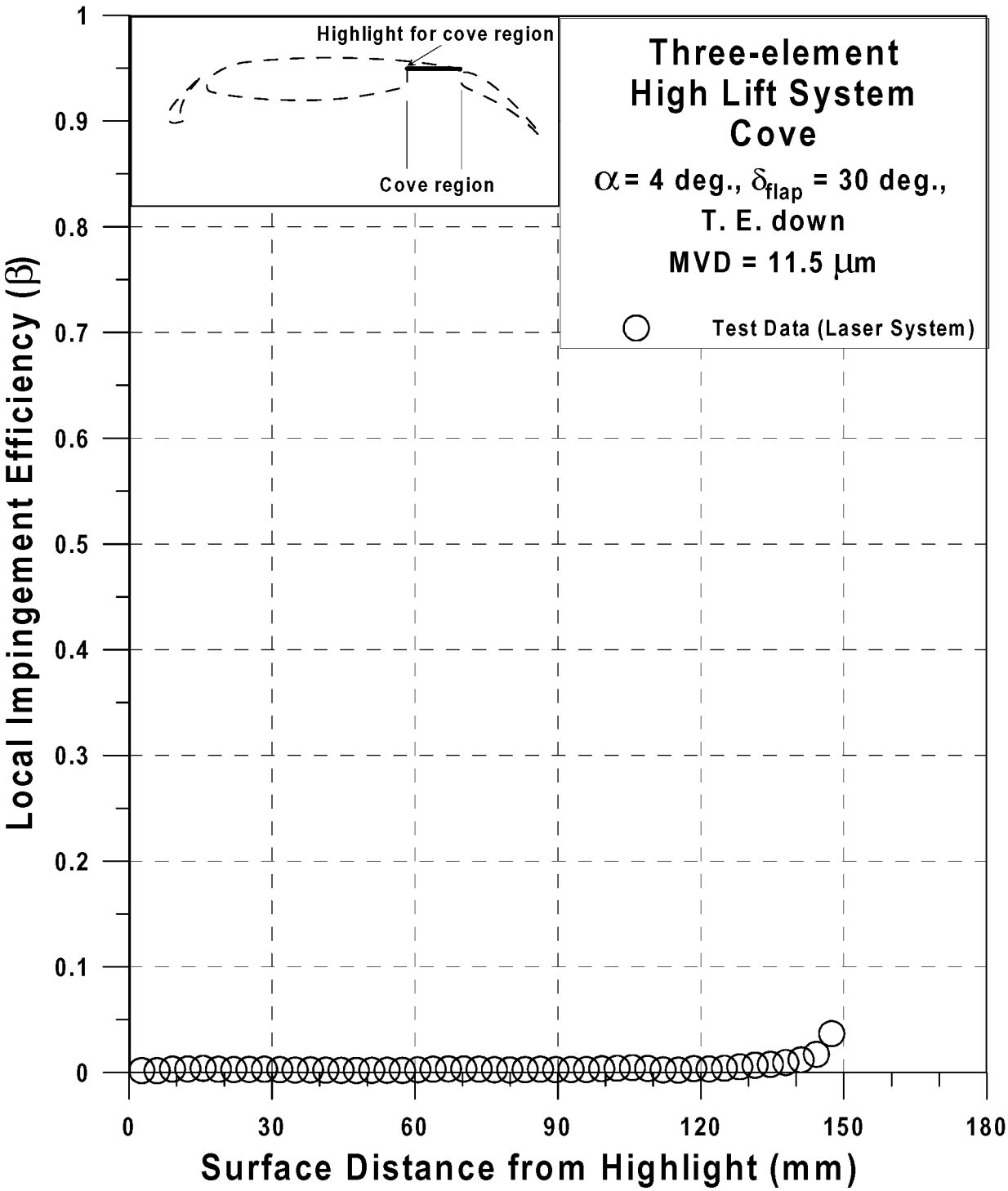

Fig. 106u Impingement efficiency distribution for three-element high lift system; cove region, TE down, V_∞ = 176 mph, α=4°, δ_{flap}=30°, MVD =11.5 μm (Continued).

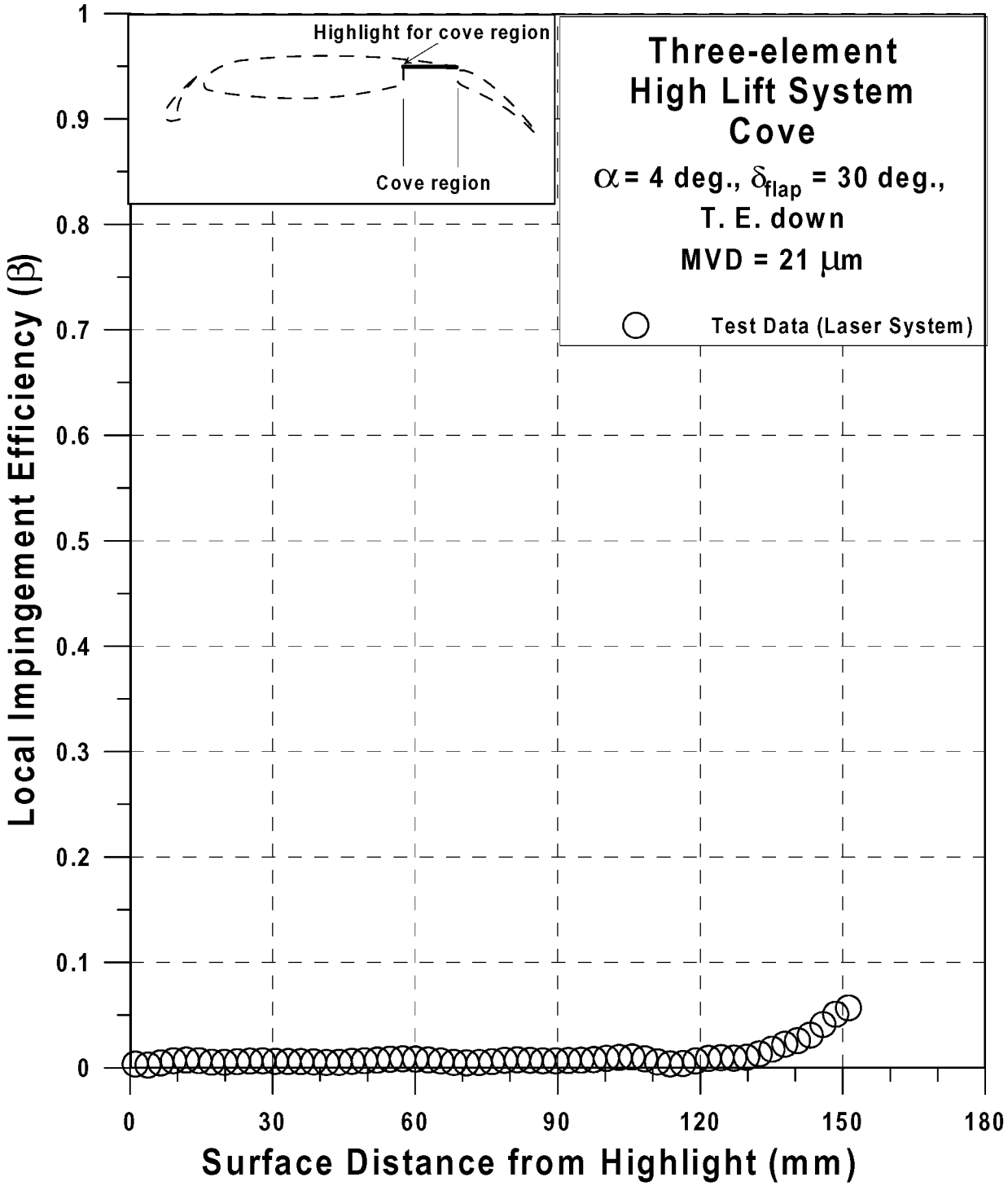

Fig. 106v Impingement efficiency distribution for three-element high lift system; cove region, TE down, V_∞ = 176 mph, α=4°, δ_{flap}=30°, MVD =21 μm (Continued).

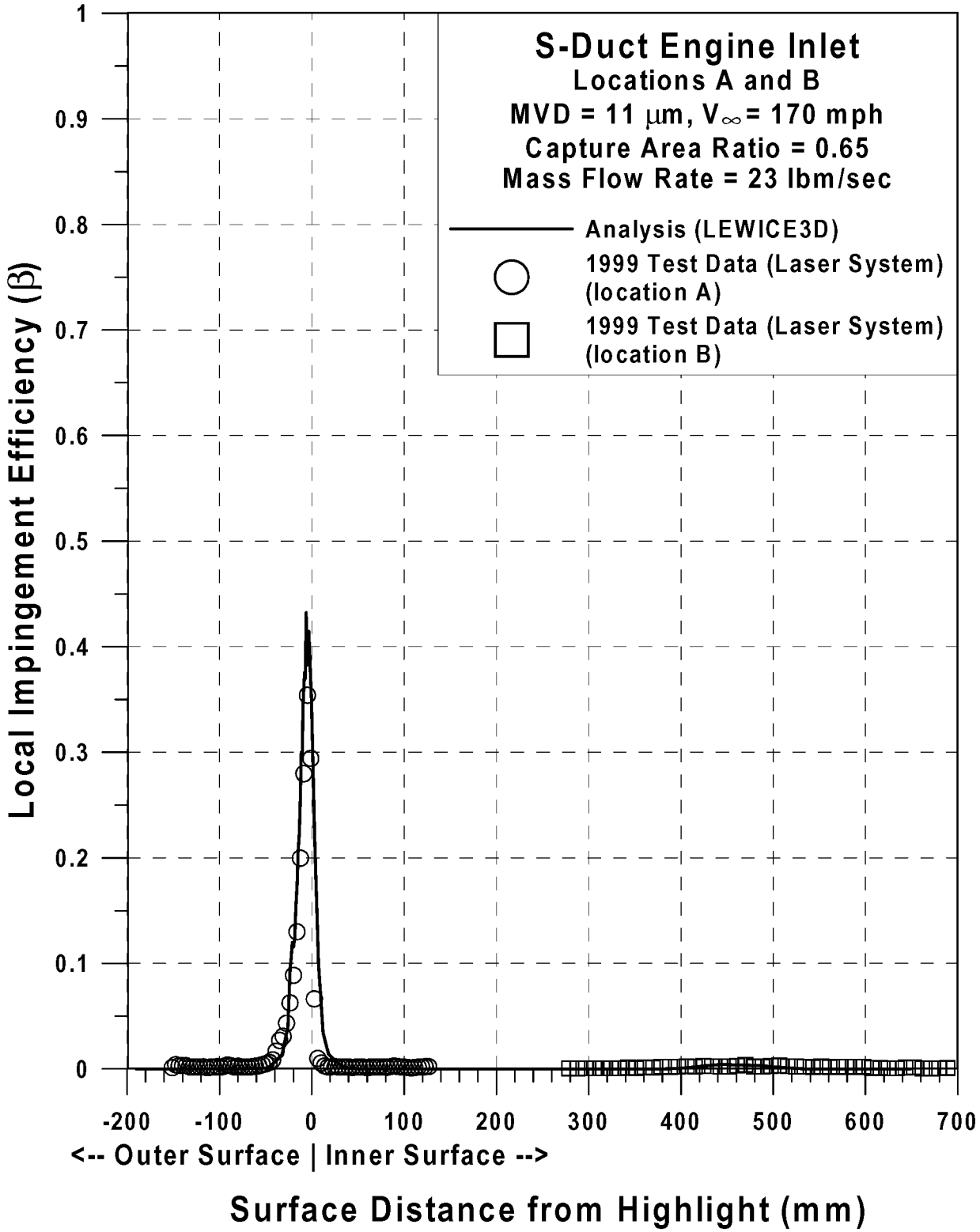

Fig. 107a Impingement efficiency distribution for S-duct engine inlet; locations A and B, V_∞ = 170 mph, $\alpha=0^\circ$, CAR=0.65, MVD =11 μm (Continued).

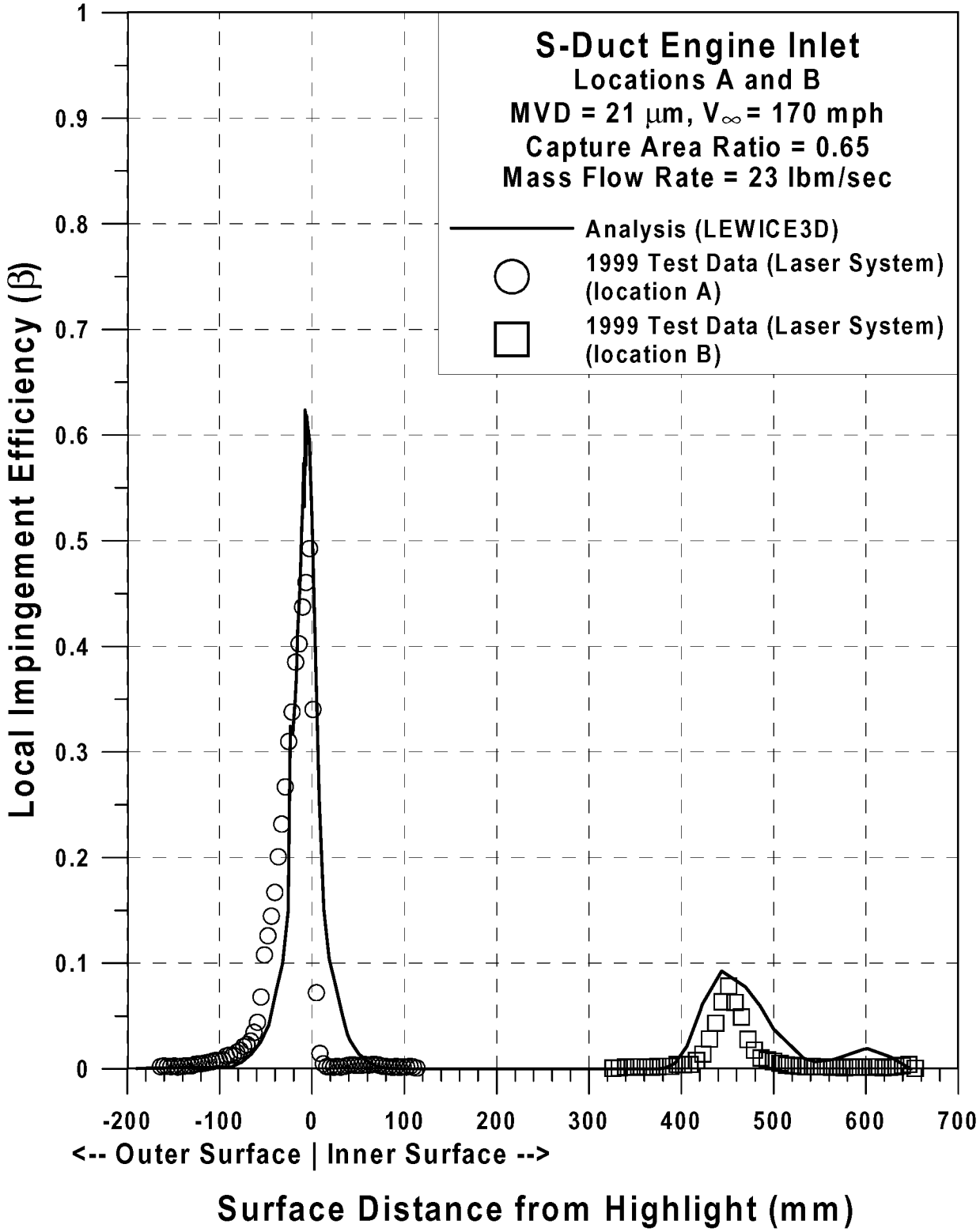

Fig. 107b Impingement efficiency distribution for S-duct engine inlet; locations A and B, V_∞ = 170 mph, $\alpha=0^\circ$, CAR=0.65, MVD =21 μm (Continued).

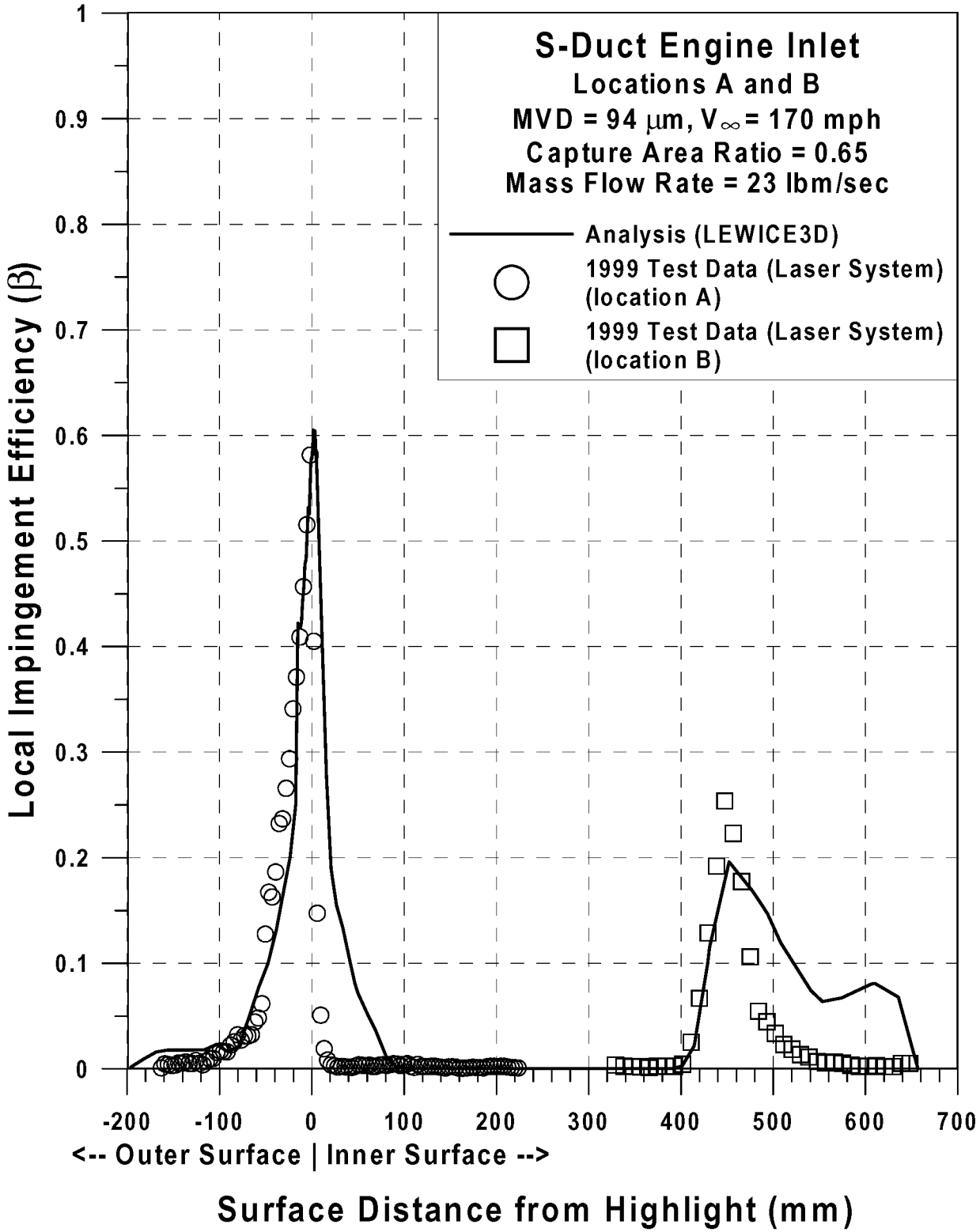

Fig. 107c Impingement efficiency distribution for S-duct engine inlet; locations A and B, V_∞ = 170 mph, $\alpha=0^\circ$, CAR=0.65, MVD =94 μm (Continued).

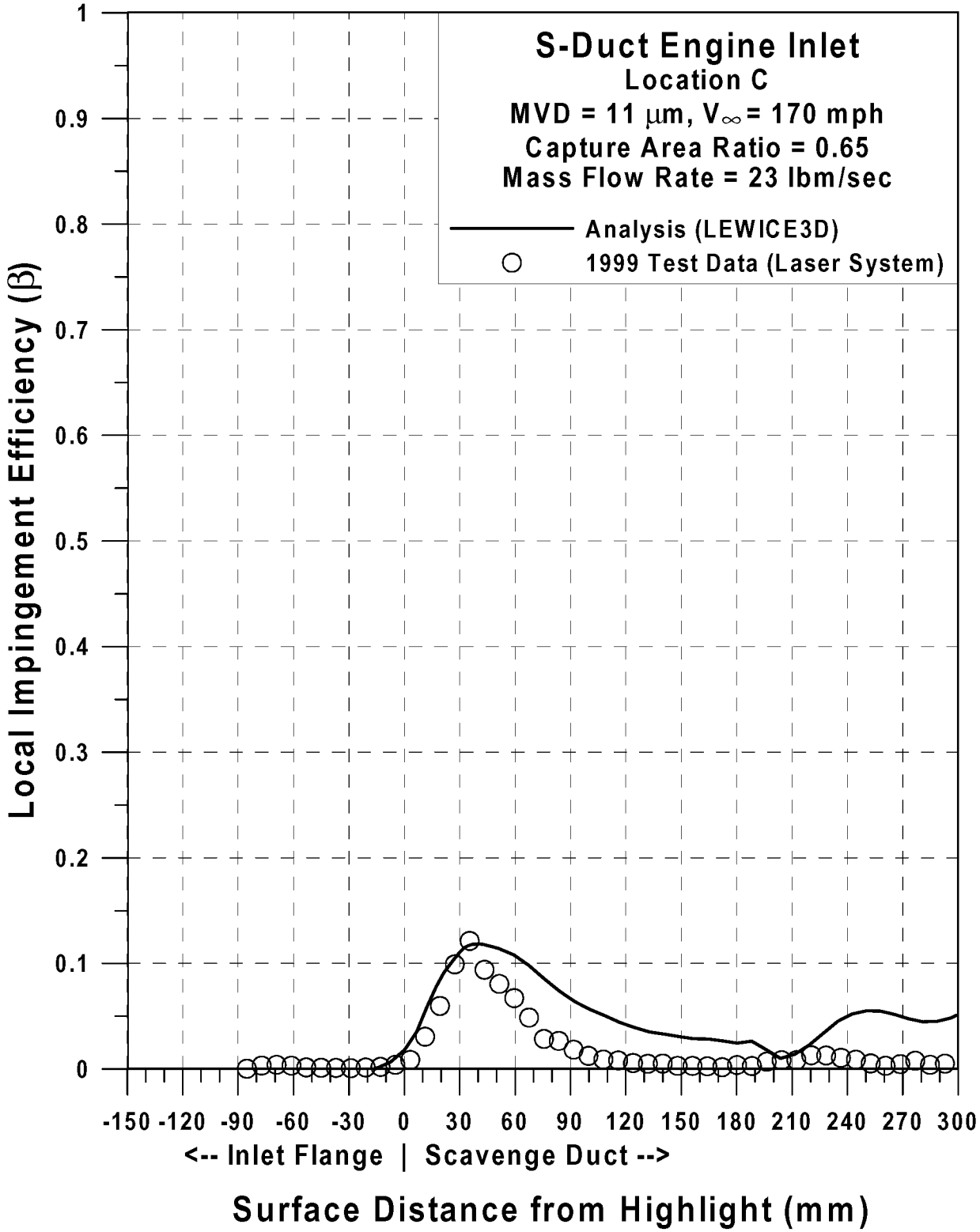

Fig. 107d Impingement efficiency distribution for S-duct engine inlet; location C, V_∞ = 170 mph, α=0°, CAR=0.65, MVD =11 μm (Continued).

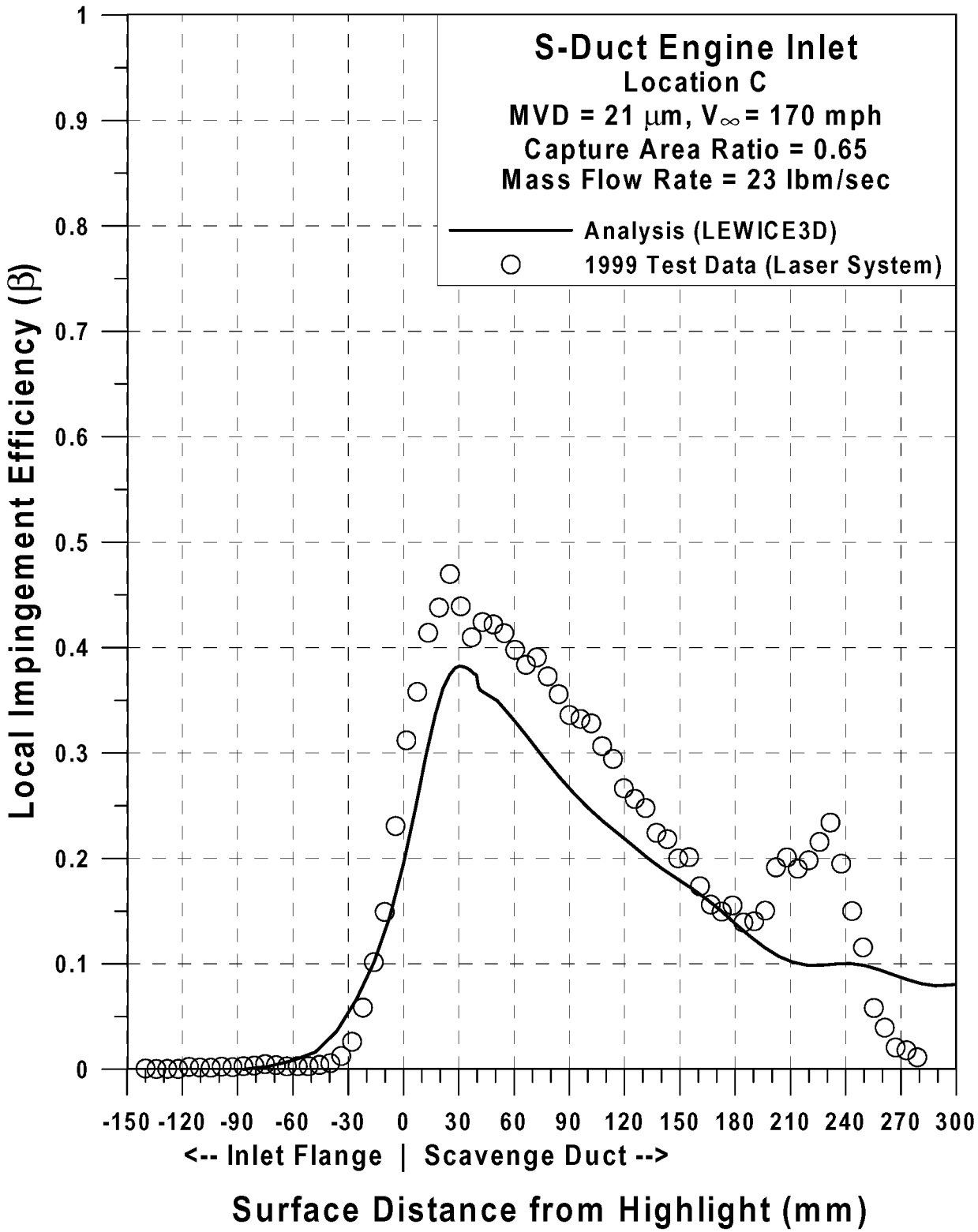

Fig. 107e Impingement efficiency distribution for S-duct engine inlet; location C, V_∞ = 170 mph, α=0°, CAR=0.65, MVD =21 μm (Continued).

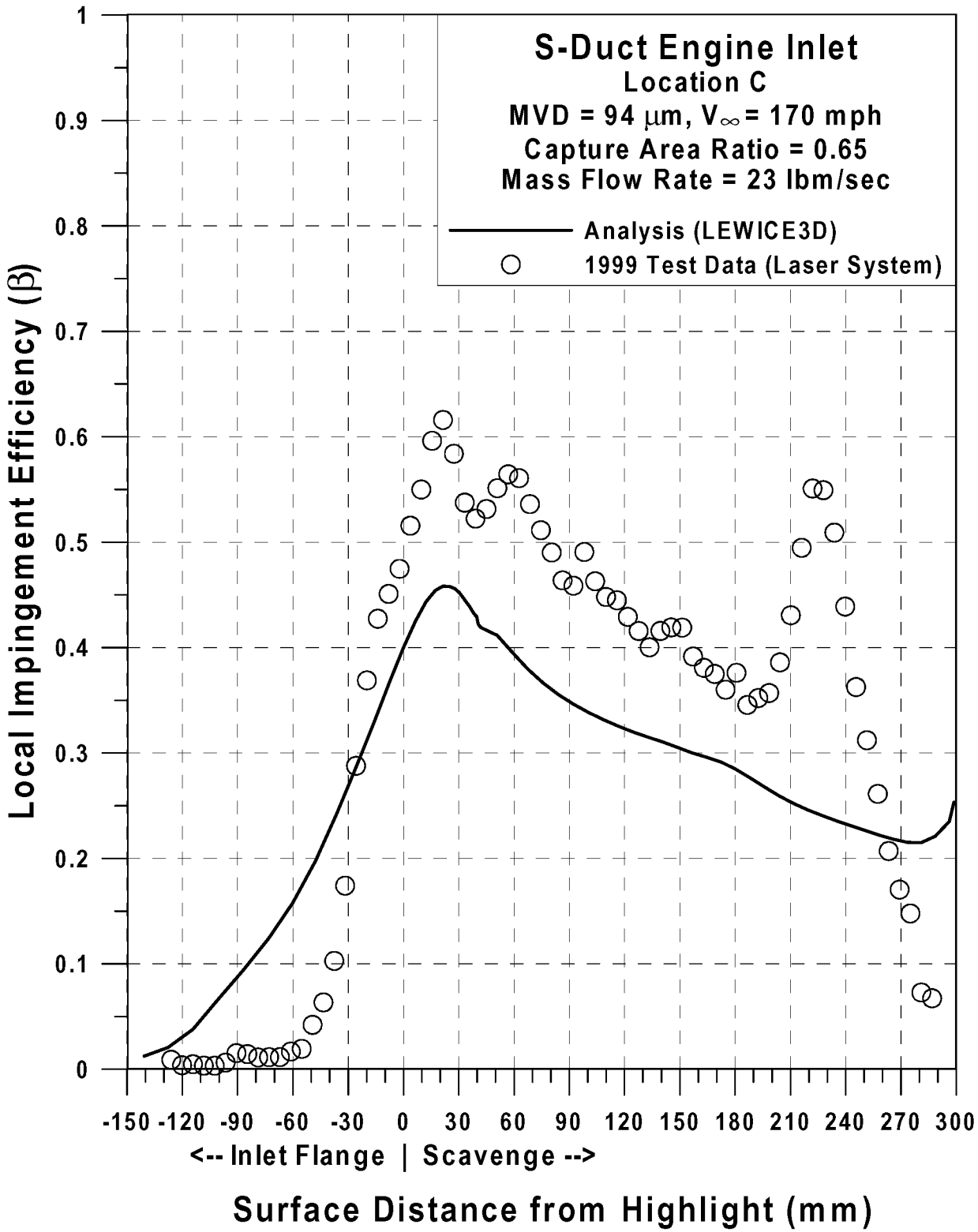

Fig. 107f Impingement efficiency distribution for S-duct engine inlet; location C, V_∞ = 170 mph, α=0°, CAR=0.65, MVD =94 μm (Continued).

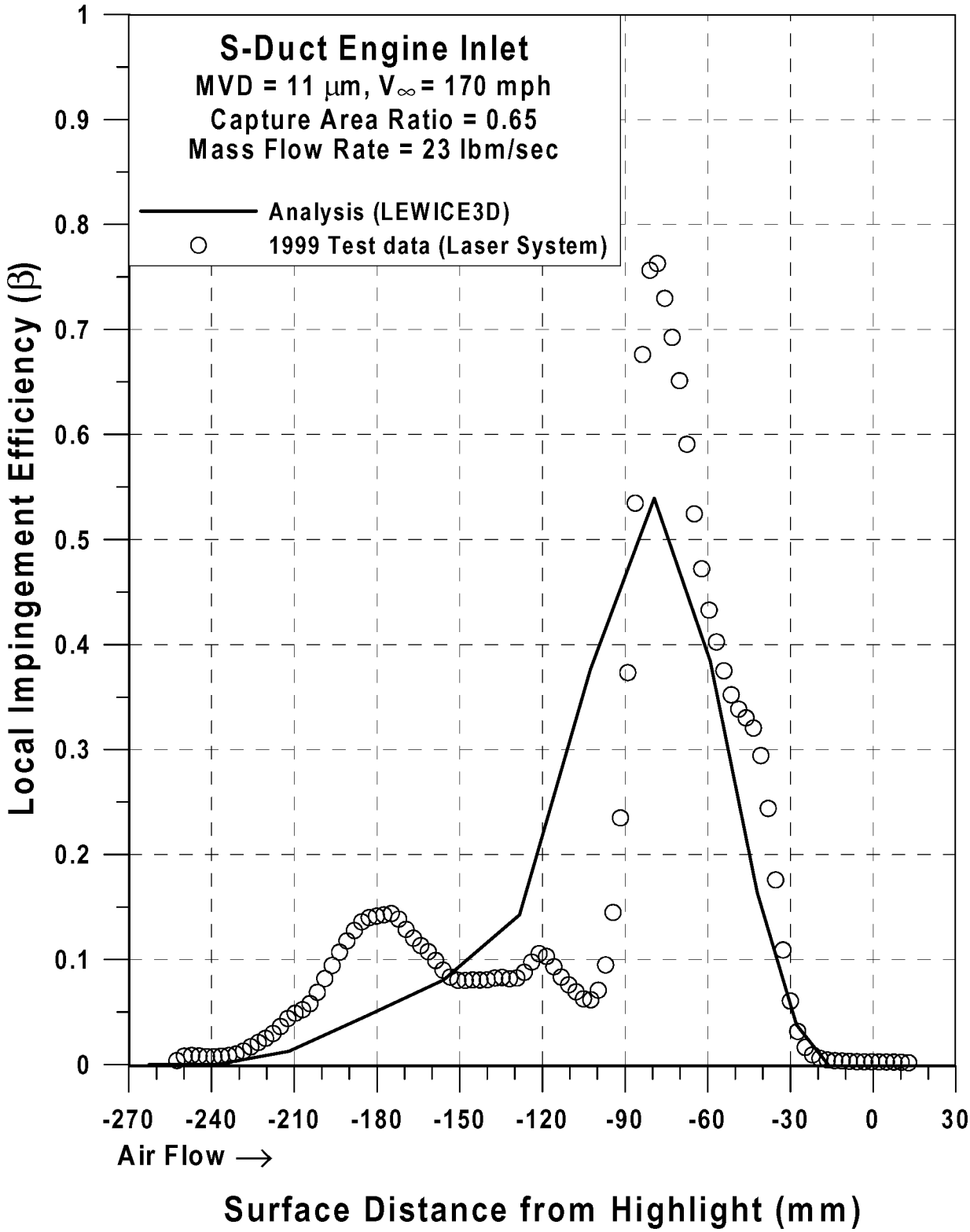

Fig. 107g Impingement efficiency distribution for S-duct engine inlet; location D, V_∞ = 170 mph, α=0°, CAR=0.65, MVD =11 μm (Continued).

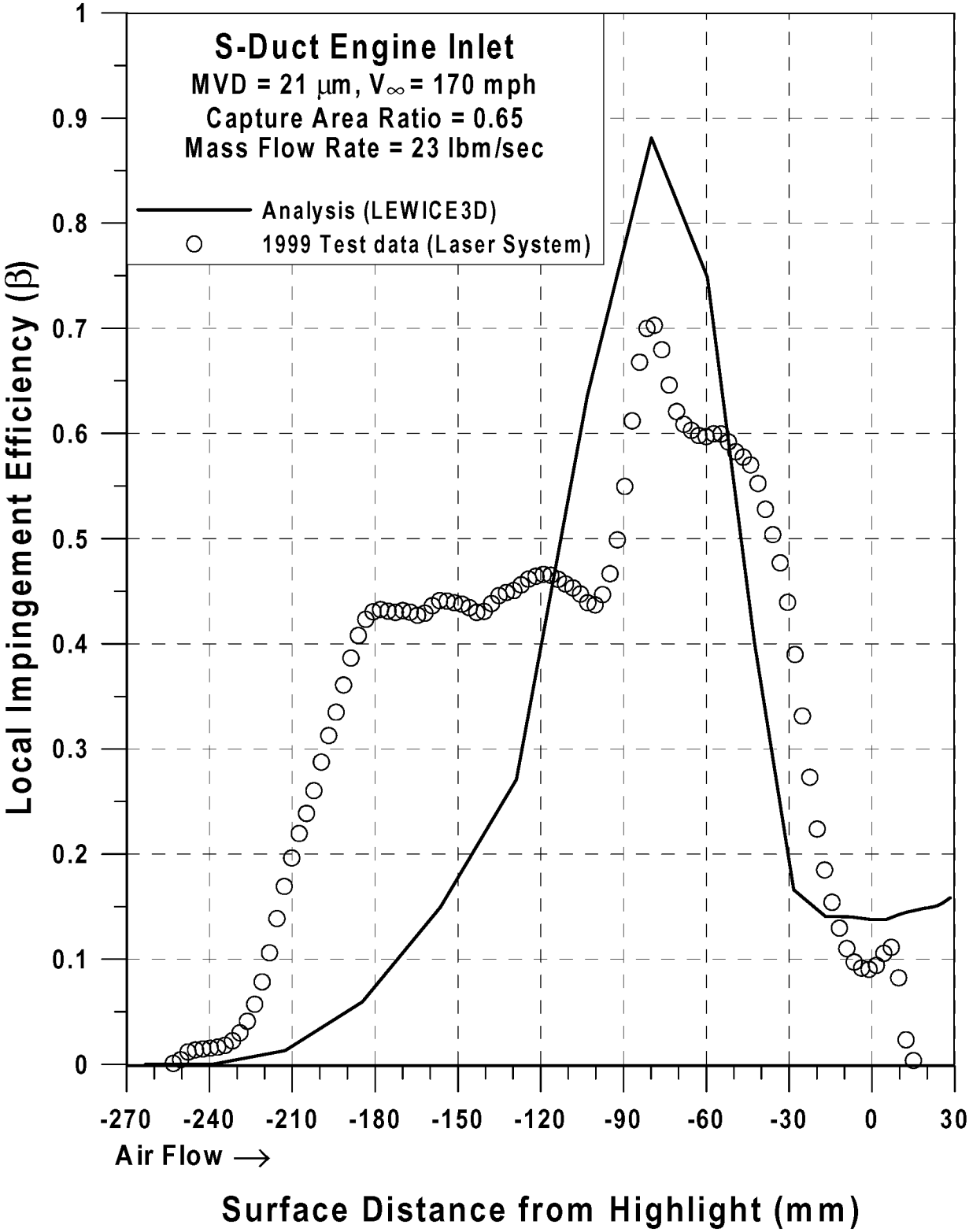

Fig. 107h Impingement efficiency distribution for S-duct engine inlet; location D, V_∞ = 170 mph, α=0°, CAR=0.65, MVD =21 μm (Continued).

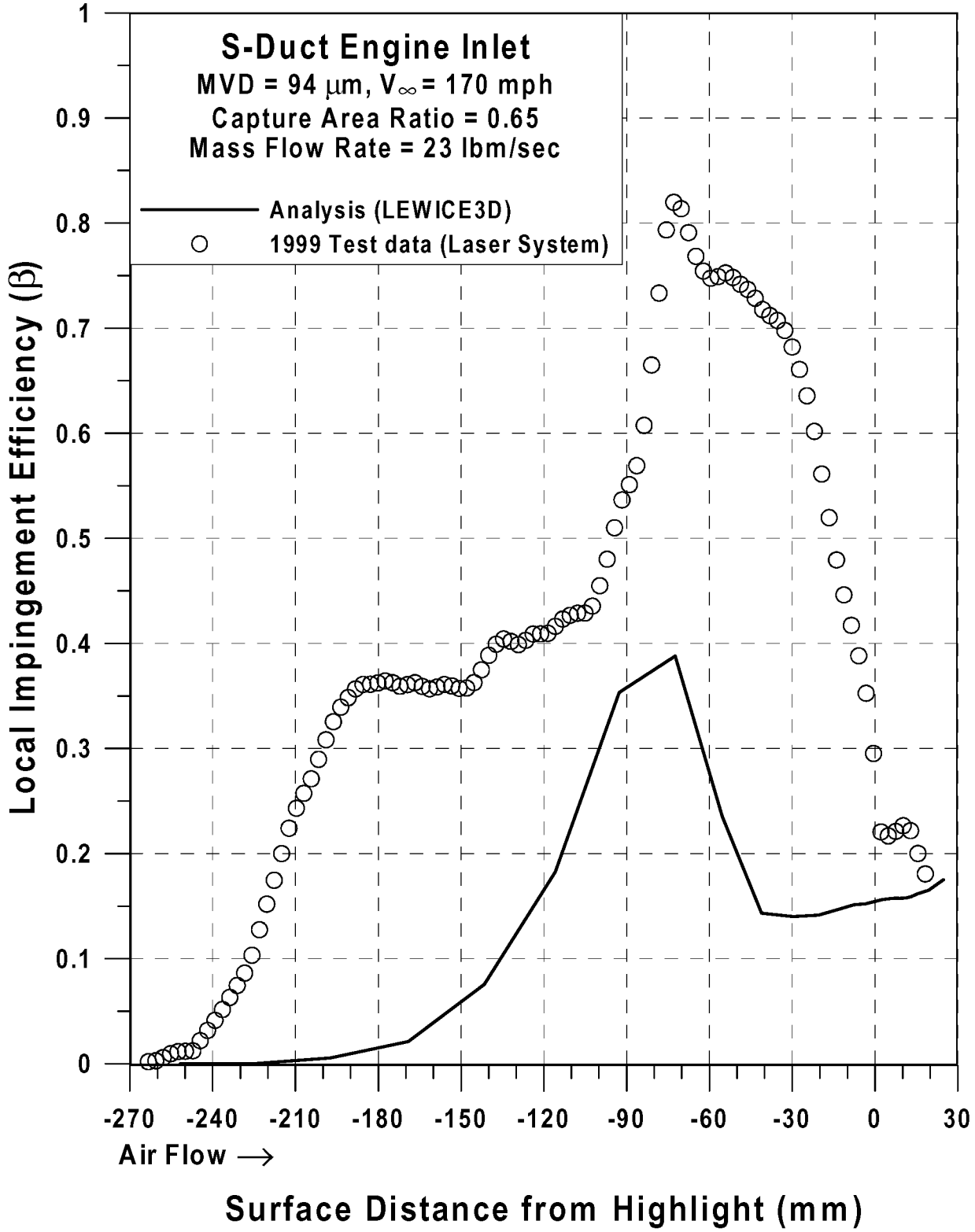

Fig. 107i Impingement efficiency distribution for S-duct engine inlet; location D, V_∞ = 170 mph, α=0°, CAR=0.65, MVD =94 μm (Continued).

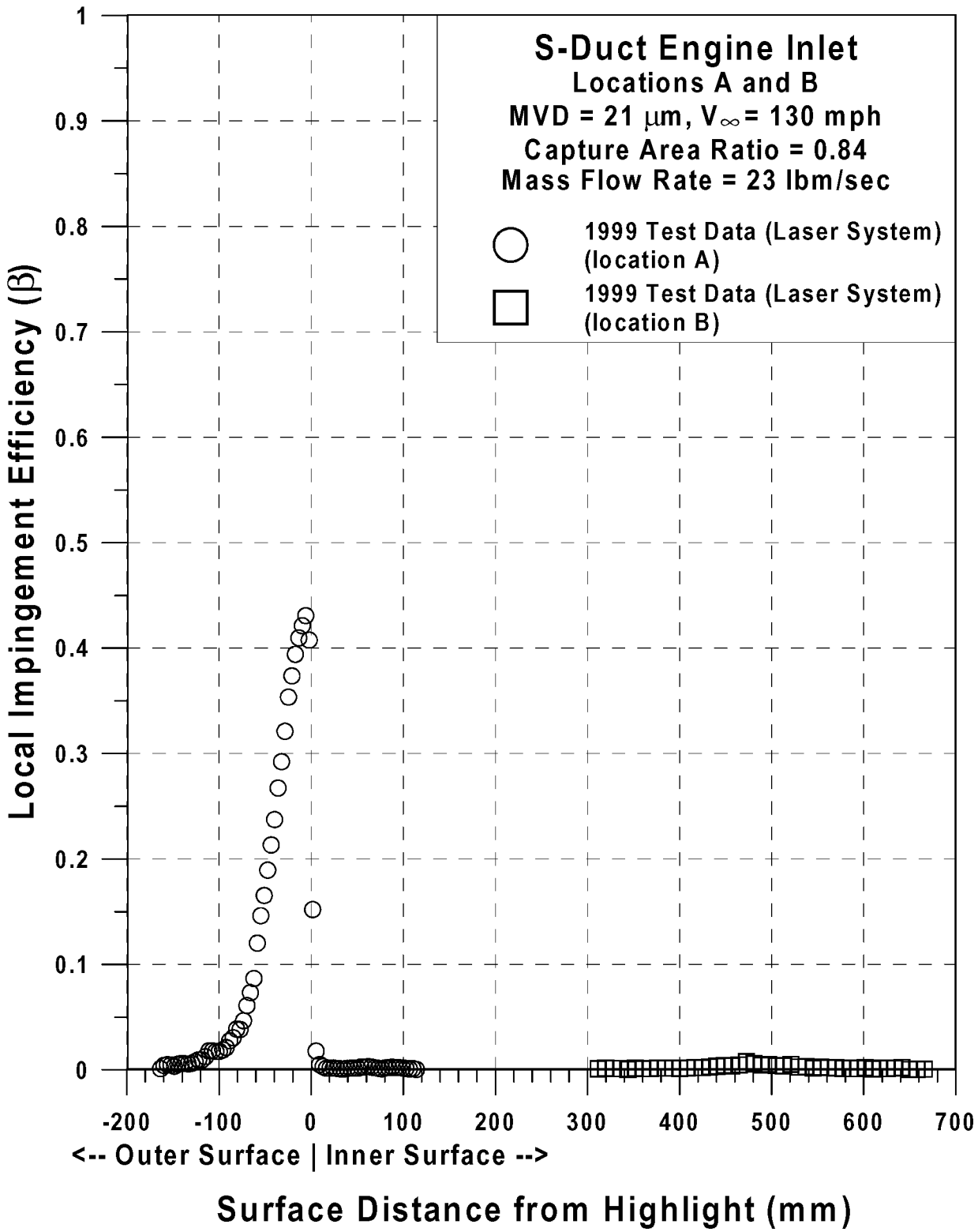

Fig. 107j Impingement efficiency distribution for S-duct engine inlet; locations A and B, V_∞ = 130 mph, $\alpha=0^\circ$, CAR=0.84, MVD =21 μm (Continued).

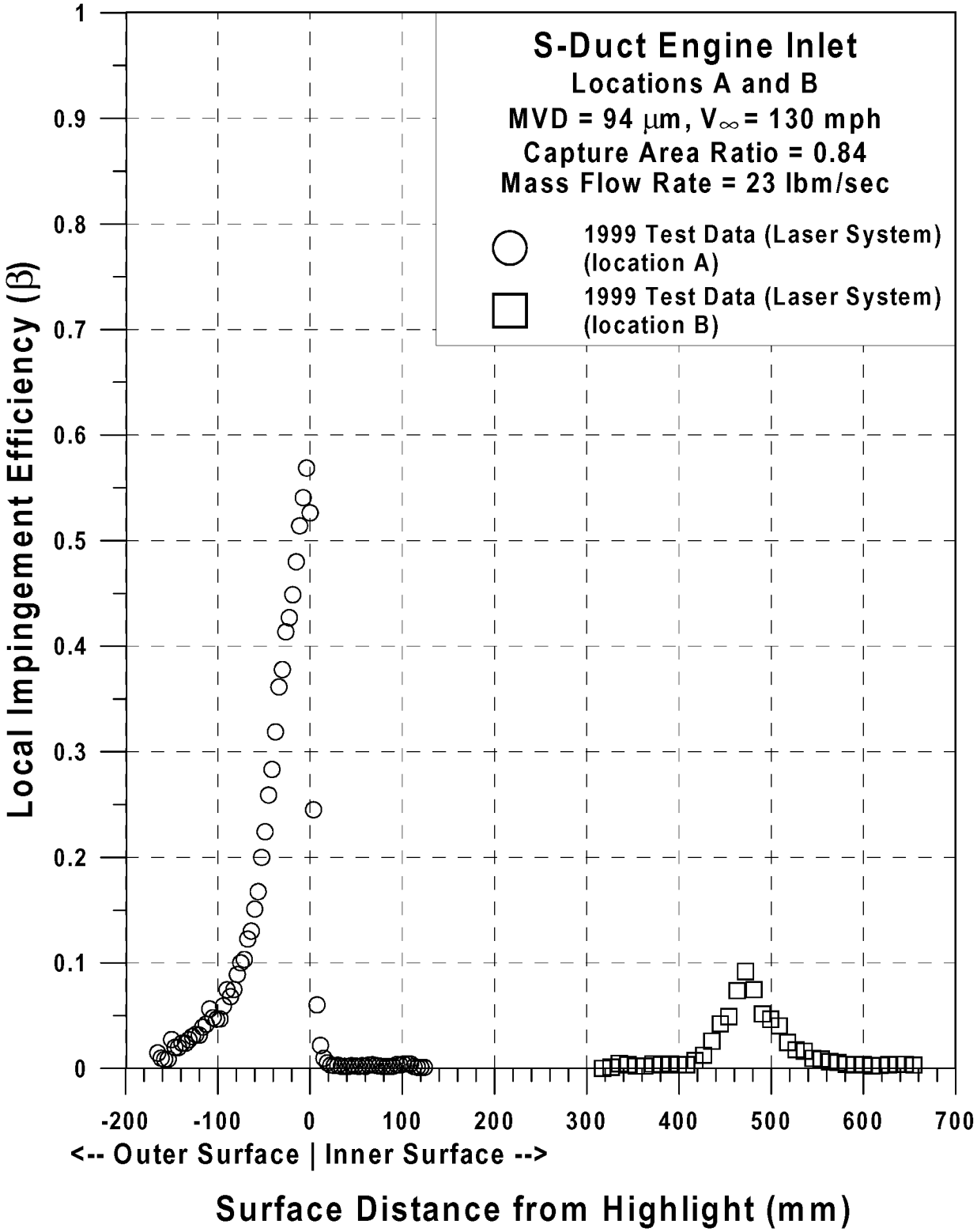

Fig. 107k Impingement efficiency distribution for S-duct engine inlet; locations A and B, V_∞ = 130 mph, α=0°, CAR=0.84, MVD =94 μm (Continued).

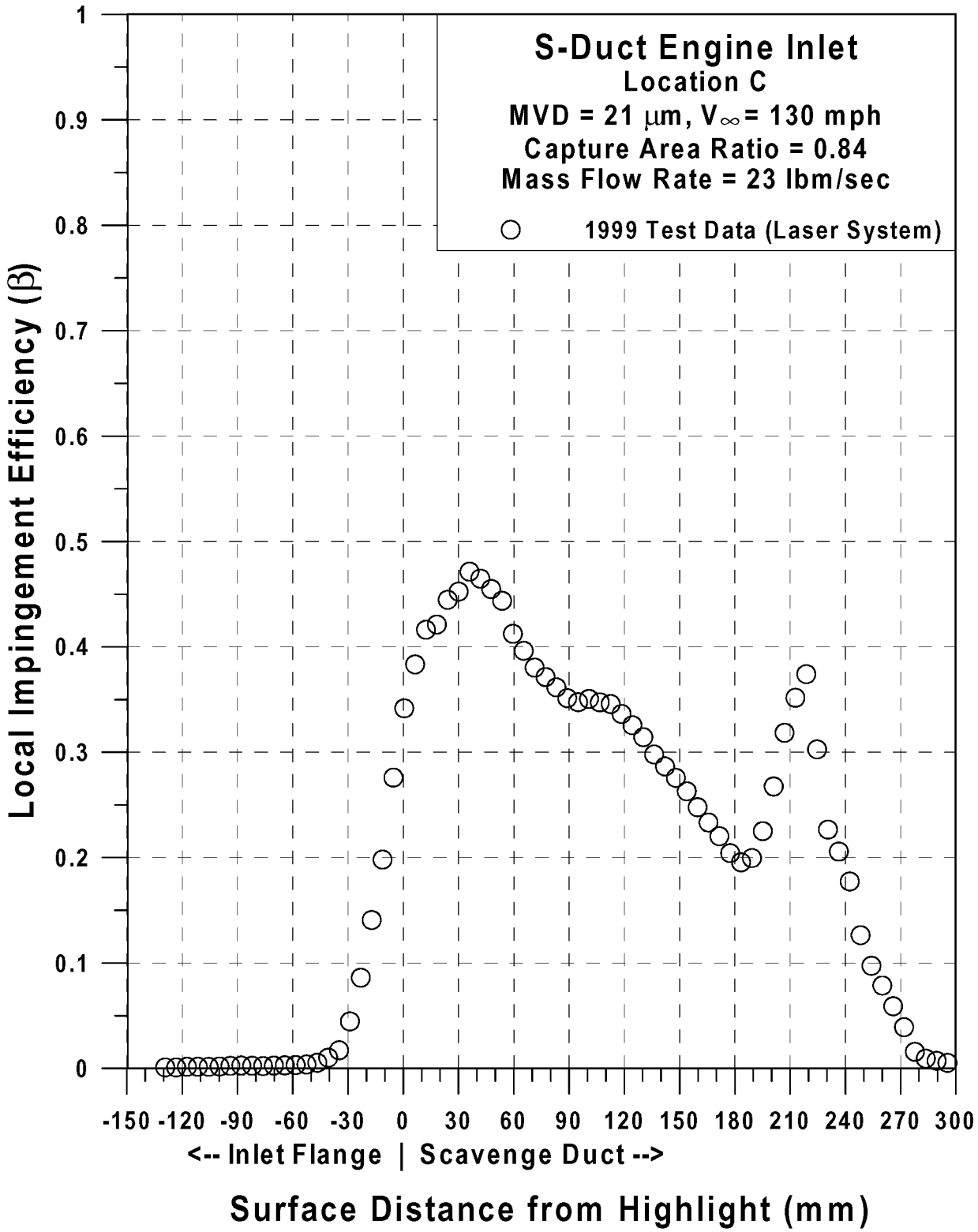

Fig. 107l Impingement efficiency distribution for S-duct engine inlet; location C, V_∞ = 130 mph, α=0°, CAR=0.84, MVD =21 μm (Continued).

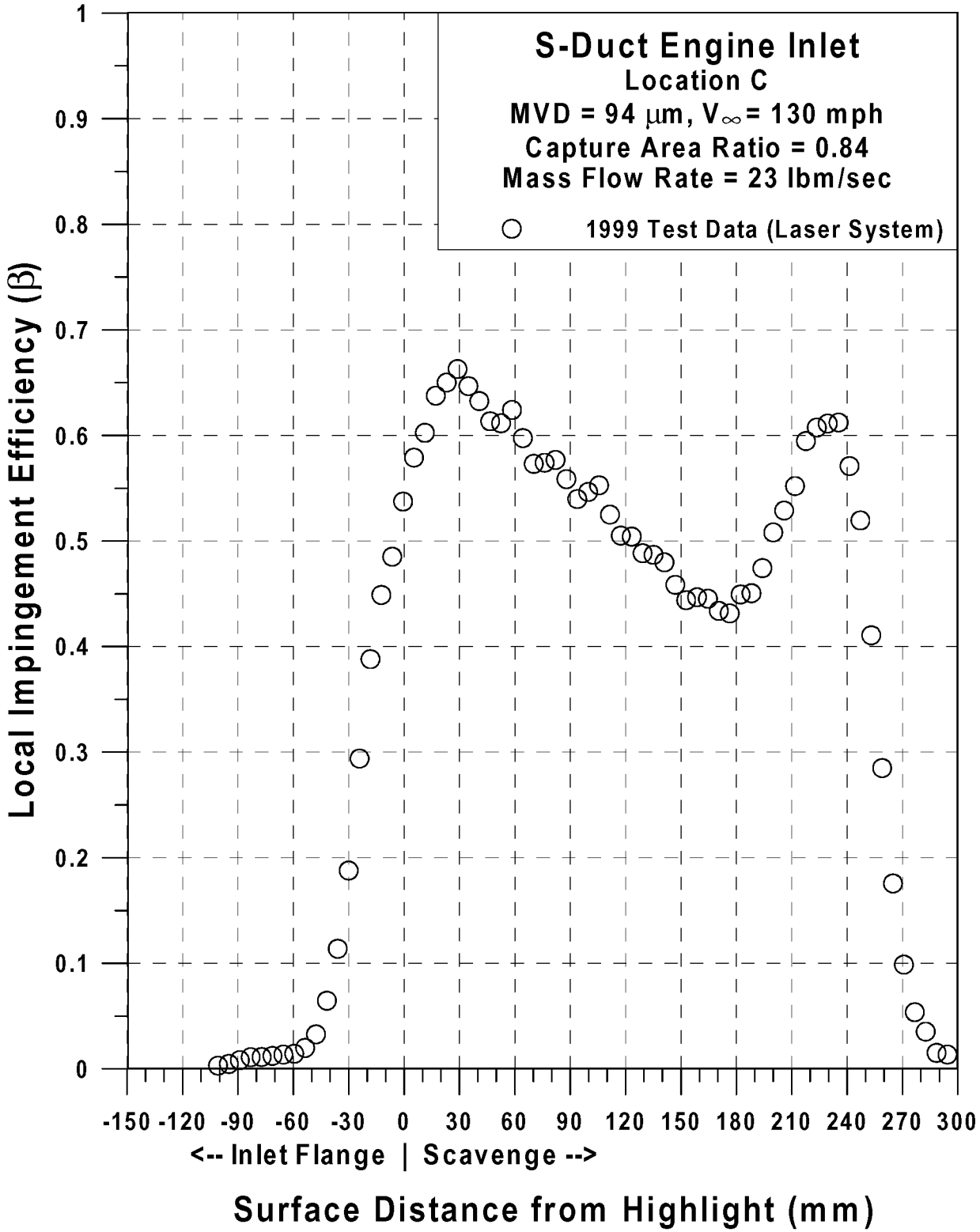

Fig. 107m Impingement efficiency distribution for S-duct engine inlet; location C, V_∞ = 130 mph, α=0°, CAR=0.84, MVD =94 μm (Continued).

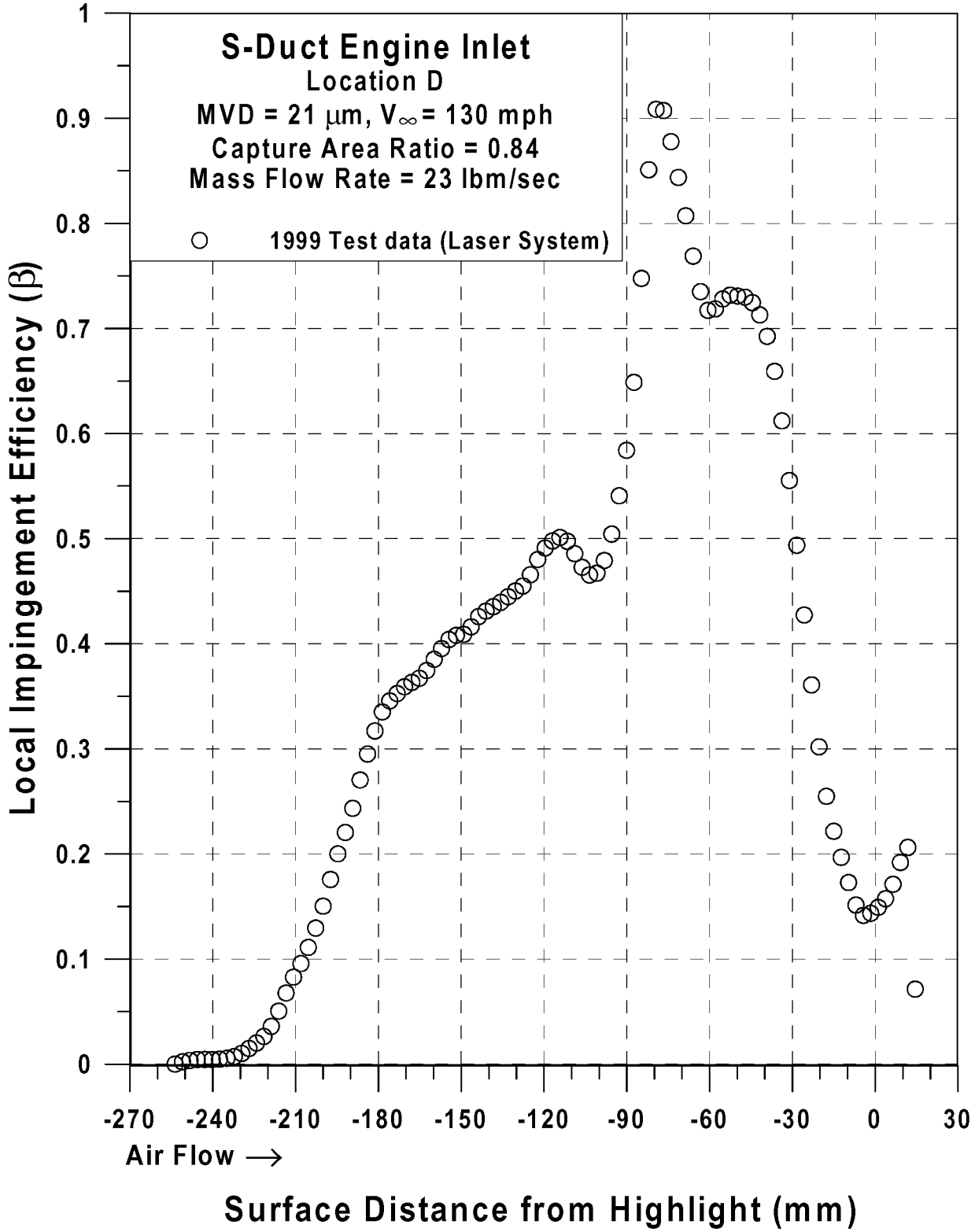

Fig. 107n Impingement efficiency distribution for S-duct engine inlet; location D, V_∞ = 130 mph, α=0°, CAR=0.84, MVD =21 μm (Continued).

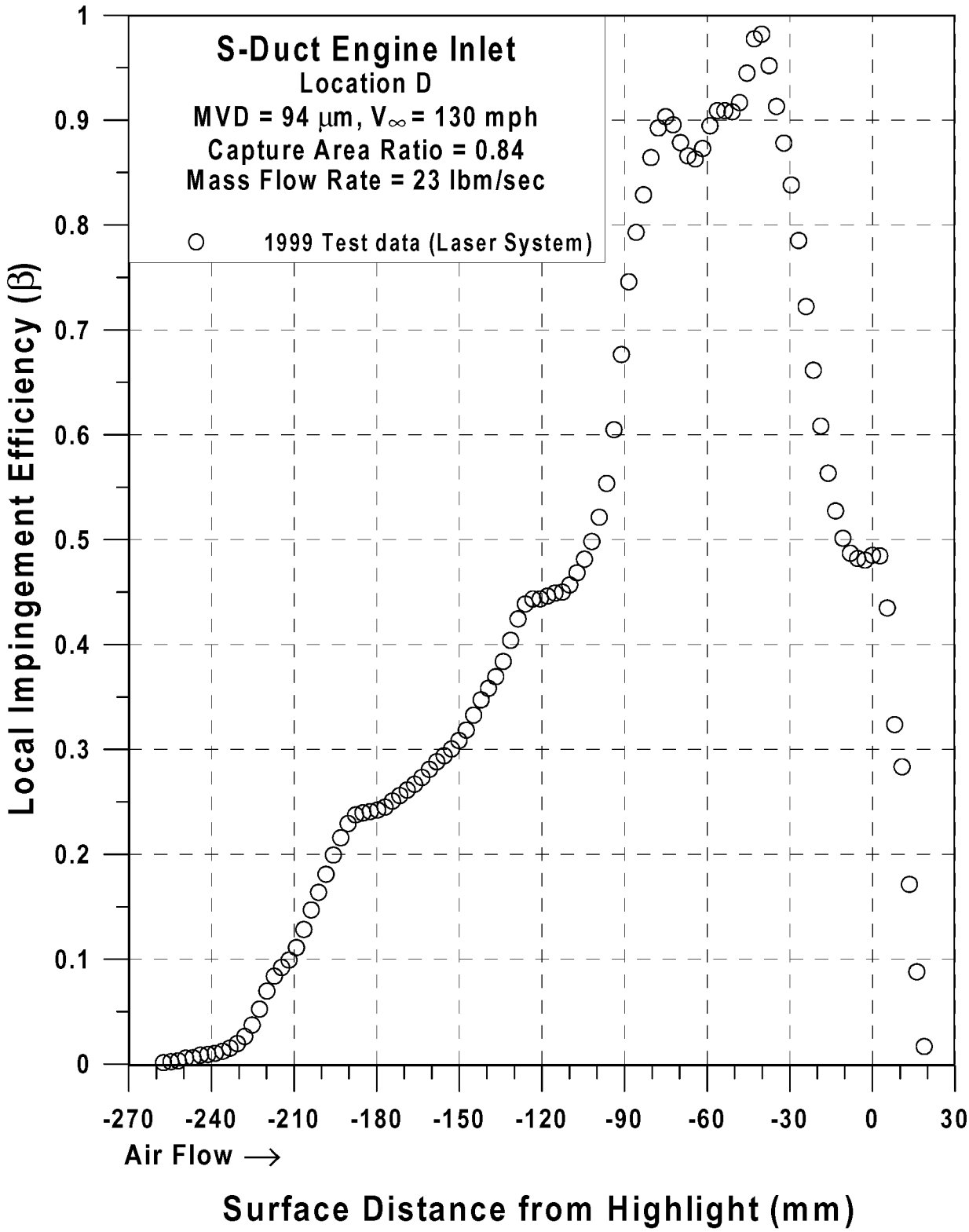

Fig. 107o Impingement efficiency distribution for S-duct engine inlet; location D, V_∞ = 130 mph, α=0°, CAR=0.84, MVD =94 μm (Continued).

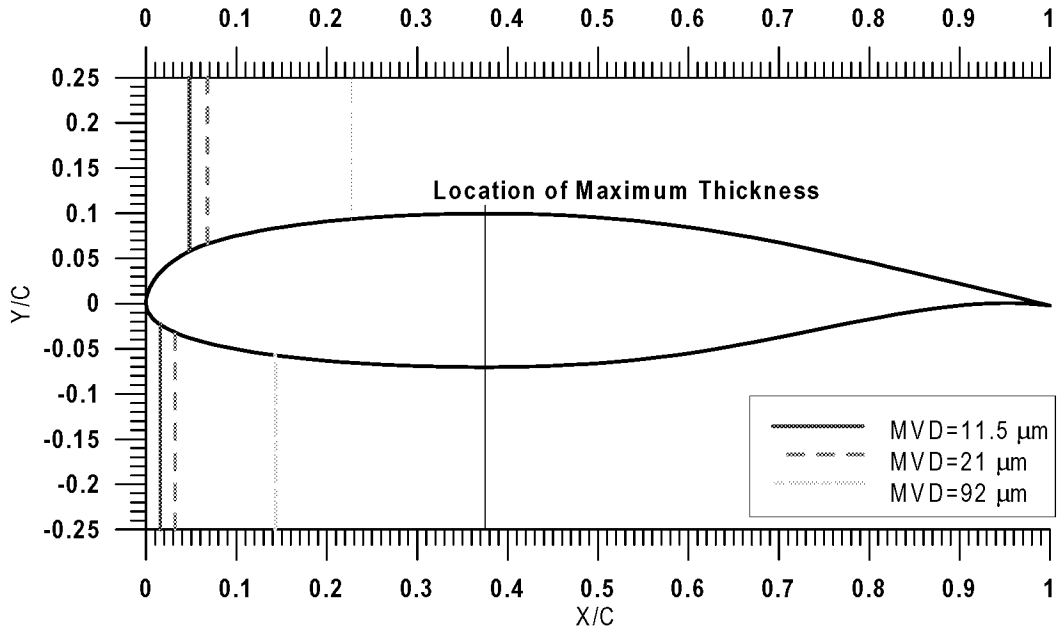

a. AOA = 0 deg.

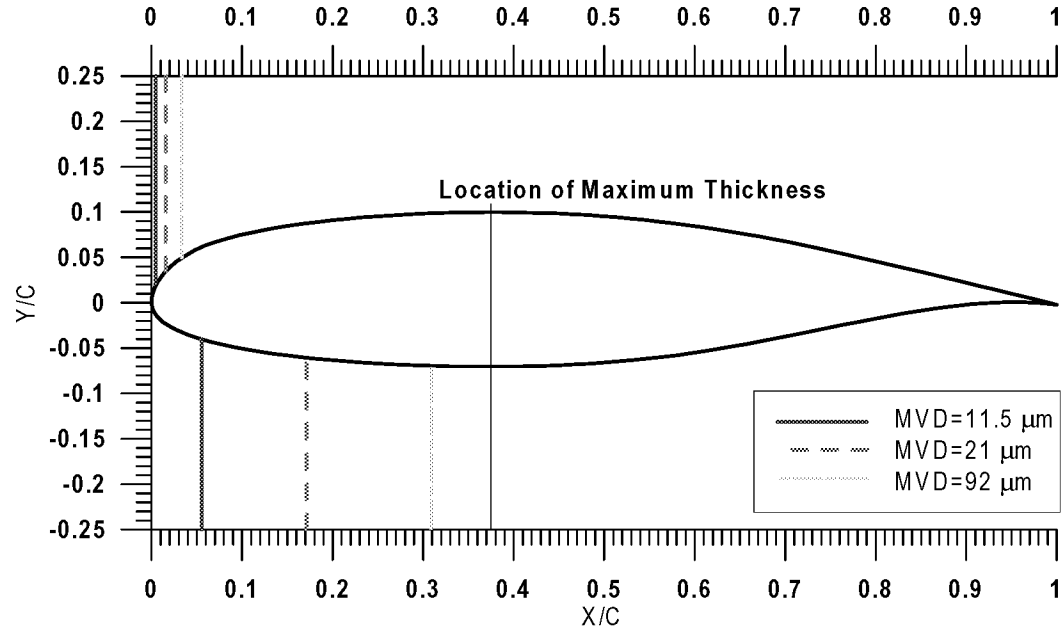

b. AOA = 8 deg.

Fig. 108 Experimental impingement limits for MS-317 airfoil - 1997 IRT tests (Continued).

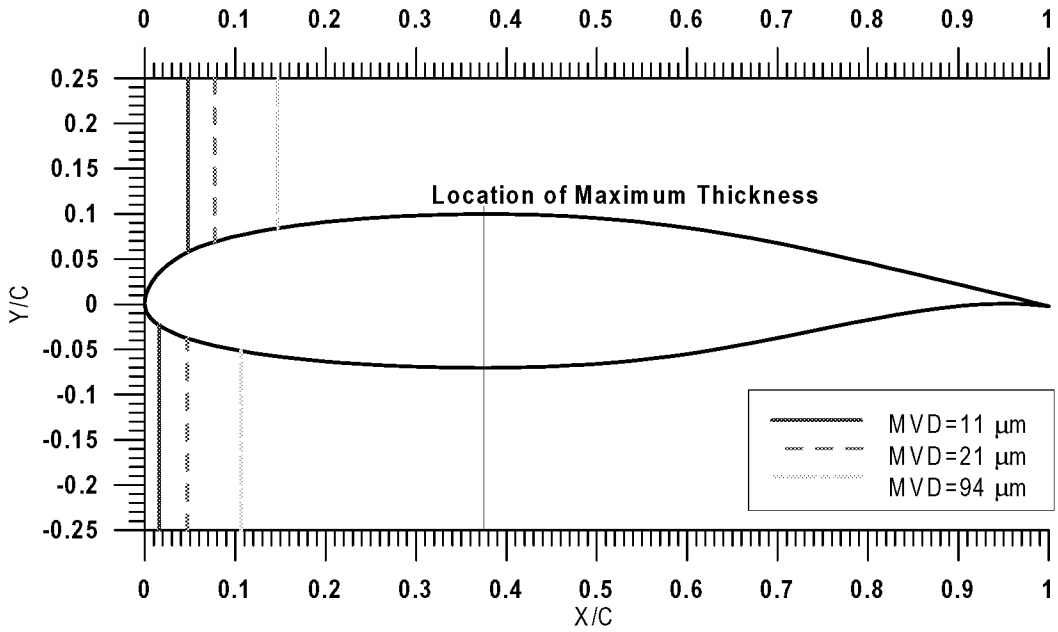

c. AOA = 0 deg.

Fig. 108 Experimental impingement limits for MS-317 airfoil - 1999 IRT tests.

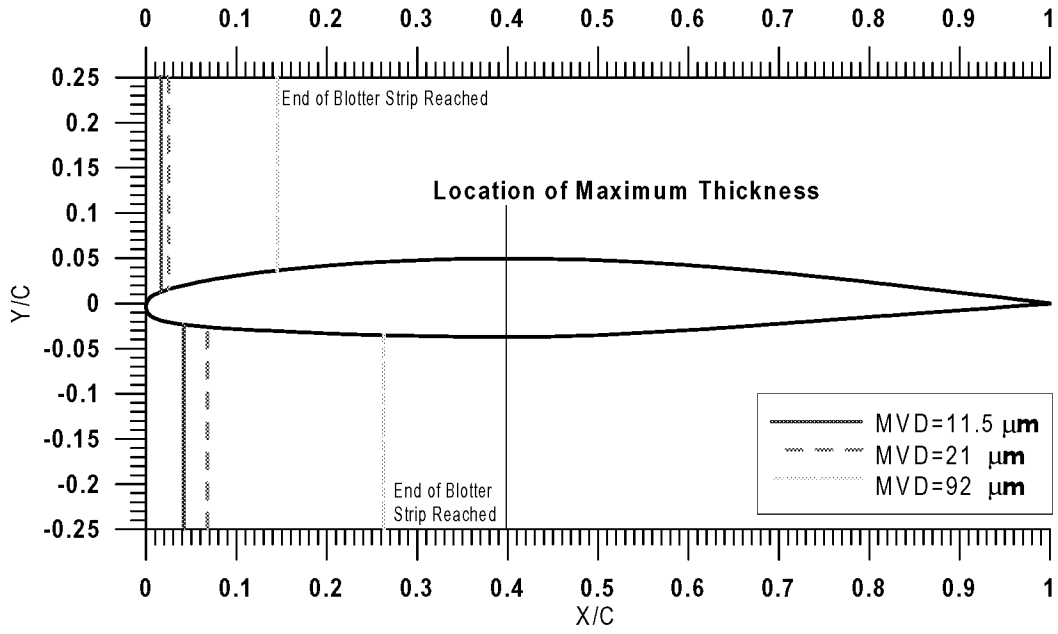

a. AOA = 1.5 deg.

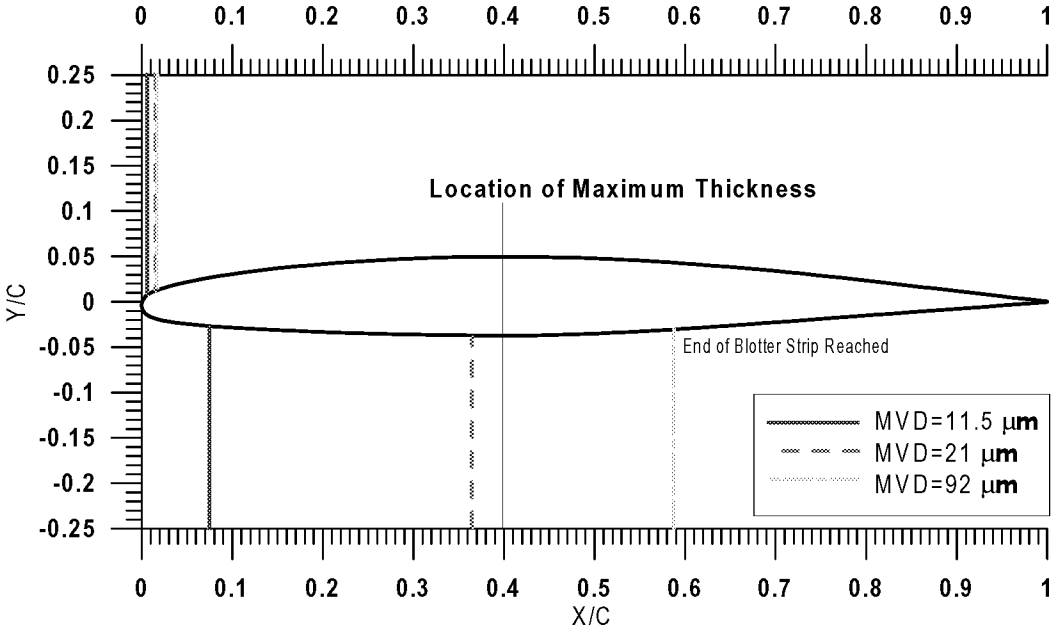

b. AOA = 6 deg.

Fig. 109 Experimental impingement limits for GLC-305 airfoil - 1997 IRT tests.

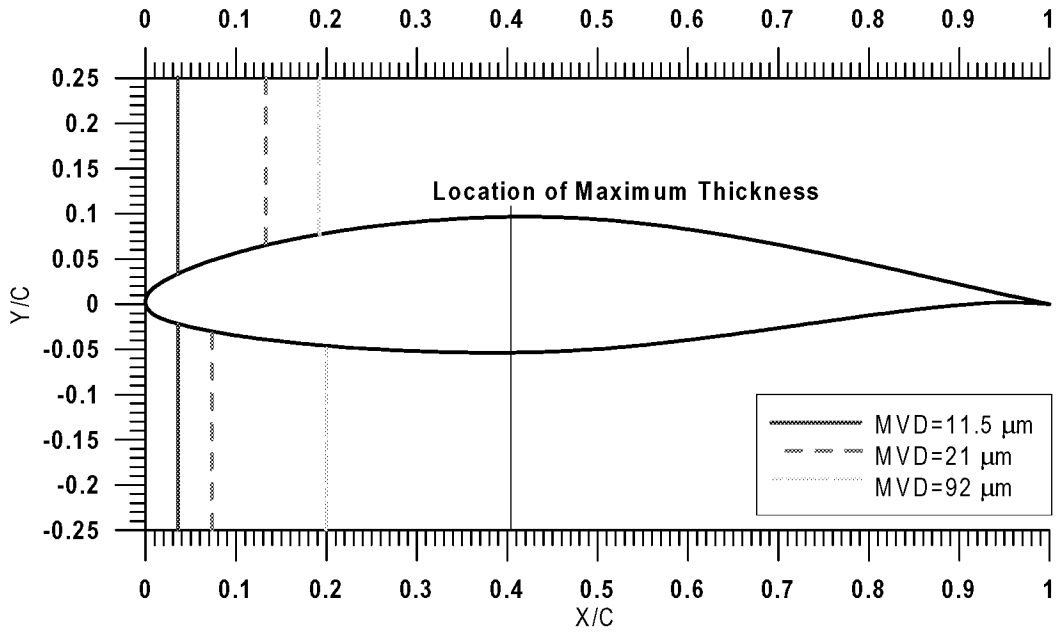

a. AOA = 0 deg.

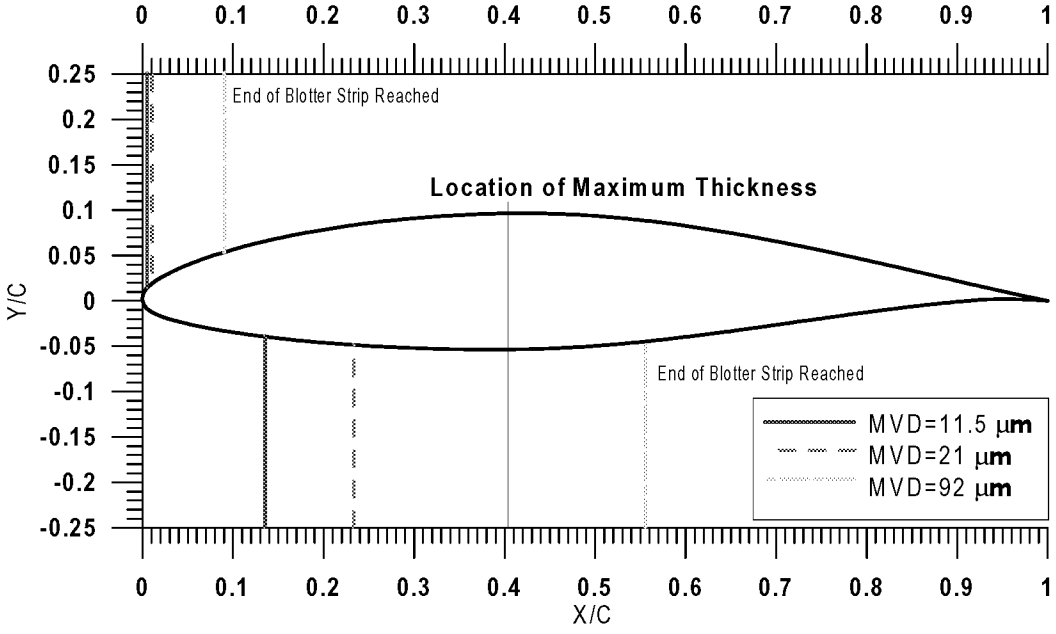

b. AOA = 8 deg.

Fig. 110 Experimental impingement limits for NACA 65_2-415 airfoil - 1997 IRT tests.

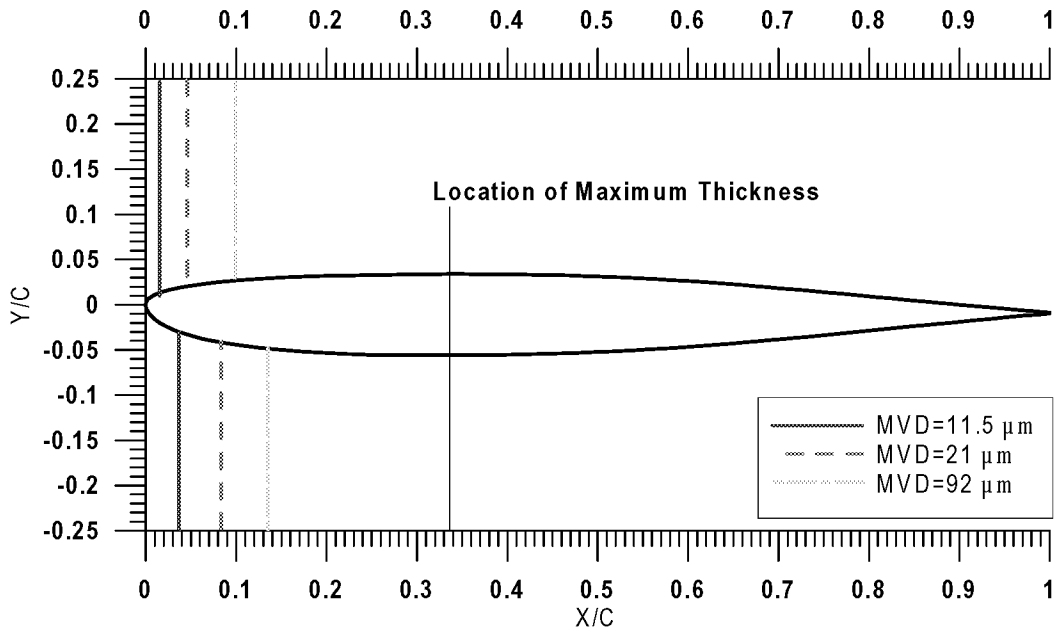

a. AOA = 0 deg.

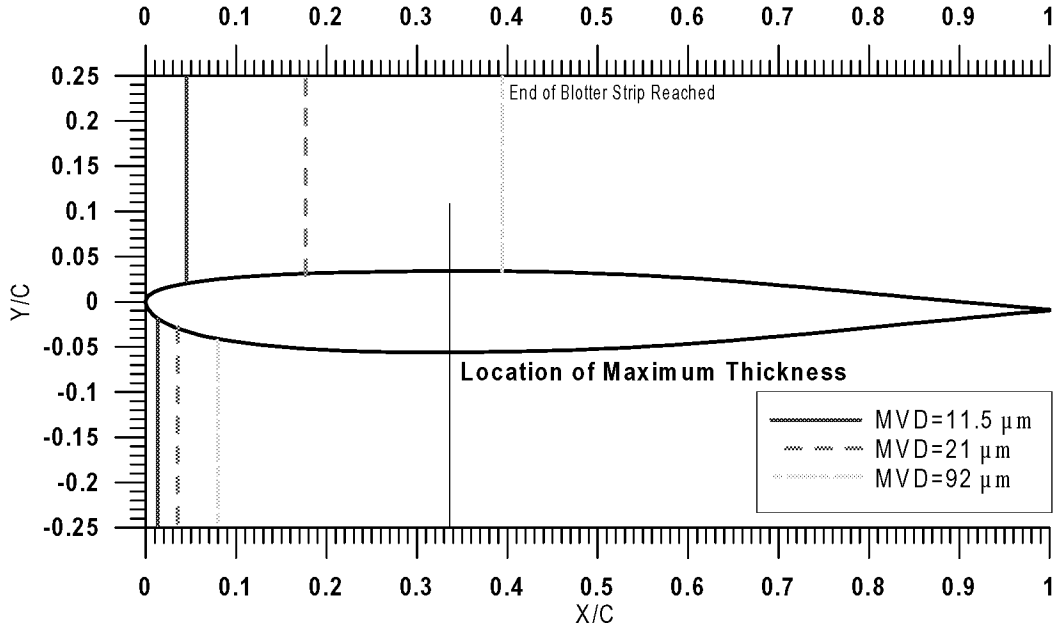

b. AOA = 4 deg.

Fig. 111 Experimental impingement limits for commercial transport tail section - 1997 IRT tests.

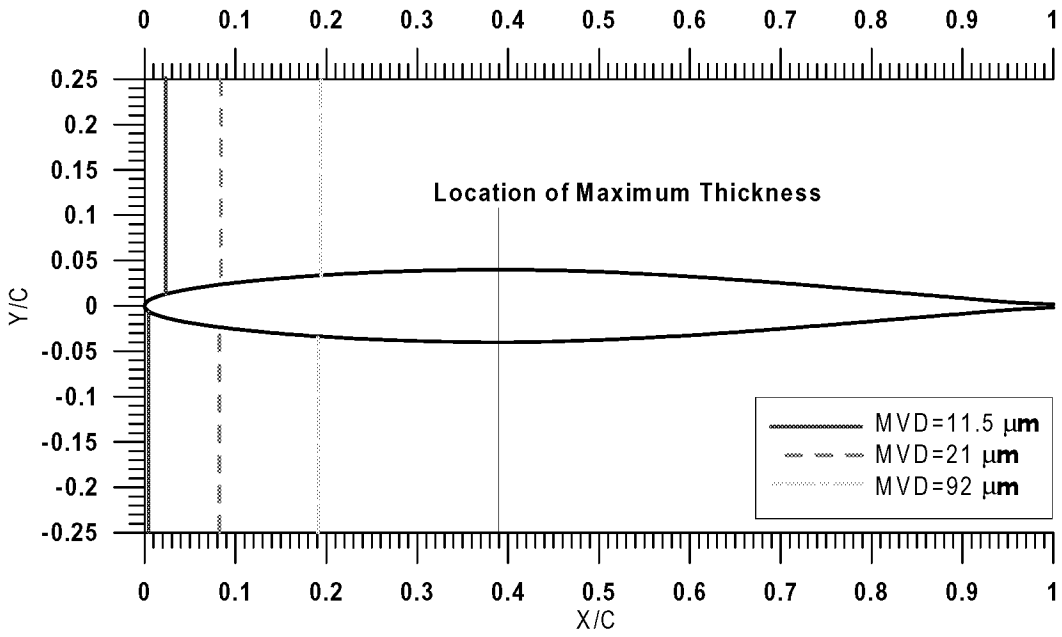

a. AOA = 0 deg.

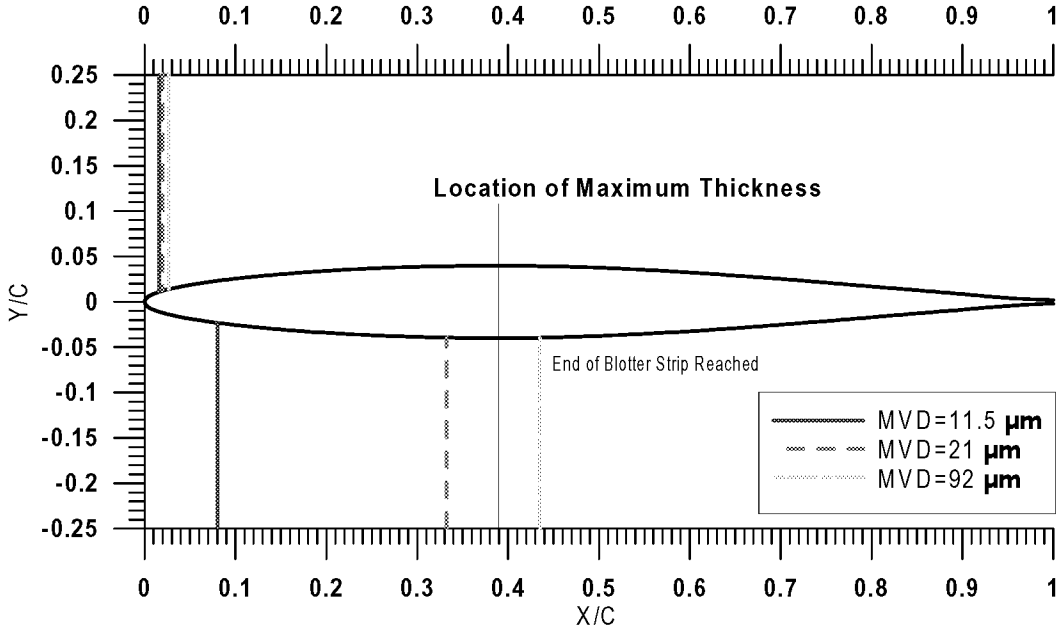

b. AOA = 6 deg.

Fig. 112 Experimental impingement limits for NACA 64A008 tail section - 1997 IRT tests.

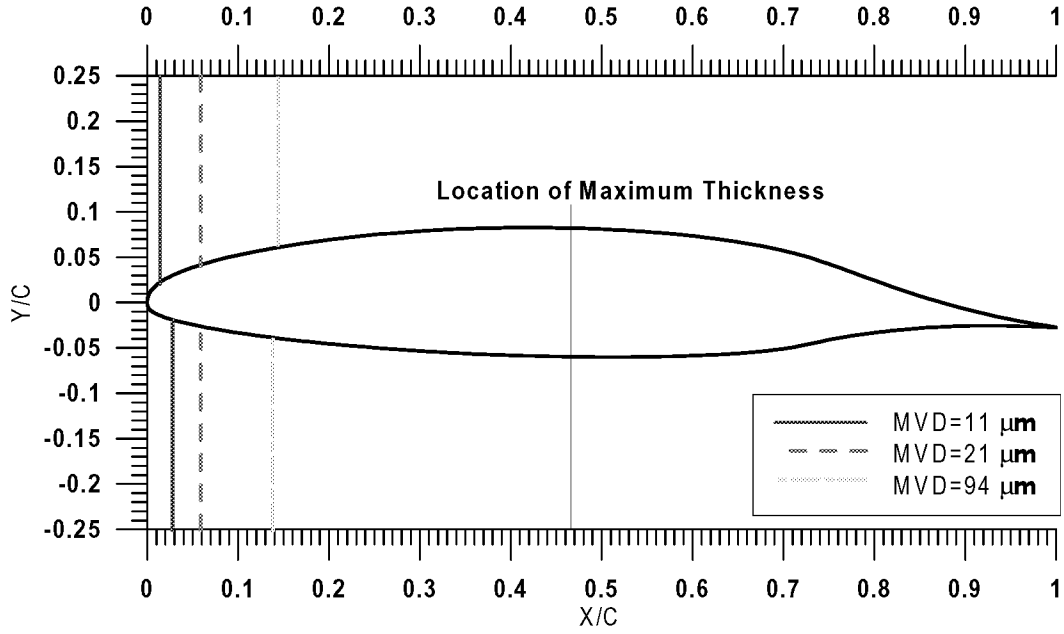

a. AOA = 0 deg.

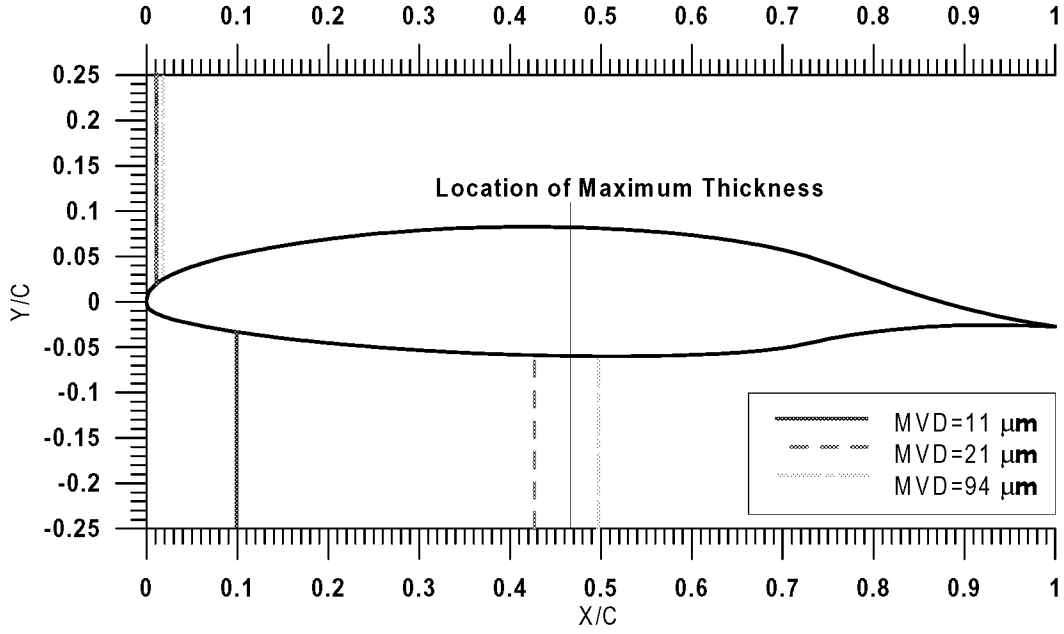

b. AOA = 8 deg.

Fig. 113 Experimental impingement limits for 36-in NLF(1)-0414 airfoil - 1999 IRT tests.

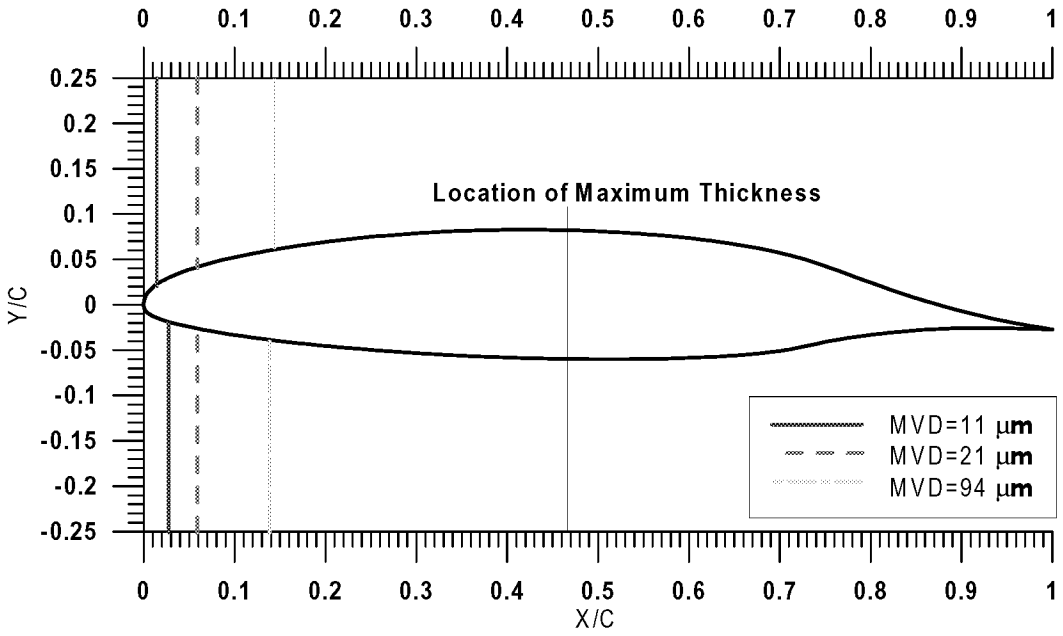

a. AOA = 0 deg., δ = 0 deg.

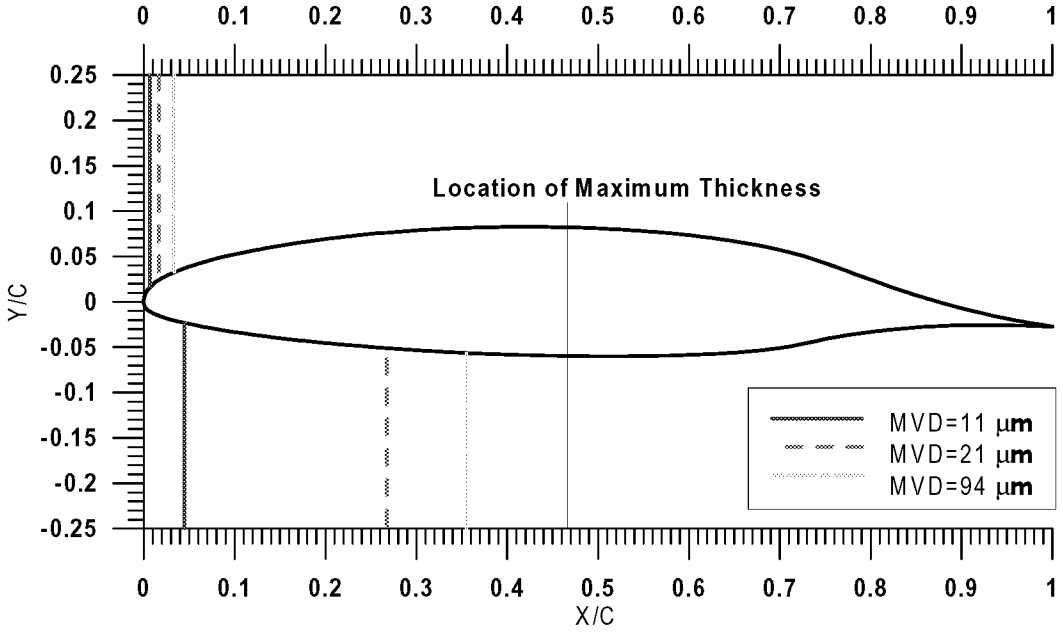

b. AOA = 4 deg., δ = 0 deg.

Fig. 114 Experimental impingement limits for 48-in NLF(1)-0414 airfoil - 1999 IRT tests (Continued).

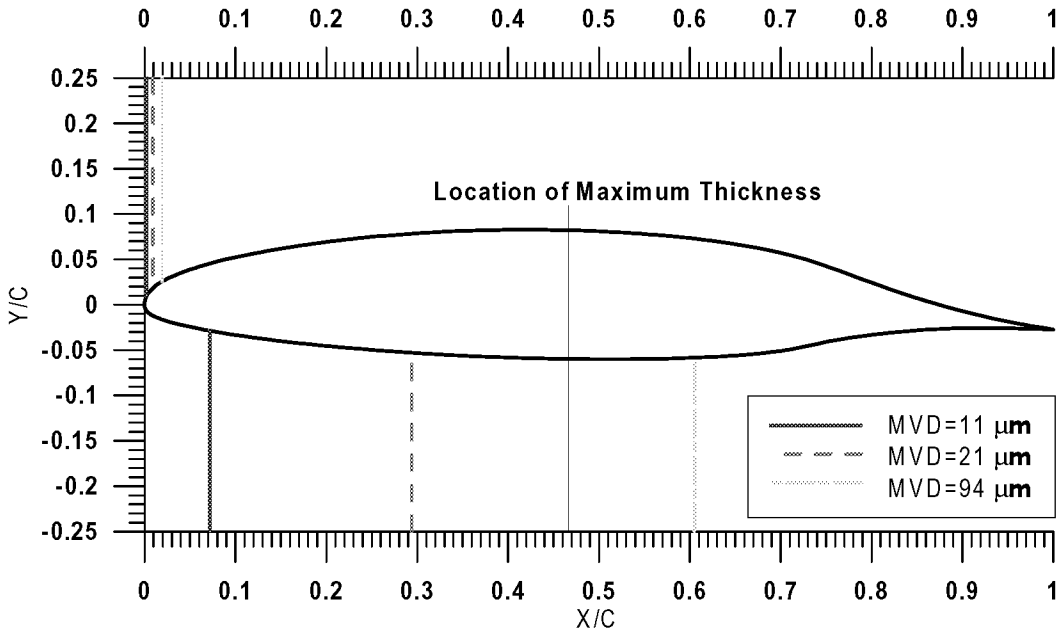

c. AOA = 8 deg., δ = 0 deg.

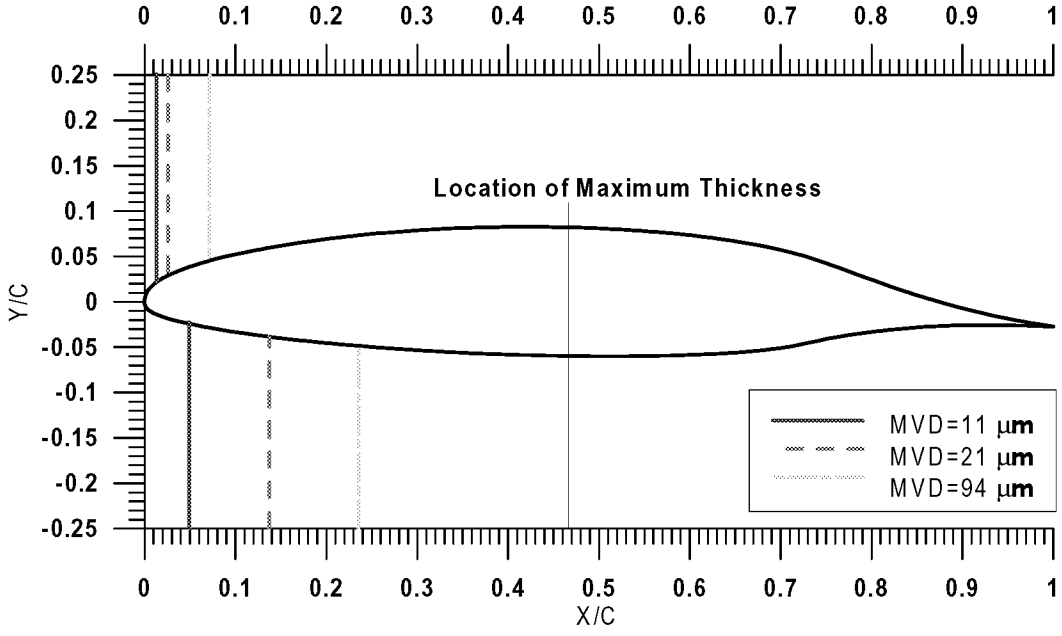

d. AOA = 0 deg., δ = 15 deg.

Fig. 114 Experimental impingement limits for 48-in NLF(1)-0414 airfoil - 1999 IRT tests.

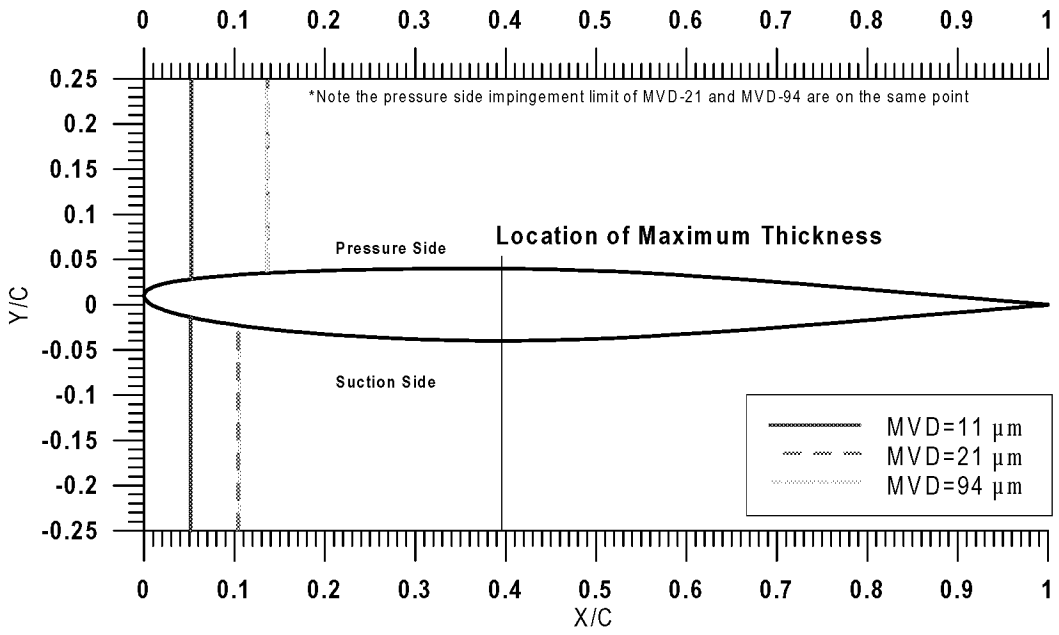

a. AOA = -1 deg., δ = 0 deg.

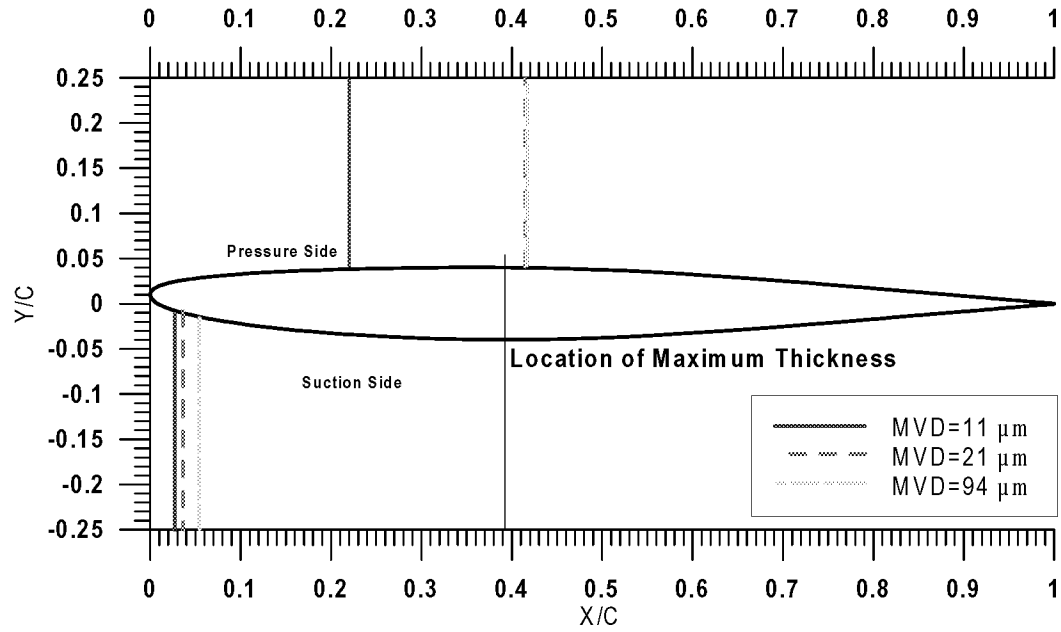

b. AOA = -6 deg., δ = 0 deg.

Fig. 115 Experimental impingement limits for 25%-scale Business Jet Empennage, Inboard, 1999 IRT tests (Continued).

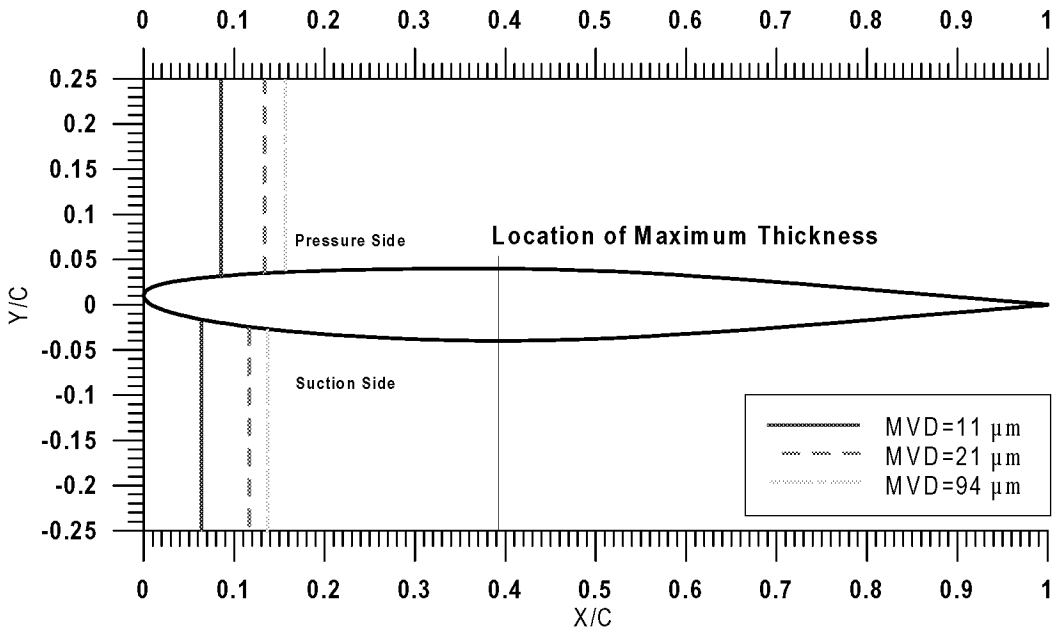

a. AOA = -1 deg., δ = 0 deg.

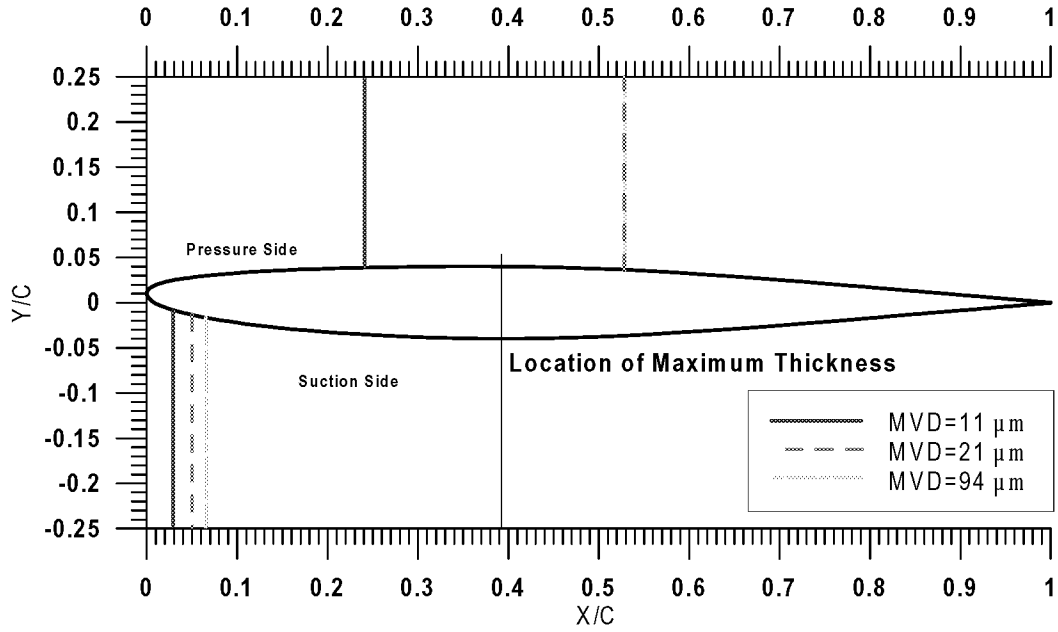

b. AOA = -6 deg., δ = 0 deg.

Fig. 115 Experimental impingement limits for 25%-scale Business Jet Empennage; Outboard, 1999 IRT tests.

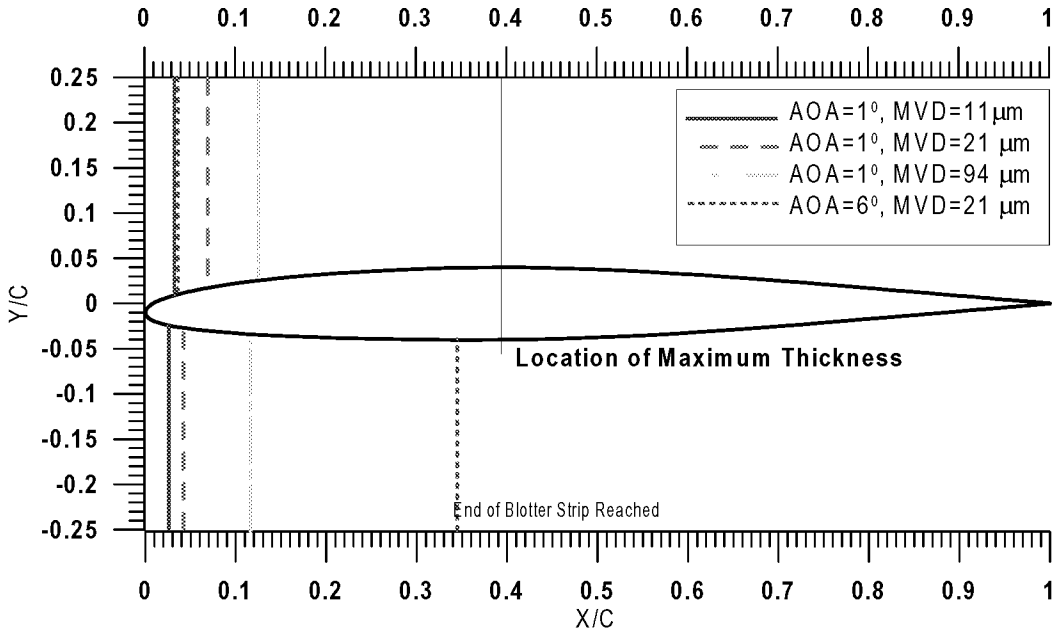

a. δ = 0 deg., Inboard

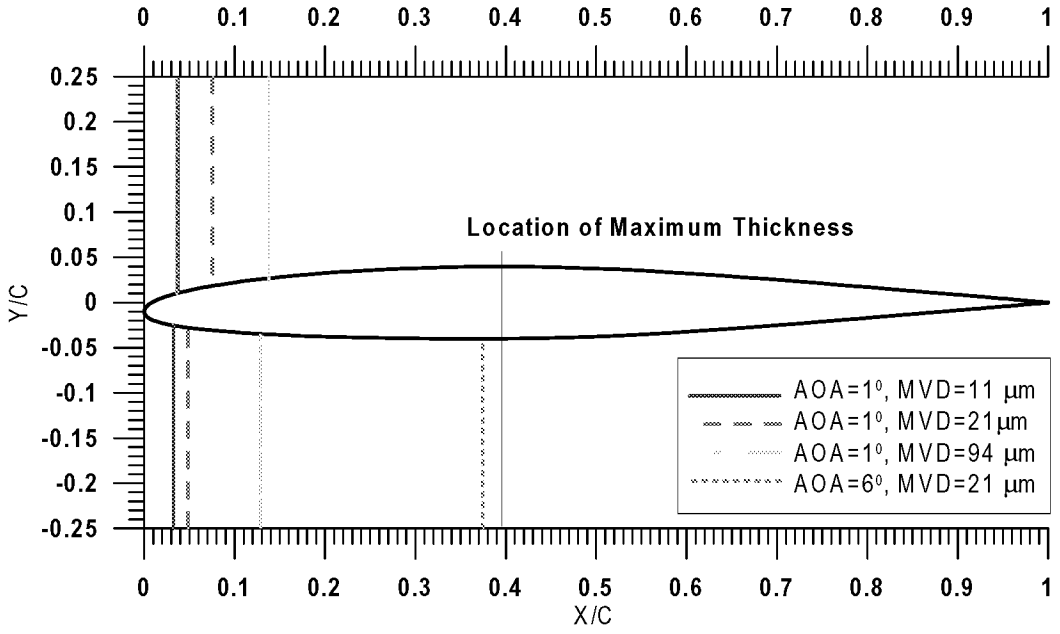

b. δ = 0 deg., Outboard

Fig. 116 Experimental impingement limits for full-scale Business Jet horizontal tail - 1999 IRT tests.

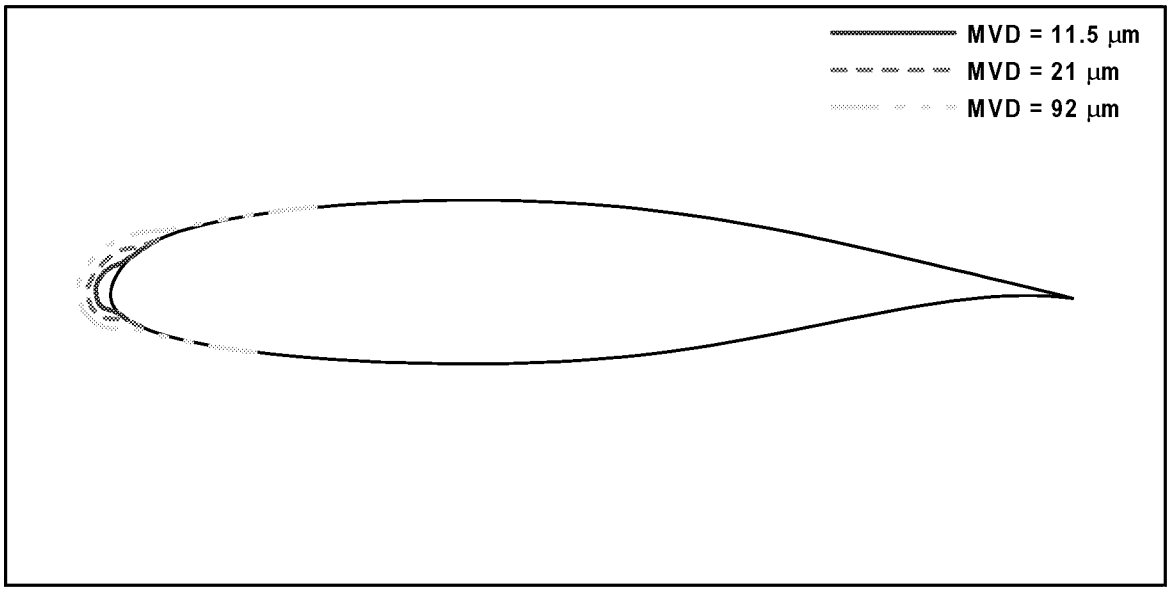

a. AOA = 0 deg.

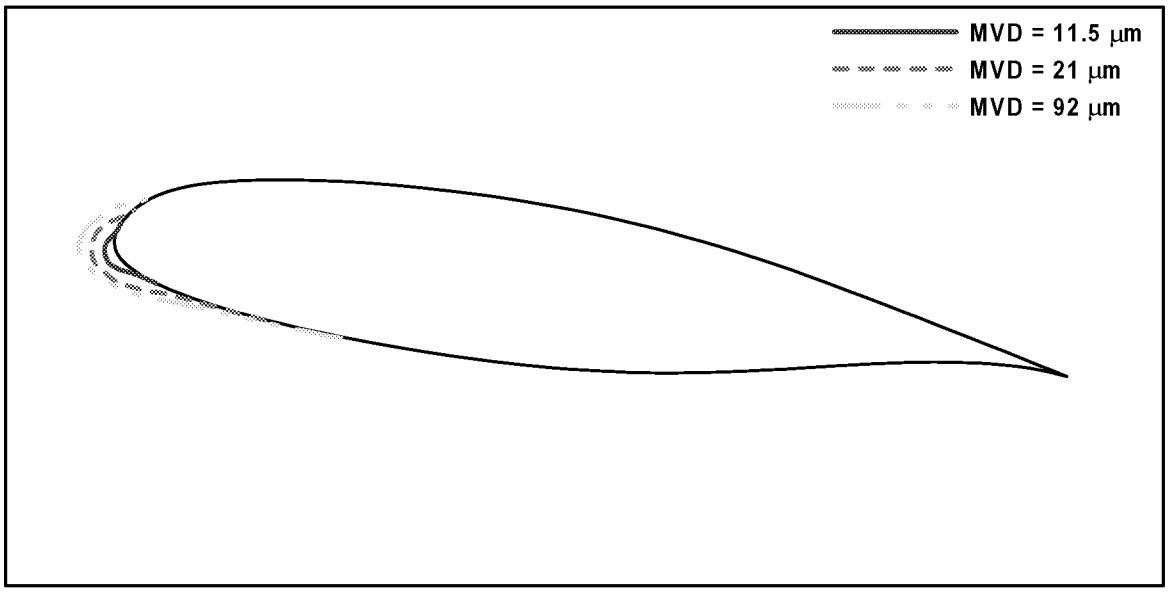

b. AOA = 8 deg.

Fig. 117 Experimental impingement efficiency surface distribution for MS(1)-0317 airfoil - 1997 IRT tests (Continued).

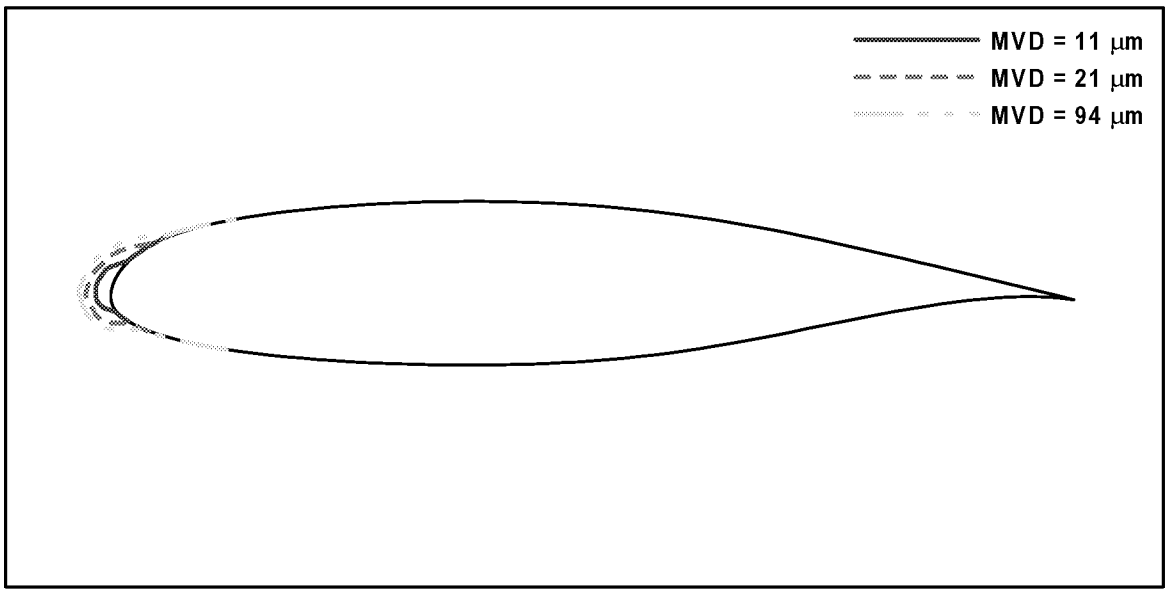

c. AOA = 0 deg.

Fig. 117 Experimental impingement efficiency surface distribution for MS(1)-0317 airfoil - 1999 IRT tests.

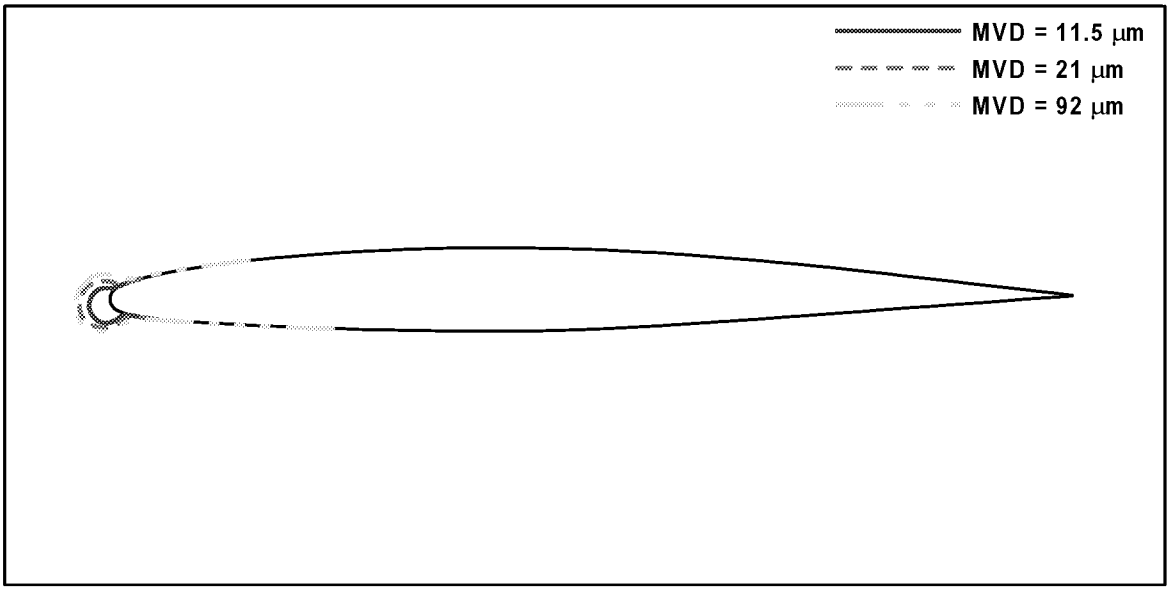

a. AOA = 1.5 deg.

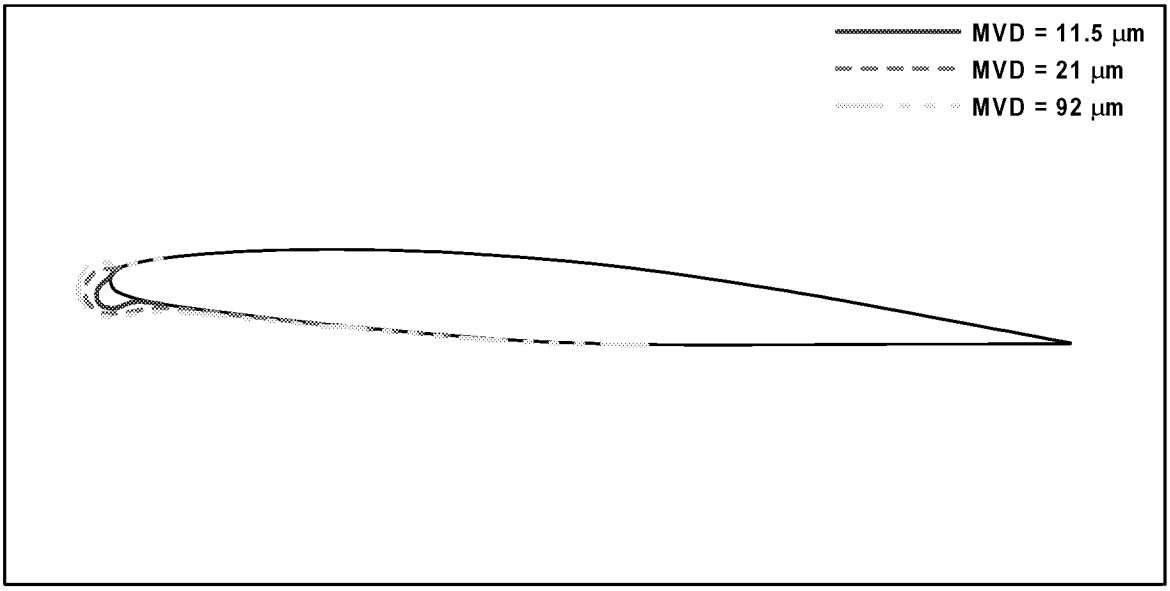

b. AOA = 6 deg.

Fig. 118 Experimental impingement efficiency surface distribution for GLC-305 airfoil - 1997 IRT tests.

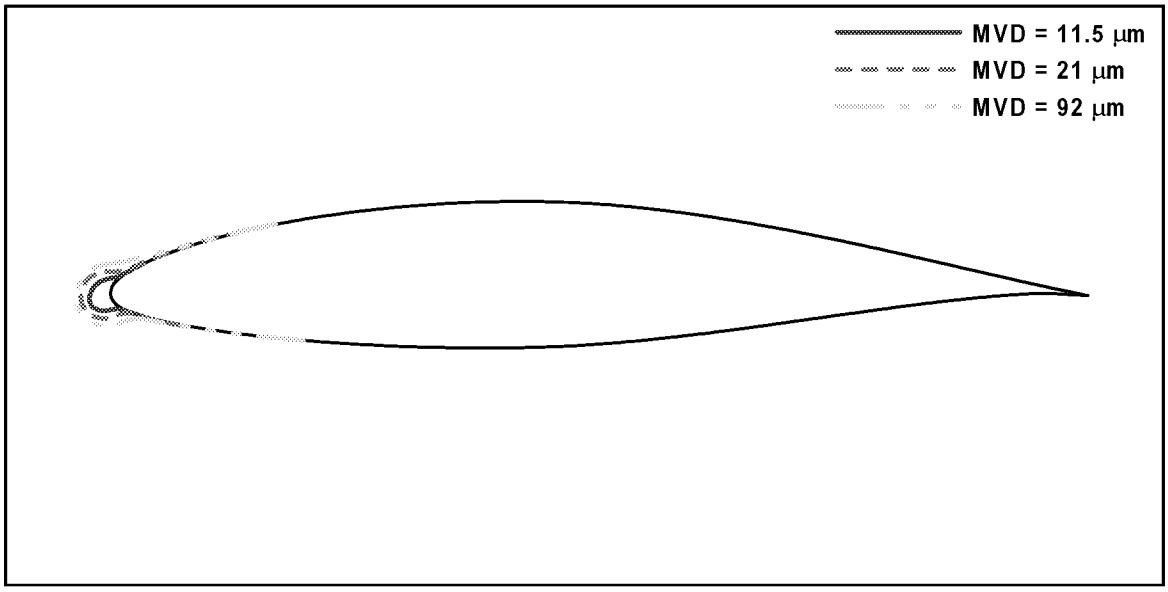

a. AOA = 0 deg.

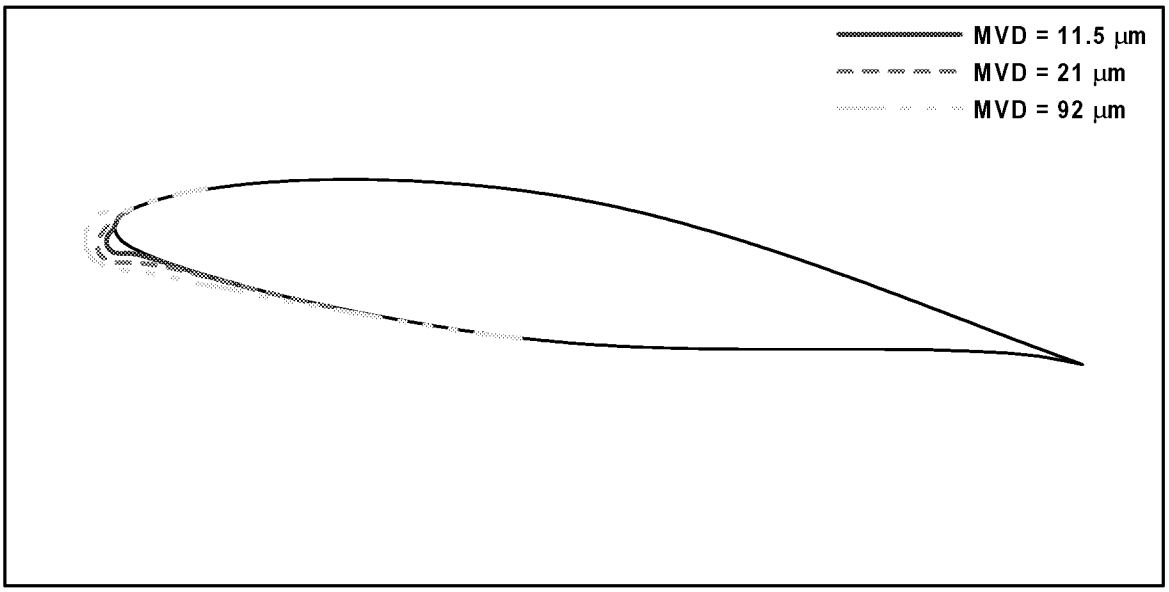

b. AOA = 8 deg.

Fig. 119 Experimental impingement efficiency surface distribution for NACA 65_2-415 airfoil -1997 IRT tests.

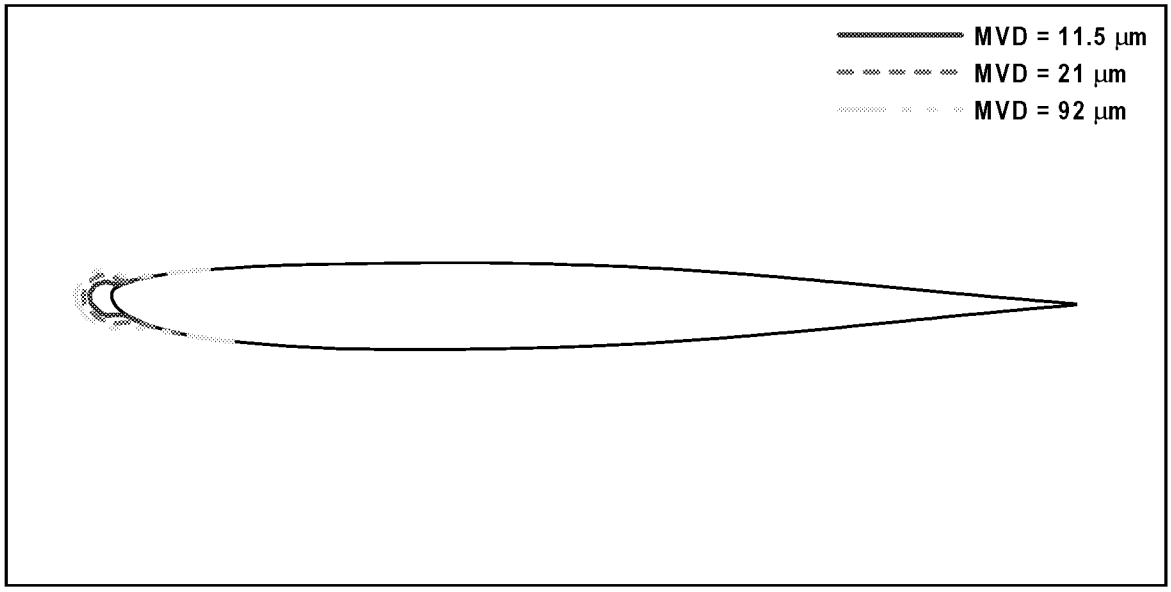

a. AOA = 0 deg.

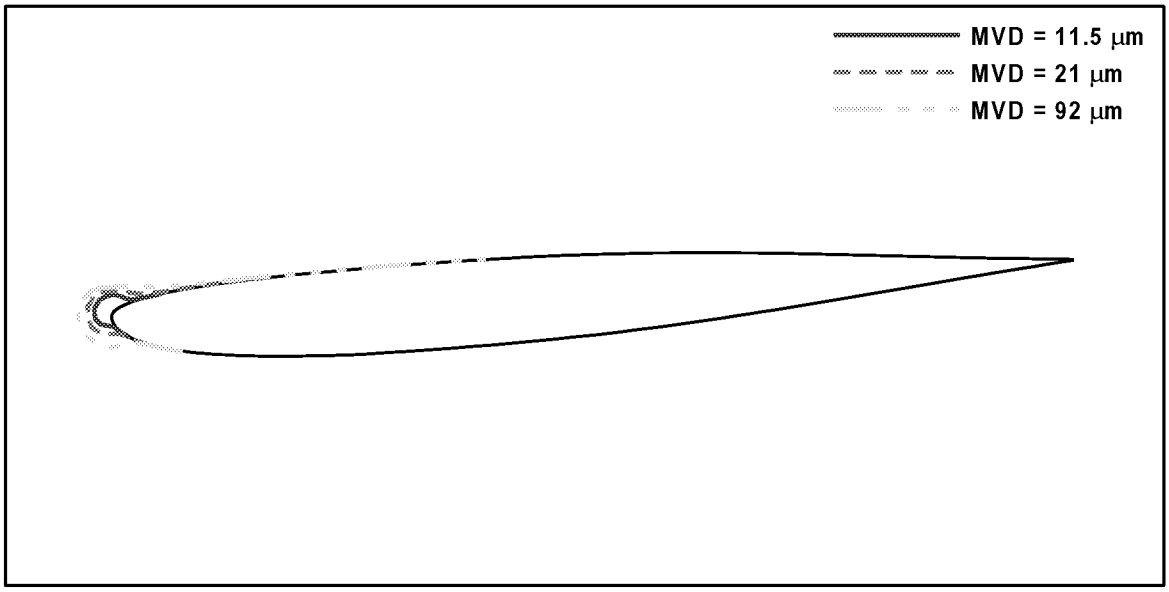

b. AOA = 4 deg.

Fig. 120 Experimental impingement efficiency surface distribution for commercial transport tail section - 1997 IRT tests.

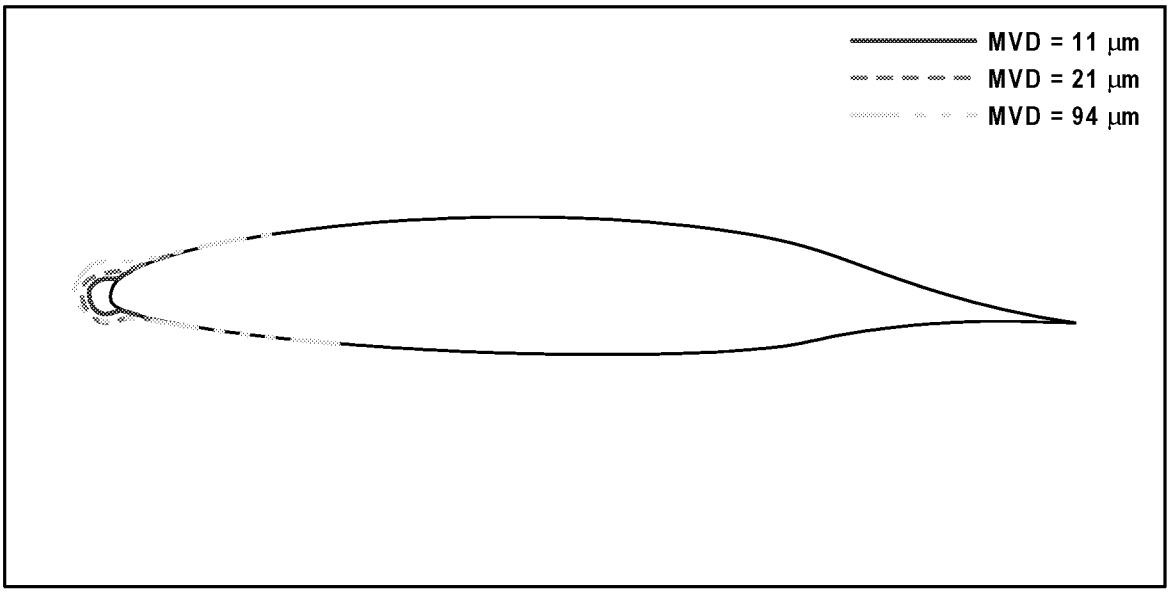

a. AOA = 0 deg.

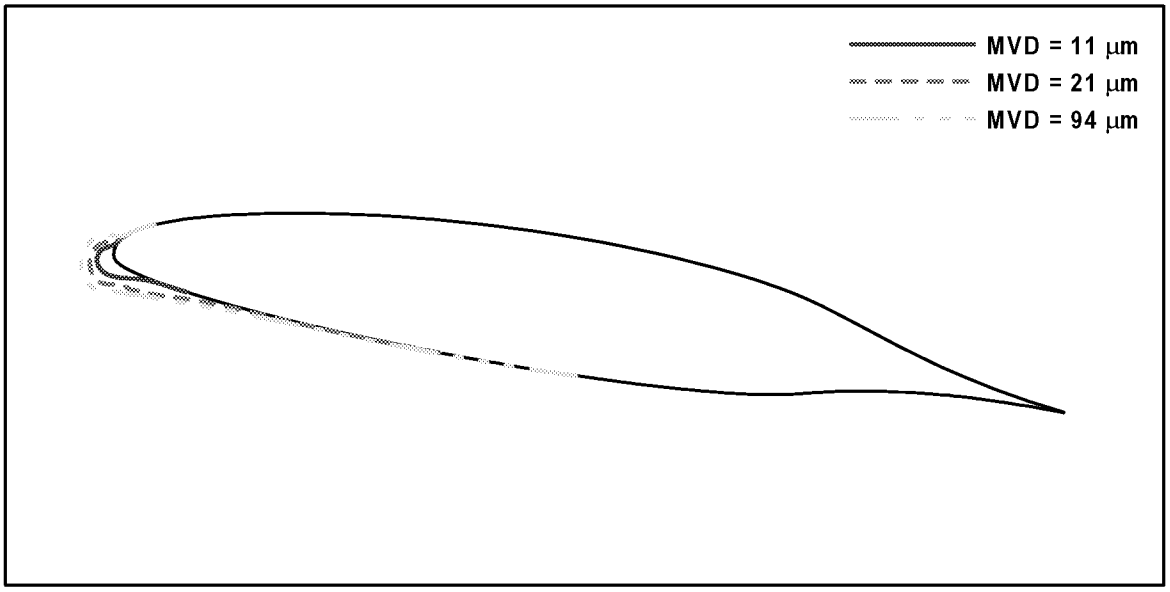

b. AOA = 8 deg.

Fig. 121 Experimental impingement efficiency surface distribution for 36-in NLF(1)-0414 airfoil - 1999 IRT tests.

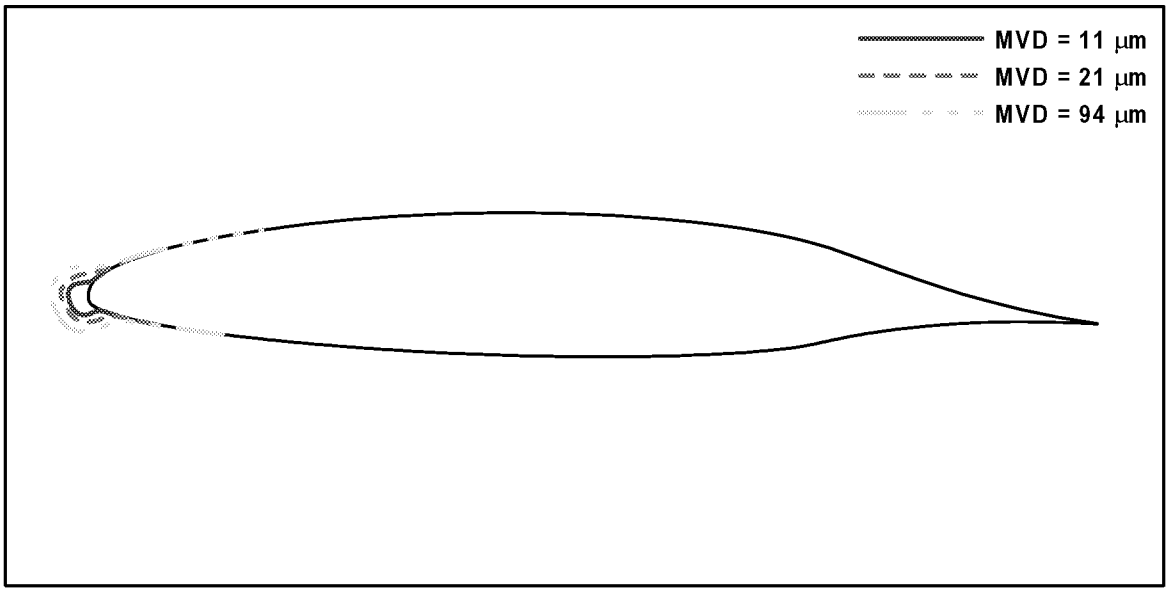

a. AOA = 0 deg., δ = 0 deg.

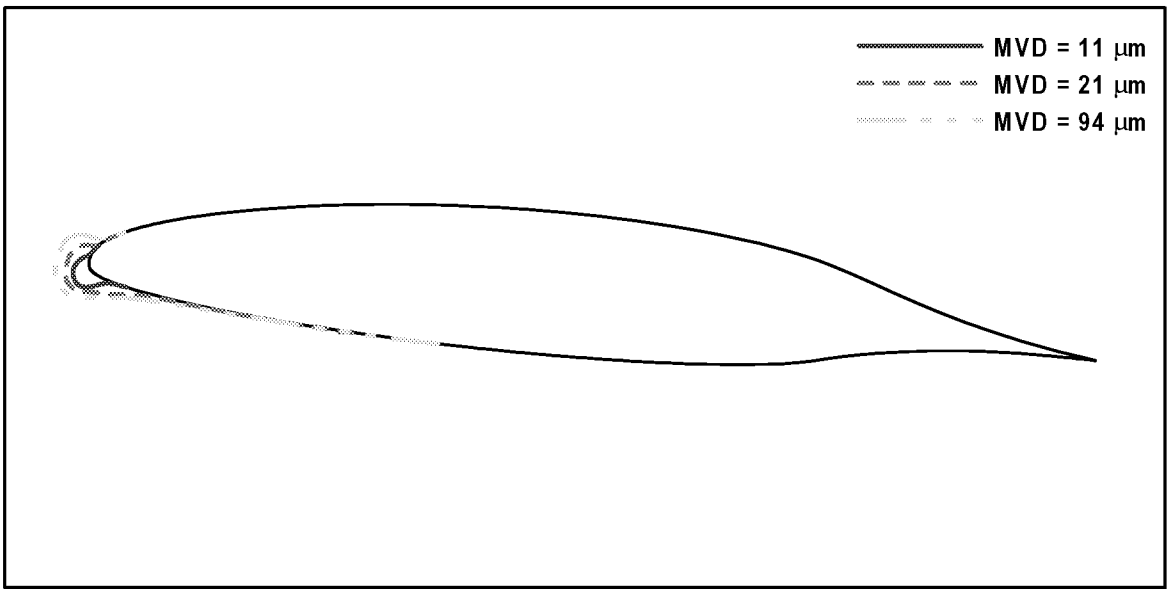

b. AOA = 4 deg., δ = 0 deg.

Fig. 122 Experimental impingement efficiency surface distribution for 48-in NLF(1)-0414 Airfoil -1999 IRT tests (Continued).

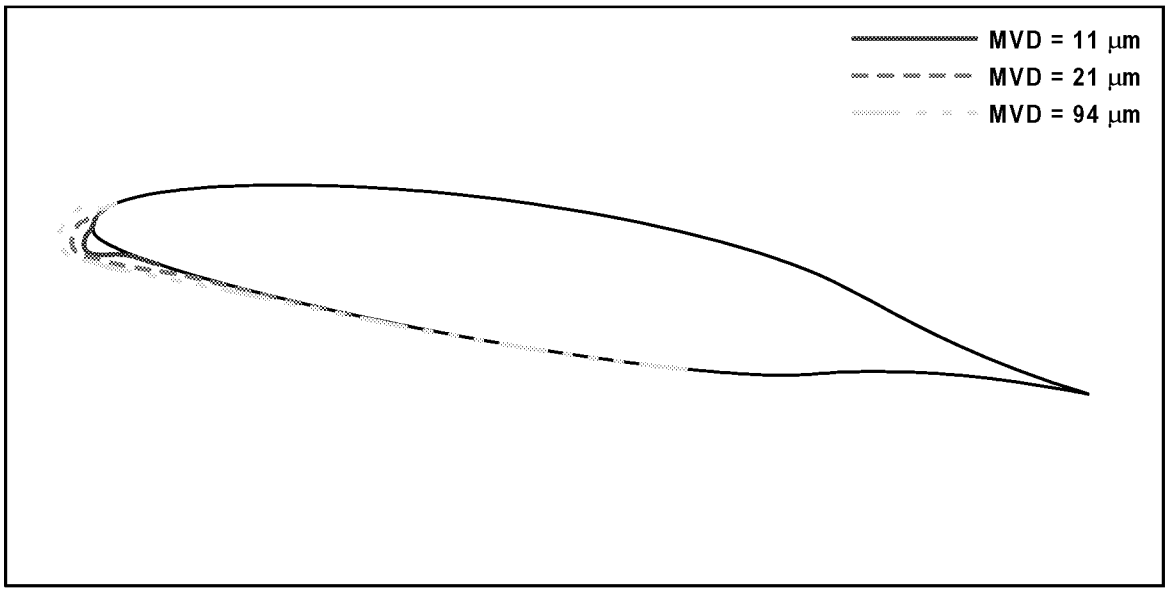

c. AOA = 8 deg., δ = 0 deg.

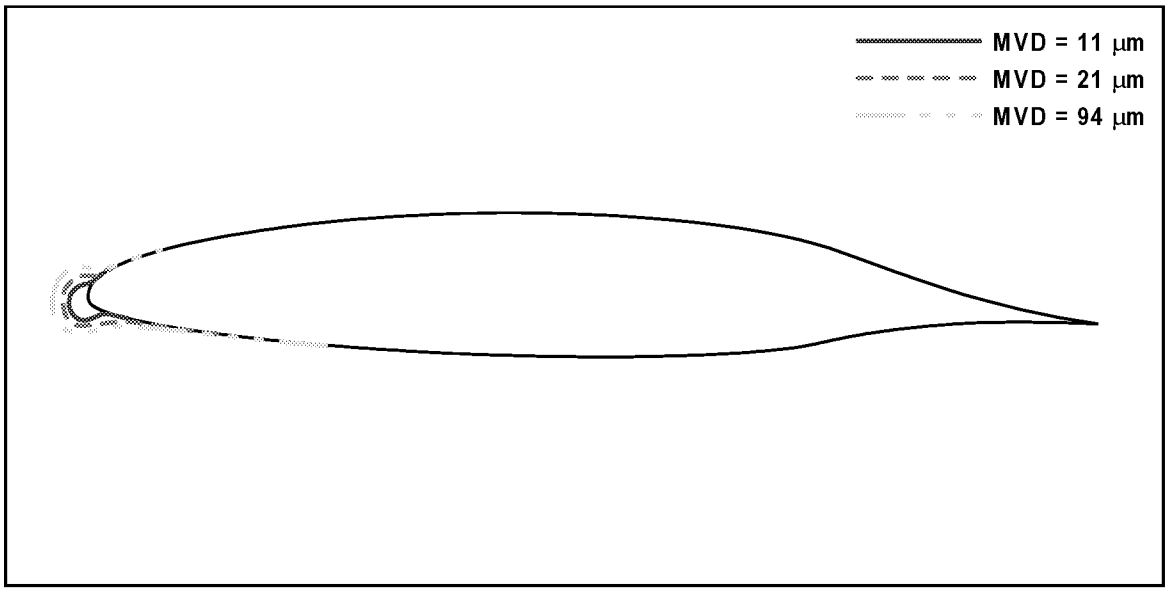

d. AOA = 0 deg., δ = 15 deg.

Fig. 122 Experimental impingement efficiency surface distribution for 48-in NLF(1)-0414 Airfoil -1999 IRT tests.

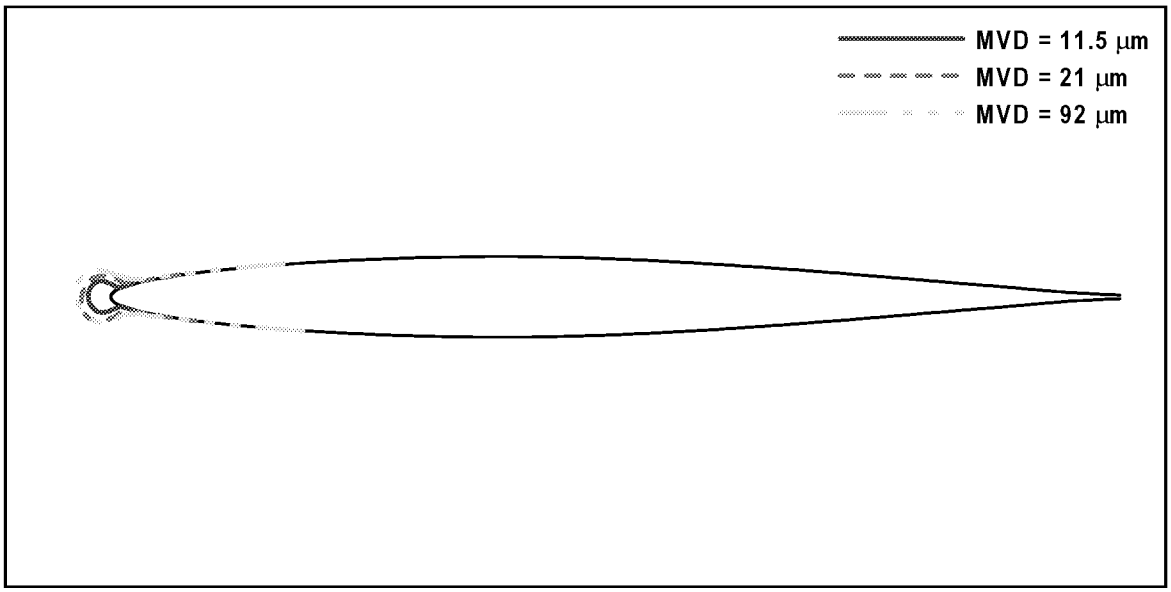

a. AOA = 0 deg.

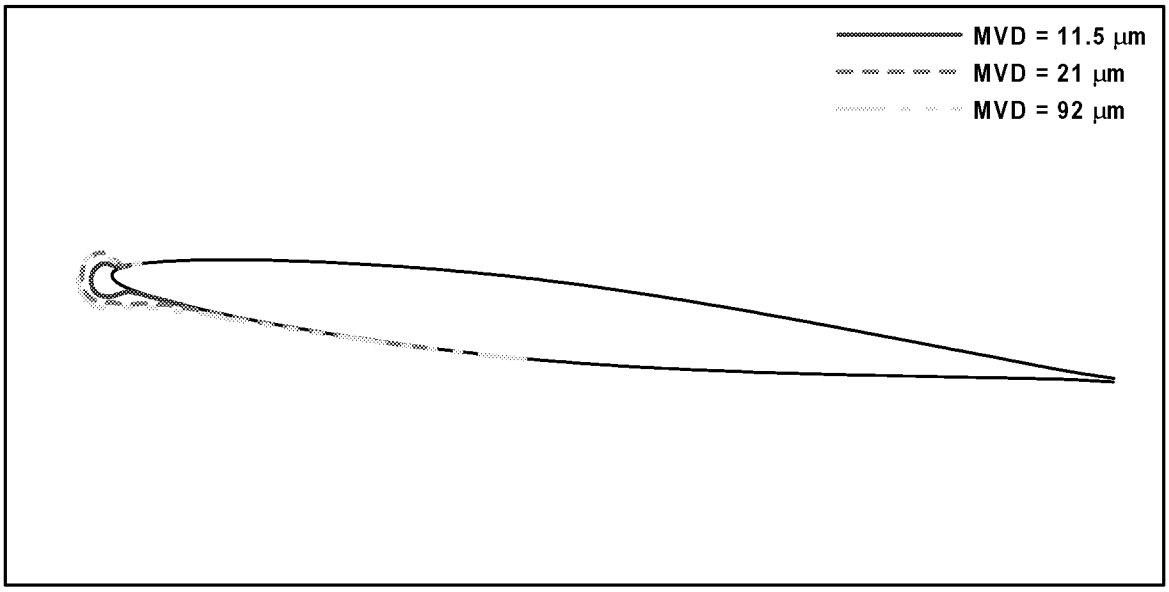

b. AOA = 6 deg.

Fig. 123 Experimental impingement efficiency surface distribution for NACA 64A008 tail section - 1997 IRT Tests.

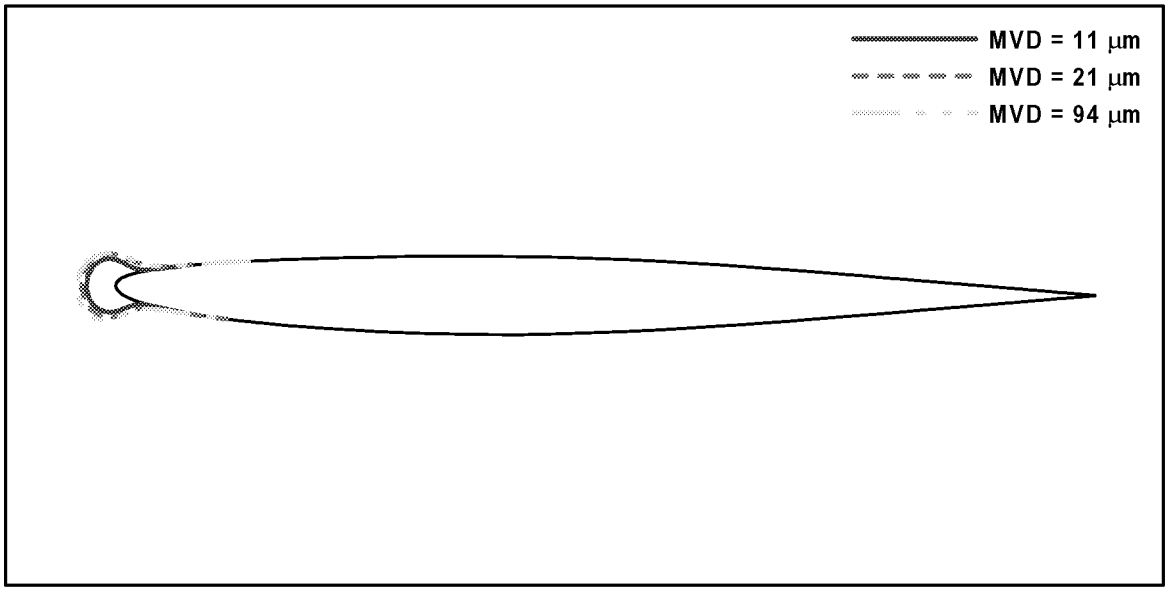

a. AOA = -1 deg., δ = 0 deg., Inboard

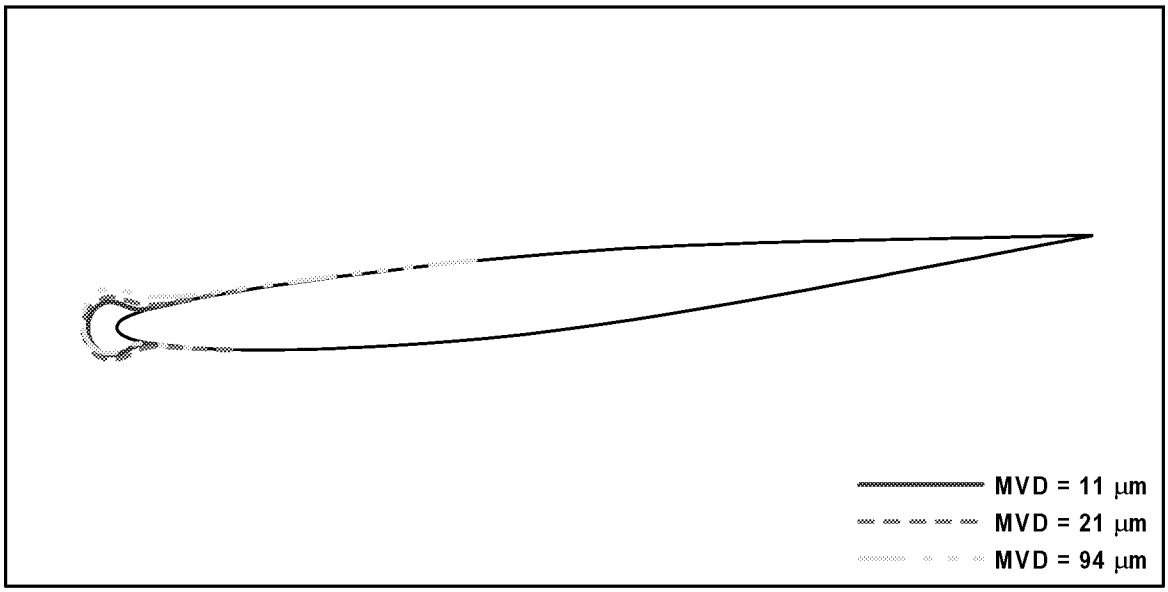

b. AOA = -6 deg., δ = 0 deg., Inboard

Fig. 124 Experimental impingement efficiency surface distribution for 25%-scale Business Jet Empennage - 1999 IRT tests (Continued).

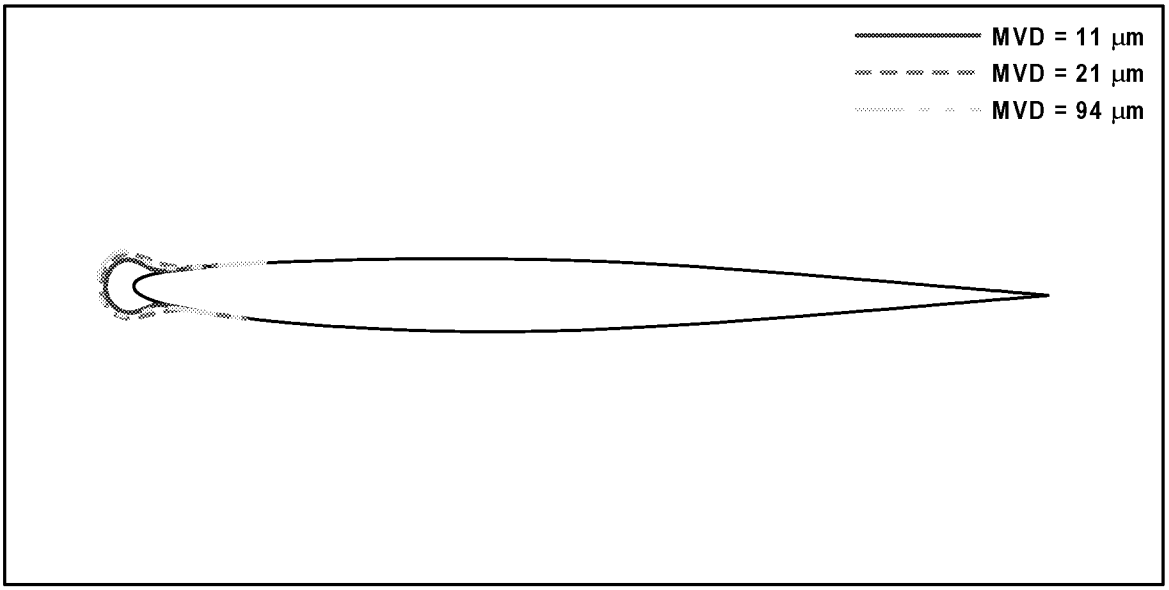

c. AOA = -1 deg., δ = 0 deg., Outboard

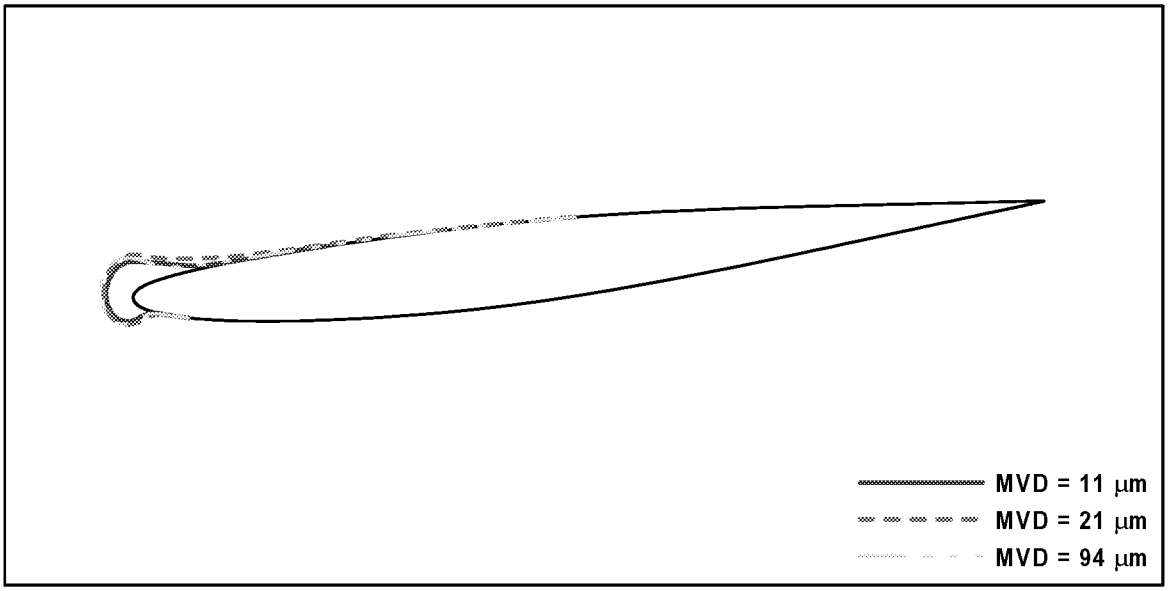

d. AOA = -6 deg., δ = 0 deg., Outboard

Fig. 124 Experimental impingement efficiency surface distribution for 25%-scale Business Jet Empennage - 1999 IRT tests.

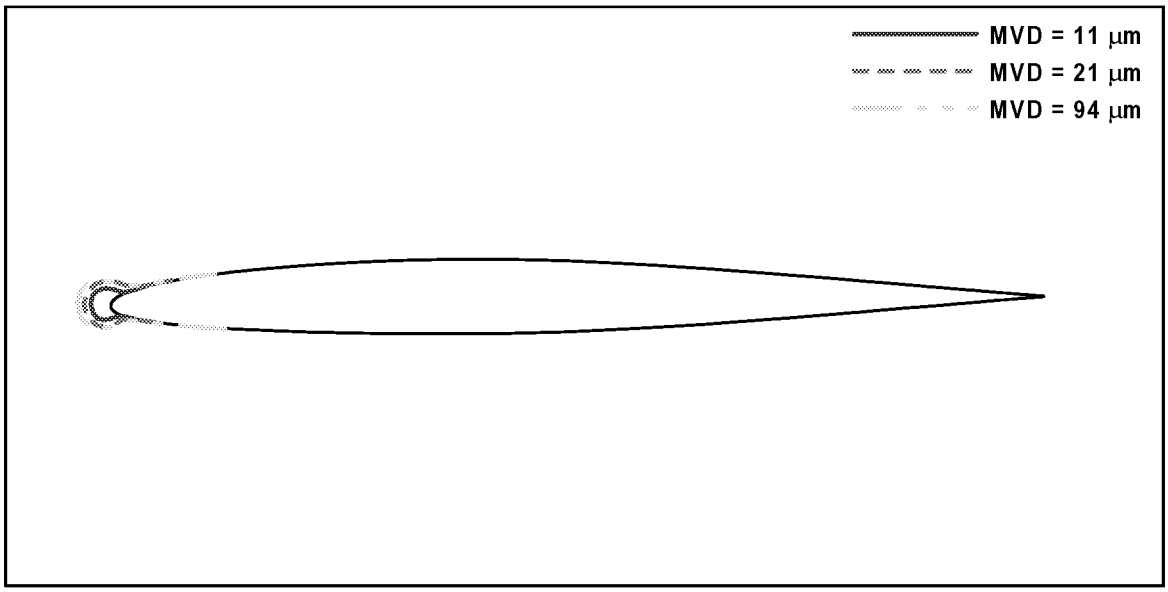

a. AOA = 1 deg., δ = 0 deg., Inboard

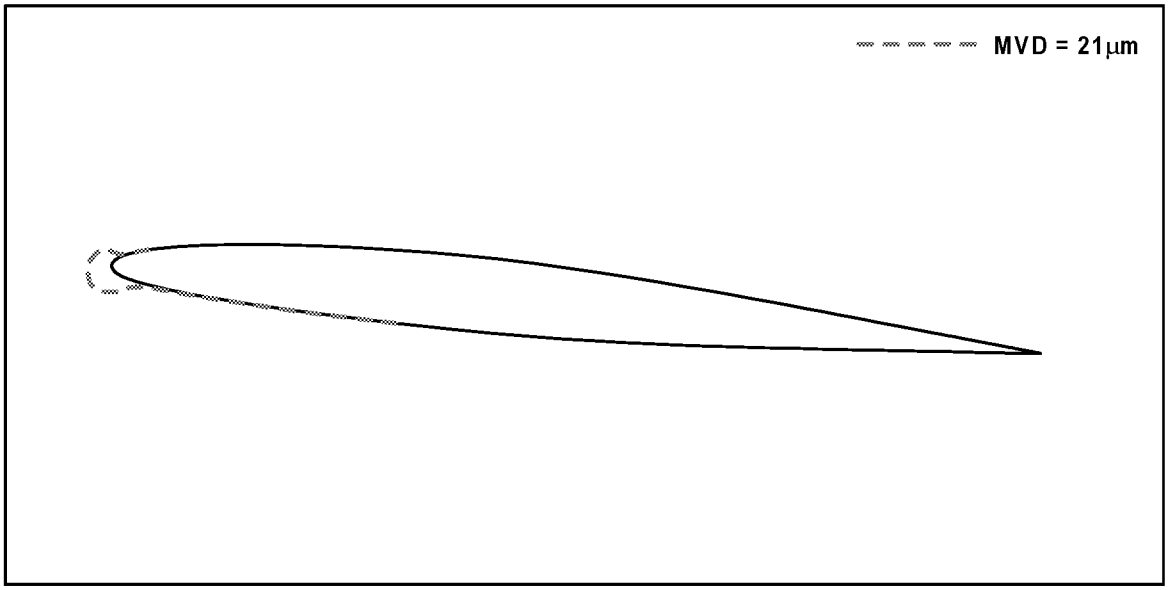

b. AOA = 6 deg., δ = 0 deg., Inboard

Fig. 125 Experimental impingement efficiency surface distribution for full-scale Business Jet horizontal tail -1999 IRT tests (Continued).

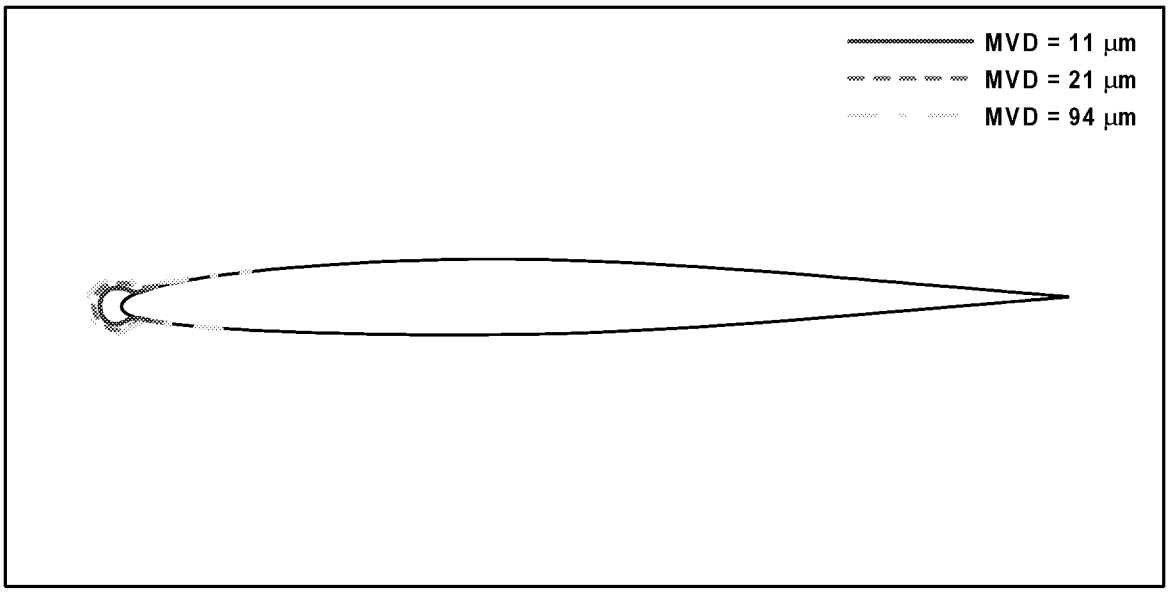

c. AOA = 1 deg., δ = 0 deg., Outboard

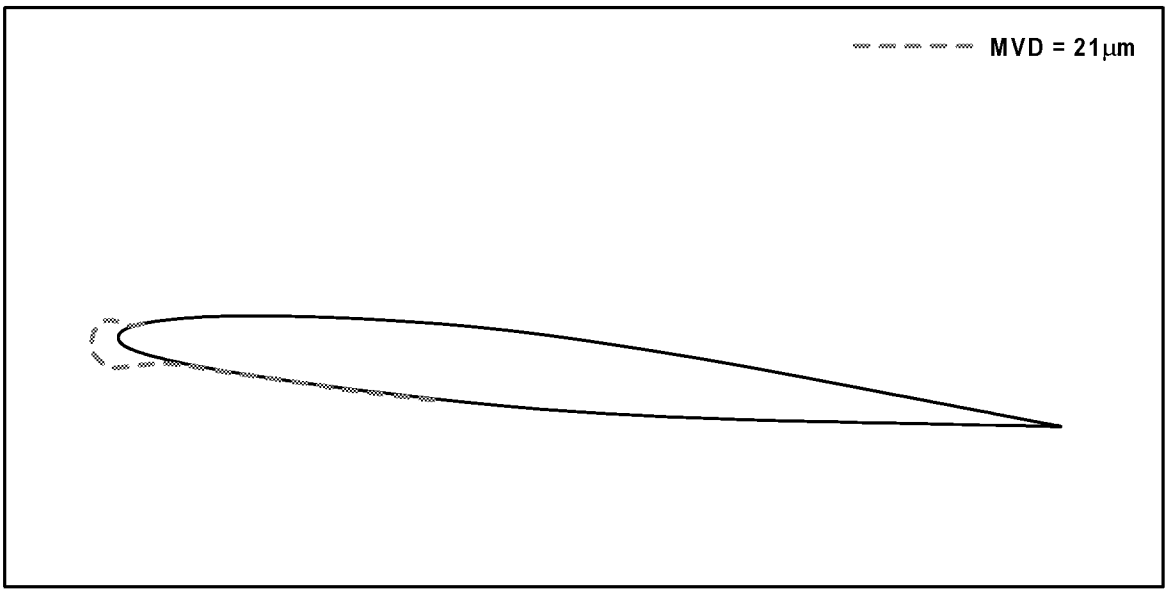

d. AOA = 6 deg., δ = 0 deg., Outboard

Fig. 125 Experimental impingement efficiency surface distribution for full-scale Business Jet horizontal tail - 1999 IRT tests.

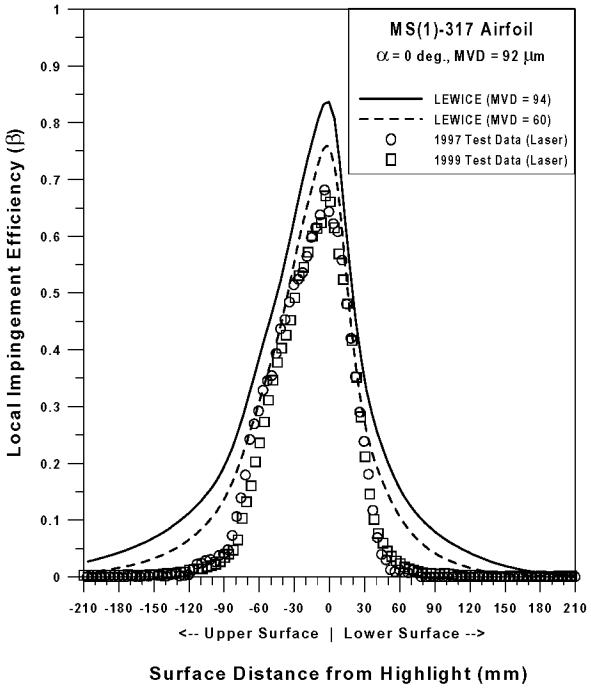

Fig. 126 Comparison of LEWICE results for MVD = 92 and 60 μm with experimental data; MS(1)-317, α = 0°, MVD = 92 μm.

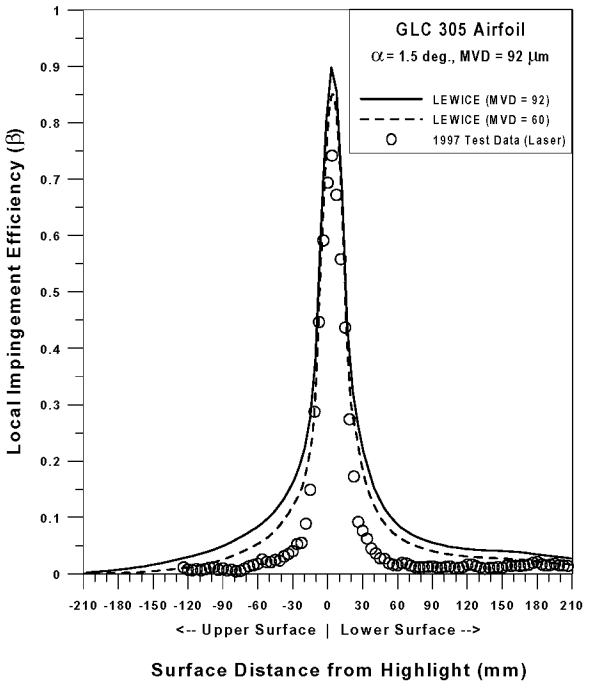

Fig. 127 Comparison of LEWICE results for MVD = 92 and 60 μm with experimental data; GLC 305, α = 1.5°, MVD = 92 μm.

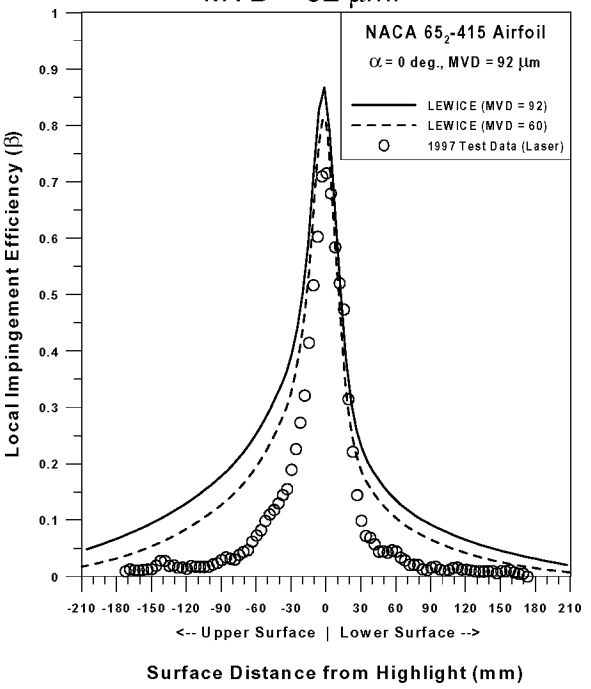

Fig. 128 Comparison of LEWICE results for MVD = 92 and 60 μm with experimental data; NACA 65_2-415, α = 0°, MVD = 92 μm.

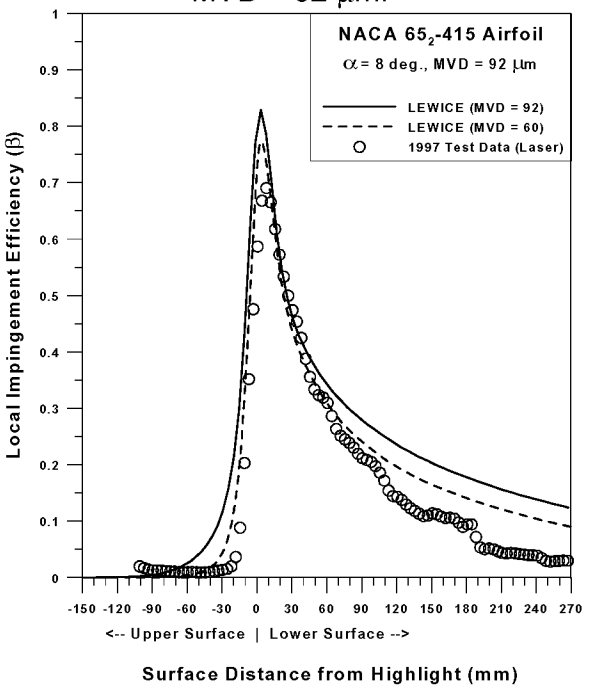

Fig. 129 Comparison of LEWICE results for MVD = 92 and 60 μm with experimental data; NACA 65_2-415, α = 8°, MVD = 92 μm.

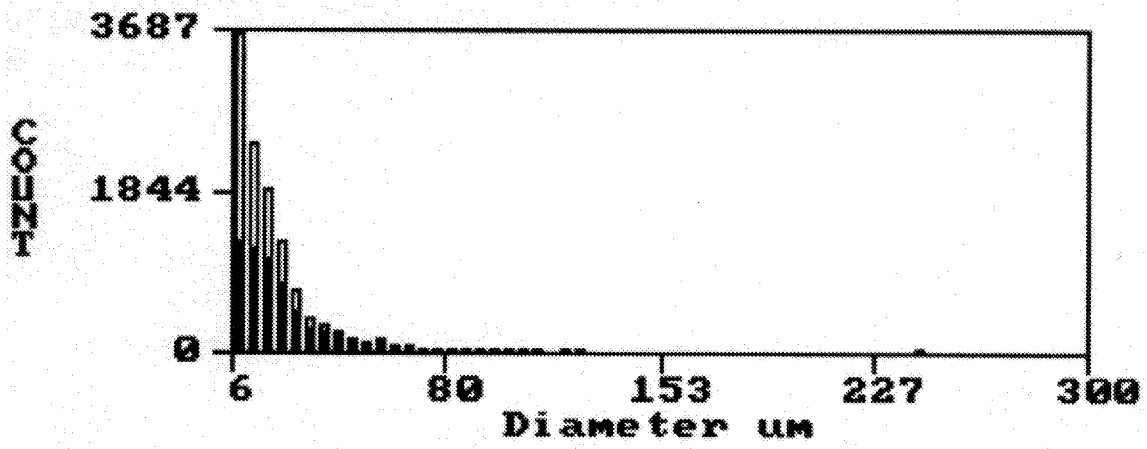

Fig. 130 Droplet distribution near LE of NACA-0012 airfoil; c=21-in, V_∞=175 mph, α = 0°, MVD = 104 μm.

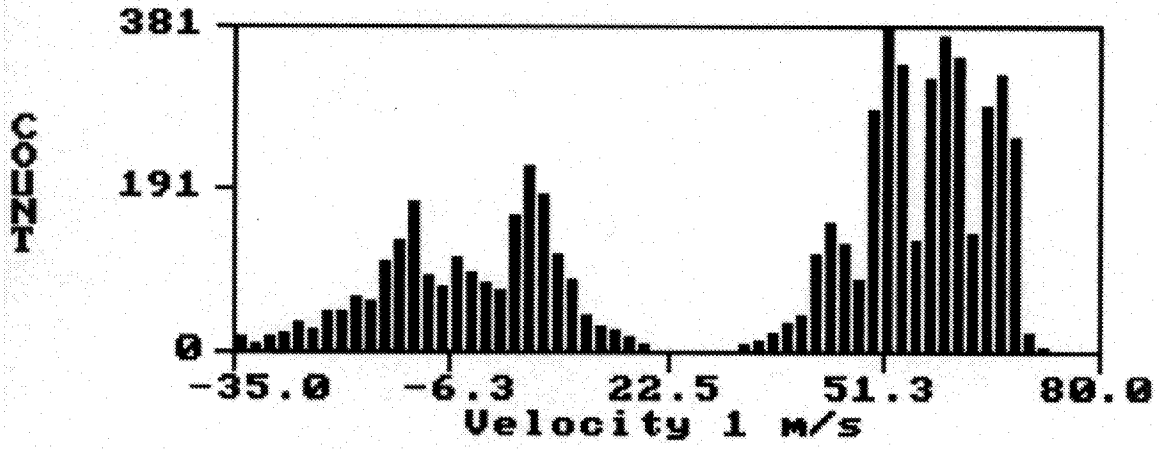

Fig. 131 Droplet velocity distribution near LE of NACA-0012 airfoil; c=21-in, V_∞=175 mph, α = 0°, MVD = 104 μm.

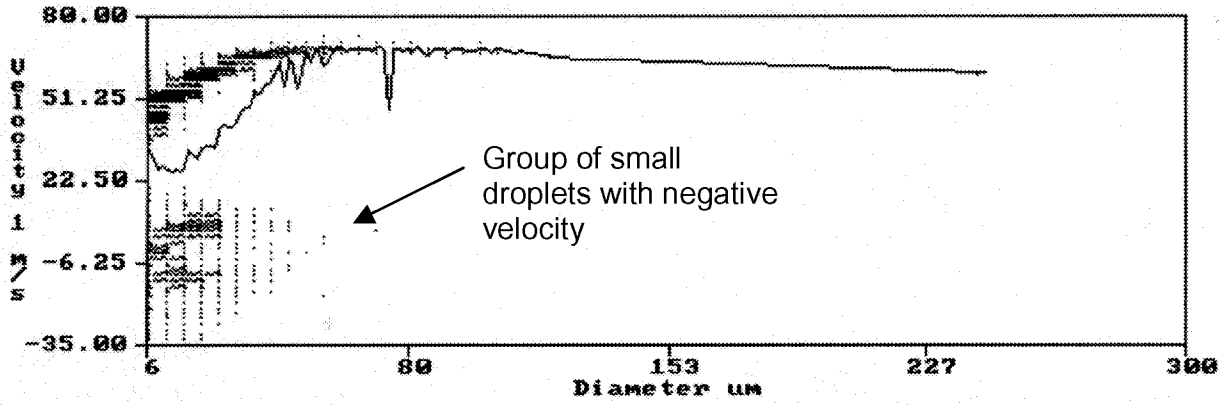

Fig. 132 Velocity versus droplet size near LE of NACA-0012 airfoil; c = 21-in, V_∞ = 175 mph, α = 0°, MVD = 104 μm.

Appendix A: Summary of Experimental and LEWICE Impingement Data

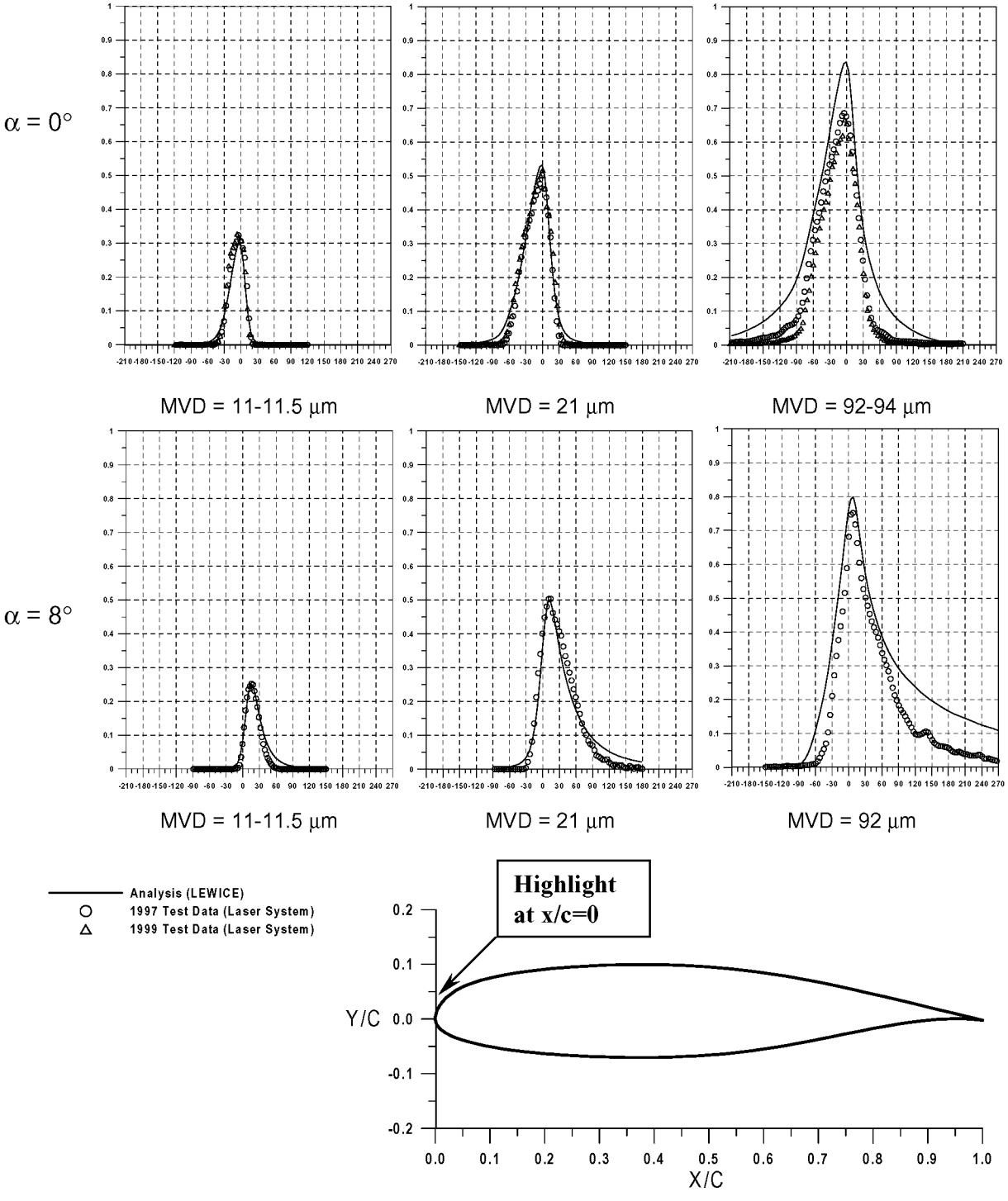

Fig. A1 Impingement data for MS(1)-0317 airfoil.

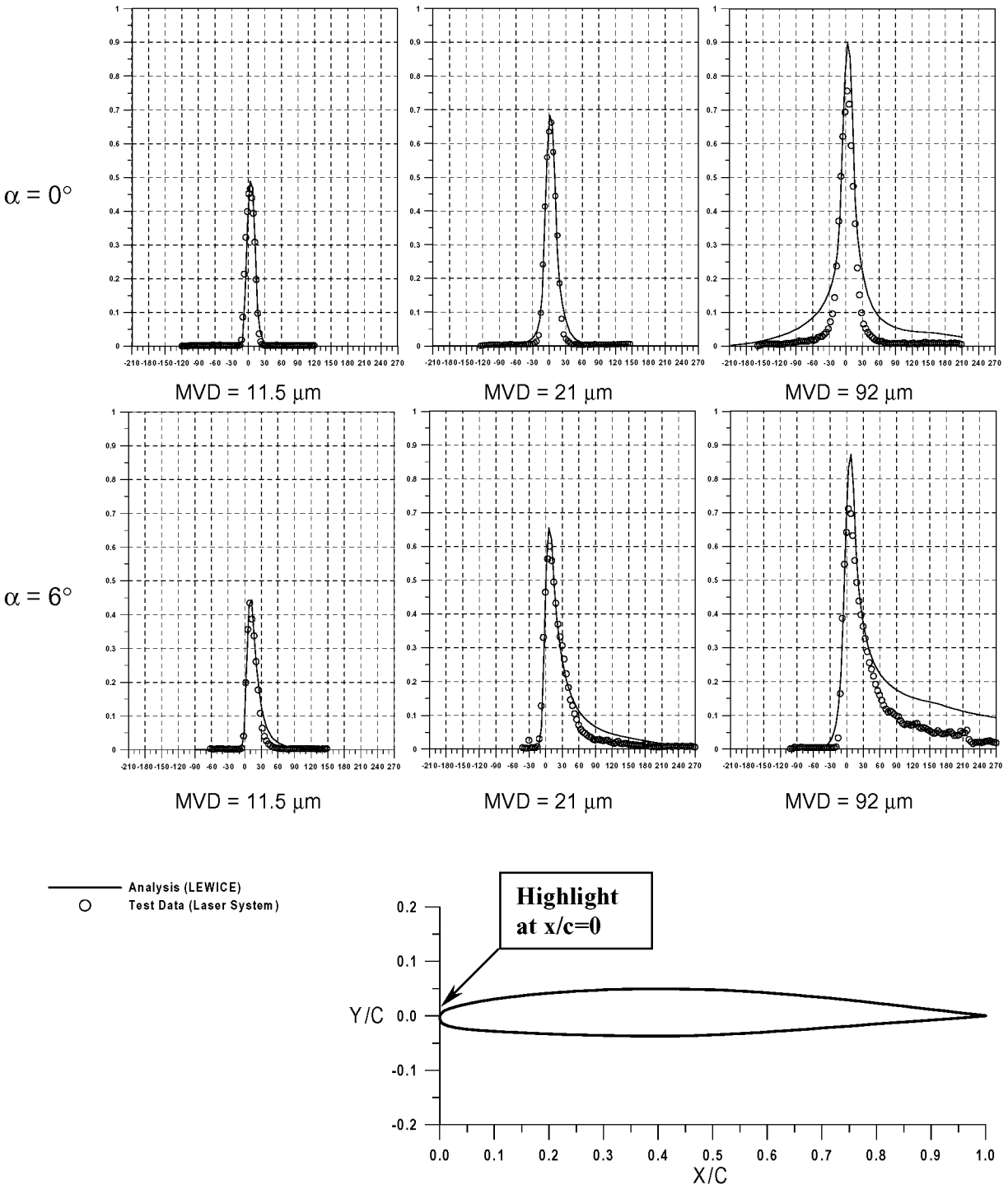

Fig. A2 Impingement data for GLC 305 airfoil.

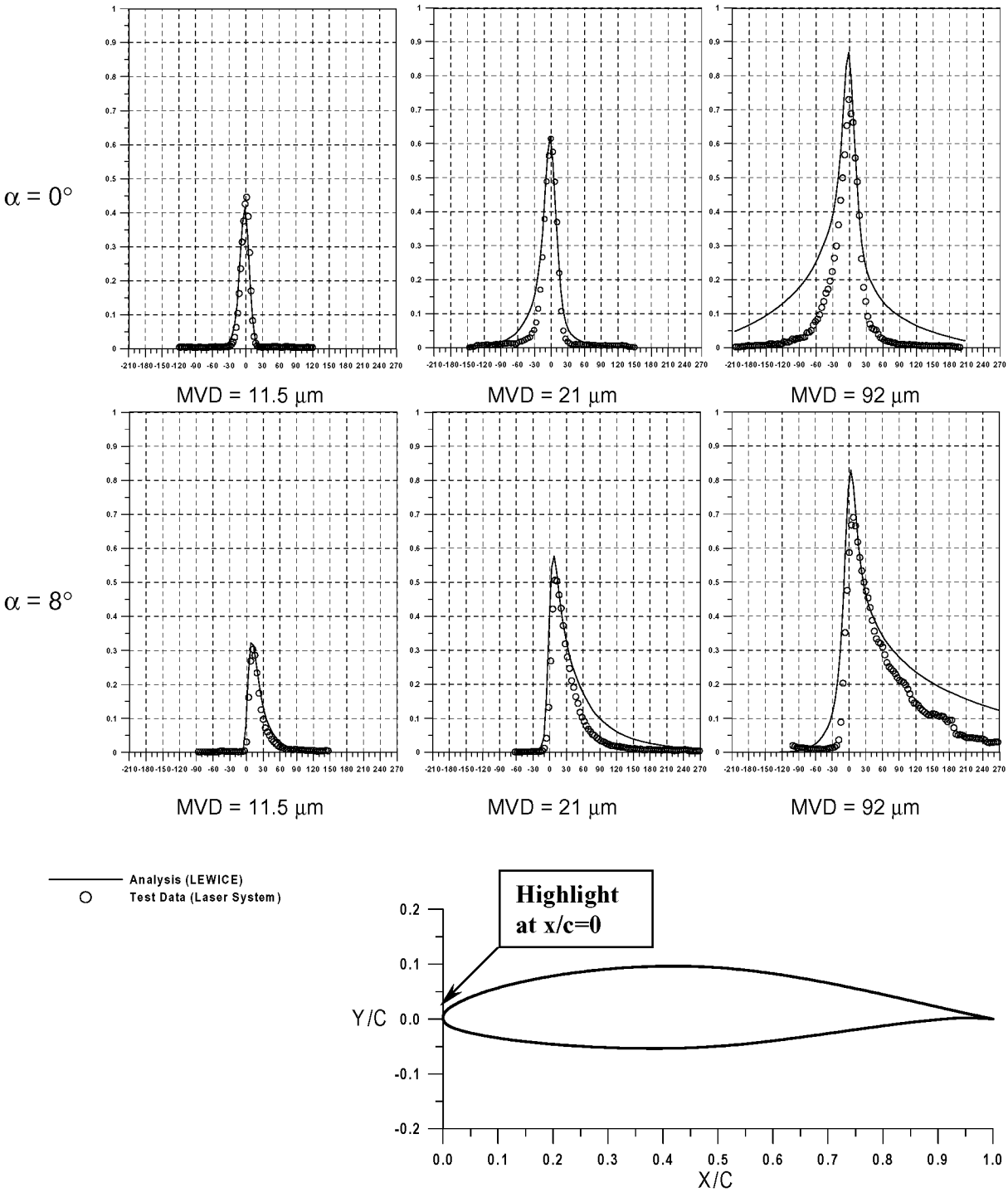

Fig. A3 Impingement data for NACA 65(2)-415 airfoil.

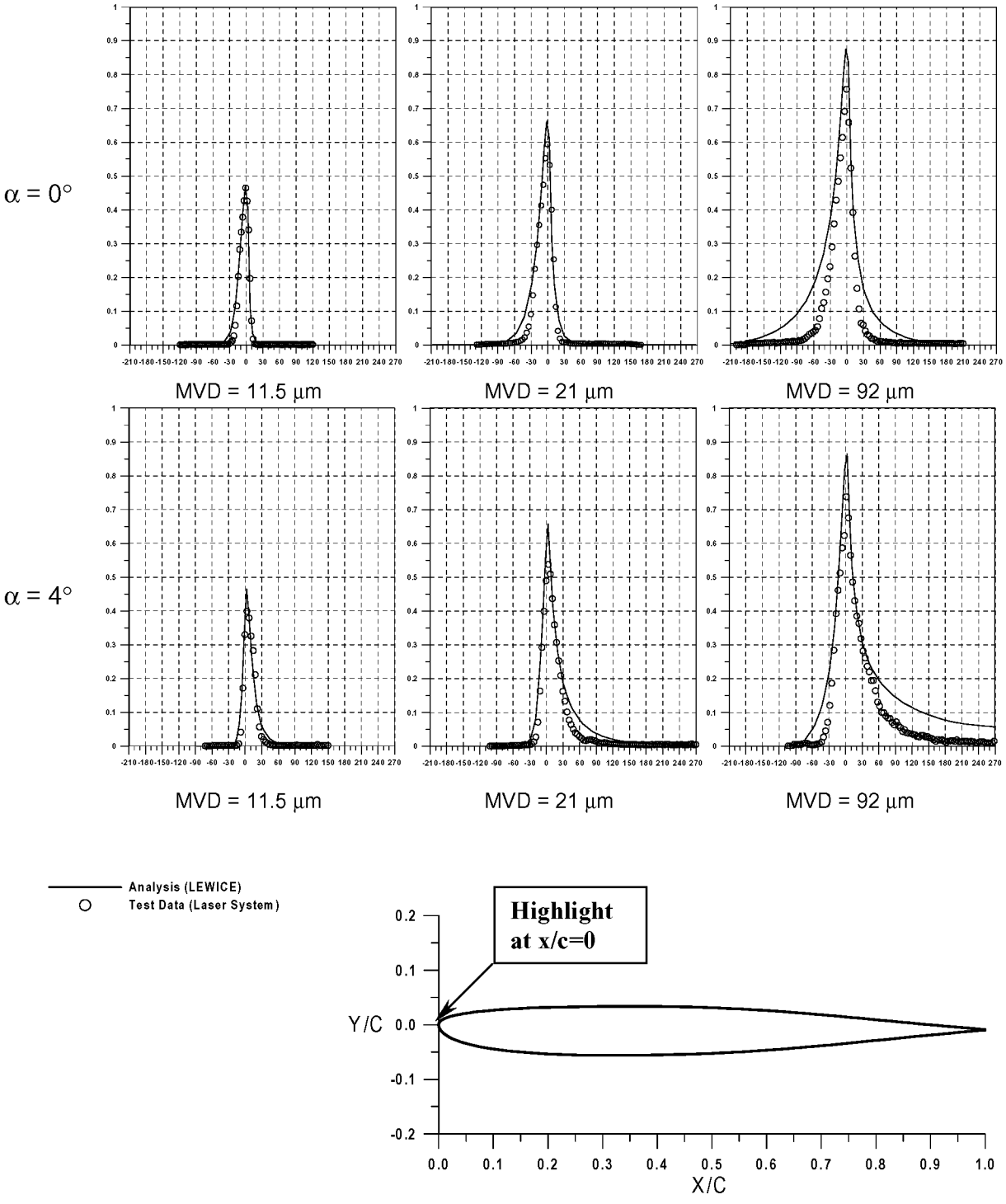

Fig. A4 Impingement data for Commercial Jet Transport Tail.

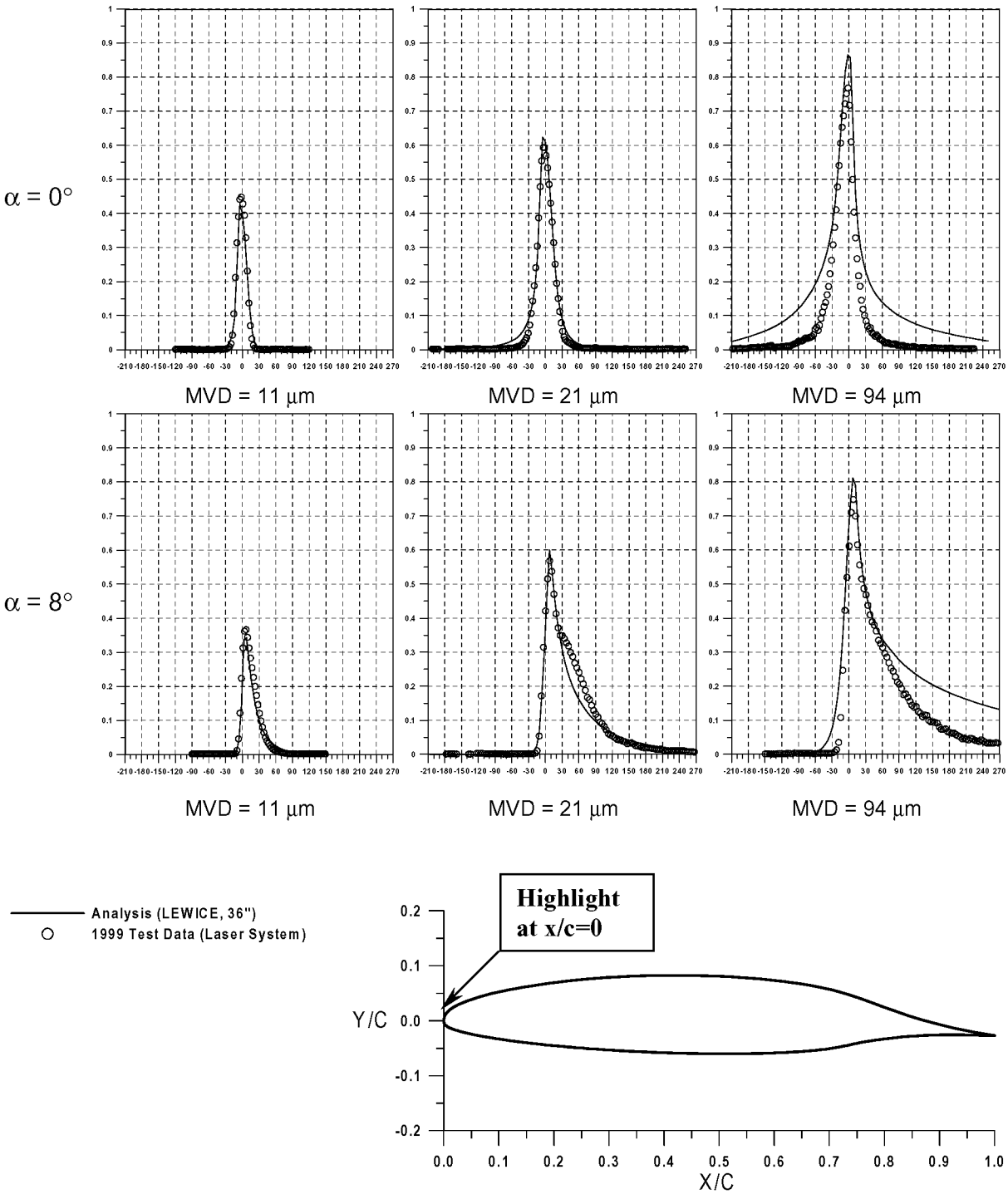

Fig. A5 Impingement data for NLF-414 36" airfoil.

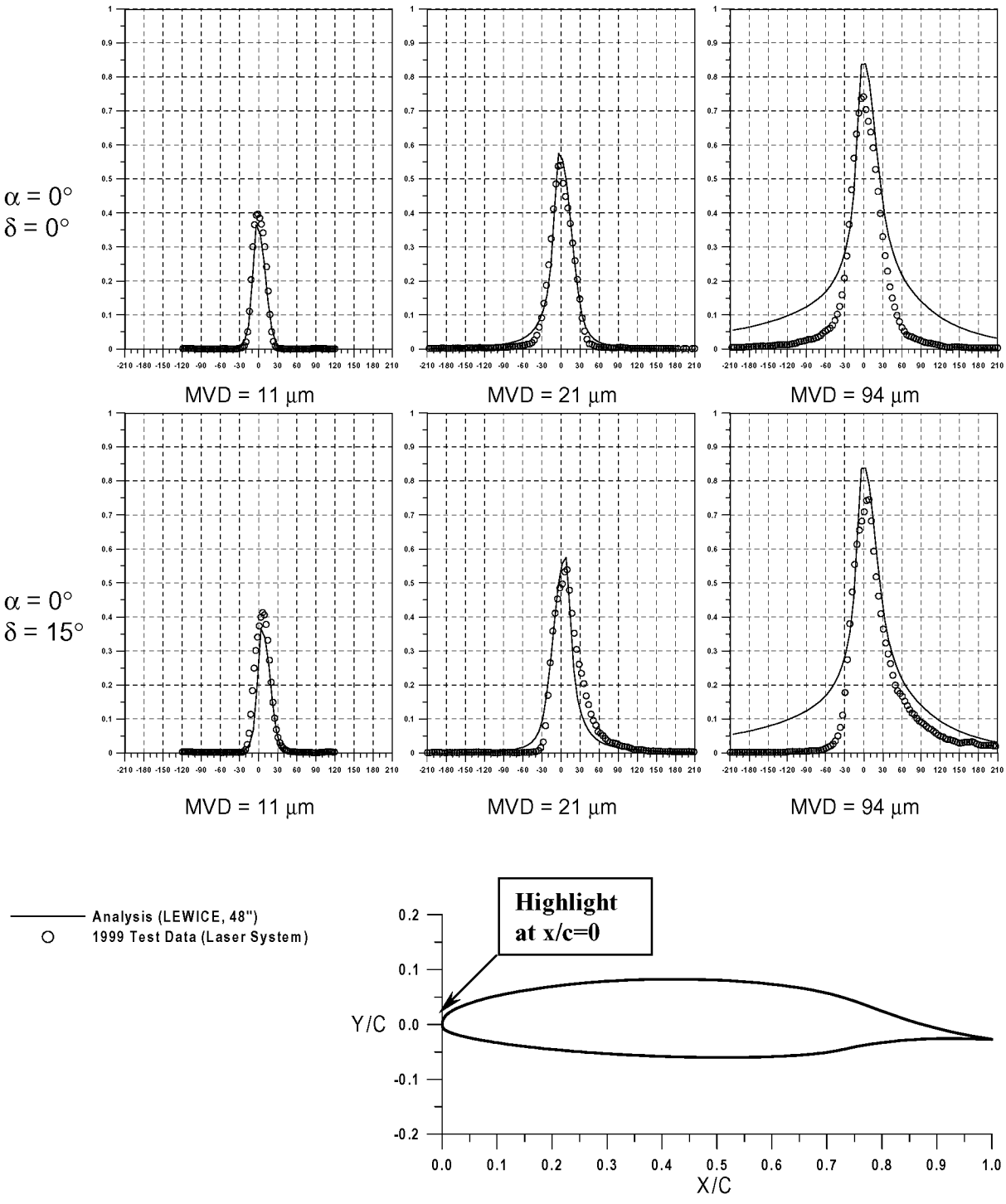

Fig. A6a Impingement data for NLF-414 48 " airfoil (Cont.)

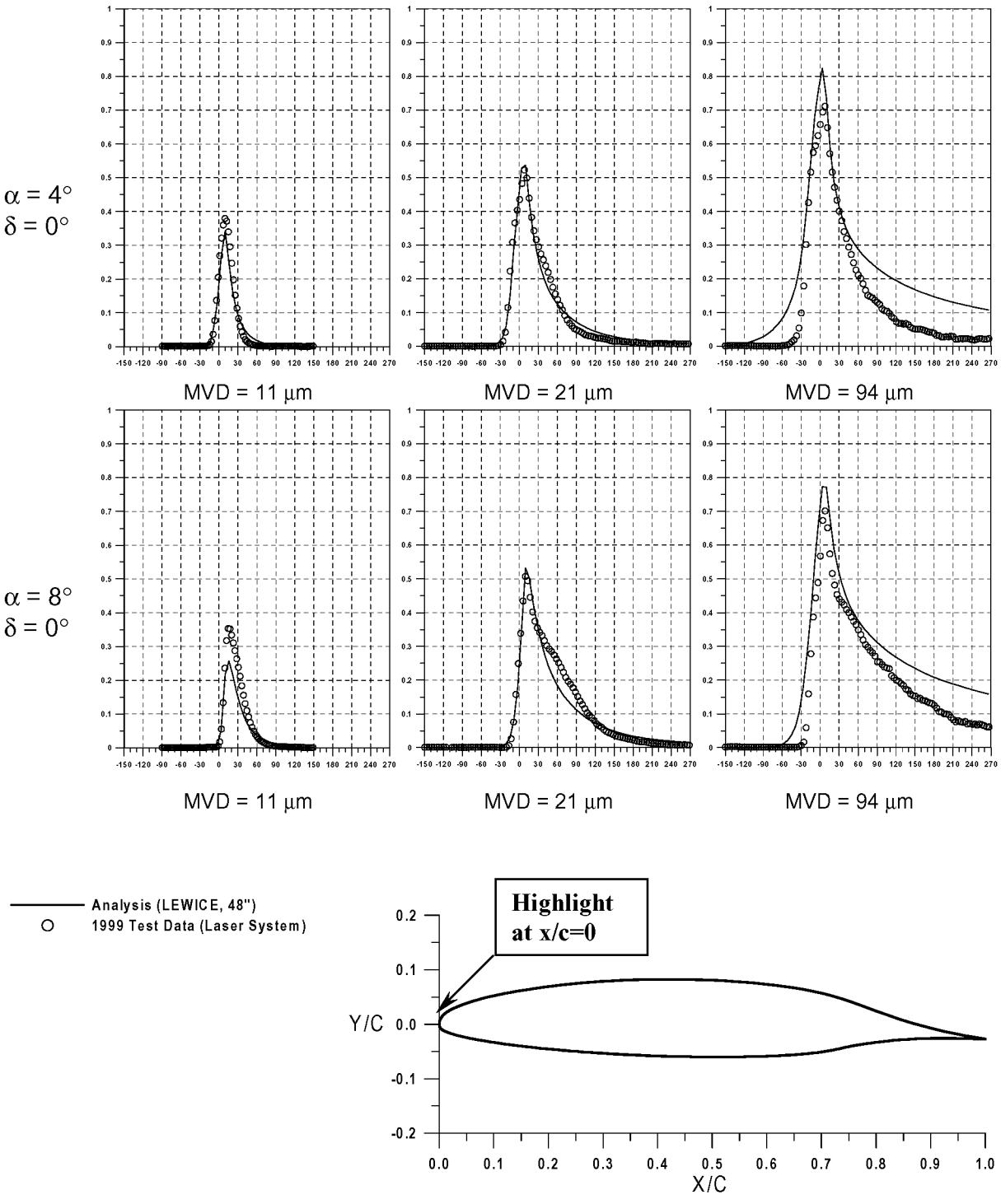

Fig. A6b Impingement data for NLF-414 48 " airfoil.

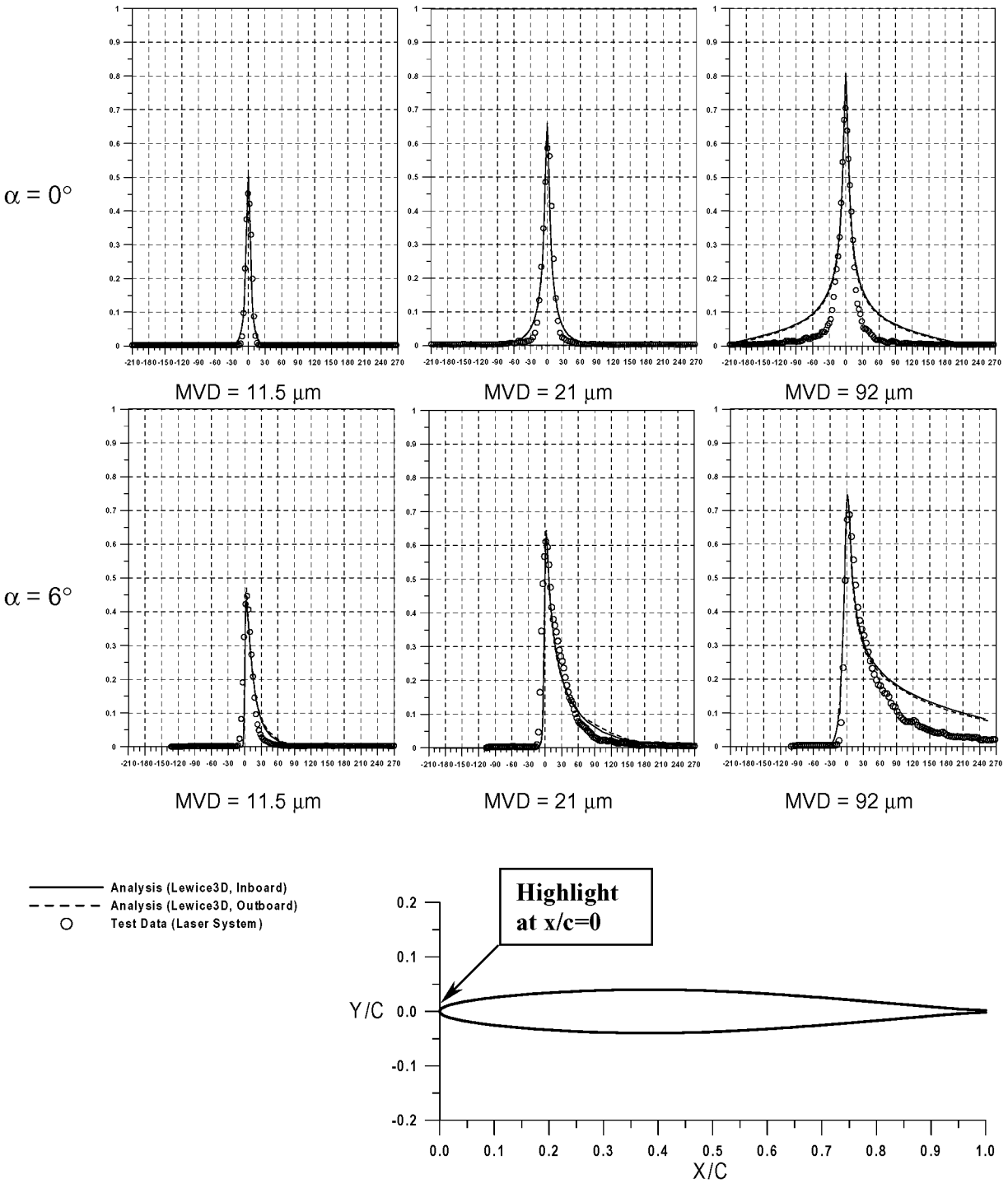

Fig. A7 Impingement data for NACA 64A008 airfoil.

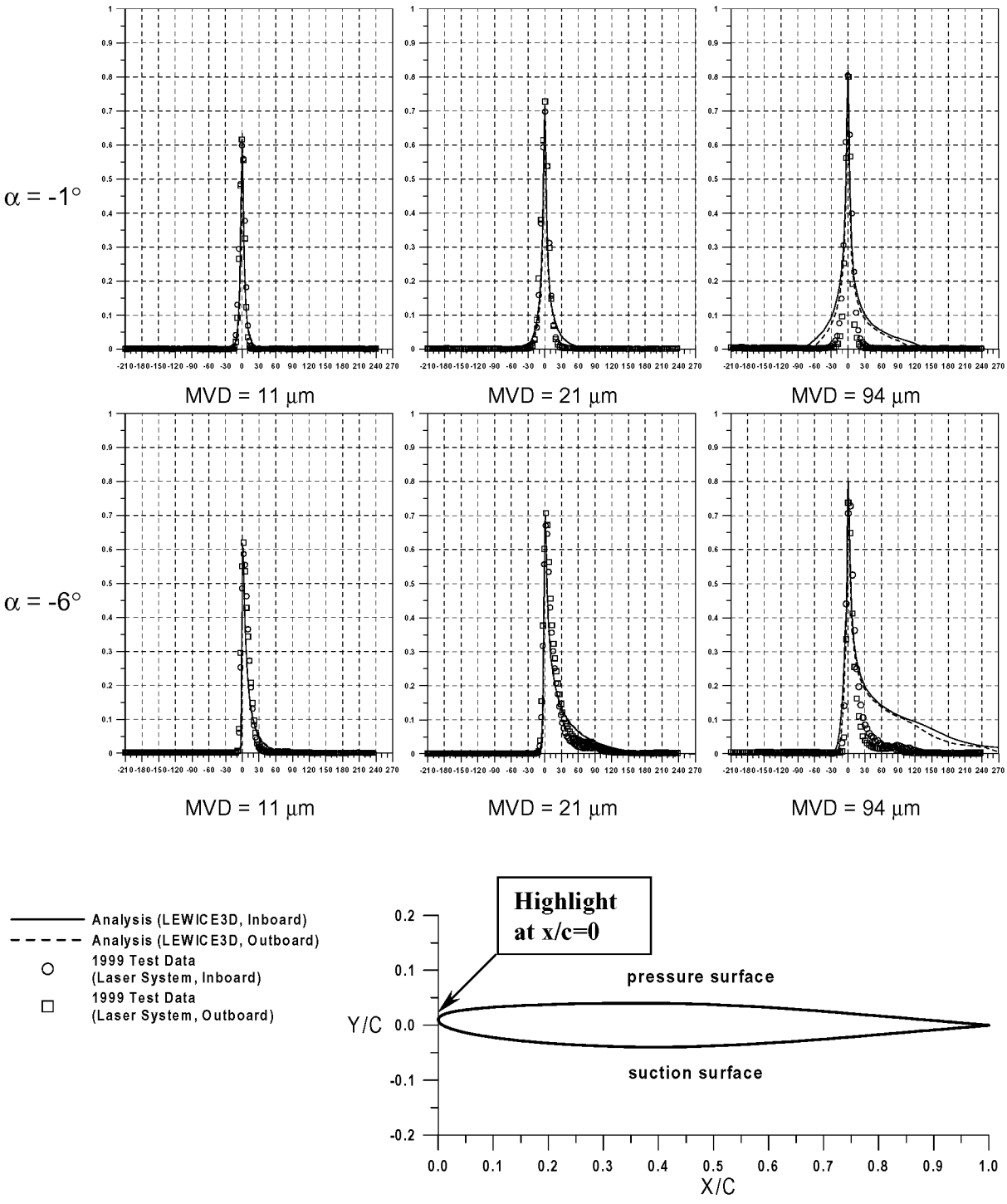

Fig. A8 Impingement data for 25% scale Business Jet Empanage.

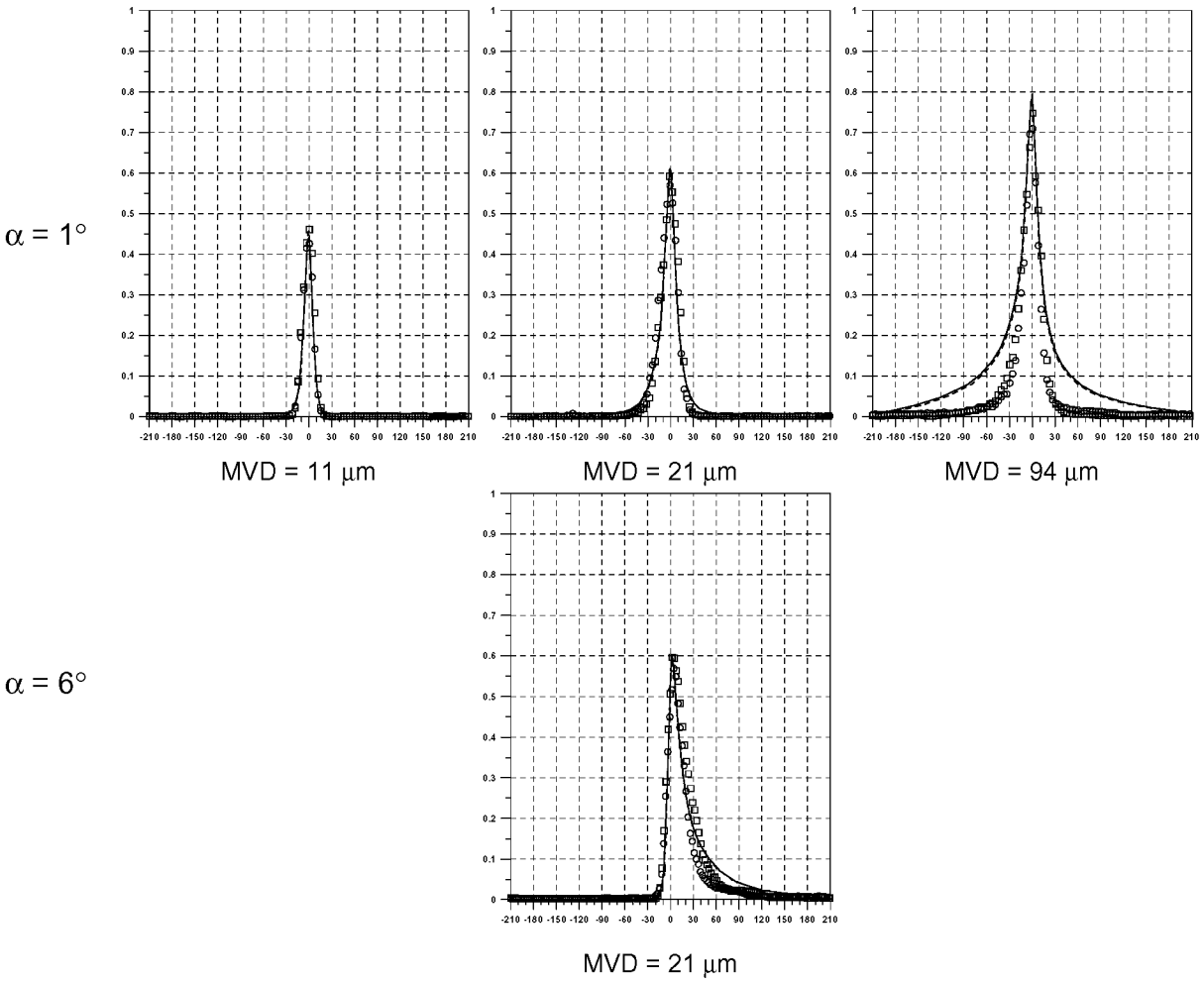

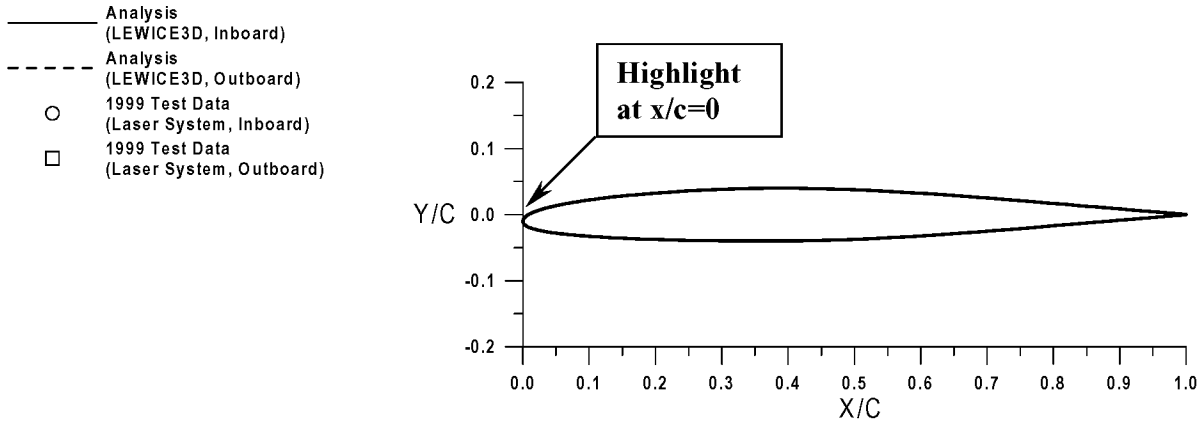

Fig. A9 Impingement data for Full Scale Business Jet Horizontal Tail.

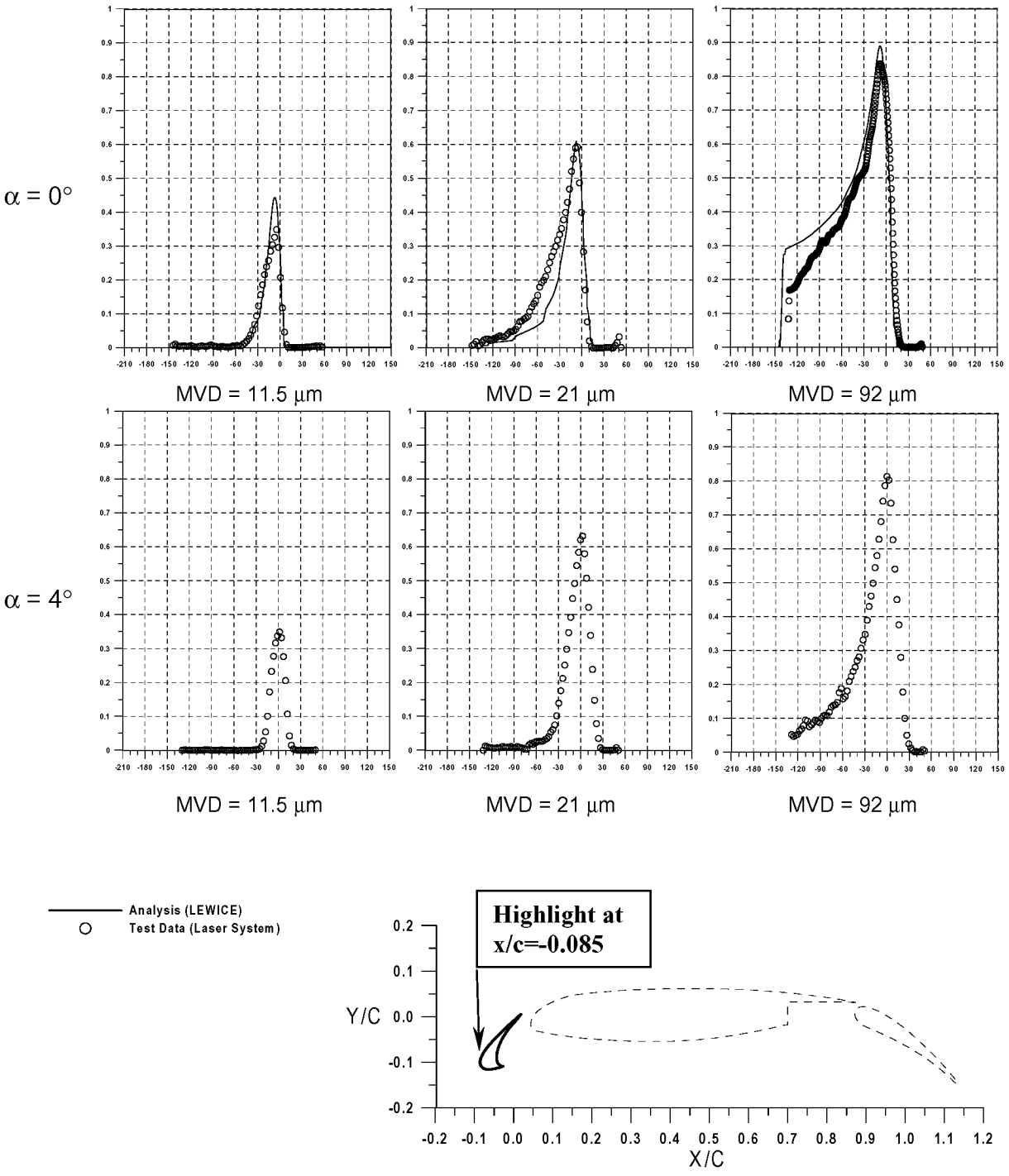

Fig. A10a Impingement data for MD 3-element (slat element).

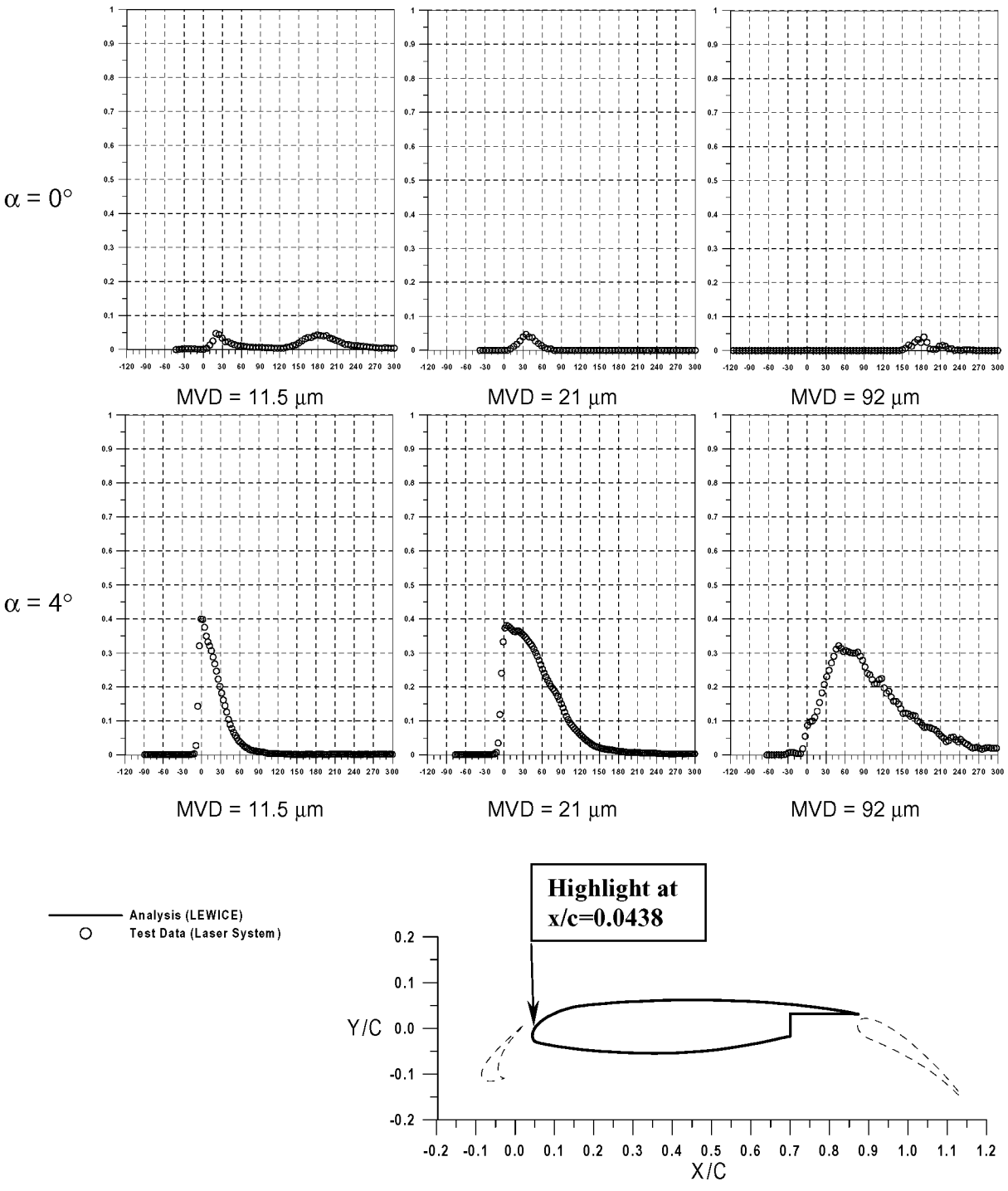

Fig. A10b Impingement data for MD 3-element (main element).

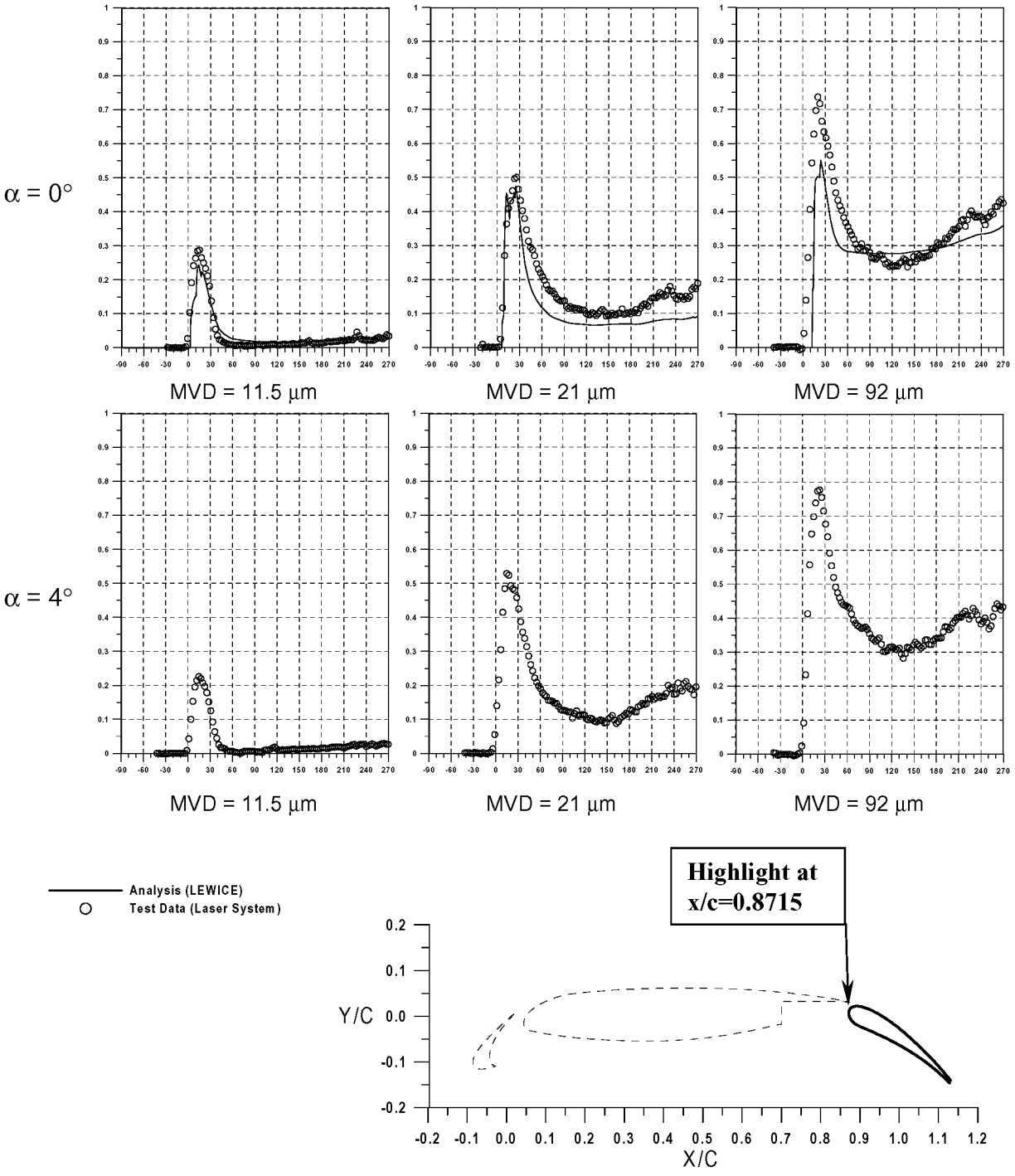

Fig. A10c Impingement data for MD 3-element (flap element).

Appendix B: Coordinates of airfoil sections

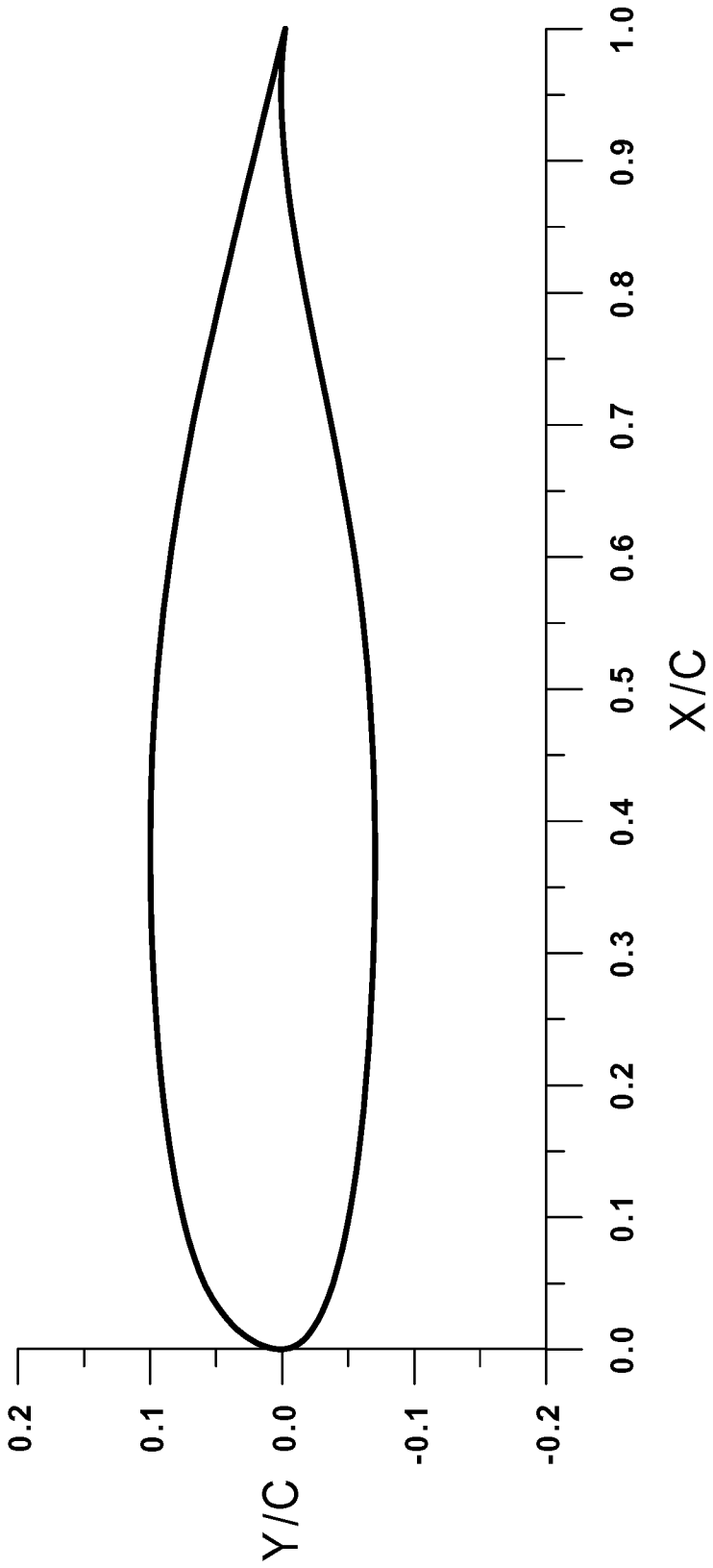

Fig. B-1 MS(1)-0317 Airfoil

Table B-1 Coordinates of MS(1)–0317 Airfoil

Lower Surface						Upper Surface					
x/c	y/c	x/c	y/c	x/c	y/c	x/c	y/c	x/c	y/c	x/c	y/c
1	-0.0024	0.3147	-0.0695			0.0000	0.0022	0.2795	0.0972	1	-0.0024
0.9848	-0.0007	0.2977	-0.0690			0.0001	0.0042	0.2959	0.0980		
0.9725	0.0002	0.2811	-0.0684			0.0004	0.0062	0.3118	0.0986		
0.9603	0.0007	0.2643	-0.0676			0.0008	0.0081	0.3251	0.0990		
0.9469	0.0007	0.2473	-0.0667			0.0013	0.0101	0.3375	0.0993		
0.9332	0.0002	0.2306	-0.0657			0.0018	0.0120	0.3527	0.0996		
0.9193	-0.0006	0.2145	-0.0645			0.0025	0.0139	0.3690	0.0997		
0.9051	-0.0017	0.1982	-0.0631			0.0032	0.0157	0.3854	0.0997		
0.8907	-0.0032	0.1814	-0.0616			0.0040	0.0176	0.4020	0.0995		
0.8760	-0.0050	0.1657	-0.0600			0.0049	0.0193	0.4183	0.0992		
0.8612	-0.0070	0.1502	-0.0582			0.0059	0.0211	0.4341	0.0988		
0.8460	-0.0093	0.1348	-0.0562			0.0068	0.0229	0.4498	0.0983		
0.8304	-0.0119	0.1199	-0.0540			0.0079	0.0246	0.4658	0.0975		
0.8145	-0.0147	0.1055	-0.0516			0.0090	0.0262	0.4818	0.0966		
0.7981	-0.0177	0.0911	-0.0489			0.0101	0.0279	0.4971	0.0956		
0.7812	-0.0210	0.0772	-0.0459			0.0113	0.0295	0.5129	0.0943		
0.7640	-0.0244	0.0640	-0.0427			0.0126	0.0311	0.5290	0.0929		
0.7443	-0.0283	0.0496	-0.0385			0.0138	0.0326	0.5446	0.0913		
0.7249	-0.0323	0.0394	-0.0350			0.0152	0.0341	0.5601	0.0896		
0.7061	-0.0361	0.0323	-0.0321			0.0165	0.0355	0.5755	0.0877		
0.6903	-0.0392	0.0273	-0.0298			0.0180	0.0370	0.5908	0.0857		
0.6732	-0.0425	0.0238	-0.0280			0.0194	0.0383	0.6063	0.0836		
0.6576	-0.0454	0.0213	-0.0267			0.0209	0.0397	0.6223	0.0812		
0.6433	-0.0479	0.0196	-0.0257			0.0224	0.0410	0.6383	0.0787		
0.6273	-0.0507	0.0179	-0.0247			0.0245	0.0428	0.6545	0.0760		
0.6112	-0.0533	0.0162	-0.0236			0.0276	0.0453	0.6713	0.0730		
0.5956	-0.0557	0.0145	-0.0225			0.0320	0.0485	0.6871	0.0701		
0.5802	-0.0578	0.0129	-0.0213			0.0384	0.0527	0.7018	0.0673		
0.5648	-0.0597	0.0113	-0.0201			0.0479	0.0579	0.7178	0.0639		
0.5488	-0.0615	0.0098	-0.0188			0.0588	0.0628	0.7353	0.0602		
0.5328	-0.0632	0.0083	-0.0175			0.0708	0.0671	0.7518	0.0565		
0.5172	-0.0646	0.0070	-0.0160			0.0835	0.0709	0.7687	0.0528		
0.5014	-0.0658	0.0056	-0.0145			0.0967	0.0743	0.7858	0.0489		
0.4851	-0.0669	0.0044	-0.0129			0.1103	0.0774	0.8025	0.0451		
0.4690	-0.0679	0.0034	-0.0112			0.1245	0.0802	0.8211	0.0407		
0.4529	-0.0687	0.0024	-0.0095			0.1391	0.0828	0.8389	0.0365		
0.4367	-0.0693	0.0016	-0.0076			0.1541	0.0852	0.8565	0.0324		
0.4202	-0.0698	0.0010	-0.0057			0.1690	0.0873	0.8758	0.0278		
0.4061	-0.0701	0.0005	-0.0038			0.1843	0.0892	0.8946	0.0233		
0.3966	-0.0702	0.0002	-0.0018			0.2001	0.0910	0.9130	0.0189		
0.3824	-0.0703	0.0000	0.0002			0.2156	0.0925	0.9312	0.0145		
0.3655	-0.0703					0.2313	0.0939	0.9486	0.0103		
0.3487	-0.0702					0.2473	0.0952	0.9658	0.0062		
0.3317	-0.0699					0.2633	0.0962	0.9827	0.0020		

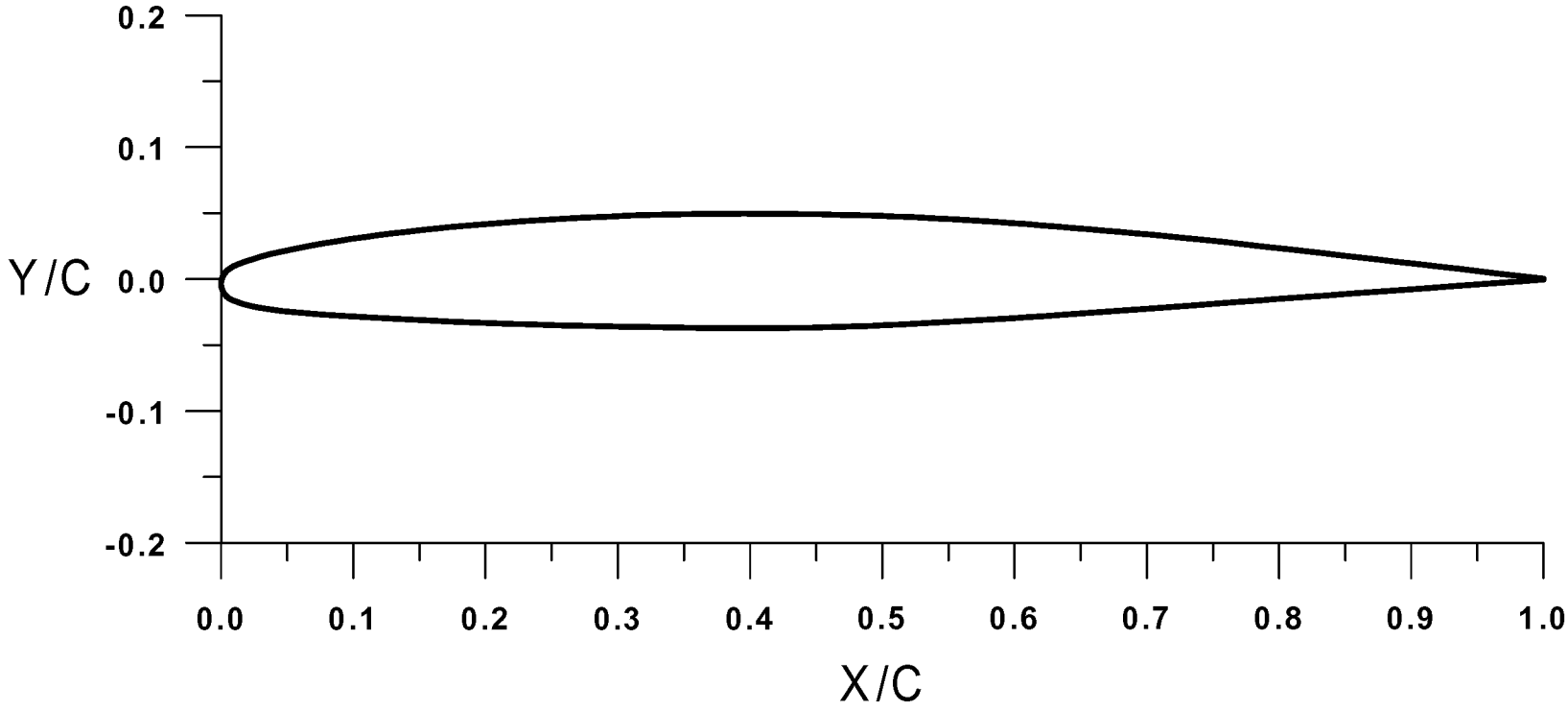

Fig. B-2 GLC 305 Airfoil

Table B-2 Coordinates of GLC 305 Airfoil

Lower Surface						Upper Surface					
x/c	y/c	x/c	y/c	x/c	y/c	x/c	y/c	x/c	y/c	x/c	y/c
1	-0.0003	0.4008	-0.0372	0.0030	-0.0119	0.0000	-0.0026	0.3178	0.0484	0.8092	0.0224
0.9832	-0.0016	0.3893	-0.0372	0.0019	-0.0103	0.0003	-0.0007	0.3288	0.0487	0.8206	0.0211
0.9676	-0.0027	0.3778	-0.0371	0.0010	-0.0085	0.0009	0.0012	0.3398	0.0490	0.8345	0.0195
0.9491	-0.0041	0.3662	-0.0370	0.0003	-0.0066	0.0018	0.0030	0.3506	0.0493	0.8488	0.0178
0.9304	-0.0054	0.3542	-0.0369	0.0000	-0.0046	0.0029	0.0047	0.3614	0.0494	0.8627	0.0162
0.9106	-0.0069	0.3421	-0.0367			0.0042	0.0062	0.3726	0.0495	0.8749	0.0148
0.8918	-0.0083	0.3299	-0.0365			0.0057	0.0075	0.3841	0.0496	0.8892	0.0132
0.8726	-0.0097	0.3177	-0.0363			0.0074	0.0086	0.3955	0.0496	0.9061	0.0112
0.8535	-0.0111	0.3052	-0.0361			0.0092	0.0096	0.4069	0.0495	0.9209	0.0095
0.8370	-0.0123	0.2930	-0.0358			0.0110	0.0104	0.4187	0.0495	0.9351	0.0078
0.8242	-0.0133	0.2809	-0.0356			0.0128	0.0112	0.4303	0.0494	0.9495	0.0062
0.8114	-0.0142	0.2689	-0.0353			0.0147	0.0120	0.4414	0.0493	0.9621	0.0047
0.7985	-0.0152	0.2565	-0.0350			0.0165	0.0127	0.4524	0.0491	0.9801	0.0026
0.7857	-0.0161	0.2437	-0.0347			0.0184	0.0134	0.4637	0.0489	1	0.0003
0.7664	-0.0175	0.2314	-0.0343			0.0211	0.0142	0.4753	0.0486		
0.7492	-0.0188	0.2197	-0.0339			0.0248	0.0154	0.4868	0.0483		
0.7325	-0.0201	0.2079	-0.0335			0.0301	0.0170	0.4979	0.0480		
0.7200	-0.0210	0.1958	-0.0331			0.0375	0.0189	0.5090	0.0476		
0.7048	-0.0221	0.1841	-0.0326			0.0480	0.0214	0.5202	0.0471		
0.6889	-0.0233	0.1728	-0.0321			0.0580	0.0235	0.5314	0.0465		
0.6729	-0.0244	0.1610	-0.0315			0.0678	0.0254	0.5428	0.0459		
0.6576	-0.0255	0.1476	-0.0308			0.0776	0.0271	0.5535	0.0453		
0.6448	-0.0265	0.1338	-0.0301			0.0876	0.0288	0.5642	0.0447		
0.6329	-0.0273	0.1214	-0.0295			0.0980	0.0304	0.5748	0.0441		
0.6214	-0.0281	0.1094	-0.0289			0.1085	0.0319	0.5859	0.0433		
0.6096	-0.0289	0.0977	-0.0282			0.1191	0.0333	0.5968	0.0426		
0.5976	-0.0297	0.0865	-0.0275			0.1298	0.0346	0.6083	0.0417		
0.5854	-0.0304	0.0758	-0.0268			0.1405	0.0359	0.6200	0.0408		
0.5733	-0.0312	0.0655	-0.0260			0.1512	0.0371	0.6319	0.0399		
0.5611	-0.0319	0.0553	-0.0251			0.1620	0.0382	0.6441	0.0389		
0.5492	-0.0326	0.0457	-0.0241			0.1726	0.0393	0.6563	0.0378		
0.5375	-0.0332	0.0366	-0.0229			0.1828	0.0402	0.6681	0.0368		
0.5256	-0.0338	0.0290	-0.0217			0.1938	0.0412	0.6795	0.0358		
0.5136	-0.0344	0.0236	-0.0206			0.2051	0.0421	0.6910	0.0348		
0.5019	-0.0349	0.0198	-0.0197			0.2164	0.0430	0.7022	0.0338		
0.4906	-0.0354	0.0171	-0.0190			0.2274	0.0438	0.7139	0.0326		
0.4793	-0.0358	0.0152	-0.0184			0.2383	0.0445	0.7261	0.0314		
0.4680	-0.0362	0.0133	-0.0178			0.2492	0.0452	0.7381	0.0302		
0.4568	-0.0365	0.0114	-0.0171			0.2605	0.0458	0.7494	0.0291		
0.4456	-0.0368	0.0095	-0.0164			0.2721	0.0464	0.7601	0.0279		
0.4345	-0.0369	0.0077	-0.0156			0.2838	0.0470	0.7710	0.0267		
0.4234	-0.0371	0.0060	-0.0146			0.2952	0.0475	0.7823	0.0255		
0.4122	-0.0372	0.0044	-0.0134			0.3064	0.0480	0.7942	0.0241		

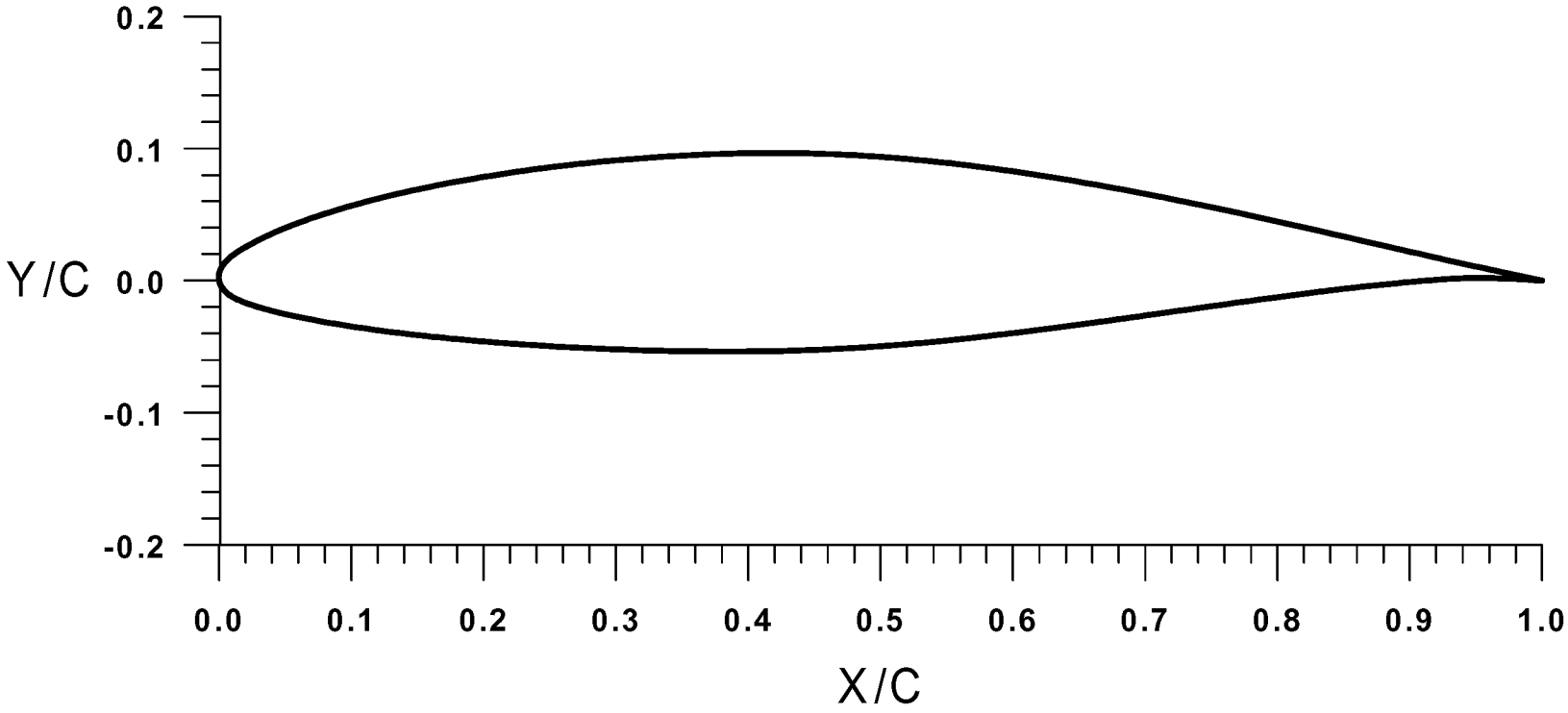

Fig. B-3 NACA 65_2-415 Airfoil

Table B-3 Coordinates of NACA 65_2-415 Airfoil

Lower Surface						Upper Surface					
x/c	y/c	x/c	y/c	x/c	y/c	x/c	y/c	x/c	y/c	x/c	y/c
1	0.0000	0.8358	-0.0078	0.6080	-0.0387	0.0000	0.0003	0.0416	0.0363	0.1891	0.0767
0.9942	0.0004	0.8311	-0.0084	0.6030	-0.0393	-0.0002	0.0013	0.0443	0.0375	0.1931	0.0774
0.9898	0.0007	0.8264	-0.0090	0.5981	-0.0399	-0.0002	0.0023	0.0470	0.0386	0.1971	0.0781
0.9856	0.0009	0.8215	-0.0096	0.5939	-0.0404	-0.0002	0.0033	0.0497	0.0398	0.2011	0.0787
0.9816	0.0011	0.8164	-0.0103	0.5902	-0.0408	-0.0001	0.0043	0.0525	0.0409	0.2052	0.0794
0.9779	0.0013	0.8112	-0.0110	0.5849	-0.0414	0.0001	0.0053	0.0554	0.0420	0.2093	0.0800
0.9742	0.0015	0.8061	-0.0117	0.5830	-0.0417	0.0003	0.0062	0.0582	0.0431	0.2133	0.0807
0.9708	0.0017	0.8011	-0.0123	0.5817	-0.0418	0.0006	0.0072	0.0612	0.0442	0.2174	0.0813
0.9674	0.0018	0.7960	-0.0130	0.5805	-0.0420	0.0010	0.0081	0.0642	0.0453	0.2216	0.0819
0.9641	0.0019	0.7906	-0.0137	0.5786	-0.0422	0.0014	0.0090	0.0672	0.0464	0.2257	0.0825
0.9612	0.0020	0.7851	-0.0145	0.5739	-0.0427	0.0018	0.0099	0.0704	0.0474	0.2298	0.0831
0.9582	0.0020	0.7798	-0.0152	0.5701	-0.0431	0.0023	0.0108	0.0735	0.0485	0.2339	0.0837
0.9551	0.0021	0.7741	-0.0160	0.5661	-0.0436	0.0028	0.0117	0.0768	0.0496	0.2381	0.0843
0.9520	0.0021	0.7685	-0.0168	0.5617	-0.0440	0.0034	0.0125	0.0800	0.0506	0.2422	0.0848
0.9490	0.0021	0.7618	-0.0177	0.5574	-0.0445	0.0040	0.0133	0.0833	0.0517	0.2464	0.0853
0.9460	0.0020	0.7555	-0.0186	0.5533	-0.0449	0.0047	0.0140	0.0866	0.0527	0.2504	0.0858
0.9432	0.0019	0.7498	-0.0194	0.5492	-0.0453	0.0054	0.0147	0.0899	0.0537	0.2544	0.0863
0.9404	0.0019	0.7438	-0.0202	0.5447	-0.0458	0.0061	0.0155	0.0933	0.0547	0.2585	0.0868
0.9372	0.0017	0.7377	-0.0211	0.5401	-0.0462	0.0068	0.0161	0.0967	0.0557	0.2626	0.0873
0.9340	0.0016	0.7317	-0.0219	0.5355	-0.0467	0.0075	0.0168	0.1000	0.0567	0.2667	0.0878
0.9307	0.0014	0.7257	-0.0227	0.5310	-0.0471	0.0083	0.0175	0.1034	0.0577	0.2708	0.0882
0.9274	0.0012	0.7196	-0.0236	0.5266	-0.0475	0.0091	0.0181	0.1069	0.0586	0.2749	0.0887
0.9239	0.0010	0.7136	-0.0244	0.5221	-0.0479	0.0098	0.0187	0.1103	0.0596	0.2790	0.0891
0.9204	0.0007	0.7076	-0.0253	0.5177	-0.0482	0.0106	0.0194	0.1138	0.0605	0.2832	0.0895
0.9167	0.0005	0.7016	-0.0261	0.5133	-0.0486	0.0114	0.0200	0.1173	0.0614	0.2873	0.0899
0.9129	0.0002	0.6955	-0.0270	0.5090	-0.0489	0.0122	0.0205	0.1209	0.0623	0.2913	0.0903
0.9090	-0.0002	0.6895	-0.0278	0.5046	-0.0493	0.0131	0.0211	0.1244	0.0632	0.2951	0.0907
0.9047	-0.0006	0.6841	-0.0286	0.5004	-0.0496	0.0139	0.0217	0.1280	0.0641	0.2992	0.0910
0.9003	-0.0010	0.6796	-0.0292	0.4960	-0.0499	0.0147	0.0222	0.1316	0.0649	0.3034	0.0914
0.8956	-0.0014	0.6742	-0.0300	0.4917	-0.0502	0.0155	0.0228	0.1353	0.0658	0.3077	0.0918
0.8914	-0.0018	0.6695	-0.0306	0.4874	-0.0505	0.0164	0.0233	0.1389	0.0666	0.3119	0.0921
0.8865	-0.0023	0.6651	-0.0312	0.4830	-0.0507	0.0172	0.0239	0.1426	0.0674	0.3162	0.0924
0.8818	-0.0027	0.6614	-0.0317	0.4786	-0.0510	0.0181	0.0244	0.1463	0.0683	0.3205	0.0928
0.8773	-0.0032	0.6574	-0.0323	0.4743	-0.0512	0.0190	0.0249	0.1500	0.0691	0.3248	0.0931
0.8726	-0.0037	0.6529	-0.0329	0.4699	-0.0515	0.0202	0.0256	0.1539	0.0699	0.3291	0.0934
0.8679	-0.0042	0.6490	-0.0334	0.4655	-0.0517	0.0219	0.0266	0.1577	0.0707	0.3333	0.0936
0.8632	-0.0047	0.6438	-0.0341	0.4612	-0.0519	0.0243	0.0279	0.1615	0.0715	0.3376	0.0939
0.8586	-0.0052	0.6390	-0.0347	0.4568	-0.0521	0.0266	0.0291	0.1654	0.0723	0.3419	0.0942
0.8540	-0.0057	0.6341	-0.0354	0.4524	-0.0523	0.0290	0.0304	0.1693	0.0730	0.3462	0.0944
0.8495	-0.0062	0.6289	-0.0361	0.4481	-0.0525	0.0315	0.0316	0.1732	0.0738	0.3505	0.0947
0.8462	-0.0066	0.6237	-0.0367	0.4438	-0.0526	0.0340	0.0328	0.1772	0.0745	0.3548	0.0949
0.8425	-0.0070	0.6183	-0.0374	0.4395	-0.0528	0.0365	0.0340	0.1811	0.0753	0.3590	0.0951
0.8398	-0.0074	0.6132	-0.0380	0.4351	-0.0529	0.0390	0.0352	0.1851	0.0760	0.3633	0.0953

Lower Surface						Upper Surface					
x/c	y/c	x/c	y/c	x/c	y/c	x/c	y/c	x/c	y/c	x/c	y/c
0.4307	-0.0530	0.2296	-0.0483	0.0520	-0.0258	0.3676	0.0955	0.5400	0.0902	0.7255	0.0606
0.4263	-0.0531	0.2249	-0.0479	0.0489	-0.0250	0.3718	0.0956	0.5440	0.0898	0.7295	0.0598
0.4219	-0.0532	0.2202	-0.0476	0.0458	-0.0243	0.3761	0.0958	0.5481	0.0894	0.7335	0.0590
0.4175	-0.0533	0.2155	-0.0473	0.0428	-0.0236	0.3803	0.0959	0.5522	0.0889	0.7389	0.0579
0.4132	-0.0534	0.2109	-0.0469	0.0399	-0.0228	0.3845	0.0961	0.5564	0.0884	0.7427	0.0571
0.4087	-0.0535	0.2062	-0.0465	0.0370	-0.0220	0.3886	0.0962	0.5603	0.0880	0.7452	0.0566
0.4043	-0.0535	0.2017	-0.0462	0.0341	-0.0213	0.3928	0.0963	0.5646	0.0874	0.7489	0.0558
0.4001	-0.0536	0.1971	-0.0458	0.0313	-0.0205	0.3969	0.0964	0.5681	0.0870	0.7536	0.0548
0.3957	-0.0536	0.1926	-0.0454	0.0286	-0.0196	0.4009	0.0964	0.5723	0.0865	0.7583	0.0538
0.3912	-0.0536	0.1880	-0.0450	0.0259	-0.0188	0.4050	0.0965	0.5766	0.0859	0.7630	0.0528
0.3866	-0.0536	0.1835	-0.0446	0.0234	-0.0180	0.4090	0.0965	0.5810	0.0854	0.7678	0.0518
0.3820	-0.0536	0.1789	-0.0441	0.0208	-0.0171	0.4130	0.0965	0.5854	0.0848	0.7721	0.0509
0.3774	-0.0536	0.1744	-0.0437	0.0189	-0.0164	0.4170	0.0966	0.5898	0.0842	0.7770	0.0498
0.3727	-0.0536	0.1699	-0.0433	0.0176	-0.0159	0.4210	0.0966	0.5943	0.0835	0.7820	0.0487
0.3680	-0.0536	0.1654	-0.0428	0.0167	-0.0155	0.4251	0.0965	0.5987	0.0829	0.7870	0.0476
0.3633	-0.0535	0.1609	-0.0423	0.0158	-0.0151	0.4291	0.0965	0.6029	0.0823	0.7920	0.0465
0.3585	-0.0535	0.1564	-0.0419	0.0149	-0.0147	0.4331	0.0965	0.6071	0.0817	0.7970	0.0454
0.3537	-0.0534	0.1520	-0.0414	0.0139	-0.0143	0.4371	0.0964	0.6114	0.0810	0.8021	0.0443
0.3489	-0.0533	0.1477	-0.0409	0.0130	-0.0139	0.4411	0.0964	0.6158	0.0804	0.8071	0.0432
0.3441	-0.0532	0.1433	-0.0404	0.0121	-0.0134	0.4451	0.0963	0.6201	0.0797	0.8121	0.0420
0.3395	-0.0531	0.1390	-0.0399	0.0113	-0.0130	0.4491	0.0962	0.6243	0.0790	0.8171	0.0409
0.3348	-0.0530	0.1348	-0.0394	0.0104	-0.0125	0.4531	0.0961	0.6287	0.0783	0.8221	0.0398
0.3301	-0.0529	0.1306	-0.0389	0.0095	-0.0120	0.4570	0.0960	0.6329	0.0777	0.8272	0.0387
0.3253	-0.0528	0.1265	-0.0383	0.0087	-0.0114	0.4609	0.0958	0.6369	0.0770	0.8322	0.0375
0.3206	-0.0527	0.1224	-0.0378	0.0079	-0.0109	0.4649	0.0957	0.6412	0.0763	0.8377	0.0363
0.3158	-0.0525	0.1183	-0.0373	0.0071	-0.0102	0.4689	0.0955	0.6457	0.0755	0.8434	0.0350
0.3110	-0.0524	0.1143	-0.0367	0.0063	-0.0096	0.4729	0.0953	0.6500	0.0748	0.8486	0.0338
0.3063	-0.0522	0.1103	-0.0362	0.0056	-0.0090	0.4769	0.0951	0.6544	0.0740	0.8547	0.0324
0.3015	-0.0520	0.1064	-0.0356	0.0048	-0.0083	0.4809	0.0949	0.6590	0.0732	0.8600	0.0312
0.2968	-0.0519	0.1025	-0.0350	0.0041	-0.0075	0.4849	0.0947	0.6635	0.0724	0.8655	0.0299
0.2920	-0.0517	0.0987	-0.0344	0.0035	-0.0068	0.4888	0.0945	0.6680	0.0716	0.8715	0.0285
0.2872	-0.0515	0.0949	-0.0338	0.0028	-0.0060	0.4928	0.0942	0.6726	0.0708	0.8787	0.0268
0.2824	-0.0512	0.0911	-0.0332	0.0023	-0.0052	0.4967	0.0940	0.6772	0.0700	0.8845	0.0255
0.2775	-0.0510	0.0873	-0.0326	0.0017	-0.0044	0.5006	0.0937	0.6818	0.0691	0.8899	0.0243
0.2727	-0.0508	0.0835	-0.0319	0.0012	-0.0035	0.5045	0.0934	0.6865	0.0682	0.8952	0.0230
0.2678	-0.0505	0.0797	-0.0312	0.0008	-0.0026	0.5084	0.0931	0.6909	0.0674	0.9003	0.0219
0.2630	-0.0503	0.0759	-0.0306	0.0004	-0.0017	0.5122	0.0928	0.6955	0.0665	0.9055	0.0207
0.2582	-0.0500	0.0722	-0.0299	0.0002	-0.0007	0.5161	0.0925	0.7002	0.0656	0.9108	0.0195
0.2534	-0.0498	0.0686	-0.0292	0.0000	0.0003	0.5201	0.0921	0.7048	0.0647	0.9164	0.0182
0.2486	-0.0495	0.0651	-0.0285			0.5240	0.0918	0.7089	0.0639	0.9218	0.0170
0.2439	-0.0492	0.0618	-0.0279			0.5280	0.0914	0.7132	0.0631	0.9270	0.0158
0.2391	-0.0489	0.0584	-0.0272			0.5320	0.0910	0.7172	0.0623	0.9321	0.0146
0.2344	-0.0486	0.0552	-0.0265			0.5361	0.0906	0.7217	0.0614	0.9370	0.0135

Lower Surface						Upper Surface					
x/c	y/c	x/c	y/c	x/c	y/c	x/c	y/c	x/c	y/c	x/c	y/c
						0.9421	0.0124				
						0.9472	0.0113				
						0.9519	0.0103				
						0.9562	0.0093				
						0.9607	0.0083				
						0.9654	0.0073				
						0.9701	0.0063				
						0.9745	0.0054				
						0.9796	0.0043				
						0.9850	0.0032				
						0.9911	0.0019				
						0.9964	0.0007				
						1	0.0000				

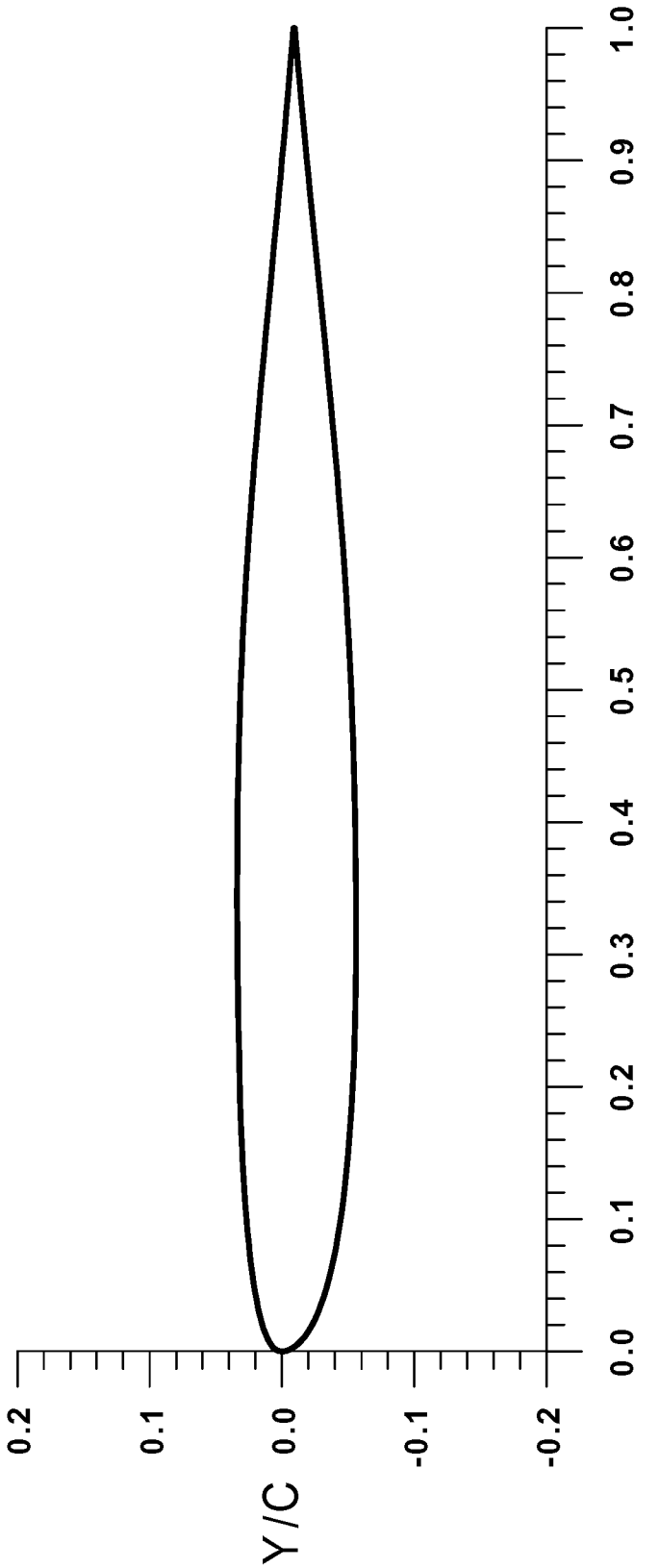

Fig. B-4 Commercial Transport Tail Section

Table B-4 Coordinates of Commercial Transport Tail Section

Lower Surface						Upper Surface					
x/c	y/c	x/c	y/c	x/c	y/c	x/c	y/c	x/c	y/c	x/c	y/c
1.0000	-0.0096	0.4474	-0.0542	0.0054	-0.0118	0.0000	0.0003	0.4170	0.0334	0.9810	-0.0071
0.9908	-0.0105	0.4340	-0.0545	0.0031	-0.0089	0.0006	0.0034	0.4306	0.0332	0.9907	-0.0079
0.9811	-0.0113	0.4205	-0.0548	0.0014	-0.0057	0.0026	0.0066	0.4441	0.0330	1.0000	-0.0086
0.9709	-0.0122	0.4071	-0.0551	0.0003	-0.0027	0.0055	0.0086	0.4576	0.0326		
0.9602	-0.0132	0.3936	-0.0553			0.0091	0.0106	0.4712	0.0323		
0.9491	-0.0142	0.3802	-0.0555			0.0131	0.0124	0.4847	0.0319		
0.9377	-0.0153	0.3667	-0.0557			0.0175	0.0140	0.4982	0.0314		
0.9258	-0.0164	0.3533	-0.0557			0.0222	0.0155	0.5117	0.0309		
0.9137	-0.0175	0.3399	-0.0558			0.0273	0.0168	0.5252	0.0303		
0.9013	-0.0187	0.3265	-0.0558			0.0328	0.0180	0.5387	0.0297		
0.8886	-0.0199	0.3131	-0.0558			0.0386	0.0192	0.5523	0.0290		
0.8758	-0.0212	0.2998	-0.0558			0.0448	0.0203	0.5658	0.0283		
0.8628	-0.0225	0.2865	-0.0557			0.0514	0.0214	0.5793	0.0275		
0.8498	-0.0237	0.2733	-0.0557			0.0585	0.0224	0.5928	0.0267		
0.8366	-0.0250	0.2602	-0.0555			0.0660	0.0234	0.6063	0.0258		
0.8233	-0.0264	0.2472	-0.0553			0.0739	0.0243	0.6198	0.0248		
0.8100	-0.0277	0.2342	-0.0549			0.0823	0.0252	0.6333	0.0239		
0.7967	-0.0290	0.2214	-0.0544			0.0912	0.0261	0.6468	0.0228		
0.7833	-0.0303	0.2087	-0.0539			0.1006	0.0269	0.6604	0.0218		
0.7699	-0.0317	0.1962	-0.0532			0.1105	0.0277	0.6739	0.0207		
0.7565	-0.0330	0.1838	-0.0525			0.1208	0.0284	0.6874	0.0196		
0.7430	-0.0343	0.1717	-0.0516			0.1315	0.0291	0.7009	0.0184		
0.7296	-0.0356	0.1598	-0.0508			0.1427	0.0297	0.7144	0.0172		
0.7162	-0.0369	0.1482	-0.0498			0.1542	0.0303	0.7280	0.0160		
0.7027	-0.0381	0.1369	-0.0487			0.1661	0.0308	0.7415	0.0148		
0.6893	-0.0393	0.1260	-0.0476			0.1782	0.0313	0.7550	0.0135		
0.6759	-0.0405	0.1154	-0.0464			0.1906	0.0317	0.7685	0.0123		
0.6624	-0.0417	0.1053	-0.0451			0.2033	0.0320	0.7820	0.0110		
0.6490	-0.0428	0.0957	-0.0437			0.2161	0.0323	0.7954	0.0097		
0.6356	-0.0439	0.0865	-0.0422			0.2291	0.0326	0.8089	0.0085		
0.6221	-0.0450	0.0778	-0.0406			0.2422	0.0328	0.8223	0.0072		
0.6087	-0.0460	0.0695	-0.0390			0.2554	0.0330	0.8356	0.0060		
0.5953	-0.0469	0.0617	-0.0373			0.2687	0.0332	0.8489	0.0047		
0.5818	-0.0479	0.0544	-0.0354			0.2821	0.0334	0.8620	0.0035		
0.5684	-0.0487	0.0476	-0.0335			0.2955	0.0336	0.8751	0.0023		
0.5550	-0.0495	0.0412	-0.0315			0.3089	0.0337	0.8880	0.0011		
0.5415	-0.0503	0.0352	-0.0294			0.3224	0.0338	0.9007	0.0000		
0.5281	-0.0510	0.0297	-0.0273			0.3359	0.0339	0.9132	-0.0012		
0.5147	-0.0516	0.0245	-0.0250			0.3494	0.0339	0.9254	-0.0023		
0.5012	-0.0522	0.0198	-0.0227			0.3629	0.0339	0.9373	-0.0033		
0.4878	-0.0528	0.0155	-0.0202			0.3764	0.0339	0.9488	-0.0043		
0.4743	-0.0533	0.0117	-0.0175			0.3900	0.0338	0.9600	-0.0053		
0.4609	-0.0538	0.0083	-0.0148			0.4042	0.0336	0.4170	0.0334		

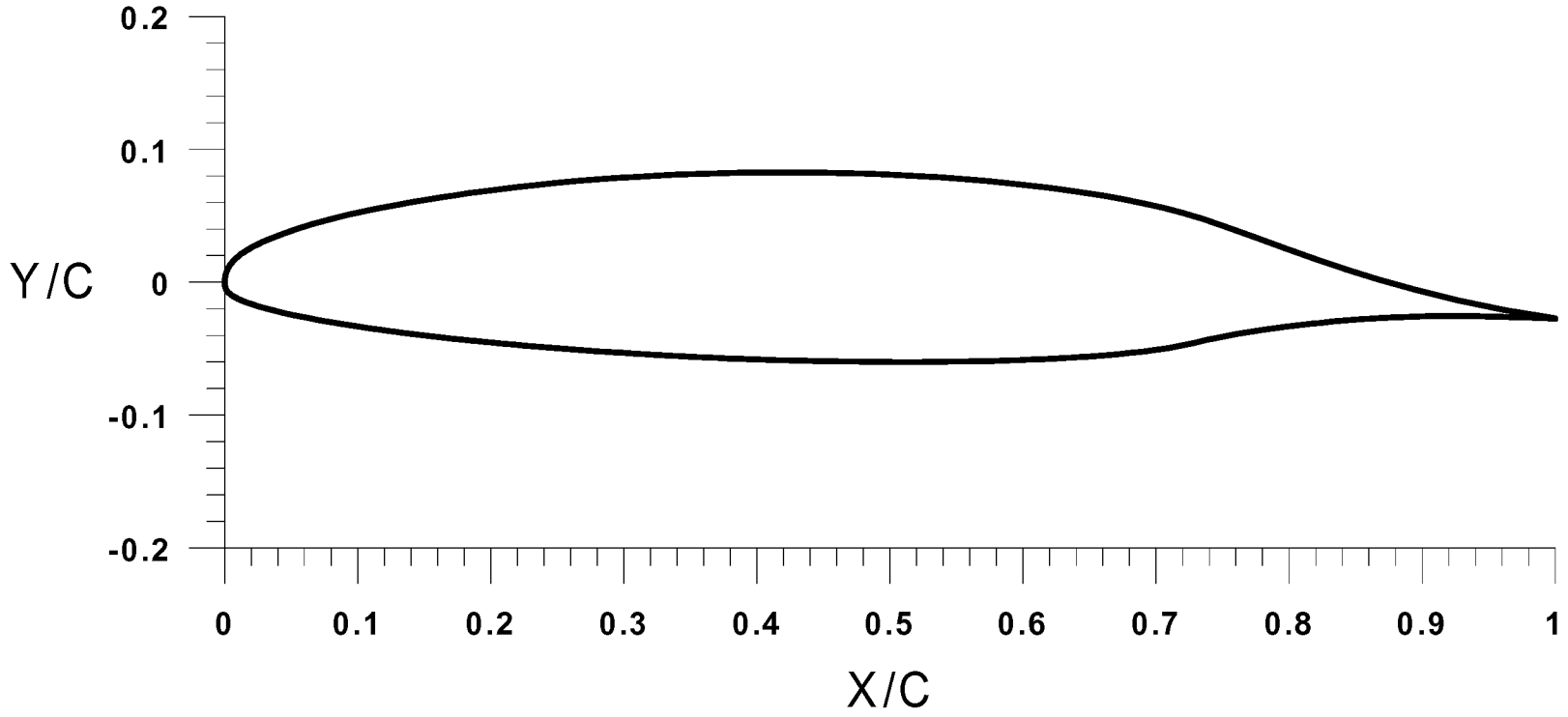

Fig. B-5 NLF(1)-0414 Airfoil (c = 36 in.)

Table B-5 Coordinates of 36-inch NLF(1)-0414 Airfoil

Lower Surface						Upper Surface					
x/c	y/c	x/c	y/c	x/c	y/c	x/c	y/c	x/c	y/c	x/c	y/c
1.0000	-0.0275	0.7548	-0.0401	0.5101	-0.0600	0.0000	0.0008	0.0617	0.0425	0.6008	0.0733
0.9943	-0.0271	0.7492	-0.0412	0.5044	-0.0600	0.0001	0.0018	0.0667	0.0440	0.6185	0.0712
0.9886	-0.0269	0.7436	-0.0423	0.4987	-0.0600	0.0002	0.0028	0.0717	0.0454	0.6303	0.0697
0.9829	-0.0267	0.7380	-0.0435	0.4930	-0.0600	0.0004	0.0038	0.0768	0.0467	0.6454	0.0675
0.9771	-0.0265	0.7324	-0.0448	0.4872	-0.0599	0.0006	0.0048	0.0818	0.0480	0.6602	0.0651
0.9714	-0.0263	0.7268	-0.0460	0.4815	-0.0599	0.0008	0.0057	0.0869	0.0493	0.6750	0.0625
0.9657	-0.0262	0.7212	-0.0472	0.4758	-0.0598	0.0011	0.0067	0.0932	0.0508	0.6903	0.0594
0.9600	-0.0260	0.7156	-0.0483	0.4701	-0.0597	0.0014	0.0076	0.0996	0.0523	0.7053	0.0560
0.9542	-0.0259	0.7100	-0.0494	0.4644	-0.0597	0.0018	0.0086	0.1088	0.0542	0.7188	0.0525
0.9485	-0.0258	0.7043	-0.0503	0.4586	-0.0596	0.0021	0.0095	0.1191	0.0563	0.7347	0.0477
0.9428	-0.0257	0.6987	-0.0511	0.4529	-0.0595	0.0026	0.0104	0.1301	0.0584	0.7528	0.0416
0.9371	-0.0256	0.6930	-0.0519	0.4472	-0.0594	0.0031	0.0113	0.1418	0.0605	0.7746	0.0337
0.9314	-0.0256	0.6873	-0.0525	0.4415	-0.0593	0.0036	0.0121	0.1543	0.0626	0.7971	0.0254
0.9256	-0.0255	0.6816	-0.0532	0.4357	-0.0592	0.0041	0.0130	0.1639	0.0641	0.8208	0.0170
0.9199	-0.0255	0.6759	-0.0537	0.4300	-0.0590	0.0047	0.0138	0.1721	0.0653	0.8434	0.0094
0.9142	-0.0256	0.6702	-0.0543	0.4243	-0.0589	0.0053	0.0146	0.1844	0.0671	0.8672	0.0020
0.9085	-0.0256	0.6645	-0.0548	0.4186	-0.0587	0.0059	0.0153	0.1938	0.0684	0.8950	-0.0058
0.9027	-0.0257	0.6588	-0.0553	0.4129	-0.0586	0.0066	0.0161	0.2061	0.0700	0.9263	-0.0135
0.8970	-0.0258	0.6531	-0.0557	0.4071	-0.0584	0.0073	0.0168	0.2200	0.0717	0.9629	-0.0211
0.8913	-0.0260	0.6474	-0.0561	0.4014	-0.0582	0.0080	0.0175	0.2329	0.0731	1.0000	-0.0271
0.8856	-0.0262	0.6417	-0.0565	0.3957	-0.0580	0.0087	0.0182	0.2468	0.0745		
0.8799	-0.0264	0.6360	-0.0569	0.3900	-0.0578	0.0095	0.0189	0.2561	0.0754		
0.8741	-0.0267	0.6303	-0.0572	0.3843	-0.0576	0.0102	0.0195	0.2658	0.0762		
0.8684	-0.0269	0.6246	-0.0575	0.3785	-0.0574	0.0110	0.0202	0.2803	0.0774		
0.8627	-0.0273	0.6188	-0.0578	0.3728	-0.0571	0.0118	0.0208	0.2955	0.0785		
0.8570	-0.0276	0.6131	-0.0580	0.3671	-0.0569	0.0126	0.0214	0.3092	0.0794		
0.8513	-0.0280	0.6074	-0.0583	0.3614	-0.0566	0.0134	0.0220	0.3237	0.0802		
0.8456	-0.0285	0.6017	-0.0585	0.3557	-0.0564	0.0142	0.0225	0.3390	0.0809		
0.8399	-0.0290	0.5960	-0.0587	0.3500	-0.0561	0.0151	0.0231	0.3543	0.0815		
0.8342	-0.0295	0.5902	-0.0589	0.3442	-0.0558	0.0159	0.0236	0.3701	0.0820		
0.8285	-0.0300	0.5845	-0.0590	0.3385	-0.0555	0.0168	0.0241	0.3836	0.0823		
0.8228	-0.0306	0.5788	-0.0592	0.3328	-0.0552	0.0176	0.0246	0.3945	0.0825		
0.8171	-0.0312	0.5731	-0.0593	0.3271	-0.0549	0.0185	0.0251	0.4056	0.0826		
0.8114	-0.0318	0.5674	-0.0595	0.3214	-0.0545	0.0194	0.0256	0.4164	0.0827		
0.8057	-0.0325	0.5616	-0.0596	0.3157	-0.0542	0.0206	0.0263	0.4279	0.0827		
0.8001	-0.0332	0.5559	-0.0597	0.3100	-0.0539	0.0223	0.0272	0.4451	0.0825		
0.7944	-0.0339	0.5502	-0.0598	0.3042	-0.0535	0.0248	0.0285	0.4632	0.0822		
0.7887	-0.0347	0.5445	-0.0599	0.2985	-0.0532	0.0282	0.0301	0.4839	0.0816		
0.7830	-0.0355	0.5388	-0.0599	0.2928	-0.0528	0.0335	0.0325	0.4993	0.0810		
0.7774	-0.0363	0.5330	-0.0600	0.2871	-0.0524	0.0403	0.0352	0.5205	0.0800		
0.7717	-0.0372	0.5273	-0.0600	0.2814	-0.0520	0.0450	0.0370	0.5375	0.0789		
0.7661	-0.0381	0.5216	-0.0600	0.2757	-0.0516	0.0496	0.0386	0.5578	0.0774		
0.7604	-0.0391	0.5159	-0.0600	0.2700	-0.0512	0.0566	0.0409	0.5763	0.0758		

Lower Surface						Upper Surface					
x/c	y/c	x/c	y/c	x/c	y/c	x/c	y/c	x/c	y/c	x/c	y/c
0.2643	-0.0508	0.0216	-0.0170								
0.2586	-0.0504	0.0197	-0.0164								
0.2529	-0.0499	0.0184	-0.0159								
0.2472	-0.0495	0.0174	-0.0156								
0.2415	-0.0490	0.0165	-0.0152								
0.2358	-0.0486	0.0156	-0.0149								
0.2300	-0.0481	0.0146	-0.0145								
0.2243	-0.0476	0.0137	-0.0142								
0.2186	-0.0471	0.0128	-0.0138								
0.2129	-0.0466	0.0119	-0.0134								
0.2072	-0.0461	0.0110	-0.0130								
0.2015	-0.0455	0.0101	-0.0125								
0.1959	-0.0450	0.0092	-0.0121								
0.1902	-0.0444	0.0083	-0.0116								
0.1845	-0.0438	0.0074	-0.0111								
0.1788	-0.0432	0.0065	-0.0106								
0.1731	-0.0426	0.0057	-0.0101								
0.1674	-0.0420	0.0049	-0.0095								
0.1617	-0.0414	0.0041	-0.0089								
0.1560	-0.0407	0.0033	-0.0083								
0.1503	-0.0401	0.0026	-0.0076								
0.1446	-0.0394	0.0020	-0.0068								
0.1390	-0.0387	0.0014	-0.0060								
0.1333	-0.0380	0.0010	-0.0051								
0.1276	-0.0372	0.0006	-0.0041								
0.1219	-0.0365	0.0004	-0.0032								
0.1163	-0.0357	0.0002	-0.0022								
0.1106	-0.0349	0.0001	-0.0012								
0.1049	-0.0341	0.0000	-0.0002								
0.0993	-0.0332										
0.0936	-0.0323										
0.0875	-0.0314										
0.0814	-0.0304										
0.0753	-0.0293										
0.0693	-0.0282										
0.0632	-0.0271										
0.0571	-0.0259										
0.0511	-0.0246										
0.0451	-0.0233										
0.0390	-0.0219										
0.0331	-0.0203										
0.0279	-0.0189										
0.0242	-0.0178										

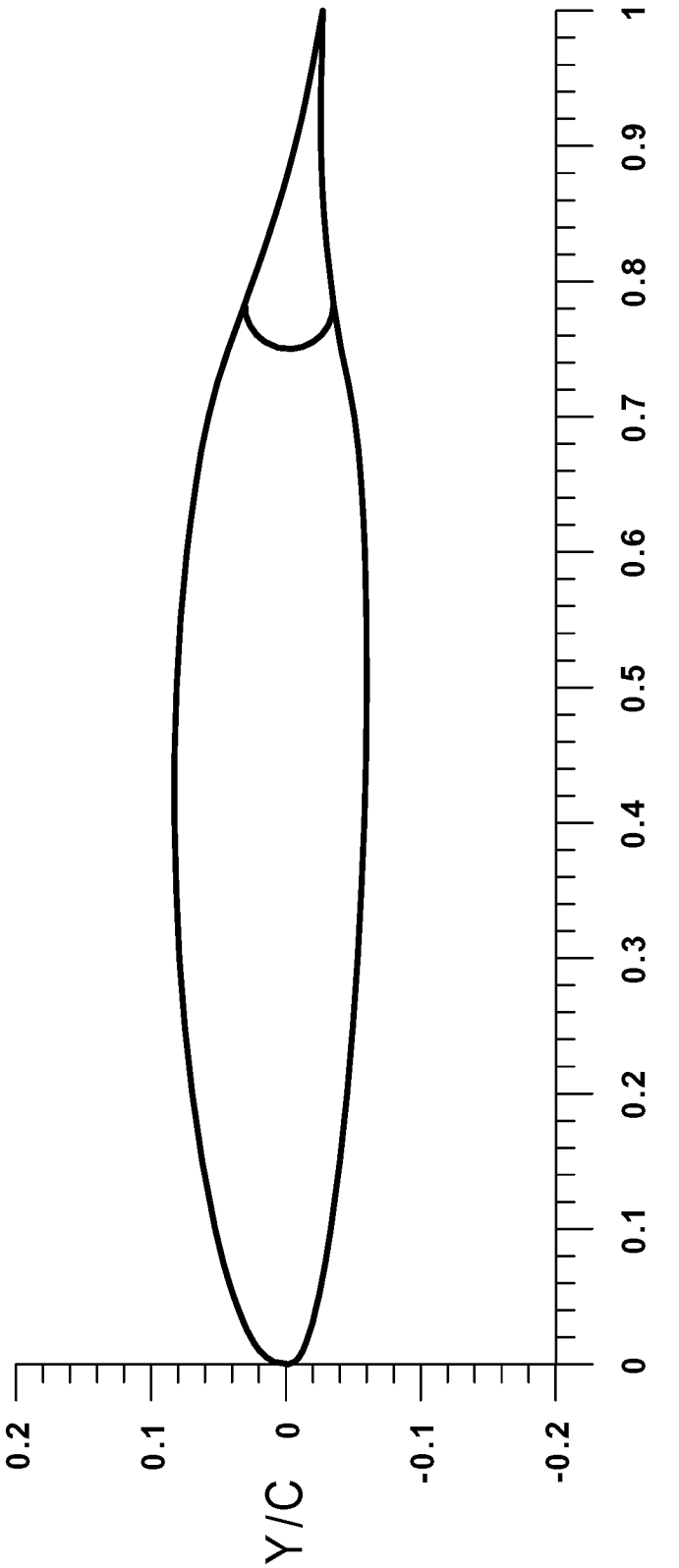

Fig. B-6 NLF(1)-0414 Airfoil (c = 48 in.)

Table B-6a Coordinates of 48-in NLF(1)-0414 Airfoil (Main Element)

Lower Surface						Upper Surface					
x/c	y/c	x/c	y/c	x/c	y/c	x/c	y/c	x/c	y/c	x/c	y/c
0.7830	-0.0355					0.0001	0.0022				
0.7499	-0.0411					0.0019	0.0090				
0.7249	-0.0464					0.0052	0.0144				
0.6999	-0.0509					0.0101	0.0195				
0.6749	-0.0539					0.0150	0.0231				
0.6499	-0.0560					0.0201	0.0261				
0.6248	-0.0575					0.0251	0.0287				
0.5999	-0.0586					0.0301	0.0310				
0.5500	-0.0598					0.0400	0.0351				
0.4999	-0.0600					0.0500	0.0387				
0.4500	-0.0595					0.0600	0.0420				
0.4001	-0.0582					0.0751	0.0463				
0.3500	-0.0561					0.1000	0.0524				
0.3000	-0.0533					0.1500	0.0619				
0.2500	-0.0497					0.2000	0.0693				
0.1999	-0.0454					0.2500	0.0749				
0.1501	-0.0400					0.3000	0.0789				
0.1001	-0.0334					0.3500	0.0814				
0.0750	-0.0293					0.4000	0.0826				
0.0600	-0.0265					0.4500	0.0825				
0.0500	-0.0244					0.5000	0.0810				
0.0400	-0.0221					0.5501	0.0781				
0.0301	-0.0196					0.6000	0.0735				
0.0250	-0.0181					0.6250	0.0704				
0.0201	-0.0165					0.6500	0.0668				
0.0151	-0.0147					0.6750	0.0626				
0.0101	-0.0126					0.7000	0.0573				
0.0053	-0.0099					0.7250	0.0508				
0.0019	-0.0067					0.7500	0.0426				
0.0001	-0.0019					0.7836	0.0303				

Table B-6b Coordinates of 48-in NLF(1)-0414 Airfoil (Flap Element)

Lower Surface						Upper Surface					
x/c	y/c	x/c	y/c	x/c	y/c	x/c	y/c	x/c	y/c	x/c	y/c
1.0000	-0.0273					0.7510	0.0058				
0.9700	-0.0269					0.7531	0.0166				
0.9625	-0.0266					0.7551	0.0153				
0.9500	-0.0263					0.7604	0.0216				
0.9370	-0.0260					0.7659	0.0286				
0.9208	-0.0259					0.7671	0.0265				
0.9000	-0.0260					0.7748	0.0296				
0.8789	-0.0267					0.7836	0.0303				
0.8638	-0.0274					0.7903	0.0280				
0.8499	-0.0283					0.8001	0.0244				
0.8420	-0.0289					0.8123	0.0201				
0.8263	-0.0304					0.8274	0.0148				
0.8112	-0.0319					0.8274	0.0148				
0.8000	-0.0333					0.8410	0.0103				
0.7889	-0.0347					0.8500	0.0074				
0.7830	-0.0355					0.8674	0.0021				
0.7748	-0.0344					0.8807	-0.0017				
0.7671	-0.0313					0.9000	-0.0068				
0.7659	-0.0335					0.9210	-0.0119				
0.7604	-0.0265					0.9345	-0.0149				
0.7551	-0.0201					0.9500	-0.0181				
0.7477	-0.0046					0.9613	-0.0202				
0.7531	-0.0214					0.9700	-0.0218				
0.7516	-0.0126					1.0000	-0.0273				
0.7501	-0.0045										

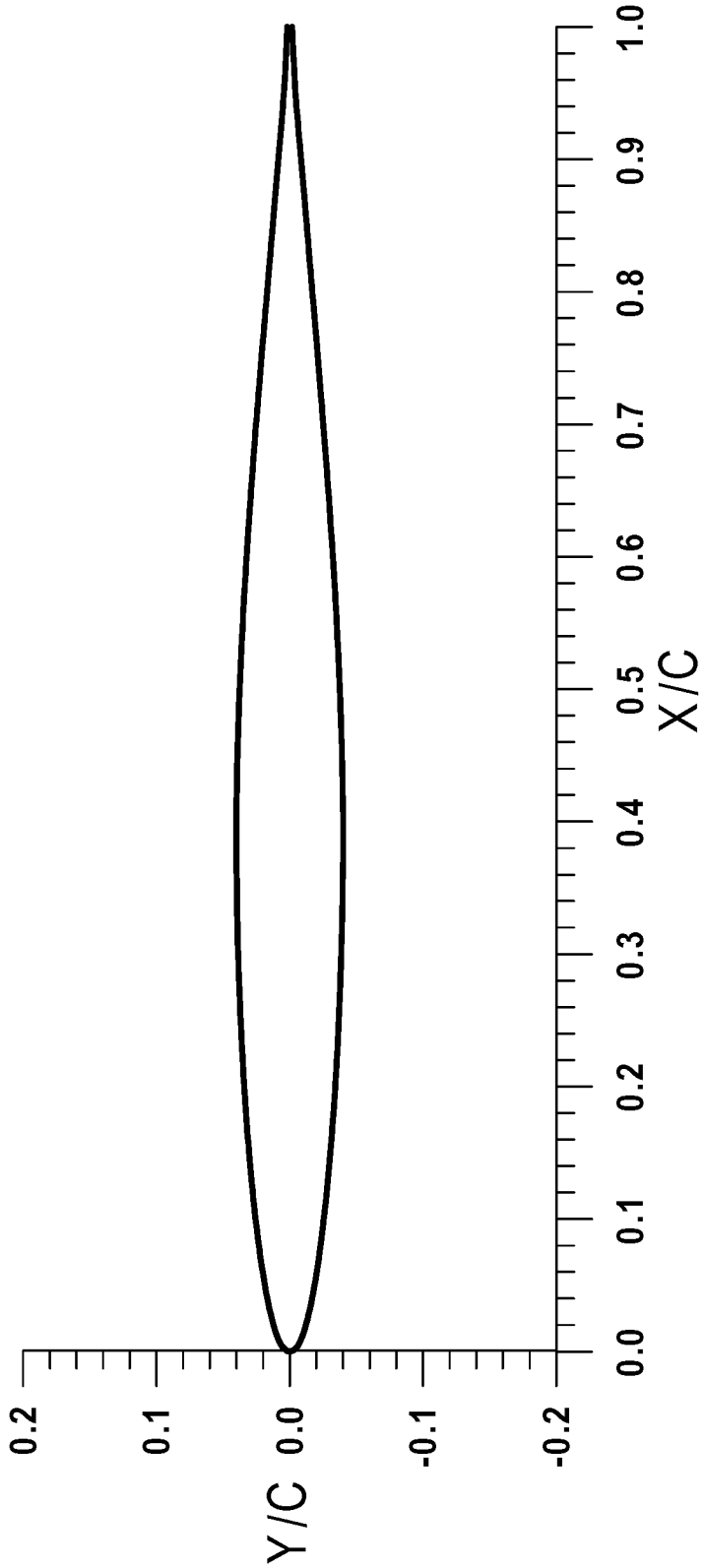

Fig. B-7 NACA 64A008 finite swept tail (c = 36 in.)

Table B-7 Coordinates of NACA 64A008 Finite Swept Tail

Lower Surface						Upper Surface					
x/c	y/c	x/c	y/c	x/c	y/c	x/c	y/c	x/c	y/c	x/c	y/c
1.0000	-0.0018	0.7872	-0.0181	0.5590	-0.0348	0.0000	0.0004	0.0913	0.0246	0.3025	0.0387
0.9943	-0.0020	0.7817	-0.0185	0.5535	-0.0351	0.0003	0.0014	0.0961	0.0251	0.3078	0.0389
0.9888	-0.0023	0.7761	-0.0190	0.5481	-0.0353	0.0007	0.0023	0.1009	0.0257	0.3132	0.0390
0.9834	-0.0025	0.7703	-0.0195	0.5428	-0.0356	0.0012	0.0031	0.1058	0.0262	0.3186	0.0391
0.9782	-0.0028	0.7658	-0.0199	0.5374	-0.0359	0.0019	0.0039	0.1107	0.0268	0.3239	0.0393
0.9731	-0.0030	0.7603	-0.0203	0.5319	-0.0362	0.0026	0.0046	0.1156	0.0273	0.3292	0.0394
0.9681	-0.0033	0.7542	-0.0208	0.5265	-0.0364	0.0033	0.0053	0.1206	0.0278	0.3346	0.0395
0.9633	-0.0036	0.7485	-0.0213	0.5211	-0.0367	0.0041	0.0059	0.1256	0.0283	0.3400	0.0396
0.9585	-0.0038	0.7427	-0.0218	0.5157	-0.0369	0.0049	0.0064	0.1307	0.0288	0.3454	0.0397
0.9537	-0.0041	0.7371	-0.0222	0.5103	-0.0371	0.0058	0.0069	0.1358	0.0292	0.3507	0.0397
0.9491	-0.0044	0.7313	-0.0227	0.5049	-0.0374	0.0067	0.0074	0.1409	0.0297	0.3560	0.0398
0.9448	-0.0048	0.7257	-0.0232	0.4995	-0.0376	0.0076	0.0078	0.1461	0.0301	0.3613	0.0399
0.9402	-0.0051	0.7198	-0.0236	0.4943	-0.0378	0.0085	0.0082	0.1512	0.0306	0.3665	0.0399
0.9358	-0.0055	0.7139	-0.0241	0.4890	-0.0380	0.0094	0.0086	0.1563	0.0310	0.3717	0.0399
0.9315	-0.0058	0.7081	-0.0246	0.4839	-0.0382	0.0103	0.0090	0.1614	0.0314	0.3769	0.0400
0.9267	-0.0062	0.7027	-0.0250	0.4789	-0.0384	0.0113	0.0094	0.1666	0.0318	0.3821	0.0400
0.9216	-0.0067	0.6971	-0.0254	0.4736	-0.0385	0.0122	0.0097	0.1717	0.0322	0.3873	0.0400
0.9164	-0.0071	0.6915	-0.0259	0.4682	-0.0387	0.0132	0.0101	0.1768	0.0326	0.3925	0.0400
0.9104	-0.0077	0.6858	-0.0263	0.4631	-0.0389	0.0141	0.0104	0.1820	0.0329	0.3976	0.0400
0.9045	-0.0082	0.6800	-0.0268	0.4579	-0.0390	0.0150	0.0107	0.1871	0.0333	0.4026	0.0400
0.8993	-0.0086	0.6743	-0.0272	0.4531	-0.0391	0.0160	0.0110	0.1921	0.0336	0.4077	0.0399
0.8941	-0.0091	0.6687	-0.0276	0.4480	-0.0393	0.0169	0.0113	0.1972	0.0340	0.4127	0.0399
0.8889	-0.0095	0.6630	-0.0280	0.4428	-0.0394	0.0179	0.0116	0.2024	0.0343	0.4179	0.0398
0.8837	-0.0100	0.6576	-0.0284	0.4376	-0.0395	0.0189	0.0119	0.2076	0.0346	0.4230	0.0398
0.8785	-0.0104	0.6522	-0.0288	0.4323	-0.0396	0.0202	0.0123	0.2128	0.0349	0.4282	0.0397
0.8737	-0.0108	0.6469	-0.0292	0.4271	-0.0397	0.0221	0.0128	0.2181	0.0352	0.4384	0.0395
0.8683	-0.0113	0.6414	-0.0296	0.4219	-0.0398	0.0248	0.0135	0.2234	0.0355	0.4333	0.0396
0.8624	-0.0118	0.6360	-0.0300	0.4167	-0.0398	0.0285	0.0144	0.2287	0.0358	0.4435	0.0394
0.8562	-0.0123	0.6305	-0.0303	0.4116	-0.0399	0.0326	0.0153	0.2340	0.0361	0.4486	0.0392
0.8501	-0.0128	0.6249	-0.0307	0.4064	-0.0399	0.0367	0.0162	0.2393	0.0363	0.4538	0.0391
0.8450	-0.0132	0.6193	-0.0311	0.4013	-0.0400	0.0410	0.0170	0.2446	0.0366	0.4590	0.0390
0.8410	-0.0135	0.6138	-0.0315	0.3961	-0.0400	0.0453	0.0178	0.2499	0.0368	0.4637	0.0388
0.8362	-0.0139	0.6082	-0.0318	0.3910	-0.0400	0.0498	0.0186	0.2551	0.0370	0.4683	0.0387
0.8315	-0.0143	0.6028	-0.0322	0.3857	-0.0400	0.0543	0.0193	0.2604	0.0373	0.4735	0.0385
0.8262	-0.0148	0.5974	-0.0325	0.3805	-0.0400	0.0587	0.0201	0.2657	0.0375	0.4787	0.0384
0.8205	-0.0152	0.5921	-0.0328	0.3753	-0.0400	0.0631	0.0207	0.2709	0.0377	0.4835	0.0382
0.8150	-0.0157	0.5866	-0.0332	0.3701	-0.0399	0.0678	0.0214	0.2762	0.0379	0.4885	0.0380
0.8094	-0.0162	0.5811	-0.0335	0.3649	-0.0399	0.0722	0.0221	0.2815	0.0381	0.4933	0.0378
0.8039	-0.0167	0.5756	-0.0338	0.3596	-0.0398	0.0770	0.0227	0.2867	0.0382	0.4981	0.0376
0.7983	-0.0171	0.5701	-0.0341	0.3543	-0.0398	0.0817	0.0233	0.2920	0.0384	0.5034	0.0374
0.7928	-0.0176	0.5645	-0.0345	0.3490	-0.0397	0.0865	0.0240	0.2972	0.0386	0.5085	0.0372

Lower Surface						Upper Surface					
x/c	y/c	x/c	y/c	x/c	y/c	x/c	y/c	x/c	y/c	x/c	y/c
0.3436	-0.0396	0.0989	-0.0255			0.5137	0.0370	0.7520	0.0210	0.9845	0.0025
0.3382	-0.0395	0.0941	-0.0249			0.5190	0.0368	0.7574	0.0206	0.9897	0.0022
0.3328	-0.0394	0.0893	-0.0243			0.5241	0.0365	0.7627	0.0201	0.9950	0.0020
0.3275	-0.0393	0.0846	-0.0237			0.5293	0.0363	0.7683	0.0196	1.0000	0.0018
0.3221	-0.0392	0.0798	-0.0231			0.5345	0.0360	0.7738	0.0192		
0.3168	-0.0391	0.0751	-0.0225			0.5397	0.0358	0.7794	0.0187		
0.3114	-0.0390	0.0706	-0.0218			0.5448	0.0355	0.7850	0.0182		
0.3061	-0.0388	0.0661	-0.0212			0.5499	0.0352	0.7906	0.0178		
0.3007	-0.0387	0.0620	-0.0206			0.5542	0.0350	0.7962	0.0173		
0.2954	-0.0385	0.0575	-0.0199			0.5594	0.0347	0.8018	0.0168		
0.2902	-0.0384	0.0530	-0.0191			0.5648	0.0344	0.8075	0.0164		
0.2849	-0.0382	0.0486	-0.0184			0.5701	0.0341	0.8131	0.0159		
0.2797	-0.0380	0.0443	-0.0176			0.5755	0.0338	0.8187	0.0154		
0.2744	-0.0378	0.0400	-0.0168			0.5809	0.0335	0.8255	0.0148		
0.2691	-0.0376	0.0358	-0.0160			0.5858	0.0332	0.8310	0.0144		
0.2637	-0.0374	0.0317	-0.0151			0.5912	0.0329	0.8360	0.0139		
0.2585	-0.0372	0.0277	-0.0142			0.5965	0.0326	0.8416	0.0135		
0.2532	-0.0370	0.0240	-0.0133			0.6015	0.0322	0.8474	0.0130		
0.2480	-0.0367	0.0213	-0.0126			0.6068	0.0319	0.8530	0.0125		
0.2426	-0.0365	0.0194	-0.0121			0.6123	0.0316	0.8587	0.0121		
0.2214	-0.0354	0.0181	-0.0117			0.6177	0.0312	0.8642	0.0116		
0.2161	-0.0351	0.0171	-0.0114			0.6231	0.0308	0.8698	0.0111		
0.2109	-0.0348	0.0162	-0.0111			0.6286	0.0305	0.8748	0.0107		
0.2057	-0.0345	0.0152	-0.0108			0.6340	0.0301	0.8801	0.0103		
0.2005	-0.0342	0.0143	-0.0105			0.6396	0.0297	0.8857	0.0098		
0.1953	-0.0338	0.0133	-0.0101			0.6449	0.0293	0.8909	0.0094		
0.1902	-0.0335	0.0124	-0.0098			0.6501	0.0290	0.8960	0.0089		
0.1850	-0.0332	0.0115	-0.0094			0.6554	0.0286	0.9014	0.0085		
0.1798	-0.0328	0.0105	-0.0091			0.6610	0.0282	0.9068	0.0080		
0.1747	-0.0324	0.0096	-0.0087			0.6664	0.0278	0.9142	0.0073		
0.1695	-0.0320	0.0087	-0.0083			0.6718	0.0274	0.9195	0.0068		
0.1644	-0.0316	0.0078	-0.0079			0.6774	0.0270	0.9247	0.0064		
0.1592	-0.0312	0.0069	-0.0075			0.6830	0.0265	0.9293	0.0060		
0.1541	-0.0308	0.0060	-0.0070			0.6884	0.0261	0.9335	0.0056		
0.1489	-0.0304	0.0051	-0.0065			0.6939	0.0257	0.9378	0.0053		
0.1438	-0.0299	0.0043	-0.0060			0.6992	0.0253	0.9422	0.0050		
0.1387	-0.0295	0.0035	-0.0054			0.7047	0.0248	0.9465	0.0046		
0.1336	-0.0290	0.0027	-0.0047			0.7104	0.0244	0.9506	0.0043		
0.1285	-0.0286	0.0020	-0.0040			0.7163	0.0239	0.9553	0.0040		
0.1235	-0.0281	0.0013	-0.0033			0.7219	0.0235	0.9600	0.0037		
0.1185	-0.0276	0.0008	-0.0024			0.7278	0.0230	0.9648	0.0035		
0.1136	-0.0271	0.0003	-0.0016			0.7340	0.0225	0.9697	0.0032		
0.1087	-0.0266	0.0001	-0.0006			0.7399	0.0220	0.9746	0.0030		
0.1038	-0.0260					0.7460	0.0215	0.9794	0.0027		

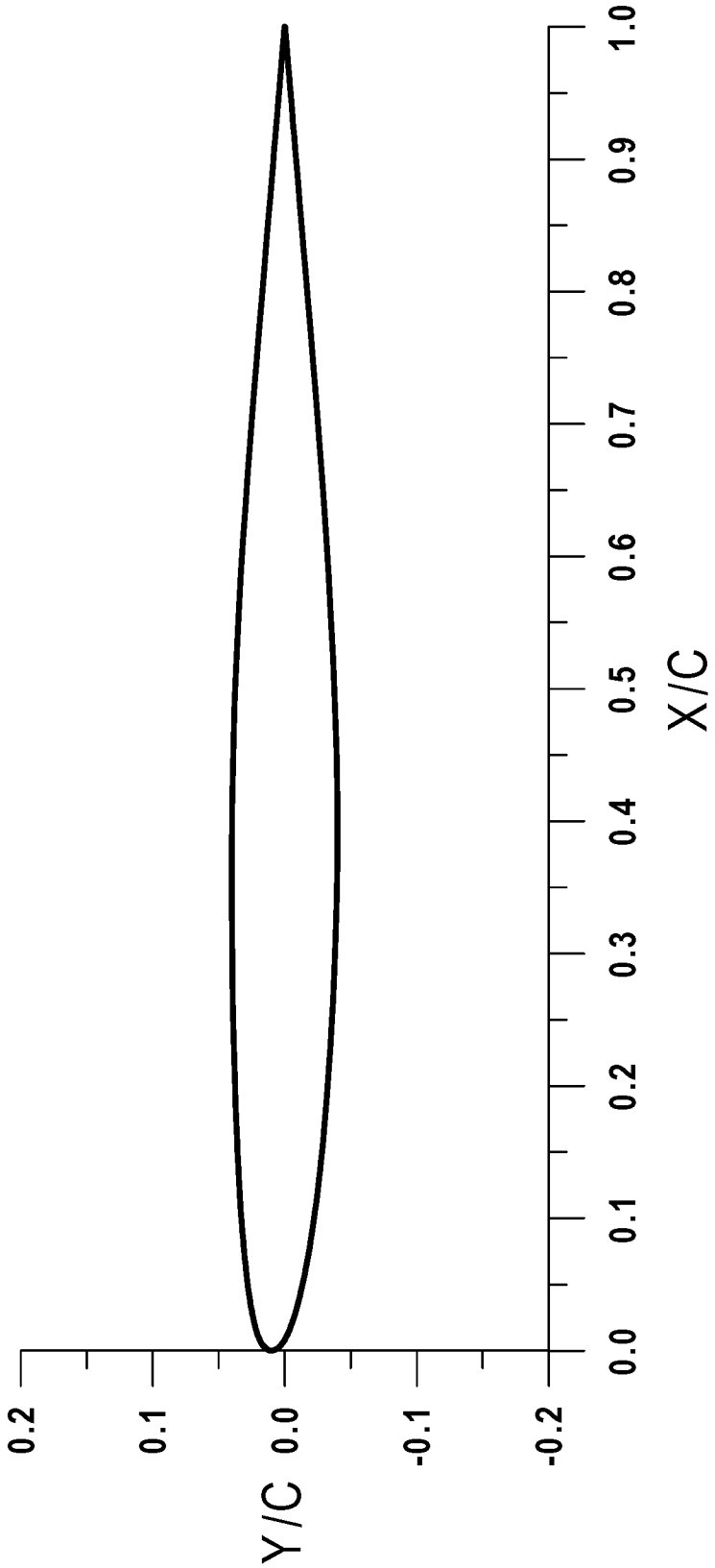

Fig. B-7 Business Jet Horizontal Tail

Table B-7 Coordinates of Business Jet Horizontal Tail

Lower Surface						Upper Surface					
x/c	y/c	x/c	y/c	x/c	y/c	x/c	y/c	x/c	y/c	x/c	y/c
1.0000	0.0000	0.9874	-0.0012	0.8419	-0.0135	0.0102	0.0010	0.1294	0.0259	0.8448	0.0132
1.0000	-0.0001	0.9864	-0.0013	0.8306	-0.0144	0.0122	0.0020	0.1362	0.0267	0.8554	0.0123
1.0000	-0.0002	0.9853	-0.0014	0.8186	-0.0154	0.0142	0.0029	0.1435	0.0275	0.8652	0.0115
0.9999	-0.0002	0.9842	-0.0015	0.8057	-0.0165	0.0163	0.0038	0.1512	0.0283	0.8743	0.0107
0.9998	-0.0002	0.9830	-0.0016	0.7919	-0.0177	0.0184	0.0046	0.1597	0.0291	0.8829	0.0100
0.9997	-0.0002	0.9817	-0.0017	0.7771	-0.0189	0.0205	0.0054	0.1688	0.0300	0.8909	0.0093
0.9996	-0.0002	0.9804	-0.0018	0.7613	-0.0202	0.0227	0.0062	0.1787	0.0308	0.8983	0.0087
0.9994	-0.0002	0.9789	-0.0020	0.7443	-0.0216	0.0249	0.0069	0.1895	0.0317	0.9052	0.0081
0.9993	-0.0002	0.9773	-0.0021	0.7260	-0.0231	0.0272	0.0076	0.2014	0.0326	0.9117	0.0076
0.9991	-0.0003	0.9756	-0.0022	0.7065	-0.0247	0.0295	0.0083	0.2146	0.0336	0.9177	0.0071
0.9990	-0.0003	0.9739	-0.0024	0.6855	-0.0263	0.0319	0.0090	0.2293	0.0345	0.9233	0.0066
0.9988	-0.0003	0.9719	-0.0025	0.6630	-0.0280	0.0343	0.0096	0.2457	0.0355	0.9286	0.0062
0.9986	-0.0003	0.9699	-0.0027	0.6389	-0.0298	0.0368	0.0103	0.2642	0.0365	0.9335	0.0058
0.9984	-0.0003	0.9677	-0.0029	0.6129	-0.0315	0.0393	0.0110	0.2853	0.0375	0.9380	0.0054
0.9982	-0.0003	0.9653	-0.0031	0.5851	-0.0333	0.0419	0.0116	0.3096	0.0384	0.9423	0.0050
0.9980	-0.0003	0.9628	-0.0033	0.5551	-0.0350	0.0445	0.0122	0.3379	0.0393	0.9463	0.0047
0.9978	-0.0004	0.9601	-0.0035	0.5230	-0.0366	0.0472	0.0129	0.3712	0.0398	0.9500	0.0044
0.9975	-0.0004	0.9573	-0.0038	0.4884	-0.0380	0.0500	0.0135	0.4112	0.0399	0.9534	0.0041
0.9972	-0.0004	0.9542	-0.0040	0.4512	-0.0391	0.0529	0.0141	0.4512	0.0392	0.9566	0.0038
0.9969	-0.0004	0.9509	-0.0043	0.4112	-0.0398	0.0558	0.0147	0.4885	0.0380	0.9596	0.0036
0.9966	-0.0005	0.9474	-0.0046	0.3712	-0.0401	0.0589	0.0153	0.5232	0.0366	0.9625	0.0033
0.9963	-0.0005	0.9436	-0.0049	0.3379	-0.0401	0.0620	0.0160	0.5555	0.0349	0.9651	0.0031
0.9959	-0.0005	0.9395	-0.0053	0.3096	-0.0399	0.0653	0.0166	0.5857	0.0332	0.9675	0.0029
0.9956	-0.0006	0.9352	-0.0056	0.2853	-0.0396	0.0687	0.0172	0.6137	0.0315	0.9698	0.0027
0.9951	-0.0006	0.9306	-0.0060	0.2641	-0.0393	0.0722	0.0178	0.6399	0.0297	0.9719	0.0025
0.9947	-0.0006	0.9257	-0.0064	0.2456	-0.0389	0.0758	0.0185	0.6643	0.0279	0.9739	0.0024
0.9942	-0.0007	0.9204	-0.0069	0.2292	-0.0385	0.0796	0.0191	0.6870	0.0262	0.8448	0.0132
0.9937	-0.0007	0.9147	-0.0073	0.2145	-0.0381	0.0835	0.0197	0.7082	0.0246	0.8554	0.0123
0.9932	-0.0008	0.9086	-0.0079	0.2013	-0.0378	0.0876	0.0204	0.7280	0.0230	0.8652	0.0115
0.9926	-0.0008	0.9021	-0.0084	0.1893	-0.0374	0.0920	0.0210	0.7464	0.0215	0.8743	0.0107
0.9920	-0.0009	0.8952	-0.0090	0.1785	-0.0370	0.0965	0.0217	0.7636	0.0200	0.8829	0.0100
0.9914	-0.0009	0.8877	-0.0096	0.1685	-0.0366	0.1012	0.0224	0.7796	0.0187	0.8909	0.0093
0.9907	-0.0010	0.8798	-0.0103	0.1594	-0.0362	0.1063	0.0231	0.7945	0.0174	0.8983	0.0087
0.9899	-0.0010	0.8713	-0.0110	0.1509	-0.0358	0.1115	0.0238	0.8084	0.0163	0.9052	0.0081
0.9891	-0.0011	0.8621	-0.0118	0.1431	-0.0354	0.1172	0.0245	0.8214	0.0152	0.9117	0.0076
0.9883	-0.0012	0.8523	-0.0126	0.1358	-0.0351	0.1231	0.0252	0.8335	0.0142	0.9177	0.0071
1.0000	0.0000	0.9874	-0.0012	0.8419	-0.0135	0.0102	0.0010	0.1294	0.0259	0.9233	0.0066
1.0000	-0.0001	0.9864	-0.0013	0.8306	-0.0144	0.0122	0.0020	0.1362	0.0267	0.9286	0.0062
1.0000	-0.0002	0.9853	-0.0014	0.8186	-0.0154	0.0142	0.0029	0.1435	0.0275	0.9335	0.0058
0.9999	-0.0002	0.9842	-0.0015	0.8057	-0.0165	0.0163	0.0038	0.1512	0.0283	0.9380	0.0054
0.9998	-0.0002	0.9830	-0.0016	0.7919	-0.0177	0.0184	0.0046	0.1597	0.0291	0.9423	0.0050
0.9997	-0.0002	0.9817	-0.0017	0.7771	-0.0189	0.0205	0.0054	0.1688	0.0300	0.9463	0.0047
0.9996	-0.0002	0.9804	-0.0018	0.7613	-0.0202	0.0227	0.0062	0.1787	0.0308	0.9500	0.0044

Lower Surface						Upper Surface					
x/c	y/c	x/c	y/c	x/c	y/c	x/c	y/c	x/c	y/c	x/c	y/c
0.1290	-0.0347	0.0123	-0.0206			0.9757	0.0022	1.0000	0.0000		
0.1227	-0.0343	0.0102	-0.0198			0.9775	0.0021				
0.1167	-0.0340	0.0082	-0.0190			0.9791	0.0019				
0.1110	-0.0336	0.0062	-0.0180			0.9806	0.0018				
0.1057	-0.0333	0.0044	-0.0168			0.9820	0.0017				
0.1007	-0.0329	0.0027	-0.0154			0.9833	0.0016				
0.0959	-0.0325	0.0013	-0.0137			0.9845	0.0015				
0.0913	-0.0322	0.0003	-0.0118			0.9856	0.0014				
0.0870	-0.0318	0.0000	-0.0097			0.9867	0.0013				
0.0828	-0.0315	0.0006	-0.0076			0.9877	0.0012				
0.0788	-0.0311	0.0017	-0.0057			0.9886	0.0011				
0.0750	-0.0308	0.0031	-0.0039			0.9894	0.0011				
0.0713	-0.0304	0.0047	-0.0025			0.9902	0.0010				
0.0678	-0.0301	0.0064	-0.0012			0.9910	0.0009				
0.0644	-0.0297	0.0083	-0.0001			0.9917	0.0009				
0.0611	-0.0294					0.9923	0.0008				
0.0579	-0.0290					0.9929	0.0008				
0.0548	-0.0286					0.9935	0.0007				
0.0518	-0.0283					0.9940	0.0007				
0.0489	-0.0279					0.9945	0.0006				
0.0461	-0.0275					0.9950	0.0006				
0.0433	-0.0271					0.9954	0.0006				
0.0406	-0.0267					0.9958	0.0005				
0.0380	-0.0263					0.9962	0.0005				
0.0354	-0.0259					0.9965	0.0005				
0.0329	-0.0255					0.9969	0.0004				
0.1290	-0.0347					0.9972	0.0004				
0.1227	-0.0343					0.9975	0.0004				
0.1167	-0.0340					0.9977	0.0004				
0.1110	-0.0336					0.9980	0.0004				
0.1057	-0.0333					0.9982	0.0003				
0.1007	-0.0329					0.9984	0.0003				
0.0959	-0.0325					0.9986	0.0003				
0.0913	-0.0322					0.9988	0.0003				
0.0870	-0.0318					0.9990	0.0003				
0.0305	-0.0251					0.9993	0.0002				
0.0280	-0.0246					0.9994	0.0002				
0.0257	-0.0241					0.9996	0.0002				
0.0233	-0.0236					0.9997	0.0002				
0.0211	-0.0231					0.9998	0.0002				
0.0188	-0.0225					0.9999	0.0002				
0.0166	-0.0219					1.0000	0.0002				
0.0144	-0.0213					1.0000	0.0001				

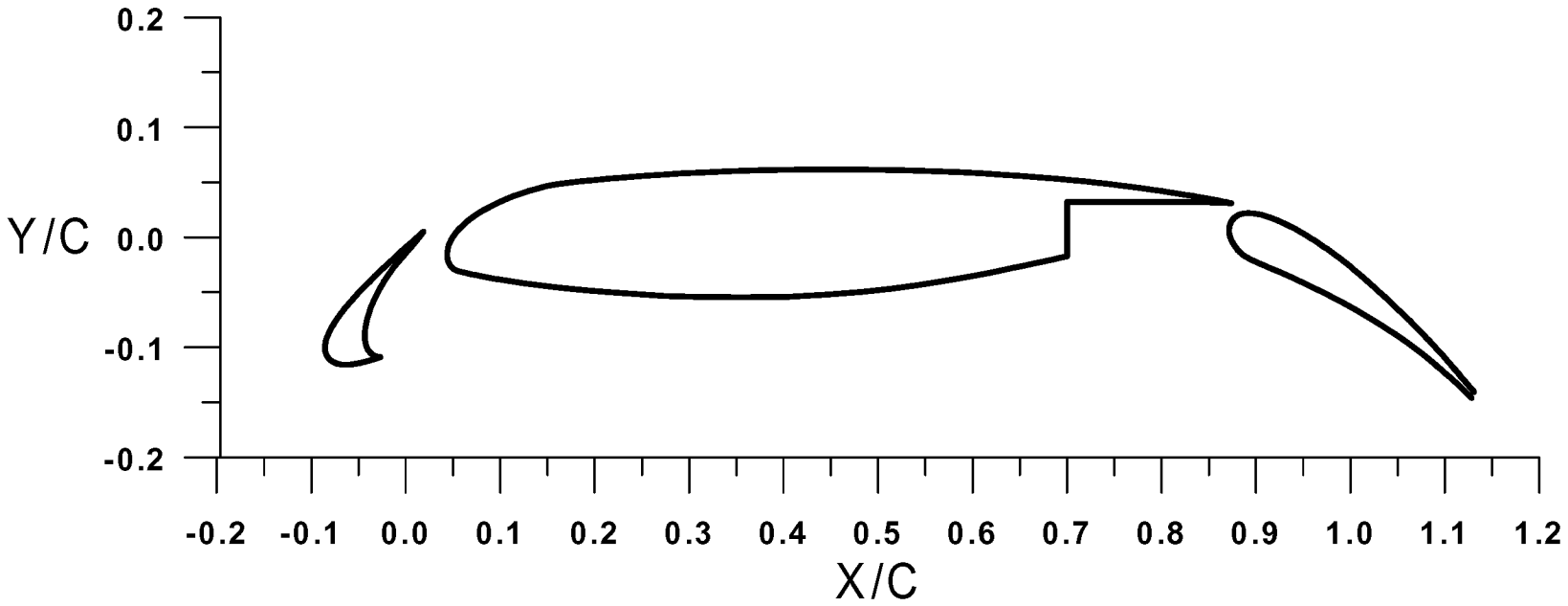

Fig. B-8 Three-element High Lift System

Table B-8a Three-element High Lift System - Slat Element Coordinates

Lower Surface						Upper Surface					
x/c	y/c	x/c	y/c	x/c	y/c	x/c	y/c	x/c	y/c	x/c	y/c
0.0188	0.0051	-0.0213	-0.0377	-0.0475	-0.1140	-0.0853	-0.0985	0.0091	-0.0023		
0.0184	0.0047	-0.0230	-0.0401	-0.0489	-0.1142	-0.0852	-0.0974	0.0103	-0.0014		
0.0181	0.0043	-0.0246	-0.0424	-0.0502	-0.1145	-0.0850	-0.0964	0.0114	-0.0005		
0.0177	0.0040	-0.0262	-0.0447	-0.0514	-0.1147	-0.0848	-0.0954	0.0124	0.0003		
0.0173	0.0035	-0.0278	-0.0471	-0.0526	-0.1149	-0.0845	-0.0944	0.0134	0.0010		
0.0169	0.0031	-0.0293	-0.0495	-0.0537	-0.1150	-0.0842	-0.0932	0.0142	0.0016		
0.0165	0.0027	-0.0307	-0.0518	-0.0548	-0.1152	-0.0838	-0.0920	0.0150	0.0022		
0.0160	0.0022	-0.0321	-0.0543	-0.0558	-0.1153	-0.0832	-0.0908	0.0157	0.0027		
0.0156	0.0017	-0.0334	-0.0567	-0.0567	-0.1154	-0.0827	-0.0894	0.0163	0.0032		
0.0151	0.0012	-0.0347	-0.0591	-0.0577	-0.1155	-0.0820	-0.0880	0.0169	0.0037		
0.0146	0.0006	-0.0359	-0.0616	-0.0585	-0.1156	-0.0812	-0.0864	0.0175	0.0041		
0.0141	0.0001	-0.0371	-0.0641	-0.0593	-0.1156	-0.0802	-0.0848	0.0179	0.0044		
0.0136	-0.0005	-0.0381	-0.0666	-0.0601	-0.1157	-0.0792	-0.0831	0.0184	0.0048		
0.0130	-0.0011	-0.0391	-0.0692	-0.0609	-0.1157	-0.0780	-0.0813	0.0188	0.0051		
0.0124	-0.0018	-0.0400	-0.0717	-0.0616	-0.1157	-0.0767	-0.0793				
0.0118	-0.0024	-0.0408	-0.0743	-0.0622	-0.1157	-0.0752	-0.0772				
0.0112	-0.0031	-0.0415	-0.0769	-0.0628	-0.1157	-0.0735	-0.0751				
0.0105	-0.0038	-0.0421	-0.0795	-0.0634	-0.1157	-0.0716	-0.0727				
0.0098	-0.0046	-0.0426	-0.0821	-0.0640	-0.1157	-0.0695	-0.0703				
0.0091	-0.0053	-0.0431	-0.0847	-0.0645	-0.1157	-0.0672	-0.0677				
0.0083	-0.0061	-0.0433	-0.0873	-0.0651	-0.1157	-0.0647	-0.0650				
0.0075	-0.0069	-0.0433	-0.0899	-0.0656	-0.1157	-0.0619	-0.0620				
0.0067	-0.0078	-0.0432	-0.0926	-0.0662	-0.1157	-0.0588	-0.0589				
0.0058	-0.0087	-0.0428	-0.0951	-0.0668	-0.1157	-0.0554	-0.0556				
0.0049	-0.0096	-0.0421	-0.0976	-0.0674	-0.1156	-0.0517	-0.0521				
0.0039	-0.0106	-0.0411	-0.1000	-0.0680	-0.1156	-0.0476	-0.0484				
0.0029	-0.0116	-0.0399	-0.1023	-0.0686	-0.1155	-0.0431	-0.0444				
0.0018	-0.0126	-0.0383	-0.1043	-0.0692	-0.1155	-0.0382	-0.0401				
0.0007	-0.0137	-0.0363	-0.1059	-0.0698	-0.1154	-0.0329	-0.0356				
-0.0004	-0.0148	-0.0341	-0.1071	-0.0704	-0.1153	-0.0280	-0.0315				
-0.0016	-0.0160	-0.0317	-0.1079	-0.0711	-0.1151	-0.0236	-0.0278				
-0.0028	-0.0172	-0.0292	-0.1084	-0.0717	-0.1150	-0.0195	-0.0245				
-0.0041	-0.0185	-0.0267	-0.1087	-0.0724	-0.1148	-0.0157	-0.0215				
-0.0055	-0.0198	-0.0291	-0.1094	-0.0731	-0.1147	-0.0123	-0.0188				
-0.0069	-0.0212	-0.0314	-0.1100	-0.0737	-0.1145	-0.0092	-0.0163				
-0.0083	-0.0227	-0.0336	-0.1106	-0.0744	-0.1142	-0.0063	-0.0141				
-0.0098	-0.0242	-0.0357	-0.1112	-0.0751	-0.1140	-0.0037	-0.0121				
-0.0113	-0.0258	-0.0376	-0.1117	-0.0758	-0.1137	-0.0014	-0.0103				
-0.0129	-0.0275	-0.0395	-0.1122	-0.0765	-0.1134	0.0008	-0.0086				
-0.0145	-0.0293	-0.0413	-0.1126	-0.0772	-0.1131	0.0028	-0.0071				
-0.0162	-0.0313	-0.0429	-0.1130	-0.0779	-0.1127	0.0046	-0.0057				
-0.0179	-0.0333	-0.0445	-0.1134	-0.0785	-0.1123	0.0062	-0.0045				
-0.0196	-0.0355	-0.0461	-0.1137	-0.0792	-0.1119	0.0077	-0.0033				

Lower Surface						Upper Surface					
x/c	**y/c**	**x/c**	**y/c**	**x/c**	**y/c**	**x/c**	**y/c**	**x/c**	**y/c**	**x/c**	**y/c**
-0.0799	-0.1114										
-0.0806	-0.1109										
-0.0812	-0.1103										
-0.0818	-0.1097										
-0.0824	-0.1090										
-0.0830	-0.1083										
-0.0834	-0.1075										
-0.0839	-0.1067										
-0.0843	-0.1059										
-0.0846	-0.1050										
-0.0849	-0.1040										
-0.0851	-0.1030										
-0.0853	-0.1020										
-0.0854	-0.1009										
-0.0854	-0.0996										

Table B-8b Three-element High Lift System - Main Element Coordinates

Lower Surface						Upper Surface					
x/c	y/c	x/c	y/c	x/c	y/c	x/c	y/c	x/c	y/c	x/c	y/c
0.8740	0.0309	0.7073	0.0320	0.5654	-0.0404	0.0497	0.0000	0.5322	0.0610		
0.8729	0.0310	0.7047	0.0320	0.5419	-0.0436	0.0504	0.0010	0.5603	0.0602		
0.8716	0.0311	0.7022	0.0320	0.5145	-0.0466	0.0513	0.0020	0.5862	0.0592		
0.8702	0.0311	0.6999	0.0320	0.4828	-0.0497	0.0522	0.0032	0.6100	0.0582		
0.8686	0.0312	0.6999	0.0297	0.4459	-0.0521	0.0533	0.0044	0.6320	0.0570		
0.8669	0.0313	0.6999	0.0273	0.4033	-0.0540	0.0545	0.0056	0.6522	0.0558		
0.8650	0.0314	0.6999	0.0246	0.3538	-0.0544	0.0558	0.0070	0.6708	0.0546		
0.8628	0.0314	0.6999	0.0218	0.3113	-0.0540	0.0573	0.0084	0.6879	0.0533		
0.8604	0.0315	0.6999	0.0188	0.2747	-0.0531	0.0590	0.0098	0.7037	0.0521		
0.8578	0.0316	0.6999	0.0156	0.2433	-0.0515	0.0609	0.0114	0.7183	0.0509		
0.8549	0.0317	0.6999	0.0122	0.2163	-0.0500	0.0630	0.0130	0.7316	0.0496		
0.8516	0.0318	0.6999	0.0085	0.1930	-0.0483	0.0653	0.0147	0.7439	0.0484		
0.8480	0.0318	0.6999	0.0050	0.1731	-0.0466	0.0679	0.0165	0.7553	0.0473		
0.8440	0.0319	0.6999	0.0017	0.1559	-0.0450	0.0708	0.0183	0.7657	0.0462		
0.8395	0.0319	0.6999	-0.0015	0.1412	-0.0435	0.0740	0.0202	0.7753	0.0451		
0.8346	0.0320	0.6999	-0.0045	0.1285	-0.0420	0.0775	0.0222	0.7842	0.0441		
0.8291	0.0320	0.6999	-0.0073	0.1176	-0.0407	0.0814	0.0242	0.7923	0.0431		
0.8230	0.0320	0.6999	-0.0100	0.1083	-0.0394	0.0857	0.0263	0.7998	0.0422		
0.8163	0.0320	0.6999	-0.0125	0.1003	-0.0383	0.0904	0.0285	0.8068	0.0413		
0.8088	0.0320	0.6999	-0.0149	0.0933	-0.0374	0.0957	0.0307	0.8131	0.0404		
0.8004	0.0320	0.6999	-0.0172	0.0874	-0.0365	0.1014	0.0330	0.8190	0.0396		
0.7912	0.0320	0.6977	-0.0176	0.0823	-0.0357	0.1077	0.0353	0.8244	0.0389		
0.7826	0.0320	0.6951	-0.0181	0.0779	-0.0349	0.1146	0.0376	0.8293	0.0382		
0.7746	0.0320	0.6921	-0.0187	0.0742	-0.0343	0.1221	0.0399	0.8339	0.0375		
0.7672	0.0320	0.6886	-0.0193	0.0709	-0.0337	0.1304	0.0422	0.8381	0.0369		
0.7603	0.0320	0.6845	-0.0201	0.0681	-0.0332	0.1395	0.0445	0.8420	0.0364		
0.7539	0.0320	0.6798	-0.0210	0.0658	-0.0328	0.1495	0.0467	0.8456	0.0358		
0.7480	0.0320	0.6744	-0.0220	0.0637	-0.0324	0.1604	0.0483	0.8489	0.0353		
0.7424	0.0320	0.6682	-0.0231	0.0619	-0.0320	0.1724	0.0496	0.8519	0.0348		
0.7373	0.0320	0.6609	-0.0245	0.0604	-0.0317	0.1855	0.0508	0.8547	0.0344		
0.7325	0.0320	0.6525	-0.0260	0.0591	-0.0315	0.1997	0.0521	0.8572	0.0339		
0.7281	0.0320	0.6428	-0.0278	0.0580	-0.0312	0.2152	0.0533	0.8596	0.0335		
0.7240	0.0320	0.6315	-0.0298	0.0567	-0.0310	0.2320	0.0546	0.8618	0.0332		
0.7201	0.0320	0.6184	-0.0321	0.0555	-0.0307	0.2503	0.0558	0.8638	0.0328		
0.7166	0.0320	0.6033	-0.0346	0.0543	-0.0303	0.2702	0.0570	0.8656	0.0325		
0.7133	0.0320	0.5858	-0.0373	0.0532	-0.0299	0.2919	0.0581	0.8673	0.0322		
0.7102	0.0320	0.7073	0.0320	0.5654	-0.0404	0.3155	0.0592	0.8689	0.0319		
0.8740	0.0309	0.7047	0.0320	0.5419	-0.0436	0.3412	0.0601	0.8703	0.0316		
0.8729	0.0310	0.7022	0.0320	0.5145	-0.0466	0.3691	0.0609	0.8717	0.0314		
0.8716	0.0311	0.6999	0.0320	0.4828	-0.0497	0.3995	0.0615	0.8729	0.0312		
0.8702	0.0311	0.6999	0.0297	0.4459	-0.0521	0.4326	0.0619	0.8740	0.0309		
0.8686	0.0312	0.6999	0.0273	0.4033	-0.0540	0.4686	0.0619				
0.8669	0.0313	0.6999	0.0246	0.3538	-0.0544	0.5017	0.0616				

Lower Surface						Upper Surface					
x/c	**y/c**	**x/c**	**y/c**	**x/c**	**y/c**	**x/c**	**y/c**	**x/c**	**y/c**	**x/c**	**y/c**
0.0521	-0.0294										
0.0511	-0.0288										
0.0502	-0.0282										
0.0493	-0.0276										
0.0484	-0.0269										
0.0476	-0.0260										
0.0468	-0.0250										
0.0460	-0.0239										
0.0454	-0.0228										
0.0449	-0.0216										
0.0445	-0.0204										
0.0442	-0.0192										
0.0439	-0.0179										
0.0438	-0.0167										
0.0439	-0.0154										
0.0440	-0.0142										
0.0441	-0.0129										
0.0443	-0.0117										
0.0446	-0.0105										
0.0448	-0.0093										
0.0452	-0.0082										
0.0456	-0.0071										
0.0461	-0.0060										
0.0466	-0.0049										
0.0472	-0.0039										
0.0477	-0.0029										
0.0484	-0.0019										
0.0490	-0.0010										

Table B-8c Three-element High Lift System - Flap Element Coordinates

Lower Surface						Upper Surface					
x/c	y/c	x/c	y/c	x/c	y/c	x/c	y/c	x/c	y/c	x/c	y/c
1.1283	-0.1458	1.0331	-0.0800	0.8749	-0.0040	0.8715	0.0067	0.9222	0.0157	1.0712	-0.0831
1.1280	-0.1455	1.0250	-0.0757	0.8745	-0.0033	0.8716	0.0077	0.9245	0.0148	1.0738	-0.0853
1.1276	-0.1453	1.0162	-0.0712	0.8740	-0.0025	0.8717	0.0087	0.9269	0.0139	1.0763	-0.0875
1.1272	-0.1451	1.0068	-0.0664	0.8736	-0.0017	0.8719	0.0096	0.9294	0.0130	1.0786	-0.0896
1.1268	-0.1447	0.9978	-0.0621	0.8732	-0.0009	0.8721	0.0105	0.9319	0.0119	1.0809	-0.0917
1.1264	-0.1444	0.9894	-0.0582	0.8728	0.0000	0.8724	0.0114	0.9345	0.0108	1.0831	-0.0937
1.1260	-0.1440	0.9814	-0.0546	0.8725	0.0009	0.8727	0.0122	0.9372	0.0097	1.0852	-0.0956
1.1255	-0.1436	0.9739	-0.0513	0.8722	0.0018	0.8731	0.0130	0.9399	0.0085	1.0873	-0.0974
1.1250	-0.1432	0.9669	-0.0482	0.8719	0.0027	0.8735	0.0138	0.9428	0.0071	1.0892	-0.0992
1.1245	-0.1427	0.9603	-0.0454	0.8717	0.0037	0.8740	0.0145	0.9456	0.0058	1.0911	-0.1009
1.1239	-0.1422	0.9540	-0.0429	0.8716	0.0047	0.8745	0.0152	0.9486	0.0043	1.0929	-0.1026
1.1232	-0.1417	0.9481	-0.0405	0.8715	0.0058	0.8751	0.0159	0.9516	0.0028	1.0946	-0.1043
1.1226	-0.1411	0.9426	-0.0383			0.8757	0.0166	0.9547	0.0011	1.0962	-0.1058
1.1218	-0.1405	0.9375	-0.0362			0.8764	0.0172	0.9579	-0.0006	1.0978	-0.1074
1.1211	-0.1398	0.9326	-0.0344			0.8771	0.0179	0.9612	-0.0024	1.0993	-0.1088
1.1202	-0.1391	0.9280	-0.0326			0.8779	0.0185	0.9646	-0.0042	1.1008	-0.1103
1.1193	-0.1383	0.9237	-0.0310			0.8788	0.0191	0.9680	-0.0062	1.1022	-0.1116
1.1183	-0.1375	0.9197	-0.0295			0.8797	0.0196	0.9716	-0.0083	1.1035	-0.1130
1.1173	-0.1366	0.9159	-0.0281			0.8807	0.0201	0.9752	-0.0105	1.1048	-0.1142
1.1161	-0.1356	0.9124	-0.0268			0.8818	0.0205	0.9789	-0.0128	1.1061	-0.1155
1.1149	-0.1346	0.9090	-0.0256			0.8829	0.0209	0.9828	-0.0151	1.1073	-0.1167
1.1136	-0.1335	0.9059	-0.0245			0.8840	0.0213	0.9867	-0.0177	1.1084	-0.1178
1.1121	-0.1324	0.9030	-0.0234			0.8853	0.0215	0.9907	-0.0203	1.1095	-0.1190
1.1106	-0.1312	0.9002	-0.0224			0.8865	0.0218	0.9948	-0.0230	1.1106	-0.1200
1.1089	-0.1298	0.8977	-0.0214			0.8879	0.0219	0.9990	-0.0259	1.1117	-0.1211
1.1071	-0.1284	0.8953	-0.0204			0.8892	0.0220	1.0034	-0.0289	1.1127	-0.1221
1.1051	-0.1269	0.8931	-0.0195			0.8906	0.0221	1.0078	-0.0321	1.1136	-0.1230
1.1030	-0.1253	0.8910	-0.0185			0.8921	0.0221	1.0123	-0.0354	1.1145	-0.1240
1.1007	-0.1236	0.8891	-0.0175			0.8936	0.0221	1.0169	-0.0389	1.1154	-0.1248
1.0983	-0.1218	0.8874	-0.0165			0.8952	0.0220	1.0217	-0.0425	1.1163	-0.1257
1.0956	-0.1198	0.8859	-0.0155			0.8968	0.0219	1.0262	-0.0460	1.1171	-0.1265
1.0927	-0.1177	0.8844	-0.0145			0.8984	0.0217	1.0306	-0.0495	1.1179	-0.1273
1.0896	-0.1155	0.8831	-0.0135			0.9001	0.0215	1.0348	-0.0528	1.1187	-0.1281
1.0863	-0.1131	0.8820	-0.0125			0.9019	0.0212	1.0388	-0.0560	1.1194	-0.1288
1.0827	-0.1105	0.8809	-0.0115			0.9037	0.0209	1.0426	-0.0591	1.1201	-0.1296
1.0788	-0.1078	0.8800	-0.0105			0.9055	0.0205	1.0463	-0.0622	1.1208	-0.1302
1.0745	-0.1049	0.8791	-0.0096			0.9074	0.0201	1.0499	-0.0651	1.1215	-0.1309
1.0700	-0.1019	0.8783	-0.0087			0.9093	0.0196	1.0533	-0.0679	1.1221	-0.1315
1.0650	-0.0987	0.8776	-0.0079			0.9113	0.0191	1.0566	-0.0706	1.1227	-0.1322
1.0596	-0.0953	0.8770	-0.0070			0.9134	0.0185	1.0598	-0.0733	1.1233	-0.1328
1.0537	-0.0917	0.8764	-0.0062			0.9155	0.0179	1.0628	-0.0759	1.1239	-0.1333
1.0474	-0.0880	0.8759	-0.0055			0.9177	0.0172	1.0657	-0.0783	1.1244	-0.1339
1.0405	-0.0841	0.8754	-0.0048			0.9199	0.0165	1.0685	-0.0807	1.1250	-0.1344

Lower Surface						Upper Surface					
x/c	y/c	x/c	y/c	x/c	y/c	x/c	y/c	x/c	y/c	x/c	y/c
						1.1255	-0.1349				
						1.1260	-0.1354				
						1.1265	-0.1359				
						1.1269	-0.1363				
						1.1274	-0.1368				
						1.1278	-0.1372				
						1.1282	-0.1376				
						1.1286	-0.1380				
						1.1290	-0.1384				
						1.1293	-0.1388				
						1.1297	-0.1391				
						1.1300	-0.1395				
						1.1303	-0.1398				
						1.1306	-0.1401				
						1.1309	-0.1405				

Appendix C: Derivation of equation (5-3) – reflectivity curve error analysis

C.1 Derivation of equation (5-3)

Consider the system of linear differential equations

$$-\frac{di}{Sdx} = -ai + j$$

$$\frac{dj}{Sdx} = -aj + i \qquad \text{(C-1)}$$

Where $a = \frac{S+K}{S}$ with boundary conditions,

$$x = 0,\ r = R_g \qquad \text{(C-2)}$$

$$x = X,\ r = R$$

Letting $r = \frac{j}{i}$ and differentiating with respect to x,

$$\frac{dr}{dx} = \frac{\frac{idj}{dx} - \frac{jdi}{dx}}{i^2} \qquad \text{(C-3)}$$

Dividing both sides of Equation (C-3) by S,

$$\frac{dr}{Sdx} = \frac{\frac{idj}{Sdx} - \frac{jdi}{Sdx}}{i^2}$$

Using Equations (C-1)

$$\frac{dr}{Sdx} = \frac{i(-aj+i)+j(-ai+j)}{i^2}$$

$$= \frac{-aij+i^2+j^2-aij}{i^2} \qquad \text{(C-4)}$$

$$= 1+r^2-2ar$$

Integrating (B-4),

$$s\int_0^X dx = \int_{R_g}^{R} \frac{dr}{r^2-2ar+1}$$

From Reference 27, page 296, integral 110,

$$S[X-0] = \left[\frac{-2}{\sqrt{-4(1-a^2)}}\tanh^{-1}\frac{2r-2a}{\sqrt{-4(1-a^2)}}\right]_{R_g}^{R}$$

Let $b = \sqrt{a^2-1}$ $\quad (b^2 = a^2-1, a^2 = b^2+1)$

$$SX = \left|\frac{-1}{b}\tanh^{-1}\frac{r-a}{b}\right|_{R_g}^{R}$$

$$SX = \left|\frac{-1}{b}\tanh^{-1}\frac{R-a}{b} - \tanh^{-1}\frac{R_g-a}{b}\right|$$

From Reference 27, page 233,

$$\tanh^{-1}x - \tanh^{-1}y = \tanh^{-1}\left(\frac{x-y}{1-xy}\right)$$

Using the above result

$$SX = \frac{-1}{b}\tanh^{-1}\left[\frac{\frac{R-a}{b}-\frac{R_g-a}{b}}{1-\left(\frac{R-a}{b}\right)\left(\frac{R_g-a}{b}\right)}\right]$$

$$\tanh(bSX) = -\frac{(R-R_g)/b}{\left[b^2-(R-a)(R_g-a)\right]/b^2}$$
$$= -\frac{b(R-R_g)}{b^2-(R-a)(R_g-a)}$$

$$tanh(bSX)\left|b^2-(RR_g-R_a-R_ga+a^2)\right| = -b(R-R_g)$$
$$\tanh(bSX)\left|b^2-(RR_g+R_a+R_ga-a^2)\right| = -b(R-R_g)$$
$$tanh(bSX)(a^2-1-RR_g+Ra+R_ga-a^2) = -b(R-R_g)$$
$$tanh(bSX)(R_ga+R(a-R_g)-1) = -bR+bR_g$$
$$tanh(bSX)(R_ga-1)-bR_g = -bR-R(a-R_g)tanh(bSX)$$

$$R = \frac{-bR_g+tanh(bSX)(R_ga-1)}{-(b+(a-R_g)tanh(bSX))}$$

$$R = \frac{R_g(-b+a\,tanh(bSX)-tanh(bSX)}{-(b+(a-R_g)tanh(bSX))}$$

dividing by *tanh(bSX)*,

$$R = \frac{R_g(-b\,coth(bSX)+a)-1}{-(a+b\,coth(bSX)-R_g)}$$

$$R = \frac{1-R_g(a-b\,coth(bSX))}{a+b\,coth(bSX)-R_g}$$

C. 2 Reflectivity Curve error analysis

Let $K = ac$ where c is the dye concentration and a is a constant. Using the above equation for K,

$$a = \frac{ac+S}{S} \qquad \text{(C-5)}$$

$$b = \frac{\sqrt{ac(ac+2S)}}{SX}$$

Let $R = \frac{N}{D}$ where,

$$N = 1-R_g(a-b\,coth(bSX)) \qquad \text{(C-6)}$$

$$D = a+b\,coth(bSX)-R_g$$

Differentiating R with respect to c,

$$\frac{dR}{dc} = \frac{D\frac{dN}{dc} - N\frac{dD}{dc}}{D^2} = \frac{1}{D}\frac{dN}{dc} - \frac{N}{D^2}\frac{dD}{dc} = F(c) \qquad \text{(C-7)}$$

where,

$$\frac{dN}{dc} = 0 - R_g\left|\frac{da}{dc} - coth(bSX)\frac{db}{dc} - b\frac{d}{dc}coth(bSX)\right|$$

$$\frac{dD}{dc} = \frac{da}{dc} + coth(bSX)\frac{db}{dc} + b\frac{d}{dc}coth(bSX) - 0$$

$$\frac{da}{dc} = \frac{a}{S}$$

$$\frac{db}{dc} = \frac{1}{S}\frac{a(ac+2S)+a^2c}{2\sqrt{ac(ac+2S)}} = \frac{a(ac+S)}{S\sqrt{ac(ac+2S)}}$$

$$\frac{d}{dc}coth(bSX) = -\frac{d(bSX)}{dc}csc\,h^2(bSX) = \frac{-SX}{sinh(bSX)}\frac{db}{dc}$$

Multiplying both sides of Equation (C-7)

$$\frac{dR}{dc}\frac{c}{R} = \frac{c}{R}F(c)$$

Rearranging

$$\frac{dR}{R} = \frac{c}{R}F(c)\frac{dc}{c}$$

where *dc*/*c* is the relative error in dye concentration due to an error in the value of reflectivity.

Solving for *dc*/*c* and normalizing the reflectance with respect to ε, the reflectance value corresponding to *c* = *0*, (zero dye concentration) yields

$$\frac{dc}{c} = \frac{R}{\varepsilon c}\frac{1}{F(c)}\frac{dR}{R} \qquad \text{(C-8)}$$

Where,

$$\varepsilon = \frac{1}{2 - R_g}$$

Appendix D: Run Log for 1997 Impingement Tests

Date : August 1, 1997
P_{BAR} : 14.40 psia
DYE CONCENTRATION : 0.0002 grams/cc
PSYCHROMETER READINGS :
:

		TUNNEL CONDITION						SPRAY CONDITIONS / MASS FLOW								REMARKS
								NOZZLE PRESSURE			TANK PRESSURE		TIME			
RUN NO.	Run I.D.	Air TEMP. (°F)	TAS (MPH)	P_∞ (PSIA)	PRESS TOTAL (PSIA)	D. C. grams/cc	Humidity %	$\frac{P_{AIR}}{P_{WATER}}$	P_{AIR} (PSIG)	P_{WATER} (PSIG)	P_{AIR} (PSIG)	P_{WATER} (PSIG)	SPRAY (SEC)	SPRAY TIME	MVD	
1	wir0001	44.5	176	13.836	14.367	0.002	59.33	0.294118	20	68	20	68	30	19:13	20	IRT air off, r11all.pmi
2	wir0002	43.8	176	13.836	14.367	0.002	59.7	0.294118	20	68	20	68	30	19:16	20	IRT air off, r11all.pmi (redo wir0001)
3	wir0003	41.4	175	13.836	14.367	0.002	53.8	0.294118	20	68	20	68	30	19:19	20	IRT air off, r11all.pmi
4	wir0004	43.9	176	13.836	14.367	0.002	64.94	0.294118	20	68	20	68	30	19:21	20	IRT air on (80 lbs pressure)
5	wir0005	45.1	176	13.836	14.367	0.002	61.23	0.294118	20	68	20	68	30	19:23	20	IRT air on (80 lbs pressure)
6	wir0006	44.2	176	13.836	14.367	0.002	54.08	0.634921	40	63	40	63	30	19:37	12	IRT air on (80 lbs pressure)
7	wir0007	43	175	13.836	14.367	0.002	57.67	0.634921	40	63	40	63	30	19:40	12	IRT air on (80 lbs pressure)
8	wir0008	44.2	176	13.836	14.367	0.002	54.91	0.634921	40	63	40	63	30	19:43	12	IRT air off
9	wir0009	42.1	176	13.836	14.367	0.002	61.5	0.634921	40	63	40	63	30	19:46	12	IRT air off
10	wir0010	45.1	176	13.836	14.367	0.002	64.36	0.151515	5	33	5	33	30	19:57	120	IRT air off
11	wir0011	44.4	176	13.836	14.367	0.002	55.23	0.151515	5	33	5	33	30	19:58	120	IRT air off
12	wir0012	39.6	176	13.836	14.367	0.002	67.26	0.151515	5	33	5	33	30	20:02	120	IRT air on (80 lbs pressure)
13	wir0013	43.5	176	13.836	14.367	0.002	61.72	0.151515	5	33	5	33	30	20:10	120	IRT air on (80 lbs pressure)
14	wir0014	43.3	175	13.836	14.367	0.002	60.35	0.151515	5	33	5	33	4	20:15	120	IRT air on (80 lbs pressure)
15	wir0015	40.4	176	13.836	14.367	0.002	63	0.151515	5	33	5	33	4	20:42	120	IRT air on (80 lbs pressure), Penetration Test
16	wir0016	44.4	176	13.836	14.367	0.002	66.6	0.151515	5	33	5	33	4	20:57	120	IRT air off
17	wir0017	47.3	176	13.836	14.367	0.002	82.06	0.151515	5	33	5	33	5	21:47	120	IRT air on (80 lbs pressure)
18	wir0018	39.2	176	13.836	14.367	0.002	84.33	0.294118	20	68	20	68	6	22:02	20	IRT air on (80 lbs pressure)
19	wir0019	41.8	175	13.836	14.367	0.002	68.4	0.294118	20	68	20	68	4	22:13	20	IRT air on (80 lbs pressure)
20	wir0020	42.7	176	13.836	14.367	0.002	68.51	0.634921	40	63	40	63	4	22:23	12	IRT air on (80 lbs pressure)
21	wir0021	46.8	176	13.836	14.367	0.002	72.17	0.151515	5	33	5	33	4	22:46	120	IRT air on (80 lbs pressure)

Date : August 4, 1997

P_{BAR} : 14.30 psia

DYE CONCENTRATION : 0.0002 grams/cc

PSYCHROMETER READINGS :

:

		TUNNEL CONDITION						SPRAY CONDITIONS / MASS FLOW								REMARKS
								NOZZLE PRESSURE			TANK PRESSURE		TIME			
RUN NO.	Run I.D.	Air TEMP. (°F)	TAS (MPH)	P_∞ (PSIA)	PRESS TOTAL (PSIA)	D. C. grams/cc (°F)	Humidity %	$\frac{P_{AIR}}{P_{WATER}}$	P_{AIR} (PSIG)	P_{WATER} (PSIG)	P_{AIR} (PSIG)	P_{WATER} (PSIG)	SPRAY (SEC)	SPRAY TIME	MVD	IRT air set to 80 lbs unless otherwise specified
1	wir0022	44.5	176	13.76	14.28	0.002	58.5	0.151515	5	33	4	39	4	20:36	120	IRT air on; all nozzles on; blotter squares used
2	wir0023	48.6	176	13.76	14.291	0.002	61.3	0.151515	5	33	4	39	4	20:56	120	IRT air on; all nozzles on; blotter strips used
3	wir0024	43.9	176	13.77	14.307	0.002	71.6	0.151515	5	33	4	39	4	21:17	120	IRT air on; all nozzles on; blotter squares used
4	wir0025	41.4	176	13.77	14.307	0.002	70.6	0.294118	20	68	22	74	4	21:46	20	IRT air on; all nozzles on except 11
5	wir0026	43.9	176	13.77	14.307	0.002	64	0.634921	40	63	43.5	67	4	22:04	12	IRT air on; all nozzles on
6	wir0027	39.1	176	13.77	14.307	0.002	73.05	0.634921	40	63	44	67	6	22:13	12	Repeat of wir0026; not enough dye on blotters.
7	wir0028	41	175	13.77	14.3	0.002	64.3	0.634921	40	63	44	67	12	22:25	12	IRT air on; all nozzles on except 11;12 seconds to accumulate dye
8	wir0029	44.7	176	13.77	14.3	0.002	71.56	0.634921	40	63	44	67	10	22:36	12	IRT air on; all nozzles on; using thin collector strips; strip 33V left on
9	wir0030	42.5	175	13.77	14.3	0.002	65.89	0.294118	20	68	22	74	4	22:51	20	IRT air on; all nozzles on; using thin collector strips
10	wir0031	42.7	177	13.77	14.3	0.002	62.01	0.151515	5	33	4	39	4	23:06	120	IRT air on; all nozzles on; using thin collector strips

Date : August 5, 1997
P_{BAR} : 14.35 psia
DYE CONCENTRATION : 0.0002 grams/cc
PSYCHROMETER READINGS : 12345 °F DB
: 12345 °F DB

Note:
1. MVD measurement methodology:
a) Optical Array Prob (OAP)
b)Forward Scrattering Spectrometer Probe (FSSP)
2. 47 MVD is the largest droplet size for FSSP system

		TUNNEL CONDITION						SPRAY CONDITIONS / MASS FLOW								REMARKS
								NOZZLE PRESSURE			TANK PRESSURE		TIME			
RUN NO.	Run I.D.	Air TEMP. (°F)	TAS (MPH)	P_∞ (PSIA)	PRESS TOTAL (PSIA)	D. C. grams/cc	Humidity %	$\frac{P_{AIR}}{P_{WATER}}$	P_{AIR} (PSIG)	P_{WATER} (PSIG)	P_{AIR} (PSIG)	P_{WATER} (PSIG)	SPRAY (SEC)	SPRAY TIME	MVD	(IRT air pressure is set to 80 lbs)
1	wir0032	38.6	176	13.82	14.352	0.002	60.42	0.634921	40	63	43.5	67	120	18:28	12	Nozzle #11 off, IRT air off, FSSP -- average MVD 12
2	wir0033	43.1	177	13.838	14.36	0.002	53.56	0.634921	40	63	43.5	67	120	18:34	12	Nozzle #11 off, IRT air on, FSSP -- average MVD 11.9
3	wir0034	43.6	176	13.819	14.362	0.002	53.91	0.634921	40	63	44	67	120	18:38	12	All Nozzles on, IRT air on, FSSP -- average MVD 11.7
4	wir0035	41.8	176	13.793	14.353	0.002	52.25	0.634921	40	63	44	67	120	18:43	12	All Nozzles on, IRT air off, FSSP -- average MVD 11.8
5	wir0036	42.3	176	13.813	14.348	0.002	48.85	0.294118	20	68	22	74	120	18:50	20	Nozzle #11 off, IRT air off, FSSP -- average MVD 21.1
6	wir0037	43.2	176	13.838	14.36	0.002	59.95	0.294118	20	68	22	74	120	18:57	20	Nozzle #11 off, IRT air on, FSSP -- average MVD 21.1
7	wir0038	38.5	175	13.838	14.362	0.002	57.3	0.151515	5	33	4	39	120	19:06	120	All Nozzles on, IRT air on, FSSP -- average MVD (not available for FSSP system)
8	wir0039	44.2	176	13.808	14.353	0.002	54.96	0.151515	5	33	4	39	120	19:13	120	All Nozzles on, IRT air off, FSSP -- average MVD (not available for FSSP system)
9	wir0040	44.1	176	13.818	14.356	0.002	57.89	0.294118	20	68	22	74	120	19:19	20	Nozzle #11 off, IRT air off, FSSP -- average MVD 20.8
10	wir0041	43.9	176	13.823	14.361	0.002	61.08	0.294118	20	68	22	74	120	19:50	20	Nozzle #11 off, IRT air off, OAP
11	wir0042	43.9	176	13.823	14.361	0.002	61.08	0.294118	20	68	22	74	120	19:55	20	Nozzle #11 off, IRT air off, OAP (repeat Runt #41)
12	wir0043	42.7	174	13.835	14.364	0.002	57.84	0.294118	20	68	22	74	120	20:02	20	Nozzle #11 off, IRT air on, OAP
13	wir0044	43.9	174	13.832	14.364	0.002	46.26	0.151515	5	33	4	39	120	20:12	120	All Nozzles on, IRT air on, OAP -- average MVD 106
14	wir0045	40.3	175	13.819	14.354	0.002	58.28	0.151515	5	33	4	39	120	20:18	120	All Nozzles on, IRT air off, OAP -- average MVD 111
15	wir0056**	39.9	176	13.815	14.366	0.002	61.40	0.634921	40	63	44	67	120	22:06	12	Nozzle #11 off, IRT air off, LWC test -- average LWC = 0.05 grams/m^3 (0.04 -- 0.06)
16	wir0057	40.7	177	13.819	14.364	0.002	61.84	0.634921	40	63	44	67	120	22:13	12	All Nozzles on, IRT air off, LWC test -- average LWC = 0.045 grams/m^3 (0.04 -- 0.05)
17	wir0058	43.6	176	13.843	14.368	0.002	57.5	0.634921	40	63	44	67	120	22:18	12	All Nozzles on, IRT air on, LWC test -- average LWC = (fail to record the reading)
18	wir0059	41.5	176	13.828	14.371	0.002	54.23	0.634921	40	63	44	67	120	22:24	12	Repeat Run #58, LWC test -- average LWC = 0.025 grams/m^3 (0.02 -- 0.03)
19	wir0060	44.4	176	13.831	14.371	0.002	51.81	0.634921	40	63	44	67	120	22:29	12	Nozzle #11 off, IRT air on, LWC test -- average LWC = 0.015 grams/m^3 (0.01 -- 0.02)
20	wir0061	43.9	174	13.826	14.369	0.002	48.10	0.294118	20	68	22	74	120	22:34	20	Nozzle #11 off, IRT air on, LWC test -- average LWC = 0.095 grams/m^3 (0.08 -- 0.011)
21	wir0062	45.3	175	13.823	14.362	0.002	49.00	0.294118	20	68	22	74	120	22:41	20	Nozzle #11 off, IRT air off, LWC test -- average LWC = 0.14 grams/m^3 (0.09 -- 0.18)
22	wir0063	43.6	175	13.821	14.36	0.002	50.73	0.151515	5	33	4	39	120	22:49	120	All Nozzles on, IRT air off, LWC test -- average LWC = 0.20 grams/m^3 (0.16 -- 0.26)
23	wir0064	43.2	176	13.89	14.368	0.002	50.44	0.151515	5	33	4	39	120	22:53	120	All Nozzles on, IRT air on, LWC test -- average LWC = 0.16 grams/m^3 (0.14 -- 0.18)
24	wir0065	44.8	176	13.826	14.364	0.002	47.4	#VALUE!			2.6	40.28	120	23:00	high	All Nozzles on, IRT air on, LWC test -- average LWC = 0.18 grams/m^3 (0.14-0.21)
25	wir0066	43.9	177	13.839	14.367	0.002	47.63	#VALUE!			2	40	120	23:05	higher	All Nozzles on, IRT air on, LWC test -- average LWC = 0.16 grams/m^3 (0.13-0.19)

** There are 10 trial runs (#46 - #55) which are not recorded in this table, but they can be found in the daily back up disk (Zip disk -- NASA #2)

Date : August 6, 1997
P_{BAR} : 14.40 psia
DYE CONCENTRATION : 0.0002 grams/cc
PSYCHROMETER READINGS :
:

Note :
1. **Test Model : MS 317**
2. **Verigood 100 New and Whatman 3MM papers strips are used.**
3. **IRT air remained on at 20 lbs to prevent the water leaking from some IRT's nozzles when the tunnel was down.**
4. **MS 317 pressure data was taken by IRT's system (record #2176 -- #2193, see Colin's notes in Aug. 7's folder)**

		TUNNEL CONDITION						SPRAY CONDITIONS / MASS FLOW								REMARKS
								PRESSURE INDICATOR			TANK PRESSURE		TIME			** IRT 80 lbs air
RUN NO.	Run I.D.	Air TEMP. (°F)	TAS (MPH)	P_∞ (PSIA)	PRESS TOTAL (PSIA)	D. C. grams/cc	Humidity %	$\frac{P_{AIR}}{P_{WATER}}$	P_{AIR} (PSIG)	P_{WATER} (PSIG)	P_{AIR} (PSIG)	P_{WATER} (PSIG)	SPRAY (SEC)	SPRAY TIME	MVD	IRT air set to 80 lbs unless otherwise specified
1	wir0067	41.6	177	13.816	14.362	0.002	57.25	0.292517	22.36	76.44	22	74	4	18:36	22	Nozzle #11 off, IRT air on, flow rate 0.31 galons/min (darker than the cllector)
2	wir0068	41.7	176	13.868	14.408	0.002	48	0.287484	22.05	76.7	22	74	4	20:42	22	Nozzle #11 off, IRT air on,
3	wir0069	43	176	13.83	14.401	0.002	54.71	0.378449	28.8	76.1	22	74	4	21:03	22	Nozzle #11 off, IRT air on
4	wir0070	45.6	176	13.86	14.409	0.002	57.42	0.293034	22.42	76.51	22	74	4	21:21	22	Nozzle #11 off, IRT air on
5	wir0071	40.5	176	13.861	14.405	0.002	52.2	0.28987	21.92	75.62	22	74	4	21:34	22	Nozzle #11 off, IRT air off
6	wir0072	40.5	176	13.868	14.415	0.002	50.58	0.103832	4.2	40.45	4	39	4	22:21	92	All Nozzles on, IRT air on (see Note #3)
7	wir0073	42.7	176	13.916	14.429	0.002	55.7	0.104223	4.22	40.49	4	39	4	22:49	92	All Nozzles on, IRT air on
8	wir0074	40.6	13.88	14.415		0.002	44.56	0.102666	4.12	40.13	4	39	4	23:00	92	All Nozzles on, IRT air on

Date : August 7, 1997
P_{BAR} : 13.90 psia
DYE CONCENTRATION : 0.0002 & 0.0003 grams/cc
PSYCHROMETER READINGS :
:

Note:

1. **WIR0075 -- WIR0084 are the flow visualization versus AOA Test, image files were saved**
2. **Concentration was changed from 0.0002 grams/cc to 0.0003 grams/cc at 20:20 - 21:20 (from WIR0099)**
3. **Both Verigood 100 New and Whatman 3MM paper were used**
4. **Test Model: MS317**

		TUNNEL CONDITION						SPRAY CONDITIONS / MASS FLOW								
								PRESSURE INDICATOR			TANK PRESSURE		TIME			
RUN NO.	Run I.D.	Air TEMP. (°F)	TAS (MPH)	P_∞ (PSIA)	PRESS TOTAL (PSIA)	D. C. grams/cc	Humidity %	$\frac{P_{AIR}}{P_{WATER}}$	P_{AIR} (PSIG)	P_{WATER} (PSIG)	P_{AIR} (PSIG)	P_{WATER} (PSIG)	SPRAY (SEC)	SPRAY TIME	MVD	REMARKS ** IRT 80 lbs air when tunnel was in operating condition ** IRT 20 lbs air when tunnel was in idle condition
1	wir0075	46.9	176	13.894	14.436	0.002	54.75	0.291159	22	75.56	22	74	30	16:54	22	Nozzle #11 off, IRT air on, AOA = -4.0 deg., filename: am4.pmi
2	wir0076	43.7	177	13.902	14.435	0.002	53.44	0.294821	22.2	75.3	22	74	30	17:04	22	Nozzle #11 off, IRT air on, AOA = 0 deg., file name: a0.pmi
3	wir0077	46.4	176	13.886	14.436	0.002	60.08	0.294651	22.09	74.97	22	74	30	17:07	22	Nozzle #11 off, IRT air on, AOA = 4.0 deg., filename: ap4.pmi
4	wir0078	38.6	176	13.891	14.437	0.002	63.79	0.296791	22.2	74.8	22	74	30	17:10	22	Nozzle #11 off, IRT air on, AOA = 8.0 deg., filename: ap8.pmi
5	wir0079	41.8	176	13.896	14.432	0.002	63.79	0.294094	21.96	74.67	22	74	30	17:13	22	Nozzle #11 off, IRT air on, AOA = 10.0 deg. filename: ap10.pmi
6	wir0080	46.0	175	13.894	14.435	0.002	57.76	0.292279	21.88	74.86	22	74	30	17:16	22	Only Nozzle #12, #10, and #2 are on, IRT air on, AOA = 10.0 deg. filename: R80.pmi
7	wir0081	46.0	175	13.894	14.435	0.002	57.76	0.292279	21.88	74.86	22	74	30	17:21	22	repeat WIR0080, filename: R81.pmi
8	wir0082	42.8	177	13.881	14.43	0.002	58.45	0.290495	21.7	74.7	22	74	30	17:24	22	Only Nozzle #1, #4, and #10 are on, IRT air on, AOA = 10.0 deg, filename: R82.pmi
9	wir0083	44.8	174	13.912	14.433	0.002	50.78	0.290551	21.71	74.72	22	74	30	17:28	22	Only Nozzle #1, #4, and #10 are on, IRT air on, AOA = 0.0 deg, filename: R83.pmi
10	wir0084	39.4	176	13.886	14.429	0.002	60.16	0.292464	21.85	74.71	22	74	30	17:30	22	Only Nozzle #12, #10, and #2 are on, IRT air on, AOA = 0.0 deg. filename: R84.pmi
11	wir0085	39.4	176	13.894	14.429	0.002	53.22	0.627197	43.17	68.83	44	67	10	17:46	12	Nozzle #11 off, IRT air on, AOA = 0.0 deg.
12	wir0086	40.6	176	13.89	14.429	0.002	59.79	0.635327	43.45	68.39	44	67	10	17:59	12	Nozzle #11 off, IRT air on, AOA = 0.0 deg.
13	wir0087	44.9	176	13.887	14.425	0.002	52.49	0.625942	43.19	69	44	67	15	18:08	12	Nozzle #11 off, IRT air on, AOA = 0.0 deg.
14	wir0088	40.8	175	13.885	14.43	0.002	65.79	0.642433	43.3	67.4	44	67	20	18:18	12	Nozzle #11 off, IRT air on, AOA = 0.0 deg.
15	wir0089	42.5	174	13.895	14.427	0.002	55.37	0.351032	23.8	67.8	44	67	20	18:32	12	Nozzle #11 off, IRT air on, AOA = 8.0 deg.
16	wir0090	43.2	177	13.89	14.127	0.002	52.81	0.640343	43.3	67.62	44	67	20	18:42	12	Nozzle #11 off, IRT air on, AOA = 8.0 deg.
17	wir0091	44.1	175	13.888	14.426	0.002	50.103	0.632051	43.7	69.14	44	67	20	18:51	12	Nozzle #11 off, IRT air on, AOA = 8.0 deg.
18	wir0092	46	175	13.894	14.427	0.002	49.46	0.286013	21.88	76.5	22	74	4	19:03	22	Nozzle #11 off, IRT air on, AOA = 8.0 deg.
19	wir0093	39.8	176	13.889	14.43	0.002	66.8	0.291503	22.3	76.5	22	74	4	19:17	22	Nozzle #11 off, IRT air on, AOA = 8.0 deg.
20	wir0094	43.1	174	13.89	14.427	0.002	56	0.294654	22.6	76.7	22	74	8	19:24	22	Nozzle #11 off, IRT air on, AOA = 8.0 deg.
21	wir0095	41.9	176	13.897	14.429	0.002	61.108	0.290743	22.3	76.7	22	74	8	19:33	22	Nozzle #11 off, IRT air on, AOA = 8.0 deg.
22	wir0096	41	176	13.881	14.427	0.002	65.01	0.109696	4.48	40.84	4	39	3	19:50	92	All Nozzles on, IRT air on, AOA = 8.0 deg.
23	wir0097	35.8	175	13.887	14.43	0.002	77.2	0.108115	4.41	40.79	4	39	4	20:00	92	All Nozzles on, IRT air on, AOA = 8.0 deg.
24	wir0098	39.5	175	13.885	14.424	0.002	59.94	0.107711	4.4	40.85	4	39	3	20:10	92	All Nozzles on, IRT air on, AOA = 8.0 deg.
25	wir0099	46.3	175	13.891	14.43	0.003	56.05	0.104028	4.21	40.47	4	39	3	22:01	92	All Nozzles on, IRT air on, AOA = 8.0 deg. (concentration 0.0003 from this run)
26	wir0100	48.9	176	13.904	14.436	0.003	59.01	0.104294	4.25	40.75	4	39	3	22:11	92	All Nozzles on, IRT air on, AOA = 8.0 deg.
27	wir0101	47.8	175	13.895	14.434	0.003	56.05	0.288626	22.23	77.02	22	74	4	22:22	22	Nozzle #11 off, IRT air on, AOA = 8.0 deg.
28	wir0102	47.1	174	13.901	14.435	0.003	48	0.290062	22.3	76.88	22	74	8	22:29	22	Nozzle #11 off, IRT air on, AOA = 8.0 deg.
29	wir0103	48.3	176	13.903	14.436	0.003	49.37	0.633577	43.4	68.5	44	67	15	22:39	12	Nozzle #11 off, IRT air on, AOA = 8.0 deg.
30	wir0104	50.6	177	13.905	14.435	0.003	53.71	0.634111	43.5	68.6	44	67	20	22:46	12	Nozzle #11 off, IRT air on, AOA = 8.0 deg.
31	wir0105	49.8	174	13.91	14.436	0.003	49.8	0.633382	43.45	68.6	44	67	20	22:57	12	Nozzle #11 off, IRT air on, AOA = 0.0 deg.

Date : August 8, 1997
P_{BAR} : 14.40 psia
DYE CONCENTRATION : 0.0003 grams/cc
PSYCHROMETER READINGS :
:

Note:
1. Test Model: MS 317
2. Continuation from August 7, 1997

		TUNNEL CONDITION						SPRAY CONDITIONS / MASS FLOW								REMARKS
								PRESSURE READING			TANK PRESSURE		TIME			
RUN NO.	Run I.D.	Air TEMP. (°F)	TAS (MPH)	P_∞ (PSIA)	PRESS TOTAL (PSIA)	D. C. grams/cc	Humidity %	P_{AIR} / P_{WATER}	P_{AIR} Display (psig)	P_{WATER} Display (psig)	P_{AIR} Gauge (psig)	P_{WATER} Gauge (psig)	SPRAY (SEC)	SPRAY TIME	MVD	** IRT 80 lbs air when tunnel was in operating condition ** IRT 20 lbs air when tunnel was in idle condition
1	wir0106	42.2	177	13.879	14.403	0.0003	58.62	0.62789	43.45	69.2	44	67	60	17:39	12	Nozzle #11 off, IRT air on, AOA = 0.0 deg.
2	wir0107	37	174	13.853	14.4	0.0003	70.53	0.629443	43.74	69.49	44	67	50	17:48	12	Nozzle #11 off, IRT air on, AOA = 0.0 deg.
3	wir0108	44.2	176	13.871	14.396	0.0003	58.08	0.61516	42.2	68.6	44	67	40	17:56	12	Nozzle #11 off, IRT air on, AOA = 0.0 deg.
4	wir0109	47	174	13.879	14.338	0.0003	54.71	0.634182	43.86	69.16	44	67	30	18:04	12	Nozzle #11 off, IRT air on, AOA = 0.0 deg.
5	wir0110	45.9	176	13.866	14.395	0.0003	54.92	0.292375	22.7	77.64	22	74	4	18:16	22	Nozzle #11 off, IRT air on, AOA = 0.0 deg.
6	wir0111	47.8	176	13.864	14.4	0.0003	51.27	0.302477	23.2	76.7	22	74	6	18:25	22	Nozzle #11 off, IRT air on, AOA = 0.0 deg.
7	wir0112	45.7	174	13.875	14.4	0.0003	53.27	0.300952	23.08	76.69	22	74	8	18:33	22	Nozzle #11 off, IRT air on, AOA = 0.0 deg.
8	wir0113	47.6	176	13.865	14.397	0.0003	49.51	0.304639	23.18	76.09	22	74	6	18:40	22	Nozzle #11 off, IRT air on, AOA = 0.0 deg.
9	wir0114	47.4	176	13.86	14.398	0.0003	50.02	0.308594	23.7	76.8	22	74	6	18:49	22	Nozzle #11 off, IRT air on, AOA = 0.0 deg.
10	wir0115	46.7	176	13.859	14.402	0.0003	50	0.309694	23.8	76.85	22	74	6	18:56	22	Nozzle #11 off, IRT air on, AOA = 0.0 deg.
11	wir0116	47.5	176	13.866	14.398	0.0003	48	0.309292	23.8	76.95	22	74	6	19:02	22	Nozzle #11 off, IRT air on, AOA = 8.0 deg.
12	wir0117	47.1	176	13.868	14.396	0.0003	47.396	0.295573	22.7	76.8	22	74	6	19:09	22	Nozzle #11 off, IRT air on, AOA = 8.0 deg.
13	wir0118	47.3	175	13.86	14.395	0.0003	43.8	0.296489	22.8	76.9	22	74	6	19:17	22	Nozzle #11 off, IRT air on, AOA = 8.0 deg.
14	wir0119	44.6	175	13.862	14.392	0.0003	50	0.296345	22.7	76.6	22	74	6	19:24	22	Nozzle #11 off, IRT air on, AOA = 8.0 deg.
15	wir0120	40.5	175	13.857	14.399	0.0003	58.394	0.643068	43.6	67.8	44	67	30	19:56	12	Nozzle #11 off, IRT air on, AOA = 8.0 deg.
16	wir0121	42.9	175	13.855	14.397	0.0003	51.56	0.645066	43.8	67.9	44	67	30	20:03	12	Nozzle #11 off, IRT air on, AOA = 8.0 deg.
17	wir0122	47.2	175	13.871	14.395	0.0003	54.59	0.636989	43.5	68.29	44	67	30	20:11	12	Nozzle #11 off, IRT air on, AOA = 8.0 deg.
18	wir0123	43.4	177	13.853	14.393	0.0003	55.44	0.642647	43.7	68	44	67	30	20:19	12	Nozzle #11 off, IRT air on, AOA = 0.0 deg.
19	wir0124	45.5	176	13.849	14.392	0.0003	49.8	0.638734	43.6	68.26	44	67	30	20:26	12	Nozzle #11 off, IRT air on, AOA = 0.0 deg.
20	wir0125	45.8	177	13.862	14.396	0.0003	48	0.109877	4.45	40.5	4	39	3	20:41	92	All Nozzles on, IRT air on, AOA = 0.0 deg.
21	wir0126	47.5	177	13.852	14.393	0.0003	50.07	0.108374	4.4	40.6	4	39	3	20:52	92	All Nozzles on, IRT air on, AOA = 0.0 deg.
22	wir0127	47.7	175	13.865	14.389	0.0003	50.51	0.112887	4.59	40.66	4	39	3	20:59	92	All Nozzles on, IRT air on, AOA = 0.0 deg.
23	wir0128	47.2	176	13.86	14.392	0.0003	40.16	0.108374	4.4	40.6	4	39	3	21:09	92	All Nozzles on, IRT air on, AOA = 8.0 deg.
24	wir0129	46.9	176	13.86	13.39	0.0003	41.9	0.107658	4.4	40.87	4	39	3	21:17	92	All Nozzles on, IRT air on, AOA = 8.0 deg.
25	wir0130	47.5	175	13.859	14.392	0.0003	43.7	0.108241	4.4	40.65	4	39	3	21:25	92	All Nozzles on, IRT air on, AOA = 8.0 deg.

Date : August 11, 1997
P_{BAR} : 14.40 psia
DYE CONCENTRATION : 0.0003 grams/cc
PSYCHROMETER READINGS :
:

Note:

1. **WIR0131 -- WIR0142 are the flow visulization tests:**
   a) **with empty test section (Run #131 -- #136)**
   b) **with collector mechanism in test section (Run #137 ~~ #142)**
2. **Image exposure time is 10 seconds.**
3. **Laser system power setting is 6 Watts**
4. **Test model : Collector Mechanism**

		TUNNEL CONDITION						SPRAY CONDITIONS / MASS FLOW								REMARKS
								PRESSURE READING Disk Digital Display Reading			TANK PRESSURE		TIME			
RUN NO.	Run I.D.	Air TEMP. (°F)	TAS (MPH)	A.O.A (deg.)	P_∞ (PSIA)	PRESS TOTAL (PSIA)	Humidity %	$\frac{P_{AIR}}{P_{WATER}}$	P_{AIR} Display (psig)	P_{WATER} Display (psig)	P_{AIR} Gauge (psig)	P_{WATER} Gauge (psig)	SPRAY (SEC)	CLOCK TIME	MVD	** IRT 80 lbs air when tunnel was in operating condition ** IRT 20 lbs air when tunnel was in idle condition
1	wir0131	48.4	174	**	13.87	14.411	N/A	0.112883	4.6	40.75	4	39	30	17:20	92	All Nozzles on, IRT air on, Empty Tunnel, filename: r131.pmi
2	wir0132	47.1	176	**	13.87	14.412	N/A	0.107527	4.4	40.92	4	39	30	17:21	92	Repeat WIR0131, filename: r132.pmi
3	wir0133	46.6	176	**	13.874	14.413	N/A	0.645185	43.55	67.5	44	67	30	17:30	12	Nozzle #11 off, IRT air on, Empty Tunnel, filename: r133.pmi
4	wir0134	47.5	175	**	13.868	14.411	N/A	0.643068	43.6	67.8	44	67	30	17:33	12	Repeat WIR0133, filename: r134.pmi
5	wir0135	46.3	176	**	13.871	14.411	N/A	0.296345	22.7	76.6	22	74	30	17:39	22	Nozzle #11 off, IRT air on, Empty Tunnle, filename: r135.pmi
6	wir0136	45.2	176	**	13.875	14.411	N/A	0.294271	22.6	76.8	22	74	30	17:42	22	Repeat WIR0135, filename: r136.pmi
7	wir0137	48.0	177	0.0	13.897	14.406	N/A	0.293734	22.5	76.6	22	74	30	18:42	22	Nozzle #11 off, IRT air on, Collector Mechansim in Test Section, filename: r137.pmi
8	wir0138	48.2	176	0.0	13.873	14.41	N/A	0.294654	22.6	76.7	22	74	30	18:44	22	Repeat WIR0137, filename: r138.pmi
9	wir0139	47.4	176	0.0	13.874	14.412	N/A	0.104423	4.25	40.7	4	39	30	18:52	92	All Nozzles on, IRT air on, Collector Mechanixm in Test Section, filename: r139.pmi
10	wir0140	47.4	176	0.0	13.879	14.411	N/A	0.106158	4.31	40.6	4	39	30	18:54	92	Repeat WIR0139, filename: r140.pmi
11	wir0141	44.8	176	0.0	13.875	14.411	N/A	0.641064	43.4	67.7	44	67	30	18:59	12	Nozzle #11 off, IRT air on, Collector Mechanism in Test Section, filename: r141.pmi
12	wir0142	46.1	175	0.0	13.876	14.409	N/A	0.643594	43.7	67.9	44	67	30	19:01	12	Repeat WIR0141, filename: r142.pmi
13	wir0143	47.4	176	0.0	13.881	14.4	61.18	0.642121	43.6	67.9	44	67	30	20:21	12	Nozzle #11 off, IRT air on, Verigood 100
14	wir0144	46	175	0.0	13.871	14.415	59.2	0.638705	43.4	67.95	44	67	30	20:31	12	Nozzle #11 off, IRT air on, Verigood 100
15	wir0145	47	176	0.0	13.881	14.412	54.79	0.642963	43.4	67.5	44	67	30	20:40	12	Nozzle #11 off, IRT air on, Verigood 100
16	wir0146	45.1	175	0.0	13.88	14.415	59.81	0.640648	43.5	67.9	44	67	30	20:50	12	Nozzle #11 off, IRT air on, Whatman 3MM
17	wir0147	46.3	176	0.0	13.884	14.413	52.42	0.641176	43.6	68.0	44	67	30	20:59	12	Nozzle #11 off, IRT air on, Whatman 3MM
18	wir0148	47.1	175	0.0	13.884	14.412	51.81	0.294271	22.6	76.8	22	74	6	21:11	22	Nozzle #11 off, IRT air on, Verigood 100
19	wir0149	46.4	177	0.0	13.885	14.413	53.59	0.295812	22.6	76.4	22	74	6	21:22	22	Nozzle #11 off, IRT air on, Verigood 100
20	wir0150	46.6	176	0.0	13.879	14.41	48.00	0.293578	22.4	76.3	22	74	6	21:31	22	Nozzle #11 off, IRT air on, Verigood 100
21	wir0151	48.1	175	0.0	13.884	14.411	52.61	0.295039	22.6	76.6	22	74	6	21:39	22	Nozzle #11 off, IRT air on, Whatman 3MM
22	wir0152	47.9	176	0.0	13.888	14.412	50.88	0.291123	22.3	76.6	22	74	6	21:49	22	Nozzle #11 off, IRT air on, Whatman 3MM
23	wir0153	45.7	175	0.0	13.881	14.412	53.4	0.105727	4.32	40.86	4	39	3	22:04	92	All Nozzles on, IRT air on, Verigood 100
24	wir0154	47.8	175	0.0	13.88	14.412	54.08	0.105651	4.3	40.7	4	39	3	22:13	92	All Nozzles on, IRT air on, Verigood 100
25	wir0155	46.4	175	0.0	13.886	14.415	54.47	0.105651	4.3	40.7	4	39	3	22:22	92	All Nozzles on, IRT air on, Verigood 100
26	wir0156	46.8	175	0.0	13.885	14.407	50.29	0.112745	4.6	40.8	4	39	3	22:30	92	All Nozzles on, IRT air on, Whatman 3MM
27	wir0157	49.5	175	0.0	13.871	14.41	50.05	0.107606	4.4	40.89	4	39	3	22:37	92	All Nozzles on, IRT air on, Whatman 3MM
28	wir0158	47.2	176	8.0	13.89	14.42	53	0.293194	22.4	76.4	22	74	6	23:04	22	Nozzle #11 off, IRT air on, Verigood 100
29	wir0159	45.1	175	8.0	13.877	14.421	59.86	0.29281	22.4	76.5	22	74	6	23:12	22	Nozzle #11 off, IRT air on, Verigood 100
30	wir0160	45.5	176	8.0	13.886	14.423	52.29	0.29281	22.4	76.5	22	74	6	23:21	22	Nozzle #11 off, IRT air on, Verigood 100
31	wir0161	47.3	175	8.0	13.886	14.416	51.81	0.295958	22.7	76.7	22	74	6	23:28	22	Nozzle #11 off, IRT air on, Whatman 3MM
32	wir0162	48.2	175	8.0	13.886	14.417	50.22	0.292969	22.5	76.8	22	74	6	23:35	22	Nozzle #11 off, IRT air on, Whatman 3MM

Date : August 12, 1997
AVERAGE P_{BAR} : 14.30 psia
DYE CONCENTRATION : 0.0003 grams/cc
PSYCHROMETER READINGS :
:

Note:

1. Strip A (Verigood 100) is 36" above the floor, strip B (3MM) is 38.5" above the floor.
2. Average 8 minutes per run
3. Pressure data of NACA652-415 was taken by IRT's Electro Scanned Pressure system. (Record #2215 ~~ #2244)
4. Test Model : NACA 65_2-415

		TUNNEL CONDITION						SPRAY CONDITIONS / MASS FLOW								
								DISK DISPLAY PRESSURE READING			TANK PRESSURE		TIME			
RUN NO.	Run I.D.	Air TEMP. (°F)	TAS (MPH)	A.O.A (deg.)	P_∞ (PSIA)	PRESS TOTAL (PSIA)	Humidity %	P_{AIR} / P_{WATER}	P_{AIR} Display (psig)	P_{WATER} Display (psig)	P_{AIR} Gauge (psig)	P_{WATER} Gauge (psig)	SPRAY TIME (sec)	CLOCK TIME	MVD	REMARKS ** IRT 80 lbs air when tunnel was in operating condition ** IRT 20 lbs air when tunnel was in idle condition
1	wir0163	44.8	174	0.0	13.781	14.31	63.1	0.108374	4.4	40.6	4	39	3	19:49	92	All Nozzles on, IRT air on
2	wir0164	47.5	176	0.0	13.714	14.313	62	0.105392	4.3	40.8	4	39	3	19:58	92	All Nozzles on, IRT air on
3	wir0165	42.6	175	0.0	13.783	14.319	73.07	0.107711	4.33	40.2	4	39	3	20:05	92	All Nozzles on, IRT air on
4	wir0166	44	176	0.0	13.776	14.313	67	0.107975	4.4	40.75	4	39	3	20:12	92	All Nozzles on, IRT air on
5	wir0167	47.6	175	8.0	13.709	14.309	65	0.106863	4.36	40.8	4	39	3	20:20	92	All Nozzles on, IRT air on
6	wir0168	51.1	175	8.0	13.782	14.304	68.21	0.106388	4.33	40.7	4	39	3	20:28	92	All Nozzles on, IRT air on
7	wir0169	50.7	174	8.0	13.79	14.309	64	0.107011	4.35	40.65	4	39	3	20:35	92	All Nozzles on, IRT air on
8	wir0170	49.6	175	8.0	13.781	14.307	66	0.104156	4.26	40.9	4	39	3	20:43	92	All Nozzles on, IRT air on
9	wir0171	49.4	176	8.0	13.797	14.311	61.94	0.633751	43.0	67.85	44	67	30	20:53	12	Nozzle #11 off, IRT air on
10	wir0172	50.7	176	8.0	14.702	14.311	55.69	0.641593	43.5	67.8	44	67	30	21:02	12	Nozzle #11 off, IRT air on
11	wir0173	49.7	176	8.0	13.79	14.31	68	0.643491	43.5	67.6	44	67	30	21:10	12	Nozzle #11 off, IRT air on
12	wir0174	47.7	175	8.0	13.788	14.308	65.07	0.641176	43.6	68.0	44	67	30	21:18	12	Nozzle #11 off, IRT air on
13	wir0175	49.3	176	0.0	13.781	14.306	55.4	0.631732	43.4	68.7	44	67	30	21:26	12	Nozzle #11 off, IRT air on
14	wir0176	48.6	175	0.0	13.787	14.307	58.8	0.643579	43.3	67.28	44	67	30	21:34	12	Nozzle #11 off, IRT air on
15	wir0177	47.4	174	0.0	13.776	14.309	61.0	0.642647	43.7	68.0	44	67	30	21:42	12	Nozzle #11 off, IRT air on (results are not good, verigood 100 paper looks bad)
16	wir0178	48.9	176	0.0	13.771	14.308	53.2	0.638643	43.3	67.8	44	67	30	21:54	12	Nozzle #11 off, IRT air on
17	wir0179	48.4	174	0.0	13.776	14.306	59.03	0.643068	43.6	67.8	44	67	30	22:04	12	Nozzle #11 off, IRT air on
18	wir0180	47.1	176	0.0	13.771	14.3	62.23	0.299213	22.8	76.2	22	74	6	22:17	22	Nozzle #11 off, IRT air on
19	wir0181	49.1	175	0.0	13.764	14.296	55.18	0.298177	22.9	76.8	22	74	6	22:24	22	Nozzle #11 off, IRT air on
20	wir0182	48.7	176	0.0	13.774	14.299	52.74	0.296654	22.7	76.52	22	74	6	22:31	22	Nozzle #11 off, IRT air on
21	wir0183	47.7	175	0.0	13.761	14.296	56.01	0.297262	22.8	76.7	22	74	6	22:37	22	Nozzle #11 off, IRT air on
22	wir0184	49.0	176	8.0	13.76	14.297	52.0	0.29765	22.8	76.6	22	74	6	22:45	22	Nozzle #11 off, IRT air on
23	wir0185	49.2	176	8.0	13.776	14.285	50.0	0.296875	22.8	76.8	22	74	6	22:51	22	Nozzle #11 off, IRT air on
24	wir0186	49.0	175	8.0	13.77	14.292	50.0	0.296875	22.8	76.8	22	74	6	22:59	22	Nozzle #11 off, IRT air on
25	wir0187	49.4	177	8.0	13.754	14.291	49.0	0.284238	22.0	77.4	22	74	6	23:06	22	Nozzle #11 off, IRT air on

Date : August 13, 1997
AVERAGE P_{BAR} : 14.30 psia
DYE CONCENTRATION : 0.0003 grams/cc
PSYCHROMETER READINGS :
:

Note:

1. Ideal condition: a) south vent door open half inches
b) total temperature 45 -- 50 deg.
c) humidity from 75% to 85%

2. Test Model: NACA 65_2-415

		TUNNEL CONDITION						SPRAY CONDITIONS / MASS FLOW								REMARKS
								DISK DISPLAY PRESSURE READING			TANK PRESSURE		TIME			
RUN NO.	Run I.D.	Air TEMP. (°F)	TAS (MPH)	A.O.A (deg.)	P_∞ (PSIA)	PRESS TOTAL (PSIA)	Humidity %	P_{AIR} / P_{WATER}	P_{AIR} Display (psig)	P_{WATER} Display (psig)	P_{AIR} Gauge (psig)	P_{WATER} Gauge (psig)	SPRAY TIME (sec)	CLOCK TIME	MVD	** IRT 80 lbs air when tunnel was in operating condition ** IRT 20 lbs air when tunnel was in idle condition
1	wir0188	49.2	174	8.0	13.772	14.299	72.9	0.645066	43.8	67.9	44	67	30	16:42	12	Nozzle #11 off, IRT air on
2	wir0189	46.2	175	8.0	13.779	14.3	65.87	0.639461	43.17	67.51	44	67	30	16:51	12	Nozzle #11 off, IRT air on
3	wir0190	45.9	175	8.0	13.778	14.301	64.5	0.627224	42.3	67.44	44	67	30	17:00	12	Nozzle #11 off, IRT air on
4	wir0191	47.1	175	8.0	13.781	14.303	67.53	0.644444	43.5	67.5	44	67	30	17:08	12	Nozzle #11 off, IRT air on
5	wir0192	45.3	174	8.0	13.775	14.298	72.07	0.641593	43.5	67.8	44	67	30	17:16	12	Nozzle #11 off, IRT air on
6	wir0193	46.2	175	8.0	13.787	14.302	58.41	0.646972	43.8	67.7	44	67	30	17:23	12	Nozzle #11 off, IRT air on
7	wir0194	47.7	175	8.0	13.775	14.296	66.0	0.644756	43.65	67.7	44	67	30	17:31	12	Nozzle #11 off, IRT air on
8	wir0195	48.4	172	8.0	13.777	14.3	64.65	0.644018	43.6	67.7	44	67	30	17:38	12	Nozzle #11 off, IRT air on
9	wir0196	47.6	174	8.0	13.781	14.299	65.45	0.641176	43.6	68.0	44	67	30	17:45	12	Nozzle #11 off, IRT air on
10	wir0197	49.1	176	8.0	13.788	14.304	60.94	0.643917	43.4	67.4	44	67	30	17:53	12	Nozzle #11 off, IRT air on
11	wir0198	61.0	176	8.0	13.788	14.303	61.77	0.640761	43.45	67.81	44	67	30	18:39	12	Nozzle #11 off, IRT air on
12	wir0199	37.0	176	8.0	13.773	14.3	80.0	#VALUE!	**	**	44	67	30	19:25	92	Nozzle #11 off, IRT air on
13	wir0200	36.8	174	8.0	13.765	14.303	58.35	0.646018	43.8	67.8	44	67	30	19:49	92	Nozzle #11 off, IRT air on
14	wir0201	39.7	173	8.0	13.771	14.304	75.76	0.644543	43.7	67.8	44	67	30	19:58	12	Nozzle #11 off, IRT air on
15	wir0202	36.8	174	8.0	13.776	14.303	97.5	0.639053	43.2	67.6	44	67	30	20:07	12	Nozzle #11 off, IRT air on (both vent doors opened about 2' each, cloud observed)
16	wir0203	35.4	174	8.0	13.765	14.298	96.19	0.64497	43.6	67.6	44	67	30	20:17	12	Nozzle #11 off, IRT air on (south vent door open for 8", no cloud observed)
17	wir0204	42.3	174	8.0	13.788	14.312	85.77	0.638002	43.55	68.26	44	67	30	21:28	12	Nozzle #11 off, IRT air on (vent doors are closed), 3MM penetrated
18	wir0205	46.9	176	8.0	13.776	14.306	81.0	0.639824	43.54	68.05	44	67	30	21:37	12	Nozzle #11 off, IRT air on (south vent door has half inches gap)
19	wir0206	48.3	172	8.0	13.805	14.312	85.0	0.634841	43.22	68.08	44	67	20	21:47	12	Nozzle #11 off, IRT air on (south vent door has half inches gap)
20	wir0207	50.1	174	8.0	13.786	14.306	75.12	0.644874	43.4	67.3	44	67	25	21:57	12	Nozzle #11 off, IRT air on (south vent door has half inches gap)
21	wir0208	48.8	175	8.0	13.79	14.31	89.04	0.115196	4.7	40.8	4	39	3	22:13	92	All Nozzles on, IRT air on (south vent door has half inches gap)
22	wir0209	47.2	175	8.0	13.778	14.313	80.7	0.110294	4.5	40.8	4	39	3	22:20	92	All Nozzles on, IRT air on (south vent door has half inches gap)
23	wir0210	40.7	174	8.0	13.772	14.311	85.0	0.640351	43.8	68.4	44	67	25	22:35	12	Nozzle #11 off, IRT air on (both vent doors opened about 2' each, cloud observed)
24	wir0211	46.4	175	8.0	13.788	14.316	92.0	0.644444	43.5	67.5	44	67	25	22:43	12	Nozzle #11 off, IRT air on (both vent doors opened about 2' each, cloud observed)
25	wir0212	42.9	177	8.0	13.791	14.319	86.2	0.64645	43.7	67.6	44	67	25	22:50	12	Nozzle #11 off, IRT air on (both vent doors opened about 2' each, cloud observed)
26	wir0213	45.5	174	0.0	13.79	14.309	77.0	0.645066	43.8	67.9	44	67	25	23:00	12	Nozzle #11 off, IRT air on (both vent doors opened about 2' each, cloud observed)
27	wir0214	44.7	174	0.0	13.794	14.318	82.2	0.646972	43.8	67.7	44	67	25	23:07	12	Nozzle #11 off, IRT air on (both vent doors opened about 2' each, cloud observed)
28	wir0215	45.6	176	0.0	13.79	14.32	80.1	0.643382	43.75	68.0	44	67	25	23:13	12	Nozzle #11 off, IRT air on (both vent doors opened about 2' each, cloud observed)

Date : August 14, 1997
AVERAGE P_{BAR} : 14.30 psia
DYE CONCENTRATION : 0.0003 grams/cc
PSYCHROMETER READINGS :
:

Note:

1. Test Model: Boeing 757 Tailplane Airfoil (stall @ -9 deg.)
2. Pressure data was taken from IRT's ESP system

		TUNNEL CONDITION						SPRAY CONDITIONS / MASS FLOW								REMARKS
								DISK DISPLAY PRESSURE READING			TANK PRESSURE		TIME			
RUN NO.	Run I.D.	Air TEMP. (°F)	TAS (MPH)	A.O.A (deg.)	P_∞ (PSIA)	PRESS TOTAL (PSIA)	Humidity %	$\frac{P_{AIR}}{P_{WATER}}$	P_{AIR} Display (psig)	P_{WATER} Display (psig)	P_{AIR} Gauge (psig)	P_{WATER} Gauge (psig)	SPRAY TIME (sec)	CLOCK TIME	MVD	** IRT 80 lbs air when tunnel was in operating condition ** IRT 20 lbs air when tunnel was in idle condition
1	wir0216	47.4	176	0.0	13.792	14.271	73.6	0.643594	43.7	67.9	44	67	25	19:40	12	Nozzle #11 off, IRT air on (south vent door opens 13 inches)
2	wir0217	48.4	176	0.0	13.741	14.276	78.7	0.645066	43.8	67.9	44	67	25	19:54	12	Nozzle #11 off, IRT air on (south vent door opens 16 inches)
3	wir0218	46.0	176	0.0	13.745	14.236	80.64	0.646539	43.9	67.9	44	67	25	20:03	12	Nozzle #11 off, IRT air on (south vent door opens 21 inches)
4	wir0219	46.2	175	0.0	13.751	14.277	76.7	0.646539	43.9	67.9	44	67	25	20:10	12	Nozzle #11 off, IRT air on (south vent door opens 21 inches)
5	wir0220	45.1	174	4.0	13.747	14.276	78.17	0.627507	43.8	69.8	44	67	25	20:27	12	Nozzle #11 off, IRT air on (south vent door opens 31 inches)
6	wir0221	44.5	176	4.0	13.755	14.279	80.6	0.640118	43.4	67.8	44	67	25	20:35	12	Nozzle #11 off, IRT air on (south vent door opens 31 inches)
7	wir0222	46.2	175	4.0	13.745	14.277	72.4	0.639053	43.2	67.6	44	67	25	20:47	12	Nozzle #11 off, IRT air on (south vent door opens 31", north vent door opens 12")
8	wir0223	44.1	174	4.0	13.76	14.277	82.2	0.645803	43.85	67.9	44	67	25	20:54	12	Nozzle #11 off, IRT air on (south vent door opens 31", north vent door opens 12")
9	wir0224	46.4	175	4.0	13.748	14.278	78.5	0.292555	22.4	76.4	22	74	6	21:12	22	Nozzle #11 off, IRT air on (south vent door opens 31", north vent door opens 12")
10	wir0225	40.7	174	4.0	13.75	14.28	76.6	0.293045	22.5	76.78	22	74	6	21:23	22	Nozzle #11 off, IRT air on (both vent doors closed -- due to heavy cloud observed)
11	wir0226	40.5	174	4.0	13.746	14.288	78.8	0.311111	23.8	76.5	22	74	6	21:31	22	Nozzle #11 off, IRT air on (vent doors were closed)
12	wir0227	43.4	174	4.0	13.74	14.28	70.3	0.294654	22.6	76.7	22	74	6	21:41	22	Nozzle #11 off, IRT air on (south vent door opens 7")
13	wir0228	47.9	175	0.0	13.744	14.28	70.5	0.291287	22.4	76.9	22	74	6	21:53	22	Nozzle #11 off, IRT air on (south vent door opens 17")
14	wir0229	44.4	176	0.0	13.743	14.278	74.3	0.292428	22.4	76.6	22	74	6	22:01	22	Nozzle #11 off, IRT air on (south vent door opens 31")
15	wir0230	43.1	177	0.0	13.729	14.277	78.7	0.29765	22.8	76.6	22	74	6	22:07	22	Nozzle #11 off, IRT air on (south vent door opens 31")
16	wir0231	45.6	177	0.0	13.746	14.277	72.0	0.290314	22.18	76.4	22	74	6	22:13	22	Nozzle #11 off, IRT air on (south vent door opens 31")
17	wir0232	43.1	177	0.0	13.749	14.285	75.7	0.104218	4.25	40.78	4	39	3	22:29	92	All Nozzles on, IRT air on (both vent doors closed)
18	wir0233	45.0	175	0.0	13.736	14.276	70.6	0.10489	4.29	40.9	4	39	3	22:38	92	All Nozzles on, IRT air on (south vent door opens 22")
19	wir0234	45.9	176	0.0	13.74	14.28	71.0	0.103704	4.2	40.5	4	39	3	22:45	92	All Nozzles on, IRT air on (south vent door opens 14")

Date : August 18, 1997
AVERAGE P_{BAR} : 13.82 psia
DYE CONCENTRATION : 0.0003 grams/cc
PSYCHROMETER READINGS :
:

Note:

1. Test Model: Collector

2. Angle Of Attack in this record was refer to IRT's AOA setting

		TUNNEL CONDITION						SPRAY CONDITIONS / MASS FLOW								REMARKS
								DISK DISPLAY PRESSURE READING			TANK PRESSURE		TIME			
RUN NO.	Run I.D.	Air TEMP. (°F)	TAS (MPH)	A.O.A (deg.) IRT	P_∞ (PSIA)	PRESS TOTAL (psia)	Humidity %	P_{AIR} / P_{WATER}	P_{AIR} Display (psig)	P_{WATER} Display (psig)	P_{AIR} Gauge (psig)	P_{WATER} Gauge (psig)	SPRAY TIME (sec)	CLOCK TIME	MVD	** IRT 80 lbs air when tunnel was in operating condition ** IRT 20 lbs air when tunnel was in idle condition
1	wir0258	46.7	175	0.0	13.82	14.362	84.1	0.2937	22.5	76.6	22	74	6	18:08	22	Nozzle #11 off, IRT air on, Verigood 100 paper (south vent door opens 31")
2	wir0259	47.4	175	0.0	13.84	14.36	82.2	0.2947	22.4	76.0	22	74	6	18:18	22	Nozzle #11 off, IRT air on, Verigood 100 paper (south vent door opens 31")
3	wir0260	45.4	175	0.0	13.82	14.362	87.7	0.2943	22.6	76.8	22	74	6	18:27	22	Nozzle #11 off, IRT air on, Verigood 100 paper (south vent door opens 31")
4	wir0261	45.7	178	0.0	13.82	14.36	97.0	0.2913	22.4	76.9	22	74	6		22	Nozzle #11 off, IRT air on, Whatman 3MM (south vent door opens 31")
5	wir0262	50.7	175	0.0	13.82	14.36	87.0	0.2992	22.8	76.2	22	74	6	18:48	22	Nozzle #11 off, IRT air on, Whatman 3MM (south vent door opens 9")
6	wir0263	52.7	176	0.0	13.81	14.35	72.0	0.6412	43.6	68.0	44	67	25	19:22	12	Nozzle #11 off, IRT air on, Verigood 100 paper (south vent door opens 9")
7	wir0264	46.5	176	0.0	13.82	14.36	73.9	0.6435	43.5	67.6	44	67	25	19:37	12	Nozzle #11 off, IRT air on, Verigood 100 paper (south vent door opens 17")
8	wir0265	42.7	175	0.0	13.82	14.35	83.0	0.6421	43.6	67.9	44	67	25	19:44	12	Nozzle #11 off, IRT air on, Verigood 100 paper (vent doors closed)
9	wir0266	50.6	175	0.0	13.83	14.36	75.5	0.6382	43.4	68.0	44	67	25	19:52	12	Nozzle #11 off, IRT air on, Whatman 3MM (vent doors close)
10	wir0267	39.4	173	0.0	13.83	14.36	85.0	0.644	43.6	67.7	44	67	25	20:01	12	Nozzle #11 off, IRT air on, Whatman 3MM (vent doors closed)
11	wir0268	43.2	175	0.0	13.83	14.36	83.4	0.105	4.23	40.3	4	39	3	20:38	92	All Nozzles on, IRT air on, Verigood 100 paper (vent doors closed)
12	wir0269	44.1	176	0.0	13.82	14.36	74.7	0.1059	4.3	40.6	4	39	3	20:45	92	All Nozzles on, IRT air on, Verigood 100 paper (vent doors closed)
13	wir0270	43.4	175	0.0	13.83	14.36	73.7	0.101	4.1	40.6	4	39	3	20:54	92	All Nozzles on, IRT air on, Verigood 100 paper (vent doors closed)
14	wir0271	49.8	176	0.0	13.82	14.36	66.2	0.1027	4.2	40.9	4	39	3	21:02	92	All Nozzles on, IRT air on, Whatman 3MM paper (vent doors closed)
15	wir0272	51.6	176	0.0	13.84	14.37	69.0	0.1078	4.4	40.8	4	39	3	21:10	92	All Nozzles on, IRT air on, Whatman 3MM paper (vent doors closed)
16	wir0273	50.9	177	0.0	13.83	14.37	62.0	0.2995	23.0	76.8	22	74	6	21:27	22	Nozzle #11 off, IRT air on, Verigood 100 paper (vent doors closed)
17	wir0274	47.7	175	0.0	13.87	14.37	70.0	0.2889	22.3	77.20	22	74	6	21:43	22	Nozzle #11 off, IRT air on, Verigood 100 paper (vent doors closed)
18	wir0275	51.1	176	-8.0	13.84	14.36	74.5	0.292	22.4	76.7	22	74	6	22:13	22	Nozzle #11 off, IRT air on, Verigood 100 paper (south vent door opens 12")
19	wir0276	46.2	176	-8.0	13.84	14.36	73.6	0.2961	22.8	77.0	22	74	6	22:20	22	Nozzle #11 off, IRT air on, Verigood 100 paper (south vent door opens 12")
20	wir0277	45.6	175	-8.0	13.83	14.36	70.6	0.3059	23.4	76.5	22	74	6	22:36	22	Nozzle #11 off, IRT air on, Verigood 100 paper (south vent door opens 25")
21	wir0278	45.1	176	-8.0	13.82	14.36	73.6	0.2917	22.4	76.8	22	74	6	22:44	22	Nozzle #11 off, IRT air on, Whatman 3MM paper (south vent door opens 25")
22	wir0279	42.2	176	-8.0	13.83	14.36	81.6	0.2939	22.6	76.9	22	74	6	22:52	22	Nozzle #11 off, IRT air on, Whatman 3MM paper (south vent door opens 25")

Date : August 19, 1997
AVERAGE P_{BAR} : 13.80 psia
DYE CONCENTRATION : 0.0003 grams/cc
PSYCHROMETER READINGS :
:

Note:

1. **Test Model: Collector**
2. **Angle Of Attack in this record was refer to IRT's AOA setting**
3. **Humidity on IRT was low, all 10 IRT's spray bars were set to spray to increase the humidity inside the IRT**
4. **Pre-spray the tunnel for about 1.5 min to 2. min before placing the strips on the collector -- to increase the humidity in IRT**

		TUNNEL CONDITION						SPRAY CONDITIONS / MASS FLOW								REMARKS
								DISK DISPLAY PRESSURE READING			TANK PRESSURE		TIME			
RUN NO.	Run I.D.	Air TEMP. (°F)	TAS (MPH)	IRT A.O.A. (deg)	P_∞ (psia)	PRESS TOTAL (psia)	Humidity %	$\frac{P_{AIR}}{P_{WATER}}$	P_{AIR} Display (psig)	P_{WATER} Display (psig)	P_{AIR} Gauge (psig)	P_{WATER} Gauge (psig)	SPRAY TIME (sec)	CLOCK TIME	MVD	** IRT 80 lbs air when tunnel was in operating condition ** IRT 20 lbs air when tunnel was in idle condition
bad	wir280-a	44.2	177	-8.0	13.7	14.3	76.0	0.6381	43.2	67.7	44	67	25	18:02	12	Nozzle #11 off, IRT air on, Verigood 100 paper (vent doors closed), trial run
1	wir0280	46.2	176	-8.0	13.79	14.33	81.5	0.6392	43.4	67.9	44	67	25	18:26	12	Nozzle #11 off, IRT air on, Verigood 100 paper (vent doors closed)
2	wir0281	48.6	175	-8.0	13.81	14.33	80.5	0.6368	43.3	68.0	44	67	25	18:34	12	Nozzle #11 off, IRT air on, Verigood 100 paper (vent doors closed)
3	wir0282	49.2	177	-8.0	13.81	14.33	69.9	0.6368	43.3	68.0	44	67	25	18:42	12	Nozzle #11 off, IRT air on, Verigood 100 paper (IRT spray for 7 min., vent doors closed)
4	wir0283	49.1	176	-8.0	13.81	14.32	77.8	0.6436	43.7	67.9	44	67	25	19:03	12	Nozzle #11 off, IRT air on, Whatman 3MM paper (vent doors closed)
5	wir0284	50.1	176	-8.0	13.8	14.33	67.0	0.6431	43.6	67.8	44	67	25	19:11	12	Nozzle #11 off, IRT air on, Whatman 3MM paper (vent doors closed)
6	wir0285	49.2	178	-8.0	13.79	14.33	73.2	0.1098	4.5	41.0	4	39	3	19:29	92	All Nozzles on, IRT air on, Verigood 100 paper (IRT spray for 3 min, vent doors closed)
7	wir0286	50.9	175	-8.0	13.8	14.33	67.9	0.1027	4.2	40.9	4	39	3	19:37	92	All Nozzles on, IRT air on, Verigood 100 paper (vent doors closed)
8	wir0287	50.4	176	-8.0	13.8	14.33	59.4	0.1051	4.3	40.9	4	39	3	19:45	92	All Nozzles on, IRT air on, Verigood 100 paper (vent doors closed)
9	wir0288	49.6	176	-8.0	13.79	14.32	79.2	0.1073	4.4	41.0	4	39	3	20:02	92	All Nozzles on, IRT air on, Whatman 3MM paper (IRT spray for 7 min, vent doors closed)
10	wir0289	50.5	176	-8.0	13.8	14.32	64.1	0.1073	4.4	41.0	4	39	3	20:10	92	All Nozzles on, IRT air on, Whatman 3MM paper (vent doors closed)
11	wir0290	48.8	176	+8.0	13.79	14.32	76.0	0.1037	4.2	40.5	4	39	3	20:39	92	All Nozzles on, IRT air on, Verigood 100 paper (IRT spray for 8 min, vent doors closed)
12	wir0291	51.2	176	+8.0	13.79	14.32	72.5	0.1073	4.4	41.0	4	39	3	20:46	92	All Nozzles on, IRT air on, Verigood 100 paper (vent doors closed)
13	wir0292	51.2	175	+8.0	13.79	14.36	59.9	0.1051	4.3	40.9	4	39	3	20:53	92	All Nozzles on, IRT air on, Verigood 100 paper (vent doors closed)
14	wir0293	47.7	175	+8.0	13.8	14.32	75.7	0.1078	4.4	40.8	4	39	3	21:10	92	All Nozzles on, IRT air on, Whatman 3MM paper (IRT spray for 8 min, vent doors closed)
15	wir0294	49.3	175	+8.0	13.8	14.32	66.5	0.1073	4.4	41.0	4	39	3	21:16	92	All Nozzles on, IRT air on, Whatman 3MM paper (vent doors closed)
16	wir0295	47.3	176	+8.0	13.79	14.32	74.0	0.6362	43.31	68.08	44	67	25	21:33	12	Nozzle #11 off, IRT air on, Verigood 100 paper (IRT spray for 10 min, vent doors closed)
17	wir0296	50.2	175	+8.0	13.8	14.32	91.5	0.6346	43.6	68.70	44	67	25	21:48	12	Nozzle #11 off, IRT air on, Verigood 100 paper (IRT spray for 10 min, vent doors closed)
18	wir0297	50.1	176	13.8	13.79	14.32	72.5	0.637	43.7	68.6	44	67	25	21:55	12	Nozzle #11 off, IRT air on, Verigood 100 paper (vent doors closed)
19	wir0298	49.9	176	+8.0	13.81	14.32	62.8	0.6332	43.11	68.1	44	67	25	22:01	12	Nozzle #11 off, IRT air on, Verigood 100 paper (vent doors closed)
20	wir0299	50.6	175	+8.0	13.8	14.32	76.3	0.6406	43.5	67.9	44	67	25	22:08	12	Nozzle #11 off, IRT air on, Verigood 100 paper (Colin Bidwell Humidity Technique, see note 4)
21	wir0300	50.0	176	+8.0	13.8	14.32	73.0	0.289	22.26	77.02	22	74	6	22:17	22	Nozzle #11 off, IRT air on, Verigood 100 paper (Colin Bidwell Humidity Technique, see note 4)
22	wir0301	49.9	177	+8.0	13.78	14.32	80.0	0.2927	22.3	76.2	22	74	6	22:25	22	Nozzle #11 off, IRT air on, Verigood 100 paper (Colin Bidwell Humidity Technique, see note 4)
23	wir0302	50.1	176	+8.0	13.8	14.32	68.2	0.298	22.8	76.5	22	74	6	22:32	22	Nozzle #11 off, IRT air on, Verigood 100 paper (Colin Bidwell Humidity Technique, see note 4)
24	wir0303	49.3	177	+8.0	13.8	14.32	80.0	0.29	22.3	76.9	22	74	6	22:44	22	Nozzle #11 off, IRT air on, Verigood 100 paper (Colin Bidwell Humidity Technique, see note 4)
25	wir0304	49.0	176	+8.0	13.79	14.32	74.2	0.294	22.7	77.2	22	74	6	22:52	22	Nozzle #11 off, IRT air on, Verigood 100 paper (Colin Bidwell Humidity Technique, see note 4)

Date : August 20, 1997
AVERAGE P_{BAR} : 13.66 psia
DYE CONCENTRATION : 0.0003 grams/cc
PSYCHROMETER READINGS :
:

Note:

1. Test Model: GLC 305
2. GLC 305 pressure data was taken by IRT's ESP system
3. Angle Of Attack in this record was refer to IRT's AOA setting
4. GLC 305's AOA is same as IRT Turntable's AOA
5. New spray time set to 18 seconds for 12 MVD

		TUNNEL CONDITION						SPRAY CONDITIONS / MASS FLOW								REMARKS
								DISK DISPLAY PRESSURE READING			TANK PRESSURE		TIME			
RUN NO.	Run I.D.	Air TEMP. (°F)	TAS (MPH)	IRT A.O.A. (deg)	P_∞ (psia)	PRESS TOTAL (psia)	Humidity %	P_{AIR} / P_{WATER}	P_{AIR} Display (psig)	P_{WATER} Display (psig)	P_{AIR} Gauge (psig)	P_{WATER} Gauge (psig)	SPRAY TIME (sec)	CLOCK TIME	MVD	** IRT 80 lbs air when tunnel was in operating condition ** IRT 20 lbs air when tunnel was in idle condition
1	wir0305	45.3	175	1.5	13.68	14.21	73.4	0.2981	22.3	74.8	22	74	6	18:25	22	Nozzle #11 off, IRT air on (both vent doors closed)
2	wir0306	43.6	176	1.5	13.68	14.2	70.8	0.29	22.3	76.9	22	74	6	18:35	22	Nozzle #11 off, IRT air on (both vent doors closed)
3	wir0307	44.3	177	1.5	13.67	14.2	68.2	0.2957	22.8	77.1	22	74	6	18:42	22	Nozzle #11 off, IRT air on (both vent doors closed)
4	wir0308	44.1	175	1.5	13.68	14.21	73.6	0.2935	22.6	77.0	22	74	6	18:55	22	Nozzle #11 off, IRT air on (both vent doors closed)
5	wir0309	45.4	177	6.0	13.66	14.2	73.6	0.2943	22.6	76.8	22	74	6	19:06	22	Nozzle #11 off, IRT air on (south vent doors open 11")
6	wir0310	45.3	176	6.0	13.68	14.21	77.1	0.2935	22.6	77.0	22	74	6	19:13	22	Nozzle #11 off, IRT air on (both vent doors closed)
7	wir0311	44.7	176	6.0	13.67	14.21	70.4	0.2965	22.8	76.9	22	74	6	19:20	22	Nozzle #11 off, IRT air on (both vent doors closed)
8	wir0312	44.3	177	6.0	13.68	14.21	68.7	0.2962	22.6	76.3	22	74	6	19:27	22	Nozzle #11 off, IRT air on (both vent doors colsed)
9	wir0313	42.5	176	6.0	13.66	14.2	85.5	0.6397	43.5	68.0	44	67	18	19:37	12	Nozzle #11 off, IRT air on (south vent doors open 11")
10	wir0314	43.9	177	6.0	13.66	14.2	77.1	0.6416	43.5	67.8	44	67	18	19:44	12	Nozzle #11 off, IRT air on (south vent doors open 5")
11	wir0315	44.9	175	6.0	13.66	14.2	74.9	0.6412	43.6	68.0	44	67	18	19:51	12	Nozzle #11 off, IRT air on (south vent doors open 5")
12	wir0316	44.4	176	6.0	13.67	14.2	76.7	0.6444	43.5	67.5	44	67	18	19:57	12	Nozzle #11 off, IRT air on (south vent doors open 6")
13	wir0317	44.0	177	1.5	13.66	14.2	75.3	0.644	43.6	67.7	44	67	18	20:03	12	Nozzle #11 off, IRT air on (south vent doors open 6")
14	wir0318	44.6	177	1.5	13.66	14.2	82.1	0.6426	43.7	68.0	44	67	18	20:15	12	Nozzle #11 off, IRT air on (south vent doors open 11")
15	wir0319	43.1	176	1.5	13.66	14.2	81.6	0.6456	43.9	68	44	67	18	20:27	12	Nozzle #11 off, IRT air on (south vent doors open 15")
16	wir0320	42.1	176	1.5	13.67	14.2	81.0	0.6406	43.5	67.9	44	67	18	20:34	12	Nozzle #11 off, IRT air on (south vent doors open 5")
17	wir0321	43.0	177	1.5	13.67	14.2	82.4	0.1034	4.20	40.6	4	39	3	20:49	92	All Nozzles on, IRT air on, (south vent doors open 5")
18	wir0322	41.7	176	1.5	13.67	14.2	81.5	0.1034	4.2	40.6	4	39	3	20:57	92	All Nozzles on, IRT air on, (south vent doors open 5")
19	wir0323	42.2	175	1.5	13.66	14.2	79.4	0.1039	4.25	40.9	4	39	3	21:03	92	All Nozzles on, IRT air on, (south vent doors open 5")
20	wir0324	41.6	177	1.5	13.67	14.2	79.4	0.1032	4.22	40.9	4	39	3	21:10	92	All Nozzles on, IRT air on, (south vent doors open 5")
21	wir0325	41.8	175	6.0	13.66	14.2	78.8	0.1057	4.3	40.7	4	39	3	21:16	92	All Nozzles on, IRT air on, (south vent doors open 5")
22	wir0326	41.7	177	6.0	13.66	14.2	78.3	0.1051	4.3	40.9	4	39	3	21:23	92	All Nozzles on, IRT air on, (south vent doors open 5")
23	wir0327	41.3	177	6.0	13.67	14.2	79.3	0.1054	4.3	40.8	4	39	3	21:29	92	All Nozzles on, IRT air on, (south vent doors open 5")
24	wir0328	41.9	176	6.0	13.67	14.2	75.1	0.1051	4.3	40.9	4	39	3	21:35	92	All Nozzles on, IRT air on, (south vent doors open 5")
25	wir0329	42.9	175	1.5	13.67	14.2	77.3	0.2904	22.3	76.8	22	74	10	21:50	22	Nozzle #11 off, IRT air on -- test for Colin Bidwell, Part I
26	wir0330	43.4	176	1.5	13.67	14.2	75.6	0.292	22.4	76.7	22	74	10	21:52	22	repeat WIR0329 except All Nozzle on
27	wir0331	41.2	176	1.5	13.67	14.2	75.3	0.2973	22.8	76.7	22	74	10	21:55	22	repeat WIR0330 except Nozzle #11 off
28	wir0332	41.3	175	1.5	13.67	14.2	78.1	0.2915	22.3	76.5	22	74	10	21:58	22	repeat WIR0331

Date : August 21, 1997
AVERAGE P_{BAR} : 13.66 psia
DYE CONCENTRATION : 0.0003 grams/cc
PSYCHROMETER READINGS :
:

Note:
1. Test Model: Collector Mechanism

		TUNNEL CONDITION						SPRAY CONDITIONS / MASS FLOW								
								DISK DISPLAY PRESSURE READING			TANK PRESSURE		TIME			
RUN NO.	Run I.D.	Air TEMP. (°F)	TAS (MPH)	IRT A.O.A. (deg)	P_∞ (psia)	PRESS TOTAL (psia)	Humidity %	$\frac{P_{AIR}}{P_{WATER}}$	P_{AIR} Display (psig)	P_{WATER} Display (psig)	P_{AIR} Gauge (psig)	P_{WATER} Gauge (psig)	SPRAY TIME (sec)	CLOCK TIME	MVD	REMARKS ** IRT 80 lbs air when tunnel was in operating condition ** IRT 20 lbs air when tunnel was in idle condition
1	wir0333	41.7	174	0.0	13.71	14.24	93.1	0.6456	43.9	68.0	44	67	18	17:09	12	Nozzle #11 off, IRT air on (vent doors closed)
2	wir0334	43.1	176	0.0	13.7	14.23	84.3	0.6426	43.7	68.0	44	67	18	17:18	12	Nozzle #11 off, IRT air on (vent doors closed)
3	wir0335	45.3	174	0.0	13.72	14.24	83.2	0.6412	43.6	68.0	44	67	18	17:32	12	Nozzle #11 off, IRT air on (vent doors closed)
4	wir035-a	49.3	174	0.0	13.72	14.23	67.0	0.6354	43.48	68.4	44	67	18	17:41	12	Nozzle #11 off, IRT air on (vent doors closed)
5	wir0336	42.0	175	0.0	13.7	14.23	84.4	0.2956	22.7	76.8	22	74	6	17:54	22	Nozzle #11 off, IRT air on (vent doors closed)
6	wir0337	43.7	174	0.0	13.71	14.23	80.1	0.2984	22.8	76.4	22	74	6	18:00	22	Nozzle #11 off, IRT air on (vent doors closed)
7	wir0338	46.4	174	0.0	13.72	14.23	77.6	0.1032	4.23	41.0	4	39	3	18:42	92	All Nozzles on, IRT air on (vent doors closed)
8	wir0339	48.0	175	0.0	13.7	14.23	74.0	0.1051	4.3	40.9	4	39	3	18:49	92	All Nozzles on, IRT air on (vent doors closed)
9	wir0340	48.0	175	-8.0	13.71	14.23	72.0	0.6406	43.5	67.9	44	67	18	19:06	12	Nozzle #11 off, IRT air on (vent doors closed)
10	wir0341	45.1	177	-8.0	13.69	14.23	70.9	0.6402	43.6	68.1	44	67	18	19:24	12	Nozzle #11 off, IRT air on (south vent door opens)
11	wir0342	41.0	176	-8.0	13.67	14.22	94.4	0.6426	43.7	68.0	44	67	18	19:42	12	Nozzle #11 off, IRT air on (pre-spray and then open south vent door 10")
12	wir0343	42.5	174	-8.0	13.7	14.22	76.8	0.2943	22.6	76.8	22	74	6	19:56	22	Nozzle #11 off, IRT air on (south vent door opens 10")
13	wir0344	43.3	176	-8.0	13.7	14.22	74.1	0.296	22.7	76.7	22	74	6	20:04	22	Nozzle #11 off, IRT air on (south vent door opens 10")
14	wir0345	43.8	175	-8.0	13.7	14.23	65.7	0.1078	4.4	40.8	4	39	3	20:15	92	All Nozzles on, IRT air on (vent doors closed)
15	wir0346	39.8	176	-8.0	13.7	14.23	75.6	0.1054	4.3	40.8	4	39	3	20:24	92	All Nozzles on, IRT air on (vent doors closed)
16	wir0347	42.7	176	+8.0	13.69	14.23	74.6	0.6397	43.5	68.0	44	67	18	20:48	12	Nozzle #11 off, IRT air on (vent doors closed)
17	wir0348	43.2	174	+8.0	13.71	14.24	73.1	0.6397	43.5	68.0	44	67	18	21:01	12	Nozzle #11 off, IRT air on (pre-spray for 45 seconds, vent doors closed)
18	wir0349	43.0	176	+8.0	13.71	14.23	70.9	0.6412	43.60	68.0	44	67	18	21:11	12	Nozzle #11 off, IRT air on (pre-spray for 30 seconds, vent doors closed)
19	wir0350	43.5	176	+8.0	13.71	14.23	63.5	0.2947	22.6	76.7	22	74	6	21:19	22	Nozzle #11 off, IRT air on (vent doors closed)
20	wir0351	42.5	175	+8.0	13.69	14.22	74.3	0.2932	22.4	76.4	22	74	6	21:29	22	Nozzle #11 off, IRT air on (vent doors closed)
21	wir0352	43.2	178	+8.0	13.69	14.23	69.0	0.1117	4.57	40.9	4	39	3	21:40	92	All Nozzles on, IRT air on (vent doors closed, IRT air only 70 lb.)
22	wir0353	43.6	173	+8.0	13.71	14.24	67.0	0.1081	4.4	40.7	4	39	3	21:51	92	All Nozzles on, IRT air on (pre-spray, vent doors closed)
23	wir0354	40.2	175	+8.0	13.7	14.24	81.4	0.6499	43.8	67.4	44	67	5	22:00	12	Nozzle #11 off, IRT air on (vent doors closed)
24	wir0355	41.3	176	+8.0	13.7	14.23	75.0	0.6451	43.8	67.9	44	67	10	22:09	12	Nozzle #11 off, IRT air on (south vent door open 11")
25	wir0356	43.7	176	+8.0	13.7	14.23	77.0	0.6382	43.4	68.0	44	67	15	22:16	12	Nozzle #11 off, IRT air on (south vent door open 11")
26	wir0357	42.1	176	+8.0	13.7	14.23	78.4	0.6425	43.5	67.7	44	67	20	22:23	12	Nozzle #11 off, IRT air on (south vent door open 11")

Date : August 22, 1997
AVERAGE P_{BAR} : 13.73 psia
DYE CONCENTRATION : 0.0003 grams/cc
PSYCHROMETER READINGS :

Note:
1. LWC measurement test (Bob Ide)

		TUNNEL CONDITION						SPRAY CONDITIONS / MASS FLOW								
								DISK DISPLAY PRESSURE READING			TANK PRESSURE		TIME			REMARKS
RUN NO.	Run I.D.	Air TEMP. (°F)	TAS (MPH)	IRT A.O.A. (deg)	P_∞ (PSIA)	PRESS TOTAL (psia)	Humidity %	P_{AIR} / P_{WATER}	P_{AIR} Display (psig)	P_{WATER} Display (psig)	P_{AIR} Gauge (psig)	P_{WATER} Gauge (psig)	SPRAY TIME (sec)	CLOCK TIME	MVD	"total temp recorded instead of static for wir 0358 thru 0376 ** IRT 80 lbs air when tunnel was in operating condition ** IRT 20 lbs air when tunnel was in idle condition
1	wir0358	58.1	177	0.0	13.73	14.27	70	0.6436	43.4	67.4	44	67	120	16:49	12	Nozzle #11 off, (vent doors closed) meas 11 mic, no IRT air
2	wir0359	52.1	177	0.0	13.73	14.26	65	0.6439	43.4	67.4	44	67	120	16:55	12	Nozzle #11 off, (vent doors closed) meas 11 mic, no IRT air
3	wir0360	49.7	177	0.0	13.73	14.27	68.0	0.2928	22.4	76.5	22	74	120	17:01	22	Nozzle #11 off, (vent doors closed) meas 19 mic, no IRT air
4	wir0361	48.6	176	0.0	13.73	14.27	68.0	0.2954	22.6	76.5	22	74	120	17:05	22	Nozzle #11 off, (south vent door open 21`") meas 19 mic, no IRT air
5	wir0362	49.3	175	0.0	13.73	14.27	81.0	0.2911	22.3	76.6	22	74	120	17:13	22	Nozzle #11 off, (south vent door open 21") meas 19 mic, no IRT air
6	wir0363	49.1	175	0.0	13.73	14.27	78.0	0.6493	43.7	67.3	44	67	120	17:19	12	Nozzle #11 off, (south vent door open 21") meas 11 mic, no IRT air
7	wir0364	49.4	177	0.0	13.73	14.27	82.0	0.6416	43.5	67.8	44	67	120	17:56	12	Nozzle #11 off, (south vent door open 21"), no IRT air , LWC = 0.12 g/cm^3
8	wir0365	49.9	174	0.0	13.73	14.27	83.0	0.6436	43.7	67.9	44	67	120	18:03	12	Nozzle #11 off, IRT air on (south vent door open 21"), LWC = 0.07 g/cm^3
9	wir0366	49.3	177	0.0	13.73	14.27	80.0	0.6435	43.5	67.6	44	67	120	18:11	12	Nozzle #11 off, IRT air on (south vent door open 21"), LWC = 0.06 to 0.07 g/cm^3
10	wir0367	47.9	176	0.0	13.73	14.27	87.0	0.2915	22.3	76.5	22	74	120	18:17	22	Nozzle #11 off, IRT air on (south vent door open 21"), LWC = 0.17 to 0.21 g/cm^3
11	wir0368	49.2	176	0.0	13.73	14.27	85.0	0.293	22.5	76.8	22	74	120	18:21	22	Nozzle #11 off, IRT air on (south vent door open 21"), LWC = 0.17 to 0.22 g/cm^3
12	wir0369	49.1	176	0.0	13.74	14.27	85.0	0.1073	4.4	41.0	4	39	120	18:30	92	all Nozzles , IRT air on (south vent door open 21"), LWC = 0.22 to 0.26 g/cm^3
13	wir0370	68.2	175	0.0	13.77	14.29	68.0	0.1069	4.35	40.7	4	39	60	19:34	92	all Nozzles , IRT air on (vent doors closed), LWC = 0.16 to 0.2 g/cm^3
14	wir0371	68.2	175	0.0	13.77	14.29	68.0	0.6459	43.6	67.5	44	67	60	19:38	12	Nozzle #11 off , IRT air on (vent doors closed), LWC = 0.01 g/cm^3
15	wir0372	68.7	175	0.0	13.77	14.29	67.0	0.2904	22.3	76.8	22	74	60	19:43	22	Nozzle #11 off , IRT air on (vent doors closed), LWC = 0.04 to 0.06 g/cm^3
16	wir0373	71.5	176	0.0	13.78	14.29	61.0	0.293	22.5	76.8	22	74	60	20:01	22	Nozzle #11 off , IRT air on (vent doors closed), LWC = 0.03 to 0.04 g/cm^3
17	wir0374	72.1	176	0.0	13.78	14.29	60.0	0.6522	43.7	67.0	44	67	80	20:05	12	Nozzle #11 off , IRT air on (vent doors closed), LWC = 0.0 to 0.005 g/cm^3
18	wir0375	72.9	175	0.0	13.78	14.29	58.0	0.1051	4.30	40.9	4	39	80	20:10	92	all Nozzles , IRT air on (vent doors closed), LWC = 0.14 to 0.18 g/cm^3
19	wir0376	65.0	175	0.0	13.78	14.29	50.0	0.115	4.6	40.0	4	39	80	20:19	92	all Nozzles , IRT air on (vent doors closed), LWC = 0.16 to 0.20 g/cm^3
20	wir0377	41.0	174	0.0	13.75	14.29	55.0	0.0983	4.0	40.7	4	39	80	20:30	92	All Nozzles on, IRT air on (vent doors closed), LWC = 0.16 to 0.2 g/cm^3
21	wir0378	38.7	175	0.0	13.76	14.29	60.0	0.2911	22.3	76.6	22	74	80	20:35	22	Nozzle #11 off, IRT air on (vent doors closed), Total T. = 44.7, LWC = 0.11 to 0.112 g/cm^3
22	wir0379	38.7	176	0.0	13.74	14.29	66.0	0.2906	22.2	76.4	22	74	80	20:50	22	Nozzle #11 off , IRT air on (south vent door open 15"), LWC = 0.12 to 0.16 g/cm^3
23	wir0380	38.2	176	0.0	13.75	14.29	74.0	0.2906	22.2	76.4	22	74	80	20:52	22	Nozzle #11 off , IRT air on (south vent door open 15"), LWC = 0.14 to 0.18 g/cm^3
24	wir0381	40.5	176	0.0	13.75	14.29	80.0	0.2913	22.2	76.2	22	74	80	20:54	22	Nozzle #11 off , IRT air on (south vent door open 15"), LWC = 0.14 to 0.18 g/cm^3
25	wir382															no data recorded
26	wir0383	39.0	176	0.0	13.74	14.29	91.0	0.2865	22	76.8	22	74	80	21:05	22	Nozzle #11 off , IRT air on (south vent door open 15"), LWC = 0.18 to 0.24 g/cm^3
27	wir0384	40.3	177	0.0	13.75	14.29	90.0	0.6389	43	67.3	44	67	80	21:10	12	Nozzle #11 off , IRT air on (south vent door open 15"), LWC = 0.10 to 0.14 g/cm^3
28	wir0385	39.6	177	0.0	13.75	14.29	95.0	0.1098	4.5	41.0	4	39	80	21:16	92	All Nozzles on , IRT air on (south vent door open 15"), LWC = 0.22 to 0.28 g/cm^3

Date : August 25, 1997
AVERAGE P_{BAR} : 13.83 psia
DYE CONCENTRATION : 0.0003 grams/cc
PSYCHROMETER READINGS :
:

Note:

1. Test Model : NACA 64A008
2. Pressure data was taken by IRT's ESP system (#2296 ~~ #2314)
3. Pressure paint tests was conducted; see Tim Benscic's image files and IRT's ESP record #2296 ~~ #2300 and #2310 ~~ #2314
**** the Whatman strip was ripped off and ruined the VG100 strip**

		TUNNEL CONDITION						SPRAY CONDITIONS / MASS FLOW								REMARKS
								DISK DISPLAY PRESSURE READING			TANK PRESSURE		TIME			
RUN NO.	Run I.D.	Air TEMP. (°F)	TAS (MPH)	IRT A.O.A. (deg)	P_∞ (psia)	PRESS TOTAL (psia)	Humidity %	$\frac{P_{AIR}}{P_{WATER}}$	P_{AIR} Display (psig)	P_{WATER} Display (psig)	P_{AIR} Gauge (psig)	P_{WATER} Gauge (psig)	SPRAY TIME (sec)	CLOCK TIME	MVD	** Only static temperature is recorded ** IRT 80 lbs air when tunnel was in operating condition ** IRT 20 lbs air when tunnel was in idle condition
1	wir0386	46.1	176	0.0	13.83	14.37	75.7	0.2988	22.8	76.3	22	74	6	21:04	22	Nozzle #11 off, IRT air off (vent doors closed)
2	wir0387	43.6	176	0.0	13.83	14.37	75.1	0.2902	22.2	76.5	22	74	6	21:24	22	Nozzle #11 off, IRT air on (one Whatman 3MM paper is placed perpendicular on the leading edge) **
3	wir0388	45.4	176	0.0	13.84	14.37	71.5	0.2924	22.4	76.6	22	74	6	21:40	22	Nozzle #11 off, IRT air on
4	wir0389	45.1	174	0.0	13.84	14.37	65.4	0.296	22.7	76.7	22	74	6	22:07	22	Nozzle #11 off, IRT air on (pre-spray for 5 minutes)
5	wir0390	44.1	176	8.0	13.83	14.37	84.4	0.299	22.9	76.6	22	74	6	22:25	22	Nozzle #11 off, IRT air on (pre-spray for 5 minutes), 46x57 cm sheet Whatman 3MM paper used
6	wir0391	45.1	178	8.0	13.82	14.37	71.0	0.2803	21.5	76.7	22	74	6	22:57	22	Nozzle #11 off, IRT air on (pre-spray for 5 minutes), 46x57 cm sheet Whatman 3MM paper used

Date : August 26, 1997
AVERAGE P_{BAR} : 13.80 psia
DYE CONCENTRATION : 0.0003 grams/cc
PSYCHROMETER READINGS :
:

Note:

1. Test Model: NACA 64A008
2. Curved strips were used; Verigood 100 paper only
3. Strip position: AA is 36" above the floor, BB is 44"
4. Gurney Flap was attached on Run #416 and #417

		TUNNEL CONDITION						SPRAY CONDITIONS / MASS FLOW								REMARKS
								DISK DISPLAY PRESSURE READING			TANK PRESSURE		TIME			
RUN NO.	Run I.D.	Air TEMP. (°F)	TAS (MPH)	IRT A.O.A. (deg)	P_∞ (PSIA)	PRESS TOTAL (psia)	Humidity %	P_{AIR} / P_{WATER}	P_{AIR} Display (psig)	P_{WATER} Display (psig)	P_{AIR} Gauge (psig)	P_{WATER} Gauge (psig)	SPRAY TIME (sec)	CLOCK TIME	MVD	** IRT 80 lbs air when tunnel was in operating condition ** IRT 20 lbs air when tunnel was in idle condition
1	wir0392	46	175	0.0	13.8	14.33	82.2	0.6455	43.7	67.7	44	67	18	17:25	12	Nozzle #11 off, IRT air on
2	wir0393	44.8	177	0.0	13.79	14.33	77.2	0.6411	43.4	67.7	44	67	18	17:40	12	Nozzle #11 off, IRT air on (south vent door open 10")
3	wir0394	44.0	176	0.0	13.8	14.34	77.6	0.6435	43.5	67.6	44	67	18	17:50	12	Nozzle #11 off, IRT air on (south vent door open 10")
4	wir0395	44.4	176	0.0	13.8	14.33	76.9	0.6401	43.4	67.8	44	67	18	18:01	12	Nozzle #11 off, IRT air on (south vent door open 10")
5	wir0396	44.9	175	+6.0	13.8	14.33	76.5	0.6411	43.4	67.7	44	67	18	18:13	12	Nozzle #11 off, IRT air on (south vent door open 10")
6	wir0397	44.3	175	+6.0	13.79	14.33	79.6	0.6435	43.5	67.6	44	67	18	13:24	12	Nozzle #11 off, IRT air on (south vent door open 11"), T_{total} = 49.8°F
7	wir0398	46.6	176	+6.0	13.8	14.33	76.2	0.6425	43.5	67.7	44	67	18	18:34	12	Nozzle #11 off, IRT air on (south vent door open 11"), T_{total} = 52.1°F
8	wir0399	43.3	176	+6.0	13.8	14.33	78.5	0.6436	43.7	67.9	44	67	18	18:41	12	Nozzle #11 off, IRT air on (south vent door open 11"), T_{total} = 49.0°F
9	wir0400	43.5	177	+6.0	13.81	14.33	76.0	0.2904	22.3	76.8	22	74	6	18:58	22	Nozzle #11 off, IRT air on (south vent door open 20"), T_{total} = 49.1°F
10	wir0401	43.3	176	+6.0	13.8	14.33	81.5	0.293	22.5	76.8	22	74	6	19:07	22	Nozzle #11 off, IRT air on (south vent door open 20"), T_{total} = 49.1°F
11	wir0402	45.5	176	+6.0	13.79	14.32	76.5	0.295	22.6	76.6	22	74	6	19:15	22	Nozzle #11 off, IRT air on (south vent door open 16"), T_{total} = 50.9°F
12	wir0403	47.2	176	+6.0	13.8	14.33	74.6	0.2907	22.3	76.7	22	74	6	19:22	22	Nozzle #11 off, IRT air on (south vent door open 16"), T_{total} = 52.9°F
13	wir0404	46.6	176	0.0	13.79	14.33	74.7	0.292	22.4	76.7	22	74	6	19:33	22	Nozzle #11 off, IRT air on (south vent door open 16"), T_{total} = 52.5°F
14	wir0405	42.6	176	0.0	13.79	14.33	81.3	0.2928	22.4	76.5	22	74	6	19:42	22	Nozzle #11 off, IRT air on (south vent door open 16"), T_{total} = 49.9°F
15	wir0406	44.6	176	0.0	13.8	14.33	76.2	0.2928	22.4	76.5	22	74	6	19:51	22	Nozzle #11 off, IRT air on (south vent door open 16"), T_{total} = 50.0°F
16	wir0407	46.6	175	0.0	13.79	14.33	73.7	0.2917	22.4	76.8	22	74	6	20:00	22	Nozzle #11 off, IRT air on (south vent door open 21"), T_{total} = 52.0°F
17	wir0408	42.8	176	0.0	13.78	14.33	80.2	0.1103	4.5	40.8	4	39	3	20:15	92	All Nozzles on, IRT air on (south vent door open 23"), T_{total} = 48.4°F
18	wir0409	45.1	177	0.0	13.81	14.33	76.1	0.1054	4.3	40.8	4	39	3	20:23	92	All Nozzles on, IRT air on (south vent door open 23"), T_{total} = 50.7°F
19	wir0410	44.3	177	0.0	13.79	14.33	76.5	0.1051	4.3	40.9	4	39	3	20:37	92	All Nozzles on, IRT air on (vent doors closed), T_{total} = 50.1°F
20	wir0411	39.6	176	0.0	13.79	14.33	75.0	0.1125	4.6	40.9	4	39	3	20:49	92	All Nozzles on, IRT air on (vent doors closed), T_{total} = 45.9°F
21	wir0412	45.1	175	+6.0	13.79	14.33	73.7	0.11	4.5	40.9	4	39	3	21:12	92	All Nozzles on, IRT air on (south vent door open 13"), T_{total} = 50.4°F
22	wir0413	41.7	176	+6.0	13.8	14.34	76.7	0.1029	4.2	40.8	4	39	3	21:23	92	All Nozzles on, IRT air on (vent doors closed), T_{total} = 47.5°F
23	wir0414	46.2	177	+6.0	13.81	14.34	78.5	0.1088	4.45	40.9	4	39	3	21:41	92	All Nozzles on, IRT air on (south vent door open 19"), T_{total} = 51.8°F
24	wir0415	45.8	176	+6.0	13.8	14.33	77.5	0.1076	4.4	40.9	4	39	3	21:54	92	All Nozzles on, IRT air on (vent doors closed), T_{total} = 51.2°F
25	wir0416	44.7	177	+6.0	13.8	14.33	73.5	0.1074	4.4	40.95	4	39	3	22:09	92	All Nozzles on, IRT air on (south vent door open 14"), T_{total} = 49.5°F; ***Gurney Flap attached***
26	wir0417	40.5	176	0.0	13.78	14.33	80.4	0.1054	4.3	40.8	4	39	3	22:17	92	All Nozzles on, IRT air on (south vent door open 14"), T_{total} = 46.0°F; ***Gurney Flap attached***

Date : August 27, 1997
AVERAGE P_{BAR} : 13.80 psia
DYE CONCENTRATION : 0.0003 grams/cc
PSYCHROMETER READINGS :

Note:

1. **Test Model: MS 317**
2. **wir0442 and wir0443 were impingment observation test -- strips were placed near the trailing edge of the airfoil**

		TUNNEL CONDITION						SPRAY CONDITIONS / MASS FLOW								REMARKS
								DISK DISPLAY PRESSURE READING			TANK PRESSURE		TIME			
RUN NO.	Run I.D.	Air TEMP. (°F)	TAS (MPH)	IRT A.O.A. (deg)	P_∞ (PSIA)	PRESS TOTAL (psia)	Humidity %	$\frac{P_{AIR}}{P_{WATER}}$	P_{AIR} Display (psig)	P_{WATER} Display (psig)	P_{AIR} Gauge (psig)	P_{WATER} Gauge (psig)	SPRAY TIME (sec)	CLOCK TIME	MVD	** IRT 80 lbs air when tunnel was in operating condition ** IRT 20 lbs air when tunnel was in idle condition
1	wir0418	43.4	175	0.0	13.73	14.26	82.4	0.6436	43.7	67.9	44	67	18	17:19	12	Nozzle #11 off, IRT air on (south vent door open 11"); T_{total} = 48.3°F
2	wir0419	43.1	175	0.0	13.73	14.26	78.9	0.6436	43.7	67.9	44	67	18	17:27	12	Nozzle #11 off, IRT air on (south vent door open 4"); T_{total} = 49.1°F
3	wir0420	43.8	177	0.0	13.73	14.26	76.4	0.6406	43.5	67.9	44	67	18	17:38	12	Nozzle #11 off, IRT air on (south vent door open 11"); T_{total} = 49.3°F
4	wir0421	43.1	175	0.0	13.74	14.27	76.0	0.6421	43.6	67.9	44	67	18	17:47	12	Nozzle #11 off, IRT air on (vent doors closed); T_{total} = 48.4°F
5	wir0422	43.1	175	8.0	13.73	14.26	74.8	0.6441	43.8	68.0	44	67	18	17:56	12	Nozzle #11 off, IRT air on (south vent door open 4"); T_{total} = 48.4°F
6	wir0423	42.9	176	8.0	13.74	14.26	75.5	0.6421	43.6	67.9	44	67	18	18:03	12	Nozzle #11 off, IRT air on (south vent door open 4"); T_{total} = 48.8°F
7	wir0424	42.4	175	8.0	13.73	14.26	76.0	0.6425	43.5	67.7	44	67	18	18:10	12	Nozzle #11 off, IRT air on (south vent door open 4"); T_{total} = 48.4°F
8	wir0425	42.5	175	8.0	13.74	14.26	75.0	0.6401	43.4	67.8	44	67	18	18:17	12	Nozzle #11 off, IRT air on (south vent door open 4"); T_{total} = 48.1°F
9	wir0426	45.2	175	8.0	13.74	14.26	73.3	0.2963	22.7	76.6	22	74	6	18:31	22	Nozzle #11 off, IRT air on (south vent door open 5"); T_{total} = 50.5°F
10	wir0427	43.6	176	8.0	13.73	14.26	79.0	0.296	22.7	76.7	22	74	6	18:40	22	Nozzle #11 off, IRT air on (south vent door open 6"); T_{total} = 49.1°F
11	wir0428	45.7	176	8.0	13.72	14.26	70.0	0.2917	22.4	76.8	22	74	6	18:56	22	Nozzle #11 off, IRT air on (south vent door open 4"); T_{total} = 51.3°F
12	wir0429	47.5	176	8.0	13.74	14.26	73.0	0.2952	22.7	76.9	22	74	6	19:10	22	Nozzle #11 off, IRT air on (vent doors closed); T_{total} = 53.1°F
13	wir0430	43.2	175	0.0	13.74	14.26	77.0	0.2947	22.6	76.7	22	74	6	19:17	22	Nozzle #11 off, IRT air on (vent doors closed); T_{total} = 48.7°F
14	wir0431	46.4	176	0.0	13.72	14.26	75.2	0.293	22.5	76.8	22	74	6	19:28	22	Nozzle #11 off, IRT air on (south vent door open 14"); T_{total} = 51.8°F
15	wir0432	45.8	176	0.0	13.72	14.26	78.3	0.2943	22.6	76.8	22	74	6	19:34	22	Nozzle #11 off, IRT air on (south vent door open 14"); T_{total} = 51.3°F
16	wir0433	45.7	177	0.0	13.71	14.25	78.5	0.2999	23	76.7	22	74	6	19:41	22	Nozzle #11 off, IRT air on (south vent door open 14"); T_{total} = 51.3°F
17	wir0434	44.2	177	0.0	13.72	14.26	70.5	0.1086	4.4	40.5	4	39	3	20:15	92	All Nozzles on, IRT air on (vent doors closed); T_{total} = 50.0°F
18	wir0435	43.6	176	0.0	13.72	14.26	74.4	0.1086	4.4	40.5	4	39	3	20:28	92	All Nozzles on, IRT air on (south vent door open 12"); T_{total} = 49.5°F
19	wir0436	43.5	176	0.0	13.72	14.26	78.0	0.1086	4.4	40.5	4	39	3	20:36	92	All Nozzles on, IRT air on (south vent door open 12"); T_{total} = 48.9°F
20	wir0437	43.5	176	0.0	13.72	14.26	75.9	0.106	4.3	40.75	4	39	3	20:42	92	All Nozzles on, IRT air on (south vent door open 12"); T_{total} = 49.4°F
21	wir0438	43.6	177	8.0	13.72	14.26	75.2	0.1076	4.4	40.9	4	39	3	20:57	92	All Nozzles on, IRT air on (south vent door open 10"); T_{total} = 49.4°F
22	wir0439	42.4	177	8.0	13.72	14.26	71.7	0.1051	4.3	40.9	4	39	3	21:06	92	All Nozzles on, IRT air on (vent doors closed); T_{total} = 48.3°F
23	wir0440	42.4	177	8.0	13.73	14.26	75.8	0.1076	4.4	40.9	4	39	3	21:18	92	All Nozzles on, IRT air on (vent doors closed); T_{total} = 47.8°F
24	wir0441	42.1	176	8.0	13.73	14.26	75.0	0.1098	4.5	41	4	39	3	21:26	92	All Nozzles on, IRT air on (south vent door open 4"); T_{total} = 48.1°F
25	wir0442	47.6	176	0.0	13.71	14.25	75.7	0.2924	22.4	76.6	22	74	360	19:50	22	Nozzle #11 off, IRT air on (south vent door open 14"); T_{total} = 53.1°F
26	wir0443	43.7	177	0.0	13.73	14.27	67.5	0.295	22.65	76.77	22	74	360	22:06	22	Nozzle #11 off, IRT air on (south vent door open 4"); T_{total} = 49.0°F

Date : September 2, 1997
AVERAGE P_{BAR} : 13.847 psia
DYE CONCENTRATION : 0.0003 grams/cc
PSYCHROMETER READINGS :
:

Note:

1. Test Model: McDonnell Douglas 3 Element Airfoil

2. Pressure data were taken by IRT's ESP system (#2324 ~~ #2328)

		TUNNEL CONDITION						SPRAY CONDITIONS / MASS FLOW								REMARKS
								DISK DISPLAY PRESSURE READING			TANK PRESSURE		TIME			
RUN NO.	Run I.D.	Air TEMP. (°F)	TAS (MPH)	IRT A.O.A. (deg)	P_∞ (PSIA)	PRESS TOTAL (psia)	Humidity %	P_{AIR} / P_{WATER}	P_{AIR} Display (psig)	P_{WATER} Display (psig)	P_{AIR} Gauge (psig)	P_{WATER} Gauge (psig)	SPRAY TIME (sec)	CLOCK TIME	MVD	** IRT 80 lbs air when tunnel was in operating condition ** IRT 20 lbs air when tunnel was in idle condition
1	wir0444	40.2	176	0.0	13.83	14.38	78.0	0.6398	43.7	68.3	44	67	18	19:40	12	All Nozzles on, IRT ari on (vent doors closed), T_{total} = 45.5°F
2	wir0445	40.2	176	0.0	13.82	14.37	77.2	0.6346	42.9	67.6	44	67	18	19:57	12	Nozzle #11 off, IRT ari on (vent doors closed), T_{total} = 44.6°F
3	wir0446	39.3	176	0.0	13.84	14.38	77.2	0.6425	43.5	67.7	44	67	18	20:13	12	Nozzle #11 off, IRT ari on (vent doors closed), T_{total} = 44.6°F
4	wir0447	39.9	176	0.0	13.84	14.38	75.9	0.6475	43.9	67.8	44	67	18	20:33	12	All Nozzles on, IRT ari on (south vent door open 6"), T_{total} = 45.3°F
5	wir0448	43.6	175	0.0	13.84	14.37	70.5	0.6445	43.7	67.8	44	67	18	20:50	12	Nozzle #11 off, IRT ari on (vent doors closed), T_{total} = 49.0°F
6	wir0449	43.0	175	0.0	13.85	14.38	73.0	0.6426	43.7	68.0	44	67	18	21:06	12	Nozzle #11 off, IRT ari on (vent doors closed), T_{total} = 48.5°F
7	wir0450	37.5	175	4.0	13.85	14.39	76.0	0.6451	43.8	67.9	44	67	18	21:25	12	Nozzle #11 off, IRT ari on (vent doors closed), T_{total} = 42.5°F
8	wir0451	38.1	174	4.0	13.85	14.4	77.2	0.644	43.6	67.7	44	67	18	21:36	12	Nozzle #11 off, IRT ari on (vent doors closed), T_{total} = 43.9°F
9	wir0452	39.8	175	4.0	13.86	14.4	76.0	0.6426	43.7	68.0	44	67	18	21:46	12	Nozzle #11 off, IRT ari on (vent doors closed), T_{total} = 45.5°F
10	wir0453	40.4	174	4.0	13.86	14.39	73.0	0.6412	43.6	68.0	44	67	18	21:56	12	Nozzle #11 off, IRT ari on (vent doors closed), T_{total} = 45.9°F
11	wir0454	41.5	174	4.0	13.87	14.4	77.2	0.2945	22.5	76.4	22	74	6	22:10	22	Nozzle #11 off, IRT ari on (south vent door open 14", and then closed before spray), T_{total} = 47.2°F
12	wir0455	39.3	176	4.0	13.85	14.4	76.0	0.2937	22.5	76.6	22	74	6	22:21	22	Nozzle #11 off, IRT ari on (vent doors closed), T_{total} = 44.9°F
13	wir0456	40.3	177	4.0	13.85	14.4	74.7	0.3095	23.8	76.9	22	74	6	22:30	22	Nozzle #11 off, IRT ari on (vent doors closed), T_{total} = 45.8°F
14	wir0457	42.0	175	4.0	13.85	14.4	72.5	0.2937	22.5	76.6	22	74	6	22:41	22	Nozzle #11 off, IRT ari on (south vent door opened 14", and the closed before spray), T_{total} = 47.3°F
15	wir0458	41.2	178	0.0	13.85	14.4	75.5	0.2934	22.5	76.7	22	74	6	22:57	22	Nozzle #11 off, IRT ari on (vent doors closed), T_{total} = 46.7°F

Date : September 3, 1997
AVERAGE P_{BAR} : 13.886 psia
DYE CONCENTRATION : 0.0003 grams/cc
PSYCHROMETER READINGS :
:

Note:

1. Test Model: McDonnell Douglas 3 Element Airfoil
2. Tim10 ~~ Tim15 were flow visualization tests (Tim Bencic)
3. wir0471 ~~ wir0472 were special tests for simulating the frost in wind tunnel
4. Pressure data was taken by IRT's ESP system (#2338 ~~ #2355)

*** The gap between slat and main element was sealed
**** Gaps between slat, main element, and flap were sealed
***** The gap between main element and flap was sealed

		TUNNEL CONDITION						SPRAY CONDITIONS / MASS FLOW								REMARKS
								DISK DISPLAY PRESSURE READING			TANK PRESSURE		TIME			
RUN NO.	Run I.D.	Air TEMP. (°F)	TAS (MPH)	IRT A.O.A. (deg)	P_∞ (PSIA)	PRESS TOTAL (psia)	Humidity %	P_{AIR} / P_{WATER}	P_{AIR} Display (psig)	P_{WATER} Display (psig)	P_{AIR} Gauge (psig)	P_{WATER} Gauge (psig)	SPRAY TIME (sec)	CLOCK TIME	MVD	** IRT 80 lbs air when tunnel was in operating condition ** IRT 20 lbs air when tunnel was in idle condition
1	wir0459	41.7	177	0.0	13.88	14.43	78.5	0.292	22.39	76.7	22	74	6	15:10	22	Nozzle #11 off, IRT air on, (south vent door open 15"), T_{total} = 47.5°F
2	Tim10	39.3	174	-4.0	13.89	14.43	74.8	0.2906	22.23	76.5	22	74	20	15:35	22	Nozzle #11 off, IRT air on, (south vent door open 15"), T_{total} = 45.0°F, image filename: am4.pmi
3	Tim11	38.5	174	0.0	13.89	14.43	78.9	0.2926	22.44	76.7	22	74	20	15:38	22	Nozzle #11 off, IRT air on, (south vent door open 15"), T_{total} = 44.1°F, image filename: a00.pmi
4	Tim12	40.1	176	+4.0	13.9	14.43	76.4	0.2918	22.37	76.7	22	74	20	15:40	22	Nozzle #11 off, IRT air on, (south vent door open 15"), T_{total} = 46.0°F, image filename: ap4.pmi
5	Tim13	38.4	175	+8.0	13.91	14.43	78.6	0.2905	22.3	76.8	22	74	20	15:43	22	Nozzle #11 off, IRT air on, (south vent door open 15"), T_{total} = 43.7°F, image filename: ap8.pmi
6	Tim14	39.0	175	+10.0	13.89	14.43	76.1	0.2924	22.4	76.6	22	74	20	15:46	22	Nozzle #11 off, IRT air on, (vent doors closed), T_{total} = 44.9°F, image filename: ap10.pmi
7	Tim15	40.1	175	+6.0	13.89	14.43	68.9	0.2928	22.43	76.6	22	74	20	15:48	22	Nozzle #11 off, IRT air on, (south vent door open 10"), T_{total} = 45.5°F, image filename: ap6.pmi
8	wir0460	38.7	176	0.0	13.9	14.43	75.8	0.2926	22.5	76.9	22	74	6	16:06	22	Nozzle #11 off, IRT air on, (south vent door open 27"), T_{total} = 44.3°F
9	wir0461	37.7	174	0.0	13.88	14.42	80.5	0.2913	22.4	76.9	22	74	6	16:20	22	Nozzle #11 off, IRT air on, (south vent door open 31"), T_{total} = 43.0°F
10	wir0462	38.1	174	0.0	13.88	14.42	76.5	0.2887	22.2	76.9	22	74	6	16:29	22	Nozzle #11 off, IRT air on, (south vent door open 31"), T_{total} = 44.1°F
11	wir0463	39.2	174	0.0	13.88	14.42	71.5	0.1076	4.4	40.9	4	39	3	16:43	92	All Nozzles on, IRT air on, (south vent door open 29"), T_{total} = 45.0°F
12	wir0464	38.0	175	0.0	13.88	14.42	75.0	0.1078	4.4	40.8	4	39	3	16:55	92	All Nozzles on, IRT air on, (vent doors closed), T_{total} = 43.5°F
13	wir0465	38.7	175	0.0	13.88	14.43	76.0	0.11	4.5	40.9	4	39	3	17:07	92	All Nozzles on, IRT air on, (south vent door open 29", and then closed before spraying), T_{total} = 43.8°F
14	wir0466	40.0	176	0.0	13.88	14.42	71.5	0.11	4.5	40.9	4	39	3	17:31	92	All Nozzles on, IRT air on, (south vent 31" & north vent 30"), T_{total} = 45.8°F
15	wir0467	38.7	176	+4.0	13.87	14.42	76.2	0.1083	4.46	41.2	4	39	3	19:07	92	All Nozzles on, IRT air on, (south vent 31" & north vent 30"), T_{total} = 44.2°F
16	wir0468	38.0	176	+4.0	13.88	14.42	72.0	0.1067	4.36	40.9	4	39	3	19:30	92	All Nozzles on, IRT air on, (south vent 31" & north vent 30"), T_{total} = 43.7°F
17	wir0469	40.7	174	+4.0	13.89	14.42	72.0	0.1074	4.4	41.0	4	39	3	19:46	92	All Nozzles on, IRT air on, (south vent 31" & north vent 30"), T_{total} = 43.6°F, 50% steam @ turning vein
18	wir0470	38.2	174	+4.0	13.88	14.43	70.0	0.1038	4.3	40.9	4	39	3	19:57	92	All Nozzles on, IRT air on, (south vent 31" & north vent 30"), T_{total} = 44.6°F, 50% steam @ turning vein
19	wir0471	38.1	177	0.0	13.88	14.43	81.0	0.3005	22.9	76.2	22	74	360	20:28	22	Nozzle #11 off, IRT air on, (vent doors closed), T_{total} = 43.7°F, 50% steam @ turning vein
20	wir0472	42.9	178	0.0	13.88	14.43	68 ~ 73	0.2849	21.9	76.9	22	74	360	21:08	22	Nozzle #11 off, IRT air off, (vent doors closed), T_{total} = 48.3°F
21	wir0473	37.9	177	0.0	13.88	14.44	72.2	0.295	22.6	76.6	22	74	6	21:36	22	Nozzle #11 off, IRT air on, (vent doors closed), T_{total} = 43.7°F ***
22	wir0474	37.1	175	0.0	13.9	14.44	76.5	0.2939	22.6	76.9	22	74	6	21:54	22	Nozzle #11 off, IRT air on, (vent doors closed), T_{total} = 42.6°F ****
23	wir0475	40.4	175	0.0	13.9	14.44	72.0	0.29	22.3	76.9	22	74	6	22:09	22	Nozzle #11 off, IRT air on, (vent doors closed), T_{total} = 42.6°F *****

Date : September 4, 1997
AVERAGE P_{BAR} : 13.869 psia
DYE CONCENTRATION : 0.0003 grams/cc
PSYCHROMETER READINGS :
:

Note:

1. Test Model: Collector Mechanism (wir0476 ~~ wir0488) and Uniformity Grid (wir0489 ~~ wir0491)
2. wir0492 ~~ wir0500 were for calibration curves
2. Hot Steam was supplied during the spray to increase the humidity. (aft test section)
3. Hot steam (50%) also installed on the turning vein (east end)

** Strips on all the blades. The capital letters (A, B, C, ...) on the strips were pointing outwards

		TUNNEL CONDITION						SPRAY CONDITIONS / MASS FLOW								REMARKS
								DISK DISPLAY PRESSURE READING			TANK PRESSURE		TIME			
RUN NO.	Run I.D.	Air TEMP. (°F)	TAS (MPH)	IRT A.O.A. (deg)	P_∞ (PSIA)	PRESS TOTAL (psia)	Humidity %	P_{AIR} / P_{WATER}	P_{AIR} Display (psig)	P_{WATER} Display (psig)	P_{AIR} Gauge (psig)	P_{WATER} Gauge (psig)	SPRAY TIME (sec)	CLOCK TIME	MVD	** IRT 80 lbs air when tunnel was in operating condition ** IRT 20 lbs air when tunnel was in idle condition
1	wir0476	38.6	175	0.0	13.88	14.42	77.5	0.6426	43.7	68.0	44	67	18	17:19	12	Nozzle #11 off, IRT air on (vent doors closed), T_{total} = 44.5°F
2	wir0477	41.6	176	0.0	13.91	14.42	73.1	0.6416	43.5	67.8	44	67	18	17:38	12	Nozzle #11 off, IRT air on (vent doors closed), T_{total} = 47.3°F
3	wir0478	40.2	177	0.0	13.86	14.41	77.9	0.6392	43.4	67.9	44	67	18	17:46	12	Nozzle #11 off, IRT air on (vent doors closed), T_{total} = 46.2°F
4	wir0479	33.9	174	0.0	13.88	14.42	80.0	0.6435	43.5	67.6	44	67	18	17:58	12	Nozzle #11 off, IRT air on (vent doors closed), T_{total} = 39.6°F ** (high humidity)
5	wir0480	41.2	173	0.0	13.88	14.41	67 ~ 76	0.651	44.2	67.9	44	67	18	18:13	12	Nozzle #11 off, IRT air on (vent doors closed), T_{total} = 47.3°F ** (no hot steam aft test section)
6	wir0481	41.4	176	0.0	13.87	14.41	73.6	0.3103	23.8	76.7	22	74	6	18:29	22	Nozzle #11 off, IRT air on (vent doors closed), T_{total} = 46.9°F
7	wir0482	39.9	174	0.0	13.87	14.41	75.9	0.3304	22.4	67.8	22	74	6	18:35	22	Nozzle #11 off, IRT air on (vent doors closed), T_{total} = 45.7°F
8	wir0483	37.8	176	0.0	13.87	14.41	75 ~ 78	0.2961	22.8	77.0	22	74	6	18:42	22	Nozzle #11 off, IRT air on (vent doors closed), T_{total} = 43.4°F
9	wir0484	41.1	176	0.0	13.87	14.41	71.7	0.2956	22.7	76.8	22	74	6	18:49	22	Nozzle #11 off, IRT air on (vent doors closed), T_{total} = 47.4°F **
10	wir0485	34.9	175	0.0	13.88	14.41	77 ~ 79	0.1155	4.7	40.7	4	39	3	19:00	92	All Nozzles on, IRT air on (vent doors closed), T_{total} = 40.8°F
11	wir0486	38.6	176	0.0	13.86	14.41	77.1	0.1149	4.7	40.9	4	39	3	19:08	92	All Nozzles on, IRT air on (vent doors closed), T_{total} = 44.8°F
12	wir0487	37.9	176	0.0	13.87	14.41	78.5	0.1125	4.6	40.9	4	39	3	19:13	92	All Nozzles on, IRT air on (vent doors closed), T_{total} = 43.1°F
13	wir0488	38.7	174	0.0	13.86	14.41	72.0	0.1146	4.7	41.0	4	39	3	19:21	92	All Nozzles on, IRT air on (vent doors closed), T_{total} = 44.3°F **
14	wir0489	39.4	175	0.0	13.85	14.4	72.5	0.1091	4.45	40.8	4	39	3	20:28	92	All Nozzles on, IRT air on (vent doors closed), T_{total} = 44.1°F
15	wir0490	40.7	175	0.0	13.86	14.41	78.0	0.6413	43.8	68.3	44	67	18	20:43	12	Nozzle #11 off, IRT air on (vent doors closed), T_{total} = 46.7°F
16	wir0491	38.4	175	0.0	13.87	14.41	78.2	0.2922	22.5	77.0	22	74	6	20:56	22	Nozzle #11 off, IRT air on (vent doors closed), T_{total} = 44.4°F
17	wir0492	37.8	175	0.0	13.87	14.41	78.0	0.3382	**23.0**	68.0	44	67	2	21:08	12	Nozzle #11 off, IRT air on (vent doors closed), T_{total} = 43.7°F ; **air pressure not right !!**
18	wir0493	38.6	175	0.0	13.87	14.41	78.0	0.4412	**30.0**	68.0	44	67	20	21:15	12	Nozzle #11 off, IRT air on (vent doors closed), T_{total} = 44.1°F ; **air pressure not right !!**
19	wir0494	40.8	175	0.0	13.86	14.42	69.0	0.647	43.8	67.7	44	67	4	21:22	12	Nozzle #11 off, IRT air on (vent doors closed), T_{total} = 44.6°F
20	wir0495	35.1	176	0.0	13.86	14.41	75.7	0.6441	43.8	68.0	44	67	18	21:29	12	Nozzle #11 off, IRT air on (vent doors closed), T_{total} = 40.4°F
21	wir0496	37.2	175	0.0	13.86	14.41	75.0	0.6422	43.8	68.2	44	67	6	21:35	12	Nozzle #11 off, IRT air on (vent doors closed), T_{total} = 40.2°F
22	wir0497	40.0	175	0.0	13.87	14.41	76.3	0.6422	43.8	68.2	44	67	16	21:40	12	Nozzle #11 off, IRT air on (vent doors closed), T_{total} = 42.6°F
23	wir0498	42.0	175	0.0	13.88	14.41	75.2	0.6402	43.6	68.1	44	67	1	21:46	12	Nozzle #11 off, IRT air on (vent doors closed), T_{total} = 45.4°F
24	wir0499	37.6	175	0.0	13.87	14.41	79.3	0.6402	43.6	68.1	44	67	8	21:51	12	Nozzle #11 off, IRT air on (vent doors closed), T_{total} = 43.4°F
25	wir0500	39.7	175	0.0	13.87	14.41	74.0	0.6402	43.6	68.1	44	67	10	21:57	12	Nozzle #11 off, IRT air on (vent doors closed), T_{total} = 45.1°F
26	wir0501	35.4	175	0.0	13.87	14.41	77.9	0.6393	43.6	68.2	44	67	12	22:02	12	Nozzle #11 off, IRT air on (vent doors closed), T_{total} = 41.0°F
27	wir0502	36.9	176	0.0	13.86	14.41	78.5	0.6435	43.5	67.6	44	67	14	22:06	12	Nozzle #11 off, IRT air on (vent doors closed), T_{total} = 42.2°F
28	wir0503	39.3	176	0.0	13.86	14.41	72.5	0.6454	43.5	67.4	44	67	2	22:13	12	Nozzle #11 off, IRT air on (vent doors closed), T_{total} = 44.8°F

Appendix E: Run Log for 1999 Impingement Tests

Date : February 2, 1999
P_{BAR} :
DYE CONCENTRATION : No dye
PSYCHROMETER READINGS :
:

Note:
Uniformity Tests.

		TUNNEL CONDITION						SPRAY CONDITIONS / MASS FLOW								
								NOZZLE PRESSURE			TANK PRESSURE		TIME			
RUN NO.	Run I.D.	TEMP. Total	TAS (MPH)	P_∞ (PSIA)	PRESS TOTAL	TEMP. Stat	Humidity %	$\frac{P_{AIR}}{P_{WATER}}$	P_{AIR} (PSIG)	P_{WATER} (PSIG)	P_{AIR} (PSIG)	P_{WATER} (PSIG)	SPRAY (SEC)	SPRAY TIME	MVD	REMARKS
1	R001	44.9	176	13.77	14.2	39.4	77.6						60	7:00	12	IRT air 80 psi, vent door close, steam on, nozzle #11 off.
2	R002	47.9	176	13.76	14.2	42.4	76.2	0.2897	3.2	11.2			60	7:05	12	IRT air off, vent door close, steam on, nozzle #11 off.
3	R003	48.5	175	13.82	14.2	43.2	69.5	0.1510	3.2	21.0			60	7:09	12	IRT air 80 psi, vent door close, steam on, all nozzles.
4	R004	47.7	176	13.78	14.3	42	67.7	0.1030	3.2	31.0			60	7:10	12	IRT air off, vent door close, steam on, all nozzles.
5	R005	48.2	176	13.84	14.2	42.7	66.5	0.0813	3.4	41.4	22	77	60	7:22	21	IRT air 80 psi, vent door close, steam on, nozzle #11 off.
6	R006	49.6	176	13.76	14.3	44.1	69.9	0.0615	3.1	51.1	22	77	30	7:25	21	IRT air off, vent door close, steam on, nozzle #11 off.
7	R007	51.6	175	13.78	14.3	46.2	73.9	0.0531	3.2	61.0	22	77	30	7:28	21	IRT air 80 psi, vent door close, steam on, all nozzles.
8	R008	51	176	13.81	14.3	45.7	66.4	0.0449	3.2	70.7	22	77	25	7:32	21	IRT air off, vent door close, steam on, all nozzles.
9	R009	47.7	173	13.84	14.2	42.2	71.4	0.0407	3.3	80.6			25	7:37	92	IRT air 80 psi, vent door close, steam on, nozzle #11 off.
10	R010	49	176	13.77	14.3	43.3	71.8	0.0678	4.9	71.9			25	7:39	92	IRT air off, vent door close, steam on, nozzle #11 off.
11	R011	50.1	174	13.79	14.2	44.7	70.9	0.1012	7.3	72.0			25	7:42	92	IRT air 80 psi, vent door close, steam on, all nozzles.
12	R012	51.1	176	13.75	14.2	45.4	70.4	0.1644	11.8	71.9			25	7:44	92	IRT air off, vent door close, steam on, all nozzles.
13	R013	52.1	175	13.84	14.3	46.6	69.2	0.2250	16.2	71.8	22	77	25	7:48	21	IRT air 80 psi, vent door close, steam on, nozzle #1 only.
14	R014	52.6	176	13.77	14.2	47.2	70.6	0.2944	20.8	70.8	22	77	25	7:50	21	IRT air off, vent door close, steam on, nozzle #1 only.
15	R015	49.5	175	13.83	14.3	44.1	63.8	0.2885	20.7	71.8	22	77	25	7:54	21	IRT air 80 psi, vent door close, steam on, nozzle #2 only.
16	R016	49.8	177	13.82	14.2	44.2	64.4	0.3559	25.5	71.6	22	77	25	7:56	21	IRT air off, vent door close, steam on, nozzle #2 only.
17	R017	50.3	175	13.8	14.3	44.8	63.6	0.4148	29.7	71.6	22	77	25	7:58	21	IRT air 80 psi, vent door close, steam on, nozzle #3 only.
18	R018	50.8	177	13.79	14.3	45.4	62.9	0.4813	34.4	71.6	22	77	25	8:04	21	IRT air off, vent door close, steam on, nozzle #3 only.
bad	R019	50.5	177	13.78	14.2	44.9	63.8				22	77	25	8:15	21	IRT air off, vent door close, steam on, nozzle #4 only.
19	R019	51.4	177	13.82	14.2	45.8	63.9	0.5444	39.0	71.7	22	77	25	8:18	21	IRT air off, vent door close, steam on, nozzle #4 only.
20	R020	49.2	177	13.79	14.3	43.8	61.1	0.6073	43.4	71.5	22	77	25	8:21	21	IRT air off, vent door close, steam on, nozzle #5 only.
21	R021	47	177	13.75	14.3	41.4	64.4	0.6732	48.3	71.7	22	77	25	8:25	21	IRT air off, vent door close, steam on, nozzle #6 only.
22	R022	48.3	177	13.75	14.3	42.7	65.4	0.7350	52.8	71.8	22	77	25	8:28	21	IRT air off, vent door close, steam on, nozzle #7 only.
23	R023	49.6	177	13.8	14.2	44.1	64.9	0.7266	52.1	71.7	22	77	25	8:30	21	IRT air off, vent door close, steam on, nozzle #8 only.
24	R024	50.5	177	13.76	14.2	44.9	64.9	0.6935	44.3	63.9	22	77	25	8:33	21	IRT air off, vent door close, steam on, nozzle #9 only.
25	R025	51.3	177	13.84	14.2	45.6	65.2	0.6764	43.5	64.4	22	77	25	8:35	21	IRT air off, vent door close, steam on, nozzle #10 only.
26	R026	52	177	13.78	14.2	46.4	67	0.3411	24.4	71.5	22	77	25	8:37	21	IRT air off, vent door close, steam on, nozzle #11 only.
27	R027	50.2	177	13.82	14.3	44.7	62.6	0.1985	7.5	37.6	22	77	25	8:39	21	IRT air off, vent door close, steam on, nozzle #12 only.
28	R028	49.7	175	13.83	14.2	44.2	63	0.3405	24.4	71.6	22	77	25	8:44	21	IRT air 80 psi, vent door close, steam on, nozzle #4 only.
29	R029	48.8	176	13.79	14.2	43.4	67.8	0.6753	43.6	64.5	22	77	25	8:46	21	IRT air 80 psi, vent door close, steam on, nozzle #5 only.
30	R030	49.3	176	13.76	14.3	43.7	78.4	0.1980	7.4	37.2	22	77	25	9:06	21	IRT air 80 psi, vent door close, steam on, nozzle #6 only.
31	R031	50.8	175	13.83	14.3	45.3	76.8	0.6753	43.5	64.4	22	77	25	9:08	21	IRT air 80 psi, vent door close, steam on, nozzle #7 only.
32	R032	52.2	176	13.85	14.3	46.6	76.3	0.1977	7.4	37.2	22	77	25	9:11	21	IRT air 80 psi, vent door close, steam on, nozzle #8 only.
33	R033	53.1	175	13.85	14.2	47.6	76.7	0.3364	24.2	71.9	22	77	25	9:15	21	IRT air 80 psi, vent door close, steam on, nozzle #9 only.
34	R034	54.1	176	13.76	14.2	48.6	77.4				22	77	25	9:16	21	IRT air 80 psi, vent door close, steam on, nozzle #10 only.
35	R035	51.5	176	13.81	14.3	46	67.7				22	77	25	9:20	21	IRT air 80 psi, vent door close, steam on, nozzle #11 only.
36	R036	51	176	13.8	14.2	45.5	67.7				22	77	25	9:23	21	IRT air 80 psi, vent door close, steam on, nozzle #12 only.

Date : February 3, 1999
P_{BAR} :
DYE CONCENTRATION : No dye
PSYCHROMETER READINGS :
:

Note:
Uniformity Tests.

		TUNNEL CONDITION						SPRAY CONDITIONS / MASS FLOW								
								NOZZLE PRESSURE			TANK PRESSURE		TIME			
RUN NO.	Run I.D.	TEMP. Total (°F)	TAS (MPH)	P_{∞} (PSIA)	PRESS TOTAL (PSIA)	TEMP. Stat (°F)	Humidity %	$\frac{P_{AIR}}{P_{WATER}}$	P_{AIR} (PSIG)	P_{WATER} (PSIG)	P_{AIR} (PSIG)	P_{WATER} (PSIG)	SPRAY (SEC)	SPRAY TIME (PM)	MVD	REMARKS
37	R037	57.2	177	13.76	14.3	51.6	57.3	0.3352	24.0	71.7	22	77	30	5:55	21	nozzle #4 moved, all nozzles spray, IRT air off, steam on.
38	R038	52.3	176	13.78	14.2	46.8	62.4	0.3351	24.1	72.0	22	77	30	7:13	21	nozzle #7 moved, all nozzles spray, IRT air off, steam on.
39	R039	53.8	176	13.8	14.2	48.2	68.4	0.3395	24.5	72.0	22	77	30	8:28	21	nozzle #2 moved, all nozzles spray, IRT air off, steam on.
40	R040	51	176	13.77	14.3	45.5	59.4	0.6694	43.5	64.9	43	67	30	8:39	11	nozzle #2 moved, all nozzles spray, IRT air off, steam on.
41	R041	53.6	176	13.75	14.3	47.9	65	0.2047	7.7	37.8			30	8:47	92	nozzle #2 moved, all nozzles spray, IRT air off, steam on.
42	R042	51.8	176	13.77	14.3	46.1	62	0.2051	7.7	37.7			30	8:52	92	nozzle #2 moved, IRT air off, steam on, nozzle #11 off.
43	R043	51.8	176	13.81	14.2	46.3	60.1	0.2015	7.7	38.2			30	9:00	92	nozzles #7, 8, 9 and 10 only. IRT air off, steam on.
44	R044	50.9	176	13.76	14.3	45.2	62.1	0.1966	7.5	38.2			30	9:03	92	nozzles #1, 6, 11 and 12 only. IRT air off, steam on.
45	R045	52.2	176	13.84	14.2	46.6	63.1	0.1873	7.2	38.3			30	9:06	92	nozzles #2, 3, 4 and 5 only. IRT air off, steam on.
46	R046	53.4	176	13.78	14.3	47.7	64.2	0.1968	7.6	38.4			30	9:10	92	nozzles #6, 7, 8 and 11 only. IRT air off, steam on.
47	R047	49.9	177	13.82	14.3	44.3	58.3	0.2024	7.6	37.6			30	9:50	92	all nozzles, with nozzle at 6 and 10 switched with each other, IRT air off, steam on.
48	R048	52.4	177	13.84	14.3	46.7	47.1	0.1946	7.4	37.8			30	10:07	92	nozzle #12 off, IRT air off, steam on.
49	R049	53.1	178	13.77	14.2	47.5	44	0.1920	7.3	37.9			30	10:13	92	repeat of run #48

Date : February 4, 1999 (cont.)
P_{BAR} :
DYE CONCENTRATION : (refer to note 2)
PSYCHROMETER READINGS :
:

Note:

1. Uniformity Tests.
2. No dye in sect. 1 (3:45pm - 5:00pm), but water for runs in sect. 2 (7:10pm - 8:50pm) and 3 (9:00pm - 10:30pm) has dye.

		TUNNEL CONDITION						SPRAY CONDITIONS / MASS FLOW								REMARKS
								NOZZLE PRESSURE			TANK PRESSURE		TIME			
RUN NO.	Run I.D.	TEMP. Total (°F)	TAS (MPH)	P_{∞} (PSIA)	PRESS TOTAL (PSIA)	TEMP. Stat (°F)	Humidity %	$\frac{P_{AIR}}{P_{WATER}}$	P_{AIR} (PSIG)	P_{WATER} (PSIG)	P_{AIR} (PSIG)	P_{WATER} (PSIG)	SPRAY (SEC)	SPRAY TIME (PM)	MVD	
50	R050															all nozzles. Nozzles #8 and #12 moved.
51	R051	46.2	176	13.76	14.2	40.6	82.2	0.1958	7.2	36.6			30	3:55	92	IRT air off, steam on. All nozzles. Nozzles #8 and #12 moved. (repeat of run #50)
52	R052	52.4	175	13.75	14.2	46.9	72.8	0.2026	7.7	37.8			30	4:09	92	IRT air off, steam on. All nozzles. Nozzles #6 "modified".
53	R053	55.3	176	13.8	14.2	50	89.5	0.3320	24.0	72.4	22	77	30	4:14	21	same as run #52
54	R054	56.4	175	13.77	14.3	48	85.4	0.3382	24.3	71.9	22	77	30	4:15	21	same as run #53
55	R055	54.1	176	13.85	14.2	48.6	87.4	0.6673	43.3	64.9	43	67	30	4:18	11	same as run #54
56	R056	53	176	13.76	14.2	47.4	61.6	0.6690	43.4	64.9	43	67	30	4:20	11	same as run #55
57	R057	54.5	175	13.77	14.3	48.9	63.8	0.3272	24.0	73.4	22	77	30	4:27	21	nozzle #1 only, IRT air off, steam on.
58	R058	53.7	176	13.81	14.3	48.4	59.8	0.3298	24.1	73.0	22	77	30	4:29	21	nozzle #2 only, IRT air off, steam on.
59	R059	52.5	175	13.78	14.2	47	59.2	0.3305	24.1	72.8	22	77	30	4:31	21	nozzle #3 only, IRT air off, steam on.
60	R060	53.1	176	13.77	14.3	47.7	61.4	0.3298	24.1	73.0	22	77	30	4:33	21	nozzle #4 only, IRT air off, steam on.
61	R061	54.2	175	13.76	14.2	48.7	61.8	0.3291	24.0	73.0	22	77	30	4:35	21	nozzle #5 only, IRT air off, steam on.
62	R062	53.5	176	13.77	14.2	48.1	57.5	0.3294	24.1	73.2	22	77	30	4:37	21	nozzle #6 only, IRT air off, steam on.
63	R063	53.5	175	13.83	14.3	48	58	0.3281	24.1	73.4	22	77	30	4:39	21	nozzle #7 only, IRT air off, steam on.
64	R064	53.4	176	13.79	14.2	48	57.5	0.3289	24.1	73.3	22	77	30	4:41	21	nozzle #8 only, IRT air off, steam on.
65	R065	51.7	175	13.82	14.3	46.2	57	0.3306	24.1	72.9	22	77	30	4:43	21	nozzle #9 only, IRT air off, steam on.
66	R066	52.2	176	13.8	14.2	48.6	58.3	0.3293	24.1	73.1	22	77	30	4:44	21	nozzle #10 only, IRT air off, steam on.
67	R067	53.2	175	13.81	14.3	47.6	60.5	0.3305	24.1	73.0	22	77	30	4:46	21	nozzle #11 only, IRT air off, steam on.
68	R068	54.1	176	13.78	14.3	48.6	61.6	0.3291	24.1	73.2	22	77	30	4:48	21	nozzle #12 only, IRT air off, steam on.
69	R069	52.7	176	13.8	14.2	47.3	58.7	0.3316	24.2	73.1	22	77	30	4:50	21	nozzle #7, 8, 9, 10 and 12, IRT air off, steam on.
70	R070	52.4	176	13.82	14.2	46.8	81.3	0.3303	24.0	72.6	22	77	30	4:52	21	nozzle #1, 5, 6 and 11, IRT air off, steam on.
71	R071	53.2	176	13.79	14.3	47.7	82.9	0.3328	24.2	72.7	22	77	30	4:55	21	nozzle #2, 3, 4 and 5, IRT air off, steam on.
72	R072	54.3	176	13.75	14.3	48.7	63.1	0.3292	24.0	72.9	22	77	30	4:57	21	nozzle #7, 8 and 12, IRT air off, steam on.
73	R073	47.2	175	13.77	14.3	41.8	74	0.6677	43.4	65.0	43	67	18	7:23	11	uniformity with grids: (3,3), (3,4), (3,5), (2,4), and (4,4), steam on, IRT air off.
74	R074	47.6	175	13.8	14.2	42	73.3	0.6673	43.3	64.9	43	67	16	7:31	11	same as above.
75	R075	49.5	175	13.75	14.3	44.1	77.8	0.6670	43.4	65.1	43	67	14	7:38	11	same as above.
76	R076	53.6	175	13.84	14.2	48	76.9	0.6692	43.4	64.9	43	67	12	7:49	11	same as above.
77	R077	53.8	175	13.78	14.2	48.3	75.4	0.6684	43.3	64.8	43	67	10	7:58	11	same as above.
78	R078	54.4	175	13.83	14.3	48.6	73.6	0.3361	24.2	71.9	22	77	6	8:04	21	same as above.
79	R079	54.7	175	13.82	14.2	48.2	71.4	0.3353	24.1	71.9	22	77	5	8:10	21	same as above.
80	R080	48.7	177	13.78	14.2	43	69.3	0.3351	24.2	72.1	22	77	4	8:39	21	same as above.
81	R081	48.7	177	13.8	14.3	43.8	70.4	0.2016	7.6	37.9			3	8:46	92	same as above.
82	R082	50.3	177	13.81	14.3	44.7	70.8	0.2007	7.6	37.7			2.5	8:51	92	same as above.

Date : February 4, 1999
P_{BAR} :
DYE CONCENTRATION : (refer to note 2)
PSYCHROMETER READINGS :
:

Note:

1. Uniformity Tests.
2. No dye in sect. 1 (3:45pm - 5:00pm), but water for runs in sect. 2 (7:10pm - 8:50pm) and 3 (9:00pm - 10:30pm) has dye.

		TUNNEL CONDITION						SPRAY CONDITIONS / MASS FLOW								REMARKS
								NOZZLE PRESSURE			TANK PRESSURE		TIME			
RUN NO.	Run I.D.	TEMP. Total (°F)	TAS (MPH)	P_{∞} (PSIA)	PRESS TOTAL (PSIA)	TEMP. Stat (°F)	Humidity %	$\frac{P_{AIR}}{P_{WATER}}$	P_{AIR} (PSIG)	P_{WATER} (PSIG)	P_{AIR} (PSIG)	P_{WATER} (PSIG)	SPRAY (SEC)	SPRAY TIME (PM)	MVD	
83	R083	48.2	174	13.82	14.3	42.7	64.4	0.3345	24.2	72.3	22	77	30	9:14	21	nozzle #1 off, IRT air off, steam off.
84	R084	47.6	175	13.83	14.2	42.2	66.5	0.3345	24.1	72.2	22	77	30	9:17	21	nozzle #2 off, IRT air off, steam off.
85	R085	48.3	175	13.77	14.2	42.8	69.8	0.3334	24.1	72.3	22	77	30	9:19	21	nozzle #3 off, IRT air off, steam off.
86	R086	49.4	175	13.76	14.3	43.9	71.9	0.3328	24.1	72.5	22	77	30	9:21	21	nozzle #4 off, IRT air off, steam off.
87	R087	50.4	175	13.8	14.2	44.9	73.2	0.3344	24.1	72.2	22	77	30	9:23	21	nozzle #5 off, IRT air off, steam off.
88	R088	50.1	175	13.8	14.2	44.7	69.1	0.3336	24.1	72.2	22	77	30	9:25	21	nozzle #6 off, IRT air off, steam off.
89	R089	48	175	13.79	14.3	43.7	68.3	0.3344	24.1	72.2	22	77	30	9:27	21	nozzle #7 off, IRT air off, steam off.
90	R090	48.1	175	13.75	14.3	43.6	68.4	0.3328	24.1	72.4	22	77	25	9:28	21	nozzle #8 off, IRT air off, steam off.
91	R091	49.5	175	13.77	14.3	44	69.5	0.3343	24.1	72.2	22	77	25	9:29	21	nozzle #9 off, IRT air off, steam off.
92	R092	50.1	175	13.8	14.2	44.6	68.9	0.3346	24.1	72.2	22	77	25	9:31	21	nozzle #10 off, IRT air off, steam off.
93	R093	50.6	175	13.77	14.3	45.1	70.1	0.3347	24.2	72.2	22	77	25	9:33	21	nozzle #11 off, IRT air off, steam off.
94	R094	51.1	174	13.82	14.2	45.7	70.2	0.3352	24.2	72.1	22	77	25	9:35	21	nozzle #12 off, IRT air off, steam off.
95	R095	49.4	176	13.78	14.2	43.9	67	0.3335	24.1	72.3	22	77	25	9:37	21	all nozzles, IRT air 80 psi, steam off.
96	R096	49.1	176	13.82	14.3	43.5	68.4	0.1977	7.5	37.7			25	9:41	92	same as above.
97	R097	48.9	176	13.8	14.2	44.5	67.5	0.6704	43.5	64.8	43	67	25	9:44	11	same as above.
98	R098	50.7	176	13.79	14.2	45.1	66.7	0.6676	43.4	65.0	43	67	25	9:46	11	all nozzles, IRT air 60 psi, steam off.
99	R099	51.2	176	13.78	14.2	45.7	66	0.3361	24.2	72.1	22	77	25	9:48	21	same as above.
100	R100	48	176	13.78	14.2	43.6	66.1	0.1992	7.5	37.6			25	9:51	92	same as above.
101	R101	48.7	175	13.8	14.2	43.2	66	0.1979	7.5	37.8			25	9:53	92	all nozzles, IRT air 40 psi, steam off.
102	R102	49.4	176	13.79	14.3	44	66	0.3358	24.2	72.1	22	77	25	9:55	21	all nozzles, IRT air 40 psi, steam off.
103	R103	50.1	175	13.76	14.2	44.6	67.4	0.6694	43.4	64.8	43	67	25	9:57	11	same as above.
104	R104	50.2	175	13.76	14.3	44.7	66.7	0.6692	43.4	64.9	43	67	25	9:59	11	all nozzles, IRT air 20 psi, steam off.
105	R105	47.8	176	13.78	14.2	42.4	64.8	0.3348	24.2	72.2	22	77	25	10:01	21	same as above.
106	R106	48	176	13.76	14.2	42.5	66.7	0.2019	7.6	37.6			25	10:03	92	same as above.
107	R107	49.2	174	13.8	14.2	44.3	66.6	0.3290	24.0	73.0	22	77	25	10:07	21	nozzle #2 and #10, IRT air off, steam off.
108	R108	50.4	175	13.78	14.3	44.8	66.8	0.3306	24.1	72.8	22	77	25	10:10	21	nozzle #1, #3 and #9, IRT air off, steam off.
109	R109	50.8	175	13.82	14.3	45.4	67	0.3303	24.0	72.7	22	77	25	10:13	21	nozzle #4, #5, #8 and #11, IRT air off, steam off.
110	R110	48.7	176	13.83	14.2	43.3	66	0.3308	24.1	72.7	22	77	25	10:15	21	nozzle #4, #5, #7 and #12, IRT air off, steam off.
111	R111	48.7	175	13.76	14.2	43.2	68.8	0.3297	24.0	72.9	22	77	25	10:17	21	nozzle #2, and #3, IRT air off, steam off.
112	R112	49.3	176	13.76	14.3	43.9	68.8	0.3297	24.0	72.9	22	77	25	10:20	21	nozzle #1, #4 and #10 IRT air off, steam off.
113	R113	50.2	175	13.83	14.3	44.6	68	0.3296	24.0	72.8	22	77	25	10:22	21	nozzle #5, #9 and #11, IRT air off, steam off.
114	R114	50.6	176	13.84	14.3	45.1	67.3	0.3299	24.0	72.9	22	77	25	10:23	21	nozzle #6, #7 and #12, IRT air off, steam off.
115	R115	48.7	176	13.79	14.3	43.3	66.7	0.3307	24.1	72.8	22	77	25	10:26	21	nozzle #2, #5, #7 and #10, IRT air off, steam off.
116	R116	49	176	13.8	14.2	43.5	69.3	0.3307	24.0	72.7	22	77	25	10:28	21	nozzle #3, #4, #6, #9, and #12, IRT air off, steam off.
117	R117	49.5	175	13.76	14.2	44	68	0.3296	24.0	73.0	22	77	25	10:30	21	nozzle #1, #8 and #11, IRT air off, steam off.

Date : February 5, 1999 (cont.)
P_{BAR} :
DYE CONCENTRATION : blue dye 0.0003 gram/cc
PSYCHROMETER READINGS :
:

Note:

1. Uniformity Tests.
2. Test starts at about 2:00pm.

		TUNNEL CONDITION						SPRAY CONDITIONS / MASS FLOW								REMARKS
								NOZZLE PRESSURE			TANK PRESSURE		TIME			
RUN NO.	Run I.D.	TEMP. Total (°F)	TAS (MPH)	P_{∞} (PSIA)	PRESS TOTAL (PSIA)	TEMP. Stat (°F)	Humidity %	$\frac{P_{AIR}}{P_{WATER}}$	P_{AIR} (PSIG)	P_{WATER} (PSIG)	P_{AIR} (PSIG)	P_{WATER} (PSIG)	SPRAY (SEC)	SPRAY TIME (PM)	MVD	
118	R118	49.8	171	13.75	14.3	44.5	73.2				22	77	25	1:43	21	all nozzles, steam on, IRT air off.
119	R119	52.6	170	13.77	14.3	47.4	55.7	0.3270	23.9	73.1	22	77	25	2:39	21	nozzle #1 only, steam on, IRT air off.
120	R120	53.6	171	13.82	14.3	48.6	56.1	0.3281	24.0	73.1	22	77	25	2:40	21	nozzle #2 only, steam on, IRT air off.
121	R121	52.3	171	13.76	14.3	47.4	53.8	0.3288	24.0	73.1	22	77	25	2:42	21	nozzle #3 only, steam on, IRT air off.
122	R122	51.4	171	13.78	14.2	46.2	52.7	0.3282	24.0	73.1	22	77	25	2:44	21	nozzle #7 only, steam on, IRT air off.
123	R123	51.6	171	13.77	14.3	46.6	55	0.3278	24.0	73.1	22	77	25	2:46	21	nozzle #8 only, steam on, IRT air off.
124	R124	52.8	171	13.8	14.2	47.5	55.5	0.3286	24.0	73.1	22	77	25	2:48	21	nozzle #9 only, steam on, IRT air off.
125	R125	53.6	171	13.76	14.3	48.4	55.5	0.3288	24.0	73.0	22	77	25	2:49	21	nozzle #10 only, steam on, IRT air off.
126	R126	52.4	171	13.84	14.2	47.4	53.3	0.3285	24.0	73.0	22	77	25	2:51	21	nozzle #12 only, steam on, IRT air off.
127	R127	51.4	170	13.75	14.2	46.2	53.8	0.3321	24.1	72.6	22	77	25	2:54	21	nozzle #1, 2, 3, 7, 8, 9, 10 and 12. Steam on, IRT air off.
128	R128	55.9	176	13.81	14.3	50.3	76.6	0.3295	24.1	73.1	22	77	25	4:11	21	nozzle #2, 5, 7, 8 and 10 after nozzle #10 was moved. Steam on, IRT air off.
129	R129	50.3	176	13.84	14.2	44.7	77.2	0.3336	24.2	72.5	22	77	25	4:20	21	all nozzles, IRT air off, steam on.
130	R130	52.9	176	13.78	14.3	47.4	72.4	0.3329	24.2	72.6	22	77	25	4:24	21	all nozzles, IRT air 80 psi, steam on.
131	R131	53.7	176	13.79	14.2	48.2	64.6	0.1972	7.4	37.8			25	4:29	92	all nozzles, IRT air off, steam on.
132	R132	53.4	175	13.78	14.2	48	64.2	0.6643	43.4	65.4	43	67	25	4:34	11	all nozzles, IRT air off, steam on.
133	R133	50.2	176	13.78	14.2	44.7	69.6	0.6533	43.4	66.5	43	67	25	4:51	11	same as above.
134	R134	51.5	177	13.8	14.2	46	69.8	0.6629	43.4	65.4	43	67	25	4:55	11	same as above.
135	R135	52.8	176	13.79	14.3	47.2	73.3	0.3335	24.2	72.4	22	77	25	5:55	21	all nozzles, after nozzle #10 moved, steam on, IRT air off.
136	R136	52	176	13.76	14.2	46.4	71	0.3335	24.2	72.5	22	77	25	5:57	21	repeat run #135
137	R137	52.9	176	13.79	14.3	47.3	70.5	0.1976	7.5	37.9			25	6:00	92	same as run #135
138	R138	53.8	177	13.78	14.3	48.3	69.6	0.6650	43.3	65.2	43	67	25	6:03	11	same as run #135
139	R139	50.8	176	13.76	14.2	45.3	71	0.3335	24.1	72.4	22	77	25	7:13	21	nozzle #2 off, IRT air off, steam off.
140	R140	52.3	176	13.82	14.2	46.7	69.1	0.3323	24.1	72.5	22	77	25	7:15	21	nozzle #1 off, IRT air off, steam off.
141	R141	53.4	177	13.77	14.3	47.8	69.2	0.3326	24.1	72.5	22	77	25	7:17	21	nozzle #3 off, IRT air off, steam off.
142	R142	54.4	177	13.82	14.3	48.8	69.4	0.3325	24.2	72.7	22	77	25	7:19	21	nozzle #4 off, IRT air off, steam off.

Date : February 5, 1999
P_{BAR} :
DYE CONCENTRATION : blue dye 0.0003 gram/cc
PSYCHROMETER READINGS :
:

Note:

1. Uniformity Tests.
2. Test starts at about 2:00pm.

		TUNNEL CONDITION						SPRAY CONDITIONS / MASS FLOW								
								NOZZLE PRESSURE			TANK PRESSURE		TIME			
RUN NO.	Run I.D.	TEMP. Total (°F)	TAS (MPH)	P_{∞} (PSIA)	PRESS TOTAL (PSIA)	TEMP. Stat (°F)	Humidity %	$\frac{P_{AIR}}{P_{WATER}}$	P_{AIR} (PSIG)	P_{WATER} (PSIG)	P_{AIR} (PSIG)	P_{WATER} (PSIG)	SPRAY (SEC)	SPRAY TIME (PM)	MVD	REMARKS
143	R143	51.4	177	13.83	14.2	46.1	62.9	0.3329	24.2	72.6	22	77	25	7:21	21	nozzle #5 off, IRT air off, steam off.
144	R144	50.4	176	13.79	14.2	44.9	67.1	0.3326	24.1	72.6	22	77	25	7:25	21	nozzle #6 off, IRT air off, steam on.
145	R145	51.7	177	13.76	14.3	46.2	68.2	0.3324	24.1	72.5	22	77	25	7:27	21	nozzle #7 off, IRT air off, steam on.
146	R146	52.7	176	13.85	14.2	47.1	38.3	0.3326	24.1	72.5	22	77	25	7:28	21	nozzle #8 off, IRT air off, steam on.
147	R147	53.5	177	13.84	14.3	47.9	68.5	0.3330	24.1	72.4	22	77	25	7:32	21	nozzle #9 off, IRT air off, steam on.
148	R148	53.9	176	13.79	14.3	48.5	67.1	0.3320	24.1	72.7	22	77	25	7:34	21	nozzle #10 off, IRT air off, steam on.
149	R149	53.2	176	13.8	14.3	47.6	63.5	0.3323	24.1	72.6	22	77	25	7:36	21	nozzle #11 off, IRT air off, steam on.
150	R150	53.1	177	13.76	14.2	47.5	64.4	0.3330	24.2	72.5	22	77	25	7:38	21	nozzle #12 off, IRT air off, steam on.
151	R151	52.1	176	13.77	14.3	46.6	60.5	0.3270	24.0	73.4	22	77	25	7:43	21	nozzle #2 only, IRT air off, steam on.
152	R152	52.1	177	13.85	14.2	46.5	62.2	0.3269	24.0	73.4	22	77	25	7:45	21	nozzle #4 only, IRT air off, steam on.
153	R153	52.5	177	13.76	14.2	47	62.4	0.3275	24.0	73.3	22	77	25	7:47	21	nozzle #5 only, IRT air off, steam on.
154	R154	53.3	176	13.78	14.3	47.8	62.6	0.3272	24.0	73.2	22	77	25	7:49	21	nozzle #6 only, IRT air off, steam on.
155	R155	53.9	176	13.81	14.3	48.4	63.1	0.3280	24.0	73.2	22	77	25	7:50	21	nozzle #11 only, IRT air off, steam on.
156	R156	52.9	176	13.8	14.2	47.5	72.9	0.3331	24.2	72.5	22	77	25	8:57	21	all nozzles, IRT air off, steam on, nozzle #2 moved.
157	R157	53.8	177	13.75	14.3	48.3	74.5	0.3268	24.0	73.4	22	77	25	8:59	21	nozzle #2 only, IRT air off, steam on.
158	R158	52.2	177	13.78	14.2	46.6	64.4	0.3341	24.2	72.4	22	77	25	9:14	21	all nozzles, IRT air off, steam on (repeat run #156)
159	R159	53	176	13.77	14.2	47.4	65.4	0.3325	24.1	72.6	22	77	25	9:16	21	nozzle #2 off, IRT air off, steam on.
160	R160	52.2	177	13.81	14.3	46.7	61.6	0.3271	24.0	73.4	22	77	25	9:19	21	nozzle #2 only, IRT air off, steam on.
161	R161	52.2	177	13.79	14.2	46.5	62.7	0.3349	24.2	72.4	22	77	25	9:39	21	all nozzles, IRT air off, steam on.
162	R162	52.9	176	13.82	14.3	47.2	63.4	0.3338	24.2	72.4	22	77	25	9:41	21	repeat of run #161
163	R163	52	176	13.8	14.2	46.5	61.4	0.1963	7.5	38.1			25	9:47	92	same as of run #161
164	R164	50.8	176	13.81	14.3	45.2	62.3	0.1979	7.5	38.0			25	9:49	92	same as of run #161
165	R165	51.9	176	13.77	14.3	46.3	75.5	0.6639	43.4	65.4	43	67	25	10:05	11	same as of run #161
166	R166	52.3	175	13.79	14.2	47.1	71.4	0.6626	43.3	65.3	43	67	25	10:12	11	same as of run #161
167	R167	47.3	175	13.77	14.2	41.7	74.5	0.3342	24.1	72.2	22	77	4.5	10:35	21	IRT air off, steam on, all nozzles, uniformity grids.
168	R168	48.7	175	13.83	14.3	43.3	75.6	0.1999	7.6	38.1			2.5	10:53	92	IRT air off, steam on, all nozzles, uniformity grids.

Date : February 8, 1999
P_{BAR} :
DYE CONCENTRATION : 0.0003 grams/cc
PSYCHROMETER READINGS :
:
:

Note:
Uniformity Tests and King's Probe

		TUNNEL CONDITION						SPRAY CONDITIONS / MASS FLOW								
								NOZZLE PRESSURE			TANK PRESSURE		TIME			
RUN NO.	Run I.D.	TEMP. Total (°F)	TAS (MPH)	P_{∞} (PSIA)	PRESS TOTAL (PSIA)	TEMP. Stat (°F)	Humidity %	$\frac{P_{AIR}}{P_{WATER}}$	P_{AIR} (PSIG)	P_{WATER} (PSIG)	P_{AIR} (PSIG)	P_{WATER} (PSIG)	SPRAY (SEC)	SPRAY TIME (PM)	MVD	REMARKS
169	R169	45.1	176	13.82	14.3	39.7	73.1	0.6666	39.5	59.3	43	67	10	7:05	11	IRT air off, steam on, all nozzles, uniformity grid.
170	R170	46	176	13.84	14.2	40.5	75	0.6626	39.3	59.4	43	67	10	7:22	11	IRT air off, steam on, all nozzles, uniformity grid.
171	R171	47.9	176	13.78	14.2	42.3	72.5	0.3045	20.2	66.2	22	77	4.5	7:32	21	IRT air off, steam on, all nozzles, uniformity grid.
172	R172	44.8	175	13.8	14.3	39.3	70.1	0.1150	3.7	32.1			3	7:52	92	IRT air off, steam on, all nozzles, uniformity grid.
173	R173	47.1	176	13.76	14.3	41.6	71.7	0.1184	3.8	32.2			1	8:02	92	IRT air off, steam on, all nozzles, uniformity grid, only one grid point (4,2).
174	R174	46	175	13.79	14.3	40.4	65.7	0.1140	3.7	32.7			1.5	8:26	92	IRT air off, steam on, all nozzles, uniformity grid, only one grid point (4,2).
175	R175	45.8	175	13.82	14.2	40.3	69.2	0.1241	4.0	32.3			2	8:33	92	IRT air off, steam on, all nozzles, uniformity grid, only one grid point (4,2).
176	R176	45.7	175	13.78	14.3	40.2	72.9	0.1189	3.7	31.5			2.5	8:37	92	IRT air off, steam on, all nozzles, uniformity grid, only one grid point (4,2).
177	R177	46	51	13.81	14.2	45.5	74.4	0.1088	3.5	32.0			2.5	8:49	92	Spash test with 1" square located at (3,3), (3,4) and (3,5) of uniformity grid; all nozzles, IRT air off, steam on.
178	R178	44	100	13.8	14.3	42.3	71.2	0.1197	3.9	32.2			2.5	8:56	92	Spash test with 1" square located at (3,3), (3,4) and (3,5) of uniformity grid; all nozzles, IRT air off, steam on.
179	R179	44	153	13.79	14.3	39.8	72.4	0.1223	3.9	31.9			2.5	9:02	92	Spash test with 1" square located at (3,3), (3,4) and (3,5) of uniformity grid; all nozzles, IRT air off, steam on.
180	R180	45.5	200	13.77	14.3	38.3	75.2	0.1263	4.1	32.3			2.5	9:07	92	Spash test with 1" square located at (3,3), (3,4) and (3,5) of uniformity grid; all nozzles, IRT air off, steam on.
181	R181	48.2	200	13.78	14.2	41	70.3	0.1173	3.8	32.1			2.5	9:14	92	Spash test with one collector strip; all nozzles, IRT air off, steam on.
182	R182	44.7	151	13.8	14.2	40.7	72.7	0.1240	3.9	31.8			2.5	9:21	92	Spash test with one collector strip; all nozzles, IRT air off, steam on.
183	R183	43.9	100	13.79	14.3	42.2	71.3	0.1206	3.9	32.2			2.5	9:27	92	Spash test with one collector strip; all nozzles, IRT air off, steam on.
184	R184	43.5	50	13.76	14.3	43.1	70.9	0.1159	3.7	32.0			2.5	9:32	92	Spash test with one collector strip; all nozzles, IRT air off, steam on.
185	R185	45.5	176	13.76	14.3	40.1	69.8	0.6632	39.4	59.4	43	67	60	10:44	11	King's probe; all nozzles, steam on, IRT air off.
186	R186	46.2	176	13.8	14.2	40.8	71.7	0.6630	39.4	59.5	43	67	60	10:47	11	Repeat of run #185
187	R187	45	176	13.77	14.3	39.6	69	0.3049	20.2	66.4	22	77	60	10:50	21	King's probe; all nozzles, steam on, IRT air off.
188	R188	44.7	176	13.8	14.2	39.1	75.8	0.3021	20.2	66.9	22	77	60	10:53	21	Repeat of run #186
189	R189	45.5	176	13.75	14.3	40.1	71.8	0.3055	20.3	66.4	22	77	4.5	10:58	21	King's probe; all nozzles, steam on, IRT air off.
190	R190	46.6	176	13.77	14.2	41.1	72.8	0.1150	3.7	32.0			60	11:00	92	King's probe; all nozzles, steam on, IRT air off.
191	R191	46.8	176	13.82	14.2	41.3	71.3	0.1121	3.6	31.9			2.5	11:02	92	King's probe; all nozzles, steam on, IRT air off.

Date : February 10, 1999 (cont.)
P_{BAR} :
DYE CONCENTRATION : 0.0003 grams/cc
PSYCHROMETER READINGS :
:

		TUNNEL CONDITION						SPRAY CONDITIONS / MASS FLOW								REMARKS
								NOZZLE PRESSURE			TANK PRESSURE		TIME			
RUN NO.	Run I.D.	TEMP. Total (°F)	TAS (MPH)	Humidity % (start)	Humidity % (end)	TEMP. Stat (°F)	Humidity %	$\frac{P_{AIR}}{P_{WATER}}$	P_{AIR} (PSIG)	P_{WATER} (PSIG)	P_{AIR} (PSIG)	P_{WATER} (PSIG)	SPRAY (SEC)	SPRAY TIME (PM)	MVD	
224	R224	53.4	177	59.7		47.9		0.3080	9.9	32.1	6	37	60	5:09	94	all nozzles, IRT air off, steam on, King and laser. King is 36" above tunnel floor.
225	R225	50.7	176	55.9		45.2		0.3159	10.1	32.1	6	37	60	5:12	94	repeat of run #224
226	R226	46.5	175	65.1	65.4	41		0.3067	9.8	31.9	6	37	3	5:15	94	all nozzles, IRT air off, steam on, King and laser. King is 36" above tunnel floor
227	R227	48.9	176	64.9	64.5	43.4		0.3070	9.9	32.3	6	37	3	5:18	94	repeat of run #226
228	R228	46.5	175	61.2	65.5	41.4		0.2700	19.6	72.6	22	77	60	5:21	21	all nozzles, IRT air off, steam on, King and laser. King is 36" above tunnel floor
229	R229	46.3	176	68.3	70.5	40.7		0.2674	19.3	72.3	22	77	60	5:25	21	repeat of run #228
230	R230	47.2	176	65.8	64.7	41.6		0.2667	19.3	72.4	22	77	4.5	5:28	21	all nozzles, IRT air off, steam on, King and laser. King is 36" above tunnel floor
231	R231	47	176	63.8	64	41.4		0.2673	19.3	72.3	22	77	4.5	5:29	21	repeat of run #230
232	R232	47.4	176	63.2	63.1	41.8		0.5084	31.6	62.1	43	67	60	5:33	11	all nozzles, IRT air off, steam on, King and laser. King is 36" above tunnel floor
233	R233	46.6	176	63.4	65.8	41.2		0.5047	31.4	62.2	43	67	60	5:34	11	repeat of run #232
233a	R233a	45.2	176	74.4	75.7	39.6		0.5059	31.5	62.4	43	67	60	5:51	11	repeat of run #233
234	R234	46.7	176	66.5	66.2	41.2		0.5042	31.4	62.3	43	67	10	6:01	11	all nozzles, IRT air off, steam on, King and laser. King is 36" above tunnel floor
235	R235	46.5	176	67.3	67.5	41		0.5044	31.4	62.2	43	67	10	6:03	11	repeat of run #234
236	R236	46.9	176	66.3	65.2	41.5		0.3120	10.0	32.1	6	37	60	6:17	94	all nozzles, IRT air off, steam on, King and laser. King is 42" above tunnel floor
237	R237	46.8	176	67.9	69.3	41.4		0.3111	10.0	32.2	6	37	60	6:21	94	repeat of run #236
238	R238	45	176	70.5	72.5	39.3		0.2704	19.5	72.3	22	77	60	6:30	21	all nozzles, IRT air off, steam on, King and laser. King is 42" above tunnel floor
239	R239	46.8	176	72.6	74.6	41.2		0.2697	19.5	72.4	22	77	60	6:32	21	all nozzles, IRT air off, steam on, King and laser. King is 42" above tunnel floor
240	R240	46.4	176	65.7	71.1	40.5		0.5097	31.9	62.5	43	67	60	6:36	11	all nozzles, IRT air off, steam on, King and laser. King is 42" above tunnel floor
241	R241	43.7	176	75.7	77.1	38.2		0.5104	31.7	62.1	43	67	60	6:40	11	repeat of run #240
241a	R241a	46.1	176	75.6	76.7	40.7		0.5038	31.4	62.3	43	67	60	6:45	11	repeat of run #241
242	R242	46.9	176	71.4	72.8	41.4		0.3130	10.0	32.1	6	37	60	6:55	94	all nozzles, IRT air off, steam on, King and laser. King is 30" above tunnel floor
243	R243	45	176	68	70	39.5		0.3150	10.0	31.9	6	37	60	6:59	94	repeat of run #242
244	R244	47.5	176	72.6	74.7	42		0.2718	19.6	72.2	22	77	60	7:07	21	all nozzles, IRT air off, steam on, King and laser. King is 30" above tunnel floor
245	R245	45.7	176	68.8	72.3	40.1		0.2728	19.7	72.2	22	77	60	7:13	21	repeat of run #244
246	R246	46.9	176	72.1	73.4	41.3		0.5108	31.7	62.1	43	67	60	7:17	11	all nozzles, IRT air off, steam on, King and laser. King is 30" above tunnel floor
247	R247	48	176	73.4	74.7	42.4		0.5080	31.5	62.1	43	67	60	7:19	11	repeat of run #246

Date : February 10, 1999
P_{BAR} :
DYE CONCENTRATION : 0.0003 grams/cc
PSYCHROMETER READINGS :
:

		TUNNEL CONDITION						SPRAY CONDITIONS / MASS FLOW								REMARKS
								NOZZLE PRESSURE			TANK PRESSURE		TIME			
RUN NO.	Run I.D.	TEMP. Total (°F)	TAS (MPH)	Humidity % (start)	Humidity % (end)	TEMP. Stat (°F)	Humidity %	$\frac{P_{AIR}}{P_{WATER}}$	P_{AIR} (PSIG)	P_{WATER} (PSIG)	P_{AIR} (PSIG)	P_{WATER} (PSIG)	SPRAY (SEC)	SPRAY TIME (PM)	MVD	
248	R248	45.5	175	54.9	55.8	40		0.3227	10.2	31.6	6	37	60	8:27	94	Humidity test: RHUM=55, King probe.
249	R249	46.7	175	55.2	56	40.6		0.2663	19.3	72.4	22	77	60	8:31	21	Humidity test: RHUM=55, King probe.
250	R250	46.9	176	55.2	55.7	41.4		0.5059	31.4	62.0	43	67	60	8:34	11	Humidity test: RHUM=55, King probe.
251	R251	46.4	176	58.7	60.6	41.1		0.3110	9.9	31.9	6	37	60	8:41	94	Humidity test: RHUM=60, King probe.
252	R252	46	176	59.5	60.3	40.5		0.2714	19.6	72.2	22	77	60	8:44	21	Humidity test: RHUM=60, King probe.
253	R253	47	176	59.7	60.3	41.4		0.5083	31.5	62.0	43	67	60	8:47	11	Humidity test: RHUM=60, King probe.
254	R254	47.4	174	67.4	68.2	41.9		0.5069	31.4	62.0	43	67	60	9:09	11	Humidity test: RHUM=65, King probe.
255	R255	49.3	174	64.5	66.6	43.9		0.2685	19.4	72.1	22	77	60	9:15	21	Humidity test: RHUM=65, King probe.
256	R256	47.7	175	65.3	65.9	42.3		0.3136	10.0	31.8	6	37	60	9:20	94	Humidity test: RHUM=65, King probe.
257	R257	48	174	75.6	73.9	42.7		0.5060	31.5	62.2	43	67	60	9:29	11	Humidity test: RHUM=75, King probe.
258	R258	47	176	72.9	73.7	41.5		0.2722	19.6	72.1	22	77	60	9:32	21	Humidity test: RHUM=75, King probe.
259	R259	47.1	176	76.7	76	41.6		0.3185	10.2	31.9	6	37	60	9:35	94	Humidity test: RHUM=75, King probe.
260	R260	46.2	177	85.2	85	40.6		0.5132	31.8	61.9	43	67	60	9:44	11	Humidity test: RHUM=85, King probe.
261	R261	47.9	176	86.3	85.8	42.4		0.2703	19.5	72.2	22	77	60	9:47	21	Humidity test: RHUM=85, King probe.
262	R262	46.7	175	85.9	85	41.4		0.3232	10.2	31.6	6	37	60	9:55	94	Humidity test: RHUM=85, King probe.
263	R263	45.4	50	77.5	78.2	45		0.2209	7.0	31.5	6	37	30	10:57	94	Refill water tank. Need to multiply LWC from King probe by 120/43, all nozzles, steam on, IRT air off.
264	R264	44.8	100	75	74.5	43.1		0.2634	8.4	31.8	6	37	30	11:00	94	Need to multiply LWC from King probe by 120/89, all nozzles, steam on, IRT air off.
265	R265	45	150	73.9	75.1	41		0.2978	9.5	31.9	6	37	30	11:02	94	all nozzles, steam on, IRT air off, King probe.
266	R266	48	200	74.1	74.7	40.7		0.3337	10.7	32.1	6	37	30	11:06	94	all nozzles, steam on, IRT air off, King probe.

Date : February 11, 1999 (cont.)
P_{BAR} :
DYE CONCENTRATION : 0.0003 grams/cc
PSYCHROMETER READINGS :
:

		TUNNEL CONDITION						SPRAY CONDITIONS / MASS FLOW								REMARKS
								NOZZLE PRESSURE			TANK PRESSURE		TIME			
RUN NO.	Run I.D.	TEMP. Total (°F)	TAS (MPH)	P_{∞} (PSIA)	PRESS TOTAL (PSIA)	TEMP. Stat (°F)	Humidity %	$\frac{P_{AIR}}{P_{WATER}}$	P_{AIR} (PSIG)	P_{WATER} (PSIG)	P_{AIR} (PSIG)	P_{WATER} (PSIG)	SPRAY (SEC)	SPRAY TIME (PM)	MVD	
267	R267	53.5	175			48	56.6	0.6082	38.1	62.6	43	67	60	3:56	11	IRT air off, steam on, to take laser image, alpha=0 deg, all nozzles. (MS-317)
268	R268	53.5	175			48.2	59.2	0.6015	37.9	63.1	43	67	60	4:04	11	IRT air off, steam on, to take laser image, alpha=10 deg, all nozzles. (MS-317)
269	R269	50.2	176			44.8	64.1	0.2599	18.9	72.9	22	77	60	4:22	21	IRT air off, steam on, to take laser image, alpha=10 deg, all nozzles. (MS-317)
270	R270	47.6	176			42.1	63.4	0.2558	18.6	72.7	22	77	60	4:26	21	IRT air off, steam on, to take laser image, alpha=0 deg, all nozzles. (MS-317)
271	R271	48.8	175			43.4	65.5	0.1460	4.8	32.8	6	37	60	4:30	94	IRT air off, steam on, to take laser image, alpha=0 deg, all nozzles. (MS-317)
272	R272	47	177			41.5	66.8	0.1370	4.4	32.3	6	37	60	4:35	94	IRT air off, steam on, to take laser image, alpha=10 deg, all nozzles. (MS-317)
273	R273	47.1	176			41.7	68	0.2497	18.5	74.0	22	77	60	4:42	21	IRT air off, steam on, to take laser image, alpha=10 deg, nozzle #1 only. (MS-317)
274	R274	48.3	176			42.7	74.1	0.2545	18.7	73.5	22	77	30	4:44	21	IRT air off, steam on, to take laser image, alpha=10 deg, nozzle #2 only. (MS-317)
275	R275	53.4	175			47.7	84	0.2551	18.8	73.8	22	77	30	5:10	21	IRT air off, steam on, to take laser image, alpha=10 deg, nozzle #12 only. (MS-317)
276	R276	55.2	176			49.8	82.9	0.2515	18.6	73.8	22	77	20	5:14	21	IRT air off, steam on, to take laser image, alpha=10 deg, nozzle #11 only. (MS-317)
277	R277	54.5	175			49.1	74.5	0.2517	18.6	73.7	22	77	20	5:16	21	IRT air off, steam on, to take laser image, alpha=10 deg, nozzle #10 only. (MS-317)
278	R278	54.6	175			49.1	73.9	0.2549	18.7	73.5	22	77	20	5:18	21	IRT air off, steam on, to take laser image, alpha=10 deg, nozzle #9 only. (MS-317)
279	R279	55	177			49.5	72.2	0.2528	18.6	73.6	22	77	20	5:21	21	IRT air off, steam on, to take laser image, alpha=10 deg, nozzle #8 only. (MS-317)
280	R280	55	176			49.6	70.8	0.2527	18.6	73.7	22	77	20	5:23	21	IRT air off, steam on, to take laser image, alpha=10 deg, nozzle #7 only. (MS-317)
281	R281	55.2	176			49.7	71.4	0.2539	18.7	73.7	22	77	20	5:24	21	IRT air off, steam on, to take laser image, alpha=10 deg, nozzle #6 only. (MS-317)
282	R282	54.8	176			49.3	68.1	0.2550	18.7	73.2	22	77	20	5:25	21	IRT air off, steam on, to take laser image, alpha=10 deg, nozzle #5 only. (MS-317)
283	R283	53.3	175			48.1	60.1	0.2536	18.5	73.1	22	77	20	5:26	21	IRT air off, steam on, to take laser image, alpha=10 deg, nozzle #4 only. (MS-317)
284	R284	49.8	177			44.2	68.9	0.2552	18.8	73.6	22	77	20	5:29	21	IRT air off, steam on, to take laser image, alpha=10 deg, nozzle #3 only. (MS-317)
285	R285	50.6	176			45.1	71.9	0.2547	18.7	73.6	22	77	20	5:32	21	IRT air off, steam on, to take laser image, alpha=0 deg, nozzle #1 only. (MS-317)
286	R286	50.9	176			45.3	71.1	0.2555	18.8	73.6	22	77	20	5:33	21	IRT air off, steam on, to take laser image, alpha=0 deg, nozzle #2 only. (MS-317)
287	R287	50	175			44.6	66.8	0.2536	18.7	73.6	22	77	20	5:35	21	IRT air off, steam on, to take laser image, alpha=0 deg, nozzle #3 only. (MS-317)
288	R288	45.5	176			39.9	70.1	0.2522	18.6	73.7	22	77	20	5:37	21	IRT air off, steam on, to take laser image, alpha=0 deg, nozzle #4 only. (MS-317)
289	R289	45.4	176			39.9	75.6	0.2546	18.8	73.7	22	77	20	5:39	21	IRT air off, steam on, to take laser image, alpha=0 deg, nozzle #5 only. (MS-317)
290	R290	46	176			40.4	79.1	0.2512	18.5	73.7	22	77	15	5:40	21	IRT air off, steam on, to take laser image, alpha=0 deg, nozzle #6 only. (MS-317)
291	R291	46.9	176			41.4	80.9	0.2524	18.6	73.8	22	77	15	5:41	21	IRT air off, steam on, to take laser image, alpha=0 deg, nozzle #7 only. (MS-317)
292	R292	48.5	176			42.9	82.3	0.2509	18.5	73.7	22	77	15	5:42	21	IRT air off, steam on, to take laser image, alpha=0 deg, nozzle #8 only. (MS-317)
293	R293	49	176			43.5	75.3	0.2482	18.3	73.8	22	77	15	5:44	21	IRT air off, steam on, to take laser image, alpha=0 deg, nozzle #9 only. (MS-317)
294	R294	48.5	177			43	70.2	0.2520	18.6	73.8	22	77	15	5:45	21	IRT air off, steam on, to take laser image, alpha=0 deg, nozzle #10 only. (MS-317)
295	R295	47.8	176			42.4	66.7	0.2565	18.9	73.8	22	77	15	5:46	21	IRT air off, steam on, to take laser image, alpha=0 deg, nozzle #11 only. (MS-317)
296	R296	47.6	176			42.2	67.7	0.2530	18.7	73.7	22	77	15	5:47	21	IRT air off, steam on, to take laser image, alpha=0 deg, nozzle #12 only. (MS-317)

Note: Taking laser image, pressure data were not recorded

Date : February 11, 1999
P_{BAR} :
DYE CONCENTRATION : 0.0003 grams/cc
PSYCHROMETER READINGS :
:
:

		TUNNEL CONDITION						SPRAY CONDITIONS / MASS FLOW								
								NOZZLE PRESSURE			TANK PRESSURE		TIME			
RUN NO.	Run I.D.	TEMP. Total (°F)	TAS (MPH)	P_{∞} (PSIA)	PRESS TOTAL (PSIA)	TEMP. Stat (°F)	Humidity %	$\frac{P_{AIR}}{P_{WATER}}$	P_{AIR} (PSIG)	P_{WATER} (PSIG)	P_{AIR} (PSIG)	P_{WATER} (PSIG)	SPRAY (SEC)	SPRAY TIME (PM)	MVD	REMARKS
297	R297	51.1	175	13.68	14.21	45.6	70.5	0.2569	18.6	72.5	22	77	4.5	6:33	21	IRT air off, steam on, blotter strips A & B, alpha=0 deg, all nozzles. (MS-317)
298	R298	49.8	176	13.68	14.2	44.4	71.3	0.2573	18.7	72.7	22	77	4.5	6:43	21	repeat of run #297.
299	R299	50.8	176	13.67	14.2	45.2	73.8	0.2601	18.9	72.6	22	77	4.5	6:50	21	repeat of run #297.
300	R300	52.3	177	13.67	14.2	46.8	78.4	0.6074	38.1	62.7	43	67	10	6:57	11	IRT air off, steam on, blotter strips A & B, alpha=0 deg, all nozzles. (MS-317)
301	R301	49.3	176	13.68	14.2	44	73.2	0.6026	38.0	63.1	43	67	10	7:04	11	repeat of run #300.
302	R302	49.6	175	13.67	14.2	44.1	73.1	0.6037	38.0	63.0	43	67	10	7:11	11	repeat of run #300.
303	R303	51.4	176	13.67	14.2	45.7	75.3	0.1476	4.8	32.4	6	37	2.5	7:20	94	IRT air off, steam on, blotter strips A & B, alpha=0 deg, all nozzles. (MS-317)
304	R304	52.5	176	13.67	14.13	47	74.2	0.1475	4.8	32.6	6	37	2.5	7:27	94	repeat of run #303.
305	R305	50.5	176	13.67	14.2	45	70.6	0.1479	4.8	32.2	6	37	2.5	7:34	94	repeat of run #303.
306	R306	52	202	13.51	14.2	44.8	69.8	0.1517	4.9	32.6	6	37	2.5	7:43	94	Splashing test, IRT air off, steam on, alpha=0 deg, only strip A, all nozzles. (MS-317)
307	R307	49	151	13.8	14.2	45	71.9	0.1469	4.8	32.4	6	37	2.5	7:49	94	Splashing test, IRT air off, steam on, alpha=0 deg, only strip A, all nozzles. (MS-317)
308	R308	49	100	14.01	14.19	47.2	68.9	0.1375	4.4	32.3	6	37	2.5	7:55	94	Splashing test, IRT air off, steam on, alpha=0 deg, only strip A, all nozzles. (MS-317)
309	R309	48.9	51	14.15	14.19	48.5	70.2	0.1494	4.8	32.4	6	37	2.5	8:02	94	Splashing test, IRT air off, steam on, alpha=0 deg, only strip A, all nozzles. (MS-317)
310	R310	50.3	174	13.67	14.19	45	72.4	0.1392	4.5	32.3	6	37	2.5	8:10	94	IRT air off, steam on, alpha=8 deg, only strip A, all nozzles. (MS-317)
311	R311	52.8	177	13.67	14.2	47.3	75.8	0.2605	18.9	72.5	22	77	4.5	8:27	21	IRT air off, steam on, alpha=8 deg, only strip A, all nozzles. (MS-317)
312	R312	50.3	174	13.67	14.2	44.9	70.6	0.6051	38.1	63.0	43	67	10	8:39	11	IRT air off, steam on, alpha=8 deg, only strip A, all nozzles. (MS-317)
313	R313	50	175	13.67	14.18	44.5	71.1	0.6027	37.9	62.9	43	67	10	9:39	11	Collector mechanism: strips at locations A, C, E, G, and I.alpha=0 deg, all nozzles, IRT air off, steam on.
314	R314	52	176	13.66	14.18	46.5	74	0.6089	38.2	62.7	43	67	10	9:47	11	Collector mechanism: I-strip.alpha=0 deg, all nozzles, IRT air off, steam on.
315	R315	48.5	176	13.66	14.18	43	76.3	0.2568	18.6	72.5	22	77	4.5	9:57	21	Collector mechanism: strips at locations A, C, E, G, and I.alpha=0 deg, all nozzles, IRT air off, steam on.
316	R316	48.5	175	13.66	14.18	43.1	72.8	0.2605	18.9	72.6	22	77	4.5	10:04	21	Collector mechanism: I-strip.alpha=0 deg, all nozzles, IRT air off, steam on.
317	R317	49.7	175	13.66	14.18	44.3	70.6	0.1513	4.9	32.7	6	37	2.5	10:15	94	Collector mechanism: strips at locations A, C, E, G, and I.alpha=0 deg, all nozzles, IRT air off, steam on.
318	R318	51.9	175	13.65	14.18	46.3	74.8	0.1462	4.7	32.4	6	37	2.5	10:23	94	Collector mechanism: I-strip.alpha=0 deg, all nozzles, IRT air off, steam on.
319	R319	51	150	13.79	14.17	47	68.3	0.1398	4.5	32.4	6	37	2.5	10:30	94	Collector mechanism: I-strip.alpha=0 deg, all nozzles, IRT air off, steam on, Splashing test.
320	R320	48.9	100	13.99	14.17	47.1	72.3	0.1446	4.7	32.4	6	37	2.5	10:37	94	Collector mechanism: I-strip. Alpha=0 deg, all nozzles, IRT air off, steam on, Splashing test.
321	R321	48.7	50	14.12	14.17	48.2	73.3	0.1343	4.4	32.6	6	37	2.5	10:43	94	Collector mechanism: I-strip. Alpha=0 deg, all nozzles, IRT air off, steam on, Splashing test.
322	R322	49	174	13.64	14.17	43.6	70.1	0.1372	4.4	32.3	6	37	2	10:50	94	Collector mechanism: I-strip. Alpha=0 deg, all nozzles, IRT air off, steam on, Splashing test.
323	R323	51	175	13.64	14.17	45.4	75.4	0.2586	18.8	72.8	22	77	3.5	10:56	21	Collector mechanism: I-strip. Alpha=0 deg, all nozzles, IRT air off, steam on.

Date : February 12, 1999
P_{BAR} :
DYE CONCENTRATION : 0.0003 grams/cc
PSYCHROMETER READINGS :
:

		TUNNEL CONDITION						SPRAY CONDITIONS / MASS FLOW								
								NOZZLE PRESSURE			TANK PRESSURE		TIME			
RUN NO.	Run I.D.	TEMP. Total (°F)	TAS (MPH)	P_{∞} (PSIA)	PRESS TOTAL (PSIA)	TEMP. Stat (°F)	Humidity %	$\frac{P_{AIR}}{P_{WATER}}$	P_{AIR} (PSIG)	P_{WATER} (PSIG)	P_{AIR} (PSIG)	P_{WATER} (PSIG)	SPRAY (SEC)	SPRAY TIME (PM)	MVD	REMARKS
324	R324		175													NLF-0414f, 48", delta=0 deg, alpha=-5,-4,-3,…,10,11,12 deg, from rdg #6634 to #6651.
325	R325		140													NLF-0414f, 48", delta=0 deg, alpha=12,8,4,0,-4 deg, from rdg #6652 to #6656.
326	R326		85													NLF-0414f, 48", delta=0 deg, alpha=-4,0,4,8,12 deg, from rdg #6657 to #6661.
327	R327		175													NLF-0414f, 48", delta=5 deg, alpha=-4,-2,-1,0,1,2,3,4,5 deg, from rdg #6662 to #6670.
328	R328		175													NLF-0414f, 48", delta=15 deg, alpha=5,4,3,2,1,0,-1,-2,-4 deg, from rdg #6671 to #6679.
329	R329	45.7	175	13.79	14.33	40.2	68.1	0.1481	4.8	32.6	6	37	2.2	9:00	94	all nozzles, IRT air off, steam on, alpha=0 deg, delta=0 deg.
330	R330	46	176	13.79	14.33	40.5	69.9	0.1491	4.8	32.2	6	37	2.2	9:08	94	repeat run #329
331	R331	46.1	175	13.8	14.34	40.7	67.5	0.1330	4.3	32.7	6	37	2.2	9:17	94	repeat run #329
332	R332	43.1	175	13.8	14.33	37.7	71.5	0.1473	4.8	32.4	6	37	2.2	9:24	94	repeat run #329
333	R333	46.6	176	13.79	14.33	40.9	74.2	0.6098	38.3	62.8	43	67	9	9:46	11	all nozzles, IRT air off, steam on, alpha=0 deg, delta=0 deg.
334	R334	44.8	177	13.77	14.32	39.2	73.5	0.6156	38.5	62.5	43	67	9	9:55	11	repeat run #333
335	R335	46.8	176	13.77	14.32	41.3	73.5	0.6159	38.5	62.5	43	67	9	10:07	11	repeat run #333 <NOTE: B-strip tape came off!>
336	R336	46.5	177	13.79	14.33	41	72.3	0.6106	38.2	62.6	43	67	9	10:15	11	repeat run #333
337	R337	44.9	176	13.79	14.33	39.3	71.9	0.6126	38.4	62.6	43	67	9	10:24	11	all nozzles, IRT air off, steam on, alpha=8 deg, delta=0 deg, B-strip only.
338	R338	44.9	177	13.8	14.33	39.4	71.6	0.6078	38.0	62.5	43	67	9	10:30	11	repeat run #337
339	R339	45.4	177	13.8	14.33	40	74.6	0.6097	38.1	62.5	43	67	9	10:36	11	repeat run #337

Date : February 13, 1999
P_{BAR} :
DYE CONCENTRATION : 0.0003 grams/cc
PSYCHROMETER READINGS :
:

		TUNNEL CONDITION						SPRAY CONDITIONS / MASS FLOW								REMARKS
								NOZZLE PRESSURE			TANK PRESSURE		TIME			
RUN NO.	Run I.D.	TEMP. Total (°F)	TAS (MPH)	P_{∞} (PSIA)	PRESS TOTAL (PSIA)	TEMP. Stat (°F)	Humidity %	$\frac{P_{AIR}}{P_{WATER}}$	P_{AIR} (PSIG)	P_{WATER} (PSIG)	P_{AIR} (PSIG)	P_{WATER} (PSIG)	SPRAY (SEC)	SPRAY TIME (PM)	MVD	
340	R340	46.1	175	14.16	14.71	40.6	76.3	0.6132	38.4	62.7	43	67	9	10:15	11	all nozzles, delta=15 deg, alpha=0 deg, steam on, IRT air off, A&B strips.
341	R341	44.7	177	14.16	14.72	39.1	74.4	0.6004	37.8	63.0	43	67	9	10:37	11	repeat run #340
342	R342	47.1	175	14.16	14.72	41.6	70.3	0.6067	38.0	62.7	43	67	9	10:57	11	repeat run #340
343	R343	45.3	175	14.17	14.73	39.8	75.4	0.2610	18.9	72.5	22	77	3.8	11:28	21	all nozzles, delta=15 deg, alpha=0 deg, steam on, IRT air off, A&B strips.
344	R344	48	175	14.18	14.73	43.8	75	0.2584	18.7	72.5	22	77	3.8	12:02	21	repeat run #343
345	R345	43.8	174	14.18	14.73	38.2	75.2	0.2607	18.9	72.3	22	77	3.8	12:21	21	repeat run #343
346	R346	43.9	175	14.19	14.74	38.6	74.4	0.2616	19.0	72.5	22	77	3.8	12:30	21	repeat run #343 (B strip only)
347	R347	46.6	173	14.18	14.73	41.2	73.8	0.1496	4.8	32.2	6	37	2.2	1:00	94	all nozzles, delta=15 deg, alpha=0 deg, steam on, IRT air off, B strip only.
348	R348	47.7	175	14.19	14.74	42.2	72.4	0.1393	4.5	32.3	6	37	2.2	2:00	94	repeat run #347
349	R349	46.3	176	14.18	14.74	40.7	70	0.1426	4.6	32.3	6	37	2.2	2:14	94	repeat run #347
350	R350	46.5	174	14.14	14.76	41.1	73.5	0.2640	19.1	72.4	22	77	3.8	2:37	21	all nozzles, delta=0 deg, alpha=0 deg, IRT air off, steam on, A&B strips.
351	R351	47.6	175	14.2	14.75	42.2	73.1	0.2593	18.8	72.6	22	77	3.8	2:50	21	repeat run #350
352	R352	43.8	176	14.2	14.75	38.4	73.7	0.2613	18.9	72.4	22	77	3.8	3:00	21	repeat run #350
353	R353	44.6	175	14.2	14.75	39.8	73.8	0.2590	18.8	72.6	22	77	3.8	3:10	21	repeat run #350
354	R354	46.4	175	14.2	14.75	40.8	73.9	0.2603	18.9	72.5	22	77	3.8	3:25	21	all nozzles, delta=0 deg, alpha=8 deg, IRT air off, steam on, B strip only.
355	R355	47.3	175	14.2	14.75	41.8	74.8	0.2608	18.9	72.5	22	77	3.8	3:37	21	repeat run #354
356	R356	45	175	14.2	14.76	39.7	73.7	0.2617	19.0	72.4	22	77	3.8	3:46	21	repeat run #354
357	R357	46.2	177	14.2	14.75	40.6	70.3	0.1275	4.2	32.7	6	37	2.2	4:01	94	all nozzles, delta=0 deg, alpha=8 deg, IRT air off, steam on, B strip only.

Date : February 16, 1999
P_{BAR} :
DYE CONCENTRATION : 0.0003 grams/cc
PSYCHROMETER READINGS :
:

		TUNNEL CONDITION						SPRAY CONDITIONS / MASS FLOW								REMARKS
								NOZZLE PRESSURE			TANK PRESSURE		TIME			
RUN NO.	Run I.D.	TEMP. Total (°F)	TAS (MPH)	P_{∞} (PSIA)	PRESS TOTAL (PSIA)	TEMP. Stat (°F)	Humidity %	$\frac{P_{AIR}}{P_{WATER}}$	P_{AIR} (PSIG)	P_{WATER} (PSIG)	P_{AIR} (PSIG)	P_{WATER} (PSIG)	SPRAY (SEC)	SPRAY TIME (PM)	MVD	
358	R358	48.6	176	13.98	14.52	43.1	70.9	0.1303	4.2	32.4	6	37	2.2	6:05	94	all nozzles, IRT air off, steam on, NLF-0414f, alpha=8 deg, delta=0 deg, long B-strip only.
359	R359	45	174	14	14.52	39.6	72.9	0.1309	4.3	32.5	6	37	2.2	7:11	94	repeat run #358
360	R360	47.2	175	13.99	14.53	41.7	72.2	0.1443	4.7	32.6	6	37	2.2	7:23	94	repeat run #358
361	R361	45.6	175	13.99	14.54	40.1	74.4	0.2574	18.7	72.5	22	77	3.8	7:42	21	all nozzles, IRT air off, steam on, NLF-0414f, alpha=8 deg, delta=0 deg, long B-strip only.
362	R362	47.2	174	13.99	14.54	41.7	70.5	0.2559	18.5	72.5	22	77	3.8	7:52	21	repeat run #361
363	R363	47.7	174	13.99	14.54	42.1	70.1	0.6098	38.2	62.6	43	67	9	8:08	11	all nozzles, IRT air off, steam on, NLF-0414f, alpha=8 deg, delta=0 deg, long B-strip only.
364	R364	44.1	174	13.99	14.54	38.7	75.1	0.6139	38.4	62.6	43	67	9	8:14	11	repeat run #363
365	R365	46.5	175	13.99	14.53	40.9	73	0.6044	38.0	62.9	43	67	9	8:25	11	all nozzles, IRT air off, steam on, NLF-0414f, alpha=4 deg, delta=0 deg, short A & B strips.
366	R366	45.7	175	13.99	14.53	40.3	70.8	0.6045	37.8	62.5	43	67	9	8:34	11	repeat run #365
367	R367	46	175	13.99	14.54	40.5	69.9	0.6075	38.0	62.5	43	67	9	8:40	11	repeat run #365
368	R368	46.7	175	13.99	14.53	41.3	69.1	0.2596	18.8	72.3	22	77	3.8	8:55	21	all nozzles, IRT air off, steam on, NLF-0414f, alpha=4 deg, delta=0 deg, long B-strip only.
369	R369	46.5	175	14	14.54	41.4	65.5	0.2593	18.8	72.3	22	77	3.8	9:14	21	repeat run #368
370	R370	44.4	175	13.99	14.54	38.9	74.8	0.2571	18.7	72.6	22	77	3.8	9:27	21	repeat run #368
371	R371	45.5	175	13.99	14.53	40	71.2	0.2572	18.6	72.3	22	77	3.8	9:38	21	repeat run #368
372	R372	46.8	175	13.65	14.19	41.1	71.4	0.1414	4.6	32.3	6	37	2.2	9:52	94	all nozzles, IRT air off, steam on, NLF-0414f, alpha=4 deg, delta=0 deg, long B-strip only.
373	R373	45	175	13.99	14.52	39.5	70.1	0.1450	4.7	32.5	6	37	2.2	10:02	94	repeat run #372
374	R374	45.6	175	13.99	14.53	40.2	71	0.1447	4.7	32.3	6	37	2.2	10:15	94	repeat run #372
375	R375	46.6	149	14.12	14.52	42.7	72.1	0.1478	4.8	32.6	6	37	2.2	10:21	94	all nozzles, IRT air off, steam on, NLF-0414f, splashing test, alpha=0 deg, delta=0 deg, short B-strip.
376	R376	45	100	14.34	14.52	43.3	70.7	0.1482	4.8	32.2	6	37	2.2	10:30	94	all nozzles, IRT air off, steam on, NLF-0414f, splashing test, alpha=0 deg, delta=0 deg, short B-strip.
377	R377	44.8	50	14.47	14.52	44.4	70.1	0.1448	4.7	32.3	6	37	2.2	10:36	94	all nozzles, IRT air off, steam on, NLF-0414f, splashing test, alpha=0 deg, delta=0 deg, short B-strip.
378	R378	44.4	50	14.47	14.51	44.2	73.2	0.1352	4.4	32.6	6	37	2.2	10:41	94	all nozzles, IRT air off, steam on, NLF-0414f, splashing test, alpha=0 deg, delta=0 deg, short B-strip.
379	R379	44.8	100	14.34	14.52	43	72.1	0.1474	4.7	32.2	6	37	2.2	10:46	94	all nozzles, IRT air off, steam on, NLF-0414f, splashing test, alpha=0 deg, delta=0 deg, short B-strip.
380	R380	45.6	151	14.11	14.52	41.6	73.5	0.1465	4.7	32.3	6	37	2.2	10:51	94	all nozzles, IRT air off, steam on, NLF-0414f, splashing test, alpha=0 deg, delta=0 deg, short B-strip.

Date : February 17, 1999
P_{BAR} :
DYE CONCENTRATION : 0.0003 grams/cc
PSYCHROMETER READINGS :
:

		TUNNEL CONDITION						SPRAY CONDITIONS / MASS FLOW								
								NOZZLE PRESSURE			TANK PRESSURE		TIME			
RUN NO.	Run I.D.	TEMP. Total (°F)	TAS (MPH)	P_{∞} (PSIA)	PRESS TOTAL (PSIA)	TEMP. Stat (°F)	Humidity %	$\frac{P_{AIR}}{P_{WATER}}$	P_{AIR} (PSIG)	P_{WATER} (PSIG)	P_{AIR} (PSIG)	P_{WATER} (PSIG)	SPRAY (SEC)	SPRAY TIME (PM)	MVD	REMARKS
381	R381	40														pressure data
382	R382	46.1	176	13.76	14.3	40.5	78.1	0.6055	37.9	62.7	43	67	9	5:08	11	NLF-414, alpha=0 deg, all nozzles, IRT air off, short A and B strips.
383	R383	47.9	176	13.75	14.29	42.2	75	0.6102	38.2	62.6	43	67	9	5:27	11	repeat run #382
384	R384	46	176	13.75	14.3	40.4	72.7	0.6083	38.1	62.6	43	67	9	5:39	11	repeat run #382
385	R385	42.2	175	13.76	14.29	42.1	72.7	0.6104	38.3	62.7	43	67	9	5:52	11	NLF-414, alpha=8 deg, all nozzles, IRT air off, short A and B strips.
386	R386	44.8	176	13.76	14.3	39.2	77.2	0.6063	38.2	63.1	43	67	9	6:19	11	repeat run #385
387	R387	41.7	177	13.75	14.29	47.2	77.8	0.6027	38.1	63.2	43	67	9	6:33	11	repeat run #385
388	R388	46.8	176	13.76	14.29	41.2	73.7	0.2632	19.1	72.5	22	77	3.8	6:46	21	NLF-414, alpha=8 deg, all nozzles, IRT air off, short A and B strips.
389	R389	46.9	177	13.76	14.29	41.3	71.6	0.2554	18.5	72.5	22	77	3.8	6:54	21	repeat run #388
390	R390	49.2	177	13.76	14.29	43.7	73.8	0.2587	18.8	72.5	22	77	3.8	7:07	21	repeat run #388
391	R391	47.4	175	13.76	14.29	41.8	72.9	0.2582	18.7	72.6	22	77	3.8	7:21	21	NLF-414, alpha=0 deg, all nozzles, IRT air off, short A and B strips.
392	R392	47.2	176	13.76	14.3	41.7	71.9	0.2567	18.6	72.4	22	77	3.8	7:35	21	repeat run #391
393	R393	48.2	176	13.77	14.3	42.7	71	0.2565	18.6	72.4	22	77	3.8	7:45	21	repeat run #391
394	R394	45.3	174	13.77	14.3	39.7	71.9	0.1358	4.4	32.5	6	37	2.2	7:57	94	NLF-414, alpha=0 deg, all nozzles, IRT air off, long B-strip and short A-strip.
395	R395	45.4	175	13.76	14.3	39.9	71.9	0.1450	4.7	32.4	6	37	2.2	8:07	94	repeat run #394, short A and B strips.
396	R396	48.1	176	13.76	14.3	42.6	74.2	0.1350	4.4	32.4	6	37	2.2	8:17	94	repeat run #394, short A and B strips.
397	R397	46.2	177	13.76	14.3	40.7	73.9	0.1591	5.2	32.5	6	37	2.2	8:38	94	NLF-414, alpha=8 deg, all nozzles, IRT air off, long B-strip and short A-strip.
398	R398	46.5	176	13.76	14.3	41.1	70.6	0.1554	5.0	32.4	6	37	2.2	8:47	94	repeat run #397, short A and B strips.
399	R399	46.9	176	13.76	14.3	41.3	70.5	0.1326	4.3	32.5	6	37	2.2	8:55	94	repeat run #397, short A and B strips.
400	R400	46.7	176	13.75	14.3	41.2	74				6	37	2.2	10:29	94	collector mechanism, all nozzles, IRT air off, I-strip only.
401	R401	48.3	176	13.76	14.3	42.7	73.2				6	37	2.2	10:36	94	repeat run #400
402	R402	47.6	176	13.77	14.3	42.1	70.3				22	77	3.8	10:45	21	collector mechanism, all nozzles, IRT air off, I-strip only.
403	R403	46.8	176	13.77	14.3	41.3	70.8				22	77	3.8	10:51	21	repeat run #402
404	R404	46.5	176	13.77	14.31	40.9	71				43	67	9	11:00	11	
405	R405	46.5	176	13.76	14.3	41.1	70.8				43	67	9	11:07	11	repeat run#404

Date : February 18, 1999
P_{BAR} :
DYE CONCENTRATION : 0.0003 grams/cc
PSYCHROMETER READINGS :
:

		TUNNEL CONDITION						SPRAY CONDITIONS / MASS FLOW								
								NOZZLE PRESSURE			TANK PRESSURE		TIME			
RUN NO.	Run I.D.	TEMP. Total (°F)	TAS (MPH)	P_∞ (PSIA)	PRESS TOTAL (PSIA)	TEMP. Stat (°F)	Humidity %	$\frac{P_{AIR}}{P_{WATER}}$	P_{AIR} (PSIG)	P_{WATER} (PSIG)	P_{AIR} (PSIG)	P_{WATER} (PSIG)	SPRAY (SEC)	SPRAY TIME (PM)	MVD	REMARKS
406	R406	46.7	177	13.78	14.32	41.2	67.4	0.2590	18.7	72.3	22	77	60	6:15	21	Collector, taking laser image, alpha=0 deg, movie (10 frames, 4 sec/frame).
407	R407	46.4	177	13.78	14.32	40.8	70.5	0.2611	19.0	72.7	22	77	3.8	6:17	21	Collector, taking laser image, alpha=0 deg, static image (exposure 4 sec).
408	R408	46.4	177	13.78	14.32	40.8	67.3	0.2625	19.1	72.7	22	77	3.8	6:20	21	Collector, taking laser image, alpha=0 deg, static image (exposure 5 sec).
409	R409	44.8	176	13.78	14.32	39.2	68.2	0.1556	5.1	32.6	6	37	60	6:26	94	Collector, taking laser image, alpha=0 deg, movie (10 frames, 2.2 sec/frame).
410	R410	45.9	176	13.78	14.32	40.2	70.9	0.1538	5.0	32.6	6	37	2.2	6:29	94	Collector, taking laser image, alpha=0 deg, static image (exposure 3.2 sec).
411	R411	43.9	178	13.78	14.32	38.3	78.6	0.6064	38.2	62.9	43	67	60	6:50	11	Collector, taking laser image, alpha=0 deg, movie (10 frames, 4 sec/frame).
412	R412	47.2	176	13.78	14.33	41.5	74.7	0.6093	38.2	62.7	43	67	9	6:55	11	Collector, taking laser image, alpha=0 deg, static image (exposure 10 sec).
413	R413	46.5	175	13.78	14.33	40.9	75.9	0.6044	38.2	63.2	43	67	60	7:19	11	No collector, taking laser image, movie (10 frames, 4 sec/frame).
414	R414	46.7	175	13.78	14.33	41.2	75	0.6035	38.0	62.9	43	67	9	7:22	11	No collector, taking laser image, static image (exposure 10 sec).
415	R415	46.4	176	13.78	14.33	40.8	72.5	0.1383	4.5	32.7	6	37	60	7:26	94	No collector, taking laser image, movie (10 frames, 2.2 sec/frame).
416	R416	46.4	175	13.78	14.33	40.9	69.8	0.1335	4.3	32.4	6	37	2.2	7:28	94	No collector, taking laser image, static image (exposure 3.2 sec).
417	R417	46.3	176	13.78	14.33	40.8	71.3	0.1267	4.1	32.5	6	37	2.2	7:31	94	No collector, taking laser image, static image (exposure 3.2 sec).
418	R418	46.3	176	13.78	14.33	40.9	71	0.2612	19.0	72.9	22	77	60	7:35	21	No collector, taking laser image, movie (10 frames, 4 sec/frame).
419	R419	45.1	176	13.78	14.33	39.6	74	0.2580	18.7	72.5	22	77	3.8	7:43	21	No collector, taking laser image, static image (exposure 5 sec).
420	R420	47.3	176	13.79	14.33	41.8	76.6	0.6107	38.3	62.7	43	67	9	8:24	11	Collector, I-strip only, alpha=0 deg.
421	R421	46.3	176	13.79	14.33	40.7	72.6	0.6079	38.0	62.4	43	67	9	8:33	11	repeat run #420
422	R422	45.8	176	13.79	14.33	40.3	71.9	0.6047	38.2	63.2	43	67	9	8:40	11	repeat run #420
423	R423	46	176	13.79	14.33	40.5	75.3	0.6057	38.2	63.0	43	67	9	8:46	11	repeat run #420
424	R424	44.7	176	13.79	14.33	39.2	74	0.1263	4.1	32.6	6	37	2.2	8:54	94	Collector, I-strip only, alpha=0 deg.
425	R425	44.4	176	13.79	14.33	38.9	70.6	0.1515	4.9	32.3	6	37	2.2	9:01	94	repeat run #424
426	R426	45	176	13.79	14.33	39.6	73.4	0.1318	4.3	32.8	6	37	2.2	9:07	94	repeat run #424
427	R427	47	176	13.79	14.33	41.4	74.4	0.1305	4.2	32.5	6	37	2.2	9:16	94	repeat run #424
428	R428	43.5	176	13.79	14.33	38	74.6	0.2639	19.2	72.7	22	77	3.8	9:26	21	Collector, I-strip only, alpha=0 deg.
429	R429	43.5	176	13.79	14.33	38	70.7	0.2611	19.0	72.6	22	77	3.8	9:32	21	repeat run #428
430	R430	44.3	176	13.79	14.33	38.8	75.2	0.2617	19.0	72.6	22	77	3.8	9:39	21	repeat run #428
431	R431	46.2	175	13.79	14.33	40.7	72.3	0.2561	18.6	72.7	22	77	3.8	9:55	21	Collector, I-strip only, alpha=8 deg.
432	R432	43.2	176	13.79	14.33	37.6	76	0.2657	19.3	72.5	22	77	3.8	10:03	21	repeat run #431
433	R433	43.3	175	13.79	14.33	37.8	72.5	0.2646	19.2	72.7	22	77	3.8	10:10	21	repeat run #431
434	R434	44.3	176	13.79	14.32	38.9	73.2	0.1382	4.5	32.6	6	37	2.2	10:20	94	Collector, I-strip only, alpha=8 deg.
435	R435	46.6	176	13.78	14.32	41.1	74.7	0.1266	4.1	32.5	6	37	2.2	10:28	94	repeat run #434
436	R436	44.4	176	13.78	14.32	38.9	73.8	0.1311	4.2	32.4	6	37	2.2	10:37	94	repeat run #434
437	R437	43.6	176	13.79	14.32	38.1	69.7	0.6105	38.3	62.7	43	67	9	10:46	11	Collector, I-strip only, alpha=8 deg.
438	R438	44.5	176	13.79	14.32	38.9	76.8	0.6094	38.3	62.9	43	67	9	10:54	11	repeat run #437
439	R439	46.4	175	13.79	14.32	40.9	73.5	0.6082	38.2	62.8	43	67	9	11:02	11	repeat run #437

Date : February 19, 1999
P_{BAR} :
DYE CONCENTRATION : 0.0003 grams/cc
PSYCHROMETER READINGS :
:

		TUNNEL CONDITION						SPRAY CONDITIONS / MASS FLOW								REMARKS
								NOZZLE PRESSURE			TANK PRESSURE		TIME			
RUN NO.	Run I.D.	TEMP. Total (°F)	TAS (MPH)	P_{∞} (PSIA)	PRESS TOTAL (PSIA)	TEMP. Stat (°F)	Humidity %	$\frac{P_{AIR}}{P_{WATER}}$	P_{AIR} (PSIG)	P_{WATER} (PSIG)	P_{AIR} (PSIG)	P_{WATER} (PSIG)	SPRAY (SEC)	SPRAY TIME (PM)	MVD	
440	R440	49.1	177	13.79	14.33	43.5	68.6	0.2606	18.8	72.0	22	77	3.8	5:33	21	IRT alpha=7.5 deg, true alpha=6 deg, L45FS, delta=3 deg, steam on, IRT air off, V-strips (A, B, C and D)
441	R441	45.2	176	13.76	14.33	39.6	70.2	0.2615	18.9	72.4	22	77	3.8	5:59	21	repeat run #440
442	R442	47	176	13.79	14.33	41.4	77.1	0.2657	19.2	72.2	22	77	3.8	6:20	21	repeat run #440
443	R443	45.3	176	13.79	14.33	39.8	72.8	0.2595	18.8	72.4	22	77	3.8	6:46	21	IRT alpha=2.5 deg, true alpha=1 deg, L45FS, delta=0 deg, steam on, IRT air off, V-strips (A and B)
444	R444	46.6	176	13.81	14.35	41	73.3	0.2634	19.1	72.5	22	77	3.8	6:56	21	repeat run #443
445	R445	46.6	176	13.81	14.34	40.9	73	0.2603	18.9	72.6	22	77	3.8	7:05	21	repeat run #443
446	R446	46.5	176	13.8	14.33	41	71.3	0.6084	38.0	62.4	43	67	9	7:20	11	IRT alpha=2.5 deg, true alpha=1 deg, L45FS, delta=0 deg, steam on, IRT air off, V-strips (A and B)
447	R447	46.7	176	13.8	14.34	41.1	71.6	0.6062	38.2	63.1	43	67	9	7:34	11	repeat run #446
448	R448	45.3	176	13.8	14.34	39.8	72.2	0.6060	38.0	62.8	43	67	9	7:44	11	repeat run #446
449	R449	45.9	176	13.8	14.34	40.5	72.8	0.1594	5.1	32.3	6	37	2.2	7:54	94	IRT alpha=2.5 deg, true alpha=1 deg, L45FS, delta=0 deg, steam on, IRT air off, V-strips (A and B)
450	R450	45	176	13.8	14.34	39.5	73.1	0.1287	4.2	32.5	6	37	2.2	8:06	94	repeat run #449
451	R451	46.2	176	13.8	14.34	40.6	71	0.1517	4.9	32.3	6	37	2.2	8:19	94	repeat run #449
452	R452	45	175	13.8	14.34	40.9	72.8	0.2593	18.8	72.5	22	77	3.8	8:41	21	IRT alpha=7.5 deg, true alpha=6 deg, L45FS, delta=0 deg, steam on, IRT air off, V-strips (A and B)
453	R453	45.1	174	13.8	14.34	39.7	71.7	0.2568	18.7	72.7	22	77	3.8	8:57	21	repeat run #452
454	R454	47.2	175	13.79	14.34	41.5	72.8	0.2619	19.0	72.5	22	77	3.8	9:10	21	repeat run #452
455	R455	45.2	176	13.8	14.34	39.9	73	0.2628	19.0	72.4	22	77	3.8	9:40	21	IRT alpha=3.5 deg, true alpha=2 deg, L45FS, delta=3 deg, steam on, IRT air off, V-strips (A and D)
456	R456	45	176	13.8	14.34	39.4	74.2	0.2591	18.8	72.7	22	77	3.8	9:55	21	repeat run #455
457	R457	44.9	175	13.8	14.34	39.4	72.8	0.2648	19.2	72.6	22	77	3.8	10:04	21	repeat run #455

Date : February 20, 1999
P_{BAR} :
DYE CONCENTRATION : 0.0003 grams/cc
PSYCHROMETER READINGS :
:

		TUNNEL CONDITION						SPRAY CONDITIONS / MASS FLOW								
								NOZZLE PRESSURE			TANK PRESSURE		TIME			
RUN NO.	Run I.D.	TEMP. Total (°F)	TAS (MPH)	P_{∞} (PSIA)	PRESS TOTAL (PSIA)	TEMP. Stat (°F)	Humidity %	$\frac{P_{AIR}}{P_{WATER}}$	P_{AIR} (PSIG)	P_{WATER} (PSIG)	P_{AIR} (PSIG)	P_{WATER} (PSIG)	SPRAY (SEC)	SPRAY TIME (PM)	MVD	REMARKS
458	R458	51.5	176	13.85	14.8	46	70.2	0.1462	4.8	32.5	6	37	2.2	10:01	94	Collector mechanism, alpha=0 deg, strips G, I and C.
459	R459	49.5	175	13.84	14.38	44	71.5	0.1440	4.6	32.2	6	37	2.2	10:10	94	repeat run #458
460	R460	47.8	175	13.84	14.38	42.2	71.3	0.1478	4.8	32.3	6	37	2.2	10:27	94	repeat run #458
461	R461	48.4	175	13.84	14.37	43	71.7	0.6162	38.4	62.4	43	67	9	10:46	11	Collector mechanism, alpha=0 deg, strips G, I and C. (A redo run, previous set of strips were wetted)
462	R462	47.8	176	13.84	14.38	42.2	71	0.6028	37.9	62.8	43	67	9	10:52	11	repeat run #461
463	R463	49.8	175	13.86	14.38	44.4	72.1	0.6101	38.2	62.7	43	67	9	11:04	11	repeat run #461
464	R464	51	176	13.85	14.38	45.7	70.9	0.2664	19.3	72.5	22	77	3.8	11:14	21	Collector mechanism, alpha=0 deg, strips G, I and C.
465	R465	48.9	176	13.85	14.38	43.4	71.2	0.2573	18.6	72.3	22	77	3.8	11:21	21	repeat run #464
466	R466	48.6	176	13.85	14.38	43.2	70.4	0.2675	19.3	72.1	22	77	3.8	11:27	21	repeat run #464
467	R467	49.3	150	13.97	14.38	45.2	71.3	0.1353	4.3	32.1	6	37	2.2	11:40	94	Collector mechanism, splashing test, alpha=0 deg, strips G, I and C.
468	R468	51.1	150	13.99	14.38	47.2	75	0.1253	4.1	32.7	6	37	2.2	11:49	94	repeat run #467
469	R469	49.1	101	14.2	14.38	47.2	70.7	0.1379	4.4	32.1	6	37	2.2	12:00	94	Collector mechanism, splashing test, alpha=0 deg, strips G, I and C.
470	R470	48.8	100	14.2	14.37	47.1	73.3	0.1265	4.1	32.3	6	37	2.2	12:05	94	repeat run #469
471	R471	48.8	50	14.33	14.38	48.4	73.8	0.1495	4.8	32.3	6	37	2.2	12:11	94	Collector mechanism, splashing test, alpha=0 deg, strips G, I and C.
472	R472	48.9	50	14.33	14.38	48.4	74.1	0.1324	4.3	32.2	6	37	2.2	12:21	94	repeat run #471
473	R473	50.9	175	13.84	14.38	45.5	72.7	0.2616	18.9	72.4	22	77	3.8	12:41	21	Collector mechanism, alpha=8 deg, strips G, I and C.
474	R474	48.7	175	13.84	14.38	43.1	73.7	0.2647	19.1	72.0	22	77	3.8	1:00	21	repeat run #473
475	R475	49.6	174	13.84	14.37	44	76	0.2556	18.6	72.6	22	77	3.8	1:07	21	repeat run #473
476	R476	49.6	175	13.84	14.38	44.2	69.7	0.2574	18.6	72.4	22	77	3.8	1:20	21	Collector mechanism, alpha=8 deg, I-strip only.
477	R477	48.5	175	13.84	14.37	42.9	73.6	0.2546	18.5	72.5	22	77	3.8	1:26	21	repeat run #476
478	R478	48	174	13.84	14.37	42.6	70.6	0.1565	5.0	32.2	6	37	2.2	1:35	94	Collector mechanism, alpha=8 deg, I-strip only.
479	R479	48.4	175	13.84	14.37	42.7	71.3	0.1599	5.2	32.3	6	37	2.2	1:42	94	repeat run #478
480	R480	51	175	13.84	14.37	45.4	75.6	0.6147	38.3	62.2	43	67	9	1:56	11	Collector mechanism, alpha=8 deg, I-strip only.
481	R481	49	174	13.84	14.36	43.5	73.5	0.6125	38.2	62.4	43	67	9	2:03	11	repeat run #480
482	R482	48.9	174	13.84	14.37	43.4	72.5	0.6118	38.1	62.4	43	67	9	2:09	11	repeat run #480
483	R483	47.3	176	13.83	14.36	41.8	71.7	0.6086	38.2	62.8	43	67	9	3:40	11	Uniformity grid with collector strips size
484	R484	48.8	176	13.84	14.37	43.2	75.1	0.2652	19.2	72.5	22	77	3.8	4:17	21	Uniformity grid with collector strips size
485	R485	49.6	176	13.84	14.37	43.8	74.2	0.1291	4.2	32.3	6	37	2.2	4:56	94	Uniformity grid with collector strips size

Date : February 22, 1999
P_{BAR} :
DYE CONCENTRATION : 0.0003 grams/cc
PSYCHROMETER READINGS :
:

		TUNNEL CONDITION						SPRAY CONDITIONS / MASS FLOW								REMARKS
								NOZZLE PRESSURE			TANK PRESSURE		TIME			
RUN NO.	Run I.D.	TEMP. Total (°F)	TAS (MPH)	P_{∞} (PSIA)	PRESS TOTAL (PSIA)	TEMP. Stat (°F)	Humidity %	$\frac{P_{AIR}}{P_{WATER}}$	P_{AIR} (PSIG)	P_{WATER} (PSIG)	P_{AIR} (PSIG)	P_{WATER} (PSIG)	SPRAY (SEC)	SPRAY TIME (PM)	MVD	
486	R486															BJE, pressure data, alpha=7, 6, 5, 4, 3, 2, 1, 0 degs.

Date : February 23, 1999
P_{BAR} :
DYE CONCENTRATION : 0.0003 grams/cc
PSYCHROMETER READINGS :
:
:

		TUNNEL CONDITION						SPRAY CONDITIONS / MASS FLOW								REMARKS
								NOZZLE PRESSURE			TANK PRESSURE		TIME			
RUN NO.	Run I.D.	TEMP. Total (°F)	TAS (MPH)	P_∞ (PSIA)	PRESS TOTAL (PSIA)	TEMP. Stat (°F)	Humidity %	$\frac{P_{AIR}}{P_{WATER}}$	P_{AIR} (PSIG)	P_{WATER} (PSIG)	P_{AIR} (PSIG)	P_{WATER} (PSIG)	SPRAY (SEC)	SPRAY TIME (PM)	MVD	
487	R487	49	176	13.87	14.41	43.5	73.2	0.6053	38.0	62.8	43	67	9	4:31	11	All nozzles, steam on, IRT air off, BJE, A and B strips, delta=0 deg, alpha=1 deg.
488	R488	47.8	176	13.88	14.42	42.2	71.9	0.6083	38.2	62.8	43	67	9	4:46	11	repeat run #487
489	R489	46.1	176	13.87	14.42	40.5	72.2	0.6123	38.4	62.7	43	67	9	5:00	11	repeat run #487
490	R490	46.5	176	13.88	14.42	41	72	0.2559	18.6	72.8	22	77	3.8	5:16	21	All nozzles, steam on, IRT air off, BJE, A and B strips, delta=0 deg, alpha=1 deg.
491	R491	50.1	176	13.88	14.42	44.6	73.2	0.2635	19.2	72.9	22	77	3.8	5:35	21	repeat run #490
492	R492	45.7	177	13.88	14.42	40	74.6	0.2591	18.8	72.6	22	77	3.8	5:51	21	repeat run #490
493	R493	45.7	175	13.88	14.42	40.1	72.9				6	37	2.2	6:06	94	All nozzles, steam on, IRT air off, BJE, A and B strips, delta=0 deg, alpha=1 deg.
494	R494	46.9	176	13.88	14.42	41.2	73.4	0.1538	5.0	32.8	6	37	2.2	6:19	94	repeat run #493
495	R495	48.5	175	13.88	14.42	43	71.6	0.1562	5.1	32.6	6	37	2.2	6:30	94	repeat run #493
496	R496	47	175	13.88	14.43	41.5	71	0.1583	5.1	32.4	6	37	2.2	6:45	94	All nozzles, steam on, IRT air off, BJE, A and B strips, delta=0 deg, alpha=6 deg.
497	R497	47.5	174	13.88	14.43	42	72.5	0.1284	4.2	32.4	6	37	2.2	7:00	94	repeat run #496
498	R498	46.4	174	13.88	14.43	40.9	71.3	0.1347	4.4	32.7	6	37	2.2	7:12	94	repeat run #496
499	R499	45.6	175	13.88	14.42	40.1	73.3	0.6013	38.0	63.2	43	67	9	7:23	11	All nozzles, steam on, IRT air off, BJE, A and B strips, delta=0 deg, alpha=6 deg.
500	R500	46	174	13.89	14.43	40.5	74.5	0.6096	38.3	62.8	43	67	9	7:40	11	repeat run #499
501	R501	47.5	175	13.88	14.42	42.1	74.9	0.6068	38.1	62.9	43	67	9	7:54	11	repeat run #499
502	R502	46.5	174	13.88	14.42	41.1	72.9	0.2606	19.0	72.8	22	77	3.8	8:07	21	All nozzles, steam on, IRT air off, BJE, A and B strips, delta=0 deg, alpha=6 deg.
503	R503	48.4	175	13.88	14.42	42.9	73.6	0.2623	19.0	72.4	22	77	3.8	8:24	21	repeat run #502
504	R504	47.4	175	13.88	14.42	41.9	71.6	0.2616	19.0	72.7	22	77	3.8	8:32	21	repeat run #502
505	R505	45.5	176	13.88	14.42	40	73.2	0.6101	38.4	62.9	43	67	9	10:18	11	All nozzles, steam on, IRT air off, BJE, A and B strips, delta=10 deg, alpha=1 deg.
506	R506	47.8	174	13.89	14.42	42.6	75.6	0.6053	38.0	62.8	43	67	9	10:30	11	repeat run #505
507	R507	46.5	175	13.89	14.42	41.2	75.2	0.6073	38.4	63.2	43	67	9	10:54	11	repeat run #505

Date : February 24, 1999
P_{BAR} :
DYE CONCENTRATION : 0.0003 grams/cc
PSYCHROMETER READINGS :
:

		TUNNEL CONDITION						SPRAY CONDITIONS / MASS FLOW								REMARKS
								NOZZLE PRESSURE			TANK PRESSURE		TIME			
RUN NO.	Run I.D.	TEMP. Total (°F)	TAS (MPH)	P_{∞} (PSIA)	PRESS TOTAL (PSIA)	TEMP. Stat (°F)	Humidity %	P_{AIR}/P_{WATER}	P_{AIR} (PSIG)	P_{WATER} (PSIG)	P_{AIR} (PSIG)	P_{WATER} (PSIG)	SPRAY (SEC)	SPRAY TIME (PM)	MVD	
508	R508	47.7	176	13.86	14.4	42.1	75.1	0.6076	38.1	62.7	43	67	30	5:27	11	10 frames, 2 sec/fr, laser image, clean tunnel, steam on, IRT air off, all nozzles.
509	R509	49	176	13.86	14.41	43.5	75.9	0.6027	37.8	62.7	43	67	9	5:30	11	1 frame, 10 sec/fr, laser image, clean tunnel, steam on, IRT air off, all nozzles.
510	R510	46.3	176	13.87	14.41	40.8	72.7	0.2610	19.0	72.7	22	77	30	5:34	21	10 frames, 2 sec/fr, laser image, clean tunnel, steam on, IRT air off, all nozzles.
511	R511	47	176	13.87	14.4	41.5	75.7	0.2583	18.7	72.5	22	77	3.8	5:36	21	1 frame, 5 sec/fr, laser image, clean tunnel, steam on, IRT air off, all nozzles.
512	R512	46.3	176	13.85	14.4	40.7	73.6	0.1322	4.3	32.4	6	37	30	5:41	94	10 frames, 2 sec/fr, laser image, clean tunnel, steam on, IRT air off, all nozzles.
513	R513	47.1	176	13.86	14.34	41.5	75.8	0.1407	4.6	32.4	6	37	2.2	5:43	94	1 frame, 3.2 sec/fr, laser image, clean tunnel, steam on, IRT air off, all nozzles.
514	R514	47.8	176	13.86	14.39	42.3	71.6	0.1572	5.1	32.5	6	37	2.2	6:43	94	Collector mechanism, BJE, all nozzles, IRT air off, steam on, I-mod strip at B-strip location.
515	R515	44	176	13.84	14.39	38.7	74.7	0.1429	4.6	32.2	6	37	2.2	6:49	94	repeat run #514
516	R516	45	176	13.84	14.39	39.2	74.1	0.1546	5.0	32.5	6	37	2.2	6:54	94	repeat run #514
517	R517	46.2	175	13.85	14.39	40.7	77.2	0.6097	38.2	62.7	43	67	9	7:03	11	Collector mechanism, BJE, all nozzles, IRT air off, steam on, I-mod strip at B-strip location.
518	R518	45.6	174	13.85	14.39	40.3	76.4	0.6089	38.2	62.7	43	67	9	7:10	11	repeat run #517
519	R519	44.2	177	13.86	14.39	38.6	75.3	0.6036	37.9	62.8	43	67	9	7:24	11	repeat run #517
520	R520	48.2	177	13.84	14.38	42.9	74.8	0.2586	18.8	72.8	22	77	3.8	7:36	21	Collector mechanism, BJE, all nozzles, IRT air off, steam on, I-mod strip at B-strip location.
521	R521	45.8	177	13.84	14.38	40.2	74.6	0.2581	18.8	72.7	22	77	3.8	7:42	21	repeat run #520
522	R522	45.8	176	13.84	14.38	40.1	75.3	0.2639	19.2	72.6	22	77	3.8	7:49	21	repeat run #520
523	R523	46	176	13.83	14.38	40.4	74.3	0.2655	19.3	72.7	22	77	3.8	8:06	21	Collector mechanism, BJE, all nozzles, IRT air off, steam on, I-mod strip at A-strip location.
524	R524	50.6	177	13.83	14.38	45.1	73.6	0.2605	18.8	72.3	22	77	3.8	8:20	21	repeat run #523
525	R525	47.6	177	13.83	14.37	41.9	75.9	0.2650	19.2	72.4	22	77	3.8	8:32	21	repeat run #523
526	R526	46.2	175	13.83	14.38	40.8	75.7	0.6052	38.2	63.2	43	67	9	8:44	11	Collector mechanism, BJE, all nozzles, IRT air off, steam on, I-mod strip at A-strip location and E-strip,
527	R527	46.2	175	13.84	14.38	40.7	74.8	0.6040	37.9	62.7	43	67	9	8:50	11	repeat run #526
528	R528	48.4	175	13.84	14.38	42.9	75.7	0.6103	38.3	62.8	43	67	9	9:00	11	repeat run #526
529	R529	46.9	174	13.84	14.37	41.4	73	0.1366	4.4	32.4	6	37	2.2	9:07	94	Collector mechanism, BJE, all nozzles, IRT air off, steam on, I-mod strip at A-strip location and E-strip,
530	R530	46.1	175	13.84	14.38	40.6	72.3	0.1380	4.5	32.5	6	37	2.2	9:14	94	repeat run #529
531	R531	45.9	175	13.83	14.38	40.4	71.7	0.1402	4.5	32.3	6	37	2.2	9:20	94	repeat run #529
532	R532	48.3	174	13.84	14.37	42.8	74.1	0.1365	4.4	32.5	6	37	2.2	9:34	94	Collector mechanism at center of turntable (normal position), I-strip, all nozzles, IRT air off, steam on.
533	R533	46.3	174	13.84	14.37	40.8	75.2	0.6059	38.2	63.1	43	67	9	9:46	11	Collector mechanism at center of turntable (normal position), I-strip, all nozzles, IRT air off, steam on.
534	R534	45.9	174	13.83	14.36	40.6	74.5	0.2535	18.4	72.7	22	77	3.8	9:54	21	Collector mechanism at center of turntable (normal position), I-strip, all nozzles, IRT air off, steam on.

Note: No run performed on February 25, 1999.

Date : February 26, 1999
P_{BAR} :
DYE CONCENTRATION : 0.0003 grams/cc
PSYCHROMETER READINGS :
:
:

		TUNNEL CONDITION						SPRAY CONDITIONS / MASS FLOW								
								NOZZLE PRESSURE			TANK PRESSURE		TIME			
RUN NO.	Run I.D.	TEMP. Total (°F)	TAS (MPH)	P_{∞} (PSIA)	PRESS TOTAL (PSIA)	TEMP. Stat (°F)	Humidity %	$\frac{P_{AIR}}{P_{WATER}}$	P_{AIR} (PSIG)	P_{WATER} (PSIG)	P_{AIR} (PSIG)	P_{WATER} (PSIG)	SPRAY (SEC)	SPRAY TIME (PM)	MVD	REMARKS
535	R535															pressure data (rdg #6725 to #6730).
																took video of laser image for MVD 21 without and with mass flow of 23 lbs/sec.
																took another few video of laser image of other MVD.
536	R536	49.1	170	13.84	14.36	43.8	74.5				6	37	2.2	8:16	94	S-duct inlet, all nozzles, steam on, strips A, B, C and D, mass flow = 23 lbs/s, scavenge flow = 2 lbs/s.
537	R537	50.5	169	13.86	14.37	45.4	71.6				6	37	2.2	8:53	94	repeat run #536
538	R538	50.2	170	13.86	14.37	44.9	73.7				6	37	2.2	9:20	94	repeat run #536
539	R539	48.8	170	13.86	14.36	43.4	72.6				22	77	3.8	9:51	21	S-duct inlet, all nozzles, steam on, strips A, B, C and D, mass flow = 23 lbs/s, scavenge flow = 2 lbs/s.
540	R540	47	169	13.86	14.36	41.8	67.1				22	77	3.8	10:21	21	repeat run #539
541	R541	50	169	13.86	14.36	44.8	72.3				22	77	3.8	10:46	21	repeat run #539

Date : February 27, 1999
P_{BAR} :
DYE CONCENTRATION : 0.0003 grams/cc
PSYCHROMETER READINGS :
:

		TUNNEL CONDITION						SPRAY CONDITIONS / MASS FLOW								REMARKS
								NOZZLE PRESSURE			TANK PRESSURE		TIME			
RUN NO.	Run I.D.	TEMP. Total (°F)	TAS (MPH)	P_{∞} (PSIA)	PRESS TOTAL (PSIA)	TEMP. Stat (°F)	Humidity %	$\frac{P_{AIR}}{P_{WATER}}$	P_{AIR} (PSIG)	P_{WATER} (PSIG)	P_{AIR} (PSIG)	P_{WATER} (PSIG)	SPRAY (SEC)	SPRAY TIME (PM)	MVD	
542	R542	49.4	131	13.97	14.26	46.5	75	0.2609	18.8	72.0	22	77	3.8	10:05	21	S-duct inlet, all nozzles, steam on, strips A, B, C and D, mass flow = 23 lbs/s, scavenge flow = 1.5 lbs/s.
543	R543	49.4	130	13.96	14.25	46.3	74.3	0.2642	19.1	72.3	22	77	3.8	10:29	21	repeat run #542
544	R544	48	130	13.96	14.25	45	74.4	0.2635	19.0	72.3	22	77	3.8	10:50	21	repeat run #542
545	R545	50.4	131	13.94	14.24	47.4	68.7	0.1438	4.7	32.3	6	37	2.2	11:27	94	S-duct inlet, all nozzles, steam on, strips A, B, C and D, mass flow = 23 lbs/s, scavenge flow = 1.5 lbs/s
546	R546	50.6	131	13.94	14.23	47.6	71.8	0.1488	4.8	32.0	6	37	2.2	11:55	94	repeat run #545
547	R547	49.1	131	13.92	14.22	46.1	74.5	0.1455	4.7	32.2	6	37	2.2	12:25	94	repeat run #545
548	R548	50.5	169	13.71	14.21	45.4	71.5	0.6150	38.4	62.4	43	67	9	12:50	11	S-duct inlet, all nozzles, steam on, strips A, B, C and D, mass flow = 23 lbs/s, scavenge flow = 2 lbs/s
549	R549	51.3	170	13.7	14.21	46	72.6	0.6066	38.4	63.2	43	67	9	1:13	11	repeat run #548
550	R550	53.2	171	13.7	14.2	47.7	74.2	0.6129	38.1	62.1	43	67	9	1:47	11	repeat run #548
551	R551	55.7	169	13.69	14.19	50.4	73.5	0.1439	4.7	32.4	6	37	2.2	2:16	94	S-duct inlet, all nozzles, steam on, strips A, B, C and D, mass flow = 23 lbs/s, scavenge flow = 2 lbs/s
552	R552	55.4	172	13.69	14.19	50.1	70.3	0.1407	4.5	32.2	6	37	2.2	2:45	94	repeat run #561

Date : March 1, 1999 (cont.)
P_{BAR} :
DYE CONCENTRATION : 0.0003 grams/cc
PSYCHROMETER READINGS :
:

		TUNNEL CONDITION						SPRAY CONDITIONS / MASS FLOW								
								NOZZLE PRESSURE			TANK PRESSURE		TIME			
RUN NO.	Run I.D.	TEMP. Total (°F)	TAS (MPH)	P_{∞} (PSIA)	PRESS TOTAL (PSIA)	TEMP. Stat (°F)	Humidity %	$\frac{P_{AIR}}{P_{WATER}}$	P_{AIR} (PSIG)	P_{WATER} (PSIG)	P_{AIR} (PSIG)	P_{WATER} (PSIG)	SPRAY (SEC)	SPRAY TIME (PM)	MVD	REMARKS
553	R553	47.4	200			40.2	63.6						120	3:33	94	Splashing test, laser sheet method. Laser sheet is normal to the chord length of MS-317. Alpha=0 deg.
																video tape = 10.
554	R554	47	200			40	62		5.0	55.0			120	3:36	175	Splashing test, laser sheet method. Laser sheet is normal to the chord length of MS-317. Alpha=0 deg.
																video tape = 11:40.
555	R555	47.6	200 to 50			40	63.5				6	37	150	3:40	94	Splashing test, laser sheet method. Laser sheet is normal to the chord length of MS-317. Alpha=0 deg.
																video tape = 13:22. Speed is reduced after about 40 sec of spray time.
556	R556	45	50 to 200			44.5	73				22	77	150	3:45	21	Splashing test, laser sheet method. Laser sheet is normal to the chord length of MS-317. Alpha=0 deg.
																video tape = 16:28. Speed is increased after about 40 sec of spray time.
557	R557	45.5	200 to 40			38.4	75.7				43	67	150	3:49	11	Splashing test, laser sheet method. Laser sheet is normal to the chord length of MS-317. Alpha=0 deg.
																video tape = 18:50. Speed is reduced after about 40 sec of spray time.
558	R558	47	175			41	78				6	37	150	3:52	94	Splashing test, laser sheet method. Laser sheet is normal to the chord length of MS-317.
																video tape = 21:44. AOA changed from 0 deg to 8 deg while spraying.
559	R559	48	175			43	75				6	37	150	3:56	94	Splashing test, laser sheet method. Laser sheet is normal to the chord length of MS-317. Alpha=8 deg.
																video tape = 24:40.
560	R560	47.7	175			42.2	71.6		2.0	24.0			150	4:00	270	Splashing test, laser sheet method. Laser sheet is normal to the chord length of MS-317. Alpha=8 deg.
																video tape = 27:33.
561	R561	45	175			39.6	70.5		2.0	24.0			120	4:06	270	Splashing test, laser sheet method. Laser sheet is normal to the chord length of MS-317. Alpha=0 deg.
																video tape = 30:39.
562	R562	45.5	200 to 10			40.2	77.8				6	37	160	4:11	94	Splashing test, laser sheet method. Laser sheet is normal to the chord length of MS-317. Alpha=0 deg.
																video tape = 33:08.
563	R563	46.8	0 to 200			46.8	78.9				6	37	200	4:16	94	Splashing test, laser sheet method. Laser sheet is normal to the chord length of MS-317. Alpha=0 deg.
																video tape = 36:47.
564	R564	47.4	130	13.86	14.15	44.6	72.4	0.2543	18.4	72.2	22	77	3.8	5:34	21	Collector, S-duct inlet, strips A, B, C, G, H and I.
565	R565	45.8	131	13.86	14.16	42.8	72.4	0.2609	18.8	72.1	22	77	3.8	5:44	21	repeat run #564
566	R566	45.4	131	13.86	14.16	42.4	72.9	0.2620	18.9	72.3	22	77	3.8	5:52	21	repeat run #564
567	R567	45.8	131	13.86	14.16	42.7	75	0.2675	19.3	72.3	22	77	3.8	6:00	21	repeat run #564

Date : March 1, 1999
P_{BAR} :
DYE CONCENTRATION : 0.0003 grams/cc
PSYCHROMETER READINGS :
:

		TUNNEL CONDITION						SPRAY CONDITIONS / MASS FLOW								
								NOZZLE PRESSURE			TANK PRESSURE		TIME			
RUN NO.	Run I.D.	TEMP. Total (°F)	TAS (MPH)	P_{∞} (PSIA)	PRESS TOTAL (PSIA)	TEMP. Stat (°F)	Humidity %	$\frac{P_{AIR}}{P_{WATER}}$	P_{AIR} (PSIG)	P_{WATER} (PSIG)	P_{AIR} (PSIG)	P_{WATER} (PSIG)	SPRAY (SEC)	SPRAY TIME (PM)	MVD	REMARKS
568	R568	47.4	131	13.86	14.16	44.4	75.4	0.1333	4.3	32.2	6	37	2.2	6:12	94	Collector, S-duct inlet, strips A, B, C, G, H and I.
569	R569	47.6	131	13.86	14.16	44.6	75.5	0.1448	4.7	32.6	6	37	2.2	6:19	94	repeat run #568
570	R570	47.8	131	13.86	14.16	44.7	74.9	0.1410	4.5	32.0	6	37	2.2	6:26	94	repeat run #568
571	R571	46.6	171	13.67	14.16	41.4	75.7	0.6184	38.5	62.3	43	67	9	6:46	11	Collector, S-duct inlet, strips A, B, C, G, H and I.
572	R572	48.8	171	13.66	14.17	43.7	76	0.6114	38.0	62.2	43	67	9	6:55	11	repeat run #571
573	R573	46.2	171	13.67	14.17	40.9	74.1	0.6132	38.1	62.2	43	67	9	7:06	11	repeat run #571
574	R574	46.5	171	13.66	14.17	41.2	72.8	0.2643	19.1	72.1	22	77	3.8	7:20	21	Collector, S-duct inlet, strips A, B, C, G, H and I.
575	R575	49	172	13.67	14.17	43.8	72.8	0.2655	19.1	71.9	22	77	3.8	7:31	21	repeat run #574
576	R576	48	171	13.66	14.17	42.8	71.8	0.2648	19.1	72.3	22	77	3.8	7:40	21	repeat run #574
577	R577	47.2	171	13.67	14.18	42	72.1	0.1343	4.3	32.3	6	37	2.2	7:50	94	Collector, S-duct inlet, strips A, B, C, G, H and I.
578	R578	47.5	170	13.67	14.17	42.3	75.3	0.1376	4.5	32.6	6	37	2.2	7:56	94	repeat run #577
579	R579	47.8	171	13.67	14.18	42.6	73.7	0.1412	4.6	32.6	6	37	2.2	8:04	94	repeat run #577
580	R580	48.8	176	13.64	14.17	43.2	72.6	0.1547	5.0	32.1	6	37	2.2	8:27	94	Collector, BJE, I-mod strip, B-location.
581	R581	46.7	176	13.64	14.18	41.2	73.4	0.1450	4.7	32.6	6	37	2.2	8:40	94	repeat run #580
582	R582	46.9	176	13.65	14.18	41.4	74.3	0.1445	4.7	32.6	6	37	2.2	8:46	94	repeat run #580
583	R583	48.3	176	13.65	14.18	42.7	76.3	0.6113	38.2	62.5	43	67	9	8:52	11	Collector, BJE, I-mod strip, B-location.
584	R584	48.4	176	13.64	14.18	43	74.5	0.6171	38.4	62.2	43	67	9	8:59	11	repeat run #583
585	R585	47.2	176	13.65	14.18	41.7	74.5	0.6093	38.2	62.6	43	67	9	9:04	11	repeat run #583
586	R586	46.8	176	13.65	14.18	41.3	74.2	0.2662	19.2	72.2	22	77	3.8	9:11	21	Collector, BJE, I-mod strip, B-location.
587	R587	46.7	176	13.65	14.18	41.1	73.2	0.2607	18.9	72.4	22	77	3.8	9:16	21	repeat run #586
588	R588	49.3	177	13.65	14.18	43.9	73.1	0.2616	18.9	72.3	22	77	3.8	9:26	21	repeat run #586
589	R589	46.6	175	13.65	14.18	41.1	74.7	0.2585	18.7	72.5	22	77	3.8	9:40	21	Collector, NLF airfoils, alpha=8 deg, I-strip only.
590	R590	46.5	175	13.66	14.18	41.1	74.5	0.2640	19.1	72.4	22	77	3.8	9:45	21	repeat run #589
591	R591	48.7	175	13.66	14.18	43	75.6	0.2575	18.6	72.2	22	77	3.8	9:53	21	repeat run #589
592	R592	48.5	175	13.65	14.18	43	74.3	0.1349	4.4	32.6	6	37	2.2	10:00	94	Splashing test, NLF-airfoil location, alpha=8 deg, I-strip only.
593	R593	47.2	174	13.66	14.18	41.8	75.4	0.1315	4.3	32.4	6	37	2.2	10:07	94	repeat run #572
594	R594	46.7	50	14.14	14.18	46.4	74.5	0.1562	5.1	32.6	6	37	2.2	10:14	94	Splashing test, NLF-airfoil location, alpha=8 deg, I-strip only.
595	R595	45.9	50	14.14	14.18	45.5	76.3	0.1348	4.4	32.5	6	37	2.2	10:17	94	repeat run #594

References

1. Von Glahn, U., Gelder, T.F., and Smyers, W.H. Jr, "A Dye Tracer Technique for Experimentally Obtaining Impingement Characteristics of Arbitrary Bodies and a Method for Determining Droplet Size Distribution," NACA TN–3338, March 1955.
2. Gelder, T.F., Smyers, W.H. Jr, and Von Glahn, U., "Experimental Droplet Impingement on Several Two-Dimensional Airfoils with Thickness Ratios of 6 to 16 percent," NACA TN–3839, December 1956.
3. Lewis, J.O. and Ruggeri, R.S., "Experimental Droplet Impingement on Four Bodies of Revolution," NACA TN–3587, 1957.
4. Lewis, James O. and Ruggeri, Robert S., "Experimental Droplet Impingement on four bodies of revolution," NACA TN–4092, December 1955.
5. Gelder, T.F., "Droplet Impingement and Ingestion by Supersonic Nose Inlet in Subsonic Tunnel Conditions," NACA TN–4268, May 1958.
6. Papadakis, M., Elangovan, R., Freund, G.A., Jr., Breer, M., Zumwalt, G.W. and Whitmer, L., "An Experimental Method for Measuring Water Droplet Impingement Efficiency on Two- and Three-Dimensional Bodies," NASA CR–4257, DOT/FAA/CT–87/22, November 1989.
7. Papadakis, M., Breer, M.D., Craig, N., and Liu, X., "Experimental Water Droplet Impingement Data on Airfoils, Simulated Ice Shapes, an Engine Inlet and a Finite Wing," NASA CR 4636, DOT/FAA/CT–TN93/18, December 1994.
8. Phillips, E.H. "ATR42/72 Review Focuses on Icing," Aviation Week and Space Technology, November 14, 1994.
9. Phillips, E.H. "FAA Lifts Icing Ban on ATR Flights," Aviation Week and Space Technology, June 5, 1995.
10. Miller, D.R., Addy, H.E., and Ide, R.F, "A Study of Large Droplet Ice Accretions in the NASA-Lewis IRT at Near-Freezing Conditions," AIAA Paper 96–0934, 34th Aerospace Sciences Meeting and Exhibit, Reno, NV, January 15–18, 1996.
11. Bragg, M.B., "Aircraft Aerodynamic Effects due to Large Droplet Ice Accretions," AIAA Paper 96–0932, 34th Aerospace Sciences Meeting and Exhibit, Reno, NV, January 15–18, 1996.
12. "FAA Inflight Aircraft Icing Plan," Federal Aviation Administration, April 1997.
13. Kim, John, "Particle Trajectory Computation on a 3-Dimensional Engine Inlet," NASA CR–175023, DOT–FAA–CT–86–1, January 1986.
14. Carlson, D.J. and Hoglund, R.F., "Particle Drag and Heat Transfer in Rocket Nozzles," AIAA Journal, Vol. 2, No. 11, pp. 1980–1984, November 1964.
15. Langmuir, I. And Blodgett, K.B., "A mathematical Investigation of Water Droplet Trajectories," Army Air Forces Technical Report No. 5418, 1946.
16. Soeder, R.H. and Andracchio, C.R., "NASA Lewis Icing Research Tunnel User Manual," NASA TM–102319, June 1990.
17. McGhee, R.J. and Beasley, W.D., "Low-Speed Aerodynamic Characteristics of a 17-Percent-Thick Medium-Speed Airfoil Designed for General Application," NASA TP–1786, 1980.
18. Addy, H.E., Jr., Potapczuk, M.G., and Sheldon, D.W., "Modern Airfoil Ice Accretions," NASA TM–107423, January 1997.

19. Torenbeek, E., "Synthesis of Subsonic Airplane Design," Delft University Press, 1982.
20. Abbott, I.H. and Von Doenhoff, A.E., "Theory of Wing Sections," Dover Publications, Inc., 1959.
21. McGhee, R.J., Viken, J.K., Pfenninger, W., Beasley, W.D., and Harvey, W.D., "Experimental Results for a Flapped Natural-Laminar-Flow Airfoil with High Lift/Drag Ratio," NASA TM–85788, May 1984.
22. Valarezo, W.O., Dominik, C.J., McGhee, R.J., Goodman, W.L., and Paschal, K.B., "Multi-Element Airfoil Optimization for Maximum Lift at High Reynolds Numbers," AIAA paper 91–3332, September 1991.
23. Valarezo, W.O., Dominik, C.J., and McGhee, R.J., "Reynolds and Mach Number Effects on Multielement Airfoils," Fifth Symposium on Numerical and Physical Aspects of Aerodynamic Flows, Long Beach, January, 1992.
24. Batra, A.B., Bennett, W.A., Vittal, B.R., and Krishnan, M.R., "Design and Development of a Compact Bifurcated Turboprop Inlet," AIAA Paper 91–2017, June 1991.
25. Canacci, V., Bencic, T., Krupar, M., and Potapczuk, M., "A Sheet Laser Flow Visualization System in NASA's Icing Research Tunnel," AIAA Paper 98–0342, January 1998.
26. Oldenburg, J.R. and Ide, R.F., "Comparison of Drop Size Distributions From Two Droplet Sizing Systems," NASA TM–102520, March 1990.
27. "CSIRO-KING Liquid Water Content Probe PMS Model KLWC-5 – Operating and Servicing Manual," Particle Measuring Systems, Inc., Boulder, Colorado.
28. Frei, R.W. and MacNeil, J.D., "Diffuse reflectance Spectroscopy in Environmental Problem Solving," CRC Press, Cleveland, Ohio, 1973.
29. Kubelka, P., "New Contributions to the Optics of Intensely Light-Scattering Materials—Part I," Journal of the Optical Society of America, Volume 38, 1955.
30. Bragg, M.B., Sweet, D., Waples,T., and Shick, R. "An Experimental Method for Water Droplet Impingement Measurement," Proceedings of the American Helicopter Society/Society of Automotive Engineers, International Icing Symposium, Montreal Canada, September 18–21, 1995.
31. Wright, W.B., "Users Manual for the Improved NASA Lewis Ice Accretion Code LEWICE 1.6," NASA CR–198355, June 1995.
32. Johnson, F., Samant, S., Bieterman, M., Melvin, R., Young, D., Bussoletti, J., and Hilmes, C., "TranAir: A Full-Potential, Solution-Adaptive, Rectangular Grid Code for Predicting Subsonic, Transonic, and Supersonic flows about Arbitrary Configurations," NASA CR–4348, December 1982.
33. Ashby, D., Dudley, M., and Iguchi, S., "Development and Validation of an Advanced Low-Order Panel Method," NASA TM–101024, October 1988.
34. Papadakis, M., Hung, K.E., Bidwell, C., and Breer, M., "Experimental Investigation of Water Impingement on Single and Multi-Element Airfoils," AIAA Paper 2000–0100, 38th Aerospace Sciences Meeting and Exhibit, Reno, NV, January 10–13, 2000.
35. Potapczuk, M. and Bidwell, C., "Swept Wing Ice Accretion Modeling," NASA TM–103114, January 1990.

36. Potapczuk, M. and Bidwell, C., “Numerical Simulation of Ice Growth on a MS-317 Swept Wing Geometry,” NASA TM–103705, January 1991.
37. Reehorst, A., “Prediction of Ice Accretion on a Swept NACA 0012 Airfoil and Comparisons to flight test Results,” NASA TM–105368, January 1992.
38. Mohler, S. and Bidwell, C., “Comparison of Two-Dimensional and Three-Dimensional Droplet Trajectory Calculations in the Vicinity of Finite Wings,” NASA TM–105617, January 1992.
39. Bidwell, C. and Mohler, S., “Collection Efficiency and Ice Accretion Calculations for a Sphere, a Swept MS(1)-317 Wing, a Swept NACA–0012 Wing Tip, an Axisymmetric Inlet, and a Boeing 737-300 Inlet,” NASA TM–106831, January 1995.
40. Bidwell, C., Pinella, D., and Garrison, P., “Ice Accretion Calculations for Commercial Transport Using the LEWICE-3D, ICEGRID3D, and CMARC Programs,” NASA/TM—1999-208895, January 1999.
41. Al-Khalil, K., Hitzigrath, R., Phillippi, O. and Bidwell, C., “Icing Analysis and Test of a Business Jet Engine Inlet Duct,” AIAA Paper 2000–1040, 38th Aerospace Sciences Meeting and Exhibit, Reno, NV, January 10–13, 2000.
42. Bidwell, C. and Potapczuk, M., “Users Manual for the NASA Lewis Three-Dimensional Ice Accretion Code (LEWICE-3D),” NASA TM–105974, December 1993.
43. Norment, H., “Calculation of Water Drop Trajectories To and About Three-Dimensional Lifting and Non-lifting bodies in Potential Airflow,” NASA CR–3935, October 1985.
44. Krogh, F., “Variable Order Integrators for Numerical Solutions of Ordinary Differential Equations,” Jet Propulsion Lab Technology Utilization Document No. CP–32308, November 1970.
45. Ide, R.F, private communication, April 16, 1996.
46. Ide, R.F., “Liquid Water Content and Droplet Size Calibration of the NASA Lewis Icing Research Tunnel,” AIAA Paper 90–0669, 28th Aerospace Sciences Meeting and Exhibit, Reno, NV, January 8–11, 1990.
47. Rogers, S.E. and Kwak, D., “An Upwind Differencing Scheme for the Steady State Incompressible Navier-Stokes Equations,” NASA TM–101051, November 1988.
48. Rogers, S.E. and Kwak, D., “An Upwind Differencing Scheme for the Time Accurate Incompressible Navier-Stokes Equations,” AIAA Journal, Vol. 28, No. 2, February 1990, pp. 253–262.
49. Power, G.D., Cooper, G.K., and Sirbaugh, J.R., "NPARC 2.2—Features and Capabilities," AIAA Paper 95–2609, 1995.
50. Papadakis, M., Vu, G.T., Hung, E.K., Bidwell, C.S., Bencic, T., and Breer, M.D., "Progress in Measuring Water Impingement Characteristics on Aircraft Surfaces," AIAA Paper 98–0488, January 1998.
51. Wright, W.B. and Potapczuk, M.G, “Computational Simulation of Large Droplet Icing,” NASA Contractor Report, May, 1996.

52. Mundo, C., Sommerfeld, M., and Tropea, C., "Droplet-Wall Collisions: Experimental Studies of the deformation and Breakup Process," International Journal Multiphase Flow, Vol. 21, No. 2, pp.151–173, 1995.
53. Mundo, C., Sommerfeld, M., and Tropea, C., "On the Modeling of Liquid Sprays Impinging on Surfaces," Atomization and Sprays, vol. 8, pp. 625–652, 1998.
54. Tan J.S.C., "Droplet Dynamics – An experimental and Numerical Study," Large Droplet Splashing research Workshop, DERA, England, UK, October 18, 2000.

REPORT DOCUMENTATION PAGE

Form Approved
OMB No. 0704-0188

Public reporting burden for this collection of information is estimated to average 1 hour per response, including the time for reviewing instructions, searching existing data sources, gathering and maintaining the data needed, and completing and reviewing the collection of information. Send comments regarding this burden estimate or any other aspect of this collection of information, including suggestions for reducing this burden, to Washington Headquarters Services, Directorate for Information Operations and Reports, 1215 Jefferson Davis Highway, Suite 1204, Arlington, VA 22202-4302, and to the Office of Management and Budget, Paperwork Reduction Project (0704-0188), Washington, DC 20503.

1. AGENCY USE ONLY (*Leave blank*)	2. REPORT DATE	3. REPORT TYPE AND DATES COVERED
	October 2002	Technical Memorandum

4. TITLE AND SUBTITLE

Experimental Investigation of Water Droplet Impingement on Airfoils, Finite Wings, and an S-Duct Engine Inlet

5. FUNDING NUMBERS

WU–708–20–13–00

6. AUTHOR(S)

Michael Papadakis, Kuohsing E. Hung, Giao T. Vu, Hsiung Wei Yeong, Colin S. Bidwell, Marlin D. Breer, and Timothy J. Bencic

7. PERFORMING ORGANIZATION NAME(S) AND ADDRESS(ES)

National Aeronautics and Space Administration
John H. Glenn Research Center at Lewis Field
Cleveland, Ohio 44135–3191

8. PERFORMING ORGANIZATION REPORT NUMBER

E–13444

9. SPONSORING/MONITORING AGENCY NAME(S) AND ADDRESS(ES)

National Aeronautics and Space Administration
Washington, DC 20546–0001

10. SPONSORING/MONITORING AGENCY REPORT NUMBER

NASA TM—2002-211700

11. SUPPLEMENTARY NOTES

Michael Papadakis, Kuohsing E. Hung, and Hsiung Wei Yeong, Wichita State University, Wichita, Kansas 67260; Giao T. Vu and Marlin D. Breer, Boeing Airplane Company, Wichita, Kansas 67277; Colin S. Bidwell and Timothy J. Bencic, NASA Glenn Research Center. Responsible person, Colin S. Bidwell, organization code 5840, 216–433–3947.

12a. DISTRIBUTION/AVAILABILITY STATEMENT

Unclassified - Unlimited
Subject Categories: 03 and 34 Distribution: Nonstandard

Available electronically at http://gltrs.grc.nasa.gov

This publication is available from the NASA Center for AeroSpace Information, 301–621–0390.

12b. DISTRIBUTION CODE

13. ABSTRACT ***(Maximum 200 words)***

Validation of trajectory computer codes, for icing analysis, requires experimental water droplet impingement data for a wide range of aircraft geometries as well as flow and icing conditions. This report presents improved experimental and data reduction methods for obtaining water droplet impingement data and provides a comprehensive water droplet impingement database for a range of test geometries including an MS(1)-0317 airfoil, a GLC-305 airfoil, an NACA 65_2-415 airfoil, a commercial transport tail section, a 36-inch chord natural laminar flow NLF(1)-0414 airfoil, a 48-inch NLF(1)-0414 section with a 25 percent chord simple flap, a state-of-the-art three-element high lift system, a NACA 64A008 finite span swept business jet tail, a full-scale business jet horizontal tail section, a 25 percent-scale business jet empennage, and an S-duct turboprop engine inlet. The experimental results were obtained at the NASA Glenn Icing Research Tunnel (IRT) for spray clouds with median volumetric diameter (MVD) of 11, 11.5, 21, 92, and 94 microns and for a range of angles of attack. The majority of the impingement experiments were conducted at an air speed of 175 mph corresponding to a Reynolds number of approximately 1.6 million per foot. The maximum difference of repeated tests from the average ranged from 0.24 to 12 percent for most of the experimental results presented. This represents a significant improvement in test repeatability compared to previous experimental studies. The increase in test repeatability was attributed to improvements made to the experimental and data reduction methods. Computations performed with the LEWICE-2D and LEWICE-3D computer codes for all test configurations are presented in this report. For the test cases involving median volumetric diameters of 11 and 21 microns, the correlation between the analytical and experimental impingement efficiency distributions was good. For the median volumetric diameters of 92 and 94-micron cases, however, the analysis produced higher impingement efficiencies and larger impingement limits than the experiment. It is speculated that this discrepancy is due to droplet splashing and breakup experienced by large droplets during impingement.

14. SUBJECT TERMS

Aircraft icing; Aircraft safety; Flight safety; Ice prevention; Deicing; Impingement; Airfoils; Wings; Swept wings; Wing flaps; Engine inlets

15. NUMBER OF PAGES

439

16. PRICE CODE

17. SECURITY CLASSIFICATION OF REPORT	18. SECURITY CLASSIFICATION OF THIS PAGE	19. SECURITY CLASSIFICATION OF ABSTRACT	20. LIMITATION OF ABSTRACT
Unclassified	Unclassified	Unclassified	